Mémoires de Géologie (Lausanne) No. 42, 2004

Mont Blanc and Aiguilles Rouges
Geology of their polymetamorphic Basement
(External Massifs, Western Alps, France-Switzerland)

with 8 new geological maps, 80 photos, 80 figures , 16 tables

Jürgen F. von Raumer and François Bussy

IMPRIMERIE CHABLOZ S.A., LAUSANNE

ISSN 1015-3578

Mémoires de Géologie (Lausanne)

Section des Sciences de la Terre
Université de Lausanne
BFSH-2, 1015 Lausanne, Suisse

42

Mont Blanc and Aiguilles Rouges
Geology of their polymetamorphic Basement
(External Massifs, France-Switzerland)

with 8 new geological maps, 80 photos, 80 figures , 16 tables

by

Jürgen F. von Raumer and François Bussy

Mémoires de Géologie (Lausanne) No. 42, 2004

Mémoires de Géologie (Lausanne)

Mémoires de Géologie (Lausanne)
Section des Sciences de la Terre
Institut de Géologie et Paléontologie
Université de Lausanne
BFSH-2, CH-1015 Lausanne

Von RAUMER Jürgen F. and Bussy François
Titre : Mont Blanc and Aiguilles Rouges – Geology of their polymetamorphic basement
Mém. Géol. (Lausanne), n° 42, 2004, 203 pp., 80 text-figs., 80 photos, 16 tabs. and 8 coloured geol. maps
ISSN: 1015-3578

Imprimeur : Chabloz S.A., Lausanne

Cover figure :
Mer de Glace and Mont Blanc massif, view from north – Col de la Terrasse
La Mer de Glace et le massif du Mont Blanc, vue depuis le Nord – Col de la Terrasse

The financial printing support by the following institutions is greatly acknowledged:
Kommission für die Stiftung Dr. Joachim de Giacomi; Fondation B. & S. Tissières, Martigny; Etat du Valais;
Instituts de Géologie-Paléontologie et de Minéralogie-Géochimie de l'Université de Lausanne

Contents

Chapter III: Metamorphism and deformation

Abstract

The Aiguilles Rouges and Mont Blanc external massifs belong to the pre-Mesozoic basement areas of the external domain of the Alps. Before their involvement into the Alpine building (basement nappes) they registered a multiple geological evolution comprising the deposition of Neoproterozoic to Cambrian sediments and emplacement of granitoid and metabasic to ultramafic magmatic rocks of Early Palaeozoic age at the Gondwanan border. After rifting and drifting (formation of Palaeotethys) all rocks underwent polyphase metamorphic and structural transformations during the Variscan orogeny, and were intruded by late Variscan granitoids. The resulting polymetamorphic basement was eroded during formation of Upper Carboniferous sedimentary troughs. New geological maps are presented in this volume, together with structural, petrological and geochemical characteristics of all lithologies. The geochemical data are presented in annexes.

Résumé

Les massifs du Mont Blanc et des Aiguilles Rouges appartiennent aux massifs dits cristallins externes de la chaîne alpine occidentale. Ils sont constitués de roches pré-mésozoïques et dessinent des nappes de socle dans le bâti alpin. Ces massifs ont enregistré une longue histoire géologique comprenant le dépôt de sédiments néoprotérozoïques à cambriens, la mise en place de roches magmatiques basiques et ultrabasiques au paléozoïque inférieur, ainsi que l'intrusion de granitoïdes ordoviciens en contexte de marge active. Ces roches sont considérées appartenir à un ensemble de blocs continentaux originaires de la marge septentrionale du Gondwana et accrétés à la marge sud-européenne après leur détachement du Gondwana et leur dérive vers le nord consécutif à l'ouverture de la Paléotéthys. Cet épisode d'accrétion correspond à l'orogenèse varisque (hercynienne), bien documentée dans les massifs du Mont Blanc et des Aiguilles Rouges, par une évolution tectono-métamorphique polyphasée essentiellement carbonifère avec formation de migmatites et intrusion de granitoïdes de types variés. Une érosion active, liée à une forte exhumation, est enregistrée au carbonifère supérieur dans les dépôts détritiques continentaux de bassins d'effondrement de type graben. Ce mémoire présente des cartes géologiques inédites et des suggestions d'excursions dans ces secteurs nouvellement cartographiés. Les lithologies sont abondamment illustrées et décrites en détail du point de vue structural, pétrologique et géochimique. Les analyses chimiques sont fournies en annexe.

Chapter I: Introduction

1. Preface

The Mont Blanc and Aiguilles Rouges massifs have been for a long time a tourist attraction, and were also preferred objects of interest for naturalists, alpinists and scientific research. Large areas of both massifs have been remapped, and a choice of new geological maps is published in this volume. Consequently, a general introduction to the knowledge of the basement underlying these areas and a choice of selected field trips will help to understand in a better way the fascinating scenery of the countryside, determined by the nature of the rocks, their evolution and transformation through surface processes.

Both massifs belong to the highest parts of the Alps, rising from a network of profound valleys. Visitors will need to walk quite a distance from public transportation, and they should allow sufficient time to do so. In most cases, a given walking-tour will focus only on one or two specific geological aspects, and a general overview of the geology will only result from several field-trips. Outcrops from both massifs have been selected to cover most of the existing rock facies. Besides known mountain trails, specific off-trail tours will need careful preparation based on detailed maps. Visitors should follow the basic rules of high mountain trekking, clothes should be adapted to extreme weather changes; safety first in all cases! Do not forget the faunal and floristic aspects; specialists at the "Chalet d'Accueil" (Col des Montets, Aiguilles Rouges massif) will be delighted to take you on guided tours.

JvR spent many years walking across these two massifs, following the footsteps of famous precursors such as de Saussure, Duparc and Mrazec, Oulianoff, Reinhard, Bellière. Global warming has an exciting side effect in these regions, in the sense that new outcrops are progressively uncovered by receding glaciers, allowing constant new observations or rediscovery of old outcrops described in the early twentieth century.

Préface

Depuis fort longtemps, touristes, naturalistes, alpinistes et scientifiques ont été attirés par les massifs du Mont Blanc et des Aiguilles Rouges. Une révision de la géologie de leurs socles a vu le jour, et un choix de nouvelles cartes géologiques est publié dans ce volume. Ce volume se veut en conséquence une introduction à la géologie de "socle" de ces deux régions, et nous souhaiterions que le paysage grandiose de ces massifs soit encore mieux appréhendé par la connaissance des roches sous-jacentes.

Les deux massifs font partie des Hautes Alpes et s'élèvent au-dessus du réseau des vallées. Le visiteur doit être prêt à marcher parfois plusieurs heures pour atteindre des affleurements éloignés de tous moyens de transport, en s'accordant suffisamment de temps pour le faire. Chaque excursion, plus ou moins longue, n'aborde que des aspects spécifiques de la géologie régionale. La compréhension de la structure entière ne peut être que le résultat de plusieurs excursions. Ces dernières ont été choisies de sorte que toutes les lithologies soient rencontrées sans trop d'effort. Par ailleurs, il existe quelques parcours balisés, ainsi que des excursions guidées à thème géologique.

Le visiteur ne doit pas oublier qu'il évolue dans un environnement alpin de haute altitude, qui requiert la prudence habituelle dans ce genre de contexte. En visitant ces régions, un regard sur la faune et la flore est recommandé, et les responsables du Chalet d'Accueil de la Réserve Naturelle des Aiguilles Rouges, au Col des Montets, se feront un plaisir de conseiller le visiteur intéressé.

JvR a parcouru ces deux massifs pendant de nombreuses années, et si nous pouvons présenter aujourd'hui une certaine vue d'ensemble, elle résulte d'une longue tradition de travail de terrain initiée par les précurseurs que sont de Saussure, Duparc et Mrazec; puis Oulianoff et ses cartes géologiques, Reinhard et Bellière, et enfin nombre de diplômants et doctorants.

2. Historical outline

The Mont Blanc and Aiguilles Rouges massifs host the highest and most famous peaks of the Alpine belt. Their discovery at the end of the 18th century resulted from reconnaissance walks along the main valleys and transverse climbing paths, as reported by local Alpine guides and early monographs by de Saussure and Goethe. The first topographic map by Imhof and Kurz (1896) is a milestone of Alpine topographic mensuration.

History of geological investigations in this region parallels the evolution of ideas in geology (details in von Raumer & Neubauer, 1993). In "Les Voyages dans les Alpes", De Saussure (1796-1803) represents a pioneering account in geology. He first mentioned the unconformity of younger sediments above older rock units, and he also recognized the general fan structure dominating the massifs, which nowadays is ascribed to be produced by Alpine shortening. Still under the influence of Neptunist ideas, the Mont Blanc granite (named "Protogine", Jurine 1806) was thought to represent the central part of a concentric structure, followed towards the exterior by crystalline schists and the layers of "petrefacts", the present-day fossils. Favre (1867) mapped large areas and discovered the unconformable Triassic sediments above the Aiguille de Belvédère in the central part of the Aiguilles Rouges. Schardt (1906) was the first to distinguish the central massifs (External Massifs) and their fan structure from the dome shaped massifs (Penninic nappes). Heim (1919) presented the first cross-section of both massifs showing their fan structure, and Collet (1924) reviewed the geology of both massifs.

After the introduction of the petrographic microscope (Zirkel 1863), Michel-Lévy (1890) abandoned the metasomatic interpretation of the "Protogine" and established the magmatic character of this granite body, thus freeing the way for a modern interpretation of geological cross-sections. Knowledge of the Mont Blanc area advanced considerably through the work of Duparc's students. Mrazec (1892) published his PhD thesis about the Mont Blanc granite, Ritter (1897) investigated the southern parts of the area, and Pearce (1898) described the rhyolites on the eastern flank of the massif. After many detailed publications (Duparc 1896, Duparc and Mrazec 1892 a,b; 1893, 1894, 1895; Duparc and Ritter 1894; Duparc and Pearce 1897), the general synthesis on the Mont Blanc massif was published by Duparc & Mrazec (1898). All these classical publications are confronted with the controversy about the interpretation of the "quartz granulitiques" (microgranular quartz), interpreted as resulting from a "second magmatic event". Alternatively, Grubenmann (1892) saw in them the result of "dynamometamorphism", he was a forerunner of interpretation of structures which, at present day, are seen as product of Alpine recrystallization. The first structural investigation (Purtscheller 1963, 1964) compared statistics of joints of the Mont Blanc granite.

In the Aiguilles Rouges area, Necker (1828) was the first to describe the eclogites and serpentinites of the Lac Cornu area, and to recognize the magmatic origin of the Vallorcine granite. Joukowski (1902) published the first petrographic data on the eclogites, and he also mentioned the serpentinites which, subsequently, were hidden under snow until recent years. The first detailed petrographic description of the Vernayaz – Salvan region (Meyer, 1916) was completed by the many observations of Reinhard (field journals 1922-1932), which served as base for the geological map Finhaut-Barberine (Collet et al. 1952), covering the Swiss part of the Aiguilles Rouges massif. The contemporaneous cartography of the French part of the massif was the meriting task of Oulianoff (Oulianoff 1924; Corbin and Oulianoff 1925, 1927, 1928 a,b,c, 1930, 1931, 1932, 1934, 1935, 1938, 1952, 1956, 1959, 1969), and his student Bellière (1958). The main conclusion from the corresponding explanations is the recognition of three superposed tectonic periods (pre-Carboniferous, Carboniferous and Alpine), and the distinction of various lithologies common to both basement areas, and only separated by the Alpine events (Oulianoff 1946, 1953, 1965).

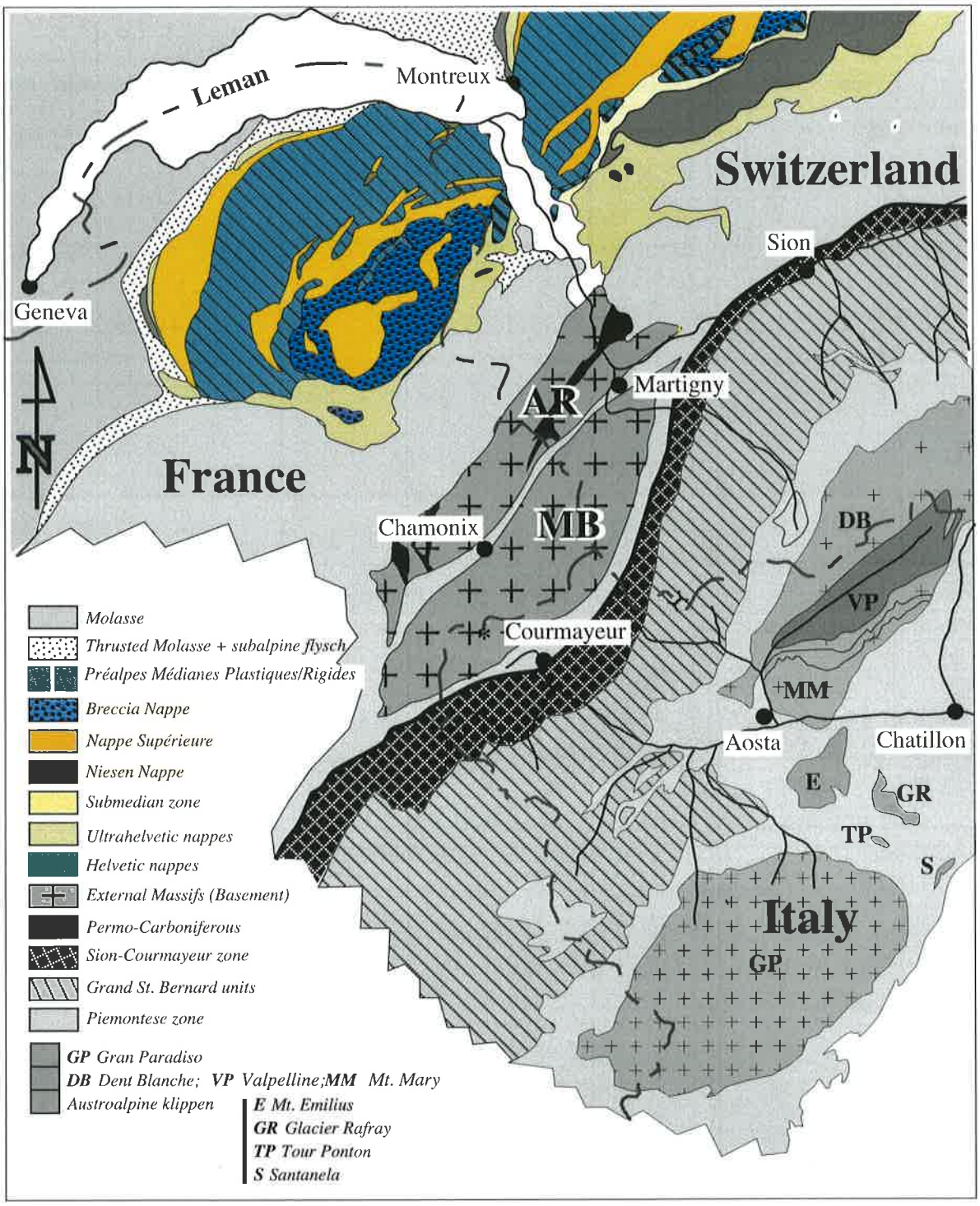

Fig. 1.01:
Geological situation of the Mont Blanc (MB) and Aiguilles Rouges (AR) massifs in the tectonic sketch map of Western Switzerland (modified from Spicher, 1980 and Dal Piaz, 1992).
Situation géologique des massifs des Aiguilles Rouges (AR) et du Mont Blanc (MB) dans le cadre des Alpes Occidentales (modifié d'après Spicher, 1980 et Dal Piaz, 1992).

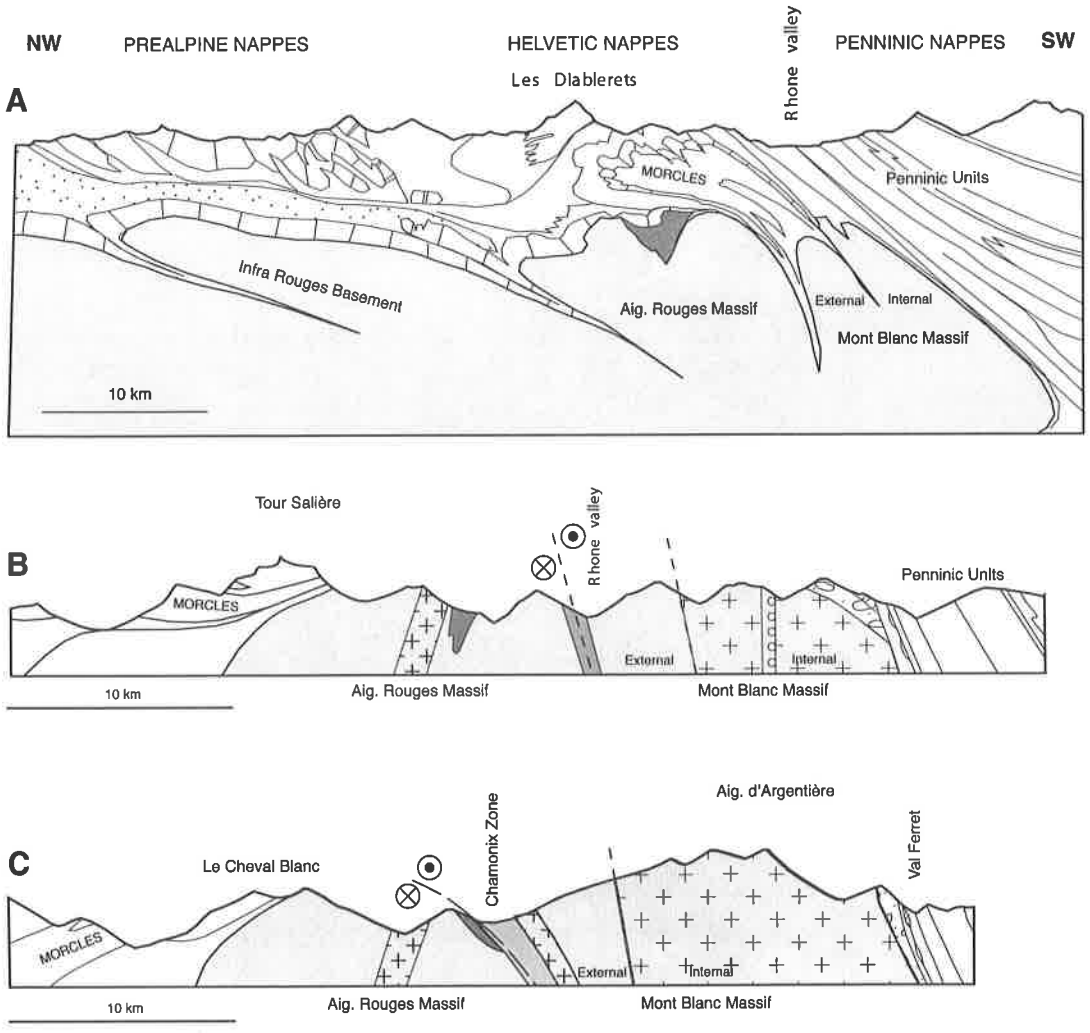

Fig. 1.02:

A:
Schematic NW-SE cross-section through the Alps, based on Escher et al. (1997) and Steck et al. (2001) The Aiguilles Rouges and Mont Blanc areas appear as Alpine basement nappes.
Coupe NW-SE schématique à travers les Alpes basée sur Escher et al. (1997) et Steck et al. (2001). Les socles des massifs des Aiguilles Rouges et du Mont Blanc apparaissent comme des plis de socle.

B,C:
NW-SE Cross-sections across the updomed Aiguilles Rouges – Mont Blanc – areas. Based on Steck et al. (2001)
Coupes NW-SE à travers les massifs surélevés des Aiguilles Rouges et du Mont Blanc surélevés - d'après Steck et al. (2001)

3. Geological framework

Geographically, the Mont Blanc massif is limited at its eastern side by the Ferret valley from Martigny to Courmayeur. From this point, the limit continues in SW direction until Col de la Seigne, and follows the Glacier torrent to Les Chapieux. From les Chapieux onwards, the limit crosses the passes Croix du Bonhomme and Col du Bonhomme, and follows the Torrent du Bonnant in northern, and after Contamines-Bionnay, in northeastern direction. Crossing Mont Lachat, the limit reaches the Chamonix valley near Les Houches.

In contrast to the Mont Blanc area, contours of the Aiguilles Rouges area are less pronounced. Its northeastern prolongation across the Rhône valley, the Fully domain, is limited in the region of Dent de Morcles by its Mesozoic cover. Following the Triassic sediments from St. Barthélémy in the Rhône valley north of Martigny, the limit crosses in southwest direction the Col de Jorat, Col d'Emaney (Salanfe), Col de Barberine, Col du Vieux (Emosson), Col de Salenton and Col d'Anterne to Servoz and St. Gervais.

Satellite pictures clearly show the regular pattern and hierarchy of valleys (Guillemot et al., 1973). The main valley of Chamonix represents a first order geological lineament visible over several hundreds of kilometers. Lateral valleys and passes also result from preferential erosion of geological features by ice and rain. Present-day morphology is essentially the result of long-lasting glaciations. Strongly retreating hanging glaciers are the only relics of a former ice cap, which was covering the whole area 10'000 years ago. Detailed cartographic work, dendrochronology, lichens and pollen analysis, as well as C14-dating have brought insight into the glacial evolution of this region (Aeschlimann 1983, Bless 1984, Wetter 1986). Many valleys contain concentric moraines, the most external of which have been dated at 1820. Authors mention ice advances in 1570, 1850/60 and 1925. Earlier stages of glaciation observed in the large valleys (Val Véni, Val Ferret) may be ascribed to late stages of major Alpine glaciations. Fluvioglacial activity locally reworked the moraines, developing erosion fans and other recent morphologies. Human colonization of these Alpine valleys was tightly related to the evolution of glaciers, as life conditions were strongly influenced by the rough climate. Interested readers are referred to Couvert du Crest (1977) and Edimontagne (1978) for the Chamonix region, and to Nebbia (1985) for the Courmayeur region.

The Mont Blanc and Aiguilles Rouges massifs consist of basement nappes appearing as eroded dome-like structures (**Fig. 1.01, 1.02**) among their Mesozoic cover in the external part of the Alpine belt. Both massifs are composed of distinct subunits (**Fig. 1.03**), as pointed out by Reinhard (Collet et al. 1952) in his general 1:25'000 map. The Aiguilles Rouges massif is mainly composed of micaschist and gneiss units with vertical fold axes and a N-S striking vertical schistosity. These structures are intersected by a large NE-SW directed mylonitic zone and the sheet-like body of the Vallorcine granite (from Miéville, Rhône valley to Vallorcine, France). First order separations are the sedimentary trough of Upper Carboniferous sediments (Dorenaz – Salvan), and the valley of Chamonix. The latter hosts the Mesozoic covers of both massifs, which are outcropping at Col du Tricot, Col de Balme, Col de la Forclaz, and in the neighborhood of Martigny.

The Mont Blanc massif also consists of strongly folded micaschist and gneiss units, which mainly outcrop in the SW end of the massif near the Miage glacier. The same units appear in the NW shoulder of the massif dominating Chamonix, separated by a sheet-like intrusion of granite (Montenvers granite) and by a zone of coarse grained K-feldspar-augengneisses, representing an Ordovician granitic intrusion. The major part of the massif is occupied by the Mont Blanc granite and associated dikes. The whole eastern side of the massif, from Mont Chemin to La Fouly, consists of a large rhyolite complex of Upper Carboniferous age. The steeply dipping Mesozoic cover around both massifs indicates the general updoming produced during Alpine orogenic events.

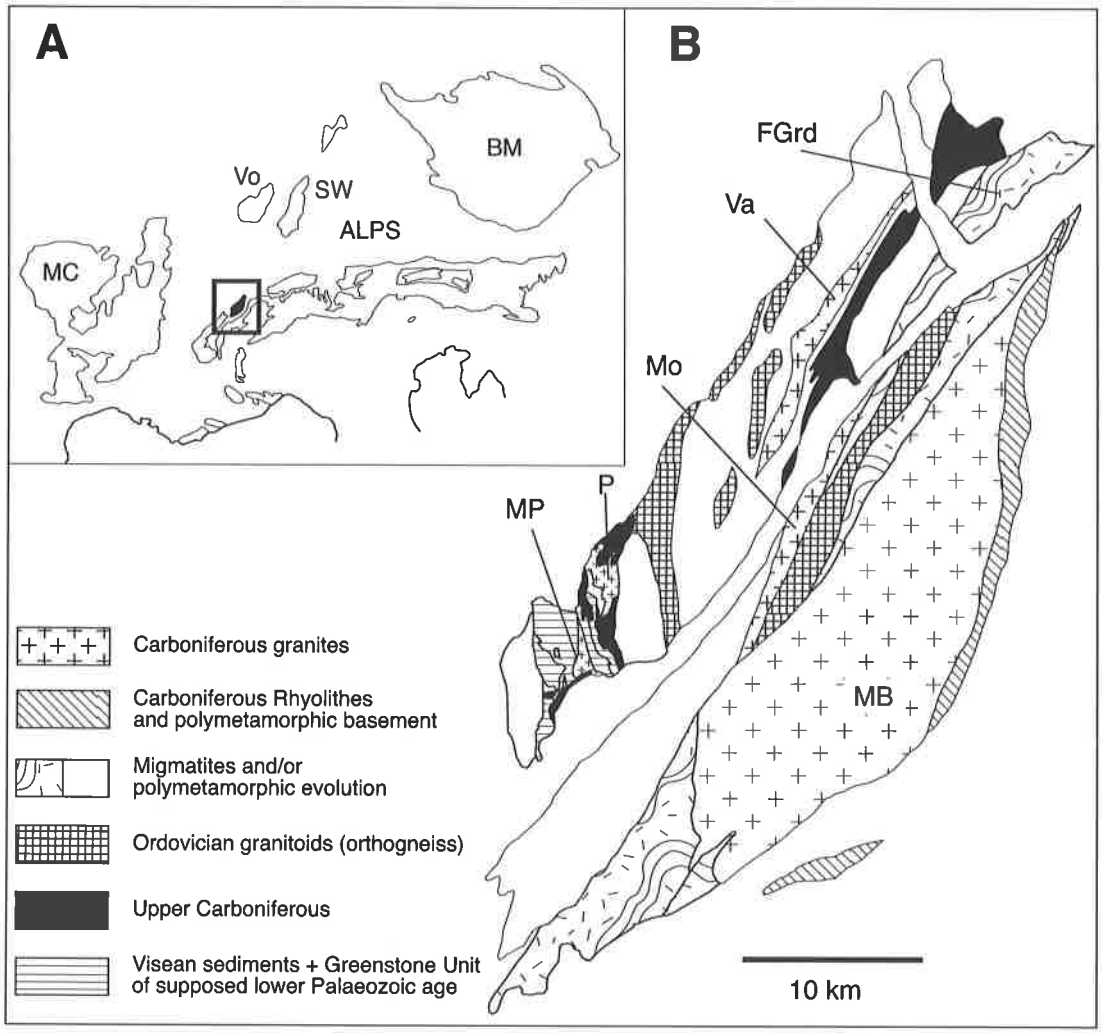

Fig. 1.03: Geological map of the Mont Blanc - Aiguilles Rouges areas, and their Alpine and Variscan framework.

A: Present-day location of Aiguilles Rouges and Mont Blanc areas (frame) in the Alpine mountain chain, and its Variscan framework: BM – Bohemian Massif; MC- French Massif Central; Vo – Vosges; SW – Black Forest (Schwarzwald);

B: Schematic geological map of the Aiguilles Rouges and Mont Blanc areas with indication of the main Variscan granite bodies: FGrd – Fully Granodiorite; MB – Mont Blanc granite; Mo - Montenvers granite; MP – Montées Pélissier granite; P –Pormenaz granite; Va –Vallorcine granite. Distribution of Viséan sediments and Greenstone unit after Dobmeier 1996.

***Fig. 1.03**: Carte géologique du Mont Blanc et des Aiguilles Rouges et reconstitution de leur contexte alpin et varisque*

***A**: Situation actuelle des Massifs des Aiguilles Rouges et du Mont Blanc dans l'arc Alpin et des massifs de socle varisque environnants. MB – Massif Bohémien; MC – Massif Central Français; Vo – Vosges; SW – Forêt Noire (Schwarzwald).*

***B**: Carte géologique schématique des Massifs des Aiguilles Rouges et du Mont Blanc et des Aiguilles Rouges avec indication des principaux corps granitiques d'âge varisque: FGrd – Fully Granodiorite; MB – Granite du Mont Blanc; Mo – Granite du Montenvers; MP – Granite des Montées Pélissier; P – Granite de Pormenaz; Va – Granite de Vallorcine. Distribution des sédiments viséens et "Greenstone Unit" après Dobmeier 1996.*

Apart from the Alpine overprint, there is no difference between the pre-Mesozoic crystalline basement of the Mont Blanc and Aiguilles Rouges and that observed in extra-Alpine domains like the French Massif Central, the Vosges or the Schwarzwald. All host Upper Carboniferous continental sedimentary troughs and are covered by estuarine detrital rocks of Triassic age (grès du Trias, Buntsandstein). All were part of the Variscan continental crust before undergoing the Triassic Tethyan marine transgression and subsequent Alpine orogeny. These basement units record a long-lasting geologic evolution, spanning from the Neoproterozoic (about 600 Ma) to the Late Carboniferous (300 Ma). Two major time periods can be distinguished: the early Neoproterozoic to lower Palaeozoic evolution (600-440 Ma), which we will call the Gondwanian period, and the middle to Upper Palaeozoic evolution (440-300 Ma), comprising continental migration and the Variscan orogeny. The following paragraphs report our current interpretation of the Paleozoic evolution of the Mont Blanc - Aiguilles Rouges area, detailed in the field-guide of the Western Alps by Stampfli (2001). More basic reading can be found in Jaquemin & Sider (1989), Delamette (1993); Eyerhalde et al., 1993 and von Raumer (1999).

The Gondwanian period (600-450 Ma)

The Atlantic ocean did not exist, and most of the continents were assembled in one very large supercontinent – Rhodinia – surrounded by older oceans. From the Neoproterozoic onwards, this continental mass began to split up into smaller pieces, representing the cores of future continents, like Laurentia (future part of North America) or Gondwana (part of future Africa). Gondwana, from around 700-600 Ma, was limited by a huge orogenic mountain chain (comparable to the Andes), the Cadomian orogen, parts of which are actually found in Central Europe (type locality Caen, Brittany). The Gondwana supercontinent was limited by vast zones of marine detrital sediments (Neoproterozoic to lower Palaeozoic), which are partly preserved in the Moroccan Anti-Atlas. Through extension, ribbon-like continental pieces, comparable to archipelagos, separated from Gondwana since the Cambrian (**Fig. 1.04**), and newly formed oceanic pieces appeared. Rifting was accompanied by eruption/intrusion of a large number of magmatic rocks, like rhyolites/ granites and/or basalts/gabbros, whereas volcanic tuffs were deposited together with other sediments. The assemblage of older metamorphic units from the Cadomian mountain chain with the magmatic and sedimentary rocks of Neoproterozoic to Ordovician age represent most of the rock units composing not only the Mont Blanc and Aiguilles Rouges massifs, but most of the basement areas of central Europe (von Raumer, 1998, von Raumer et al. 2003). During the Ordovician, the continental block of Gondwana was surrounded by vast marine sedimentary areas interrupted by Archipelago-like volcanic islands. Such Volcanic arcs indicate that part of the oceanic crust was subducted under Gondwana, and during this evolution part of oceanic crust was transformed into eclogites. The subduction of oceans triggered the separation of continental blocks, which began to drift across the ocean to join the continental mass of Laurentia.

The second period (440-300 Ma)

From 440 Ma onwards, the new oceanic domain of Palaeotethys (back-arc basin) opened in relation with the southeastward subduction of the Rheic ocean underneath Gondwana, and the migration of microcontinents from Gondwana towards Laurentia. These microcontinents finally collided obliquely with Laurentia or Laurentia-derived blocks in a California-like tectonic situation (**Fig. 1.04**) around 380 Ma (see Stampfli et al., 2002), generating the Ligerian and Variscan orogenies. As a result developed nappe tectonics, high grade metamorphism and polyphase deformation. As for the Himalayan belt, the resulting thick continental crust was unstable and underwent consecutive exhumation and erosion, bringing lower granulitic crust (30-40 km) up to the surface. Contemporaneous sedimentary basins collected detritus of the eroding mountain chain during the Upper Carboniferous. All these rocks compose the present-day Aiguilles Rouges and Mont Blanc areas.

Post-Palaeozoic evolution (245-25 Ma):

Since 245 Ma began the Triassic transgression (245 Ma), but some parts of the Mont Blanc area remained at surface and were preserved as islands in a marine environment. The earliest sediments represent fluvial deltaic fans, where Dinosaur footprints (Emosson) testify the presence of animals (Demathieu et Weidmann, 1982). Sediments from the Triassic to the Cretaceous are described in detail by Amberger (1960), Ayrton (1980), Epard (1990, 2001) and Stampfli (2001). Sedimentation was interrupted by the Alpine orogenic events, and cross-sections (Escher et al. 1996) illustrate well the resulting complications. During this period, the Mont Blanc and Aiguilles Rouges massifs were again tectonically affected, but the nature of the older rock series is still well recognizable.

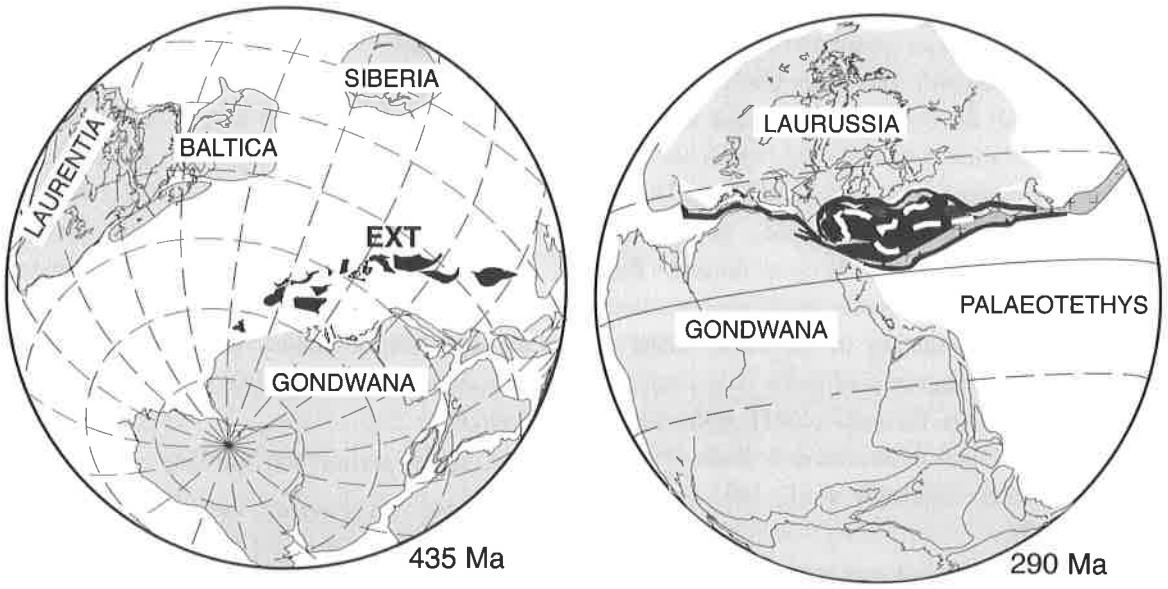

Fig.1.04 :
Palaeotectonic reconstructions after Stampfli and Borel (2002)

A: Palaeotectonic situation during the Silurian (435 Ma). Most of the basement areas of Central Europe (black) were located at the Gondwana border, forming the "Hun-terrane" assemblage (Stampfli, 1996) in the former eastern continuation of Avalonia (von Raumer et al., 2002). Beginning of their separation from Gondwana and drifting toward their future location at the border of Laurussia (see B). **Ext**: approximate location of the Alpine External Massifs including Mont Blanc and Aiguilles Rouges areas.

B: Approximate location of most of the European basement areas (black) during the Early Permian (290 Ma). The final collision of Gondwana with Laurussia produced the supercontinent Pangea. The assemblage of basement areas (black), Alps included, is dominated by continuing oblique subduction and strike-slip regime (Stampfli et al., 2002).

Reconstructions paléotectoniques d'après Stampfli et Borel (2002)

***A:** Situation géologique au Silurien (435 Ma). La plupart des futurs massifs de socle européens (en noir), formant l'assemblage (Terrane) "Hun" (Stampfli, 1996), situés au Nord du continent Gondwana et dans la prolongation orientale d'un ancien continent appelé Avalonia (von Raumer et al. 2002), se détachent du Gondwana et commencent leur dérive vers leur future localisation au bord de Laurussia (voir B). **Ext** - Situation approximative des Massifs Externes incluant les Massifs du Mont Blanc et des Aiguilles Rouges.*

***B:** Situation approximative au début du Permien (290 Ma), inspirée des reconstructions de Stampfli et al. (2002). Le continent Gondwana entre en collision avec Laurasia pour former le futur supercontinent Pangea. L'ensemble des socles (en noir et gris foncé) indiqué sous A, inclus les Alpes, se trouve en situation de cisaillement dextre entre les continents et sera graduellement incorporé jusqu'à la formation des Alpes définitives.*

Les grandes périodes d'évolution géologique

Les massifs du Mont Blanc et des Aiguilles Rouges constituent avec les massifs de l'Aar-Tavetsch-Gotthard, de Belledonne-Tête Rousse-Pelvoux et de l'Argentera, ce qu'on appelle les Massifs Cristallins Externes de l'arc alpin. Ils sont caractérisés par un socle pré-mésozoïque commun et semblable à celui rencontré dans le Massif Central Français, dans les Vosges ou dans la Forêt Noire (Schwarzwald), notamment au niveau de leur évolution carbonifère supérieure, caractérisée par des dépôts grossièrement détritiques et des lits charbonneux. Leur évolution mésozoïque précoce est également commune, marquée par une transgression triasique de la mer tethysienne (grès du Trias, Buntsandstein). Il apparaît ainsi que tous ces massifs cristallins appartenaient à une croûte continentale varisque continue dans le cadre élargi de la Pangée, puis qu'ils suivirent des destinées différentes au cours du Mésozoïque et de l'orogenèse alpine.

Les massifs du Mont Blanc et des Aiguilles Rouges consistent essentiellement en lithologies de socle, par contraste avec les roches sédimentaires mésozoïques et tertiaires déposées dans le bassin de la Téthys alpine et actuellement localisées sur le pourtour de ces massifs et dans la profonde vallée de Chamonix. Ce socle pré-mésozoïque recèle une histoire géologique beaucoup plus longue et complexe que supposée initialement, qui semble débuter voici près de 600 millions d'années. En termes de tectonique des plaques, nous devons nous faire à l'idée que ces éléments de socle ont probablement subi de grands déplacements horizontaux et que leur patrie est sans doute à chercher dans le continent africain (ancien Gondwana). Pour la clarté du propos, nous allons subdiviser ces 600 millions d'années en trois périodes principales: du Précambrien à l'Ordovicien (600-440 Ma), ou période Gondvanienne, du Paléozoïque moyen au Paléozoïque supérieur (440-310 Ma), comprenant les grands bouleversements de l'orogenèse varisque (hercynienne), et enfin du Trias à l'actuel avec la formation des Alpes. Le lecteur non initié est renvoyé au petits ouvrages de Jaquemin et Sider (1989) et von Raumer (1999) sur les Aiguilles Rouges et le Mont Blanc, ainsi qu'aux guides naturalistes de Delamette (1993) et Eyerhalde et al. (1993). Les questions plus spécifiques relatives au métamorphisme sont abordées dans von Raumer et al. (1999), alors qu'une interprétation générale récente de la chaîne alpine est donnée dans le guide des Alpes Occidentales de Stampfli (2001).

***Au cours de la période gondwanienne (600-440 Ma)**, la configuration des continents était sensiblement différente de l'actuel; l'océan atlantique n'existait pas et il faut imaginer une immense masse continentale entourée d'océans anciens aujourd'hui disparus. Ce supercontinent appelé Rhodinia allait se segmenter en plusieurs morceaux, futurs cœurs des continents actuels, notamment Laurentia (partie de la future Amérique du Nord) et Gondwana (partie du futur continent Africain). Ce dernier était limité, il y a environ 700-600 Ma, par une vaste chaîne de montagnes représentant l'orogène Cadomien (comparable aux Andes), dont les traces sont préservées,parmi d'autres, en Bretagne (localité type: Caen). Le continent Gondwana était entouré par de très larges zones de sédiments détritiques marins, constituant les couches sédimentaires d'âge précambrien et paléozoïque inférieur préservées aujourd'hui dans la région de l'Anti-Atlas. Une extension lente des domaines océaniques et continentaux permit l'éruption en surface et l'intrusion en profondeur de nombreuses roches magmatiques de type rhyolite ou granite, ainsi que basalte ou gabbro. L'ensemble de ces roches métamorphiques provenant de l'ancien continent Gondwana, ainsi que sédimentaires et magmatiques d'âge précambrien à ordovicien, forment l'essentiel des socles des massifs cristallins externes des Alpes, du Massif central français, des Vosges et de la Forêt-Noire (von Raumer 1998, von Raumer et al., 2002, 2003). A l'Ordovicien, on peut imaginer un bloc continental entouré de vastes domaines sédimentaires interrompus par des îles volcaniques en archipels. Ces arcs volcaniques étaient l'expression en surface d'une subduction de croûte océanique sous le continent Gondwana, processus au cours duquel un métamorphisme de haute pression affecta cette dernière (éclogitisation).*

Pendant la deuxième période (440-300 Ma), *cette subduction induisit la formation de structures d'extension (rift) en arrière de la marge continentale, conduisant à sa rupture et à la dérive de microcontinents (fragments de Gondwana correspondant à peu près aux massifs de socle trouvés aujourd'hui en Europe) se déplaçant à travers les espaces océaniques (comme des icebergs) vers les côtes de Laurentia (**Fig. 1.04**).*

*Autour de 380 Ma (Dévonien), la collision entre les microcontinents mentionnés ci-dessus (Stampfli et al. 2002), et le supercontinent Laurasia (Laurentia et Baltica, se fait dans un contexte tectonique comparable à celui existant aujourd'hui en Californie (**Fig. 1.04**). Cette collision engendra une profonde transformation des roches (métamorphisme et déformations multiples), initiant l'orogenèse ligérienne et varisque. Des parties importantes de la croûte allaient être subductées sous Laurussia, conduisant à un épaississement de la croûte continentale. Devenue instable, cette dernière fut soumise à une forte exhumation et érosion (comme actuellement en Himalaya), induisant la remontée en surface de lithologies de la croûte inférieure (env. 30-40 km de profondeur). Simultanément, des sédiments détritiques (schistes et grès du Carbonifère inférieur et du Carbonifère supérieur (Houiller) se déposaient en surface, témoignant de ces événements tectoniques. Ces roches feront l'objet d'une description plus détaillée dans le chapitre suivant.*

La troisième période *commence par l'ennoiement progressif (quelques îles subsisteront un certain temps dans le futur massif du Mont Blanc) des terres par la mer téthysienne dès le Trias (254 Ma). Localement se forment de larges zones de deltas fluviatiles, tels celles du Vieux Emosson abritant les fameuses traces de dinosaures (Demathieu et Weidmann, 1982). Les lithologies sédimentaires du Trias au Crétacé décrites par Amberger (1960), Ayrton (1980), Epard (1990, 2001) et Stampfli (2001) forment souvent de belles falaises. Cet épisode de sédimentation est interrompu par la formation des Alpes. A nouveau, de vastes domaines sont soumis à subduction, avec formation de nappes et transformations métamorphiques (Escher et al. 1996). De grandes écailles de socle furent chevauchées, entassées, plissées, ou basculées à différentes périodes. En ce qui concerne les massifs du Mont Blanc et des Aiguilles Rouges, les transformations métamorphiques alpines furent suffisamment faibles pour préserver l'identité antérieure des roches, mais assez fortes pour engendrer la croissance d'une grande quantité de nouveaux minéraux. Les événements mentionnés ci-dessus feront l'objet des chapitres suivants.*

4. An introduction to metamorphism of rocks

As stated above, rocks of the Alpine basement underwent repeated metamorphic transformations during successive orogenic cycles. Non-specialist readers will find a basic introduction to the concept of metamorphism below.

Sedimentary and magmatic rocks are mineral aggregates. These aggregates were originally stable during rock formation, but underwent transformations or reequilibration during their subsequent geological evolution. Apart from surface processes (such as alteration and erosion), these transformations are essentially linked to the pressure and temperature changes within the earth crust. Indeed, pressure P (expressed as kilobars (Kb) or Pascals (Pa)) increases regularly with depth (equivalent to the weight of the overlying rock column) as does temperature T. The mean rate is about 0.3 Kb and 30°C per km of burying. As a consequence, any rock being buried through tectonic processes will progressively adapt to the new P and T conditions through crystallization of new mineral assemblages at the expend of the old, unstable ones. These recrystallization processes can be fully or only partly successful. In the latter case, relicts of the old mineral assemblage (or paragenesis) are present and can be identified within the metamorphic rock. In the same way, several successive orogenic events will induce repeated recrystallization stages, with or without mineral relicts.

The main interest in the study of metamorphic mineral assemblages is that each of them grew in a restricted range of P and T conditions. Detailed analysis of mineral parageneses thus allows reconstitution of the physical conditions (i.e. depth) under which the metamorphic rock recrystallized. If mineral relics are present, the corresponding P and T conditions can sometimes be established, allowing reconstitution of the P-T-time path of the rock. If P-T conditions increase with time, the path is prograde; it is retrograde in the opposite case.

During metamorphic recrystallization, rocks often develop a schistosity resulting from the preferred orientation of minerals recrystallizing in an external stress-field. Weakly metamorphosed rocks (greenschist facies) are characterized by a well developed schistosity and many green minerals, such as chlorite, epidote and actinolite, as well as biotite and locally garnet. Medium-grade metamorphism (amphibolite facies) is characterized by coarser-grained minerals, which often give a nodulous aspect to the rock. The main metamorphic minerals growing in rocks of argillaceous composition are (depending of the P and T conditions): garnet, staurolite, andalusite, kyanite, sillimanite, cordierite, feldspars (both plagioclase and alkali feldspar), amphibole. In high-grade metamorphic conditions (4 kb and >650°C), graywackes (detrital rock with feldspar, quartz and argillaceous minerals) begin to melt forming liquid of granitic composition. These rocks, named migmatites, often display a banded aspect with clear veins of granitic material within relict material of the original lithology (e.g.**Photo 3.07**).

Une petite introduction au métamorphisme des roches

Comme mentionné plus haut, les roches composant le socle alpin ont subi des transformations métamorphiques répétées au cours des cycles orogéniques successifs. Les concepts du (poly)métamorphisme seront donc brièvement rappelés ci-dessous.

Les roches sédimentaires et magmatiques ne sont autres que des assemblages de différents minéraux. Ces assemblages originellement stables au moment de la formation des roches, vont subir des transformations ou rééquilibrations au cours de leur évolution géologique. Mis à part l'altération et l'érosion, processus de surface, ces transformations seront liées aux changements de température et/ou de pression rencontrés au sein de la croûte terrestre. En effet, la pression P (exprimée en Kilobars (Kb) ou Pascals (Pa)) augmente régulièrement avec la profondeur (du poids de la colonne de roche sus-jacente) tout comme la température T. On compte en moyenne une augmentation de 0.3 Kb et 30°C par km d'enfouissement. Ainsi, une roche d'origine quelconque soumise à enfouissement par des processus tectoniques va-t-elle progressivement s'adapter aux nouvelles conditions de P et T en cristallisant de nouveaux assemblages de minéraux au détriment des anciens, devenus instables. Ces processus de recristallisation peuvent être plus ou moins achevés; si tel n'est pas le cas, des "reliques" de l'ancien assemblage (ou paragenèse) peuvent encore être observées et identifiées au sein de ce qui est désormais appelé une roche métamorphique. De même, si plusieurs événements orogéniques se succèdent, on peut s'attendre à des recristallisations répétées au sein des roches (polymétamorphisme), avec ou sans reliques minérales d'un ou plusieurs des événements en question.

Le grand intérêt des assemblages de minéraux du métamorphisme réside dans le fait qu'à un assemblage donné correspond une gamme restreinte de conditions de P et T. L'analyse détaillée des paragenèses permet ainsi de reconstituer les conditions physiques (donc de profondeur) par lesquelles la roche métamorphique a passé. Si des reliques sont présentes, il est parfois possible de déterminer également les conditions P-T correspondantes et ainsi de suivre l'évolution métamorphique de la roche dans le temps. Une évolution des paragenèses vers des conditions P-T plus élevées est dite prograde; elle est dite rétrograde dans le cas inverse.

*Lors de leur recristallisation métamorphique, les roches acquièrent souvent une structure schisteuse résultant de l'orientation préférentielle des minéraux dans un champ de contraintes externe. Les roches faiblement métamorphiques (faciès schistes verts) se caractérisent par une schistosité très marquée et par la présence de beaucoup de minéraux verts, tels la chlorite, l'épidote ou l'actinote, et la présence de biotite, mais localement aussi de grenat. Le degré de métamorphisme moyen (faciès amphibolite) s'exprime par une taille plus grande des minéraux, qui déforment la schistosité et donnent un aspect noduleux à la roche. Les minéraux les plus importants des roches d'origine argileuse sont (en fonction de P et T): le grenat, la staurotide, l'andalousite, le disthène, la sillimanite, la cordiérite, les feldspaths (plagioclase et feldspath potassique), l'amphibole. Finalement, dans le domaine du métamorphisme élevé (4 Kb et plus de 650°C), les roches ayant une composition de grauwackes (roche détritique à feldspath, quartz et minéraux argileux) commencent à fondre en formant un liquide de composition granitique. Ces roches appelées migmatites ont un aspect souvent rubané (voire **Photo 3.07**), avec des veines de matériel granitique et des reliques de la roche originale.*

Chapter II: Lithologies

The present-day Aiguilles Rouges and Mont Blanc areas are identical in their origin and their pre-Alpine geological evolution. They appear as separate massifs, resulting from distinct Alpine basement fold structures (**Fig. 1.03**). All basement rocks are older than their mesozoic cover and consist of metamorphosed sedimentary or magmatic lithologies, such as. metagraywackes, micaschists, marbles or orthogneisses, metagranites, amphibolites, metabasites, respectively (see preceding chapter). Different units can be distinguished, on the basis of their metamorphic evolution (**Fig. 2.01**):

Polymetamorphic basement

The largest parts of both massifs are underlain by high-grade polymetamorphic rocks, whose first metamorphic recristallisation was pre-Ordovician in age and reached amphibolite facies conditions (see preceding chapter). Their original composition and presumed age are reported in **Tab. 2.01**:

Tab. 2.01 Lithologies of the polymetamorphic basement
Séquence lithologique du socle polymétamorphique

Interpretation *Interprétation*	presumed age *âge présumé*	observed petrography *pétrographie observée*
Magmatic origin *roches d'origine magmatique*		
granites	Ordovician	coarse grained Kf-augengneisses - orthogneiss *gneiss oeillés grossiers à feldspath potassique*
granodiorites	Cambro-Ordovician	gneiss with plagioclase, biotite ± amphibole *gneiss à plagioclase, biotite ± amphibole*
acidic volcanites	Lower Palaeozoic	finegrained Kf-sillimanite gneisses *gneiss microgrenus à feldspath potassique et sillimanite*
basic volcanites	Lower Palaeozoic	amphibolites, eclogites
ultramafic rocks	Lower Palaeozoic	serpentinites
Sedimentary origin *roches d'origine sédimentaire*		
Al-rich argillaceous sediments	Neoproterozoic to Lower Palaeozoic	garnet-sillimanite ± kyanite ± staurolite *micaschistes à grenat-sillimanite ± disthène ± staurotide*
carbonates	Lower Palaeozoic	diopside-garnet-marbles *marbres à diopside-grenat*
layered units of graywackes and Al-rich units	Neoproterozoic to Lower Palaeozoic	gneiss with biotite-plagioclase-quartz and micaschists ± staurolite ± kyanite ± sillimanite *rubans à biotite-plagioclase-quartz et micaschistes ± staurotide ± disthène ± sillimanite*
sandstones	Lower Palaeozoic	garnet-kyanite quartzite *quartzite à grenat ± disthène*

A large variety of sedimentary rocks actually consist of mixtures of the endmember compositions reported in **Table 2.01**; in the same way, many magmatic rocks have chemical composition inbetween the granite and gabbro endmembers.

On the basis of cartographic work we suppose that the original sedimentary pile had a reduced thickness, and that these sediments were deposited on a continental platform, presumably during the Neoproterozoic to lower Palaeozoic.

All these metamorphic lithologies are found in the entire polymetamorphic basement of the Aiguilles Rouges (see field trips), as well as in the SW part (Miage glacier) and NW shoulder (St. Gervais – Martigny) of the Mont Blanc massif.

Greenstone Unit

Besides the polymetamorphic basement mentioned above, the SW part of the Aiguilles Rouges – (i.e. Zone St. Gervais-Les Houches) – is underlain by another rock unit, the so-called "Greenstone Unit" (GSU, see **Fig. 2.01**), characterized by Dobmeier (1996) and Dobmeier et al. (1999). It lies on both sides of the Arve valley and is composed of a variety of greenish, calc-alkaline volcanic rocks of rather low metamorphic grade, presumably representing a lower Palaeozoic arc environment (Dobmeier et al. 1999), but a Devonian or Silurian age cannot be excluded.

Visean sediments

A younger and weakly metamorphosed sedimentary sequence outcropping in the St. Gervais – Les Houches area had originally been attributed to the Lower Carboniferous and/or Devonian (Laurent 1968), and subsequently to the Visean by Bellière and Streel (1980) on the basis of microfossils (*Reitlingeridae*). This sedimentary series is composed of metagraywackes and argillaceous schists with interlayers of calc-alkaline metabasalts and former iron-rich basalts. It is considered to be entirely lower Carboniferous (Dobmeier 1996, Dobmeier et al. 1999).

Upper Carboniferous

The entire Aiguilles Rouges massif is intersected by a long, narrow sedimentary basin containing detrital continental sediments of Upper Carboniferous age. They are well known in Fully (Dorénaz) and Salvan, where they have been exploited for coal (Fehlmann 1919), as well as in Les Houches. Such rocks are also known in the higher levels of the Mont Blanc domain (Col de Miage, Vernet 1969). These sediments have been attributed to the Westphalien B – Stephanien A (Jongmanns 1960). U-Pb zircon ages ranging between 308-295 Ma have been obtained on interlayered volcanic ash-fall deposits (Capuzzo & Bussy 2000). Interpretation of depositional environment has been proposed by Sublet (1969, Pilloud (1991), Niklaus and Wetzel (1996), and the tectonic setting has been discussed by Lox and Bellière (1993) and Dobmeier and von Raumer (1995). Capuzzo (2000) and Capuzzo & Wetzel (2000) invoked a half-graben structure dominated by transtension along with dextral strike-slip movements.

Mesozoic cover

The last period of sedimentation is recorded at different locations (mostly passes) along the Chamonix valley. Detailed information can be found in Amberger (1960), Grasmück (1961), Badoux (1971), Huggenberger (1985), Epard (1989, 1990, 2001), and Stampfli et al. (2001).

II.1 Lithologies composing the polymetamorphic basement

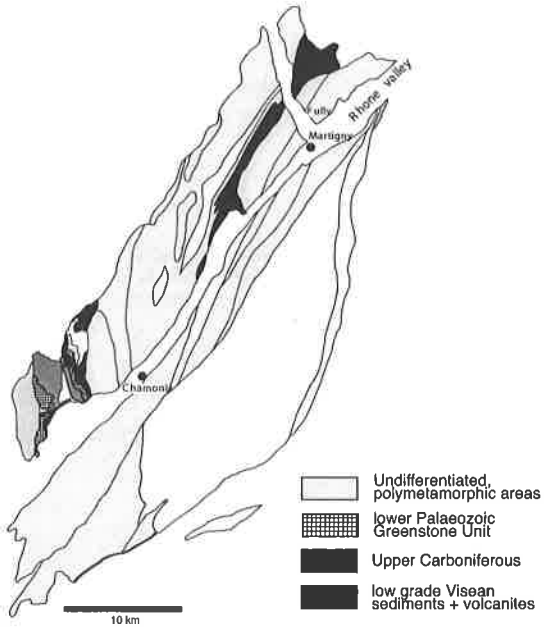

In both massifs, the constituents of the polymetamorphic basement are well preserved (see adjacent **figure 2.01**, grey areas). They represent the metamorphosed products of former protoliths of Precambrian (Neoproterozoic) to lower Palaeozoic age. Strongly transformed by Variscan metamorphic events (Carboniferous age), their nomenclature is necessarily that of metamorphic rocks (see Tab. 2.01, preceding section).

Fig. 2.01
Schematic geological map indicating the polymetamorphic areas (gray)
Carte géologique schématique des massifs du Mont Blanc et des Aiguilles Rouges avec le socle polymétamorphique (en grisé).

Metamorphism reached high amphibolite facies grade, i. e. conditions above 500-600°C and 5-8 kbars (pressures corresponding to depths of 15 to 25 km (see chapter III, about metamorphism). The metamorphic products of former magmatic rocks are orthogneisses (former granitic rocks), amphibolites (metamorphosed basalts and gabbros) and eclogites (former basalts or gabbros from crustal levels deeper than 25 km, subduction zone). Former sediments are found as metagreywackes (former litharenites, greywackes), micaschists or metapelites (former argillaceous sediments), paragneisses (gneisses resulting from former mixed sediments), quartzites (former sandstones ± argillaceous material), and calc-silicate marbles (former carbonate sediments with varying admixtures of sand and/or argillaceous material).

Mapping lithostratigraphic units in the Aiguilles Rouges and Mont Blanc areas was facilitated by the presence of marker horizons like orthogneisses or amphibolites, or even certain assemblages of micaschists with quartzites and metagreywackes. Corbin and Oulianoff (1925) already noticed the distribution of amphibolites across both massifs. The various constituting lithologies will be described successively.

II.1.1. Orthogneisses – the Lower Palaeozoic granitoids

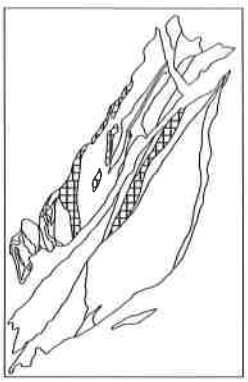

Orthogneisses, which represent magmatic events of Cambro-Ordovician age, are widespread in both massifs (hatched areas in **figure 2.02**, adjacent). They are mostly represented by augen gneisses which, in the Aiguilles Rouges, are accompanied by less frequent granodioritic gneisses.

Fig. 2.02
Schematic geological map indicating distribution of Ordovician orthogneisses (hatched areas). *Carte géologique schématique des Massifs du Mont Blanc et des Aiguilles Rouges avec la distribution des orthogneiss d'âge Ordovicien (hachuré).*

Augengneisses have been mentioned in the explanation notes accompanying Oulianoff's maps (see references Ch. I.3), and they have been mapped as "gneiss rubano-lenticulaires" by Bellière (1958) in the Aiguilles Rouges massif. In the NW shoulder of the Mont Blanc massif (**Fig. 1.03**), they appear as large rock units defined as orthogneiss of probably lower Palaeozoic age (von Raumer 1976). Their Ordovician age has been confirmed by zircon U-Pb dating at 453±3 Ma (Bussy and von Raumer 1994). Of variable aspect in the field, such rock units can be followed up in the zone of Chamonix – Martigny from the Mer de Glace to Alpe Bovine above Martigny. Petrographic details can be found in Bauer (1993), Nähr (1993), and Morard (1998). Orthogneisses of supposedly comparable age have a wide distribution in the Aiguilles Rouges basement following the contours of km-scale folds (von Raumer, 1984). Such rocks, observed from the Salanfe area across Val Bérard and Lac Cornu to Planpraz above Chamonix, have been subject of detailed descriptions by Joye (1989), Chiaradia (1993), Fracheboud (1997), Marquis (1997), and Wirsing (1997). They are labeled "orthogneisses of lower Palaeozoic age" in the new metamorphic map of the Alps by Frey et al. (1999).

Although less evident, granodioritic gneisses also form elongated units parallel to the augengneisses in the Salanfe area (Chiaradia 1993). Also called "Gneiss du Luisin", they can be followed from Mt. Luisin to the rock units along the trail arriving to the Salanfe area. Comparable rocks appear along the road connecting Gorges du Trient to Salvan. A first age determination (457±2 Ma, U/Pb zircon; unpublished data, F. Bussy) confirms their Ordovician age. Biotite-amphibole gneisses appear in a large area near Col de Salenton (Wirsing, 1997), where they are supposed to be slightly older than the augengneisses and the granodioritic gneisses mentioned above.

Petrography of augengneisses

Type-locality: Mont Blanc massif: outcrops along the road from Croix de Lognan to the entrance of the EDF galeries near the Argentière glacier (coord Fr: 957.500/118.020; see also field-trip Lognan); Aiguilles Rouges massif: at the bottom of the dam Vieux Emosson (coord CH: 558.250/101.350; see field-trip Emosson).

The petrographic composition of augengneisses corresponds to that given by von Raumer (1976), a granitic microcline-perthite orthogneiss with albitic plagioclase, quartz, biotite and muscovite (**Photos 2.01-2.02**). Accessory garnet is locally observed (Aig. à Bochard, Fr.: 956.870/115.820). The best outcrop areas on the Mont Blanc side are the regions Pointe des Grands – Croix de Bérons, near the alpine refuge Albert I, and Lognan – Glacier d'Argentière. On the Aiguilles Rouges side, large areas of such gneisses are found at the bottom of Mt Luisin near Lac Salanfe, in the rocks dominating the northwestern part of Lac Emosson and the dam site of Vieux Emosson, and the large areas near Col de Salenton, Col de Bérard, and farther west, at Combe de Floriaz – Pointe de la Glière and in the neighborhood of Lac Noir.

The augengneisses are not homogeneous. An interlayering of very coarse-grained units with microgranular banded ribbons and microgranular leucocratic gneisses, locally containing small nodules of sillimanite, is observed. These various facies may contain different quantities of coarse K-feldspar crystals. Through gliding or abrupt changes rock may change from normal lensoid gneisses to very coarse augengneisses locally containing K-feldspars of up to 15 cm long (Petoudes, von Raumer 1971). The concentration of large K-feldspars is not necessarily constant or continuous and may be concentrated in lenses. Part of the observed fine-grained gneisses limiting such lenticular concentrations of K-feldspar zones may have resulted from high temperature shearing, but irregularities of distribution may also result from folding. Nice examples of large-scale folds are found on the eastern shore of lake Emosson (**Photo 2.03, 2.04**) near the former dam site of Barberine (von Raumer 1984; see field-trip Emosson) and in the Salanfe region, at the foot of Mt Luisin and near Col d'Emaney (Chiaradia 1993 a, b, see field-trip Salanfe).

The difficulty to recognize the original rocks results from high temperature deformation during the Late Carboniferous, with or without partial melting. Where partial melting occurred, deformation-driven melt segregation yielded many spots and veins of newly formed granular mobilisates of granitic composition, giving the rock a migmatic aspect (**Photo 2.05**). Such migmatites may still contain relicts of former K-feldspars, thus corresponding to the gneiss "rubano-lenticulaires" of Bellière (1958) (**Photo 2.06**). The gradual mobilisation is well observed in the Lognan region (see field-trip Lognan) and near Pointe des Grands (see field-trip Trient), where microgranular mobilisates containing plagioclase-K-feldspar-quartz-muscovite first appear as veinlets parallel to small shear zones (coord. Fr: 958.320/117.900; von Raumer 1976, **Photo 2.07**), accompanied by formation of sillimanite. Mobilisates progressively become larger until the entire rock of the former augengneiss (remaining as ghost-structure) is completely replaced by mobilisates (**Photo 2.08**). Some large black K-feldspar crystals are sometimes the only unmelted relics in the rock.

At an advanced stage of anatexis, discordant veins of muscovite-bearing granite crosscut pre-existing structures (**Photo 2.08**). A radiometric age for such granite veins yielded a Carboniferous age (317±2 Ma, U/Pb monazite, Bussy and von Raumer 1994). Consequently, reheating and formation of migmatites have to be attributed to Late Carboniferous regional events.

Where K-feldspar-augengneisses were deformed without partial melting, biotite often developed, generating dark colored biotite gneisses, such as at the eastern shore of Lac Emosson or at Val Bérard (Wirsing 1997). Rocks are strongly schistose, contain relict elongated K-feldspars and might even host newly grown andalusite (Emosson, coord. CH: 560.080/102.940).

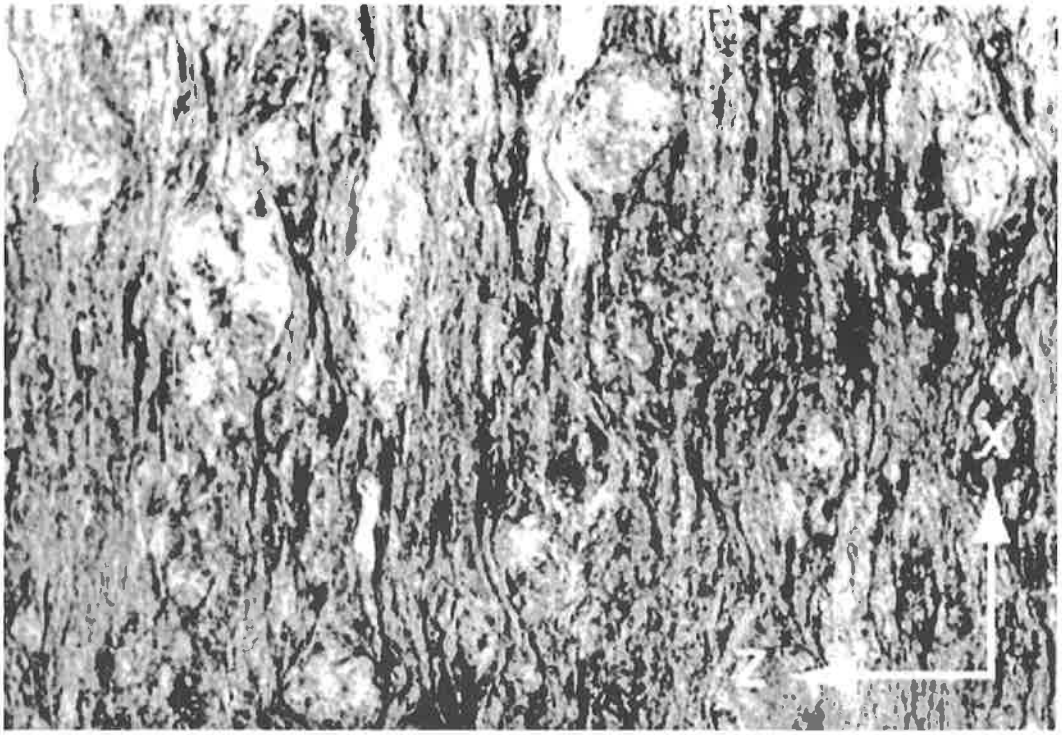

Photo2.01
Coarse-grained orthogneiss, x-z-section; moraine Pointe des Grands, Mont Blanc massif
Orthogneiss grossier, section x-z; moraine de la Pointe des Grands, massif du Mont Blanc
Coord CH:565.100/95.650; (scale 1:1)

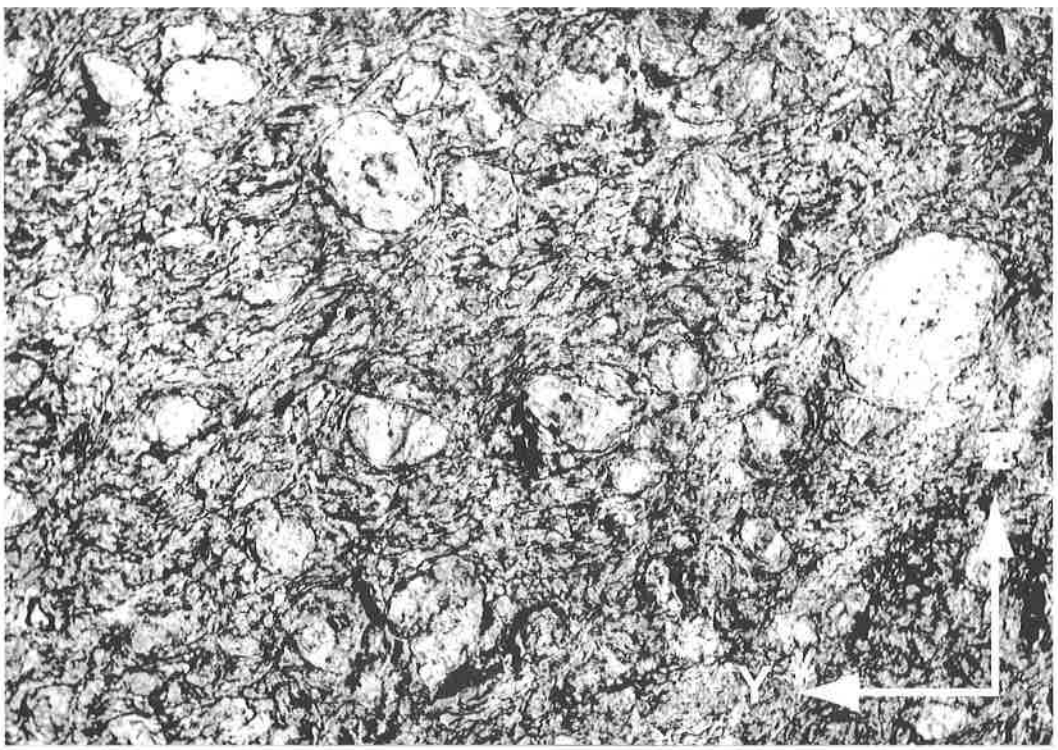

Photo2.02
Coarse-grained orthogneiss, y-z-section; moraine Pointe des Grands, Mont Blanc massif
Orthogneiss grossier, section y-z; moraine de la Pointe des Grands (scale 1:1)

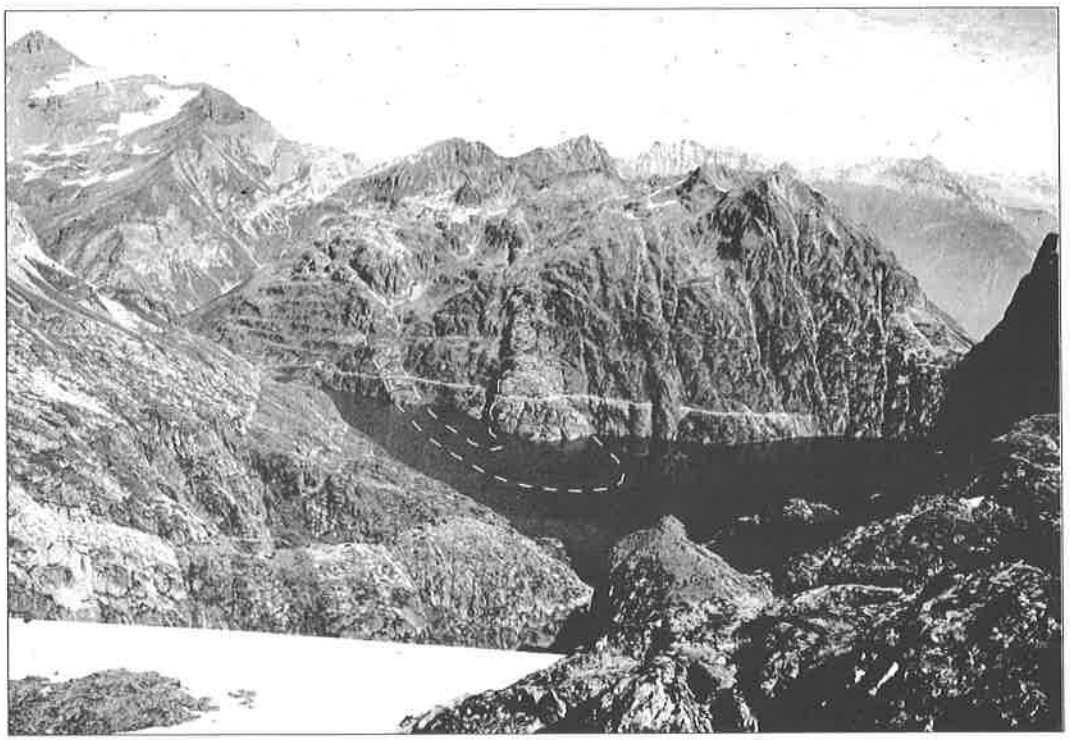

Photo2.03
Major fold structure in orthogneisses at the eastern shore of Lake Emosson;
Plis d'orthogneiss au bord oriental du Lac d'Emosson (Coord CH: 560.000/103.000)

Photo2.04
Detail of Variscan fold hinge in orthogneiss; Salanfe area (Coord CH: 563.075/108.225)
Tête de pli varisque dans un orthogneiss, détail; domaine de Salanfe (scale 1:15)

Photo2.05
Migmatized orthogneiss, Petoudes area, Mont Blanc massif (Coord. CH: 565.610/96.020; 2430)
Orthogneiss migmatique, région des Petoudes, massif du Mont Blanc

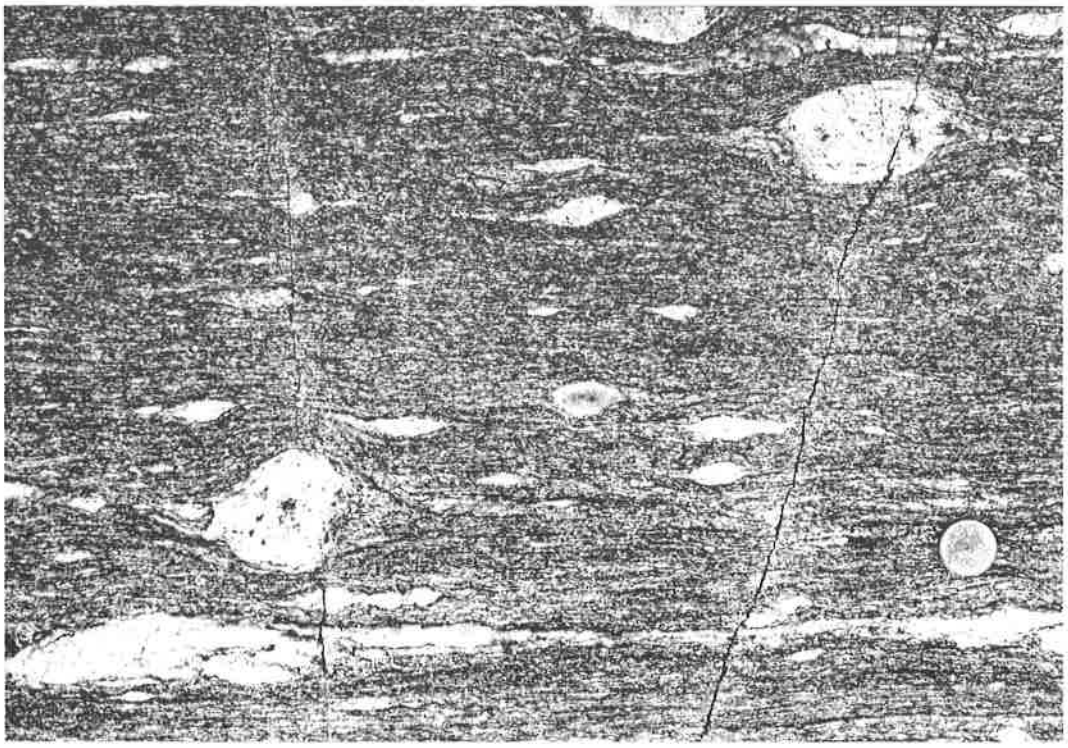

Photo2.06
Strongly deformed orthogneiss; Vieux Emosson region, Aiguilles Rouges
Orthogneiss déformé, Vieux Emosson, Aiguilles Rouges (Coord. CH:518.600/101.030)

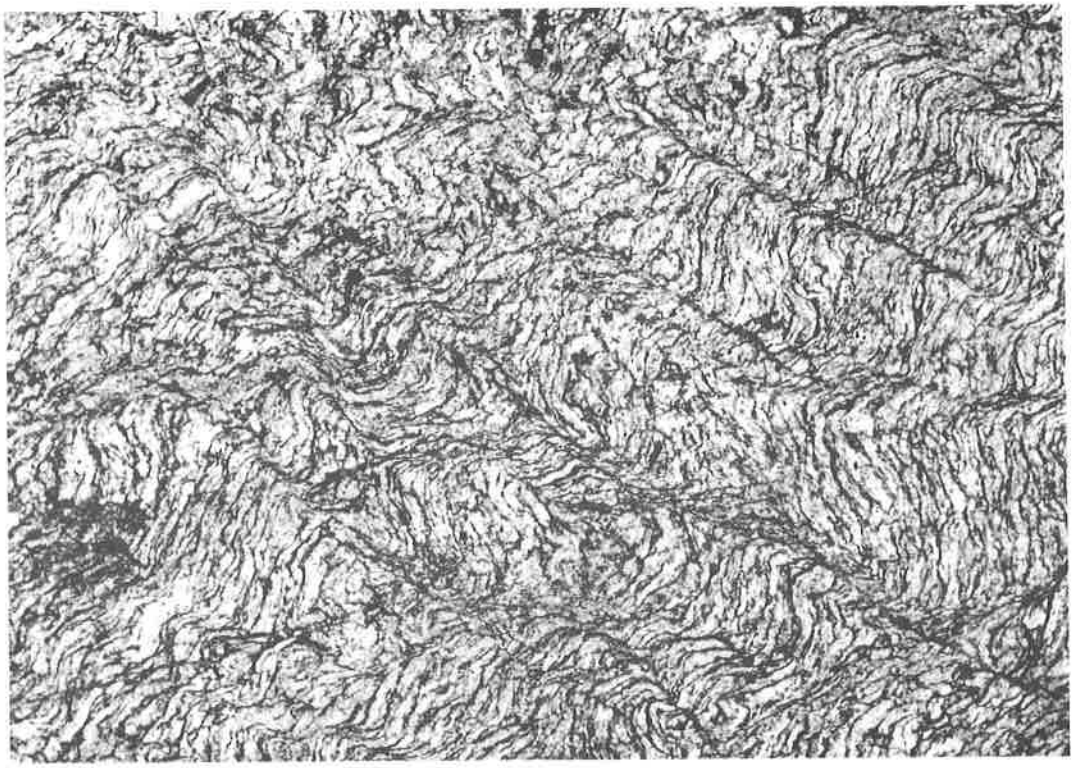

Photo2.07
Beginning of anatectic melting along shear-zones, Lognan, Mont Blanc massif; *Début d'anatexie parallèlement aux zones de cisaillement, Lognan, Massif du Mont Blanc* (scale 1:4)
(Coord. FR: 958.320/117.900, 2290);

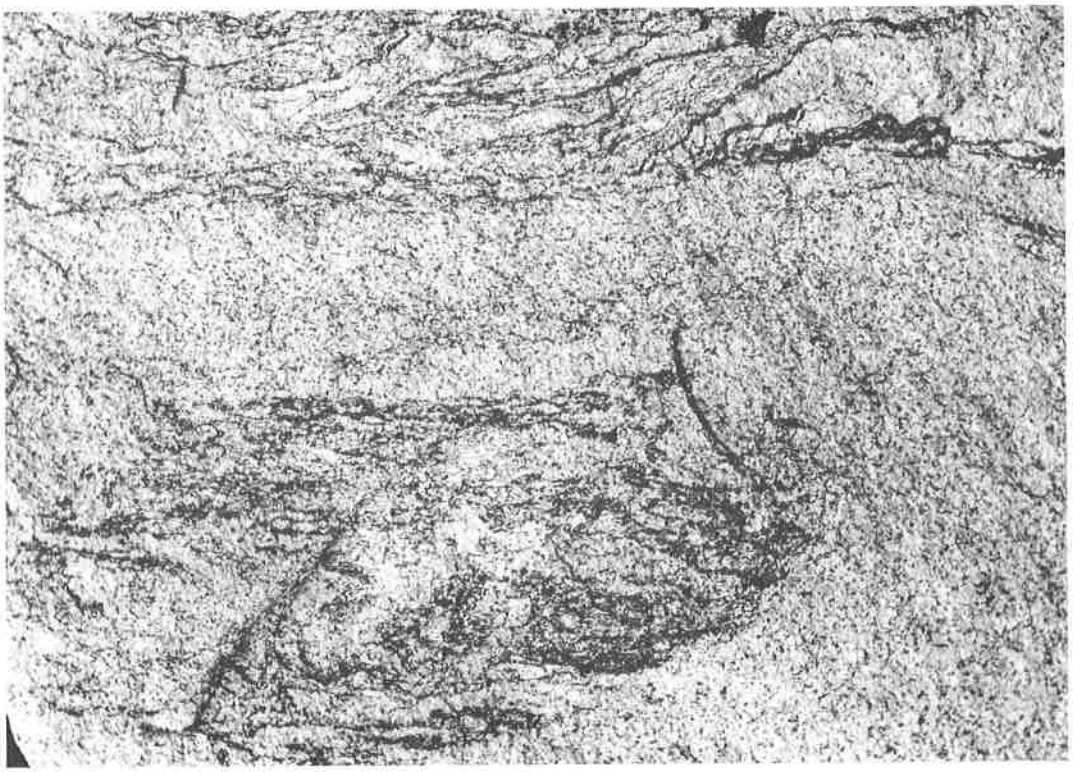

Photo2.08
Intrusion of newly formed granitic melt into the strongly mobilised orthogneisses, Lognan region, Mont Blanc massif. *Intrusion de filons granitoïdes néoformés dans un orthogneiss fortement migmatisé, environs de Lognan, massif du Mont Blanc* (Coord FR: 958.130/117.370; 2700) (scale 1:3)

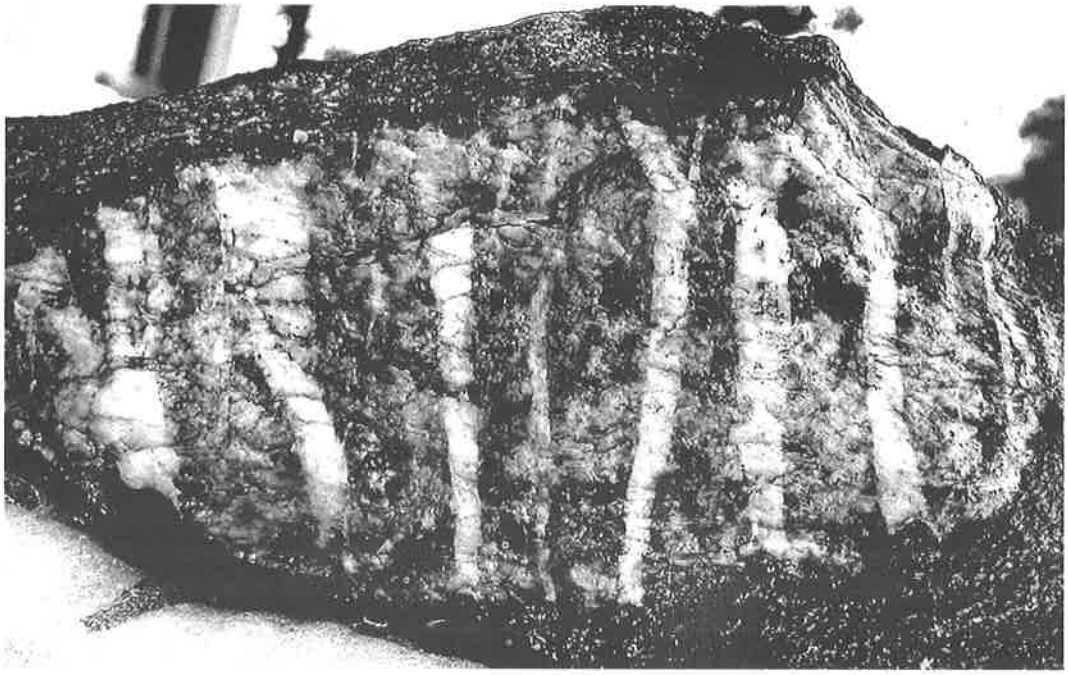

Photo2.09
Kf-feldspar crystal (size 20 cm) from an orthogneiss with Alpine tension-gashes (white) filled by albite and quartz; Petoudes area, Mont Blanc massif. *Cristal de feldspath potassique (20 cm long) dans un orthogneiss, traversé par des fissures alpines remplies d'albite et de quartz, Environs de Petoudes, massif du Mont Blanc*

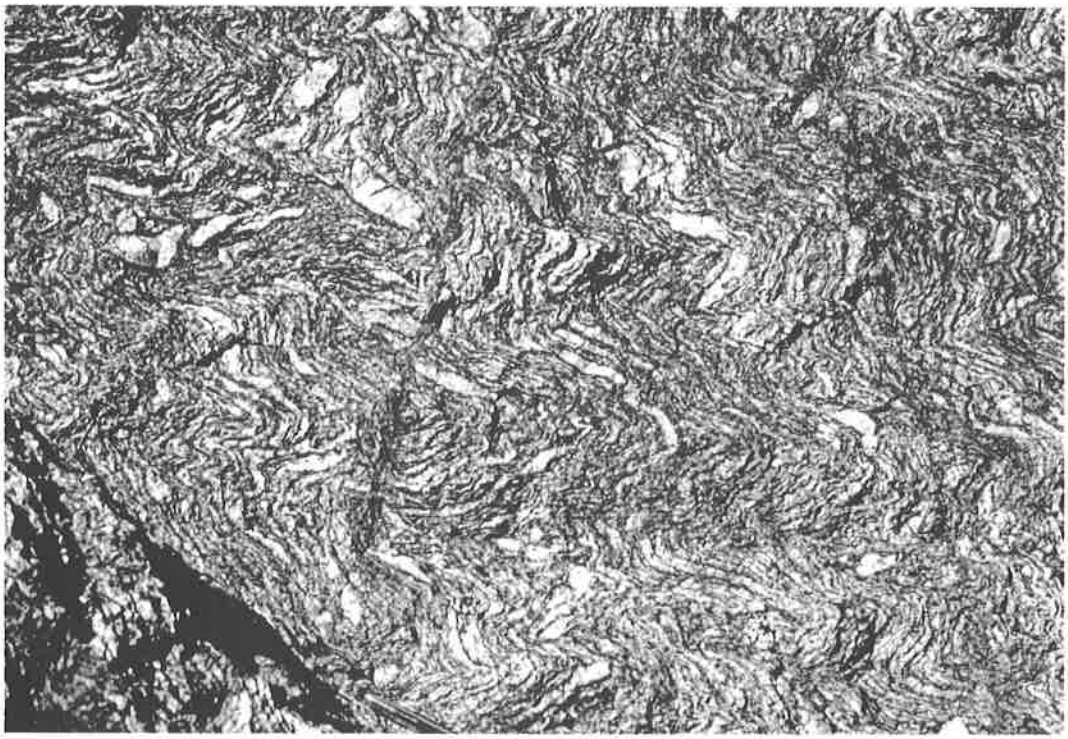

Photo2.10
Alpine fold structures in orthogneisses at Vieux Emosson; Aiguilles Rouges
Plis d'âge alpin dans un orthogneiss au Vieux Emosson, Aiguilles Rouges (Coord CH: 558.300/101.380)
(scale/*échelle* 1:5)

Such transformations are probably due to strong shear along the limbs of large-scale folds. Locally transformation into a fine-grained, leucocratic gneiss goes in parallel with the formation of a marked foliation and crystallization of muscovite and sillimanite (Marquis 1997). In both cases, chemical composition remains unchanged (Wirsing, 1997). An extreme deformation is visible in a large mylonite zone on the western border of the Emosson dam site (coord. CH: 560.520/101.635), where strongly deformed relics of K-feldspar are the only evidence for a former K-feldspar augengneiss origin.

Spectacular deformation resulted from Alpine metamorphism (von Raumer 1984, 1987). In the Emosson area, different stages of deformation show the growing influence of Alpine tectonics when approaching the base of the Alpine Morcles nappe. Orthogneisses have a shining gray-greenish foliation surface, and brittle deformation is visible through a large number of tiny fissures filled with quartz and chlorite (coord. CH: 558.750/101.650). Their statistic distribution in conjugate en échelon systems shows the narrow relationship to shear accompanied by general flattening. Alpine crenulation folds (**Photo 2.10**) are observed when approaching the base of Morcles nappe (coord. CH: 558.310/101.390) near the Vieux Emosson dam site.

Alpine transformations are even more spectacular in the Mont Blanc area (von Raumer 1971). In the neighborhood of Petoudes (coord. CH: 567.650/ 98.900), on the western side of Trient river, rather large cliffs are formed by K-feldspar augengneisses, where black coloured K-feldspars reach a size of 15 cm. The stretched original feldspars are broken, and the healed fractures are filled with stretching fibers of quartz and albite, growing normal to the fracture (**Photo 2.09**). When recomposing the separated fragments of the former K-feldspars, an elongation of about 300% can be deduced (von Raumer 1984), but matrix probably suffered even a stronger elongation reacting as more plastic material during recrystallization of quartz and white mica, under overall greenschist facies conditions.

Petrography of granodioritic gneisses

Type locality: Aiguilles Rouges: The "Gneiss du Luisin" type outcrops at the foothill of Mt Luisin, Lac de Salanfe area (coord. Ch: 562.350/108.450).

In the Salanfe area, the transition between augengneisses and granodioritic gneisses is not sharp and part of the "Luisin"-type gneisses may represent former augengneisses, having suffered a strong foliation with formation of biotite through deformation. In this case, part of the gneisses would correspond to the biotite-K-feldspar gneisses observed in the Val Bérard and Emosson areas (see above). The "Luisin"-gneisses are characterized by abundant biotite marking a good schistosity and by numerous mafic microgranular enclaves. Plagioclase, K-feldspar and quartz appear only as reduced grains among the well crystallized biotite crystals. Microscopy does not allow to distinguish clearly between augengneisses and biotite-gneisses as two rock types (see also geochemistry, Chap. 2.1.3), and their age confirms that the biotite gneisses are older than the augengneisses.

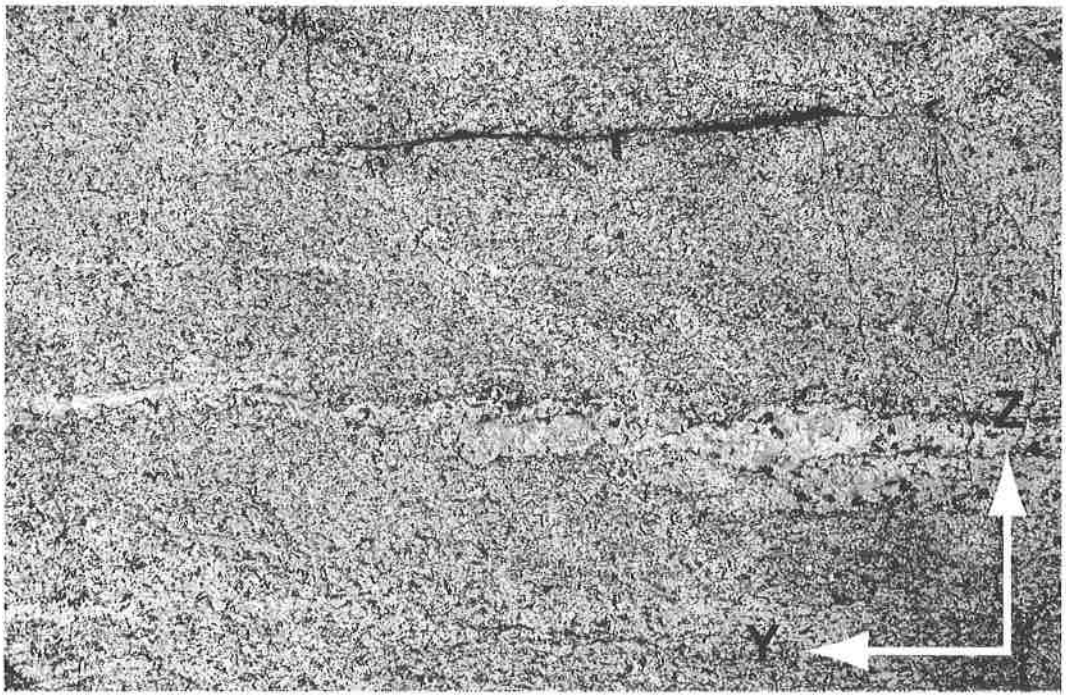

Photo2.11
Hornblende-biotite-gneiss (Col de Salenton), horizontal view, y-z section; (Coord Fr: 950.125/121.855)
Gneiss à hornblende-biotite (Col de Salenton), aspect horizontal, section y-z. Scale/*échelle: 1:2*

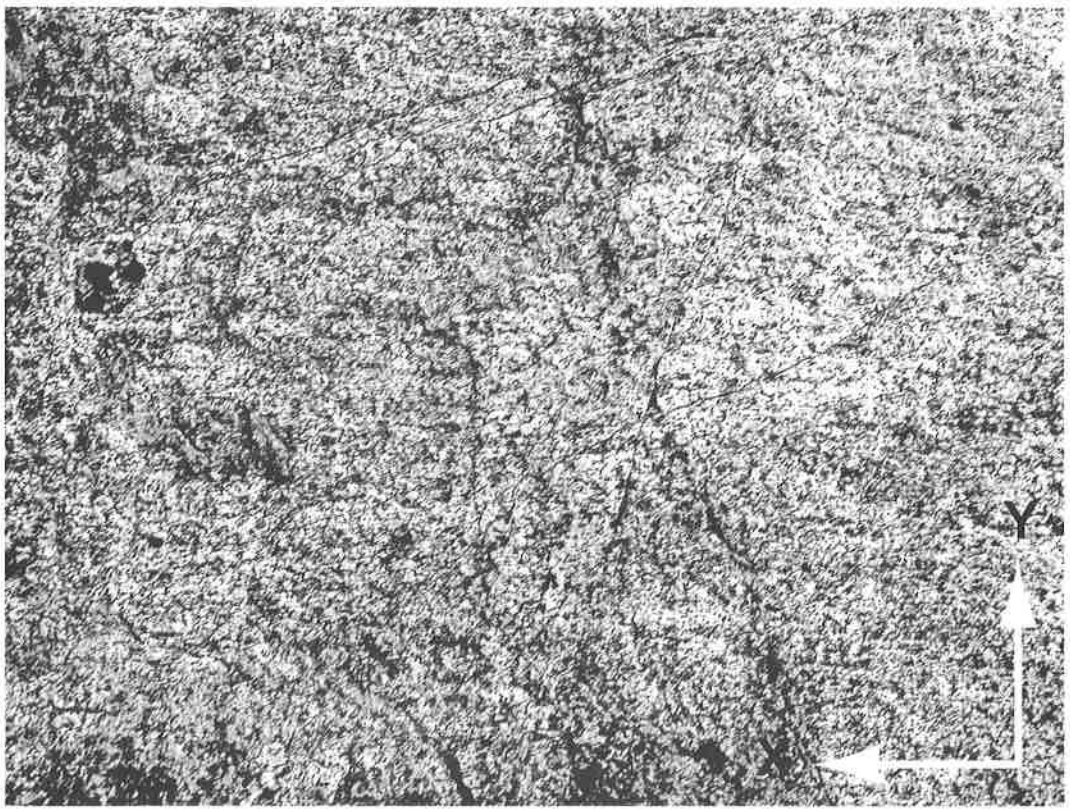

Photo2.12
Hornblende-biotite-gneiss (Col de Salenton) with vertical stretching lineation, vertical view, top at left, x-y section. Scale/échelle: 1:2 *Gneiss à hornblende-biotite avec linéation d'étirement (Col de Salenton), aspect vertical, bout supérieur à gauche, section x-y (Coord Fr: 950.125/121.855)*

Petrography of biotite-amphibole gneisses

Type locality: outcrops situated east of Col de Salenton (coord. Fr: 950.125/121.855).

Biotite-amphibolte gneisses appear to the east of Col de Salenton and they look quite different from the augengneisses and granodioritic gneisses. They are homogeneous medium-grained gneisses with a well expressed biotite foliation and isolated grains of amphibole (**Photos 2.11-2.12**). In the well organised foliation plane, biotite and amphibole follow a clear linear structure indicating a considerable vertical stretching of this rock unit. This structure is also underlined by the alignment of biotite and amphibole patches (microlithes, autoliths).

Textures point to granoblastic to nematoblastic recrystallization of all components (Wirsing, 1997). Brown-green tschermakitic hornblende I of maximum 4 mm size is in most cases elongated parallel to the main linear structure of the rock. Locally corroded, they could represent a magmatic generation of hornblende. A second generation of actinolitic hornblende attains a maximum size of 3 mm and has grown parallel to foliation plane S_2, locally intergrown with biotite.

The first generation of biotite is red-brown and attains a size of 1 mm; it may be the expression of an older foliation plane and defines the main foliation plane S_1. Ilmenite and sphene are observed as unmixing products. Biotite generation II is light-brown and up to 3mm in length; it follows the main foliation and replaces hornblende I with crystallization of idiomorphic sphene. A third generation of tiny biotites could be the expression of a more recent schistosity.

Plagioclase (An_{25-40}) up to 1.5 mm in size is intergrown with quartz. Quartz grains up to 1.5 mm in size with faint signs of undulatory extinction display first stages of very tiny recristallized grains due to weak Alpine overprint. K-feldspar appears only as accessory tiny grains (0.4 mm) among the assemblage of quartz and plagioclase. Zircon crystals appear in both biotite generations and in hornblende I.

The origin of this rock unit should be re-discussed. Located in the central part of a large fold hinge, these rocks either may represent a former magmatic unit of granodioritic composition, or they resulted from probably Variscan anatectic melting with contemporaneous stretching in a fold-hinge of a former granodioritic unit.

II.1.2 Zircon typology

Zircon typology after Pupin (1980, 1988) was applied to granitoid gneisses (Bauer 1996, Trient region; Wirsing 1997, Val Bérard region; Morard 1998, Lognan – Rachasses region). Unpublished results show, that zircon morphology for the different regions is comparable (**Fig. 2.03**). Biotite-hornblende gneisses occupy field 4 of Pupin's classification (**Fig.2.04**) corresponding to calc-alkaline granites (Pupin 1988).

Granitoid gneisses from Val Bérard (augengneisses and biotite-K-feldspar gneisses) plot just across the limit between field 4 and field 3 corresponding to aluminous monzogranodiorites. Augengneisses from Lognan also plot into field 3, although some of their zircons host cores of calc-alkaline morphology (Morard 1998).

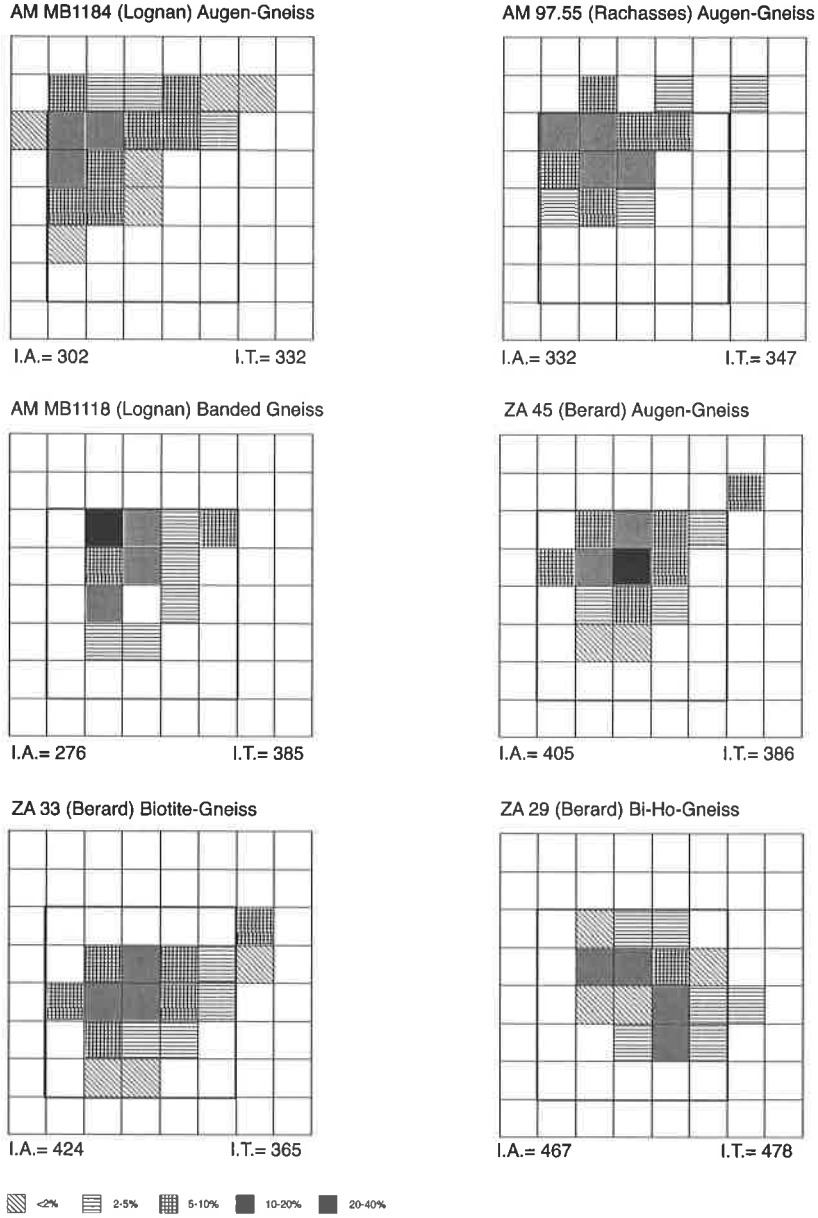

Fig. 2.03
Zircon typology (Pupin 1988) of granitoïd gneisses (orthogneisses and bi-ho-gneisses) from the Mont Blanc and Aiguilles Rouges areas, coordinates indicating mean values of IA and IT. ZA: Wirsing 1997; AM, Morard 1998.

Diagrammes de distribution typologique du zircon (Pupin 1988) des gneiss granitoïdes (orthogneiss et gneiss à bi-ho) des massifs du Mont Blanc et des Aiguilles Rouges avec indication des indices moyens IA et IT. Echantillons: ZA (Wirsing 1997); AM, (Morard 1998).

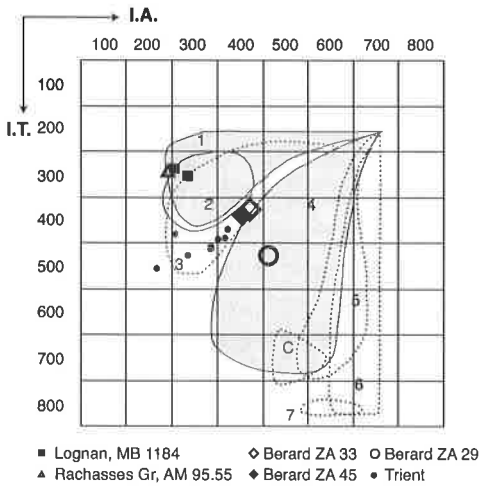

Fig. 2.04
Typological indices of zircon populations (after Pupin 1988) of Ordovician orthogneisses from Mont Blanc and Aiguilles Rouges areas (unpublished results from Bauer 1993, Wirsing 1997, Morard 1998; information about specimens see preceding figure **2.03**).

*Indices typologiques des populations de zircons (projection d'après Pupin 1988) du orthogneiss ordovicien des massifs du Mont Blanc et des Aiguilles Rouges (Résultats non publiés tirés de Bauer 1993, Wirsing 1997, Morard 1998 (information sur les échantillons, voir figure **2.03** précédente).*

Crustal origin
1. Aluminous leucogranites, authochtonous or intrusive
2. Monzogranites and granodiorites (sub)authochtonous
3. monzogranodiorites and intrusive porphyric granodiorites

Hybrid origin
4. calc-alkaline and calc-alkaline MgK granites
5. SubalkalineFeK granites
C. Tholeiitic continental granites (charnockites)

Mantellic
6. Alkaline and hyperalkaline granites (hypersolvus > I.T. 640)
7. Tholeiitic oceanic granites (plagiogranites)

II.1.3 Geochemistry of granitoïd gneisses

A wealth of mostly unpublished chemical data are available (Mont Blanc massif: Bauer 1993 and Nähr 1993 for the Trient area; Morard 1998 for the Lognan area; Aiguilles Rouges massif: Wirsing 1997 for Val Bérard; unpublished analyses, Favre and von Raumer, Emosson region), of which representative analyses are reported in Annex I (**Tab. VI.1-VI.7**). Some general chemical features will be reported and discussed below in a number of conventional diagrams. As all these rocks underwent a complex polymetamorphic history, their concentrations in some of the reputedly mobile elements such as Ca, Na, K, Rb, Sr and Ba might have been modified, which would affect their position in some diagrams. For example, some of the samples show dubiously high A/CNK ratios in **Fig. 2.08**, which might be related to a loss of Ca.

Hornblende-biotite gneisses (Val Bérard)

These rocks depart quite strongly from all other orthogneisses in diagrams based on major elements. They are relatively silica- (and Ti)-poor (**Fig. 2.05**), plot in the field of tonalites to granodiorites in the R1-R2 classification (**Fig. 2.06**), have a K_2O/Na_2O < 1 and are essentially metaluminous (**Fig. 2.07** and **2.08**), which is in keeping with a relatively low P_2O_5 content (**Fig. 2.09** and Bea et al 1992). Their REE content is moderate (ΣREE=136 ppm) and their weak negative Eu anomaly (mean Eu/Eu* = 0.89) points to limited fractional crystallization processes. These characteristics and the zircon typology (**Fig. 2.04**) are typical of low- to medium-K calc-alkaline rocks (ACG granites; Amphibole-bearing Calc-alkaline Granites) in Barbarin's (1999) classification, typical of subduction-related environments.

Augengneisses (Bérard-Emosson)

These are moderately evolved rocks with silica contents mostly between 64 and 70 wt% SiO_2 (**Fig. 2.05**), which plot in the granodiorite to monzogranite fields in the R1-R2 classification diagram (**Fig. 2.06**). They are definitely peraluminous (**Fig. 2.07** and **2.08**) and plot in the Biotite>Muscovite field of the A-B diagram of Debon and Lefort (**Fig. 2.07**). Their P_2O_5 content corresponds to equilibrium temperatures above 950 to 1000°C (see Bea et al., 1992) (**Fig. 2.09**), which is certainly too high for this kind of magma and rather denotes low Ca activity, a feature typical of peraluminous melts (Bea et al. 1992). Their REE content is much higher than that of the hornblende-biotite gneisses (ΣREE=250 ppm), as well as their negative Eu anomaly (mean Eu/Eu* = 0.52) (**Fig. 2.10**), pointing to a more fertile source and a probably more differentiated character.

Augengneisses (Trient-Lognan)

Orthogneisses from the Mont Blanc massif are globally more differentiated than those from the Aiguilles Rouges; ranging between 71 and 77 wt% SiO_2 (**Fig. 2.05**). They plot in the syenogranites field in the R1-R2 classification diagram (**Fig. 2.06**). Otherwise, they are equally peraluminous as the Bérard-Emosson augengneisses (**Fig. 2.07** and **2.08**). Their P_2O_5 content corresponds to equilibrium temperatures mostly above 1000°C, which are even higher than those obtained for the Bérard-type rocks. This feature reflects the very low Ca activity of these evolved magmas, preventing crystallization and fractionation of apatite (Bea et al., 1992). Moderate LREE contents and a strong negative Eu anomaly (mean Eu/Eu* = 0.40) also evidence the highly differentiated character of the Trient-Lognan augengneisses.

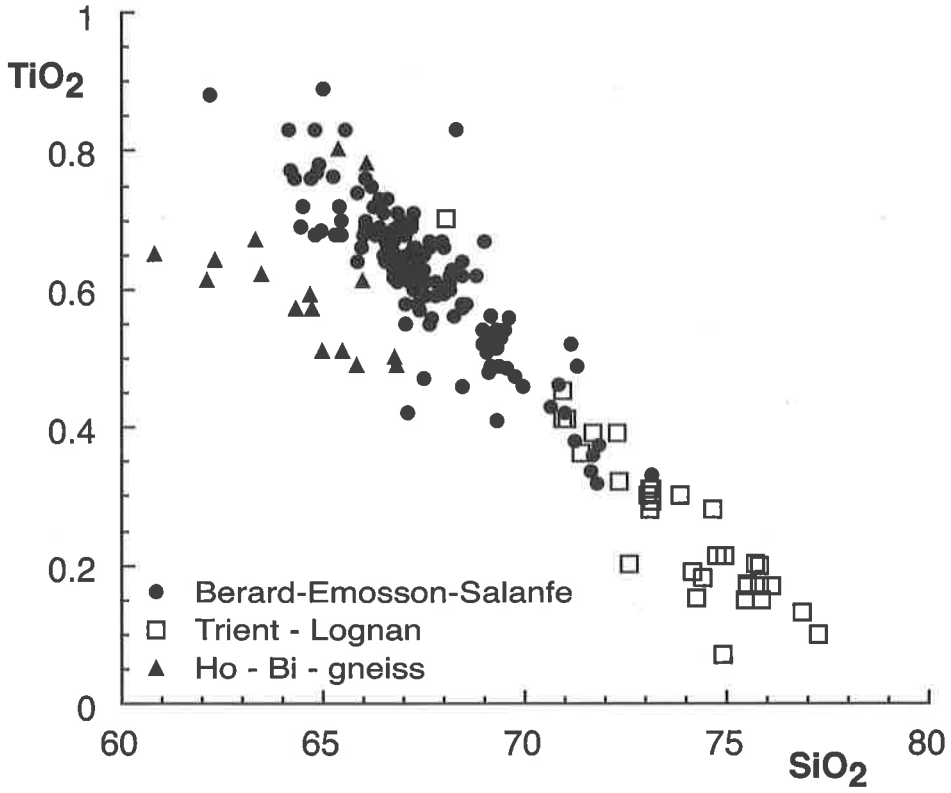

Fig. 2.05 Comparison of chemical composition (TiO_2 - SiO_2) of metagranites (orthogneiss of lower Palaeozoic age) from Mont Blanc (Trient-Lognan) and Aiguilles Rouges (Bérard-Emosson-Salanfe). Luisin granodiorite, Salanfe (4 analyses); gneiss à biotite-hornblende, Bérard (14); orthogneiss Emosson - Bérard (123); orthogneiss Salanfe (6); orthogneiss Trient - Lognan (31).

Comparaison du chimisme (TiO_2 - SiO_2) de méta-granitoïdes (orthogneiss d'âge Paléozoïque inférieur) du Massif du Mont Blanc (Trient-Lognan) et des Aiguilles Rouges (Bérard-Emosson-Salanfe) Granodiorites du type Luisin, Salanfe (4 analyses); gneiss à biotite-hornblende, Bérard (14); orthogneiss Emosson - Bérard (123); orthogneiss Salanfe (6); orthogneiss Trient - Lognan (31).

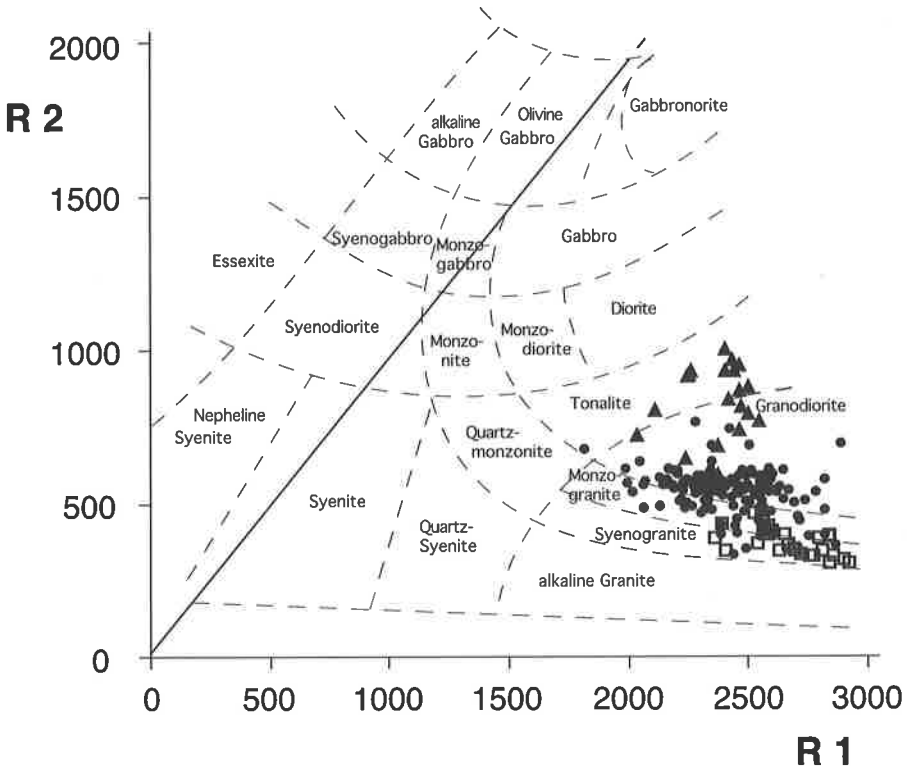

Fig. 2.06
Classification of plutonic rocks after De La Roche et al. (1980)

Diagramme de classification paramétrique des roches plutoniques d'après De La Roche et al. (1980)

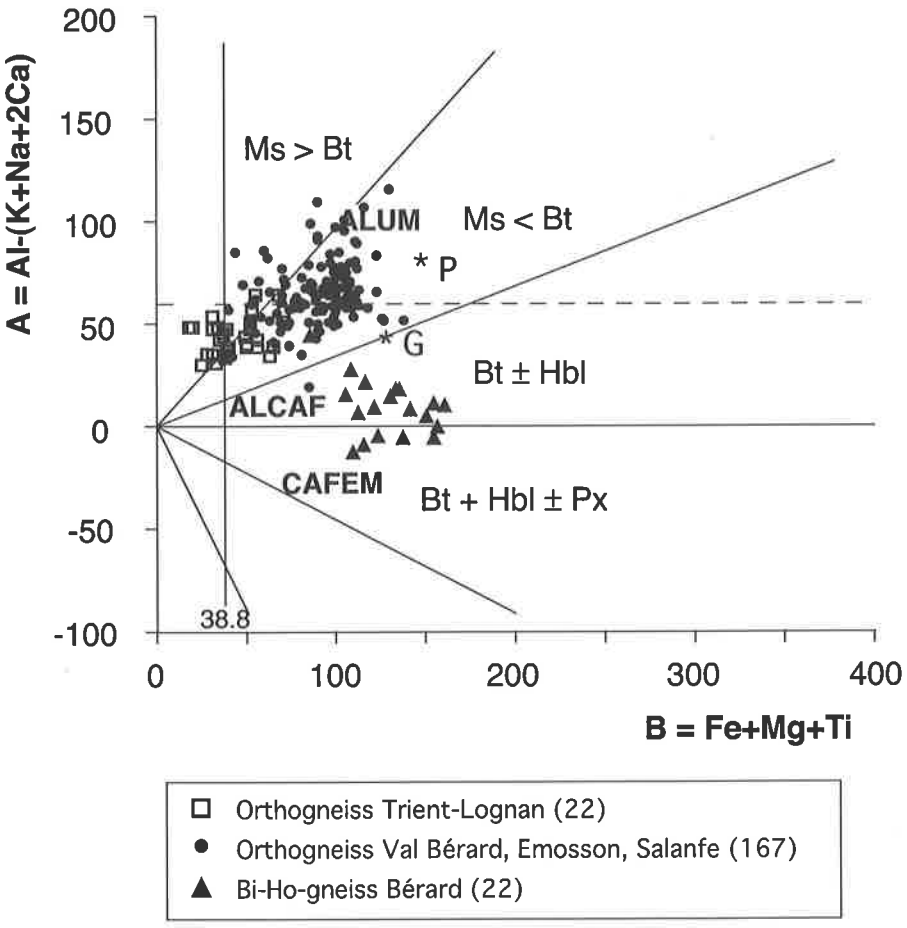

Fig. 2.07
A-B discriminant diagram after de Debon & Le Fort (1988)

Diagramme A-B de Debon & Le Fort (1988) et champs de repartition des associations magmatiques

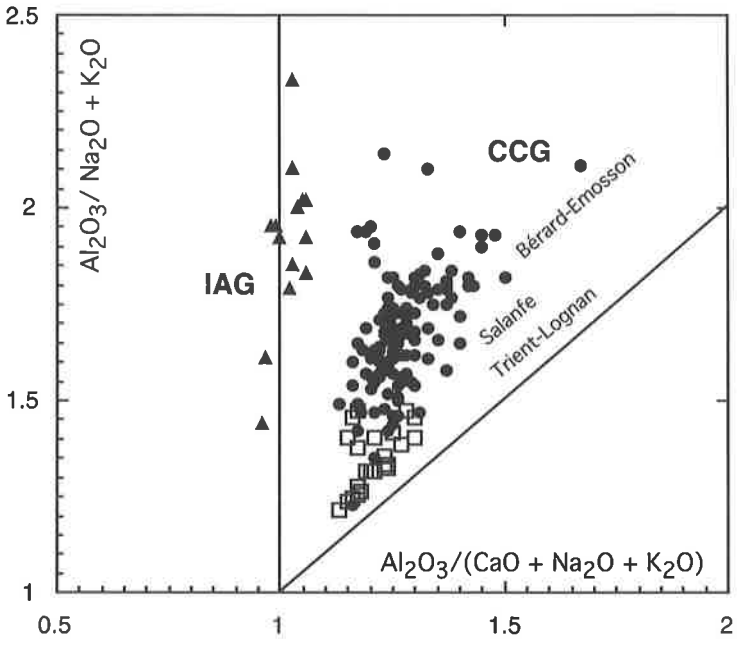

Fig. 2.08
Origin of lower Palaeozoic metagranites from Aiguilles Rouges and Mont Blanc areas. Plate tectonic interpretation after Maniar and Piccoli (1989).
IAG Arc volcanic granites, CCG Continental collision typ granites.

Origine des métagranitoïdes du Paléozoïque inférieur des massifs du Mont Blanc et des Aiguilles Rouges dans le diagramme discriminant de Maniar et Piccoli (1989). IAG: granites de type arc volcanique, CCG: granites de type collision continentale.

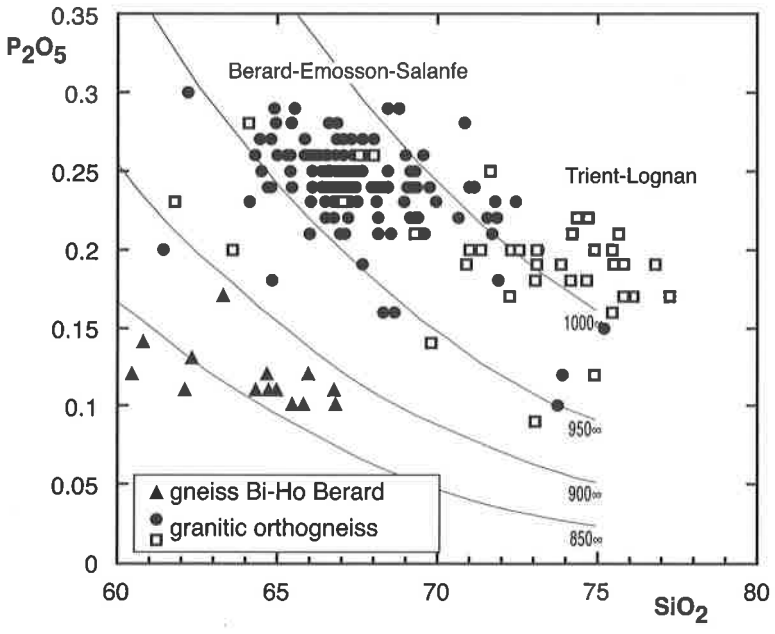

Fig. 2.09
P_2O_5 contents in lower Palaeozoic granitoids from Aiguilles Rouges and Mont Blanc areas. See text for explanation

Concentrations en P_2O_5 des méta granitoïdes d'âge Paléozoïque inférieur. Les granitoïdes du massif du Mont Blanc ont, en moyenne, des concentrations en P_2O_5 plus basses que les orthogneiss des Aiguilles Rouges.

Overall, augengneisses from both massifs have a peraluminous character, which is confirmed by zircon typology (**Fig. 2.04**). They mainly differ in their degree of differentiation, but might derive from similar crustal sources. Whether they are of MPG (muscovite-bearing peraluminous granitoids) or CPG (cordierite-bearing peraluminous granitoids) type (Barbarin, 1999) is a difficult question, considering that their high present-day muscovite content is of metamorphic origin. A slight decrease of the A/CNK index with differentiation favour a genetic link with the CPG (Barbarin, 1999). Both MPGs and CPGs are typical of continental collision geodynamic environments.

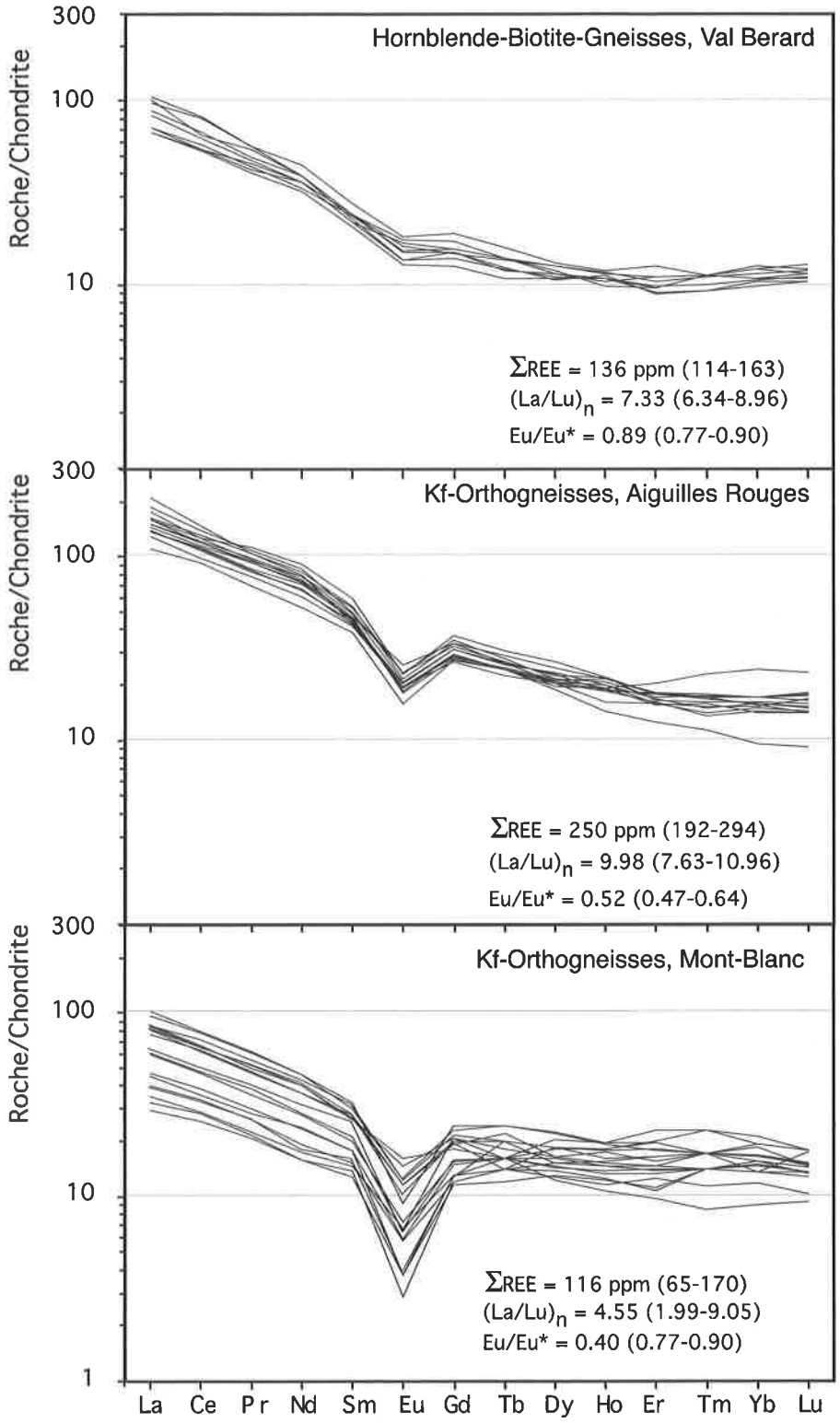

Fig. 2.10
REE concentrations of AR and MB gneisses (Chondrite normalized values) unpublished data (Annex I, Tab VI.7) from Bauer 1993, Morard 1998; Wirsing 1997).
Composition en terres rares des gneiss paléozoiques du AR et du MB (valeurs normalisées à la composition de chondrite; données non publiées (Annexe I, Tab. VI.7), d'après Bauer 1993, Morard 1998; Wirsing 1997). Chiffres en paranthèeses, gamme de variation des teneurs.

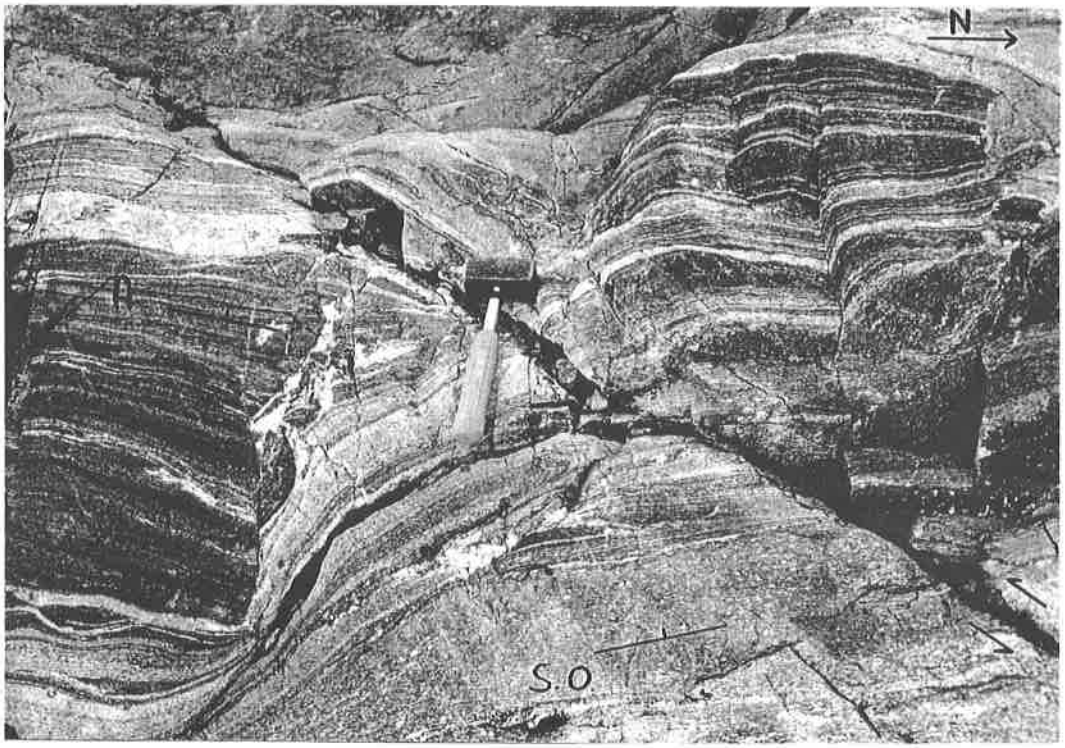

Photo 2.13
Boudinized isoclinal amphibolite layer in plagioclase-rich micaschists. VaL Bérard, Aiguilles Rouges (Coord. Fr.: 949.975/120.670). (Photo 3.4 in Fracheboud 1997). *Amphibolite boudinée dans des micaschistes à plagioclase. Val Bérard, Aiguilles Rouges. (Coord. Fr. 949.975/120.670). (Photo 3.4 dans Fracheboud 1997).*

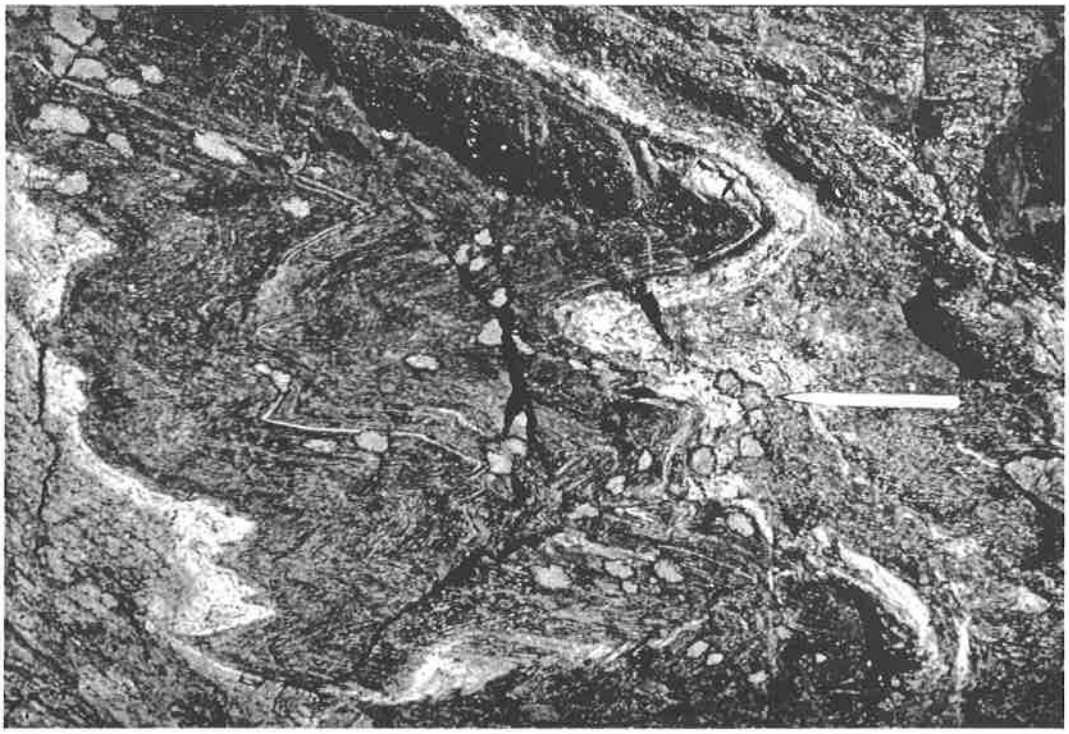

Photo 2.14
Foliated garnet amphibolite layer with plagioclase-rich rim at the contact with micaschists (scale 1:10). Fontanabran area, Aiguilles Rouges (Coord. CH: 561.750/105.140, 2560m). *Amphibolite à grenat rubanée et plissée avec bordure riche en plagioclase au contact avec des micaschistes. Fontanabran, Aiguilles Rouges*

II.2. Metabasic rock units

2.1 Petrography of metabasic rocks

Metabasic rocks, representing metamorphosed rocks of basaltic composition (basalts, gabbros) are found in many places as amphibolites (products of medium to high amphibolite grade metamorphism), or as high pressure eclogites first mentionned by Necker (1828). Both rock types occur as dispersed boudins within the basement lithologies of the Aiguilles Rouges and Mont Blanc massifs. This volumetrically insignificant rock type is the only record of Palaeozoic basaltic magmatism in the area.

Amphibolites

Type localities: outcrops at the northern border of Lac d'Emosson (coord. CH: 559.400/101.960), and many outcrops in the neighbourhood of Col de la Terrasse (coord. CH: 557.470/100.000).

Relicts of amphibolite boudins are mostly preserved in micaschists or migmatites of both massifs. In the Aiguilles Rouges, where migmatisation is less intense, massive amphibolites appear as boudin trails where only fold hinges are preserved (**Photo 2.13, 2.14**). They can be easily mapped like pearls of a giant necklace (Corbin & Oulianoff 1925), around large-scale km-size folds (von Raumer et al. 1990). In the SW part of Aiguilles Rouges, amphibolites are locally observed in the polymetamorphic basement situated in the SE of the St.-Gervais-Les Houches zone (WG, Dobmeier 1996).

In the central part of Aiguilles Rouges, amphibolites appear preferentially in a micaschist unit, and their distribution seems to indicate the presence of one or two original "layers" (strata or dikes) of reduced size. Crosscutting relationships with quartzite bands (Fontanabran region; coord. CH: 561.040/104.630), or metagreywacke layers (Lac Vert area; coord. CH: 557.500/100.075), suggest that these basaltic layers were dykes intruded into the former sediments (now micaschists, metagreywackes, and quartzites) rather than subaerial volcanic flows.

In the strongly migmatized border zone of the Mont Blanc granite (Combe des Fonds, Mt. Dolent glacier, coord. CH: 571.700/85.125), amphibolites appear as strongly brecciated bodies in a migmatitic environment (**photo 2.15**), indicating a brittle behaviour of amphibolites in a strongly mobilized environment.

The mineralogy of amphibolites is characterized by the classical amphibolite facies assemblage amphibole – plagioclase ± garnet ± zoisite (cm-long needles, **photo 2.16**; coord. CH: 558.830/100.630; 560.920/103.780). Zoisite is mostly replaced by clinizoisite, white mica and plagioclase. The transition from plagioclase- to garnet-amphibolites, best observed under the microscope, may be gradual, and two types of evolution are found. On the one hand, an original coexistence of both types of amphibolites seems to exist with plagioclase amphibolites representing former olivine-tholeiites, and garnet amphibolites representing more evolved quartz- or hypersthene-bearing tholeiites (von Raumer et al. 1990) (see chapter geochemistry). On the other hand, a gradual transformation from garnet amphibolites to plagioclase amphibolites is also possible, accompanied by changes of Fe and Mg during hornblende and garnet destabilisation (see Ch. III.1).

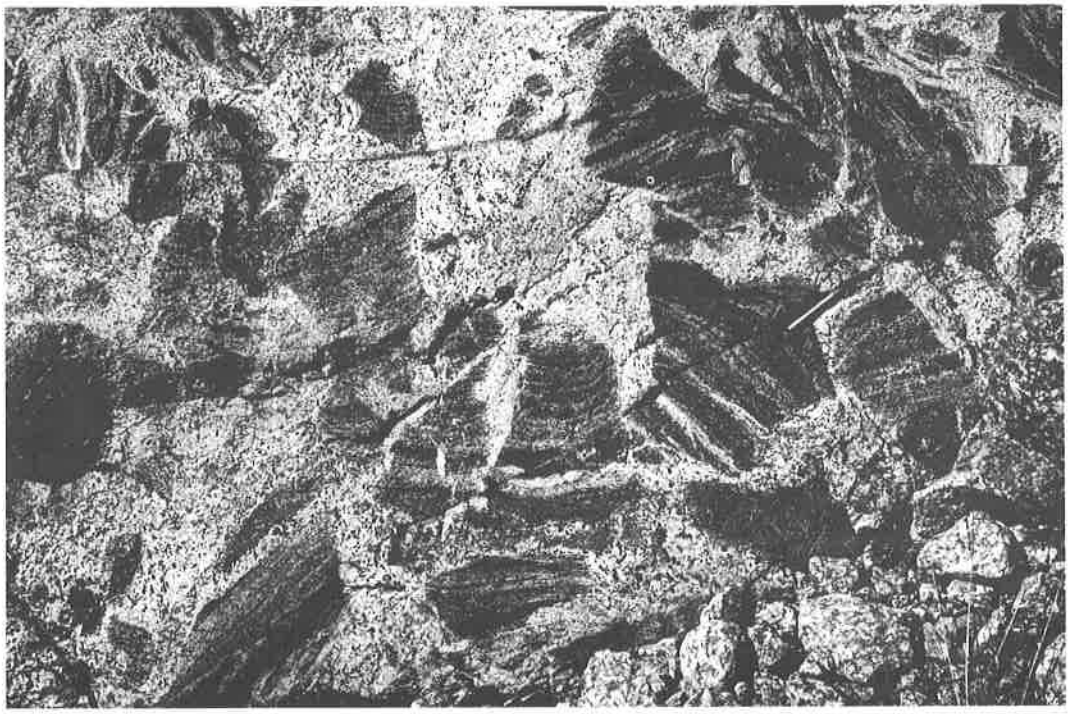

Photo 2.15
Brecciated layered amphibolite in a migmatic matrix (scale 1:20). Combe des Fonds, Mt. Dolent glacier, Mont Blanc massif (Coord. CH: 571.840/85.265, 2480m). *Amphibolite bréchique dans une matrice de migmatite, Combe des Fonds, glacier du Mt. Dolent, Massif du Mont Blanc.*

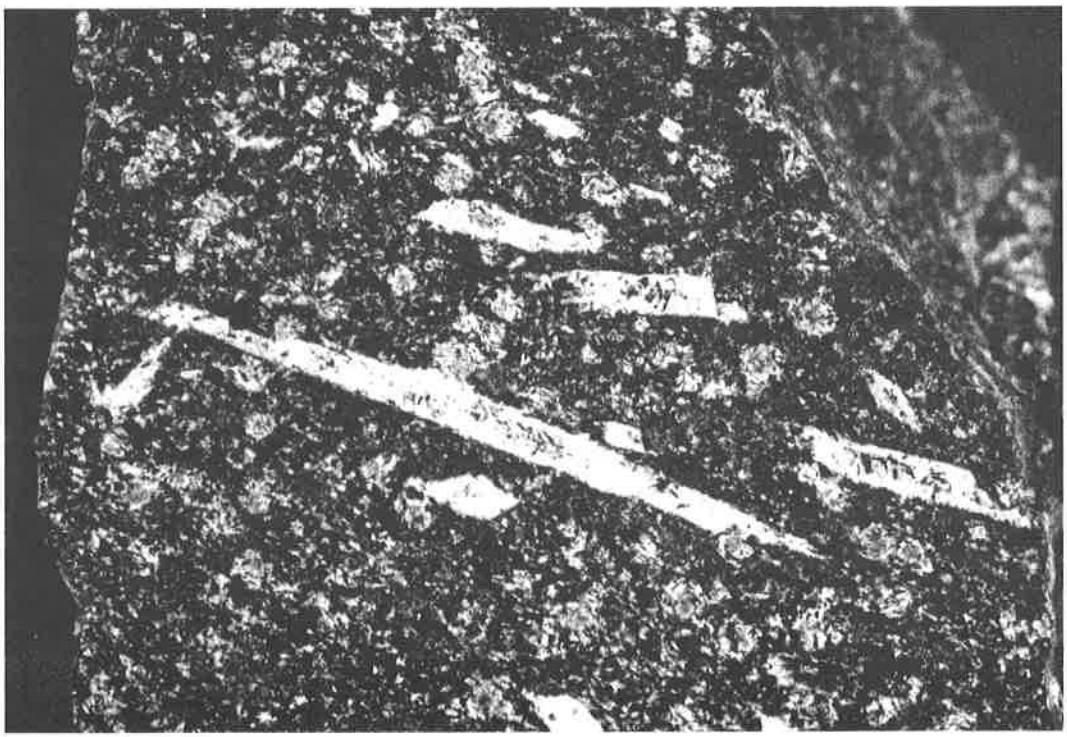

Photo 2.16
Garnet amphibolite with pseudomorphs of clinozoisite after zoisite. Vieux Emosson, Aiguilles Rouges (Coord. CH: 558.830/100.630). (scale 1:2)
Amphibolite à grenat avec pseudomorphose de zoisite en clinozoisite. Vieux Emosson, Aiguilles Rouges. (Echelle 1 : 2).

The observed mineral phases indicate an amphibolite facies metamorphic recrystallization at medium pressure, which occurred some time between the Ordovician and the Carboniferous. The local presence of zoisite needles suggests an evolution from higher to medium pressures, and kelyphitic reaction rims around garnet may indicate the former existence of eclogites.

A special type of garnet amphibolites appears at the contact between amphibolite boudins and micaschists, where a leucocratic plagioclase-rich border zone develops with growth of large zoned garnets (**Photo 2.14, 3.18**). Plagioclase-bearing layers parallel to the foliation, containing tiny garnets, also occur within some amphibolite boudins (**Photo 3.17**). Such observations indicate metamorphic reactions accompanied by segregation of leucocratic material. Very locally layers as wide as several centimetres consist of a granular intergrowth of plagioclase-biotite with clusters of either small hornblende or garnet crystals. In addition, the plagioclase matrix may contain large crystals of kyanite and/or staurolite. In the Emosson area, Dupasquier (1996) described for the first time such leucocratic segregations, which may have resulted from metasomatic processes or early stages of partial melting. These features are very similar to those observed around eclogite boudins at Lac Cornu, interpreted as decompression melting phenomena (von Raumer et al. 1996).

Secondary transformations are observed as reaction rims at the contact with quartz-andalusite veins, where former garnet amphibolites are completely transformed into a brownish coloured, mica-rich rock. Strong changes result from Alpine metamorphic transformations (von Raumer 1974). In the Aiguilles Rouges, the assemblage pumpellyite, prehnite and laumontite shows anchimetamorphic or lowest greenschist facies recrystallization, whereas in the Mont Blanc area, the assemblage actinolite-chlorite-epidote (±clinozoïsite±zoïsite)-albite-sphene indicates lower greenschist facies grade.

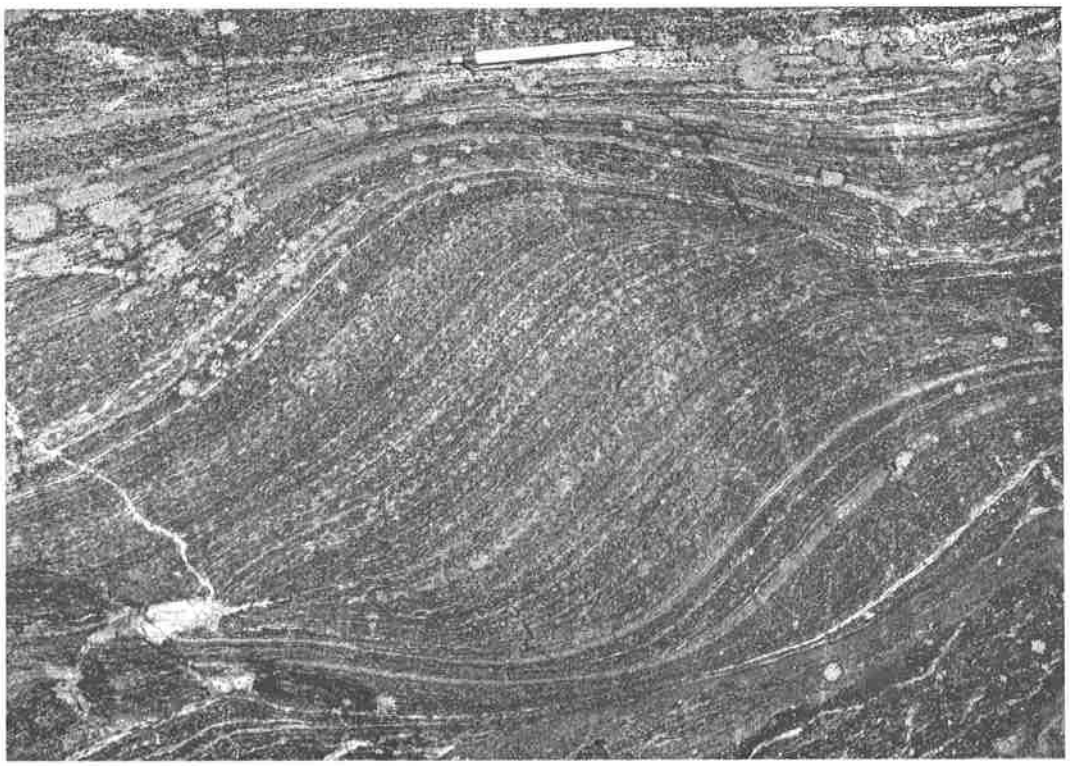

Photo 2.17
Coarse grained eclogite shear-lens, western lakeside of Lac Cornu, Aiguilles Rouges (pencil as scale)
Eclogite rubanée à grain grossier. Rivière ouest du Lac Cornu, Aiguilles Rouges. (crayon comme échelle)

Photo 2.18
Garnet-plagioclase felses of tonalitic composition from western lakeside of Lac Cornu, Aiguilles Rouges (scale 1:4), interpreted as product from dehydration melting of meta-eclogites.
Gneiss tonalitique à plagioclase-grenat, formé par fusion de déhydratation de méta-eclogites. Rivière ouest du Lac Cornu, Aiguilles Rouges.

Eclogites

Eclogites were first mentioned by Necker (1828) in the Aiguilles Rouges, and after the short notes made by Favre (1867) and Michel-Lévy (1890) followed a more detailed description by Joukowski (1902). In the Mont Blanc massif, the eclogite locality from the Petoudes area (coord. CH: 567.200/95.790} was first mentioned by Duparc & Mrazec (1893,1894), and more localities were discovered in the neighbourhood of Pointe des Grands (Coord. CH: 565.640/95.680).

The Lac Cornu eclogites, formerly interpreted as a "vein" of neptunistic origin (Corbin et Oulianoff 1928a), form part of a complex assemblage of elongated amphibolite bodies. Besides the main outcrop area at Lac Cornu, distinct, minor eclogite boudins and granulite bodies can be followed up in northern direction across Tête de Béchat, Col de Barme and the Upper Val Bérard to the region of Lac d'Emosson (foot of Fontanabran, coord. CH: 561.400/105.020), and tiny relicts are even observed among the migmatites above Miéville (Plancherel 1960). The metabasites hosting the eclogites correspond to amphibolites as described above (Liégois and Duchesne, 1981), including the boudin-shaped massive eclogites. The main structures are dominated by a repetition of distinct amphibolite layers which may correspond to distinct large-scale, isoclinal folds, where flanks of the folds have been strongly sheared and transformed. Eclogite boudins seem to represent an assemblage of elongated fold hinges. Many of the fine grained, massive eclogites probably represent former basaltic layers, and locally such lensoid, very fine grained bodies are interlayered with banded eclogitic layers reminiscent of former tuffitic banding. Local occurrences of very coarse grained assemblages recall the relicts of former gabbroic protoliths.

The gradual decomposition of eclogites to amphibolites is accompanied by a multitude of tectonic phenomena. One very nicely preserved lensoid shaped eclogite body (**Photo 2.17**) is limited by dextral shear zones filled with plagioclase. The preserved parallel structures of very coarse eclogite, representing the oldest strutural relict in eclogites of this region, had induced Corbin & Oulianoff (1928a) to see a sedimentary origin fort his assemblage. Outwards, the eclogites are gradually replaced by sheared amphibolitic rocks, which are accompanied by fine grained biotite-plagioclase rocks containing cataclastic relicts of hornblende, which could be interpreted as fine grained mylonites accompanying the eclogite bodies. Inside the eclogite bodies appear locally narrow, red coloured, vein-like bands filled by fine grained garnet and quartz.

The main eclogite body and the many isolated boudins are embedded in migmatites. Among the massive banded eclogitic to granulitic rocks appear, near to the migmatites, vein-like structures of homogeneous, plagioclase-garnet gneiss looking like granulites (**Photo 2.18**), (coord. Fr: 949.280/117.190). Composed by plagioclase-biotite-garnet-kyanite and reaction rims of hercynite-cordierite around kyanite, such rocks correspond, in their chemical composition, to tonalitic melts produced through dehydration melting of amphibolites (Wolf and Wyllie, 1994), and may be the product of decompression melting during uplift from lower crustal to upper crustal conditions (von Raumer et al. 1996, see Chapter III, metamorphism). The age of such melts is supposed to be Carboniferous, but remains to be determined through radiometric dating.

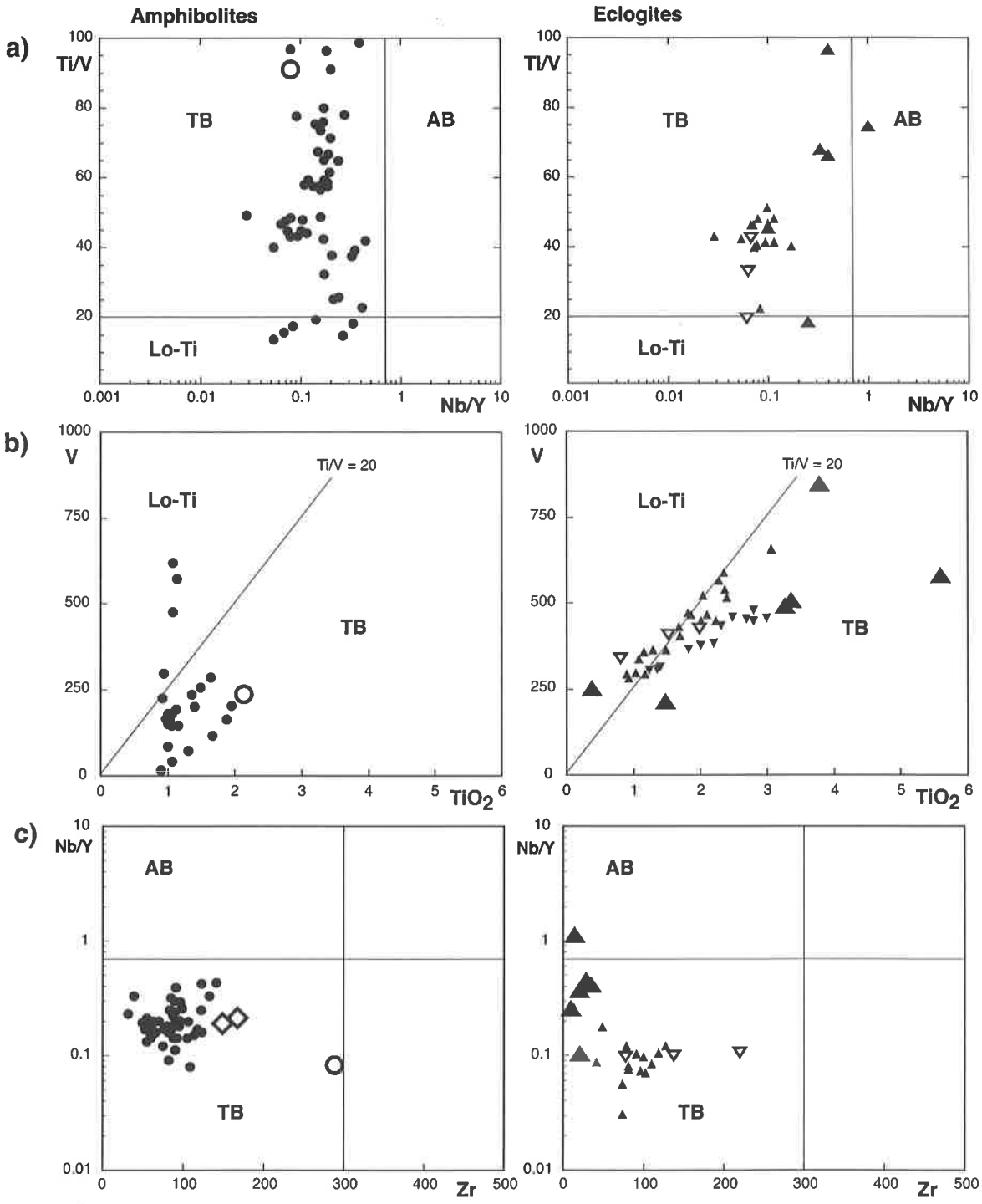

Fig. 2.11
Chemical discrimination of amphibolites and eclogites from Aiguilles Rouges (see text) on the basis of Ti/V-Nb/Y, V-TiO_2, Nb/Y-Zr (Floyd et al., 2000). Dots: Emosson amphibolites (von Raumer et al., 1990), Circle: strongly contaminated amphibolite in metagreywackes (1527, von Raumer et al., 1990); Diamonds: Metasomatically transformed garnet amphibolites at the contact with micaschists (1601, 1604; von Raumer et al., 1990); Small triangles, upside: unpublished eclogite data from massive eclogites (Tête du Bechàt locality, Aiguilles Rouges); Small triangles, downside: eclogite series I (Liégois and Duchesne, 1981); Large triangles: data from banded eclogites, Lac Cornu, Aiguilles Rouges (Coord. FR. 949.810/116.570). Open triangles: Paquette et al. (1989); AB-alkali basalts, TB-tholeiitic basalts, Lo-Ti- Low-titanium tholeiitic basalts . (Data: Annex I, Tab. VI.9)
Discrimination chimique d'amphibolites et eclogites des Aiguilles Rouges (voir texte) basée sur Ti/V-Nb/Y, V-TiO_2, Nb/Y-Zr (Floyd et al., 2000). Points: Amphibolites d 'Emosson (von Raumer et al., 1990), Cercle: Amphibolite fortement contaminée (1527, von Raumer et al., 1990) : losanges: Amphibolites contaminées au contact avec des micaschistes (1601, 1604; von Raumer et al., 1990); Petits triangles, pointe en haut: données non publiées sur les amphibolites de la Pointe de Béchat; Triangles, pointe en bas: eclogites série I (Liégeois and Duchesne, 1981); Grands triangles: nouvelles analyses d'éclogites rubanées, voisinage du Lac Cornu, Aiguilles Rouges (Coord. FR. 949.810/116.570). Triangles ouverts: Paquette et al. (1989); AB – Basalte alcalin; TB – Basalte tholéiitique, Lo-Ti - Basalte tholéiitique pauvre en Ti. (données: Annexe I, Tab. VI.9)

II.2.2 Geochemistry of metabasites

Many metabasic rocks underwent retromorphic reactions, such as recrystallisation of plagioclase into albite and white mica, supposing hydrothermal processes of Late Variscan and/or Alpine age. Consequently, few valid analytical data are available (Annex I, Tab.VI,9).

Von Raumer et al. (1990) classified amphibolites from the Aiguilles Rouges massif, using CIPW normative compositions, AFM values, major (de La Roche et al. 1980; Pearce, 1984) and trace elements diagrams (Pearce 1980; Pearce and Cann, 1976; Pearce and Norry, 1979; Shervais, 1982; Beccaluva, 1983). They distinguished between plagioclase-bearing amphibolites interpreted as former spinel- and olivine-bearing tholeiites (high in Cr and Ni), and garnet amphibolites, interpreted as more evolved quartz hypersthene tholeiites (high in V and P). These differences were ascribed to a magmatic differentiation mechanism.

As for eclogites, Liégois and Duchesne (1981) distinguished between series-I massive eclogites and series-II, banded eclogites, the latter representing a more heterogeneous assemblage. They interpreted the series-I eclogites from the Lac Cornu area as products of fractional cristallisation from continental tholeiites of noritic composition (same as for the amphibolites), and the banded series-II eclogites as of volcano-sedimentary origin. More recently, an assemblage of banded eclogites has been investigated in the neighbourhood of Lac Cornu, and massive-type eclogites have also been discovered at Tête de Béchat (Dobmeier 1997, unpubl.).

As the eclogites and amphibolites are considered to represent an early Palaeozoic magmatic event (von Raumer et al., 2002), it is tempting to compare the data with the large data-base for the Sudetan early Palaeozoic metabasic rock series (Crowley et al., 2000; Floyd et al., 2000). As many of the minor and trace elements were not systematically determined in early geochemical analyses, comparison has to be restricted to TiO_2-, Cr-, Zr- and V concentrations. Using the discrimination diagrams Ti/V vs Nb/Y, V vs TiO_2 and Nb/Y vs Zr (**Fig. 2.11**), most of the Emosson amphibolites are identified as former tholeiites, corresponding to the "main tholeiitic metabasalts series" of Floyd et al. (2000).

Comparing chondrite-normalized REE patterns (**Fig. 2.12**) (Paquette et al., 1989; von Raumer et al., 1990; Morard 1997; new data, annex I, Tab. VI,9) most amphibolites display a relatively flat N-type MORB trend, either with slightly enriched LREE (La_N/Sm_N = 1.0-1.5, mostly garnet-amphibolites) or slightly empoverished LREE (La_N/Sm_N = 0.65-0.8, mostly plagioclase-amphibolites). Plagioclase- and garnet-amphibolites have overall normalised abundances around 10 (Ce/Yb_N = 1.0) and 10-20 (Ce/Yb_N = 1.3), respectively. The contaminated amphibolite (1527), hosted in a metagreywacke, has an overall normalised abundance around 40 (Ce/Yb_N = 0.8), and the reaction rims of amphibolites with micaschists (1601,1604) have overall normalised abundances of 20-30 (Ce/Yb_N = 1.4). For the massive Lac Cornu eclogites (453 Ma; U/Pb zircon upper intercept age; Paquette et al. 1989), these authors published comparable N-MORB type flat patterns (Ce/Yb_N = 0.9), with overall normalised abundances between 10 and 30 (**Fig.2.12**), and a small negative Eu-anomaly (Eu/Eu*= 0.86-0.94). The corresponding high E_{Nd} (O.5 Ga) values of +5.9 to +6.8 (Paquette et al. 1989) plead for formation of Cambro-Ordovician oceanic crust for the metaeclogites. In contrast, the banded meta-eclogites from Lac Cornu (new data, annex I, Tab. VI,9) have very low REE concentrations with overall normalized abundances between 2 - 10 (Ce/Yb_N =.6-3.5) and extreme positive Eu-anomaly (Eu/Eu*= 1.4-3.3), thus confirming the primary difference between the massive and the banded eclogites, suggesting a contrasting origin of these two rock series.

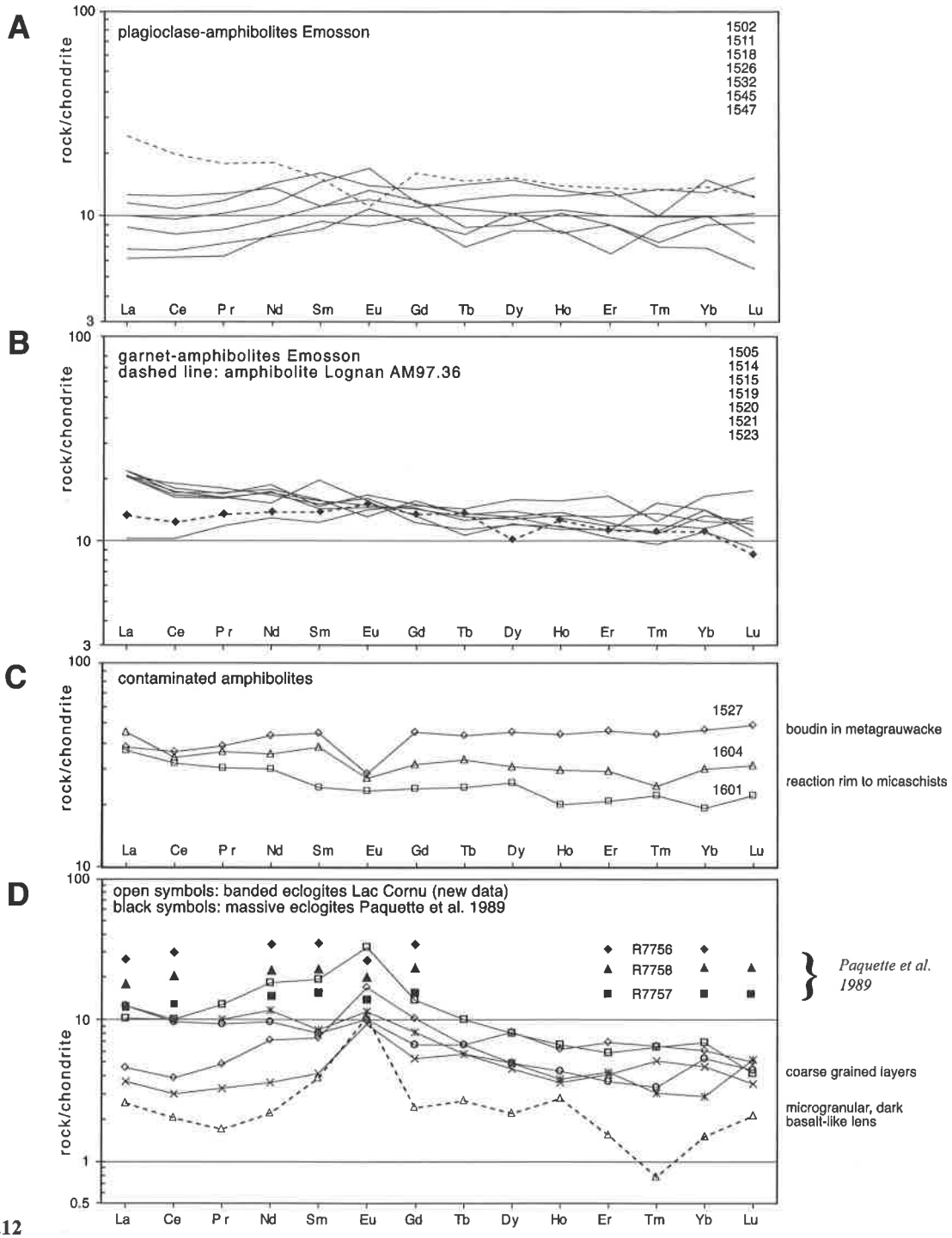

Fig. 2.12
Chondrite-normalized REE compositions of amphibolites and eclogites from the Aiguilles Rouges massif, data from Liégois et Duchesne, 1981; Morard 1997; Paquette et al., 1989; and new La-ICP-MS data, F. Bussy, Uni Lausanne, annex I, Tab. VI,9). **A,B**: plagioclase- and garnet-amphibolites, Emosson, new data, and for comparison: unpublished data from Lognan, Mont Blanc (unpubl. Morard 1997); **C**: contaminated amphibolites (von Raumer et al. 1990): 1527 amphibolite in metagreywackes 1601, 1604: garnet-rich reaction rims with micaschists; **D**: Black symbols without lines: data from massive eclogites, Lac Cornu (Paquette et al., 1989). Open symbols: new data from banded eclogites (Lac Cornu), dashed line (triangles): fine grained, dark eclogite (metabasalt?) among coarse grained eclogitic layers.

Composition en terres rares (normalisées au chondrite) d'amphibolites et éclogites des Aiguilles Rouges, données de Liégeois et Duchesne, 1981; Morard 1997; Paquette et al., 1989; et nouvelles analyses LA-ICP-MS, F. Bussy, Uni Lausanne, annexe I, Tab. VI,9).

***A,B**: amphibolites à plagioclase et grenat, Emosson, nouvelles analyses, et pour comparaison, analyse non publiée de Morard (1997); **C**: amphibolites contaminées (von Raumer et al. 1990): 1527 dans des métagrauwackes; 1601, 1604: riches en grenat au contact aves des micaschistes; **D**: symboles noirs sans lignes:éclogites massives, Lac Cornu (Paquette et al., 1989), symboles ouverts: nouvelles analyses d'éclogites rubanées (Lac Cornu); ligne interrompue: éclogite noire, microgrenue (Basalte?) entre des couches plus grossières.*

Following the comparision with the Sudetan data (Crowley et al., 2000; Floyd et al., 2000), trace element discrimination Zr/Ti – Nb/Y (Floyd and Winchester, 1978) places the metabasic rocks mostly in the field of subalkaline basalts (**Fig. 2.13 a**). Comparing evolution of TiO_2 and Cr with fractionation indicators like FeO*/MgO resp. Zr (Floyd et al., 2000), an elongated field of amphibolites can be distinguished (TiO_2-FeO*/MgO; Cr/Zr; **Fig. 2.13b,c**) which seems to plead for one melting batch undergoing differentiation. The higher TiO_2-values, located outside the cluster, correspond to samples having undergone metasomatic transformations, such as an amphibolite boudin located in a metagreywacke matrix, or the contact zone between amphibolite and micaschists. Among eclogites, two trends become visible in the Zr/Cr-diagram which seem to represent differences in magmatic differentiation. 6 points, located in the field of Zr<100, correspond to a banded complex with lensoid, finegrained eclogite bodies interlayered with coarser grained eclogite bands, the latter seeming to represent a tuffitic banding. Most of the points are situated in the field between 100 and 200 ppm Zr and show an evolution between lower and higher values of Cr. The corresponding rocks comprise the series-I massive eclogites (Liégois and Duchesne 1981) from Lac Cornu and from the Tête du Béchat locality. TiO_2-trends could be the mirror of metasomatic processes during eclogitization. In the TiO_2-FeO*/MgO-diagram, the eclogites follow with some exceptions identical trends as the amphibolites.

Comparison of variable partial melting of lherzolite mantle sources and high-pressure eclogite fractionation in a chondrite-normalized Ce/Yb – Sm diagram, **Fig. 214.a** (Floyd et al, 2000): eclogites and amphibolites seem to represent an homogeneous batch of melt, forming sills an/or dykes and extrusive flows into sediments. Comparing magmatic evolution of amphibolites and eclogites with an array between depleted N-MORB and an enriched OIB plume source (Zr/Y – Ti/Y, **Fig. 2.14 b**), most of the points extend on a line subparallel to the mantle array, but with lower Zr/Y values, and only the strongly contaminated amphibolite 1527 shows the strong influence of sediments. In a Y/Nb – Zr/Nb (**Fig. 2.14c**) projection, the amphibolites plot on a line, which corresponds to the N-MORB range (Floyd et al, 2000), whereas the eclogites occupy a subparallel line, which could correspond to an E-MORB range shown by Floyd et al. (2000). Using the correlation between enrichment factors (La/Sm and Zr/Nb, **Fig. 2.14d**), all amphibolites plot into an area characterized by rather low enrichment factors La/Sm on a Mid Atlantic ridge MORB array.

In the Aiguilles Rouges, the discordant intersection of amphibolites with hosting metasediments supposes intrusion, thus representing a volcanic event. Also the appearance as fine grained amphibolites pleads for originally volcanic rocks, and concentrations of TiO_2 (>0.5%) and V (>100 ppm) exclude a gabbroic origin (Pfeifer et al. 1989). Their original chemical composition pleads for a transitional MORB type, which has been compared by von Raumer et al. (1990) to continental rift magmatism before oceanic opening (e.g. Bellieni et al., 1984; Fodor and Vetter, 1984; Upton et al., 1984).

The age of this continental magmatism is unknown; it could be Cambrian or Ordovician-Silurian, depending on the age of the host metasediments. From a geotectonic point of view, it could correspond to a continental rifting situation (see above), comparable to that experienced by Africa and south America during the Jurassic opening of the Atlantic ocean, with intrusion of tholeiitic plateau basalts. Liégois and Duchesne (1981) interpreted the series-I eclogites from the Lac Cornu area as differentiated products of continental tholeiites, which agrees well with the above interpretation for amphibolites.

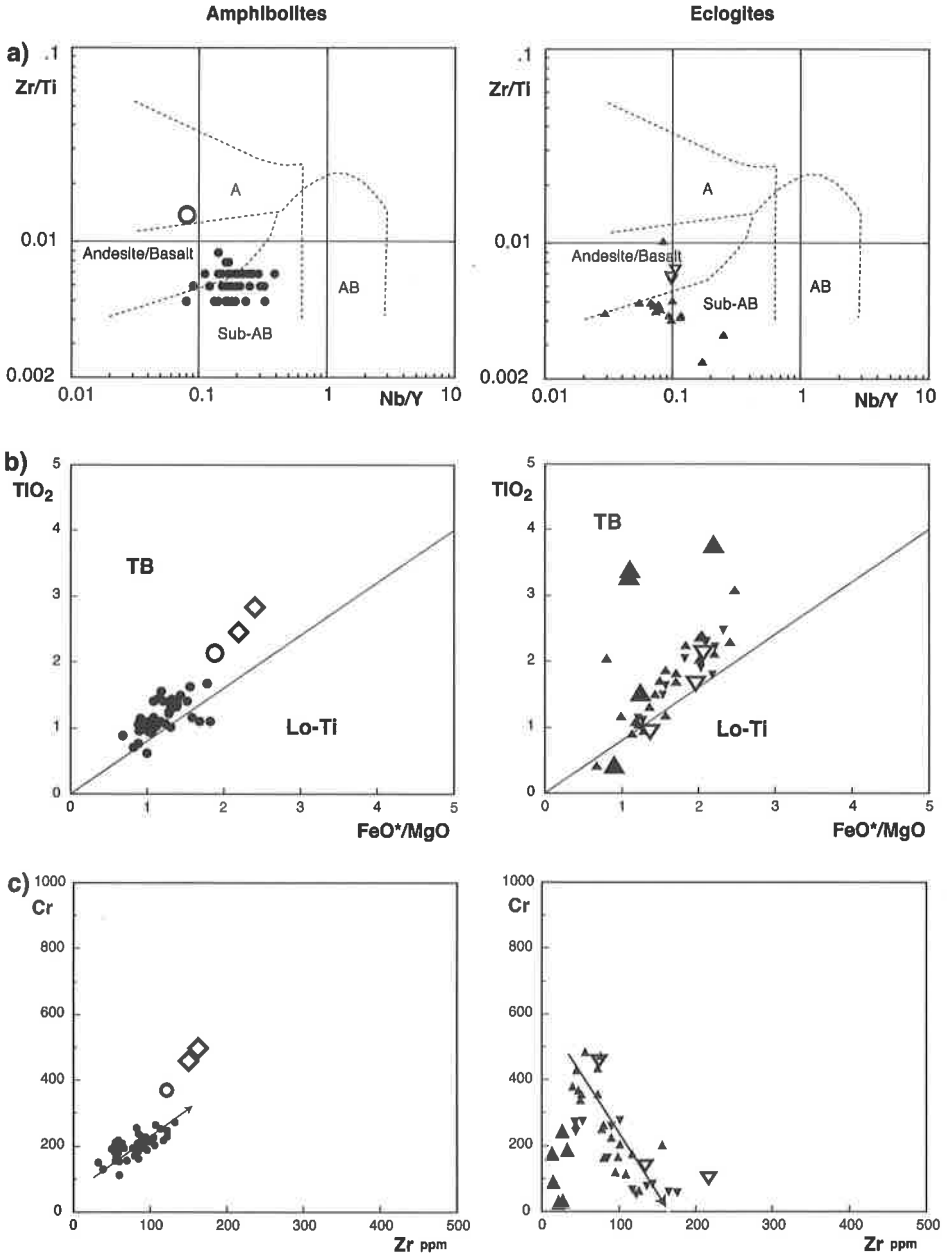

Fig. 2.13
Chemical discrimination of amphibolites and eclogites from Aiguilles Rouges (see text) - symbols as Fig. 2.11
a) Trace element discrimination (Zr/Ti-Nb/Y) and classification after Floyd and Winchester (1978); A- alkaline, AB- alkaline basalts;
b,c) Variation of fractional cristallization in TiO2- FeO*/MgO, Cr-Zr diagrams after Floyd et al. (2000). Lo-Ti: field of Lo-ti tholeiites, TB: field of theoleiitic basalts.

Discrimination chimique d'amphibolites et eclogites des Aiguilles Rouges (voir texte) - symboles: voir Fig. 2.11
***a)** Discrimination sur la base d'éléments traces (Zr/Ti-Nb/Y) et classification d'après Floyd and Winchester (1978);*
A- alcalin, AB- basaltes alcalins;
***b,c)** Variation et cristallisation fractionnée dans les diagrammes TiO2- FeO*/MgO, Cr-Zr après Floyd et al. (2000). Lo-Ti: champ des tholéiites Lo-ti, TB:champ des basaltes tholéiitiques.*

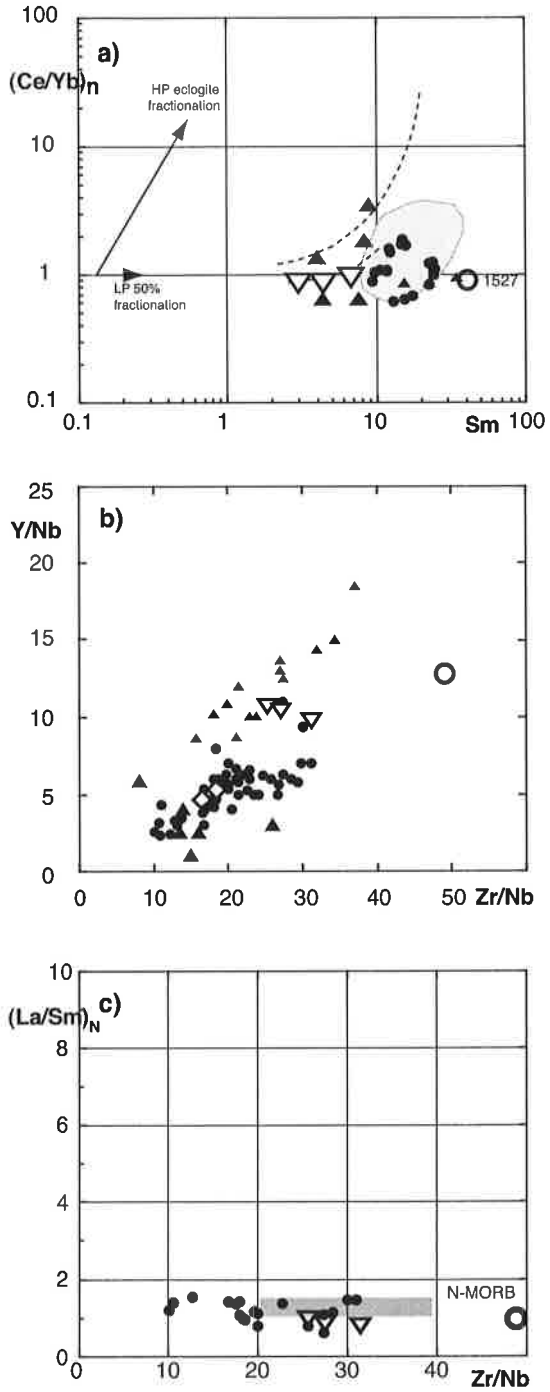

Fig. 2.14
Chemical discrimination of amphibolites and eclogites from Aiguilles Rouges (see text) on the basis of $(Ce/Yb)_N$, Zr/Y-Ti/Y, Y/Nb-Zr/Nb, $(La/Sm)_N$-Zr/Nb (after Floyd et al., 2000, – symbols as Fig. 2.11)
a) Homogeneity of amphibolite/eclogite protoliths concerning mantle source $(Sm)_N$ and pressure of fractionation $(Ce/Yb)_N$, grey area: data from Floyd et al. 2004
b) Comparison of HFSE. Amphibolites envelop a line corresponding to a N-MORB source
c) Correlation between enrichment factors $(La/Sm)_N$ and Zr/Nb ratios. Amphibolites and eclogites plot on a line indicating formation at lower ridge segments (enriched MORB) to deep depleted MORB localities. Grey area: Mid Atlantic ridge S of 60 N (Floyd et al. 2000)

Discrimination chimique d'amphibolites et eclogites des Aiguilles Rouges (voir texte) basée sur $(Ce/Yb)_N$, Zr/Y-Ti/Y, Y/Nb-Zr/Nb, $(La/Sm)_N$-Zr/Nb (Floyd et al., 2000) - symboles: voir Fig. 2.11
***a)** Homogénéité de provenance de source mantellique $(Sm)_N$ des protolithes et de pression de fractionation $(Ce/Yb)_N$, champ gris: données de Floyd et al. 2004.*
***b)** Comparaison d'élements HFS. Les amphibolites se groupent autour d'une ligne correspondant à des sources N-MORB*
***c)** Corrélation entre facteurs d'enrichissement (La/Sm)n et relations Zr/Nb). Amphibolites et eclogites occupent une ligne entre formation sur une ride de basse profondeur (MORB enrichi) et grande profondeur (MORB appauvri). Barre grise:: Ride atlantique au S de 60 N (Floyd et al. 2000)*

Photo 2.19
Northern slope of Lac Noir area, with the Aiguille du Pouce (2474m) in the background. Major ultramafitic body (dark spot, about 20 m diameter) surrounded by migmatitic metagreywackes and K-feldspar-gneisses.
Les pentes nord en-dessous du Lac Noir, en arrière l'Aiguille du Pouce (2474m). Un bloc majeur d'ultramafite (surface grise, diamètre à peu près 20 m) entouré par des métagrauwackes et des gneiss à feldspath potassique migmatisés.

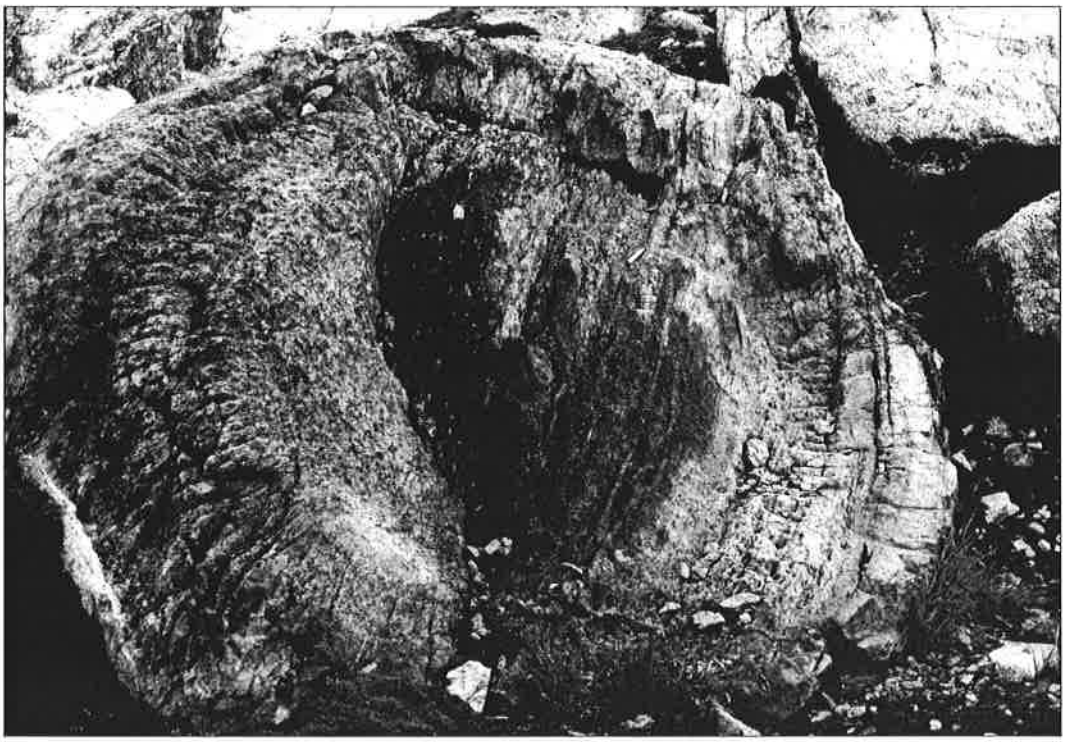

Photo 2.20
Strongly foliated ultramafic lens (interior) with a prominent metasomatic black wall zone, tremolite and talc, 5 m diameter; Lac Cornu area, Aiguilles Rouges (Coord Fr: 949.570/117.640, 2405m).
Roche ultramafique schisteuse (intérieur) entourée par des zones métasomatiques de trémolite-talc. Diamètre 5m, region du Lac Cornu, Aiguilles Rouges. (Coord Fr: 949.570/117.640, 2405m).

II.3 Ultramafic rocks

Necker (1828) observed for the first time the occurrence of ultramafic rocks from the Aiguilles Rouges area (p.8): "... des amas plus ou moins considérables d'une stéatite ollaire, verte, très tendre, ... paraissant passer à une chlorite compacte ou lamellaire, très tenace, et même dure dans les environs du Lac Cornu." Favre (1867) also knew about this occurrence, writing (p. 319): "... une matière voisine de la serpentine, associée à de la chlorite en paillettes brillantes, arrangée en rognons alignés, allongés, joints entre eux par des crins de la même substance, plus ou moins épais et accompagnés de matières stéatiteuses." Joukowsky (1902) has been the last to confirm the presence of such rocks from the Aiguilles Rouges (p.7): "un certain nombre d'amas lenticulaires de roches serpentineuses formant comme une traînée de pointements elliptiques un peu à l'E des roches basiques précédentes (eclogites and amphibolites), dans le voisinage du lac Noir (NE of Lac Cornu)." After that time, the trace of these ultramafic lenses has been lost, although Corbin and Oulianoff (1928) had mapped the amphibolite bodies of that region. Bellière (1958) just mentioned one block of serpentinite from the moraine, notifying a new occurrence of serpentinite (serpentine-talc-chlorite-tremolite rock) near Pointe de Brévent. In the Mont Blanc area, Favre (1867) mentioned for the first time the occurrence of "blocs de serpentine", and Duparc & Mrazec (1893) made a comparable observation in the moraines of glacier du Bois and glacier des Bossons.

Geology and petrography

These historical observations provide already many structural details about the ultramafic lenses found in the Lac Cornu – Lac Noir region (**Photos 2.19, 2.20**). After many years, these occurrences have been re-discovered during our field campaigns (**Fig. 2.15**), due to the disappearance of an important snow cover sitting there during the first (cold) half of the 20th century. Some small serpentinite lenses have been recently observed in the upper Val Bérard region, in the northern prolongation of Lac Cornu (Fracheboud 1996).

The ultramafic rocks, mostly serpentinites, appear as irregular boudin-shaped lenses of 10 cm to 100 m in size, tracing a more than 2 km long synform, which may seem to have formed by disintegration of a relatively rigid peridotite layer embedded in a more ductile felsic material (**Fig. 2.16**). Most of the boudins are found near Lac Cornu and on the northern slope of Lac Noir, and can be followed up in northern direction to the valley of Floriaz, and to the upper Val Bérard. The host lithologies are banded migmatites containing large K-feldspars, reminiscent of migmatites of Ordovician K-feldspar augengneisses (**see Photo 2.05**), biotite-plagioclase migmatites (probably former metagraywackes), and biotite-rich augenschists with garnet and sillimanite (probably former Al-rich sediments). Independent of external structures, the internal structures of the lenses are oblique to the host rocks, which may be interpreted as the breaking down of a major rigid body in a plastic matrix. In some of the ultramafic bodies tension gashes vertical to the external foliation appear, filled with serpentine or talc stretching-fibres. Minor fragments have been rotated in the migmatite matrix indicating dextral strike-slip of the host rock (**Photo 2.21**, coord Fr.: 949.570/117.640). Occasionally metasomatic black walls develop at the contact to the felsic country rocks, forming concentric layers of actinolite-chlorite-talc-carbonate (magnesite) (e.g. **Photo 2.20**).

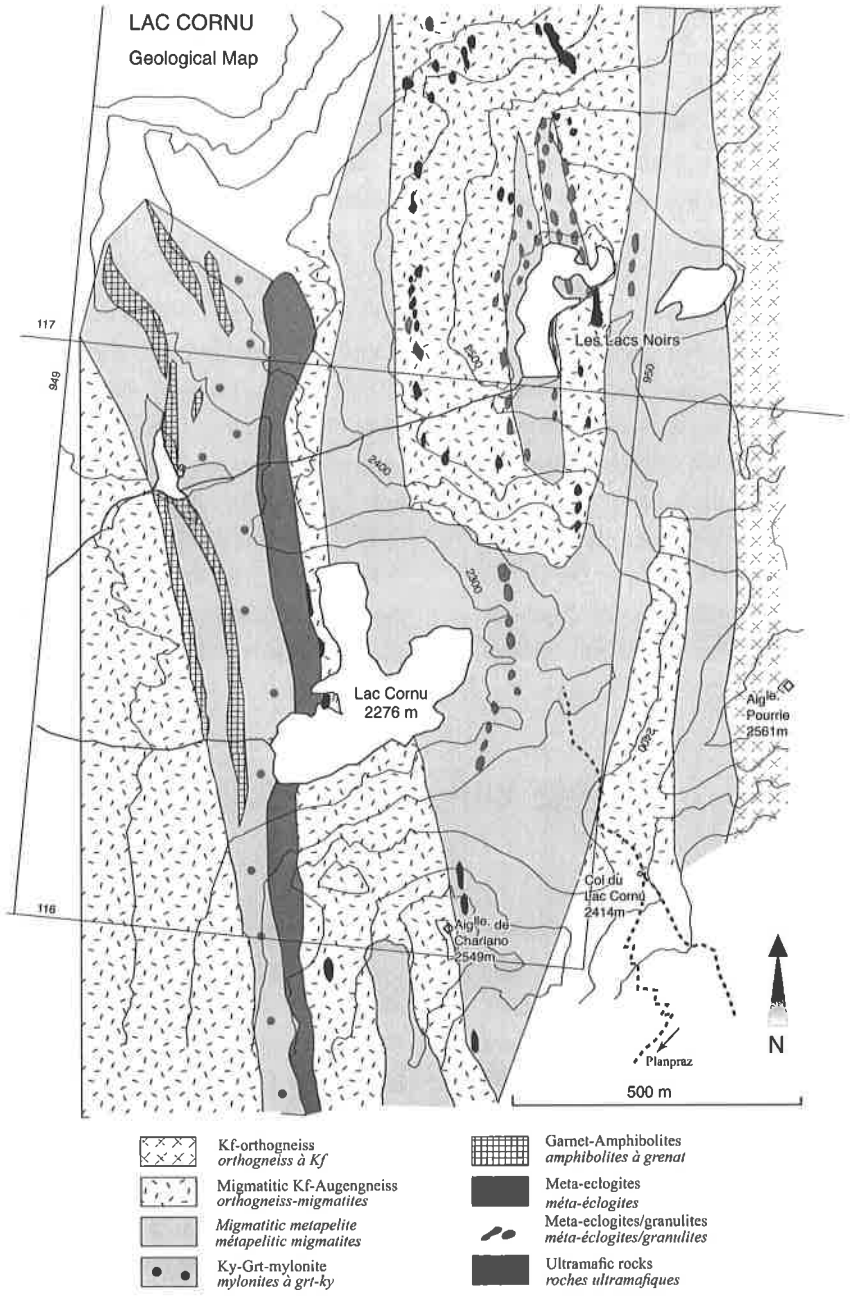

Fig. 2.15
Geological detailed map of the Lac Cornu – Lac Noir area, Aiguilles Rouges. Exaggerated size of ultramafite and meta-eclogite/granulite lenses. *Carte géologique de la région du Lac Cornu – Lac Noir, Aiguilles Rouges. Taille des lentilles d'ultramafite et de méta-éclogite/granulite exagérée.*

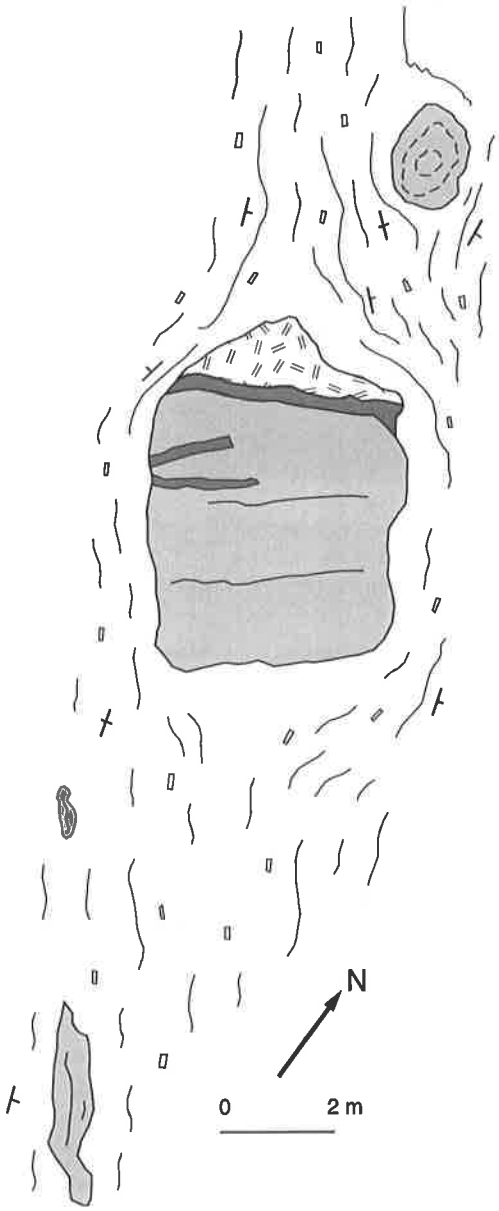

Fig. 2.16
Detailed map of ultramafic lenses surrounded by migmatitic K-feldspar augengneisses with subvertical foliation moulding the different blocks. Large serpentinite block (grey) with talc tension gashes (dark grey) and coarse grained pegmatoids in the pressure shadow.
Détail géologique de blocs d'ultramafite moulés par des gneiss oeillés migmatisés à foliation subverticale. Large bloc (gris) avec des fentes d'extension remplies de talc (gris foncé), et avec des pegmatoïdes dans l'ombre de pression.

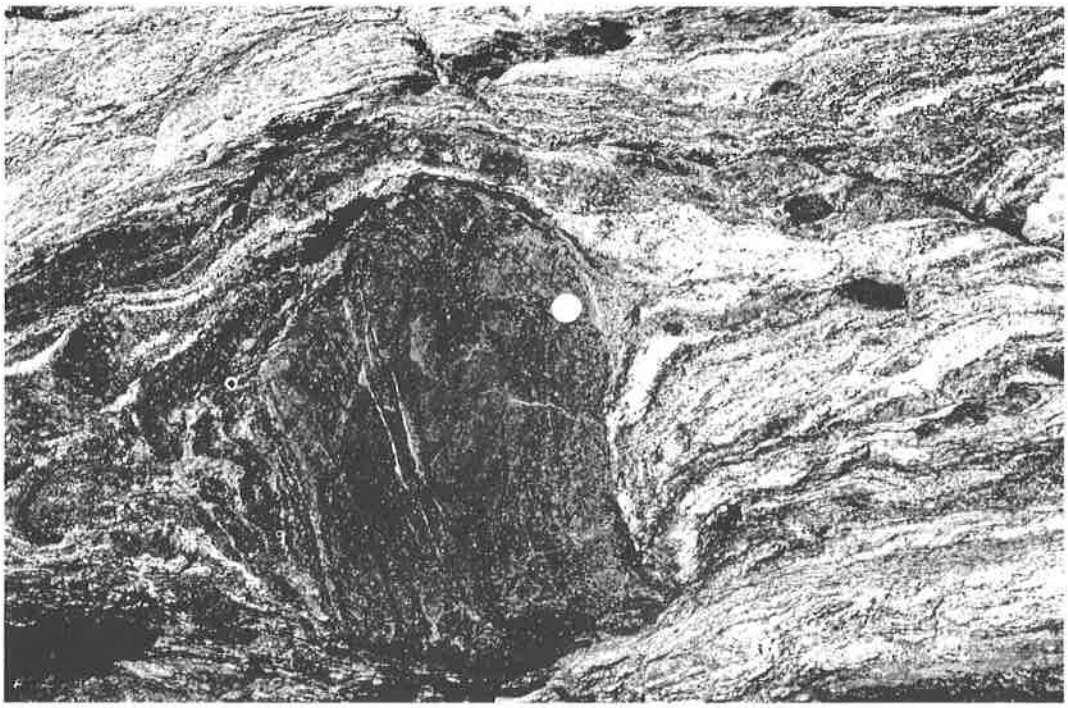

Photo 2.21
Rotated fragment of ultramafic rock embedded in migmatite, scale 1:3; western lake-side of Lac Cornu, Aiguilles Rouges (Coord Fr: 949.450/116.215)
Fragment d'ultramafite ayant subi une rotation, entourée par des migmatites, échelle 1:3; Rivière ouest du Lac Cornu, Aiguilles Rouges.

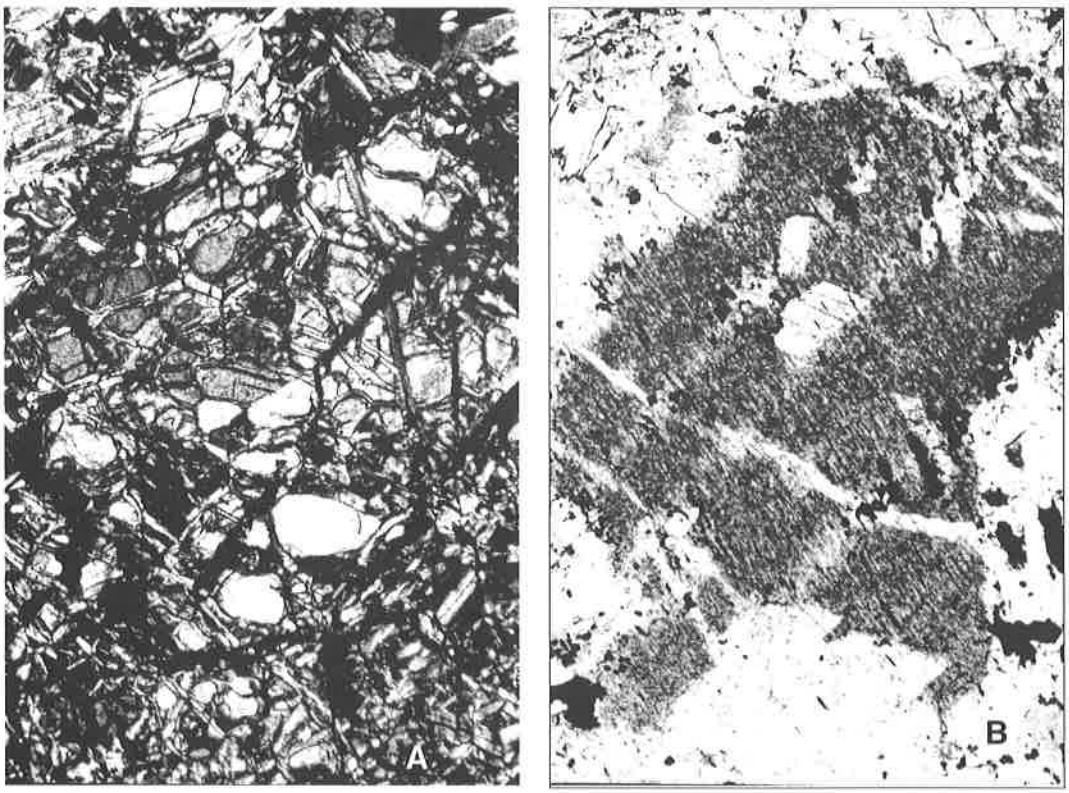

Photo 2.22
Microscopic view of mineral relics in ultramafic rocks (microphotographs from H.R. Pfeifer, Lausanne): A: olivine-relics of 0.2 to 0.5 mm width. B: Pseudomorphs of talc and Ca-amphibole after clinoyroxene (width: approx. 3 mm). *Aspect microscopique de reliques minéralogiques dans les ultramafites (Photos de H.R. Pfeifer, Lausanne): A: reliques d'olivine de 0.2 - 0.5 mm de diametre; B: pseudomorphoses de pyroxène en talc et en amphibole calcique (à peu près 3 mm large).*

The actual mineralogy of the ultramafic rocks is dominated by chlorite and the two serpentine minerals chrysotile and lizardite, indicating a low temperature serpentinization event. In the central part of larger lenses, relics of the former mantle assemblage are preserved: olivine, orthopyroxene, pseudomorphs of talc and Ca-amphibole after clinopyroxene (**Photo 2.22, Table. 2.02, Figs. 2.17, 2.18**; Pfeifer and von Raumer 1996). Modal and bulk-rock analyses reveal two major mantle protoliths (**Fig. 2.17, rock analyses: annex I, Tab. VI.8**): minor, dike-like occurrences of former pyroxenites with SiO_2-contents around 48 wt%, high in CaO, Al_2O_3, TiO_2 and low in H_2O with abundant tremolite, and the more abundant former lherzolites, dominated by serpentine-minerals and relics of mantle minerals, with SiO_2-contents around 39 wt%, considerably lower in CaO and Al_2O_3 and high in H_2O. Only one sample appears to be a former harzburgite and no dunite-relics have been found. The bulk Al_2O_3-MgO and the CaO-MgO-ratios indicate a wide spectra ranging from primitive, undepleted lherzolites to considerably evolved ones, indicating a subcontinental mantle composition (**Fig. 2.18**, Pfeifer and von Raumer 1996).

Two interpretations may be put forward about the age and palaeotectonic situation of these ultramafic rocks. They may have a Late Carboniferous age, if related to the Late Carboniferous gabbros, granites and migmatites of the Fully region (Bussy et al., 2000). More probably, these ultramafic rocks are related to the general subduction and rifting regime of this region during the Cambrian-Early Ordovician (Pfeifer and von Raumer 1996). They subsequently underwent large-scale transformations during the Late Carboniferous strike-slip and anatexis.

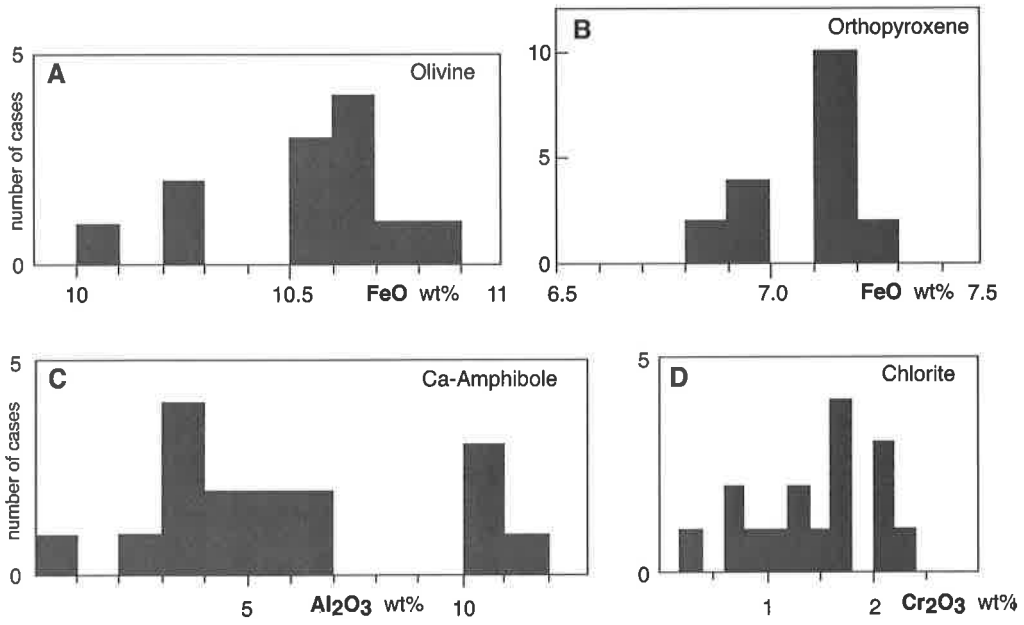

Fig. 2.17:
Fe-, Al- and Cr-variation of various minerals of the ultramafic rocks. A: olivine, B: orthopyroxene, C: Ca-amphibole (Al-tremolite), D: Mg- chlorites. *Variation en Fe, Al et Cr dans les minéraux composant les ultramafites: A: olivine, B: orthopyroxene, C: Ca-amphibole (Al-trémolite), D: Mg- chlorites.*

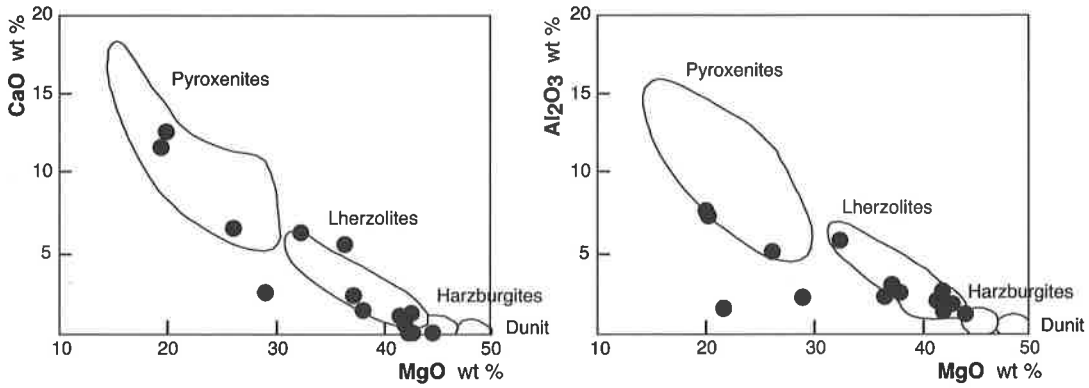

Fig. 2.18:

CaO and Al_2O_3- bulk rock contents of ultramafic rocks from the Lac Cornu area plotted against MgO (recalculated on an anhydrous basis) compared to compositional fields of typical pyroxenites and peridotites based on about 200 analyses (Pfeifer 1990). Apart from one metasomatically changed sample and another one plotting in the field of harzburgites, almost all samples plot within the field of pyroxenites and spinel-lherzolites, indicating a subcontinental, only lightly depleted, mantle protolith.

Compositions globales d'ultramafites du Lac Cornu en CaO et Al_2O_3 comparées aux compositions en MgO (calculées sur une base anhydre) et au champs de composition de pyroxenites et péridotites basés sur 200 analyses (Pfeifer 1990). Mis à part un échantillon changé par métasomatisme et un échantillon situé dans le champ des harzburgites, la plupart des échantillons se trouve dans les champs des pyroxenites et lherzolites, indiquant une provenance mantellique subcontinentale peu apauvrie.

Table 2.02: Mineralogy of the ultramafic rocks. *Minéralogie des roches ultramafiques*

A Typical modal compositions of the two main rock types.
Compositions modales des deux types de roches principales.

Minerals	Oliv	Opx	Cpxpm	Spin	Chl	Serp	Tc	Am
Lherzolites	10	5	10	2	8	45	10	10
Pyroxenites	5	0	20	2	8	10	10	45

Oliv: olivine; Opx: orthopyroxene; Cpxpm: pseudomorphs after clinopyroxene, mainly talc and amphibole; Sp: spinel; chl: chlorite; serp: serpentine; tc: talc; Am: Ca-amphibole

B Mean FeO, Al_2O_3 and Cr_2O_3-contents of the various minerals (based on microprobe analysis by H.R.Pfeifer and F. Bussy). *Moyennes des compositions en FeO, Al_2O_3 et Cr_2O_3 des minéraux principaux (analyses microsonde par H.R. Pfeifer et F. Bussy)*

Olivine:	FeO = 10.6 wt%, Xforst. 0.89
Orthopyroxene:	FeO = 7.2 wt%, Xenst. 0.89
Clinopyroxene:	completely replaced by Fe and Al-rich talc and Ca-amphibole
Spinel:	chromite with 50 wt% Cr_2O_3, 15% Al_2O_3 and 25% FeO
Serpentine:	chrysotile and lizardite, Feo = 4 wt%
Talc:	FeO = 2%, pseudomorph after Cpx: FeO = 6-7 wt%
Ca-amphibole:	Al-tremolite, Al_2O_3 0-10 wt%
Mg-chlorite:	Cr_2O_3: 1.5 wt%

II.4 Rocks of sedimentary origin

Most of the so-called "gneisses" and micaschists, composing the polymetamorphic basement, have a sedimentary origin, where compositional variation can be described in terms of end-members (see **Tab. 2.1**), like quartzites, metagreywackes, metapelites, meta-carbonates (marbles), and metavolcanites (acidic and/or basic). As mentioned in the introduction, most of these former sediments have a Neoproterozoic to Early Palaeozoic age, and are believed to represent detrital platform sediments of the former Gondwana supercontinent. Their high-grade metamorphic transformation, accompanied by several deformation phases, is a consequence of their involvement in the Variscan orogeny. This complication does not facilitate the determination of former sedimentological environments; consequently, interpretation on age and deposition environments of these rocks mainly rely on comparison with better known/preserved areas in Europe on a lithostratigraphic basis.

Lithostratigraphy is a tricky way of investigating highly metamorphosed sedimentary rock units, as recrystallisation might erase original specificities, but it was the only one at hand in the early period of mapping of these areas. Field observation enabled to establish three mappable lithological units of unknown polarity (**Fig. 2.19**), easy to follow over several kilometres: 1) a unit of finely banded metagreywackes (biotite-plagioclase-quartz-gneisses) (**Photo 2.23**) containing some lenses of former carbonates (calc-silicate lenses); 2) a unit of dark brown coloured micaschists (**Photo 2.24**) with two interlayers of amphibolite, inclusions of rather large lensoid bodies of carbonates (calc-silicate marbles), and a locally coarse-grained quartzite unit (**Photo 2.25**); 3) a pile of finely banded interlayers of micaschists and metagreywackes (**Photo 2.27**), easily recognizable through its rusty weathering, probably due to the presence of former pyrite. After the first discovery of scheelite (Frey, 1977), ore exploration field campaigns (Della Valle et al. 1987) revealed that most of the calc-silicate rocks contained traces of scheelite, ascribed to a volcanic component. More massive

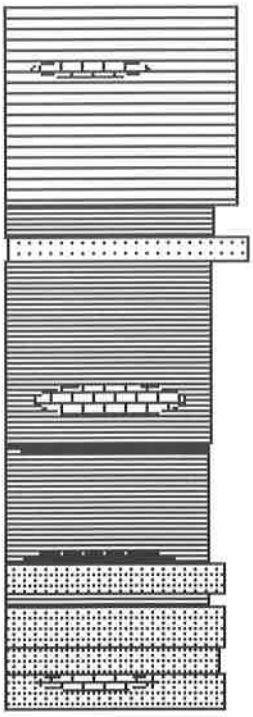

Finely banded, rusty weathering metagreywackes and micaschists with carbonate lenses and graphite nodules
métagrauwackes et métapélites finement rubanés et à patine rouille, contenant des lentilles de carbonates et de nodules de graphite

Garnet-bearing quartzite, *Quartzite à grenat*

Micaschists with intercalations of carbonates and metabasic rocks
micaschistes avec des rubans de carbonates et d'amphibolites

metagreywackes with calc-silicate interlayers
métagrauwackes avec des nodules à calcsilicates

Fig. 2.19
Reconstructed lithostratigraphic column of metasediments from the Emosson area (Aiguilles Rouges), unknown polarity. *Reconstruction d'une colonne lithostratigraphique pour les métasédiments de la region du Lac Emosson (Aiguilles Rouges), polarité inconnue.*

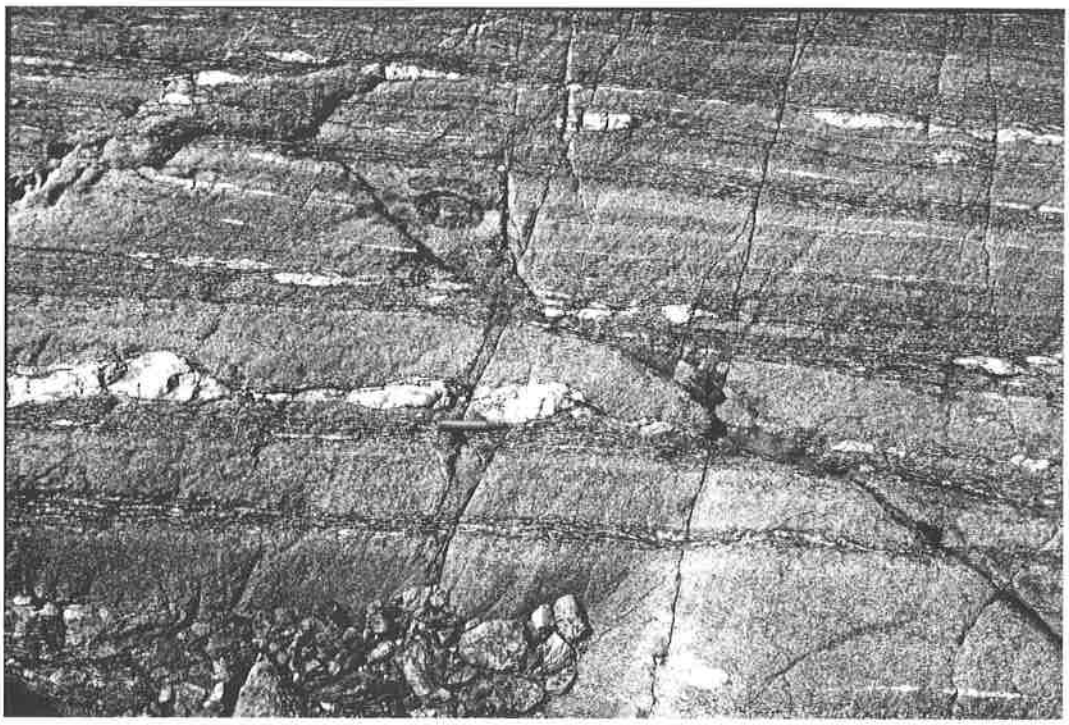

Photo 2.23
Metagreywackes, isoclinally folded, eastern border of Lac Emosson (Aiguilles Rouges) (scale 1:10).
Métagrauwackes répétées par plissement isoclinal. Rivière est du Lac Emosson, (Aiguilles Rouges) (échelle (1.10) (Coord CH: 567.850/103 720; 2000 m).

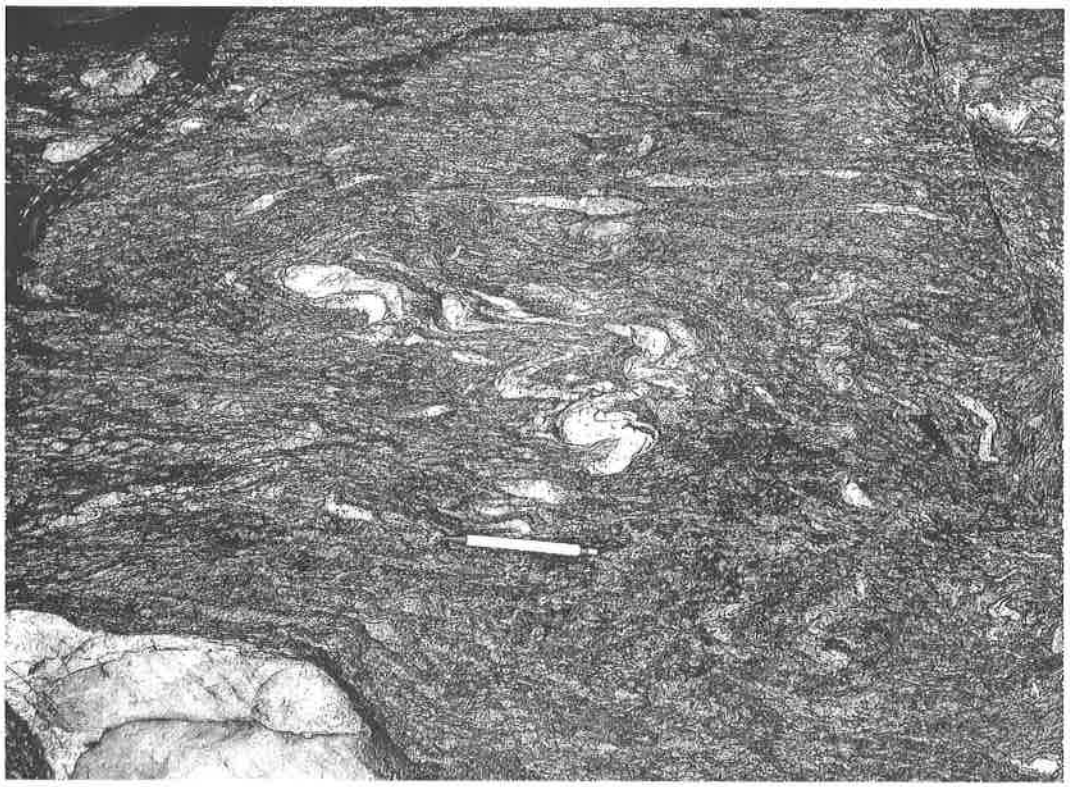

Photo 2.24
Strongly folded micaschists with quartz segregations, showing fold hinges of third generation (pencil 15 cm), Lac Vert area, Aiguilles Rouges.
Micaschistes fortément plissés avec des veines de quartz, indiquant des plis de 3e génération ouverts. Lac Vert, Aiguilles Rouges. (Coord. CH: 557.850//100.100; 2540 m).

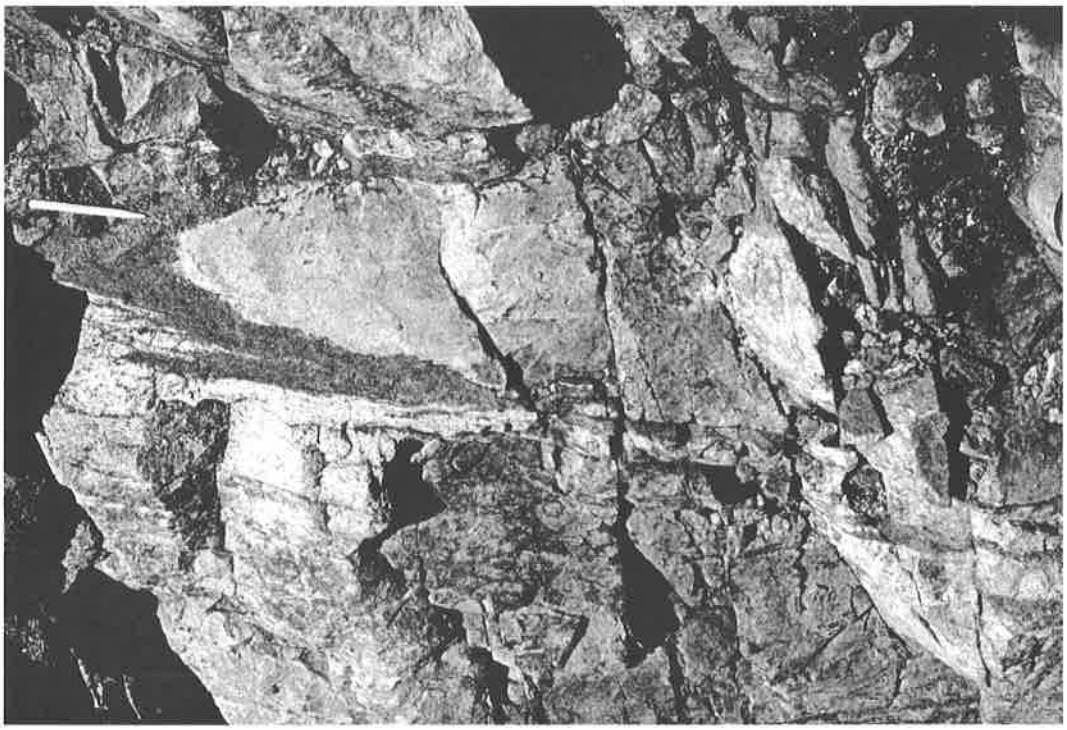

Photo 2,25
Fold hinge of isoclinal quartzite fold, Fontanabran area, Emosson, Aiguilles Rouges (pencil 15 cm).
Pli isoclinal d'un quartzite, environs de Fontanabran, Emosson, Aiguilles Rouges (crayon 15 cm).
(Coord CH: 561.040/104.620; 2520 m).

Photo 2.26
Finely banded interlayers of metagreywacke and turmaline rich bands (pencil 15 cm), Vieux Emosson, Aiguilles Rouges *Métagrauwackes et rubans enrichis en tourmaline (crayon 15 cm), Vieux Emosson, Aiguilles Rouges*. (Coord CH: 558.320/100.250; 2380 m).

deposits of secondary origin are locally found in diopside-scheelite skarns, formed by metasomatic remobilisation of tungsten during Late Variscan metamorphism and anatexis (Chiaradia, 1993). The presence of scheelite in the calc-silicate rocks is a strong argument in favour of a Neoproterozoic-Lower Palaeozoic age for the Aiguilles Rouges metasediments. Indeed, similar scheelite-bearing rocks have been described in Cambrian carbonates from the Appalachian Mountains (Einaudi et al., 1981), as well as in drill-cores from NE-Germany (Ehling 1994, Röllig et al. 1994), well-dated by Archaeocyathidae fossils. This age attribution is further supported by lithostratigraphic similarities among metasedimentary piles across the European Variscides (von Raumer & Chiaradia 1992, von Raumer 1998).

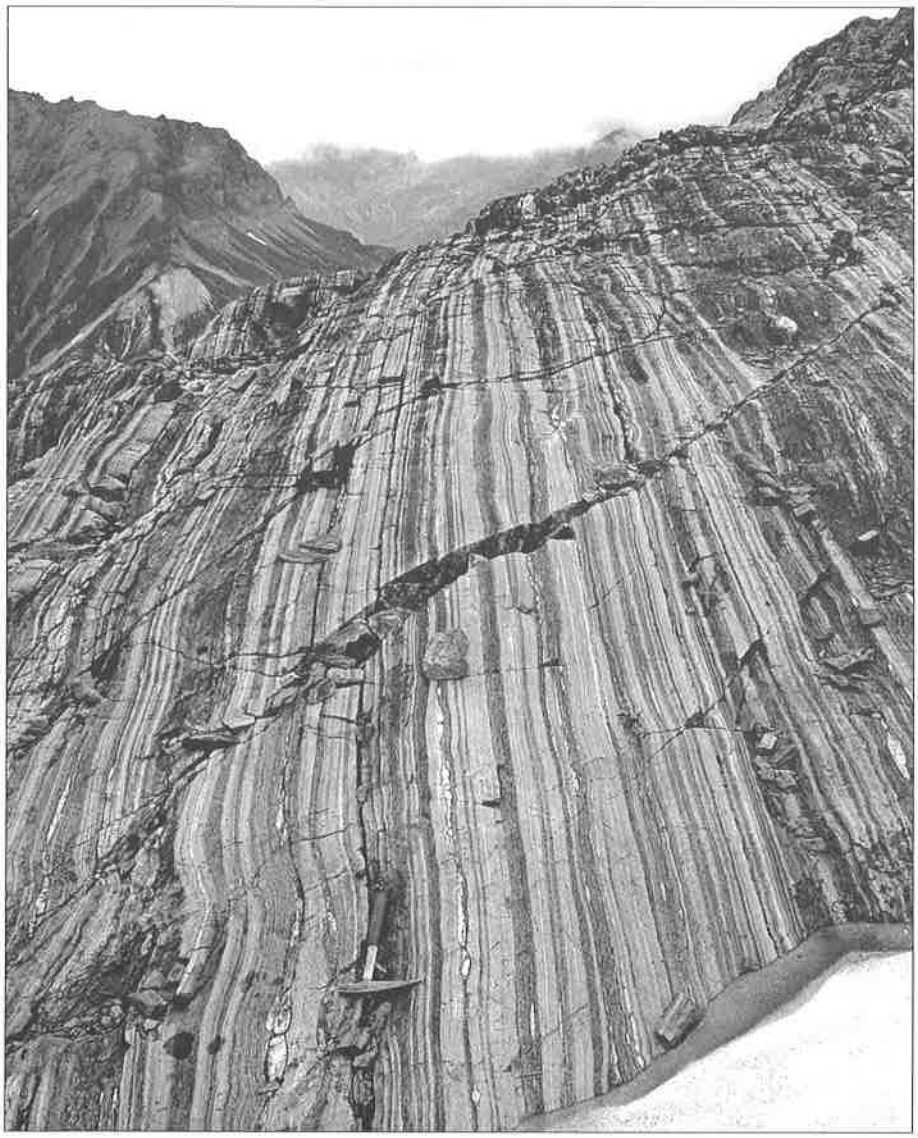

Photo 2.27
Strongly foliated and isoclinally folded banded gneisses (metagreywackes, micaschists and amphibolites), Lac Vert domain, Vieux Emosson, Aiguilles Rouges (hammer as scale) (Coord. CH: 457.480/100.000;2540 m).
Gneis rubanés (métagrauwackes, micaschistes et amphibolites), répétés par plissement isoclinal. Lac Vert, Vieux Emosson, Aiguilles Rouges. (échelle: marteau) (Coord. CH: 457.480/100.000;2540 m).

II.4.1. Petrography of meta-sedimentary rock units

As mentioned above, we will distinguish among quartzites, metagreywackes, micaschists and carbonate rocks, representing the main fields of chemical composition in an ACF-diagram, but all variations between these endmembers may have existed.

Micaschists

Micaschists are essentially composed of biotite with some quartz and plagioclase. Additional phases like kyanite, sillimanite, staurolite, and garnet indicate that amphibolite facies grade has been attained. Fine intercalations of quartz-rich layers and transitions towards metagreywackes are frequent. A large number of mineral parageneses (von Raumer 1983) mirror compositional variation and superposition of distinct mineral assemblages through time, indicating a polyphase metamorphic evolution from higher greenschist to amphibolite facies grade and anatexis. A remarkable type of garnet-bearing micaschist, originally described by Reinhard (in Collet et al. 1952), is characterized by large plagioclase porphyroblasts (up to 10 cm in length, **Photo 2.28**), which gives the rock an unusual patchy structure.

Metagraywackes and quartzites

In contrast to micaschists, metagreywackes are mainly composed of variable amounts of biotite, plagioclase and quartz. Higher contents in biotite are found in compositions transitional to micaschists, and higher quartz contents indicate compositions transitional to quartzites. Few additional minerals like kyanite and/or garnet may occur. A rhythmic layering of pyrite-tourmaline is locally observed in metagreywackes (**Photo 2.26**), which may indicate submarine exhalative activity, as postulated in the Salanfe area (Chiaradia 1993a,b).

Quartzites constitute the quartz-rich endmember, where biotite, plagioclase, garnet, and kyanite may appear as minor phases, representing former argillaceous components among the quartz grains.

Carbonates

Most of the carbonates are represented as calcite with some additional phases like diopside, garnet and amphibole. They appear as lensoid bodies (**Photo 2.29**), boudins among the micaschists, or as fine, extremely thinned layers in the neighbourhood of mylonite zones. An omnipresent accessory mineral is scheelite.

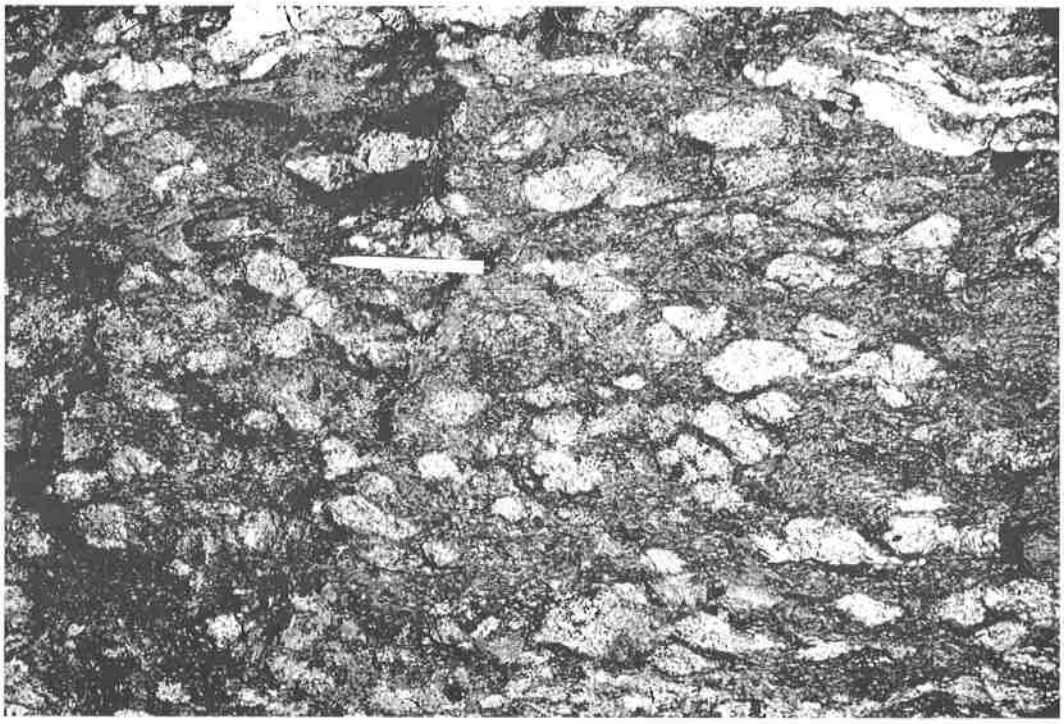

Photo 2.28
Plagioclase porphyroblasts in micaschist, Vieux Emosson area, Aiguilles Rouges (pencil 15 cm).
Porphyroblastes de plagioclase dans micaschiste, Vieux Emosson, Aiguilles Rouges)
(Coord. CH: 558.460/100.060; 2320 m).

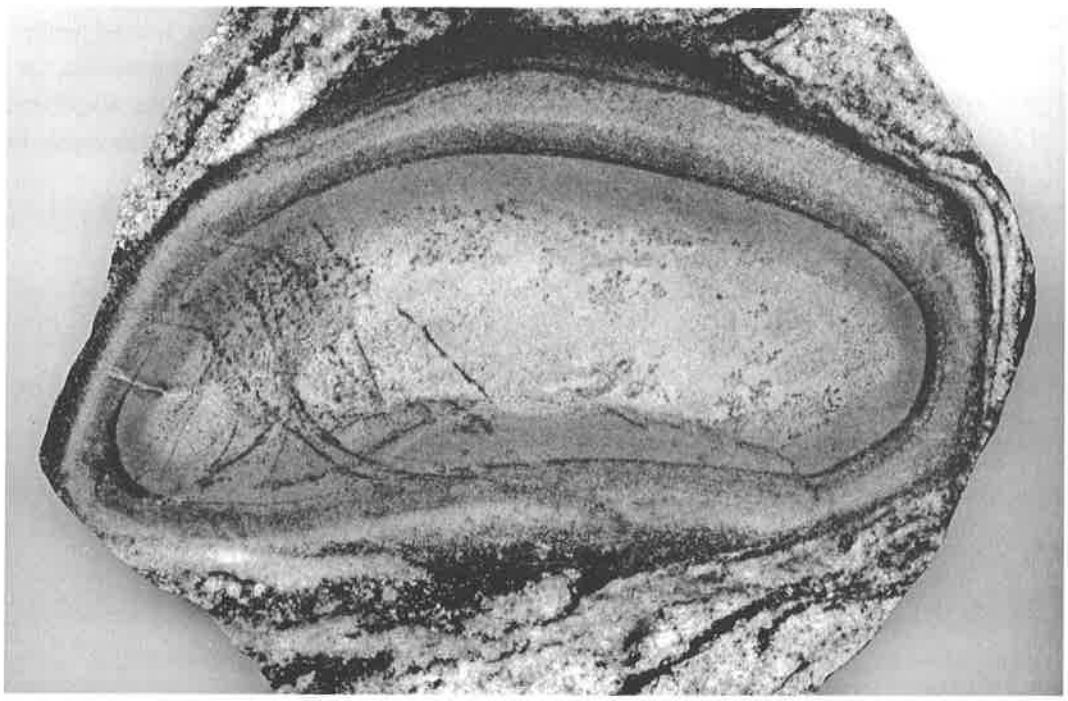

Photo 2.29
Calcsilicate boudin in migmatite, with reaction rims. Boulder from Estelette glacier, Val Veny, Mont Blanc area (horizontal size: 17cm)
Boudin de roche calcsilicatée avec zone réactionelle, entouré par des migmatites. Bloc de la moraine du glacier d'Estelette, Val Veny, massif du Mont Blanc (largeur horizontale 17 cm).

II.4.2. Chemical composition of metasedimentary rocks

Chemical analyses of the Aiguilles Rouges metasediments confirm field observations when plotted in the Wimmenauer (1984) classification diagram (**Fig. 2.20**). Dominant lithologies are quartzites (sandy greywackes), greywackes/arkoses and the groups of argillaceous greywackes to pelites, representing the Al-rich sediments. In the TiO_2-Ni diagram of Floyd et al. (1989), we observe (**Fig. 2.21**) rising Ni- and Ti-values from quartzites to greywackes and to micaschists, which supposedly indicate increasingly basic magmatic sources. Micaschists are locally high in Ni (Fracheboud, 1997), which might be due to higher maturity of the former sediments (Floyd et al. 1989), to the presence of an ultrabasic detrital component (known in that region) or to submarine alteration of metabasic bodies. A higher maturity of micaschists with respect to metagreywackes is also demonstrated in a Sr-Ba diagram (**Fig. 2.22**) (Mingram 1996).

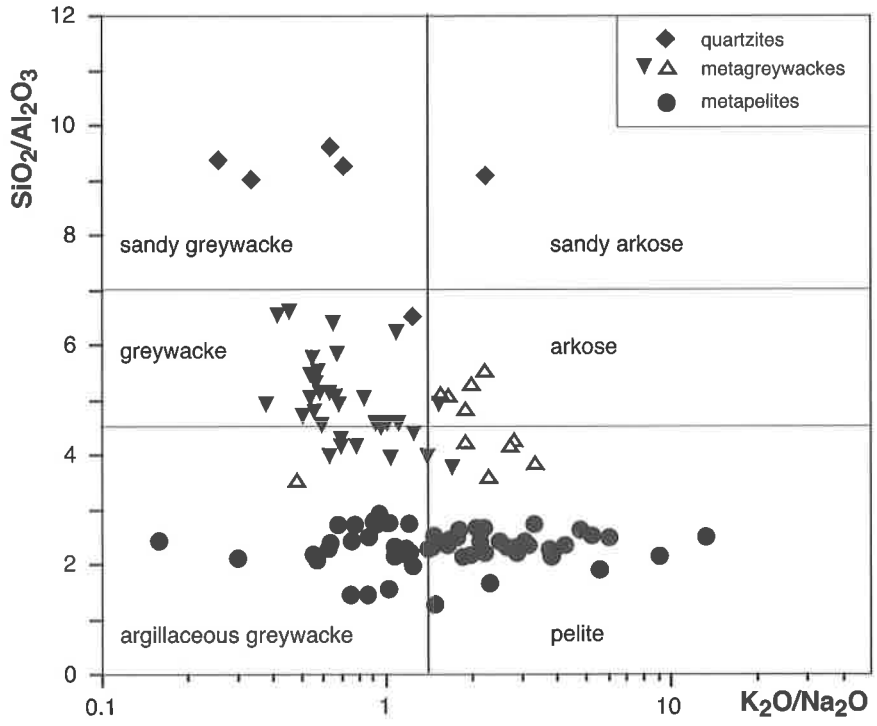

Fig. 2.20
Classification of detrital metasediments (Aiguilles Rouges area) after Wimmenauer (1984).
Classification des métasédiments détritiques (Aiguilles Rouges) d'après Wimmenauer (1984).

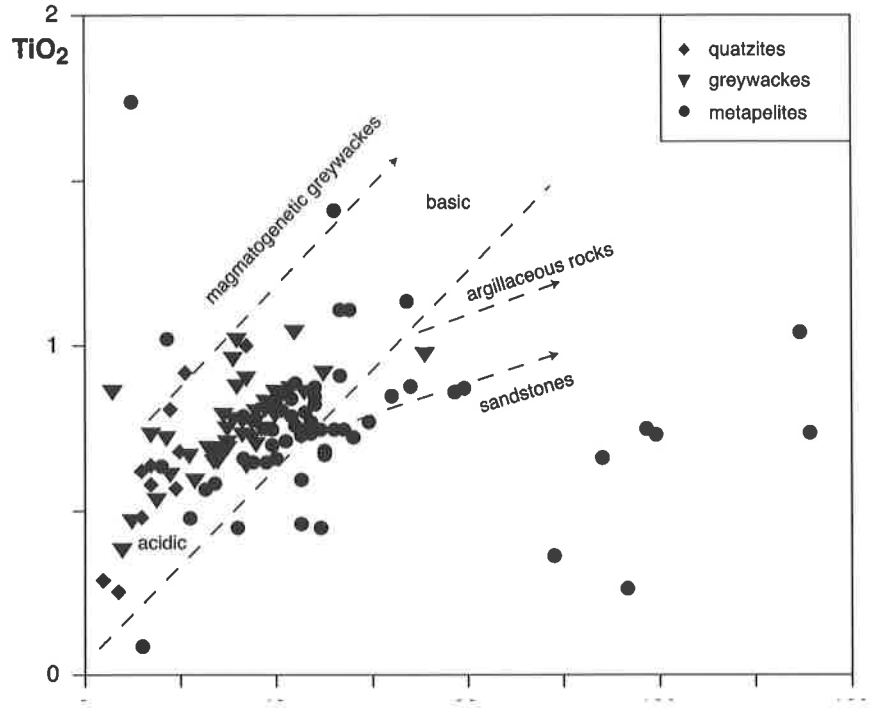

Fig. 2.21
Chemical classification of detrital metasediments (Aiguilles Rouges area) after Floyd et al. (1989).
Classification chimique des métasédiments détritiques (Aiguilles Rouges) d'après Floyd et al. (1989).

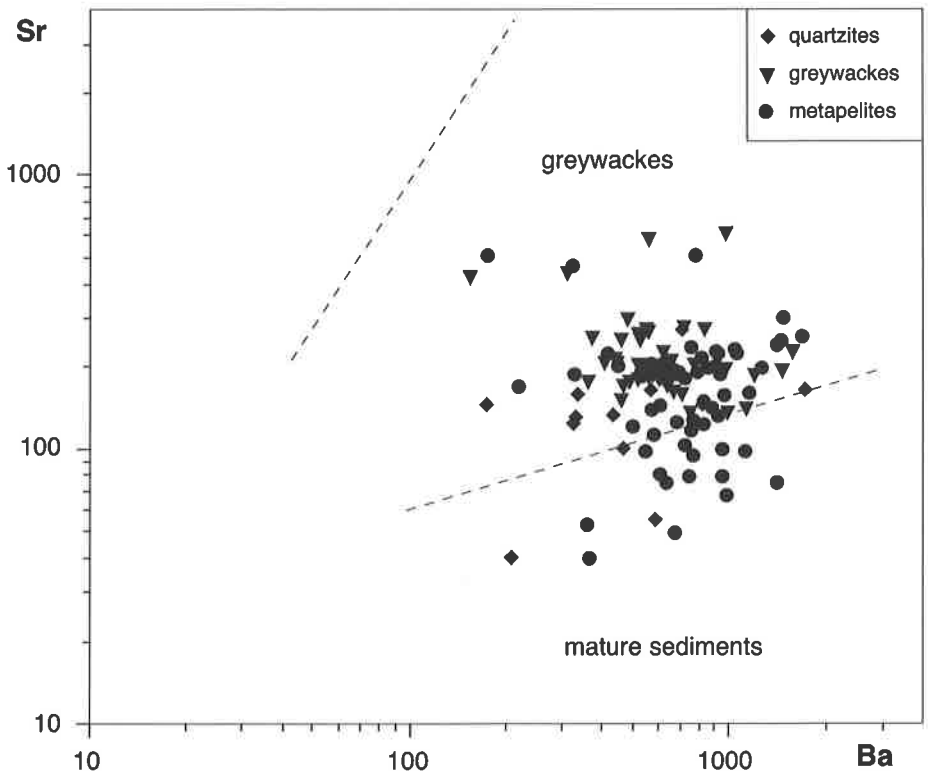

Fig. 2.22
Chemical classification of detrital metasediments (Aiguilles Rouges area) after Floyd et al. (1989).
Classification chimique des métasédiments détritiques (Aiguilles Rouges) après Floyd et al. (1989).

In a diagram reporting the alteration index (CIW, Harnois 1988) versus K_2O/Na_2O (**Fig. 2.23**) (Mingram, 1996), all metagreywackes and quartzites from the Emosson region are characterized by a moderate alteration index (CIW 70-85) and low K_2O/Na_2O values (< 3), coinciding with the values observed by Mingram (1996) for comparable rock units. Among the metapelites, a subgroup coincides more or less with the field occupied by the metagreywackes, and a second subgroup occupies a field characterized by CIW-values > 85 and K_2O/Na_2O values between 2-25. To be noted is an irregular enrichment in K_2O of the metagreywackes colleted at the Salanfe mining site (Chiaradia 1993) (not shown in figure **2.23**). This feature is ascribed to a strong hydrothermal alteration of plagioclase into white mica and calcite.

Chemical analyses of Emosson metasediments reported in diagrams discriminating geotectonic environments yield contradictory results. In the SiO_2-K_2O/Na_2O diagram of Roser & Korsch (1986) (**Fig. 2.24**), most points plot in fields of active continental margin or oceanic island arc settings. In **Fig. 2.25** (Fe_2O_3tot + MgO) versus TiO_2 or Al_2O_3/SiO_2 (Bhatia and Crook, 1986), metagreywackes predominantly plot in the continental island arc field, whereas quartzitic rocks lie in the field of a passive continental margin setting.

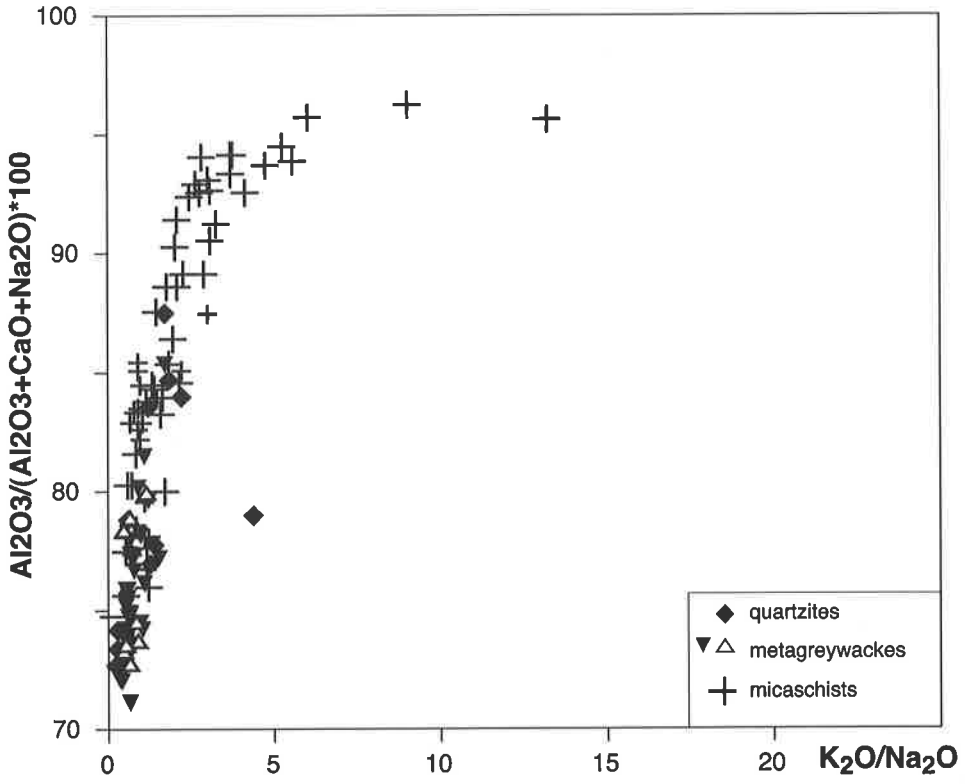

Fig. 2.23
Differentiation of detrital metasediments (Aiguilles Rouges area) after their alteration index CIW (Harnois, 1988). *Différenciation des métasédiments détritiques (Aiguilles Rouges) d'après leur indice d'altération CIW(Harnois, 1988).* **A**:

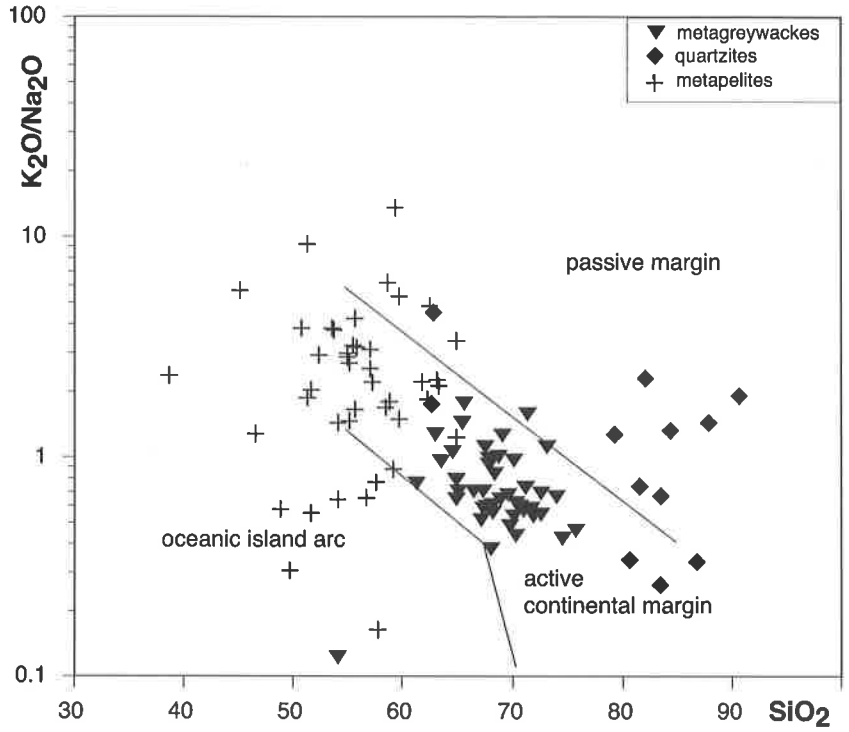

Fig. 2.24
Discrimination of detrital metasediments (Aiguilles Rouges area) after their source areas (Roser and Korsch, 1986) *Différenciation des métasédiments détritiques (Aiguilles Rouges) d'après leur région d'origine (Roser et Korsch, 1986)*

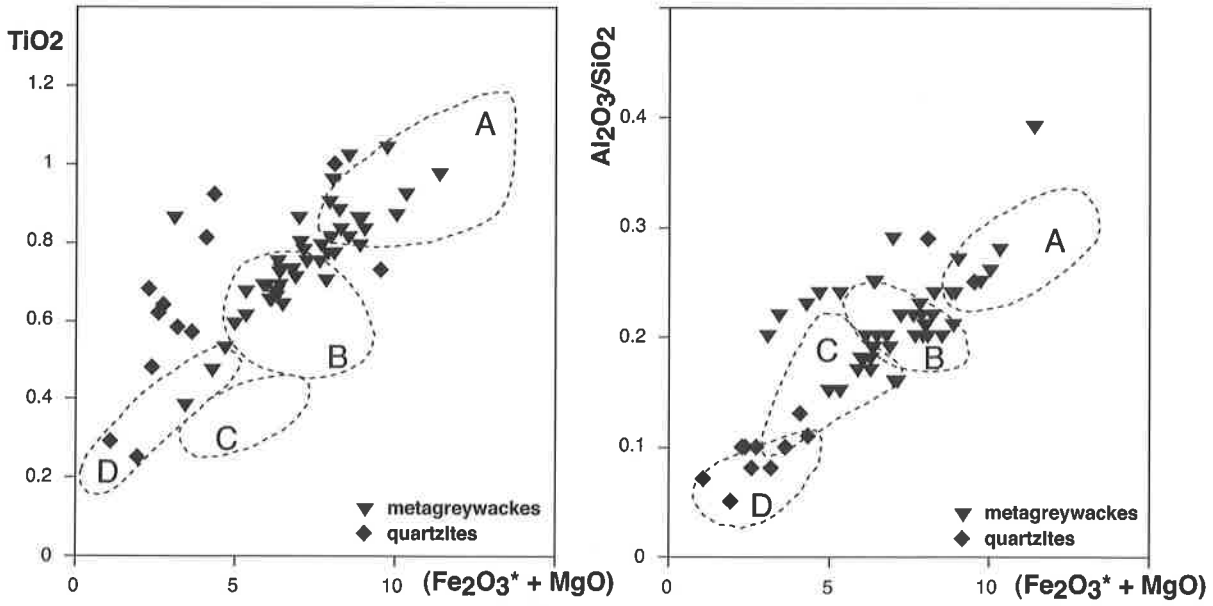

Fig. 2.25
Discrimination of sandy metasediments (Aiguilles Rouges area) after the geotectonic situation of their source areas (Bhatia and Crook, 1986). A: Oceanic island arc; B: Continental island arc; C: active continental margin; D: passive margin.
Discrimination des métasédiments gréseus (Aiguilles Rouges) d'après la situation tectonique de leur région d'origine (Bhatia et Crook, 1986). A: arc volcanique océanique; B: arc volcanique continental; C: marge continentale active; D: marge passive.

Chapter III.
Metamorphism and Deformation

III.I Metamorphism of the polymetamorphic basement

The basement areas appearing in the Aiguilles Rouges–Mont Blanc massifs represent an assemblage of lithological units with contrasting metamorphic histories including, besides Alpine metamorphism, non-, mono- and polymetamorphic units. Such associations might represent former basement-cover relationships (e.g. Late Carboniferous cover) or the tectonic juxtaposition of slices (e.g.SW part of Aiguilles Rouges, Dobmeier 1996), which experienced different metamorphic paths. Among the polymetamorphic units (older than the Upper Carboniferous sedimentary cover), most contain predominantly amphibolite grade mineral assemblages, but locally appear relicts of granulite or eclogite facies grade. Although successive parageneses are observed, a clear attribution to specific orogenic events is difficult. For convenience, Alpine mineral parageneses will be distinguished from late Variscan and earlier relict assemblages, re-evaluated by von Raumer et al. (1999).

III.1.1 Alpine mineral assemblages

In the Aiguilles Rouges area, pumpellyite, prehnite and laumontite are found in weakly retrograded amphibolites; and stilpnomelane is observed in the matrix of nearly undeformed Late Carboniferous rhyolites (Coord CH: 563.575/108.660). Orthogneisses yield chlorite-albite mineral assemblages, and quartz shows the first stages of low angle boundary crystallisation (polygonisation) and undulation (von Raumer 1974, 1984). Near the overlaying Mesozoic sediments of the Morcles nappe, small-scale folds with a nearly horizontal axial plane (**Photo 2.10**) appear in the pre-Variscan orthogneisses. Characteristic healed fracture patterns appear in specific lithologies (**Photo 3.01, 3.02**), and Alpine foliation is expressed in detrital rocks of Late Carboniferous age (Triège, **Photo 3.03**) by tiny white mica leaflets grown in the pressure shadows of detrital quartz grains, the latter transformed by contemporaneous pressure solution. In the Mont Blanc area, K-feldspar crystals from pre-Variscan orthogneisses are strongly stretched, and their fractures are healed by albite-quartz fibres (**Photo 2.09**). In the Mont Blanc granite, a penetrative foliation developed (leading to the name of "protogine" of early authors, Jurine 1806; **Photo 2.01, 4.09**). The mineral paragenesis [green biotite–chlorite–epidote-albite] indicates lower greenschist facies conditions (von Raumer 1967, 1971). Stilpnomelane is omnipresent (von Raumer 1969), and is observed as detrital crystals in the "Molasse grise" (Aquitanian, Lower Freshwater Molasse) near Lausanne (von Raumer, 1971). Neoformation of chlorite, garnet and/or epidote is observed along joint surfaces and slicken sides in the granite. Poty et al. (1974) determined conditions of 400°C and 0.25 Gpa from fluid inclusions in quartz from tension gashes.

Photo 3.01
Fiber-growth of quartz in Alpine tension gash in lower palaeozoic metasediments, Lac Noir area, Aiguilles Rouges (Coord FR: 949.980/117.150; vertical scale : 10 cm). Original at the Musée Cantonal de Lausanne.
Croissance de quartz en fissure alpine dans des métasédiments paléozoïques, région Lac Noir, Aiguilles Rouges (Coord. FR: 949.980/117.150 ; échelle verticale: 10 cm). Original au musée cantonal de Lausanne.

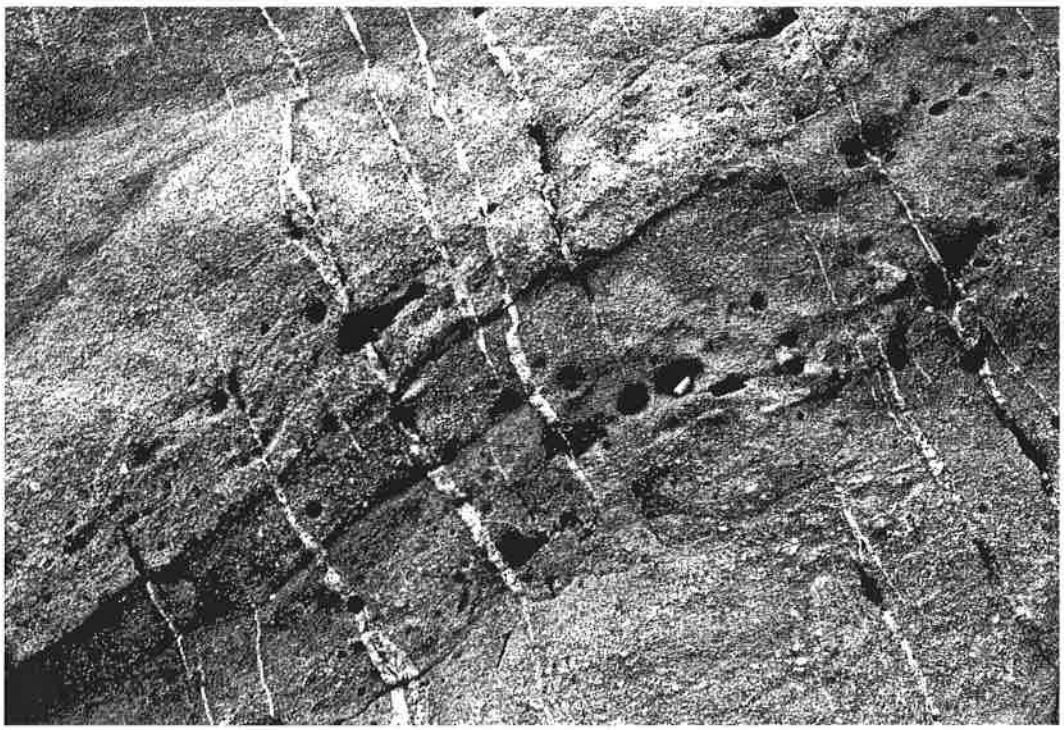

Photo 3.02
Quartz-bearing tension gashes of Alpine age in Triassic sandstones, Col de la Terrasse, Aiguilles Rouges (Coord CH: 557.500/99.125).
Fissures alpines remplies de quartz dans les grés d'âge triasique, Col de la Terrasse, Aiguilles Rouges (Coord CH: 557.500/99.125).

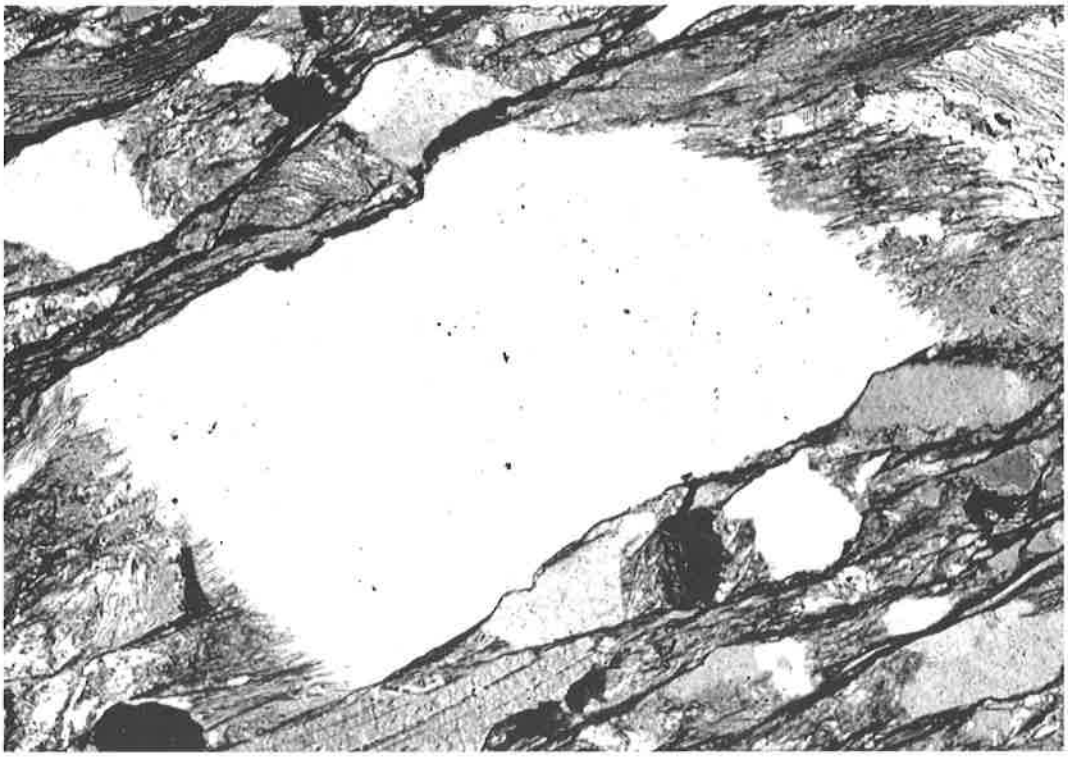

Photo 3.03
Alpine very low grade metamorphic overprint of Alpine age in metagreywacke of late Carboniferous age at Triège, Aiguilles Rouges massif (Coord CH: 565.960/105.925). A rhomb shaped quartz grain (white, 1 mm size) reduced by surfaces (NW and SE) of pressure solution, representing the main foliation, whereas the SW and NE surfaces show a very fine intergrowth of newly formed white mica flakes with quartz in the pressure shadow. Oblique polarisers.
Grain de quartz détritique polygonal (blanc, 1mm de large) dans un grauwacke d'âge carbonifère, Triège, Aiguilles Rouges (Coord CH: 565.960/105.925). La schistosité alpine est marquée par des surfaces de dissolution sous pression d'orientation NE-SW, remodelant le grain de quartz originellement rond, et les surfaces SW et NE, dans l'ombre de pression, sont marquées par l'intercroissance de fines feuilles de mica blanc parallèles à la schistosité avec du quartz. Nicols croisés.

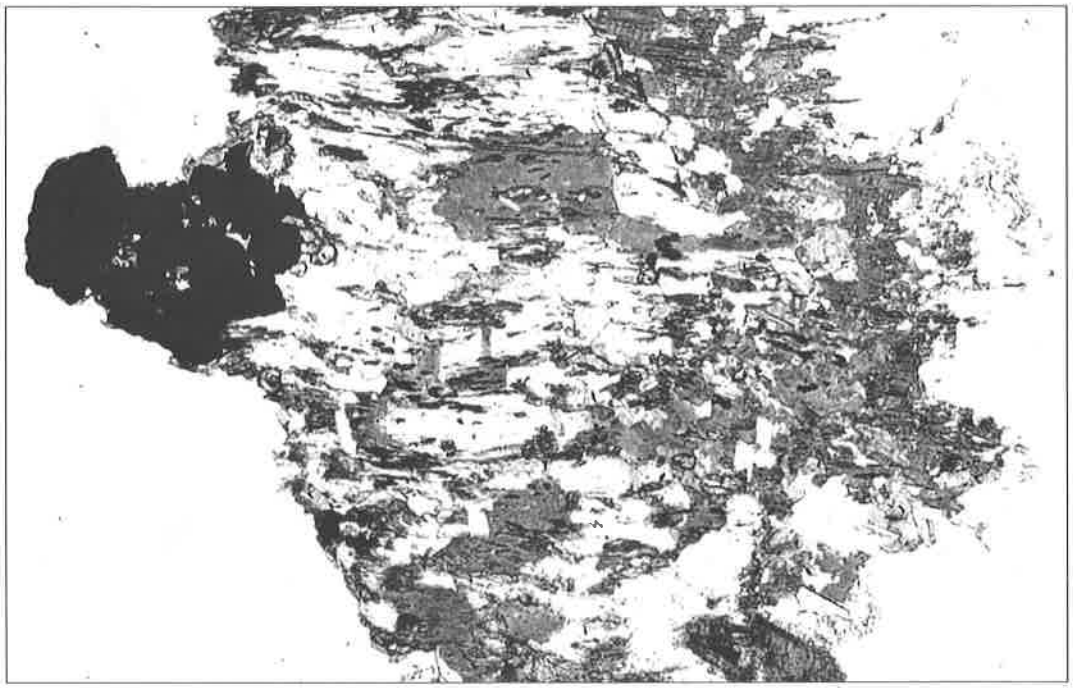

Photo 3.04
Microscopic picture of a former biotite flake (0,5 mm large) from the Mont Blanc granite (Coord CH.: 573.690/96.230). The primary grain has been replaced by Alpine minerals: opaque – ilmenite; white and gray – new growth of green biotite, gray flakes – view on the cleavage plane; tiny, gray elongated grains elongated E-W- sphene crystals parallel to the former clivage plane of magmatic biotite. *Vue microscopique d'une biotite (largeur 0.5 mm) du granite du Mont Blanc (Coord CH.: 573.690/ 96.230), remplacée par des minéraux d'âge alpin. Opaque: ilmenite; Gris et blanc: biotite verte alpine néoformée, formation de sphène suivant le clivage de la biotite originelle (grains gris allongés E-W).*

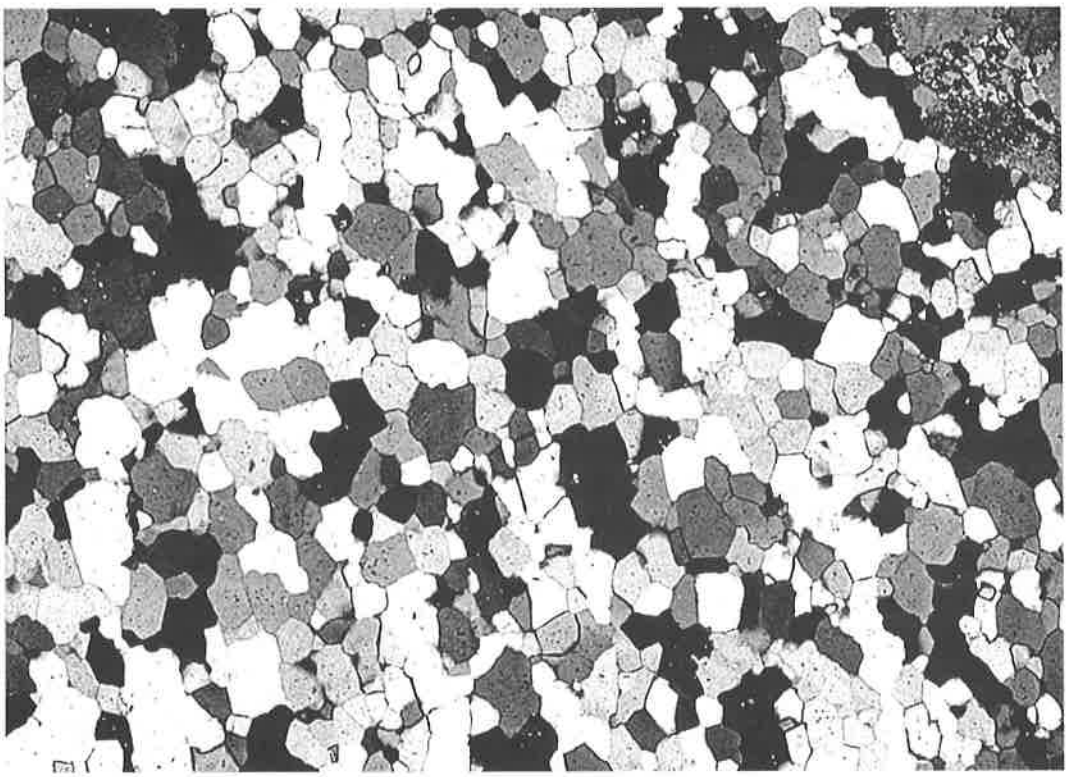

Photo 3.05
Alpine, polygonal recrystallisation of magmatic quartz in the Mont Blanc granite (compare **Fig. 3.18**) – picture 2.75 mm large (Coord CH.: 567.455/95.695) *Recristallisation alpine polygonale de quartz magmatique dans le granite du Mont Blanc- largeur de photo 2.75 mm.*

Photo 3.06
Alpine stilpnomelane grown in K-feldspar of the Mont Blanc granite – picture size 1mm
(Coord CH.: 573.795/96.565).
Stilpnomélane alpin dans feldspath potassique, granite du Mont Blanc, largeur de la photo 1 mm.

The 303 Ma-old Mont Blanc granite is a good recorder of the Alpine greenschist facies overprint, where each group of original magmatic constituents is characterized by specific, newly formed minerals (von Raumer 1967, 1984). The original dark brown biotite is replaced either by chlorite or by a mosaic of small, oriented flakes of green biotite, and the former cleavage planes of the host are underlined by concentrations of tiny sphene crystals (**Photo 3.04**). Biotite flakes and sphene are overgrown by newly formed clinozoisite-epidote, preserving the alignment of sphene crystals. Chlorite either replaces biotite or appears at interstices of former constituents. The large K-feldspar phenocrysts are replaced locally by patch-perthite and chess-board albite, and the former sharp 110-cleavage planes are strongly enlarged through growth of vein perthite. Former plagioclase is replaced by a felt of phengite-paragonite with microliths of zoisite-clinozoisite, and albite. Former subround grains of primary quartz display all stages of polygonization and are replaced by aggregates of new hexagon-shaped quartz grains (**Photo 3.05**), showing distinct maxima of c-axis orientation (additional details in Ch. 3.2, deformation). The above-cited neoformation of stilpnomelane (von Raumer, 1969) is mainly observed in areas with faint Alpine deformation. Newly formed leaflets are concentrated either in small tension-gashes of K-feldspar, or at the border of primary biotite in contact with quartz (**Photo 3.06**). With stronger deformation and recrystallization, mainly chlorite, phengite and epidote appear. The famous minerals found in Alpine tension gashes of the Mont Blanc granite have been subject of specific descriptions (Poty, 1969, 1999; von Raumer, 1974; Bayle, 1999; Gautron, 1999; Meisser, 1999; Arlt, 2004). A statistical research on composition of sandy chlorite formed in Alpine tension gashes in the Mont Blanc cross-section shows that chlorite composition across the entire cross-section is rather constant, representing rhipidolithes with Fe/Mg ratios between 0.5-0.6 (see **Table 3.01**).

Specific transformations are observed on slicken sides, which may be composed by actinolite-quartz fibres, quartz-chlorite aggregates, epidote, or newly formed pink garnet. These phenomena are certainly influenced by the fluid regime, similarly to the neoformation of minerals in tension gashes (Poty et al., 1974). Alpine fluids are characterized by > 80 mol% H_2O, and < 10 mol% CO_2 (Mullis, 1983, 1995). Unpublished observations about the distribution of garnet slicken sides will be briefly reported.

Garnet-bearing slicken sides are systematically observed in steeply dipping N60-80° quartz veins at the NE border of the Mont Blanc granite (Aiguille du Tour - Bovine, and Montenvers cross-sections). They consist of a thin coating (mostly < 1mm) of tiny garnet grains on a quartz surface, and may be locally accompanied by a thin layer of epidote. Garnet has a very specific composition high in spessartite molecule, besides grossular and minor almandine (analyses **Tab. 3.02**). It must have been produced by fluid circulation from the granitic host. Ca (grossular component) may have been supplied by the decaying plagioclase (An_{20-30}), whereas Mn (spessartite component), Fe (almandine component) and Mg (pyrope component) were mobilized during decay of brown biotite and/or chlorite in the granite host. Mass-balance calculations based on Mn show that about 15 cm of granitic host rock on both sides of the veins may have been sufficient to supply all the necessary components. Similar Alpine garnets have been described in the Aar massif (Steck, 1966; Steck and Burri, 1971).

Distribution of Alpine minerals in the area has been described by Parker (1973) and Stalder et al. (1998). Although less spectacular in size, many tiny tension gashes containing a great number of Alpine minerals were described by Frey (1974, 1977, 1981) from very different localities in the metamorphic basement where, besides quartz, albite, adularia and chlorite, minerals like fluorite, anatas, brookite, monazite, xenotime, aeschinite and synchisite have been observed.

Meters	Coord. CH.	host-rock	nb	001	b°
00 426	573 190/87 590	rhyolite	1.630	14.1617	9.2892
00 800	573 150/87 900	rhyolite	1.636	14.1618	9.2927
00 850	573 150/87 960	rhyolite	1.633	14.1462	9.2929
00 865	573 160/87 980	rhyolite	1.631	14.1530	9.3029
01 715	573 350/88 790	rhyolite	1.633	14.14.82	9.3053
02 101	573 450/89 170	rhyolite	1.635	14.1414	9.30699
02 568	573 560/89 630	rhyolite	1.6371	14.1480	9.308
02 603	573 560/89 660	rhyolite	1.6361	14.149	9.305
02 720	573 590/89 770	microgranite	1.632	14.158	9.2962
02 790	573 610/89 840	rhyolite	1.636	14.1529	9.30486
02 843	573 620/89 880	microgranite	1.643	14.1434	9.3153
03 390	573 730/90 420	rhyolite	1.622	14.1542	9.2836
03 570	573 660/90 590	rhyolite	1.635	14.156	9.308
05 480	572 920/92 360	granite	1.642	14.137	9.313
05 575	572 850/94 420	granite	1.644	14.145	9.325
05 960	572 550/92 660	granite	1.637	14.1455	9.309
06 000 - 11 590		granite	-	no data	-
11 597	568 210/96 040	granite	1.634	14.142	9.303
12 425	567 460/96 620	Kf-orthogneiss	1.641	14.1350	9.3185
12 427	567 460/96 620	Kf-orthogneiss	1.639	14.1502	9.30465
12 579	567 350/96 720	Kf-orthogneiss	1.632	14.1469	9.29706
12 647	567 290/96 770	mylonitic gneiss	1.632	14.1319	9.3042
12 850	567 130/96 900	mylonitic schist	1.626	14.1568	9.2935
13 715	566 950/97 070	Kf-orthogneiss	1.645	14.1664	9.3194
13.820	566 580/97 690	Kf-orthogneiss	1.643	14.1268	9.3210
13 887	566 560/97 750	Kf-orthogneiss	1.655	14.1329	9.33609
13 965	566 510/97 830	Kf-orthogneiss	1.6501	14.1484	9.3225
13 989	566 500/97 850	Kf-orthogneiss	1.637	14.1433	9.30999
14 170	566 410/98 000	Kf-orthogneiss	1.645	14.1574	9.3295
14 333	566 280/98 060	Kf-orthogneiss	1.656	14.1117	9.3357
14 370	566 250/98 080	Kf-orthogneiss	1.6288	14.1433	9.29919
14 470	566 150/98 110	Kf-orthogneiss	1.632	14.1480	9.292
14 588	566 050/98 150	Kf-orthogneiss	1.632	14.1619	9.2951
15 737	564 960/98 500	Kf-orthogneiss	1.636	14.1424	9.3104
15 853	564 850/98 550	Kf-orthogneiss	1.634	14.1500	9.2974

Tab. 3.01
Cristallographic and optical data on sand-chlorites (platy habit) in Alpine tension-gashes from the cross-section through the Mont-Blanc massif, water power line La Fouly – Trient, current meters counted from La Fouly in the southern section. nb optical properties determined by comparing with refractive liquids with sodium-light source and precision thermometric corrections. (001) and b° X-ray powder data were produced by a Jagodzinsky high precision powder camera.
Données cristallographiques et optiques des chlorites sableux (à habitus tabuleux) trouvées dans les fissures alpines de la section à travers le massif du Mont Blanc (conduite d'eau La Fouly – Trient), distance en mètres mesurés depuis le début de la galerie à La Fouly au sud. Les propriétés optiques nb déterminées par comparaison avec des liquides refractaires et une source de lumière sodium, corrections thermométriques de haute précision. Constantes de resaux (001) et b° obtenues par caméra radiographique de poudres de haute précision Jagodzinsky.

Coord. CH.	a_0	Py	Alm	Grs	Spess
566 640/ 93 125	11.74268	0.9	18.3	47.3	33.5
571 920/101 875	11.74637	1.1	15.9	46.7	36.3

Tab. 3.02
Lattice constants and chemical composition of spessartite-rich garnets in Alpine slicken sides from the Mont Blance granite. *Constante de reseau et composition chimique de grenats de miroirs de faille alpins dans le granite du Mont Blanc.* Analyst microprobe H. Schwander (Basel); radiometric data: von Raumer, Jagodzinski powder camera.

III.1.2 Pre-Variscan and Variscan mineral assemblages

The main rock types have been characterised in the preceeding chapter and, besides field observations, the classical approach to metamorphic rocks is based on chemical analyses and their representation in triangular projections like ACF/A'KF and AFM diagrams (**Fig. 3.01, 3.02**). Compared to Winkler (1979), rocks like metasediments (shales, marine clays and greywackes with variable amounts of CaO) and amphibolites (former basaltic and andesitic rocks) occupy a specific area in the ACF-diagram. As the main field aspect between micaschists and metagreywackes is their difference in quartz contents, both rock types coincide with the field of greywackes in the ACF projection. A specific series of greywackes, observed in the Salanfe area (Chiaradia, 1993), have less Al and plot in an elongated field stretching from the greywackes to marls and/or amphibolites and, in the A'KF-projection, they show an enrichment of potassium, which could indicate either hydrothermal changes or a certain admixture of acidic tuffs. The corresponding projections in the AFM-diagram (**Fig. 3.02**) plot mainly on a line characterized by a rather constant Fe/Mg-relation around 0.5. Metagreywackes and shales plot mainly in the field characterized by an average pelagic shale, whereas the metagreywackes from the Salanfe area (Chiaradia, 1993) have lower Al-values, and may represent former Al-poor shales or siltstones, which may have contained chlorite and K-feldspar.

The strongest metamorphic imprint of the polymetamorphic units in the Aiguilles Rouges and Mont Blanc massifs reached high amphibolite facies grade and locally anatectic conditions (**Photos 3.07; 3.08; 3.09; 3.10**). Consequently, besides migmatites, all rocks should contain minerals like kyanite, sillimanite, staurolite, garnet, plagioclase, biotite, diopside, amphibole, and quartz. These mineral assemblages are well preserved in the Aiguilles Rouges area (**Fig. 3.02**), but were totally destroyed by the Alpine overprint in the Mont Blanc. On the other hand, migmatitic structures are nicely preserved in both massifs.

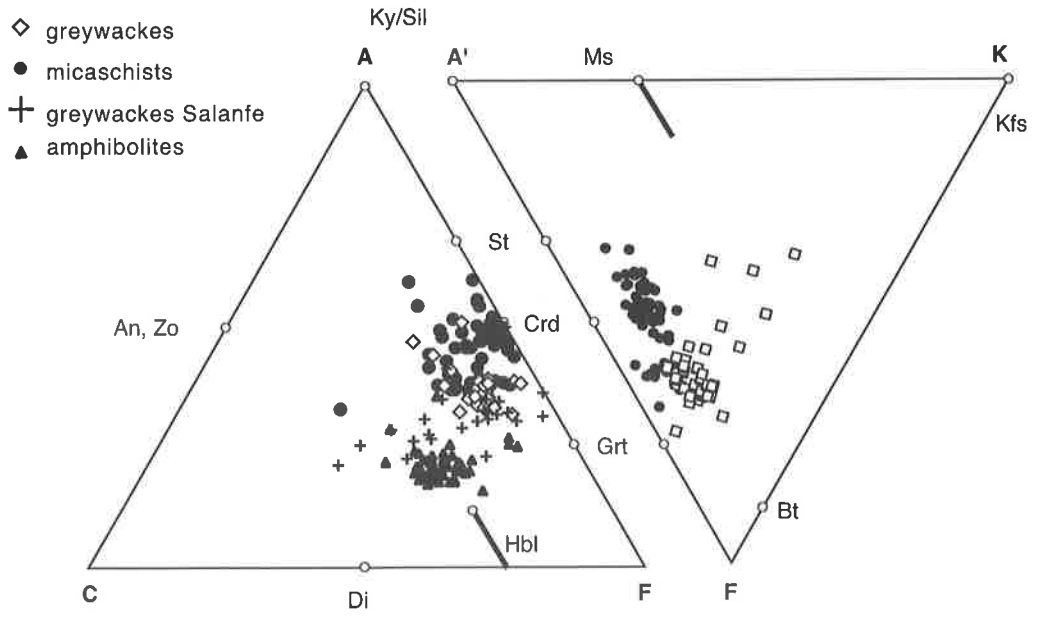

Fig. 3.01
ACF – A'KF projections of metamorphic rocks from the Aiguilles Rouges massif, unpublished analyses von Raumer (Annex I, Tab. VI.10, 11), and from Chiaradia (1993), Fracheboud (1997), Marquis (1997).
Minerals: An – Anorthite, Bt – Biotite, Crd – Cordierite, Di – Diopside, Grt – Garnet, Hbl – Hornblende, Ky – Kyanite, Kfs – K-feldspar, Ms – Muscovite, Sil – Sillimanite.
Projections ACF - A'KF des roches métamorphiques du massif des Aiguilles Rouges. Analyses non publiées de von Raumer (Annexe I, Tab. VI.10, 11), et de Chiaradia (1993), Fracheboud (1997), Marquis (1997).
Minéraux: An – Anorthite, Bt – Biotite, Crd – Cordiérite, Di – Diopside, Grt – Grenat, Hbl – Hornblende, Ky – Kyanite (disthène), Kfs – Feldspath potassique, Ms – Muscovite, Sil – Sillimanite.

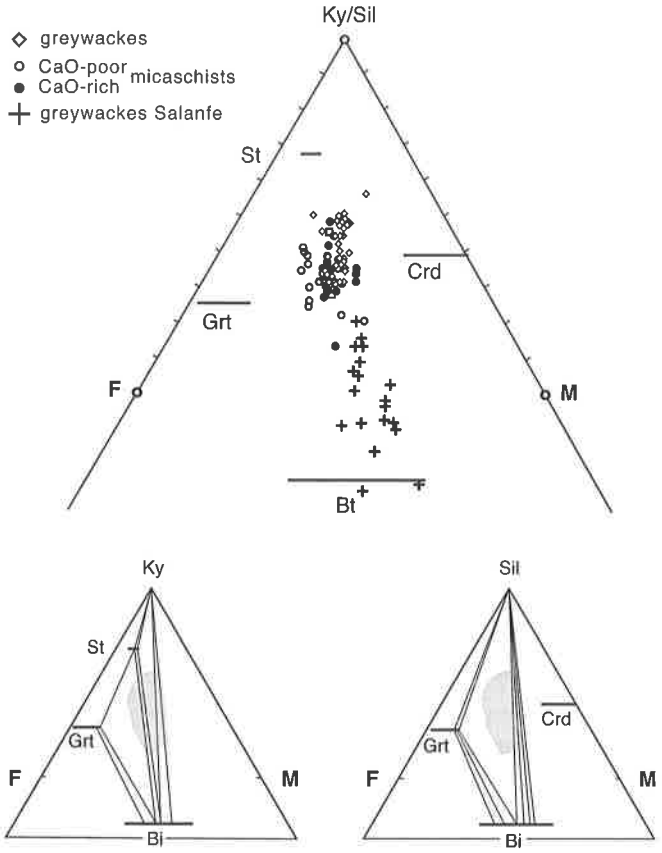

Fig. 3.02
AFM projections of metamorphic rocks from the Aiguilles Rouges massif, indicating the succession from kyanite-bearing to sillimanite-bearing parageneses, shaded area: field occupied by the metasediments.
Projection AFM des roches métamorphiques des Aiguilles Rouges, illustrant l'évolution des paragenèses à disthène (gauche) aux paragnèses à sillimanite (droite), en gris: projection des métasédiments.

Relics of pre-Variscan minerals

The available isotopic ages point to a late Variscan high-T event, i.e. a monazite-in reaction in Emosson micaschists at 327±2 Ma and a monazite crystallization in a leucosome vein at 320 ±1 Ma (Bussy et al., 2000). As lower Palaeozoic migmatites are documented in other External Massifs, it is suspected that some high grade rocks in the Aiguilles Rouges-Mont Blanc area could also be pre-late Variscan in age. For example, some large isolated garnets in micaschists or gneisses from Val Bérard (**Photo 3.11**) are reminiscent of kinzigite garnets and may represent relicts of an earlier metamorphic event. Pseudomorphosed zoisite in amphibolites (e.g. **Photo 2.16**), and relicts of hercynite-rimmed muscovite pseudomorphs after kyanite indicate that the high-pressure field has been traversed before attaining the HT conditions. Following Proyer (2003), the horizons of plagioclase nodules in micaschists (e.g. **Photo 2.18**) may indicate decay of former omphacite-bearing horizons containing paragonite and phengite. But so far, only meta-eclogites can be safely related to a pre-high-T Variscan metamorphic phase.

Preserved eclogites are found in the Lac Cornu (Liégeois & Duchesne, 1981) and Val Bérard (Schulz & Von Raumer, 1993) areas. Despite a slight Variscan retrogression, the following paragenesis is observed (all mineral abbreviations after Bucher & Frey, 1994):

[Grt + symplCpx + Am + Pl]

Liégois & Duchesne (1981) estimated conditions of 0.11GPa/780°C and a thermogradient around 15-20°C/Km. Relict omphacite Jd_{26} within garnet; or Jd_{22-25} to Jd_{7-15} in symplectitic pyroxenes associated with plagioclase, yield T-P estimates of 700°C/0.14 GPa and 700°C/0.08 GPa, respectively (Schulz and von Raumer, 1993).

Variscan mineral assemblages

Migmatites: metagranites and metagraywackes (**Photos 3.07, 3.08, 3.09, 3.10**) experienced partial melting of variable intensity ascribed to isothermal decompression during exhumation processes. Early stages of melting are expressed by the mineral assemblage muscovite, sillimanite and K-feldspar, observed from areas near the glacier d'Argentières (Lognan) to the neighbourhood of Pointe des Grands (Photos **2.07; 2.08**). Typical mineral assemblages are:

[Pl + Qtz + Kfs + Bt ± Sil ± Ms ± Grt ± Crd]

Monazite from a leucosome vein of a migmatitic graywacke at Emosson yielded a U-Pb crystallization age of 320 ± 1 Ma (Bussy et al., 2000), whereas monazite from a migmatitic granite in the Mont Blanc massif (Lognan) yielded 317 ± 2 Ma (Bussy and von Raumer, 1994). Locally, small, elongated spots of sillimanite (fibrolite) are parallel to the main foliation of the orthogneiss (**Photo 3.12**).

Metagreywackes and metapelites

Metapelites and metagreywackes are characterized by sillimanite-bearing assemblages (**see Fig. 3.02**):

[Bt + Pl + Qtz + Sil ± Grt ± Crd ± Ms ± Kfs]

Monazites from such micaschists yielded a U-Pb isotopic age of 327 ± 2 Ma at Emosson, interpreted as the peak temperature age (Bussy et al. 2000).

Paragneisses of various compositions display monotonous assemblages (Schulz & Von Raumer, 1993, Dobmeier, 1998):

[Qtz + Bt + Pl(olig) ± Ms ± Grt ± Sil ± Kfs]

As this late Variscan high-T/anatectic event represents the thermal peak of metamorphic evolution, relict parageneses containing kyanite, staurolite and older garnet, are supposed to indicate former higher pressure conditions. These undated parageneses are currently attributed to an early stage of the Variscan evolution, pointing to a clockwise decompression path illustrated by the transition from kyanite to sillimanite, typical of a Barrowian metamorphic evolution (see **Fig. 3.07**).

Such relicts have been found in metapelites and paragneisses in the central part of the Aiguilles Rouges (Emosson, Val Bérard; von Raumer, 1983; von Raumer & Schwander 1985; Schulz & von Raumer 1993). Additional observations were reported in unpublished theses (Joye 1989, Dupasquier 1996, Schmocker 1996, Fracheboud 1997, Marquis 1997, Wettlaufer 1998). Relicts of kyanite and/or staurolite were already mentioned by Bellière (1954, 1958) in the whole region between Lac Cornu and Val d'Emaney:

1) garnet 1 – staurolite – kyanite ± biotite
2) garnet 2 – sillimanite - biotite
3) Late stage andalusite

Schulz & von Raumer (1993) observed a sequence of mineral parageneses appearing in the neighbourhood of Val Bérard in Al-silicate-rich rocks (with additional kyanite and andalusite appearing in quartz veins):

Relic paragenesis
1) Qtz + Bt + Oligoclase ± Grt ± St ± Ky
Followed by:
2) Qtz + Bi + Oligoclase ± Grt ± Sil
Late stage:
3) andalusite

In the SW of the Aiguilles Rouges (St-Gervais-Les Houches), metasediments yielded the following parageneses (Dobmeier 1996,1998):

Western gneiss unit (WGU):
in S1: Qtz + Bt + Oligoclase + Grt + Ky + Kfs
in S2: Qtz + Bt + Ms + Oligoclase + Grt ± Sil ± Kfs
Eastern gneiss unit (EGU):
pre-S2: Qtz + Bt + Ms + Pl + Grt + Ky + Sil + Kfs
in S2: Qtz + Bt + Ms + Oligoclase + Grt + Sil + Kfs

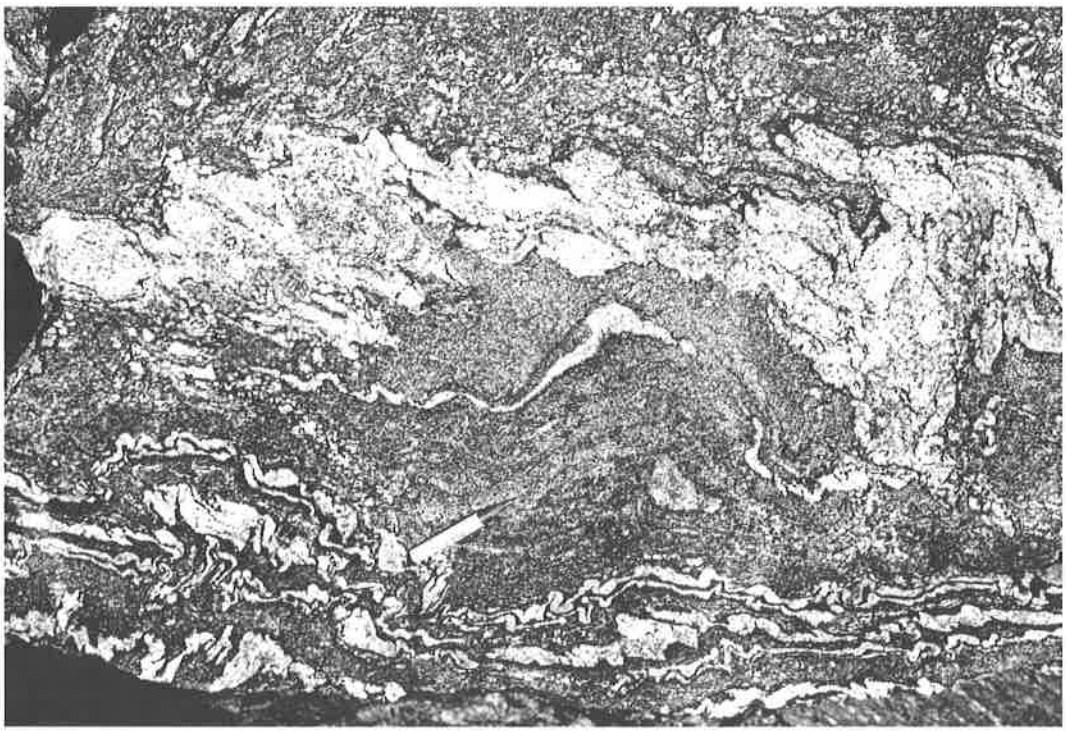

Photo 3.07
Migmatite with relic structures, indicating three phases of deformation. On the way between Planpraz / Altitude 2000 and Col Cornu, Aiguilles Rouges (Coord Fr.: 950.050/115.750). *Migmatite avec reliques de trois générations de déformation, sur le chemin entre Planpraz/ Altitude 2000 et Col Cornu, Aiguilles Rouges (Coord (fr.: 950.050/115.750).*

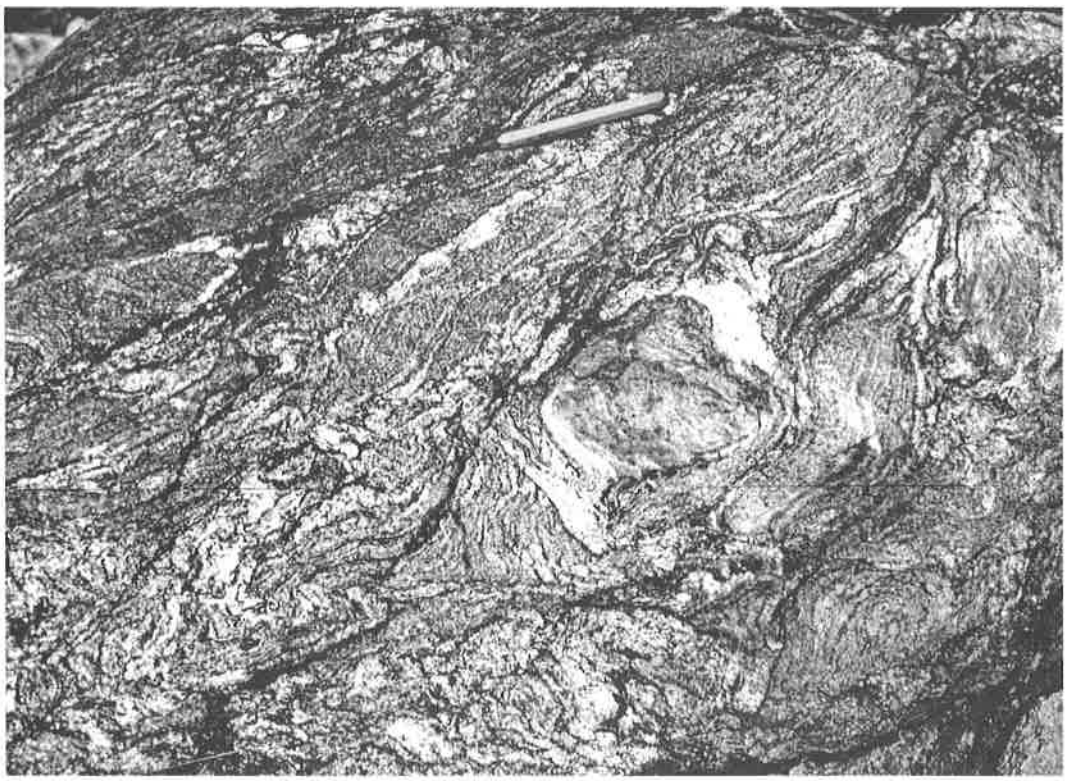

Photo 3.08
Migmatite with relics of a former carbonate rock, at present a calcsilicate rock, Alpe Bovine area (Mont Blanc massif) (Coord CH: 568.285/97.795) *Migmatite avec relique d'une roche carbonatée transformée en silicates calciques, Alpe Bovine (Massif du Mont Blanc) (Coord CH.: 568.285/97.795).*

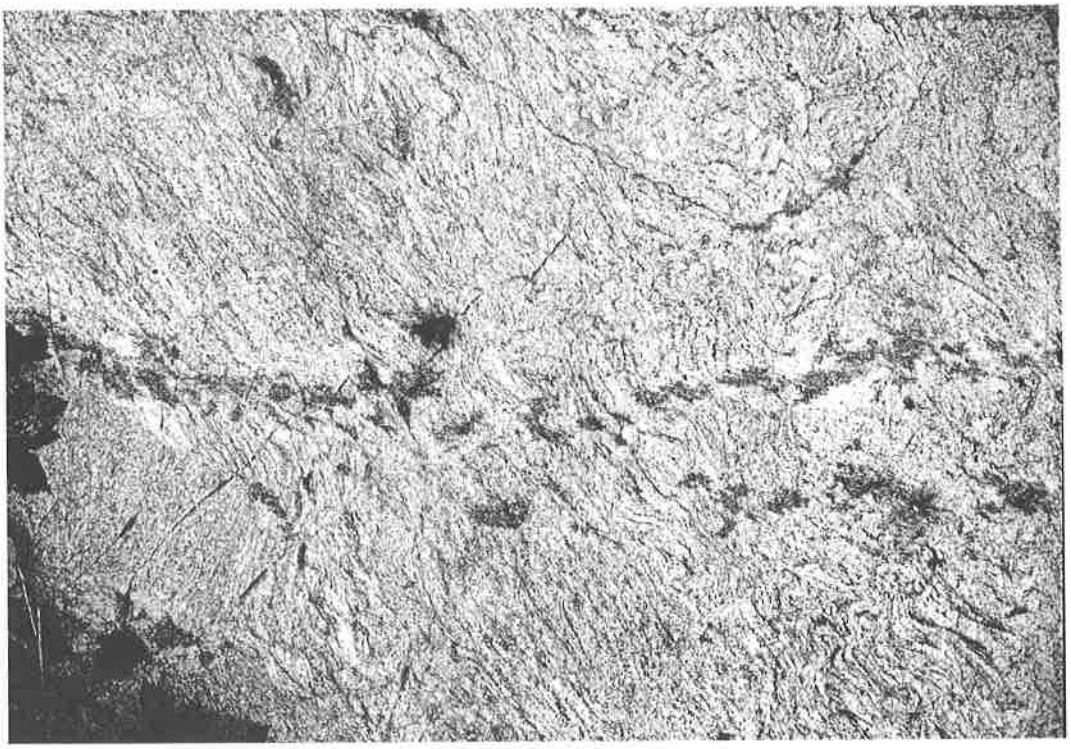

Photo 3.09
Migmatite with formation of cordierite-bearing tension gashes, leaching of host-rock. Col de la Seigne region, Mont Blanc massif (Coord FR: 946.130/93.400)
Migmatite avec formation de fissures d'extension à cordiérite (pinite) avec lessivage de la roche encaissante; Région du Col de la Seigne,massif du Mont Blanc (Coord Fr. 946.130/93.400).

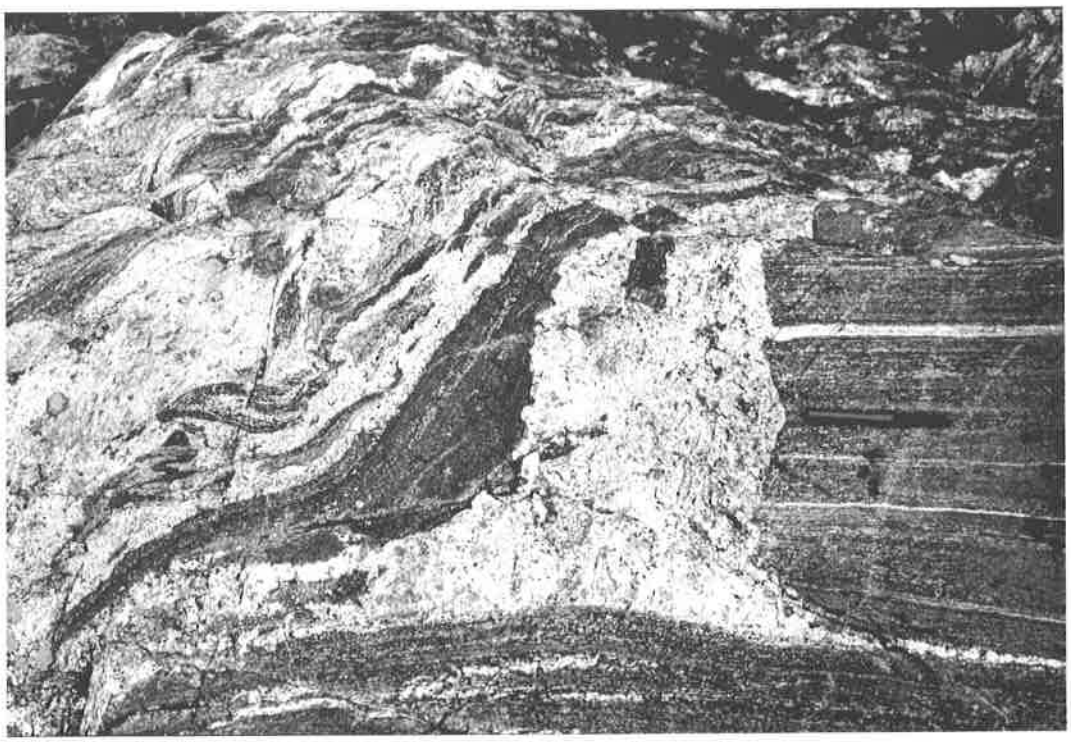

Photo 3.10
Mobilisate at the rim around amphibolitic granulite, Lac Cornu area, Aiguilles Rouges (Coord Fr.: 949.810/116.570) *Mobilisat anatectique au bord d'une granulite amphibolitique, Lac Cornu, Aiguilles Rouges (Coord Fr.: 949.810/116.570).*

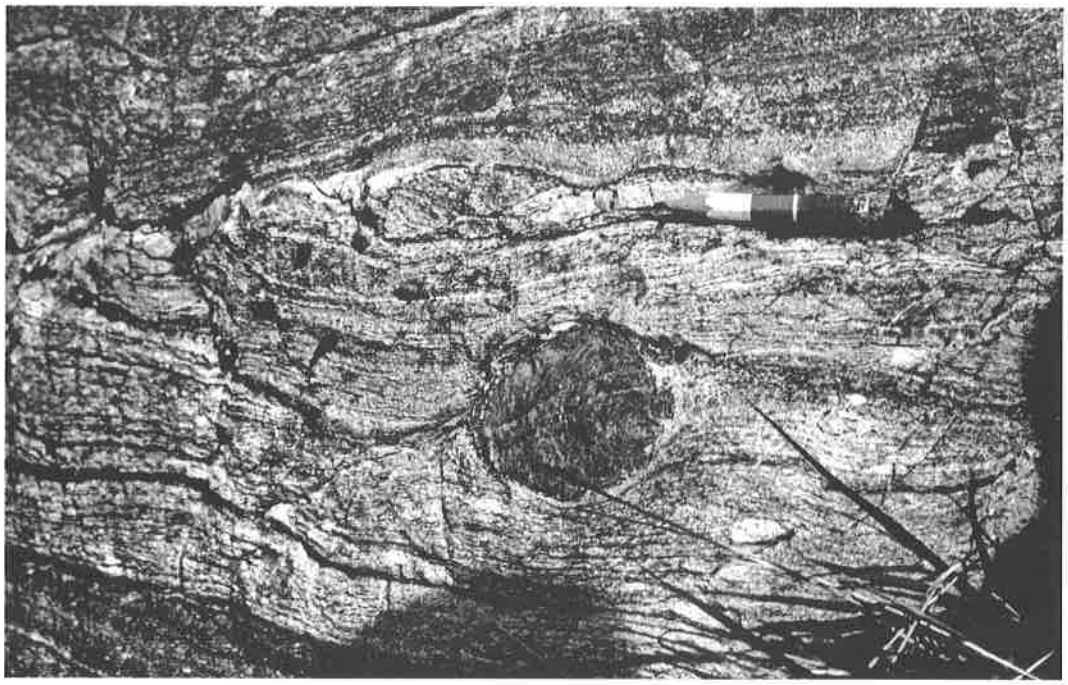

Photo 3.11
Garnet (Ø 5 cm) in biotite-gneiss, Val Bérard, Aiguilles Rouges (Coord FR: 950.170/121.080)
Grenat (Ø 5cm) dans gneiss à biotite, Val Bérard, Aiguilles Rouges (Coord FR: 950.170/121.080).

Photo 3.12
Sillimanite blasts in orthogneisses, neighbourhood of Col de la Terrasse, Aiguilles Rouges (Coord. CH: 557.150/99.020) vertical scale/*échelle verticale:* 40 cm
Croissance de nodules à sillimanite dans un orthogneiss, voisinage du Col de la Terrasse, Aiguilles Rouges (Coord CH: 557.150/99.020).

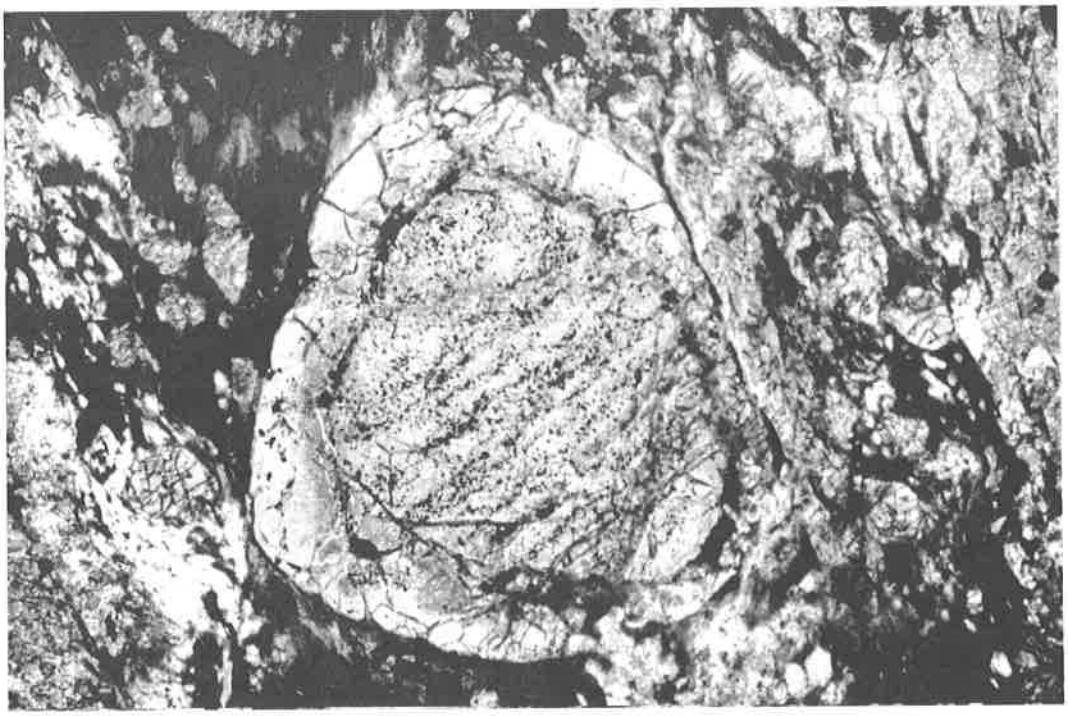

Photo 3.13
Zoned garnet (Ø 6mm), sample 1124, Emosson, Aiguilles Rouges (Coord CH: 558.150/101.730)
Grenat zoné (Ø 6mm), éch. 1124, Emosson, Aiguilles Rouges (Coord CH: 558.150/101.730).

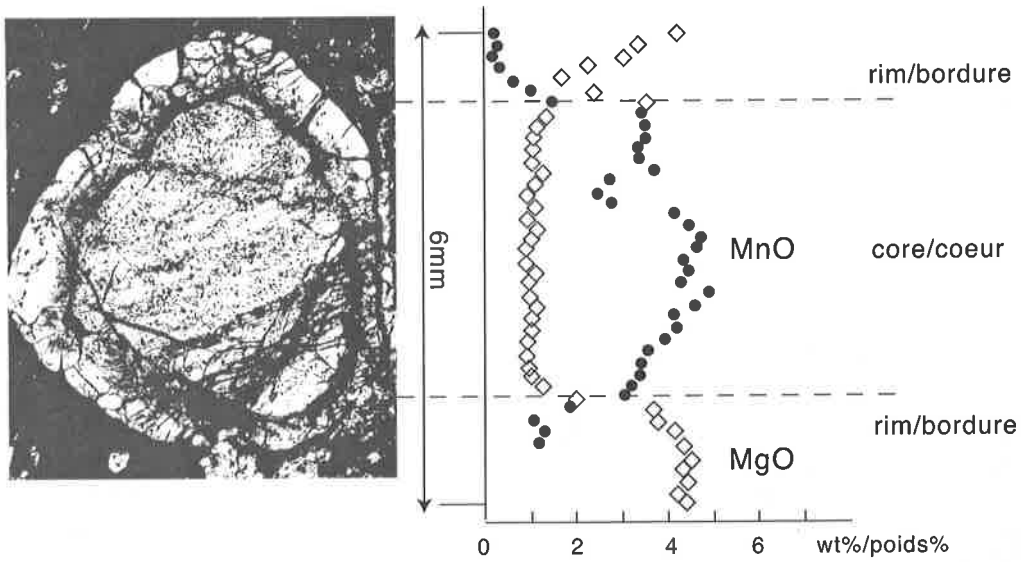

Fig. 3.03
Microscopic cross-section of garnet (6 mm diameter, see Photo 3.13) in garnet-micaschists from Lac Emosson (Coord CH.: 558.150/101.730) with indication of chemical changes of MnO and MgO across the garnet (from von Raumer and Schwander, 1985; 1124). *Section microscopique d'un grenat (diamètre 6 mm, Photo 3.13) de micaschiste à grenat de la région du Lac Emosson, Aiguilles Rouges (Coord Ch.: 558.150/101.730), avec indication des changements de composition chimique en MnO et MgO à travers le grenat (de von Raumer et Schwander, 1985; 1124).*

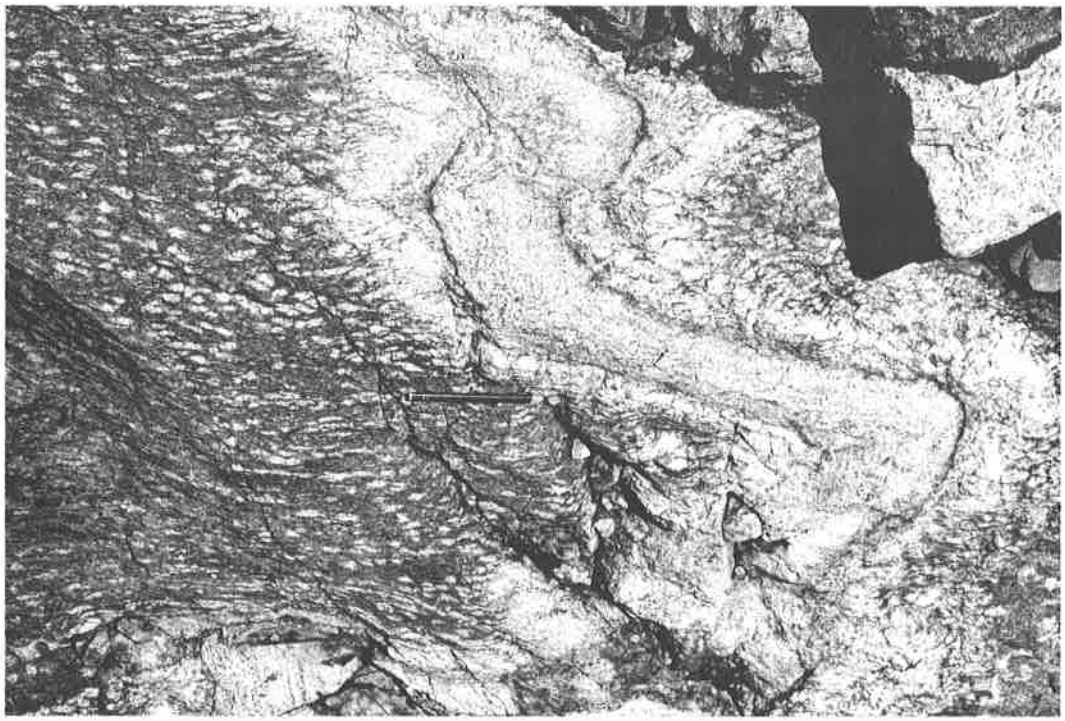

Photo 3.14
Micaschist-metagreywacke fold, plagioclase growth in micaschist parallel to foliation of the axial plane, Vieux Emosson area, Aiguilles Rouges (Coord Ch: 558.480/100.070, 2480m), width: 90 cm
Pli affectant un assemblage de micaschiste-metagrauwacke avec croissance de plagioclase parallèlement à la foliation du plan axial, Vieux Emosson, Aiguilles Rouges (Coord Ch: 558.480/100.070, 2480m), largeur: 90 cm.

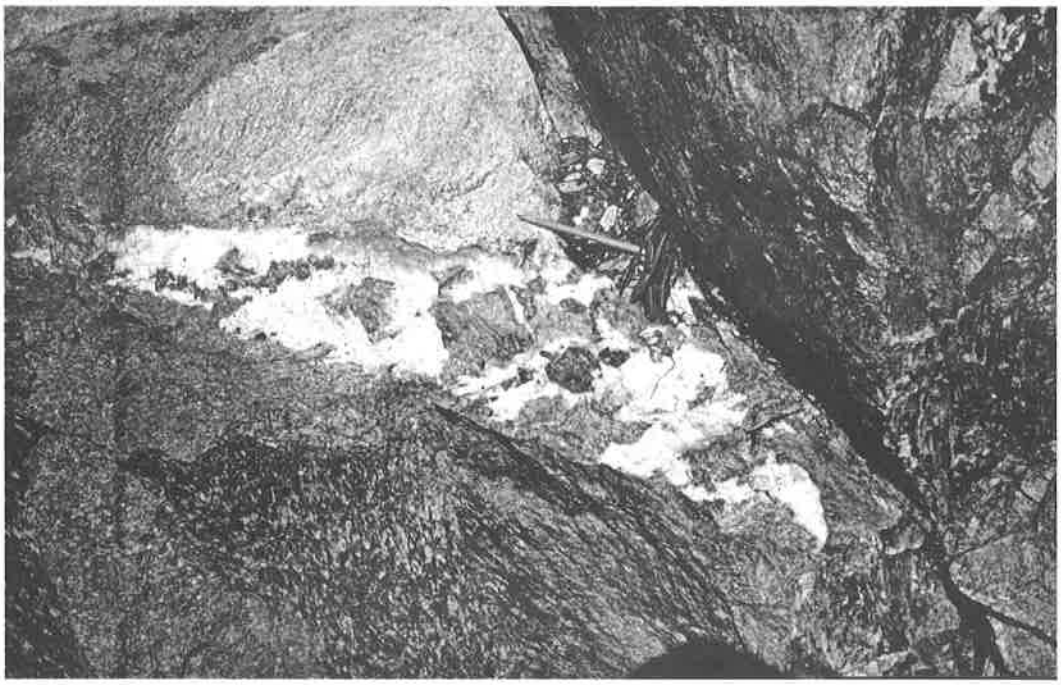

Photo 3.15
Andalusite-bearing tension gash, Emosson, Aiguilles Rouges (Coord CH: 559.300/101.800)
Fissure à andalousite, Lac Emosson, Aiguilles Rouges (Coord CH: 559.300/101.800)
Horizontal size/ *largeur : 1m*

Metapelitic rocks have been thoroughly investigated by von Raumer (1983). Sillimanite (fibrolite) and kyanite are known in wide areas of the central part of the Aiguilles Rouges massif, especially between the Lac Cornu and Emosson areas. Staurolite is often observed in rocks higher in Fe (Hoschek, 1984) than normal micaschists (von Raumer, 1983). Garnet is abundant either as homogeneous, zoned, or atoll-like grains (von Raumer, 1983; von Raumer and Schwander, 1995). **Fig. 3.03** shows a zoned garnet (compare with **Photo 3.13**) with the corresponding chemical composition in terms of Mg, Fe, Ca and Mn. Two garnet types may occur in one thin section; i.e. large zoned garnets with a Mn-rich core containing many tiny dark inclusions, and a very low-Mn rim, and smaller homogeneous garnets low in Mn. This clearly indicates an evolution during growth. Atoll garnets are observed as relicts in plagioclase porphyroblasts in micaschists.

Two series of micaschists were distinguished (von Raumer, 1983); those low in CaO (<1.0 wt%), and those containing 1-3 wt % CaO (**Fig. 3.01**), all having a rather limited Fe/Mg compositional range (**Fig. 3.02**). In the low-Ca rocks, with plagioclase around An_{10-30}, garnets appear mostly as atolls or corroded relics rimmed by plagioclase and biotite, whereas in the more CaO-rich micaschists with plagioclase An_{30-45}, garnets appear as larger, zoned crystals. During evolution to higher temperature, a second generation of garnet might appear besides the biotite and the sillimanite. Growth of sillimanite is accompanied by growth of plagioclase (von Raumer 1983, 1984), the latter being related to axial planes of major folds (**Photo 3.14**), and elongated parallel to the corresponding fold axis.

Andalusite is a late mineral related to Late Variscan extensional tectonics. It occurs in tension gashes (locally vertical to the late stage fold axes F3, **Fig. 304**) together with quartz and K-feldspar (**Photo 3.15**), or as pink coloured nodules (von Raumer 1984). Contact metamorphism phenomena are locally observed, either in the Montenvers granite at the contact with the Mont-Blanc granite, where biotite flakes grow (von Raumer, 1984), or along the contact of the Vallorcine granite with quartz recrystallisation (Joye, 1989).

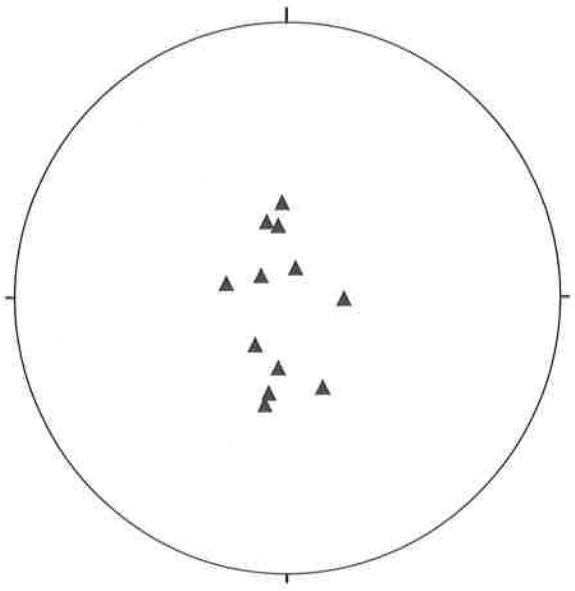

Fig. 3.04
Projection of subhorizontal tension gashes from the western Emosson and Tré les Eaux areas (Aiguilles Rouges massif). Equal area projection, lower hemisphere.
Projection de surfaces à andalousite des domaines Tré les Eaux et Emosson ouest (Aiguilles Rouges) dans l'hémisphère inférieur, avec conservation des surfaces.

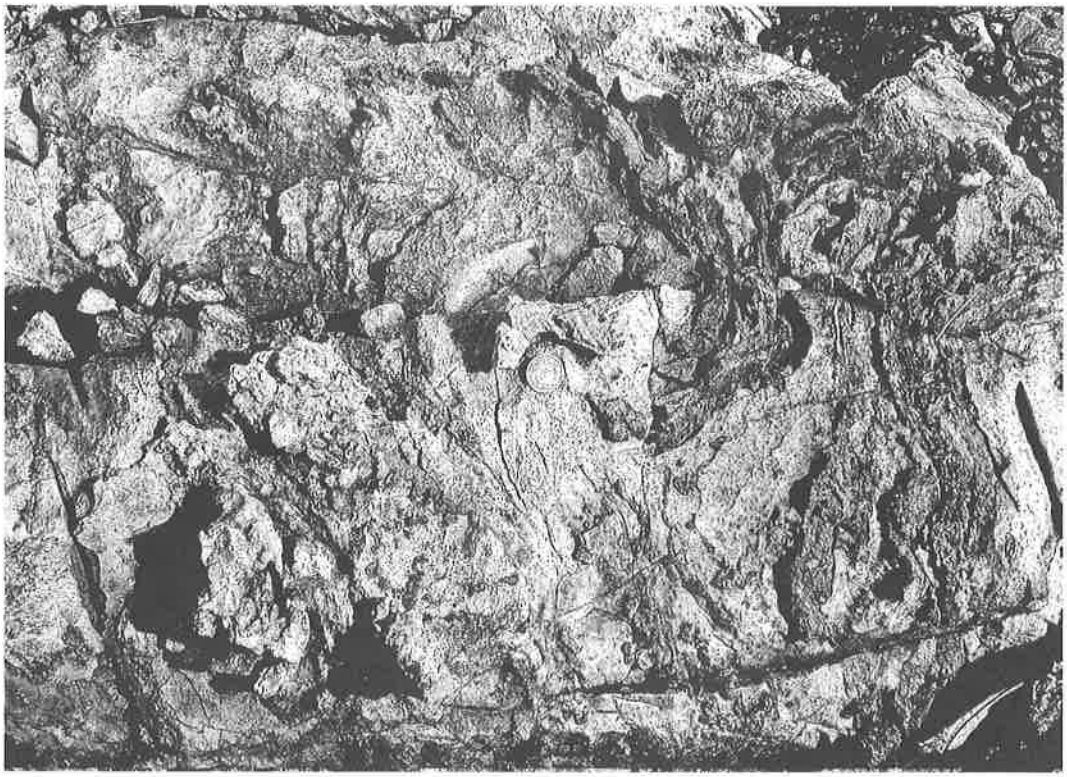

Photo 3.16
Diopside marble, diopside-bearing layers appearing as hard layers in the weaker carbonate host-rock. Lac Blanc-Chésérys area, Aiguilles Rouges (Coord Fr: 953.030/120.040/2406).
Marbre à diopside, les couches à diopside plus dures ressortent de la roche encaissante carbonatée, moins dure. Région Lac Blanc - Chésérys, Aiguilles Rouges (Coord FR: 953.030/120.040/2406).

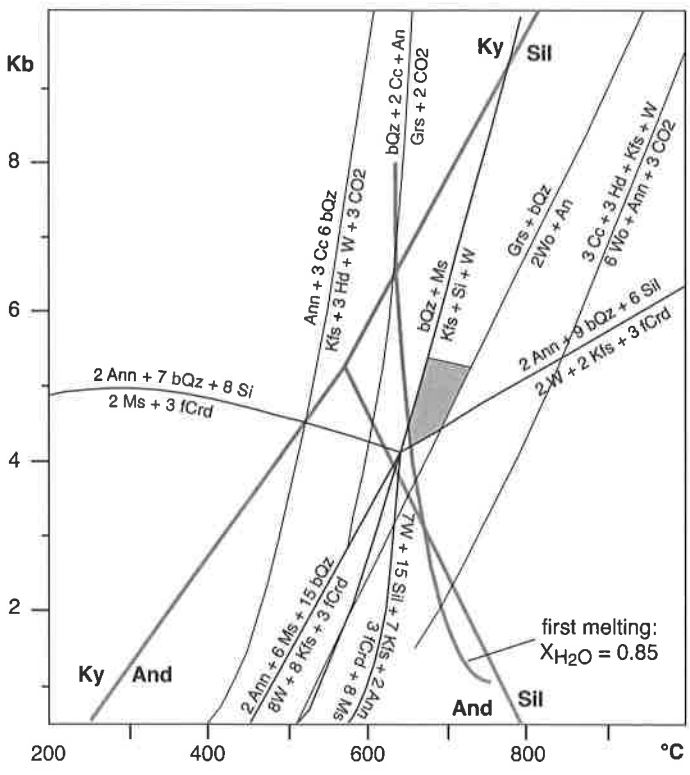

Fig. 3.05
Reconstruction of a petrogenetic grid for the late Variscan skarn formation in carbonate lenses at Salanfe, from Chiaradia (1993). P-T conditions of the D3 high temperature metamorphic event, defined by the stability field of mineral parageneses observed in metagreywackes and in calcsilicate lenses, and by the first melting curve for XH2O = 0.85. Triple-point of andalusite, sillimanite and kyanite after Greenwood (1976). Reaction curves calculated with MacIIPtax and GridlocII computer programs written by J. Liebermann (Inst. of Earth Sciences – The Hebrew University of Jerusalem); thermodynamic data for minerals from Berman (1988).
Diagramme pétrogénétique pour la formation tardi-Varisque des skarns dans les marbres de Salanfe. Tiré de Chiaradia (1993). Conditions P-T pour la phase de haute température définies par la stabilité des paragenèses minéralogiques observées dans les métagrauwackes et les lentilles calciques, et par la courbe de première fusion pour XH2O = 0.85. Point triple andalousite, sillimanite et disthène d'après Greenwood (1976). Courbes de réactions calculées par les programmes MacIIPtax et GridlocII, formulés par J. Liebermann (Dept. of Earth Sciences – The Hebrew University of Jerusalem); données thermodynamiques pour les minéraux de Berman (1988)

Carbonate rocks

Carbonate rocks have a typical composition of calc-silicate-bearing marbles (**Photos 2.29, 3.08, 3.16**), appearing as lenses among the micaschists and/or migmatites, and containing the mineral assemblage:

[Cc ± Qtz ± Grt ± Di]

Scheelite is present in most marbles of the region (first observed by Frey, 1977), and abundant in calc-silicate marbles from Salanfe (Chiaradia, 1993).

A striking example of the Late Variscan evolution of carbonate rocks is known from the Salanfe area (Chiaradia, 1993, see field-trip Salanfe area, Ch. V), where the main thermic and metasomatic event has been dated around 300 Ma (total Pb dating, Chiaradia, 1997). Besides normal calcsilicate minerals, a skarn mineralization has developed, leading to a well known ore site. Chiaradia (1993) reported the following mineral parageneses in the marbles hosting the skarn ores (more details Ch. V, field-trips):

S1: qtz – plag – Kfs – white mica
S2: qtz – plag – Kfs – white mica – biotite – Fe-grt
Static event:
qtz – plag – Kfs – biotite – sill – and
Skarn: Ca-garnet – hedenbergite - diopside
S3: qtz – plag – Kfs – biotite – sill – Fe-grt

Chiaradia (1993) established a petrogenetic grid defining the main conditions of evolution (**Fig. 3.05**):

Metabasic rocks

Metabasites of basaltic or gabbroic origin are found as boudins of variable size in the metasediments, mostly metapelites. They often contain relicts of early high-P events (see above), and currently record amphibolite facies conditions with the mineral assemblage:

[Pl + Am + Ilm ± Grt ± Ca-cpx ± Zo]

The pervasive foliation of the amphibolite (**Photo 3.17**) is underlined by narrow plagioclase-rich layers containing tiny garnets. Joye (1989) reported four generations of amphibole from actinote (Amph 1) to ferropargasite or ferropargasitic hornblende (Amph2), and to edenite or ferroedenitic hornblende (Amph 3,4), indicating a prograde P-T path to about 10Kb/700°C (formation of Amph 2) and a consecutive retrograde evolution to about 3Kb/600°C (see **Fig. 3.08**). In the amphibolites of Emosson (von Raumer et al., 1990), most amphiboles are magnesiohornblende and few zoned amphiboles show an evolution from actinolite to magnesiohornblende (nomenclature after Leake, 1978) through Tschermak substitution. According to Laird and Albee (1981), these amphiboles plot in a field, where sillimanite-bearing parageneses are stable in metasediments, as observed in the field.

In the southwestern part of the Aiguilles Rouges (Western Gneiss Complex), Dobmeier (1996) observed the following sequence of amphibolitic parageneses:

1) as relicts: Grt – Cpx (Jd?, Di?) – Plg – Rt
2) syn-S1: Am – Plg(An_{30-60}) – Qtz – Ttn – Ilm ± Bt
3) syn-S2: Am – Plg(Ab-An_{30}) – Bt – Chl – Qtz – Ttn - Rt ± Ep

Amphiboles of paragenesis 2) have ferrotschermakite or ferropargasite composition in the core with a rim of ferrohornblende, yielding estimated conditions of core formation of about 5-7 Kb/>800°C.

Photo 3.17
Strongly foliated garnet-amphibolite with plagioclase-bearing layers containing tiny garnets; Lake Emosson, Aiguilles Rouges (Coord CH: 558.400/101.940)..
Amphibolite à grenat, foliation marquée par des couches riches en plagioclase avec des petits grenats, Lac Emosson, rive ouest, Aiguilles Rouges (Coord CH: 558.400/101.940)

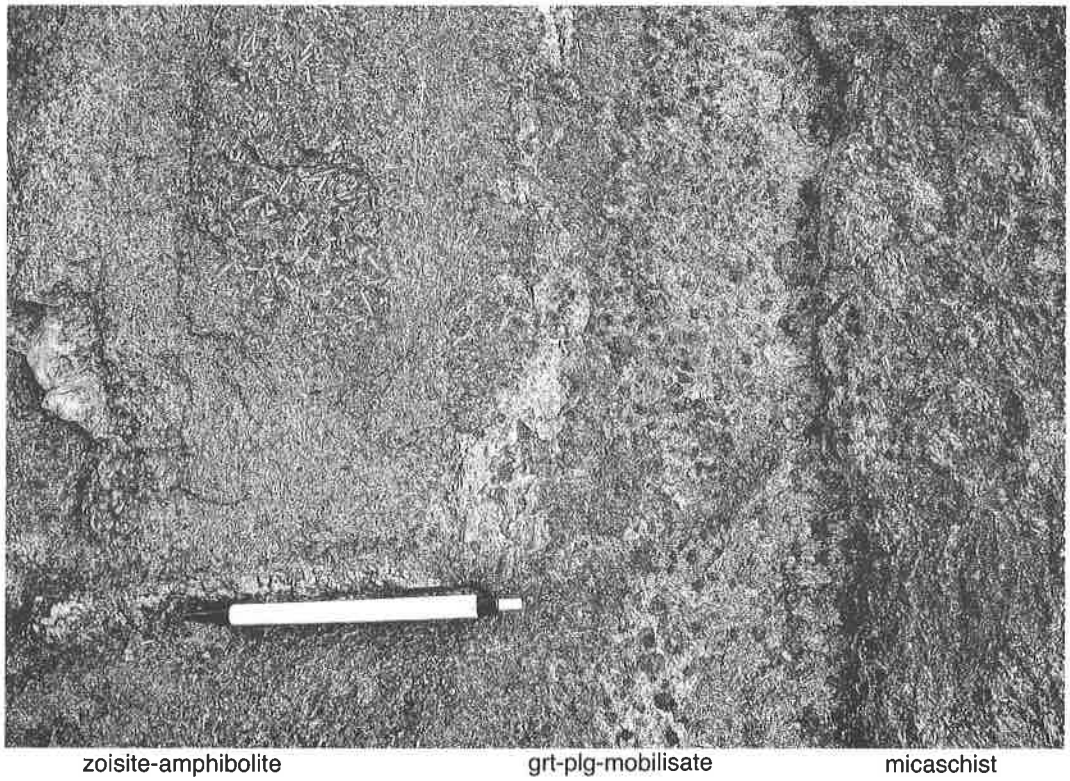

Photo 3.18
Zoisite amphibolite – micaschist transition, Vieux Emosson, Aiguilles Rouges
(Coord CH: 558.810/100.620/2317m). *Transition micaschiste–amphibolite à zoïsite, Vieux Emosson, Aiguilles Rouges (Coord CH: 558.810/100.620/2317m).*

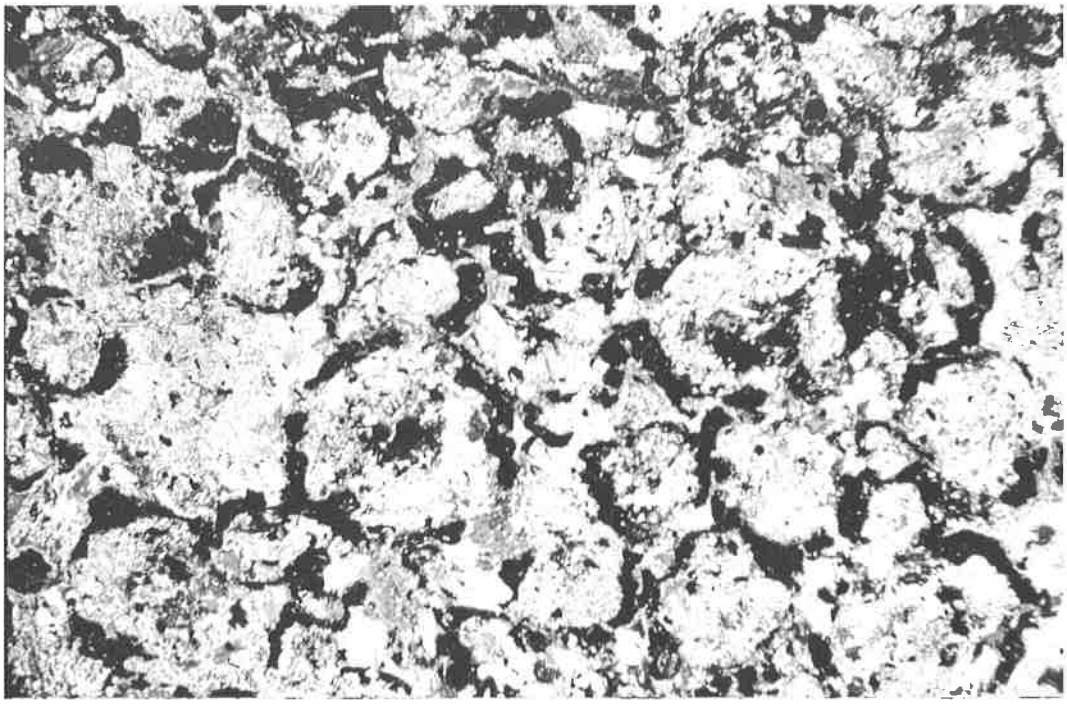

Photo 3.19
Microgranular coronitic metagabbro as rounded relics in migmatites, Lac Noir area, Aiguilles Rouges (Coord. FR: 949.820/116.890). Microscopic aspect of black garnet rims around a microgranular matrix with symplectitic structures containing some amphiboles and/or pyroxenes. Horizontal scale 10 mm.
Metagabbro coronitique microgranulaire en relique dans les migmatites du Lac Noir, Aiguilles Rouges (Coord. Fr. 949.820/116.890). Sous le microscope on reconnaît des bordures de grenat (en noir) dans une texture microgranulaire symplectitique avec des grains d'amphibole et/ou de pyroxène.

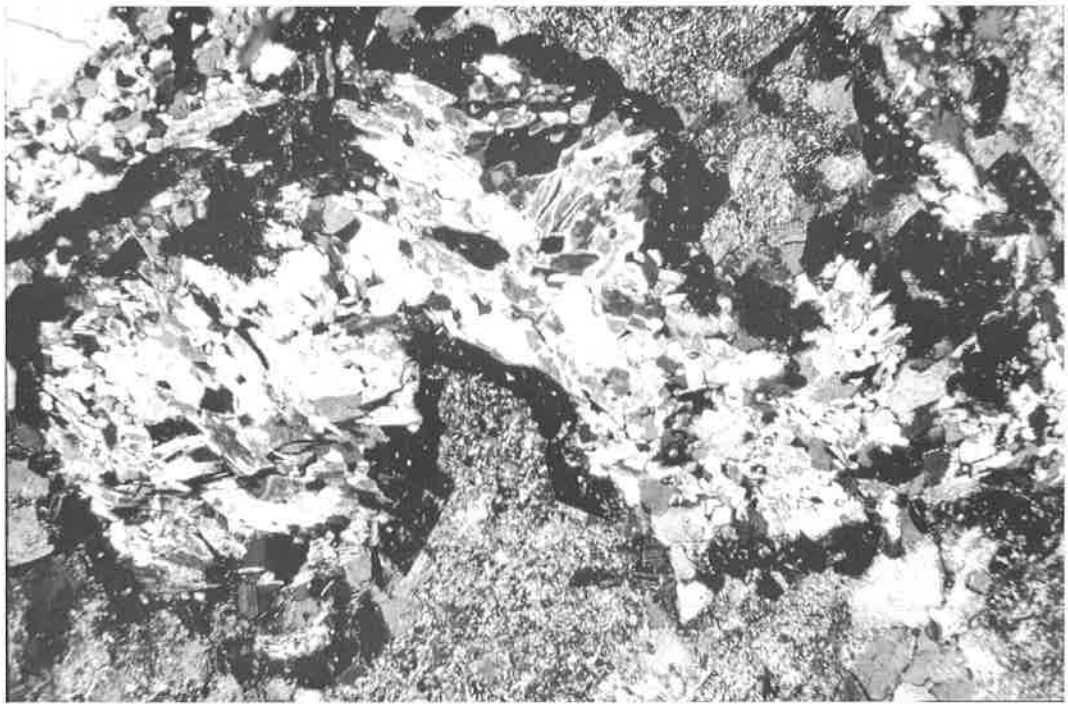

Photo 3.20
Major bloc of coronitic metagabbro in a migmatized zone, detailed microscopic view. Combe de Balme, Aiguilles Rouges (Coord. Fr: 92.050 / 554.670). Black garnet rims around a microgranular matrix of amphiboles. Horizontal scale 2mm. *Bloc de métagabbro coronitique dans des migmatites de la Combe de Balme, Aiguilles Rouges (Coord. Fr: 92.050 / 554.670). Bordure de grenat (en noir) et une texture microgranulaire composée de grains d'amphibole.*

As mentioned in chapter II, amphibolites can be rimmed by a plagioclase-rich layer. A detailed cross-section through the boudin of **Photo 3.18** shows an evolution from the metapelitic host on the right side of the picture (a garnet-bearing micaschist) across a plagioclase-rich whitish layer (central part of the picture) with larger garnets, kyanite and/or staurolite, to the massive garnet-amphibolite containing small whitish needles of zoisite (see also **Photos 2.15, 2.16**). We thus observe in a narrow transition the mineral parageneses:

garnet – plagioclase – biotite,
(towards the rim with larger, zoned garnets)
plagioclase – garnet – kyanite – staurolite – biotite
amphibole – zoisite – garnet

Kyanite from the plagioclase-rich layer is locally transformed into a cordierite-hercynite-K-feldspar assemblage (Dupasquier 1997, see also Ch. II), which corresponds to a heating-decompression reaction at rather high temperatures and pressures (**Fig. 3.06**, equations 2 and 4).

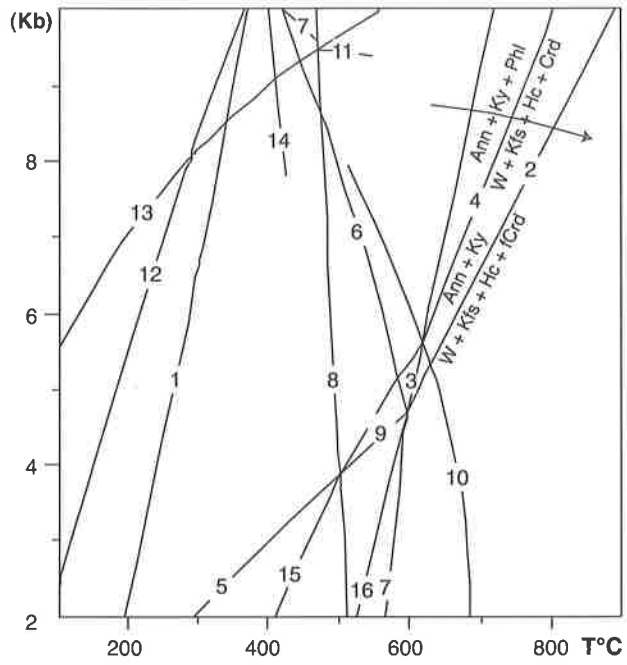

Reactions of Fig. 3.06
1) hCrd = 2W + Crd
2) 5Ann + 15 Ky = 5W + 5Kfs + 3Hc
3) Ann + 3Ms = 4W + 4Kfs + 3Hc
4) 3Ann + 15Ky + 2Phl = 5W + 5Kfs +)Hc + 3Crd
5) 5Ann + 20Ky = 5Ms + 7Hc + 4fCrd
6) 7W + /Kfs + 15Ky + 2Ann = 3fCrd + 9Ms
7) fCrd + 5Ms = 5W + 5Kfs + 5Ky + 2Hc
8) 3Crd + 2Ann = 3fCrd + 2Phl
9) 7Ann + 60Ky + 8Phl = 15Ms + 21Hc + 12Crd
10) 7W + Kfs + 2Phl + 15Ky = 3Crd + 9Ms
11) 14Kfs + 30Ky + 7 hCrd + 4Ann = 7Crd + 6fCrd + 18Ms
12) 2Ann + 3hCrd = 6W + 2Phl + 3fCrd
13) 14Kfs + 4Phl + 30Ky + 7hCrd = 13Crd + 18Ms
14) 3hCrd + 9Ms = 13W + 7Kfs + 2Phl + 15Ky
15) 7fCrd + 40Ky + 10Phl = 10Ms + 14Hc + 15Crd
16) 3fCrd + 6Ms + 2Phl = 8W + (Kfs + 6Hc +3Crd
17) 42Kfs + 90Ky 21hCrd + 26Ann = 39fCrd + 54Ms + 14Phl

Fig. 3.06
Reconstruction of a petrogenetic grid, program PTAX (system KFMASH, Bt,Crd,Hc,Ky,Ms,Kfs,W) defining the high temperature-decompression evolution of kyanite to hercynite and cordierite (Dupasquier, 1997).
Grille pétrogénétique etablie avec le programme PTAX (sytème KFMASH, Bt,Crd,Hc,Ky,Ms,Kfs,W) pour la transformation à haute température et en décompression du disthène en hercynite et cordiérite (Dupasquier, 1997).

Leucocratic rocks are also associated with some eclogite or amphibolite boudins in the Lac Cornu area (see Ch. II; field trip **V.3**). The equigranular garnet-biotite-plagioclase rocks (**Photo 2.18**) have a chemical composition of tonalites and have been interpreted as decompression melting products linked to the exhumation of high-pressure units (Von Raumer et al., 1996). A preliminary U-Pb zircon dating from one of these leucosomes yielded an age of c. 325 Ma (Bussy & Schaltegger, work in progress). The following mineral parageneses have been observed:

Included in garnet: 1) St + intergrowth Bt + Pl (Phe?)
Main paragenesis: 2) Bt + Pl + Grt + Ky ± St
reaction rim
around kyanite: 3) Hc + Crd;
in biotite: Sil as fibrolite
tension gashes
or rock-forming: 4) andalusite

Stable isotopes and phase chemistry indicate melting conditions for such tonalitic melts around 14Kb and maximum temperatures of 700-800°C (von Raumer et al., 1996, **Fig.3.07**).

Xenolith-like lumps of coarse-grained mafic rocks appear locally in the migmatites with coronitic textures at the microscopic scale. **Photos 3.19 and 3.20** illustrate coronitic textures around garnet, in what looks like a former gabbro. Several generations of minerals are observed. Such rocks are reminiscent of early Palaeozoic gabbros observed in the Gotthard area (Biino 1994), but this needs confirmation.

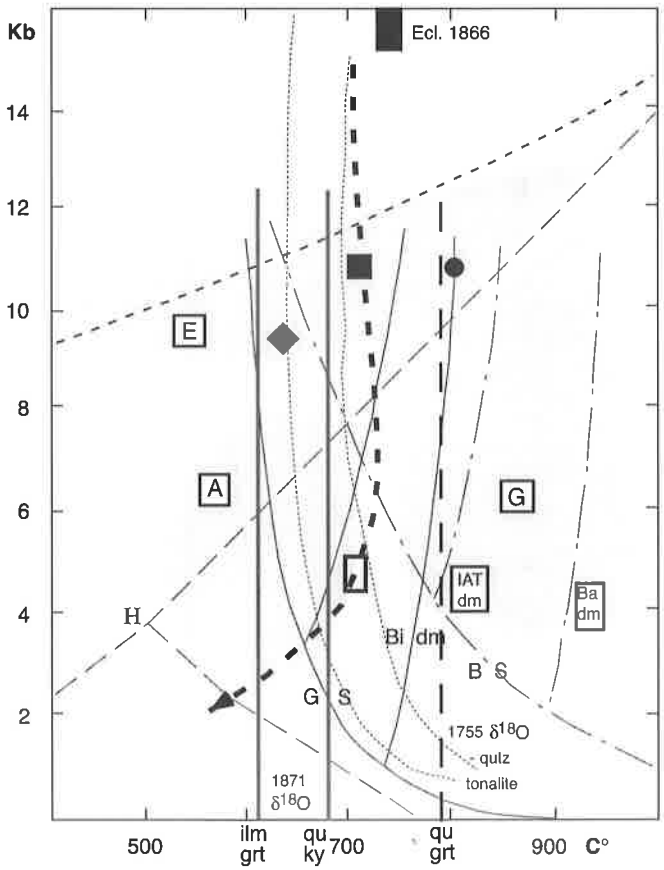

Fig. 3.07
Reconstruction of a pressure-temperature (P-T) path for dehydration melting of amphibolitic/ metaeclogitic rocks from the Lac Cornu area (von Raumer et al., 1996).
Fields of eclogite- (E), granulite- (G), amphibolite-facies (A), solidus of basalts B/S and granites G/S with dehydration melting curves (IAT- island arc tholeiites; B – basalts; Bi - biotite), after A.B. Thompson (1990); tonalite after Wyllie (1977); P-T-path and black rectangle ecl. 1866: from Schulz & von Raumer (1993);
Dot: Eclogite Lac Cornu Liegeois & Duchesne (1981); Rectangle: Salanfe, Chiaradia (1993), see Fig. 3.04 ;
diamond: 1731; square: 1871; H: Al-silicate triple point after Holdaway (1971).
Reconstruction des conditions de pression-température (P-T) pour la fusion d'amphibolites/ éclogites retrogrades par déhydratation, Lac Cornu, Aiguilles Rouges (von Raumer et al., 1996).
Les champs des éclogites (E), granulites (G), du faciès amphibolite (A), les solidus des basaltes (B/S) et granites (G/S), et les courbes de fusion par déhydratation (IAT- tholeyiites d'arc insulaire; B – basaltes; Bi - biotite) sont reprises de A.B. Thompson (1990); tonalite d'après Wyllie (1977); chemin P-T et rectangle noir (ecl. 1866): de Schulz & von Raumer (1993); Point noir: éclogite du Lac Cornu Liégeois & Duchesne (1981); Rectangle: Salanfe, Chiaradia (1993), voir Fig. 3.04 ; losange: 1731; carré: 1871; H: point triple des silicates d'alumine d'après Holdaway (1971).

Evolution through time

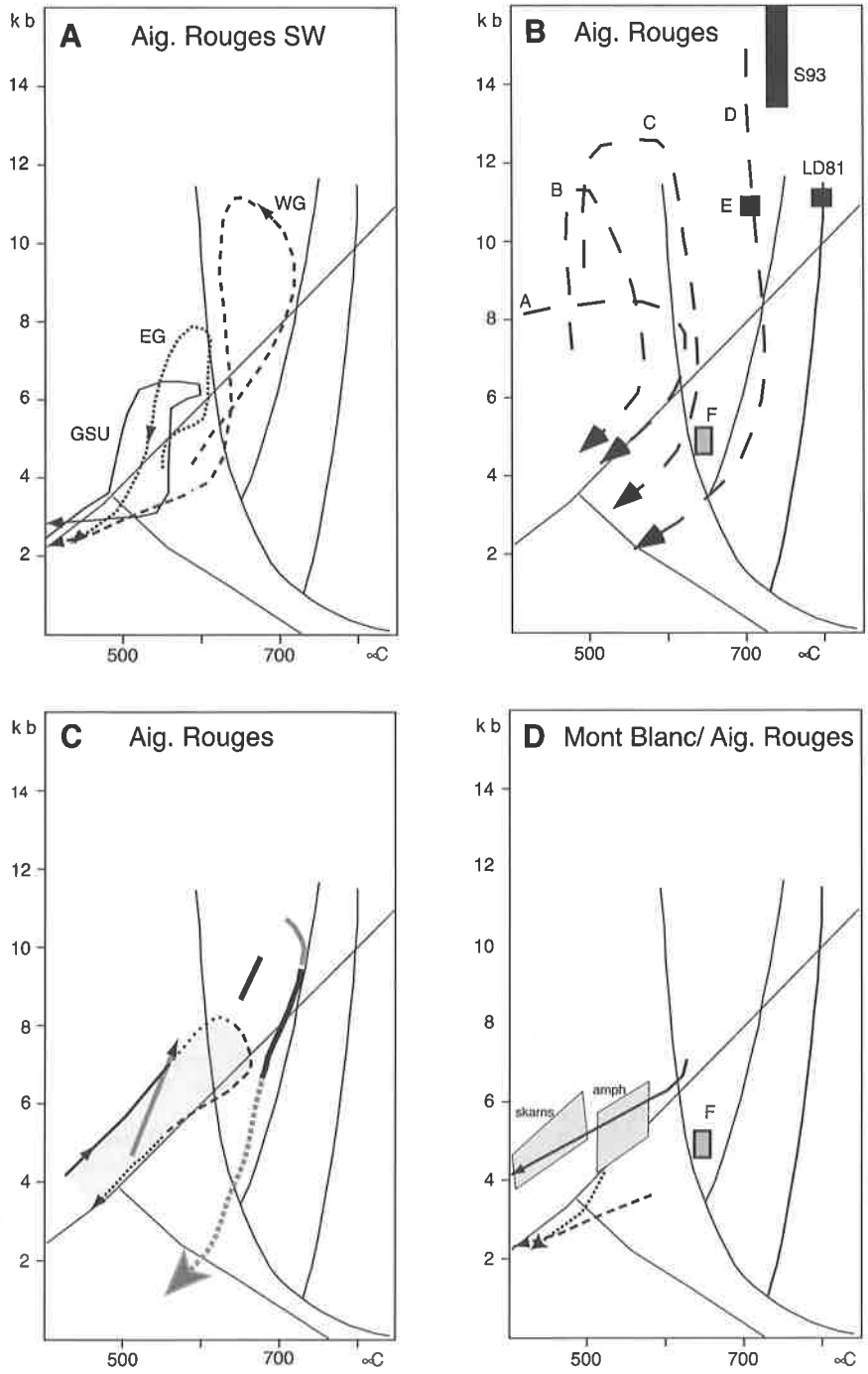

As the eclogite protolith in Lac Cornu has been dated at 453 +3/-2 Ma (U-Pb zircon, Paquette et al, 1989), we assume that the kyanite-bearing parageneses preceded the high-temperature phase without major cooling in-between, thus representing a Variscan evolution. Although this assumption has to be verified through precise dating, P-T paths have been established from mineral assemblages of various lithologies (**Fig. 3.08**). They point to contrasting metamorphic histories, with both counterclockwise (south of the Aiguilles Rouges, Dobmeier, 1998, Fig. **3.08A**) and clockwise (central part of the Aiguilles Rouges, Joye 1989, (**Fig. 3.08C**); Schulz & Von Raumer, 1993; **Fig. 3.08B**) paths.

For the southwestern part of the Aiguilles Rouges massif, Dobmeier (1996) derived a two-stage model, beginning with Visean rifting of older crust, with subsequent compression and nappe transport, leading to the prograde branches of the p-t-paths (**Fig. 3.08A**). The general shortening ended before the Upper Carboniferous, when large-scale strike-slip was accompanied by decompression and subsequent cooling of all units. In contrast, the central part of the Aiguilles Rouges seems to represent distinct parts of a nappe pile (**Fig. 3.08B**, paths A-C) which, as a consequence of their different initial crustal levels, followed different heating and decompression paths, where former eclogites (**Fig. 3.08B**, path D) follow an isothermic decompression path, when joining up the other crustal units. The position of the leucosomes associated with the Lac Cornu eclogites is reported on the isothermal decompression path deduced for the central part of the Aiguilles Rouges. The Mont Blanc and Aiguilles Rouges areas experienced contrasting late Variscan evolutions. Marshall et al. (1997) proposed a Variscan P-T-t cooling path for the northeastern part of the Mont Blanc massif, which differs by about 2 Kb from those depicted from the Aiguilles Rouges areas (**Fig. 3.08D**) which may indicate different uplift-erosion histories for both massifs.

Fig. 3.08
Pressure-temperature evolution in the Mont-Blanc and Aiguilles-Rouges areas during the Variscan events. Reaction curves: Al-silicate stability fields after Holdaway (1971); solidus of granites and corresponding dehydration melting curves after Thompson (1990).
A: Variscan P-T evolution in the southwestern parts of the Aiguilles Rouges massif (St. Gervais - Les Houches area; Dobmeier, 1996, 1998); EG – Eastern Gneiss unit,WG – Western Gneiss unit, GSU: Greenstone unit (see Fig. 2.01).
B: Variscan P-T evolution of the central part of the Aiguilles Rouges massif (Val Bérard area, Schulz and von Raumer, 1993): Paths A, B, C: p-t-paths of garnet-bearing gneisses; D: Retrograded eclogites: LD81- Liégeois and Duchesne (1981); S93: Schulz and von Raumer (1993); E: Ky-bearing tonalitic melts from the Lac Cornu area (see Fig. 3.07, von Raumer et al., 1996); F: formation of W-Au-skarns, and formation of leucogranites, ± 300Ma (Salanfe area; Fig. 3.05, Chiaradia, 1993).
C: Variscan P-T evolution of the central part of the Aiguilles Rouges massif after Joye (1989). Thin line around the grey field: prograde and retrograde p-t- paths estimated from garnet-bearing gneisses, prograde evolution during deformation D1, retrograde evolution during deformation D2. Thick lines: prograde and retrograde evolution of amphibolites.
D: Late Variscan evolution in the Mont-Blanc and Aiguilles-Rouges areas. Arrow and fields of skarns and amphibolites (amph): Late Variscan P-T-path after Marshall et al. (1997) in the north-eastern Mont-Blanc area. Dashed and stippled arrows: p-t estimations after Dobmeier (1996) for the southwestern part of the Aiguilles Rouges massif, paths EG,WG (see Fig. 3.08A). F: see Fig. 3.08B

Evolution pression-température (P-T) varisque dans les massifs des Aiguilles Rouges et du Mont Blanc. Stabilité des silicates d'alumine d'après Holdaway (1971); solidus des granites et des courbes de fusion par déhydratation d'après Thompson (1990).
***A**: Evolution P-T dans la région St.Gervais – Les Houches d'après Dobmeier (1996, 1998) EG – Eastern Gneiss unit, WG – Western Gneiss unit, GSU: Greenstone unit (voir Fig. 2.01).*
***B**: Evolution P-T de la partie centrale des Aiguilles Rouges (Val Bérard, Schulz & von Raumer, 1993): Chemins A, B, C: Chemins P-T-de gneiss à grenat; D: Chemin P-T d'eclogites retrogrades: LD81- Liégois et Duchesne (1981); S93: Schulz et von Raumer (1993); E: Métatonalites à disthène de la region du Lac Cornu (voir Fig. 3.07, von Raumer et al., 1996); F: formation des skarns à W-Au et de leucogranites, ± 300Ma (Salanfe area; Fig. 3.05, Chiaradia, 1993).*
***C**: Evolution P-T de la partie centrale des Aiguilles Rouges d'après Joye (1989). Lignes fines autour du champs gris: chemins P-T prograde et rétrograde des gneiss à grenat; évolution prograde pendant la déformation D1, évolution rétrograde pendant la déformation D2. Lignes épaisses: évolution prograde et rétrograde des amphibolites.*
***D**: Evolution tardi-varisque dans les massifs du Mont-Blanc et des Aiguilles-Rouges. Flèche et champs des skarns et amphibolites (amph): Evolution P-T tardi-Varisque d'après Marshall et al. (1997) dans la partie nord-est du massif du Mont-Blanc. Flèches à trait interrompu et pointillés: estimations P-T d'après Dobmeier (1996) pour le domaine St.Gervais – les Houches des Aiguilles Rouges, chemins P-T EG,WG (voir Fig. 3.08A). F: voir Fig. 3.08B.*

Chapter III.2

Deformation of the polymetamorphic basement

Two major periods of deformation have to be distinguished in the polymetamorphic basement of both massifs. The most important is related to the Variscan high-grade metamorphic evolution, which blurred the inferred structures linked to earlier events (e.g. intrusion of Ordovician granitoids). The second period of deformation is Alpine; the related structures are often discrete at the outcrop scale, as they appear as microstructures or fracture patterns. They are more evident in the Mesozoic cover.

III 2.1 Variscan structures

So far, only few structural data have been published on the polymetamorphic basement of the southwestern and central parts of the Aiguilles Rouges Massif (Schulz and von Raumer 1993; Dobmeier 1996). The many unpublished data (partly from unpublished theses, e.g. Joye 1989, Chiaradia 1993, Wirsing 1997, Fracheboud 1997, Marquis 1997), collected in the high-grade metamorphic domains of both massifs, are discussed here in some more detail. The different regions of the polymetamorphic basement are dominated by pervasive, subvertical foliations in N-S to NE-SW direction (mostly a composite set of superposed foliations S_2/S_3) appearing as axial plane in large-scale folds (**Fig. 3.09, Photo 3.14).** Structures resulted from deformation of a highly plastic environment. Early fold-axes (F_1, F_2) and kyanite-bearing mylonites containing sheath-folds (Joye 1989) are refolded by sub-vertical F_3-folds, accompanied by growth of sillimanite, and a more recent deformation (F_4) produced subhorizontal folds in NE-SW direction. Predominance of F_3 fold-axes has been demonstrated in the Emosson and Salanfe areas (von Raumer 1984, Chiaradia 1993, see geological maps: **annexes IV,V,IX**), where Ordovician orthogneisses and metagreywackes appear as vertical large-scale folds (**Photo 2.03**). In some cases a complex pattern of superposed fold generations is preserved in migmatites and micaschists (**Photos 3.07, 3.23**). In most areas the open F_3 folds represent different hierarchies of parasitic folds (**Photo 3.21**), and quartz segregations record earlier fold generations (**Photos 3.22, 3.23**). The corresponding axial plane is locally underlined by a biotite-foliation, which generate microlithons (**Photo 3.23, 3.24**). Deformation style changes in rocks submitted to rather high stretching. Development of sheath-fold has been observed in Emaney (Joye, 1989) and in the Vieux Emosson area (**Photos 3.25, 3.26**), where quartzitic layers embedded in micaschists are submitted to extreme buckling and stretching.

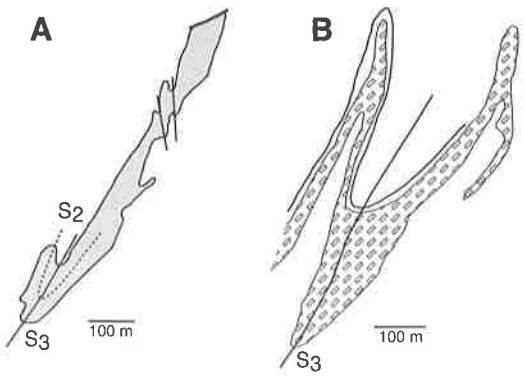

Fig. 3.09
Major D3 folds observed in micaschists at Lac Vert (A) (annex VI and Fig. 5.05) and in augengneiss at Salanfe (B) areas (annex IX, Fig. 5.12).
Plis D3 observés dans les micaschistes du Lac Vert (A) (annexe VI et Fig. 5.05) et dans les gneiss oeillés de Salanfe (B) (annexe IX, Fig. 5.12).

Photo 3.21
D3 folds in high grade metamorphic gneisses from the Vieux Emosson area. P*lis D3 observés dans la région du Vieux Emosson.*

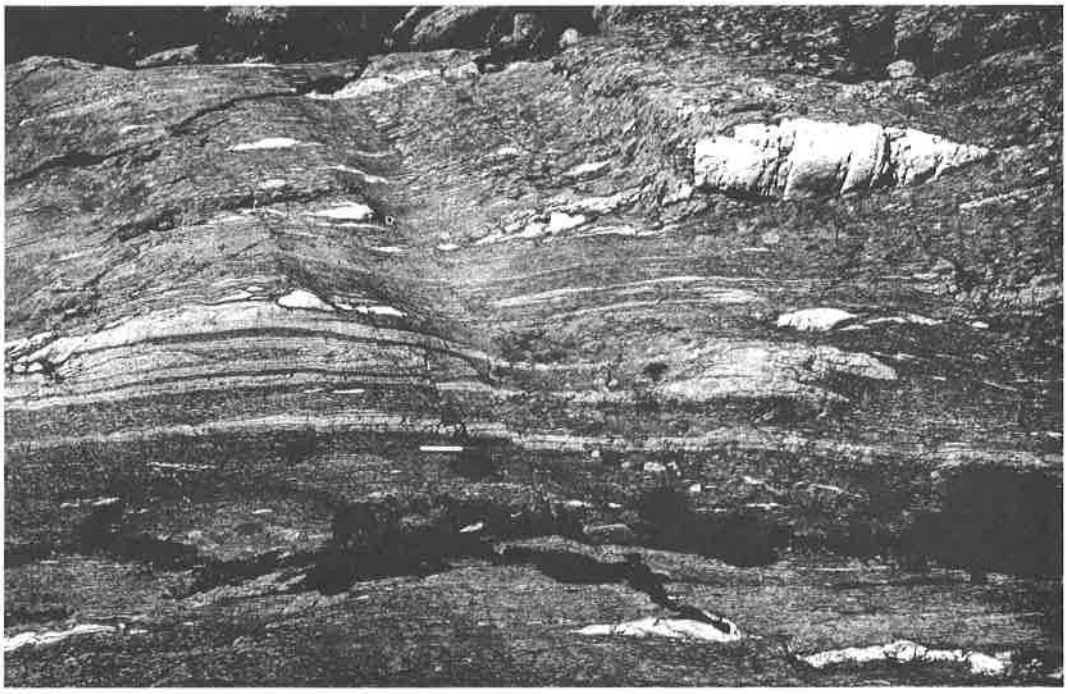

Photo 3.22
Superposed fold generations in metasedimentary gneisses with quartz-nodules, Fontanabran region, eastern part of Emosson area. (Coord. CH: 560.510/103.460). *Plis superposés dans des gneiss métasédimentaires avec veines de quartz, environs de Fontanabran, domaine oriental du Lac Emosson. (Coord. CH: 560.510/ 103.460)*

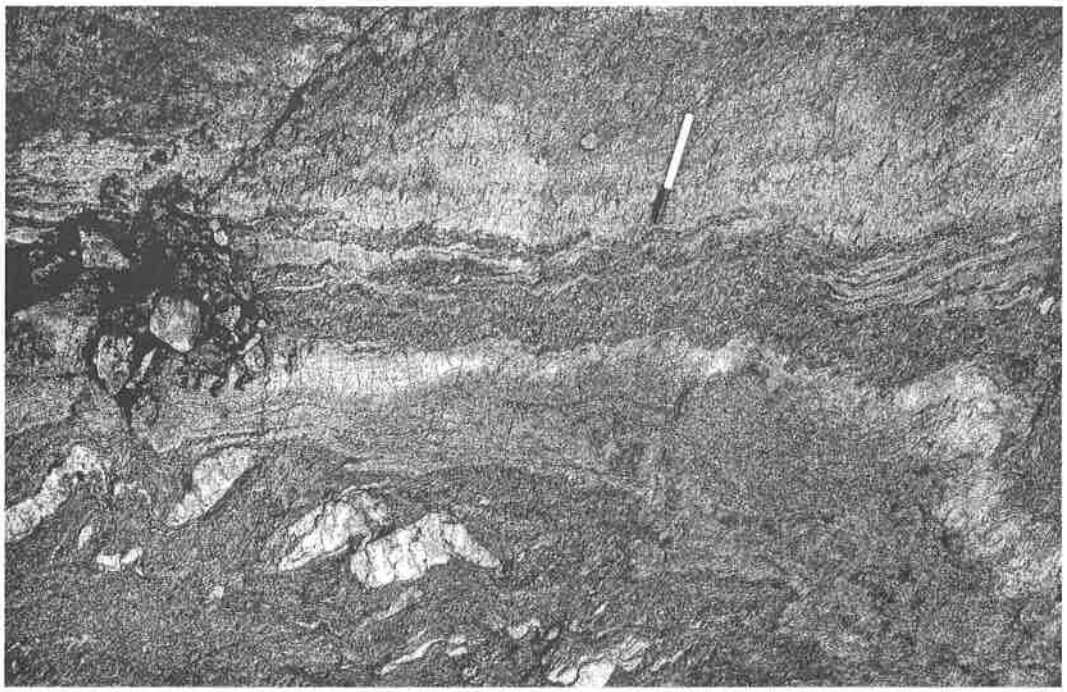

Photo 3.23
Superposed folds in micaschists from the Vieux Emosson/Lac Vert area, foliation S3 in the axial plane marked by biotite. (Coord. CH: 557.670/ 99.770). *Plissement superposé dans des micaschistes du Vieux Emosson/Lac Vert, foliation S3 du plan axial marquée par la biotite. (Coord. CH: 557.670/ 99.770)*

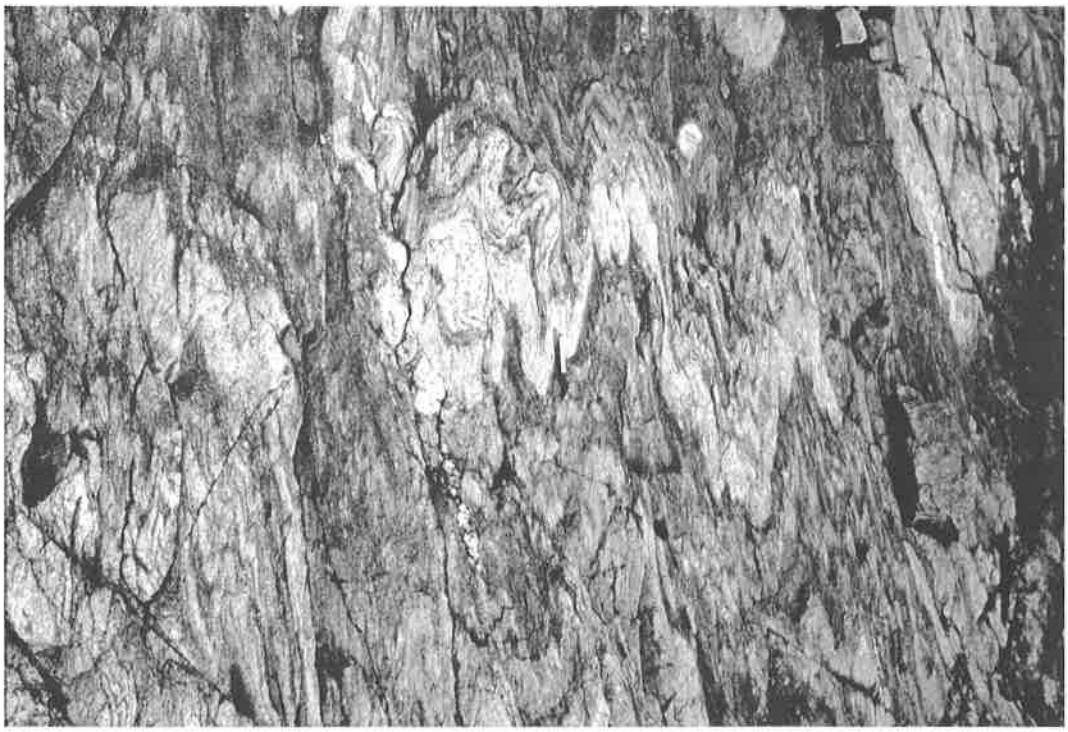

Photo 3.24
Strongly expressed fracture cleavage with formation of microlithons in S3 from metagreywackes in the Vieux Emosson/Lac Vert area. (Coord. CH: 557.800/99.810). *Microlithons marqués par la schistosité S3 dans des métagrauwackes du Vieux Emosson/Lac Vert. (Coord. CH: 557.800/99.810).*

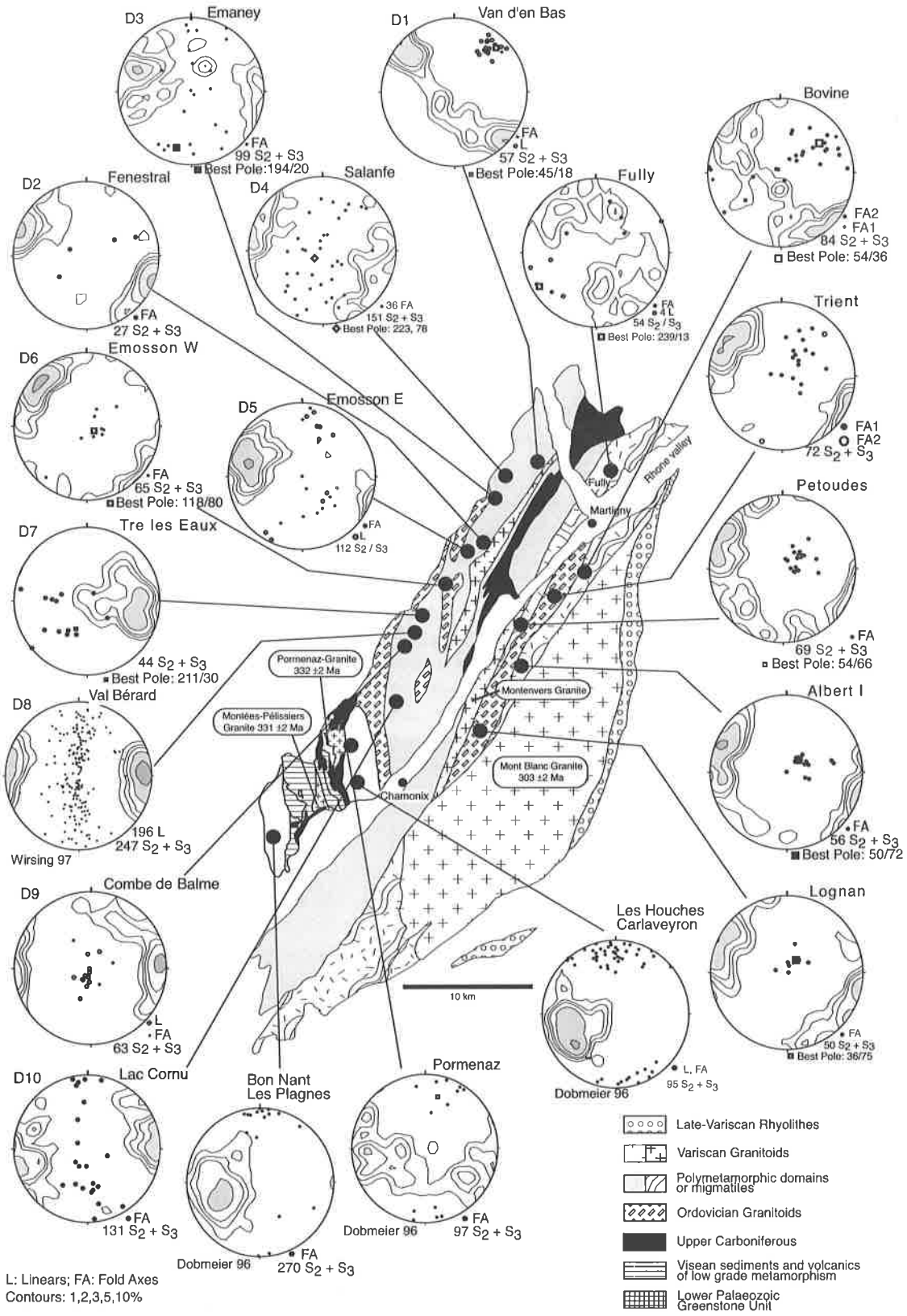

Fig. 3.10
Distribution of Late Variscan structures in the polymetamorphic basement of Aiguilles Rouges and Mont Blanc. Statistics of dominant metamorphic, composite surfaces S_2/S_3, lineation and fold axes. (Numbered diagrams: additional data in Annex III). *Distribution des structures tardi-varisques dans le socle polymétamorphique des Aiguilles Rouges et du Mont Blanc. Statistique de l'orientation des plans de foliation composites S_2/S_3, linéations et axes de plis (diagrammes numérotés: données supplémentaires dans l'annexe III)*

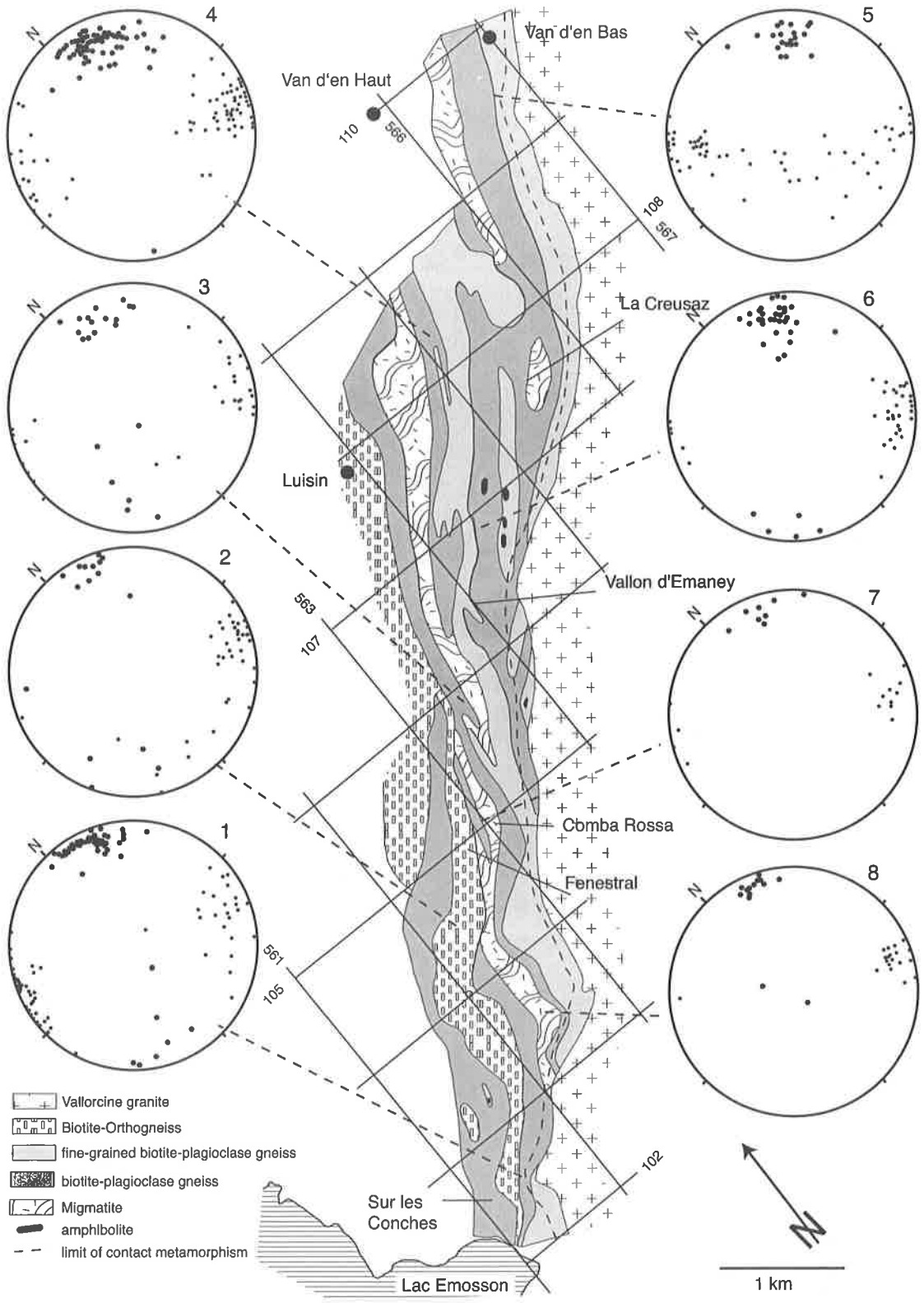

Fig. 3.11
Geology of the mylonite zone and adjacent area between Van d'en Bas and Emosson (geological sketch map with main lithologies after Joye 1989). Orientation statistics of foliation planes (S_2/S_3, small points) and lineation (dots) for specific areas. *Géologie de la zone à mylonites entre Van d'en Bas et Emosson (d'après l'esquisse géologique des unités lithologiques de Joye 1989). Statistique d'orientation des surfaces de foliation (S_2/S_3, petits points) et structures linéaires (grands points) dans des domaines choisis.*

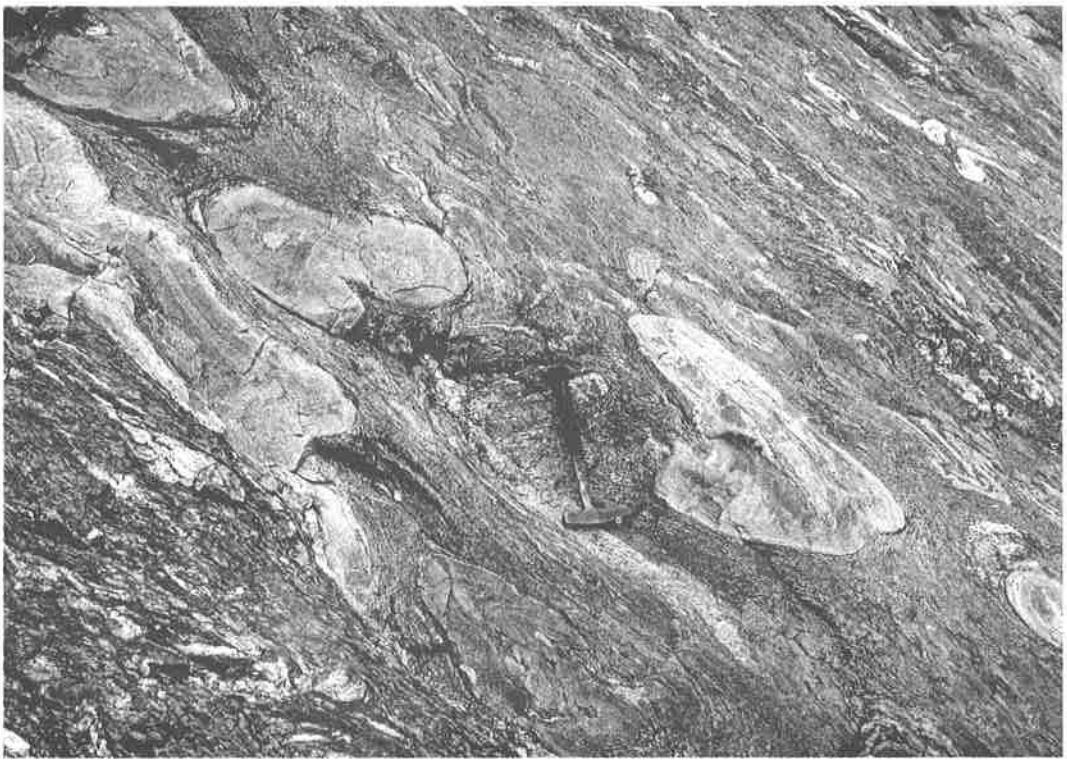

Photo 3.25
Extreme buckling or sheath folds of metaquartzites among micaschists, Lav Vert/Vieux Emosson area, Aiguilles Rouges, see detail Photo **3.26**. (Coord. CH: 557.870/100.150).
Interférence extrême de plis ou plis en fourreau de métaquartzites au sein de micaschistes, Lac Vert/Vieux Emosson, Aiguilles Rouges, voir photo détaillée ***3.26****. (Coord. CH: 557.870/100.150).*

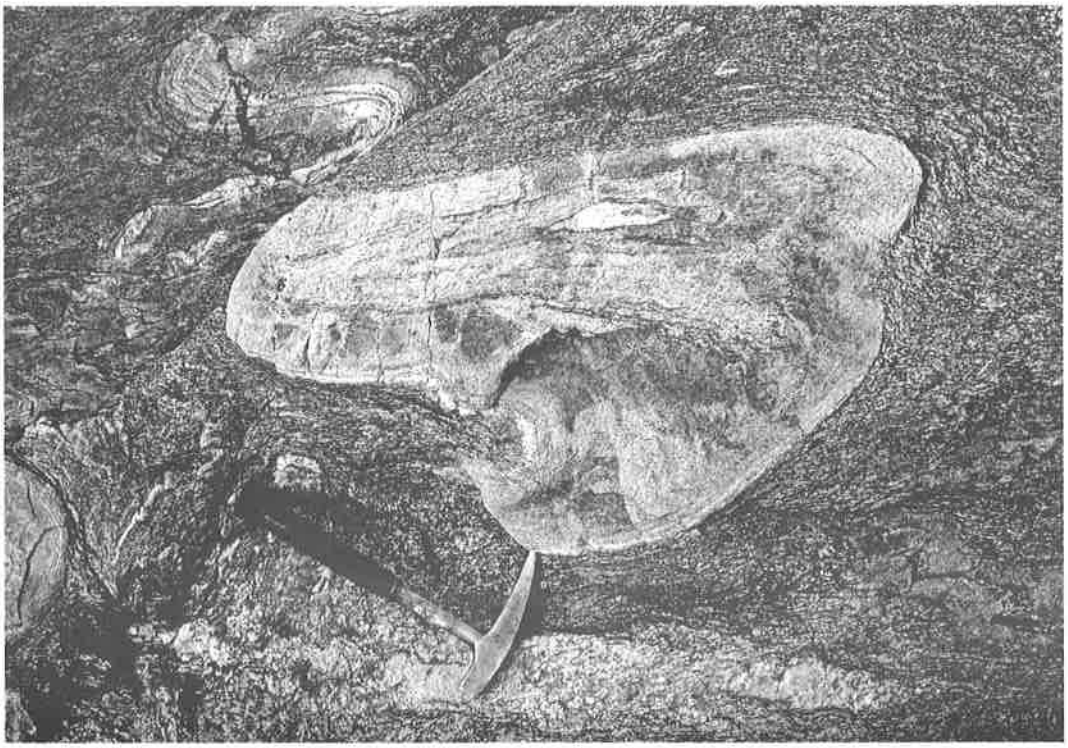

Photo 3.26
Detail of Photo 3.25 with isoclinal folding (quartz vein) overprinted by a strongly stretched, cigar-shaped vertical F3 fold. *Détail de la photo 3.25 avec micaschistes plissés isoclinalement (veine de quartz), puis fortement étirés par un pli F3 vertical en forme de cigare.*

The synoptic diagrams (pervasive foliation planes S_2+S_3, fold axes; additional data: **Annex III**) show a rather homogeneous distribution of the fabrics, where several domains of homogeneity can be distinguished (**Fig. 3.10**). In the central Aiguilles-Rouges massif (Lac Cornu, Val Bérard), the generally steep pervasive composite foliation (S_2-S_3) trends N-S. The plunge of associated fold-axes, which are located on a N-S directed great circle, varies considerably between subhorizontal and subvertical. Several domains (Combe de Balme, Emosson W, Petoudes, Albert I, Lognan) are dominated by subvertical, N-S to NE-SW trending composite foliation planes, deformed by tight to isoclinal folds of various magnitude (cm to km-scale) with steeply plunging fold axes. The corresponding diagrams reveal poles of foliation planes on horizontal great circles, and the corresponding vertical fold axes and linear structures plot on the π-pole of these great circles. A third type of distribution pattern occurs in the neighborhood of granite bodies (Pormenaz, Trient, Van d'en Bas), where a late set of fold axes, dipping subhorizonally to the NE, probably formed during the emplacement of these plutons (e.g. **Photo 3.27, Fig. 3.12**).

Mylonites represent another major tectonic feature in the Aiguilles Rouges and Mont Blanc massifs. Besides the famous Miéville ultramylonite affecting the southeastern side of the Vallorcine granite, another 500 m wide mylonite zone is limiting the same granite along its northwestern side (**Fig.3.11**). There, most lithologies have been strongly and rather homogeneously deformed, often into very fine-grained material, which locally shows subhorizontal fold axes (see **Photo 3.27**). Drag-folds with strongly stretched plagioclase-blasts parallel to the fold-axes (**Photo 3.28**) highlight a plastic behavior in the entire shear-zone. A difference of timing appears, when comparing lineations from mylonites and migmatites (**Fig. 3.13**), as lineations of stretched plagioclases occupy mainly subvertical directions in the mylonites, whereas NW-dipping lineations and folds are common to mylonites and migmatites.

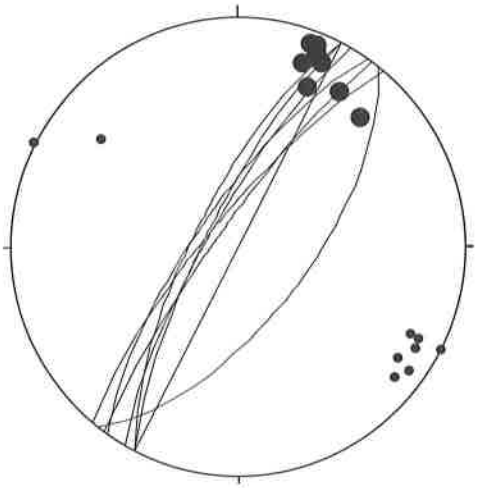

Fig. 3.12
Subvertical foliation planes (poles and great circles) and horizontal fold axes (dots, see **Photo 3.27**) from the mylonite zone (compare with **Fig. 3.11**, Joye 1989).
Diagramme des foliations subverticales (pôles de projection et grands cercles) et axes de plis horizontaux (grands points, voir exemple Photo 3.27) de la zone à mylonites (à comparer avec Fig. 3.11, Joye 1989).

Photo 3.27
Subhorizontal fold (F3 or F4) overprinting isoclinally folded mylonites near the contact of the Vallorcine granite, Van d'en Bas.
Pli à axe subhorizontal (F3 ou F4) affectant des mylonites plissées isoclinalement, voisinage du contact du granite de Vallorcine, Van d'en Bas.

Original lithologies are difficult to identify; in the northeastern part (Van d'en Bas – Emosson area), they consist in biotite-orthogneisses, migmatites and two types of biotite-plagioclase paragneisses, the latter representing different types of mylonitic rocks in this zone (**Fig. 3.11**) (Joye, 1989). The biotite orthogneisses (**Fig. 3.11**) might partly represent former Ordovician granitoids, although syntectonic granitoids of Variscan age are not excluded (e.g. Gneiss des Perrons, dominating the western dam site, and the granitoid gneisses exposed in the northern prolongation at Dt. de Fenestral). The migmatites are still undated; they could be related to the 320 Ma-old Variscan thermal event, or be older. In the Mont-Blanc massif, mylonites transformed granitoid veins into strongly stretched linear gneisses with porphyroclasts of former garnet or kyanite(?) (**Photo 3.29**).

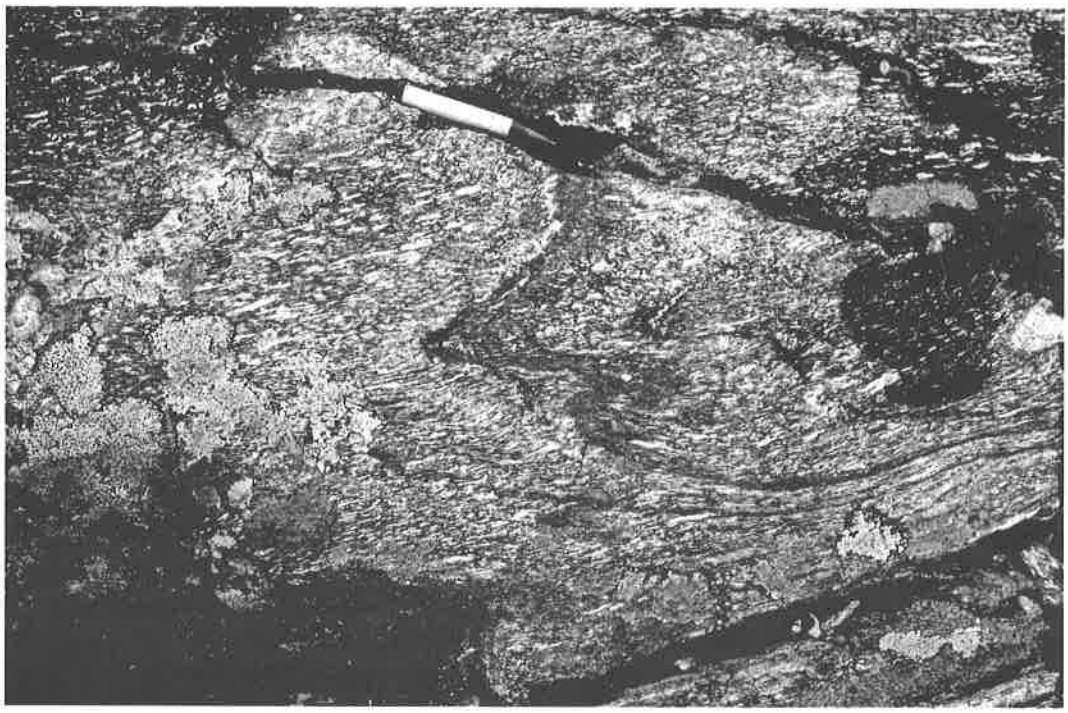

Photo 3.28
Drag-fold in mylonitic gneisses, axial plane expressed by cylindrical stretched plagioclase blasts, Lac Blanc area, Aiguilles Rouges massif. *Plis de cisaillement dans des gneiss mylonitiques avec plan axial marqué par des plagioclases fortement étirés. Environs du Lac Blanc, Aiguilles Rouges.*

The observed structures can be correlated with the Variscan metamorphic and magmatic evolution. Precise age data define a sequence of thermal events, where the oldest granitoids (Pormenaz, Montées Pélissiers) yield ages of 332-331 Ma (U/Pb Zr, Bussy et al. 2000). Structural criteria indicate that the sheet-like Montées-Pélissiers granite intruded into a transcurrent N-S directed vertical shear-zone after the formation of a tight upright synform during strong dextral transpression (Dobmeier 1996, 1998). As shown in the preceding chapter, partial melting affected most of the early Palaeozoic lithologies; leucosomes were dated at 320±1 Ma and 317 ±2 Ma in the Aiguilles Rouges and the Mont Blanc massifs, respectively (U/Pb on monazite, Bussy et al. 2000; Bussy and von Raumer 1994). These leucosomes were plastically deformed by the F3-folds (with vertical axes). Sheet-like intrusion of peraluminous granitic melts occurred at 307 Ma (Fully, Vallorcine, Montenvers; Bussy et al. 2000), contemporaneously to the beginning of coarse volcano-detrital sedimentation within the Salvan-Dorénaz trough (Capuzzo & Bussy, 2000). These events occurred in a context of fast exhumation/erosion, controlled by crustal-scale transcurrent faults, delimiting horst and graben structures.

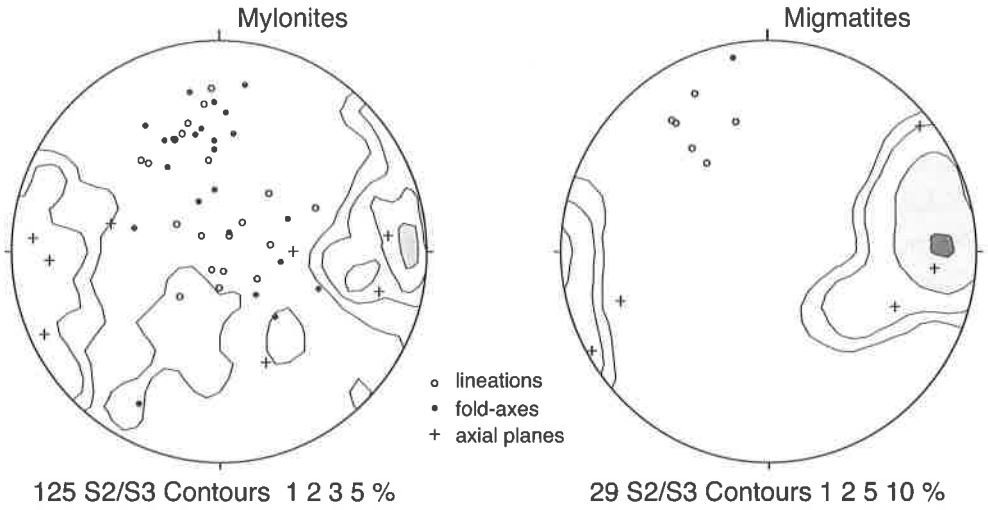

Fig. 3.13
Structural data from the Chéserys region (additional information to Fig. 3.10 + 3.11). "Blastomylonite"-type rocks and migmatites share NW-dipping folds and lineations, whereas mylonites also contain steeply dipping lineations of spindle-type plagioclases.
Structures dans la région de Chéserys (en complément de la figure 3.10 + 3.11). Des roches de type "blasto-mylonite" et les migmatites également ont des axes de plis et des linéations de direction NW communs, tandis que les mylonites présentent des linéations subverticales formées par des plagioclases étirés.

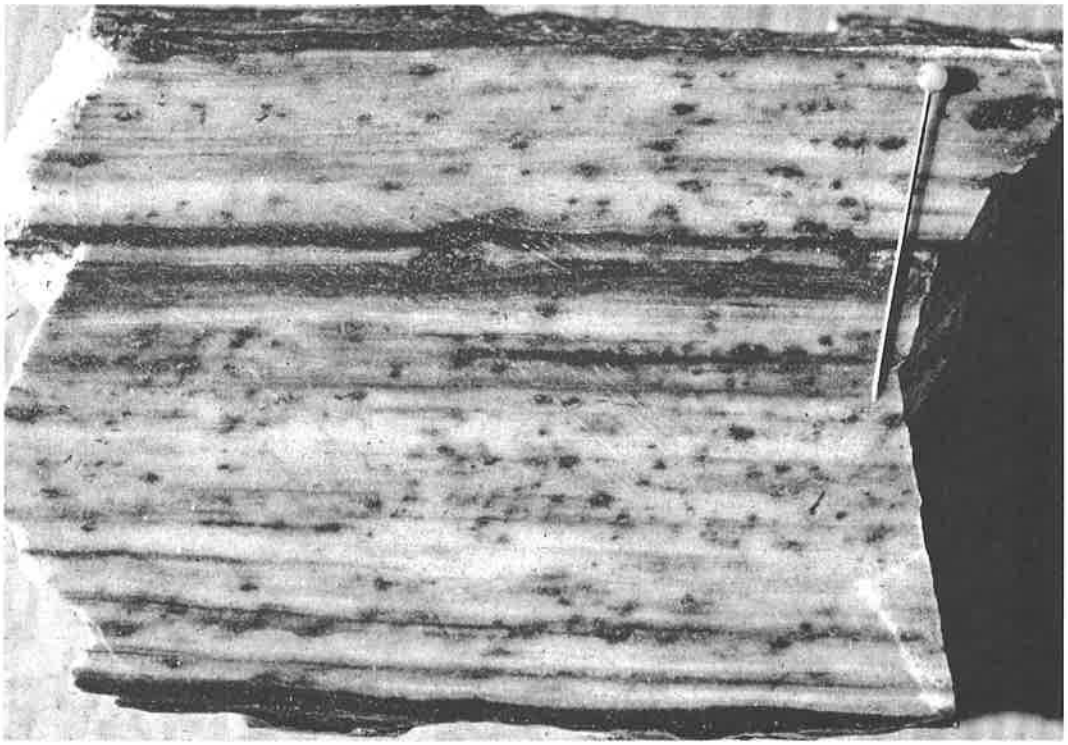

Photo 3.29
Mylonite with pseudomorphs of chlorite after garnet, Trient area, Mont Blanc massif.
Cord. CH: 567.965/98.110; 2480m. *Mylonite dans des gneiss granitoïdes avec pseudomorphose de grenat en chlorite, Val de Trient, massif du Mont Blanc. Cord. CH: 567.965/98.110; 2480m.*

In conclusion, most of the Variscan metamorphic and structural evolution occurred during a rather short time span of about 25 Ma (von Raumer et al. 2003), which can be summarized as follows. An inferred early stage of thrusting buried the lithologies and induced a prograde metamorphism attaining high amphibolite facies conditions (**Fig. 3.08**). Later on, the tectonic regime switched to transpressional, then to transtensional conditions (gravitational collapse?), which favored decompression, exhumation and erosion of the rocks, i.e. a retrograde metamorphic evolution (Joye 1989, Dobmeier 1996, 1998, Bussy et al., 2000). Early fold axes have been rotated into the main direction of stretching with formation of coaxial sheeth-folds and a steeply dipping composite S_2-S_3 pervasive foliation with parallelization of all former structures. After the end of the magmatic evolution (Mont Blanc granite at 303 Ma), erosion continued (last sedimentary record in the Salvan-Dorénaz basin at 295 Ma, Capuzzo & Bussy, 2000) until complete peneplanation of the Variscan relief. Permian(?) rubefaction is still recognizable in Emosson or Val Bérard, as well as low temperature brittle structures and strike-slip faults delimiting tectonized blocks, many of which having been reworked during the Alpine orogenesis.

III 2.2 Alpine structures

Although Alpine metamorphism and structures are omnipresent in the entire region, they will not be subject of detailed discussion in this volume. Alpine deformation is well examplified by the strongly north dipping Triassic cover near Mex (in the Rhone valley; but also at Fontanabran, Emosson region; Col Salenton, Val Bérard) and its south dipping counterparts in the Martigny region. Together with the horizontal sediment layers at higher levels (e.g. Col de la Terrasse or Mt. Oreb (Swiss-French border; and Aiguilles de Belvédère at 2600m), they represent a huge dome structure, which is well illustrated in the Alpine cross sections of this region (Escher et al., 1995; Steck et al. 2001; **Fig. 1.03**).

Besides detailed investigations in the SW part of the Aiguilles Rouges (Gourlay 1986; Dobmeier, 1996), local observations were collected at some points in the central part of the Aiguilles Rouges (Gourlay 1986, Chamonix zone; Fracheboud 1997, Val Bérard; Marquis 1997, Tré-les-Eaux), but few statistical work on Alpine deformation has been published. In the Aiguilles Rouges basement, Alpine deformation is expressed as discrete fracture patterns or, at microscopic scale, as a faint fracture cleavage, all developed in very low grade metamorphic conditions.

In the Aiguilles Rouges area, horizontal, NW-SE oriented fold-axes of Alpine age can be observed in the entire polymetamorphic basement, such as in Ordovician orthogneisses near the thrust plane of the Morcles Nappe (**Photo 2.10**). Other examples were documented from the interface basement/Triassic cover at Col de la Terrasse and Mt. Oreb (Fracheboud, 1997; Marquis, 1997; see **Photo 3.30**).

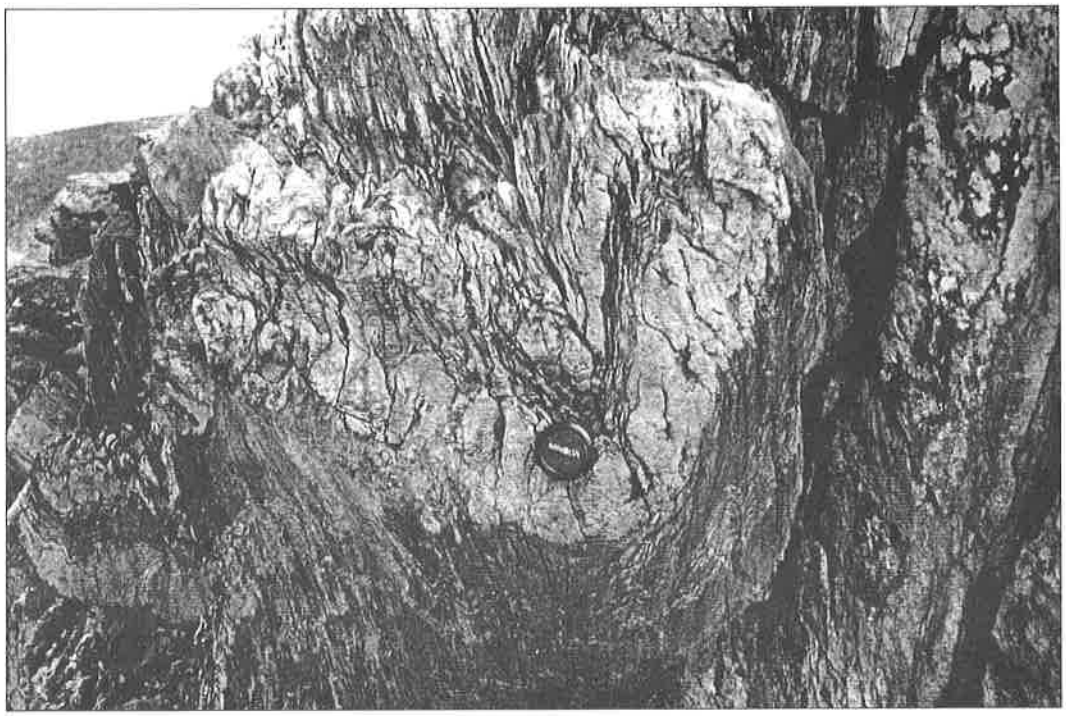

Photo 3.30
Subhorizontal cylindrical fold of Alpine age in Triassic quartzites and metapelites with well expressed pressure-solution planes, photo from Fracheboud (1997), Mt. Oreb, Aiguilles Rouges (Coord Fr.: 123.450/951.450).
Pli cylindrique à axe subhorizontal d'âge alpin dans les quartzites et métapélites du Trias, avec plan axial marqué par un phénomène de dissolution sous pression, Photo tirée de Fracheboud (1997), Mt. Oreb, Aiguilles Rouges (Coord Fr.: 123.450/951.450).

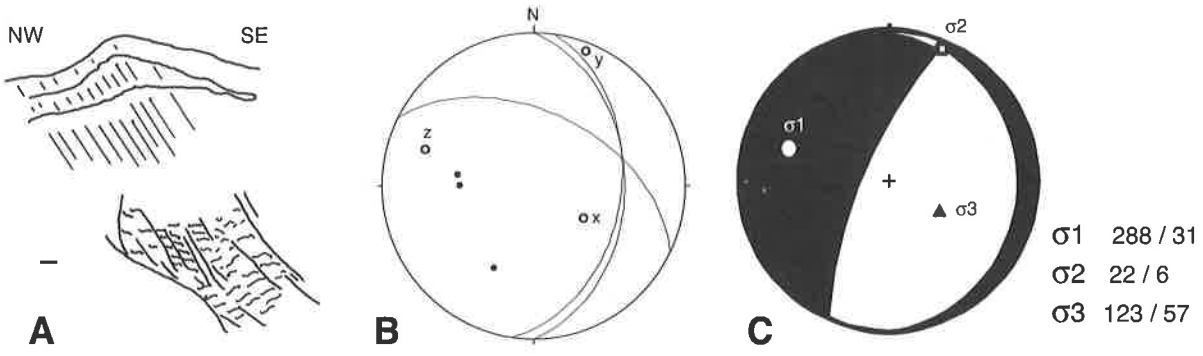

Fig. 3.14
Foliation of Alpine age in micaschists of the basement (Vieux Emosson, Aiguilles Rouges, coord. CH.: 558.505/100.050, see Photo 3.31). **A**: sketch of a NW-SE cross-section with foliation dipping towards SE and subhorizontal lithologies. Detail: coarse fracture cleavage (10-15 cm spacing) dipping to SE, with crenulated interspaces. **B**: Projection of fracture cleavage in an equal area projection, lower hemisphere (3 poles and great circles, and x,y,z coordinates from the deformation ellipsoid (see C). **C**: Statistics of 61 slicken-sides of Alpine age from the Emosson area, σ3 is dipping 123/57.
Foliation d'âge alpine dans les micaschistes (Vieux Emosson, Aiguilles Rouges, coord. CH: 558.505/100.050, à comparer avec photo 3.31). A: esquisse d'une section NW-SE avec des lithologies en position subhorizontale et une foliation avec pendage vers le SE. Détail: clivage de fracture grossiere (espacement 10-15 cm) avec un pendage vers le SE, avec crenulation. B: Projection du clivage de fracture dans la sphère inférieure du canevas Schmidt (3 pôles et grands cercles, et coordonnées x, y, z de l'ellipsoïde de déformation (voir C). C: statistique de distribution de 61 stries de miroirs de failles d'âge alpin de la région d'Emosson, s3 a une direction 123/57 .

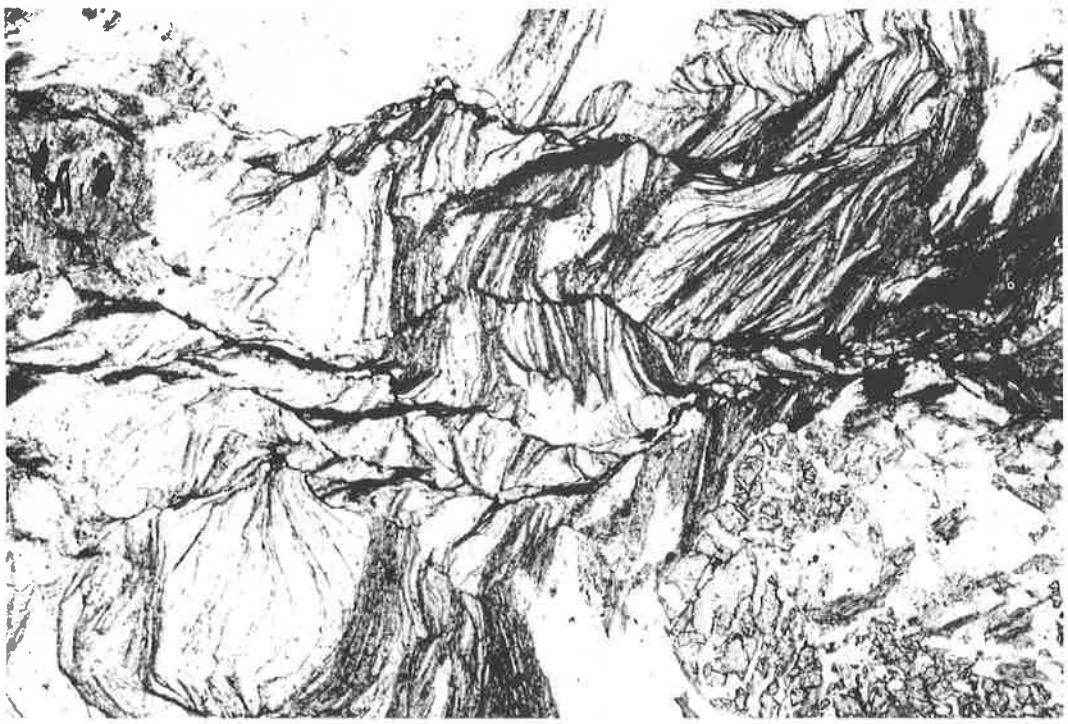

Photo 3.31
Microscopic view of alpine fracture cleavage from microlithons in micaschists (see Fig. 3.14A)
Vue microscopique de schistosité de fracture alpine dans des microlithons de micaschistes du socle (voir Fig. 3.14A)

In Emosson micaschists, a coarse fracture cleavage with 10 cm spacing is locally observed (**Fig. 3.14**), where microlithons are deformed by 1cm spaced kinks containing a microscopic foliation produced by pressure solution (**Photo 3.31**). Most evident are brittle structures like fractures with chlorite – quartz slicken-sides. A statistic plot for the Emosson region evidences a deformation ellipsoid with σ3 dipping 60° to the SE, which is related to the thrusting and general shortening induced by the Morcles Nappe emplacement (von Raumer, 1987). Comparable observations were made in the SW domain of the Aiguilles Rouges (Dobmeier, 1996). Microscopic observations are less evident; a foliation is well observed in the Aiguilles Rouges sedimentary cover of Carboniferous (e.g. **Photo 3.03**) and Triassic age, and folds in Triassic sediments show a strong axial cleavage (**Photo 3.30**).

In the Mont Blanc area, dominated by metamorphic conditions of low greenschist facies grade, deformation is expressed through a well marked foliation plane, distinct fracture patterns and quartz recrystallization.

The Alpine foliation plane carries in most cases a vertical stretching lineation. The progressive rotation of stretching direction is recorded in the basement and the Mesozoic cover (Gurlay 1986), corresponding to the general deformation plan drawn by Steck (1990).

A typical example of the vertical stretching lineation is observed in Late Carboniferous rhyolithes at the foot of the Mer de Glace glacier (Coord. Fr.: 954.280/115.840). Oriented sections parallel to the main foliation and lineation (x-y section) show the recristallization of former quartz phenocrysts, transformed into stretched aggregates of quartz grains. **Photo 3.32** shows a core-mantle structure, and the statistical orientation of quartz c-axes measured on a universal stage in a thin section oriented parallel to the foliation plane (orientation x-y, **Fig. 3.15**) shows three main maxima, one independent (coloured in black, **Fig. 3.16**), dipping about 10° to North, represented by the core crystals, plotted also in the pole-**figure 3.15**. Two symmetrical, more inclined maxima (coloured in gray in **Fig. 3.16**) represent the orientation of new grains recrystallised during dextral shear[1)].

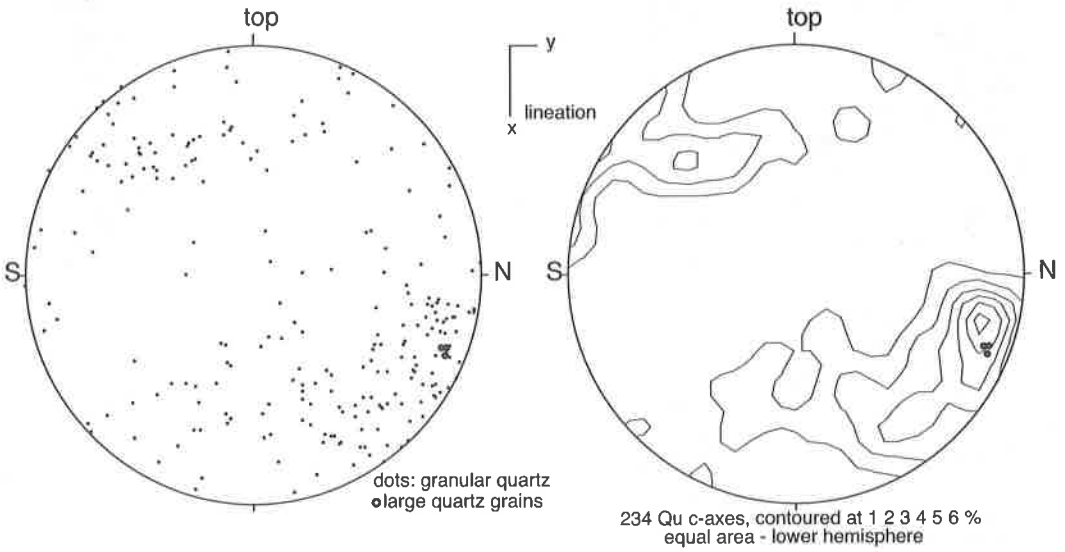

Fig. 3.15
Statistical plot of quartz c-axes in an equal area projection, lower hemisphere, and contour-lines. The black dots show the orientation of three large quartz-grains filling the central part of the elongated aggregate (compare **Photo 3.32** and **Fig. 3.16**).
*Distribution de pôles des axes c de grains de quartz dans une projection stéréographique avec conservation des surfaces, hémisphère inférieur, et contours de densité de distribution. 3 points noirs: orientation de 3 grains de quartz larges (Fig. 3.16) compsant le centre du aggrégat (**Photo 3.32, Fig. 3.16**).*

---

1) H. Stünitz and R.Heilbronner (Basel) are thanked for their constructive discussion of the structural patterns

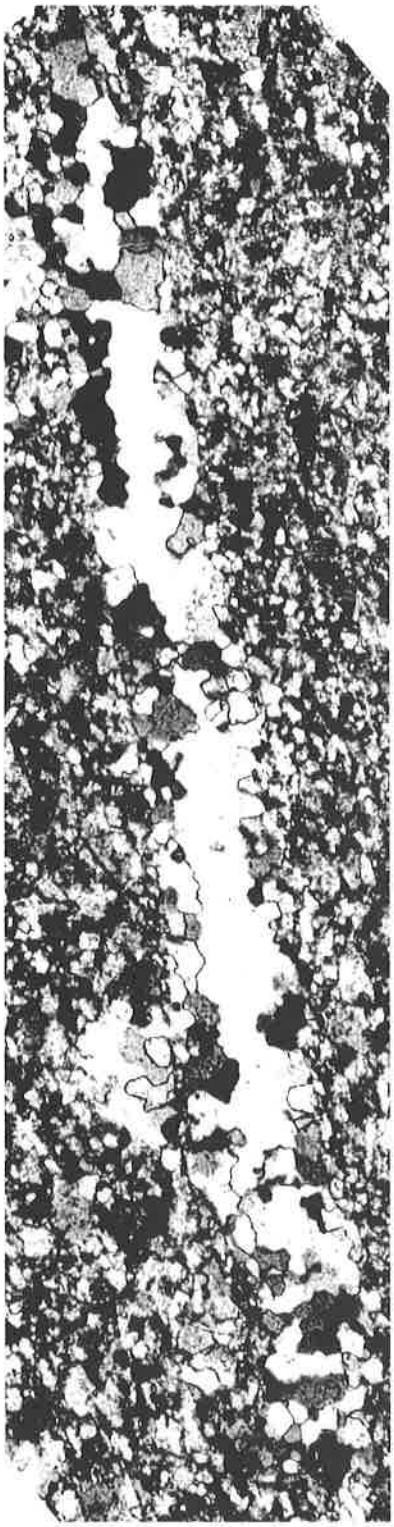

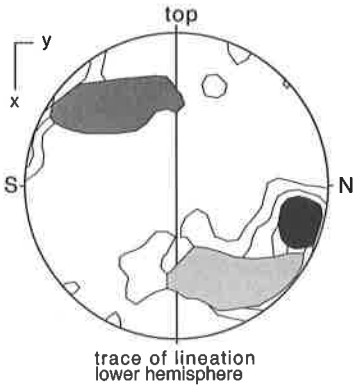

Fig. 3.16

Photo 3.32
Elongated quartz-aggregate with a core-mantle structure, (3mm length), recrystallisation of a former quartz phenocryst from a Carboniferous rhyolite in an Alpine stretching lineation. (Mont Blanc massif, Montenvers, Cord Fr.: 954.280/115.840, oriented thin section x-y). *Aggrégat de grains de quartz avec structure coeur-manteau, (longueur 3mm), resultant de la recristallisation d'un phénocristal rhyolithique dans une linéation d'étirement alpin. (Massif du Mont Blanc, Montenvers, Cord Fr.: 954.280/ 115.840, lame mince orientée x-y).*

Fig. 3.16
Orientation statistics of quartz c-axes in a recrystallised and stretched quartz aggregate, core-mantle structure (compare with Photo **3.32**). Black: older core-orientation of c-axes; grey: orientation of recristallised quartz grains during dextral shearing. *Statistique d'orientation d'axes C du quartz dans un aggrégat coeur-manteau de quartz recrystallisé et étiré (voir **Photo 3.32**). Noir: grains du coeur, plus anciens; gris: grains recristallisés pendant un cisaillement dextre.*

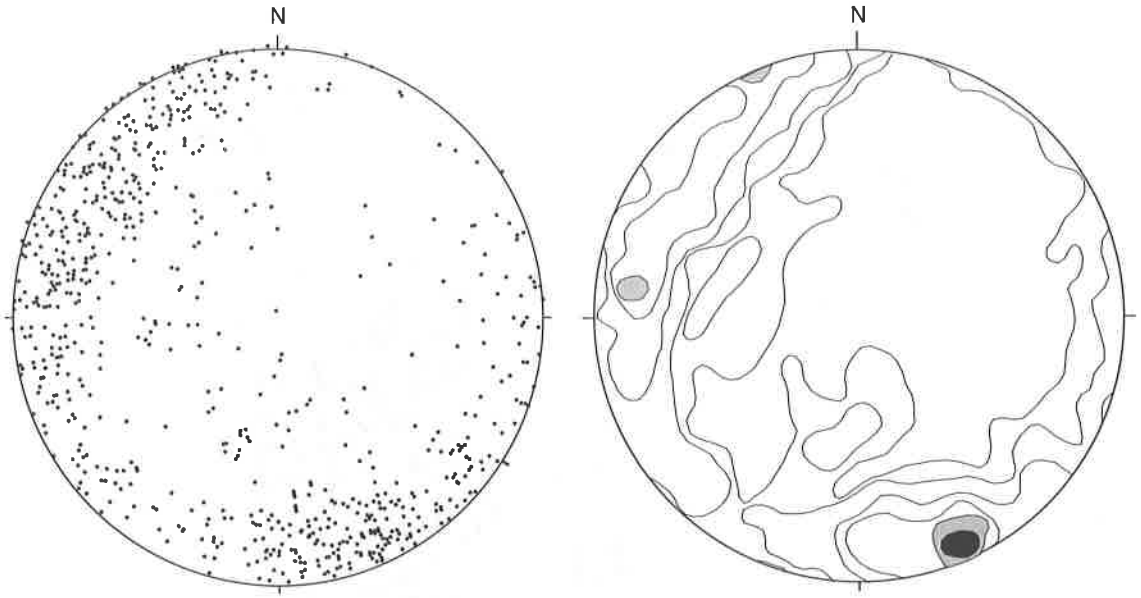

Fig. 3.17
Distribution of quartz c-axes in an aggregate of polygonal quartz replacing a former granitic quartz (compare with **Photo 3.33**). Projection of 733 quartz c-axes in a lower hemisphere, density counts: 1/2, 1, 2, 3, 4 (grey), 5 (black) %. *Distribution d'axes c de 733 grains d'un aggrégat de quartz polygonaux (voir **Photo 3.33**), remplaçant un ancien grain de quartz granitique. Densité de comptage: 1/2, 1, 2, 3, 4 (gris), 5 (noir) %.*

When applying the same procedure to polygonal quartz grains recrystallised during the Alpine greenschist facies overprint of the Mont Blanc granite (**Photo 3.32**), a different kind of pole figure is observed. Statistics of quartz c-axes in an elongated polygonal quartz-aggregate replacing a former drop-like quartz shows the distribution in well defined maxima (**Fig. 3.17**). The distribution analysis of optical c-axes (**Fig. 3.18**) shows a relic of clustering produced by small-angle relationships, indicating the presence of former larger subgrains. An ideal polygonal recristallisation would produce a completely random distribution of grains, oriented in certain maxima, comparable to the picture presented by **Photo 3.15**. Flattening of the quartz aggregate and pole-figures indicate relationship to the alpine foliation plane.

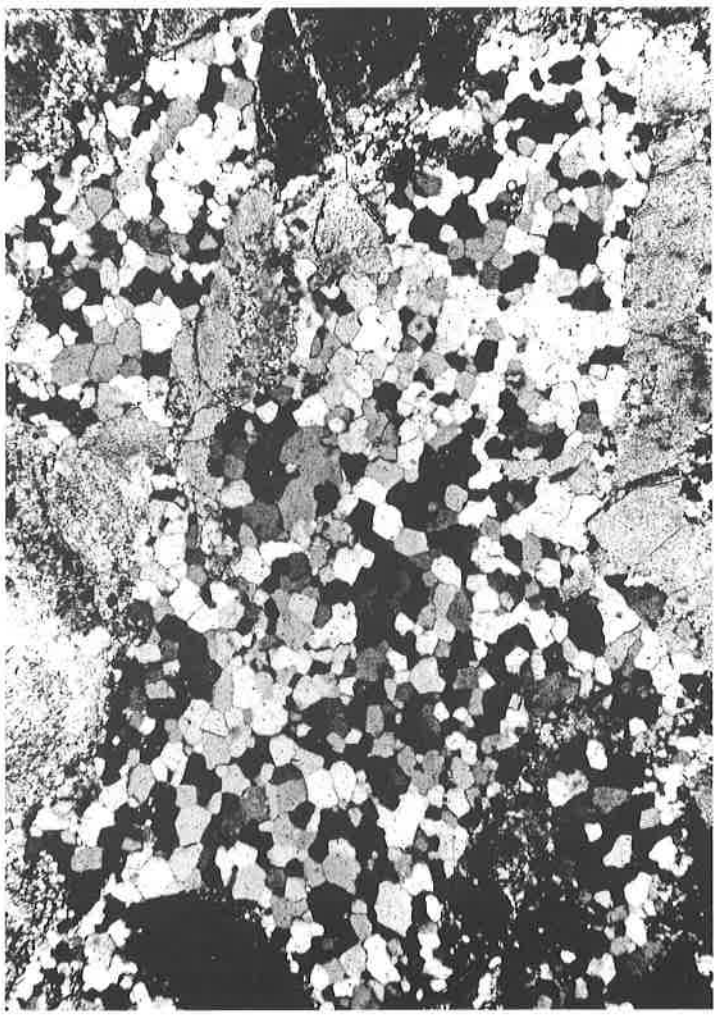

Photo 3.33
Elongated aggregate (length 1 cm) of polygonal quartz-grains from the Mont-Blanc granite (Coord. CH: 567.455/95.695).
Aggrégat de grains de quartz polygonaux allongé (longueur 1 cm) du granite du Mont Blanc (Coord. CH: 567.455/95.695).

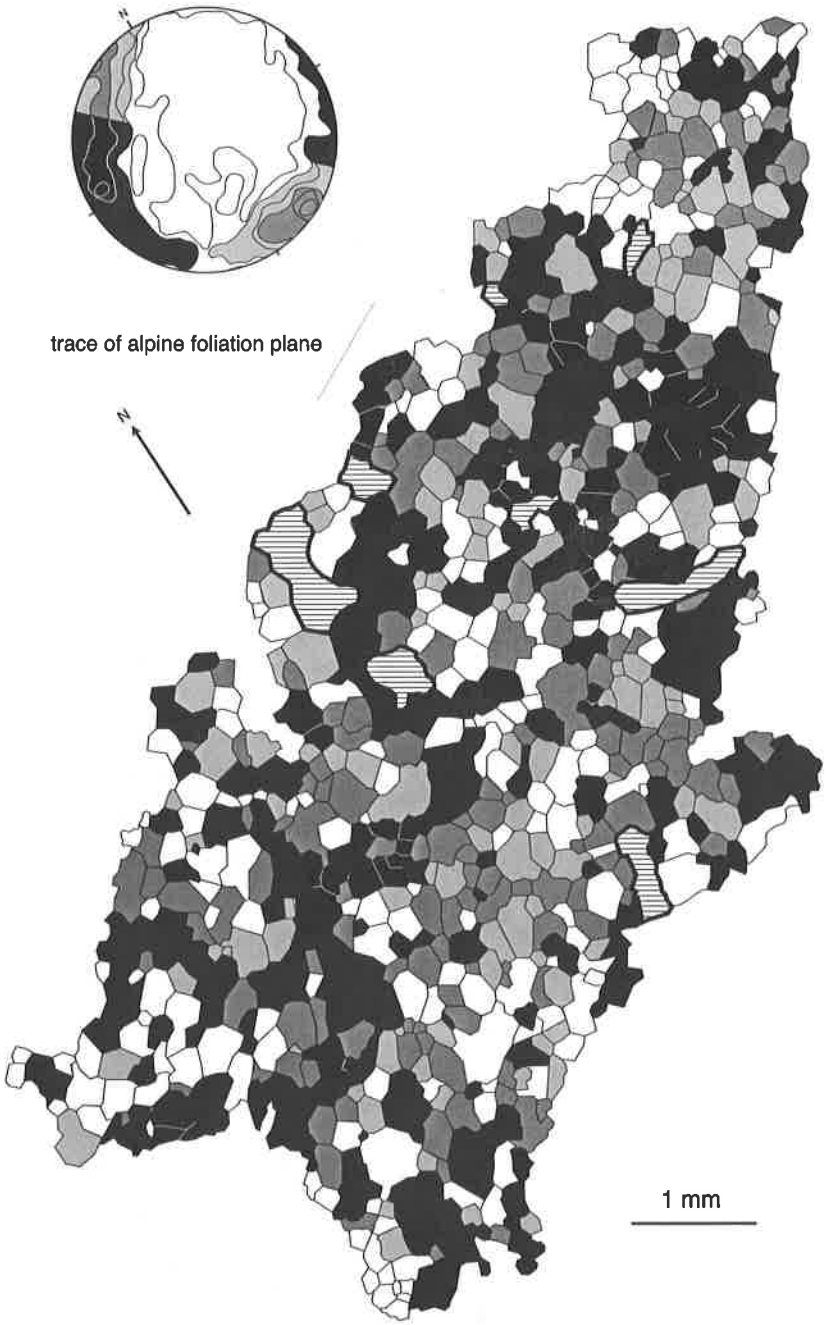

Fig. 3.18
Recrystallisation of a former subround granitic quartz grain into a flattened quartz aggregate (length 1 cm) of polygonal quartz grains of Alpine age (see **Photo 3.33**). Statistical distribution analysis of optical c-axes (733 measures on optical universal stage), showing distribution in two main plot maxima (170°, 270°). Colouring: for the 170° maximum: black: 3-5% densities, dark grey 1-2% densities; for the 270° maximum: middle grey: maximum 3-5% densities, very light grey: 1-2% densities. White: oblique grains. Horizontal pattern: plagioclase. (Coloured diagram: annex III).
*Recristallisation d'un ancien grain de quartz granitique arrondi en un aggrégat allongé (1 cm de longueur) de grains polygonaux (**Photo 3.33**). 733 grains de quartz, Analyse statistique d'orientation d'axes optiques c (733 mesures sur platine universelle optique), indiquant une distribution en deux maxima (170°, 270°). Couleurs: Maximum à 170°: Noir - densités de comptage 3-5%, gris foncé - densités 1-2% correspondantes. Maximum à 270°: gris moyen - densités 3-5%, gris très clair - densités 1-2% correspondantes. Blanc: Grains obliques. Hachure horizontale: grains de plagioclase. (Diagramme en couleur annexe III).*

Chapter IV
The Carboniferous Magmatic Rocks

Wide areas of the polymetamorphic basement described in the foregoing chapters were intruded by a series of Variscan granitoids and volcanites (**Fig. 4.01**) which, in many cases, show only traces of Alpine metamorphism. They occur as syntectonic intrusive granites, locally associated with subvolcanic facies, acidic sub-aerial lava flows and volcanic/volcaniclastic ash-fall deposits. High-precision U-Pb dating evidenced three short-lived magmatic pulses at 330 Ma, 307 Ma and 303 Ma (Bussy & von Raumer, 1993; Bussy et al., 1998b; Bussy et al., 2000). Still undated granite bodies, like the Fenestral-les Perrons granite, the hb-bearing anatectic granites and xenolith-rich anatectic granites from the Lac Cornu-Chéserys areas, and the microgranular granitoids occurring in the SW part of the Mont Blanc massif, are also considered to be of Carboniferous age on the basis of structural criteria

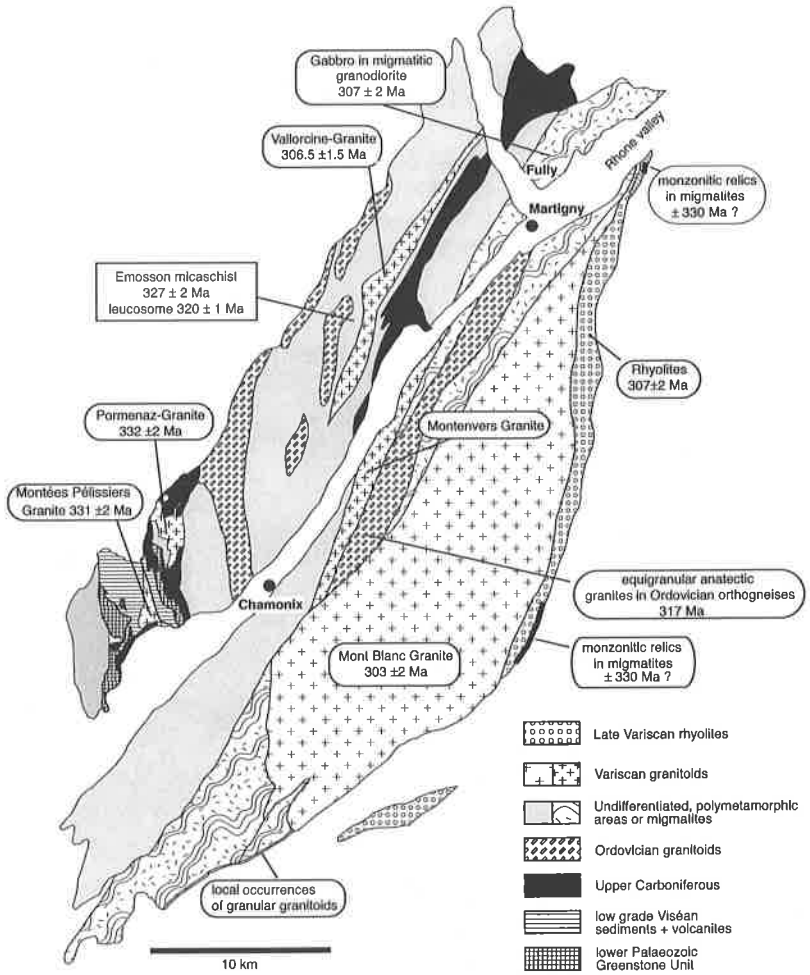

Fig. 4.01
Geological map of the Mont Blanc and Aiguilles-Rouges areas with indication of the main Variscan granite bodies and their ages (data after Bussy et al., 2000). *Carte géologique des massifs du Mont Blanc et des Aiguilles-Rouges avec les granites d'âge varisque (âges d'après Bussy et al., 2000).*

Photo 4.01
Folded durbachite rocks (K-feldspar amphibolites) from Reuses du Dolent at the foot of the Mt. Dolent glacier (corresponding to photograph 3.15 in Gay 1998). Width of picture corresponds to 70 cm. (Coord CH.: 571.900/85.230). *Durbachites (amphibolites à K-feldspath) plissées affleurant dans les Reuses du Dolent au pied du glacier du Dolent (photo 3.15 de Gay 1998). Largeur de la photo correspondant à 70 cm. (Coord CH.: 571.900/85.230).*

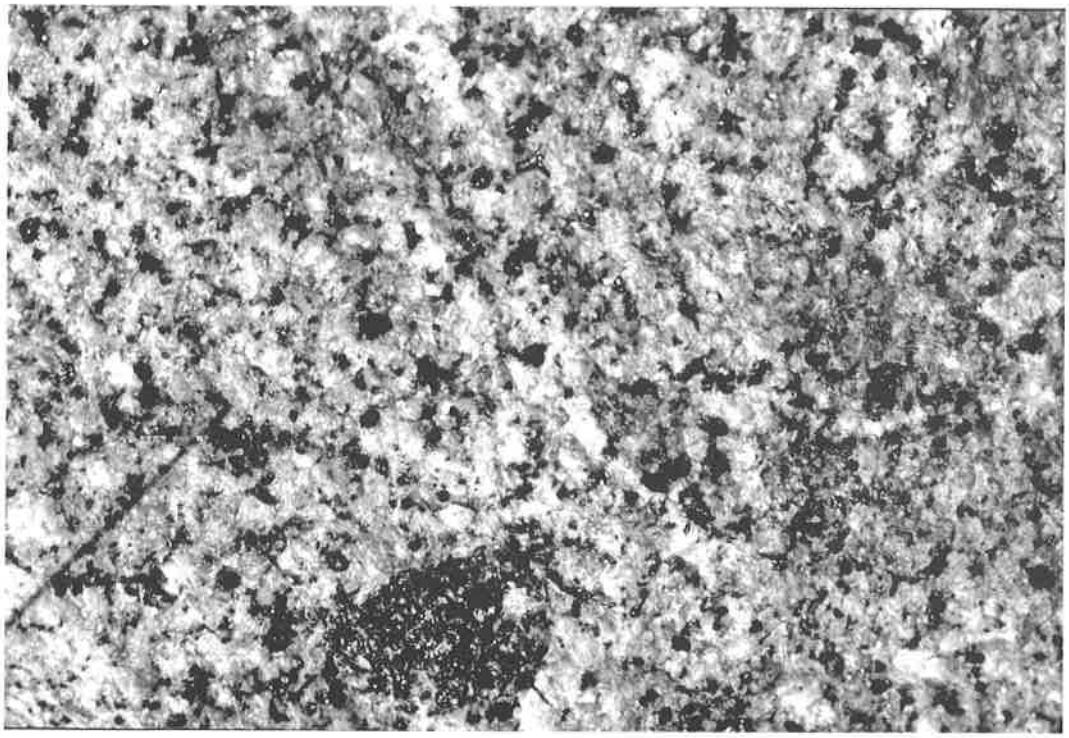

Photo 4.02
Vallorcine granite (lower facies) from the Miéville quarry (type locality; Coord. CH: 568.300/111.000). *Faciès profond du granite de Vallorcine de la carrière de Miéville (localité type; Coord. CH: 568.300/111.000).*

IV.1. Characteristics of rock types

The various granite intrusions will be described in a chronological order according to the succession of magmatic pulses mentioned above. Petrographic details can be found in the cited literature .

1.1. The 330 Ma magmatic pulse

The oldest group of Variscan granitoids is represented by the 330 Ma magmatic pulse, characterized by high-K calc-alkaline to shoshonitic plutons, which are documented in the southwestern part of the Aiguilles-Rouges massif by the Pormenaz monzonite (333 ± 2 Ma, Bussy et al., 1998a, 2000) and the Montées Pélissier granite (331 ± 2 Ma; Bussy et al., 2000). High-K calc-alkaline to shoshonitic plutonic enclaves are also found in the migmatites of Fully near Martigny and on the eastern side of the Mont Blanc massif at the base of the Mt. Dolent (Val Ferret).

Monzonitic-durbachitic rocks

These rocks are best represented by the Pormenaz monzonite, a 1.4 by 2.5 km porphyritic funnel-shaped mass in vertical cross-section, which intruded amphibolite-facies metamorphic rocks and Lower Carboniferous metagraywackes (Délitroz & Fellay 1997) in the Servoz-Les Houches region. Although a complex contact relationship led Laurent (1973 a,b) to infer a metasomatic origin, the shape and internal structures of the intrusion rather suggest a syntectonic emplacement of the magma and post-crystallization mylonitic deformation along a long-lasting dextral transpressive fault. The main facies is a porphyritic to equigranular monzonite with large pink or white K-feldspar megacrysts (up to 4 cm) in a dark gray-green amphibole-rich matrix. Euhedral crystals of brown sphene are clearly visible on hand specimen. Plurimetric bodies of durbachites (Holub 1977; Rock 1991) are found as dark green, equigranular, magmatic enclaves.

Rocks comparable to the Pormenaz monzonites and durbachites are located in the SE shoulder of the Mont Blanc massif parallel to the Val Ferret, occurring as irregular lumps in migmatites (Type localities: Coord CH: 571.300/83.925, Arête des Grépillons; 571.680/84.810, Reuses du Dolent). At the foot of the Mt. Dolent glacier, strongly deformed "K-feldspar amphibolites" represent the current type of durbachitic rocks, composed mainly of K-feldspar, actinolite and biotite, largely recrystallized into an actinolite-chlorite-K-feldspar assemblage through Alpine metamorphism. Shortly described by Gay (1998), they appear as blocks, lenses, or boudins up to 20 m in size among migmatites; they are mainly characterized by a strong alignment of K-feldspar crystals of 3-5 cm in size (**Photo 4.01**), showing microscopic recrystallization and formation of new, tiny K-feldspar grains. Few crystals of plagioclase (An_{30}) are only visible under the microscope. Among the colored phases appear dark red-brown biotite and actinolite, and sphene crystals up to 5mm in length. Among the darkest banded units appear locally small ultrabasic lumps, mostly transformed into chlorite-actinolite assemblages. Large morainic blocks of syenite-looking granitoids with actinolite, sphene and large K-feldspar are likely to represent differentiated products of the durbachitic magmatic series, and could be compared to the Pormenaz quartz-monzonites. These rocks have also been observed in the water gallery near La Fouly. Durbachitic rocks appear also as irregular lumps among migmatites at the eastern contact of the late Variscan Mont-Blanc granite and rhyolites (crest of Catogne, Champex; Tièche 1969), and in the late Variscan migmatites and granodiorites of Fully near Martigny.

Montées-Pélissier granite

The Montées-Pélissier granite is a vertical, 3 km-long by 500 m-wide sheet-like pluton in tectonic contact with its country-rock. A transpressive regime induced subhorizontal movements with extreme elongation, subsequently reoriented into subvertical displacements (Dobmeier 1998). The granite intruded syntectonically along ductile shear-zones during the transcurrent stage and recorded the subsequent vertical movements during cooling (Dobmeier 1996). Primary magmatic flow fabrics are mostly superimposed by low-T ductile to brittle deformation. The Montées-Pélissier granite is a fine-grained foliated two-mica monzogranite, which hosts rare biotite-rich restites, mafic microgranular enclaves and biotite-bearing lamprophyres.

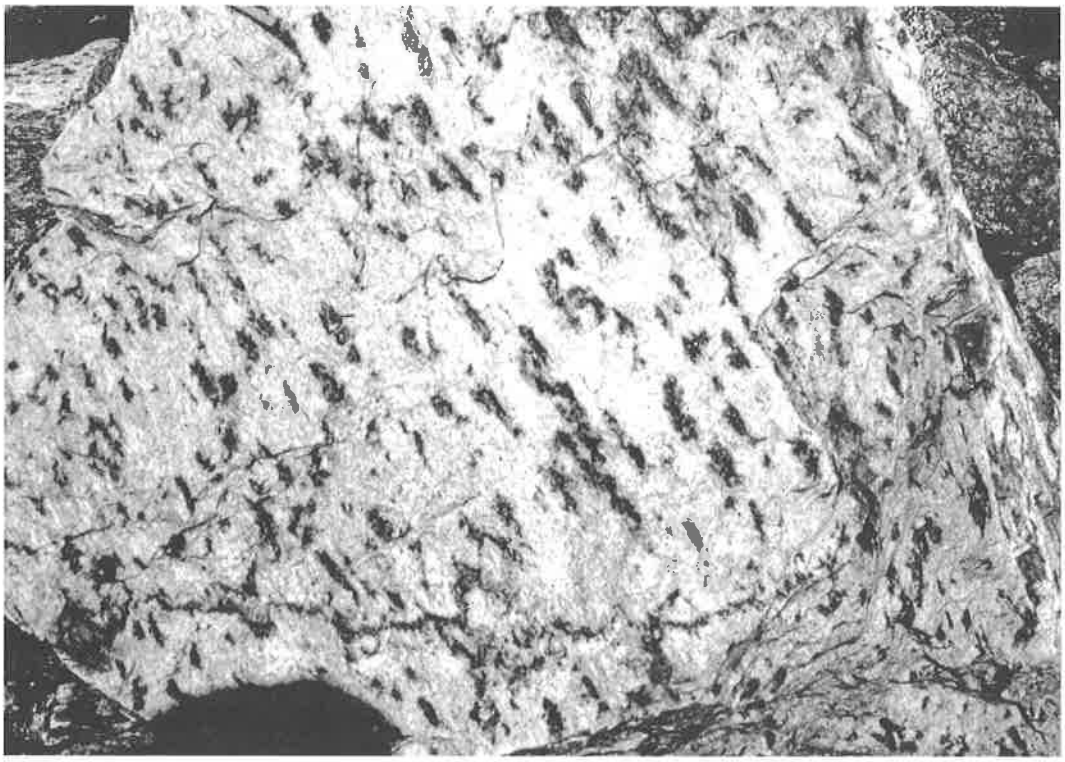

Photo 4.03
Pinite-bearing leucogranite. Patches: former cordierite transformed into pseudomorphs of chlorite and white mica (pinite) after cordierite (Miéville quarry; Coord. CH: 568.300/111 000). Width of picture equals 15 cm. *Leucogranite à pinite. Taches: pseudomorphoses de cordiérite en chlorite et mica blanc (pinite); (carrière de Miéville; Coord. CH: 568.300/111.000) Largeur de photo égale à 15 cm.*

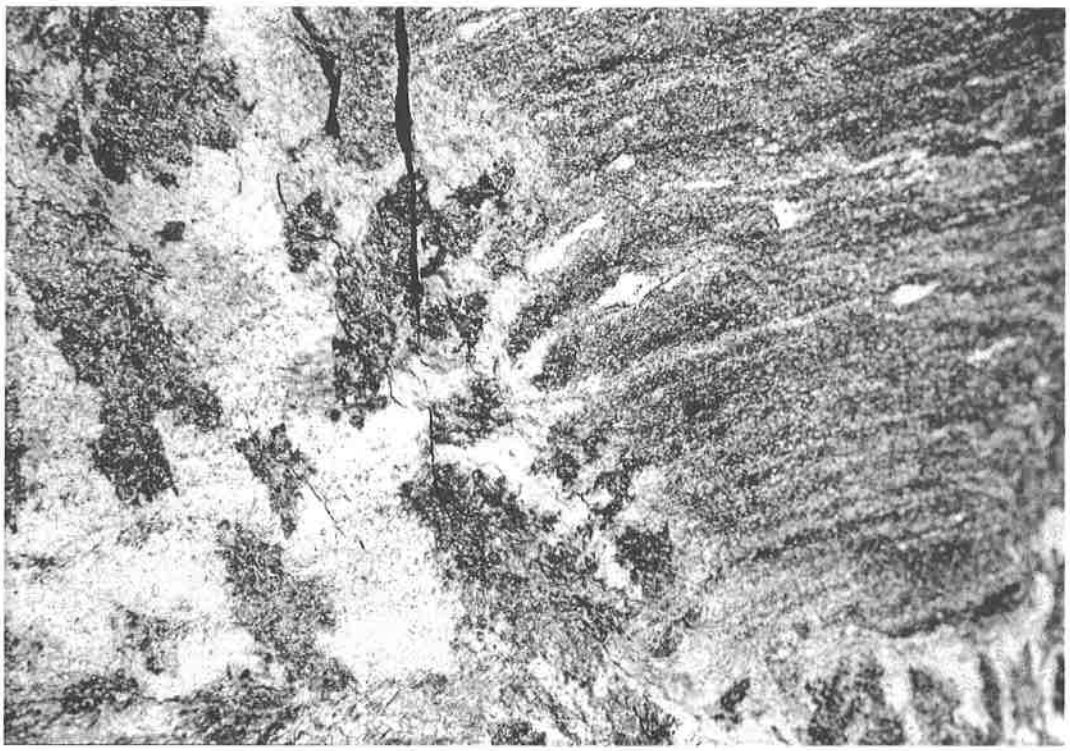

Photo 4.04
In-situ formation of pinite-bearing leucogranite with patches of former cordierite at the contact with the host-rock. Road-cut near La Balmaz (Coord. CH: 568.500/111.575). Width of picture equals 10 cm. *Formation in situ de leucogranite à pinite avec des taches d'anciennes cordiérites (pinite) au contact avec la roche mère, voisinage de La Balmaz (Coord. CH: 568.500/111.575). Largeur de photo égale à 10 cm.*

Fenestral – les Perrons granites

Nearly parallel to the Chamonix valley, the Aiguilles Rouges polymetamorphic basement contains a series of undated, irregular, lens-shaped bodies, mapped by Joye (1989) as granite gneisses **(Fig. 3.10)**. They are tentatively included in the same age group. In the structural map, they appear as irregular folded bodies of biotite-rich K-feldspar augengneisses. They might represent early Carboniferous syntectonic intrusions, comparable to the Viséan granites observed in the Belledonne area (Debon et al., 1998), which have been strongly sheared during the Variscan tectonics and are accompanied by migmatites. Alternatively, they may represent Ordovician augengneisses as described in chapter II.

1.2. The 307 Ma magmatic pulse

During the 307 Ma event, three peraluminous granites intruded simultaneously in the Aiguilles Rouges/ Mont Blanc area: the Vallorcine granite, the Fully granodiorite and the Montenvers granite.

Vallorcine granite

Type locality: old quarry near Miéville, Rhone valley (Coord. CH: 568.300/111.000).

Necker (1828) was the first to establish the magmatic origin of the Vallorcine granite, a 15-km-long by 1-km thick sheet-like pluton (see map, **Fig. 4.01**), stretching along the SE border of the Aiguilles-Rouges massif from Miéville (Rhone valley) to the village of Vallorcine (Chamonix valley). The granite body intruded at 306.5 ± 1.5 Ma (Bussy et al., 2000) along a steeply dipping, NE-SW trending, dextral strike-slip shear zone (Brändlein 1991; Brändlein et al. 1994). Syntectonic intrusion is inferred on the basis of structural analysis, which documents long-lasting strike-slip shearing both in the country rocks (pre- and post-intrusion fabrics), and in the granite. The latter developed an early NE-SW trending magmatic flow structure, evolving locally into a post-solidus foliation. The Vallorcine granite was subsequently affected along its SE contact by intense low-T ductile shearing leading to the well-known "Miéville ultramylonite" (Reinhard and Preiswerk 1927; Steck and Vocat, 1973; Kerrich et al. 1980) of Late Variscan age (see Thöni in Joye, 1989), but reworked during the Alpine orogeny. Alpine relief provides a 2000 m-high natural cross-section through the pluton, first described by Meyer (1916). Brändlein (1991) distinguished a lower and an upper facies. The lower facies is a biotite-rich monzogranite (**Photo 4.02**) hosting numerous enclaves up to 30 cm in size; including gneiss xenoliths from the country rock, hornfelses, micaceous restites with sillimanite and hercynite, early cordierite-bearing leucogranite (**Photos 4.03,4.04**) blocks and mafic microgranular enclaves. The upper facies is finer-grained with less biotite and almost no enclaves, pointing to an enclave unmixing process during upward motion of the magma (Bussy et al., 2000). Aplitic and subvolcanic dykes are concentrated within the wall rocks of the upper contact. The Vallorcine intrusion is a typical S-type granite, as confirmed by zircon typology, stable isotopes (Brändlein et al. 1994) and the presence of Al-rich minerals (andalusite, e.g Einfalt 1979; cordierite, muscovite). Disequilibrium of stable isotopes from feldspars suggests the formation of a late hydrothermal convection system (500- 280°C), which led to crystallisation of tourmaline and topaz (Brändlein 1991).

Fully granodiorite

Type localities: cliffs along the road side between Fully and Dorénaz and vineyards (Coord. CH.: 575.460/110.830); Chéserys region north of Chamonix (Coord. FR.: 952.280/119.720).

The Fully granodiorite is located in the vineyards of the northern end of the Aiguilles Rouges massif (Krummenacher 1959), but comparable rocks appear in the Aiguilles-Rouges massif north of Chamonix. It is a highly heterogeneous, coarse-grained granodiorite of migmatitic aspect with cordierite clots (up to 10 vol.%, now greenish pinite), dispersed K-feldspar megacrysts and numerous small biotite-rich restitic enclaves, with garnet, schlieren and nebulitic structures. Micaschists, gneisses, marbles and amphibolites are found as dm-long xenoliths, whereas mafic magmatic enclaves can reach one meter in diameter. Cordierite-bearing leucogranitic dykes and stocks crosscut the main facies. No systematic internal structure is observed. Despite the migmatitic structures, the whole mass has a clear intrusive character. It is a typical peraluminous, anatectic granitoid with a large restitic component

Photo 4.05
Anatectic granite of Fully or Lauterbrunnen type with a restitic gneiss-marble band from the Lac Blanc – Chéserys area (Coord. FR: 952.280/119.720; 2491 m). Width of picture equals 60 cm. *Granite d'anatexie de type Fully ou type Lauterbrunnen de la région du Lac Blanc – Chéserys (Coord. FR: 952.280/119.720; 2491 m). Largeur de photo égale à 60 cm.*

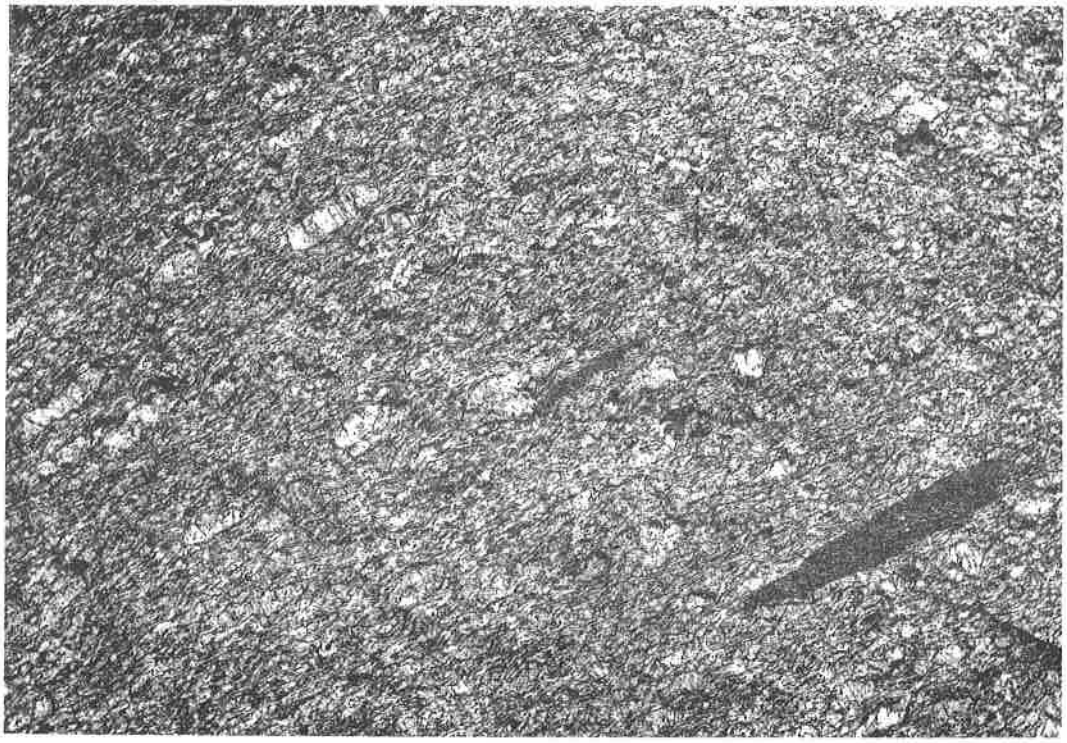

Photo 4.06
Stretched Montenvers granite (Alpine deformation) from Lognan area (Mont Blanc massif) south of Argentières (Coord. FR: 957.220/117.560). Width of picture equals 40 cm. *Granite de Montenvers étiré par la déformation alpine (Lognan, Massif du Mont Blanc) au S d'Argentières (Coord. FR: 957.220/117.560). Largeur de photo égale à 40 cm.*

and abundant Al-rich minerals (garnet, cordierite, muscovite, hercynite). Zircons preferentially develop the {211} crystallographic form (low A index) and plot in the expected field of intrusive aluminous granites in the typological grid of Pupin (1988, **Fig. 4.03, 4.04**). The mafic magmatic enclaves include typical mafic microgranular enclaves of intermediate composition (quartz-dioritic to granodioritic), as well as angular to rounded pieces of fine- to coarse-grained gabbros, up to one meter in size (Bovay 1988). The latter preserve clear, locally pegmatitic, undeformed igneous textures, but experienced hydrothermal alteration. Pyroxene recrystallized into Mg-hornblende with minor Mg-biotite, and plagioclase (An_{60}) is strongly sericitized. The angular shape and absence of chilled margins indicate that these gabbro enclaves are pieces of a larger mafic body, which were incorporated as solid-state fragments into the mobile migmatitic mass. They have chemical characteristics of calc-alkaline type similar to those found in other Variscan acid-basic associations (e.g. Corsica, Pyrenees). Interactions with crustal material, possibly during hydrothermal retrogression, are evidenced by high LILE contents like K, Ba and Rb. Zircon and monazite, extracted from granodioritic, leucogranitic and gabbro samples, yielded ages of 307 ± 2 Ma for all rock types (Bussy et al., 2000). Although solid at time of incorporation into the anatectic mass, the gabbro enclaves are thus contemporaneous with the acid magmatism within errors. In other words, a mantellic basic magmatism was active at time of enhanced crustal anatexis. Comparable rocks with all stages of migmatization of a former metasedimentary sequence (**Photo 4.05**) can be observed north of Chamonix in the upper part of the Chéserys region (Coord. FR: 952.280/119.720). They are strongly reminiscent of the Lauterbrunnen migmatites (Rutishauser, 1973, Olsen et al. 2000).

Montenvers granite

Type locality: cliffs at the base of the Mer de Glace glacier, Montenvers/Chamonix (Coord FR: 955.300/113.550).

In the Mont Blanc massif, the peraluminous Montenvers granite was emplaced syntectonically at 307 ± 3 Ma (Bussy and von Raumer, 1994) as a sheet-like intrusion, in a similar way and at the same time as the Vallorcine granite. It is now a strongly deformed, often mylonitic leucocratic orthogneiss (**Photo 4.06**), hosting both microgranular and restitic enclaves (Morard, 1998). Equivalents are observed in the northwestern prolongation near Croix de Prelayes (above Col de la Forclaz) and in the Grandes Otanes area southwest of Col de Balme. Most primary minerals recrystallized in Alpine greenschist facies, but zircon typology and whole-rock chemistry still point to an S-type granite.

Microgranular granites – Col de la Seigne

In the neighborhood of the Col de la Seigne, the polymetamorphic basement of the Mont Blanc massif is widely transformed into migmatites and accompanied by long, narrow bodies of a microgranular S-type granite (Coord. IT.: 29.825/70.125), resembling the granitoid dikes from the Lognan region (Coord. FR: 958.200/117.400) dated at 317 ± 2 Ma (Bussy and von Raumer, 1994). It is probable that these granite bodies result from the same anatectic event dated in Lognan.

Hornblende-bearing granitoids – Lac Noir

In the neighborhood of Lac Cornu (Coord. FR: 949.425/117.270), the strongly migmatized basement is locally crosscut by small diffusive bodies of a hornblende-bearing leucogranite. Comparable mobilisate veins (**Photo 4.07**) can be observed in anatectic metasedimentary units at the northern prolongation of Lac Noir (Coord. FR: 949.640/117.285; 949.890/117.290) and in the Chéserys area. These undated mobilisates might by contemporaneous with the 320-317 Ma anatectic event or with the 330 Ma event. The hornblende-biotite-bearing gneisses of the Val Bérard area (Wirsing, 1997; see Ch. II) look very similar to the Lac Noir mobilisates; consequently, these gneisses might be of Variscan anatectic origin rather than of Ordovician age.

Sub-aerial dacitic flows

Sub-aerial dacitic flows outcropping at the base of the Salvan-Dorénaz sedimentary basin erupted at 308 ± 3 Ma (Capuzzo & Bussy, 2000). They represent the surface equivalent of the nearby Vallorcine granite and associated rhyolitic dykes, and present porphyritic textures with large euhedral and subhedral quartz and plagioclase phenocrysts. These lava flows are

Photo 4.07
Anatectic mobilisates of hornblende-bearing granitoids north of Lac Noir (Aiguilles Rouges) (Coord. FR: 949.890/117.290). Width of picture equals 60 cm *Mobilisats anatectiques de granites à hornblende au nord du Lac Noir (Aiguilles Rouges) (Coord. FR: 949.890/117.290). Largeur de photo à peu près 60 cm.*

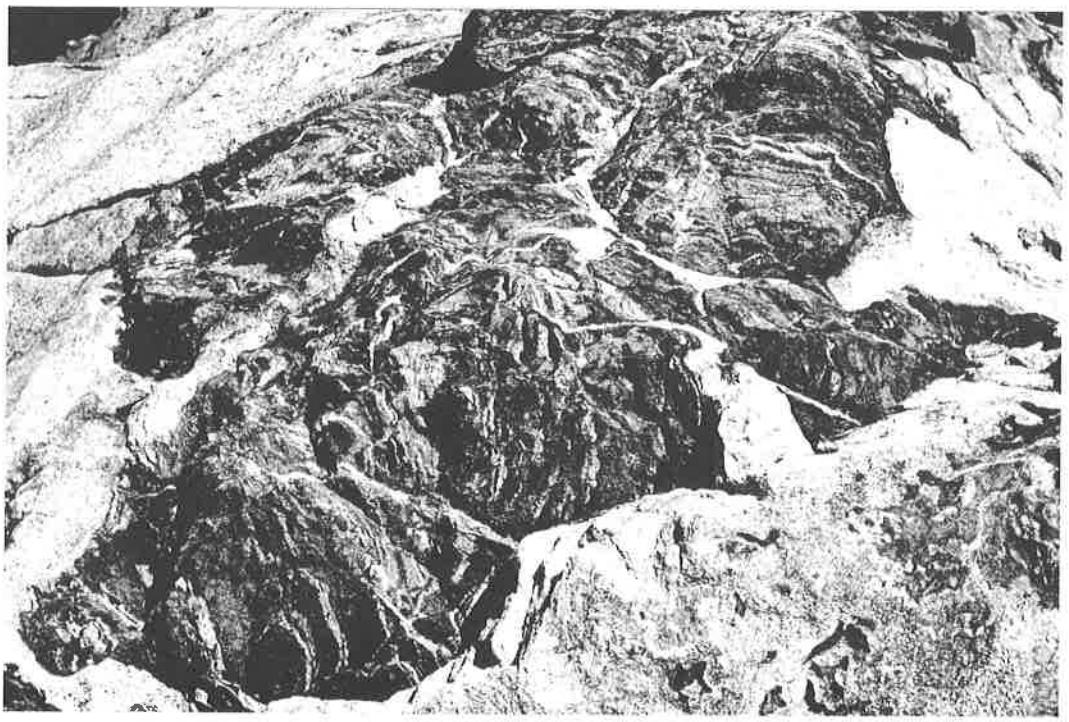

Photo 4.08
View of the northern magmatic contact area of the Mont Blanc granite near Plan de l'Aiguille above Chamonix. (Coord. FR: 953.200/110.230). *Contact magmatique à l'ouest du granite du Mont Blanc dans le voisinage du Plan de l'Aiguille au dessus de Chamonix (Coord. FR:953.200/110.230).*

characterized by variable proportions of coherent and autoclastic scoriaceous volcanic facies interlayered toward the top with Upper Carboniferous sediments, and are presumably related to the emplacement of a rhyodacitic lava dome along the north-western margin of the half-graben sedimentary basin. In the Mont Blanc massif, calc-alkaline **rhyolitic dykes** were emplaced simultaneously (307 ± 2 Ma) at shallow crustal levels, but they derive from different, deeper magma sources.

1.3. The 303 Ma magmatic pulse

Mont-Blanc granite

The 303 Ma magmatic pulse is represented by the voluminous Mont Blanc granite (303 ± 2 Ma, Bussy et al. 2000), located in the Mont Blanc massif. Named "Protogine" (Jurine 1806, see historical remarks, chapter I), because of its Alpine deformation, its magmatic character was first recognized by Michel-Lévy (1890). It is a foliated, porphyritic monzo- to syenogranite with K-feldspar megacrysts and Fe-rich biotite as the only mafic mineral (von Raumer, 1967; Marro 1988; Bussy 1990); it hosts numerous mafic microgranular enclaves, calc-alkaline micromonzodioritic stocks and synplutonic dykes of mantellic origin, which record magma mingling processes (Bussy 1990).

The main body is composed of a very coarse-grained granite, which shows a clear parallel alignment of large K-feldspars (**Photo 4.09**) indicating internal flow structures (von Raumer 1967). Towards the contacts, the granite grades into a finer grained border facies (Marro 1986) and, near the margins appear biotite-rich schlieren (**Photo 4.11**), recording former internal flow structures (von Raumer, 1967). In the Mt. Dolent area (SE part of Arête Gallet), Gay (1998) observed a huge intrusion breccia (**Fig. 4.02**), and comparable pictures may be observed in the glacial outcrops below Mt. Dolent, as well as at the northwestern contact at Plan des Aiguilles above Chamonix (**Photo 4.08**). Near the contact occur swarms of rounded xenoliths (**Photo 4.12**). The main granite body is interpreted (Marro 1986) as a coupola-like intrusion, and its emplacement might have been triggered by a pull-apart structure during Variscan strike-slip. Marro (1986) distinguished two main magmatic pulses; the first one corresponding to the porphyritic central facies (**Photo 4.09**) and associated equigranular border facies, and the second to leucocratic, equigranular to porphyritic dikes crosscutting the main granite body, and characterized by "droplets" of quartz (**Photo 4.10**). This distinction holds also for the Dolent region (Gay 1998).

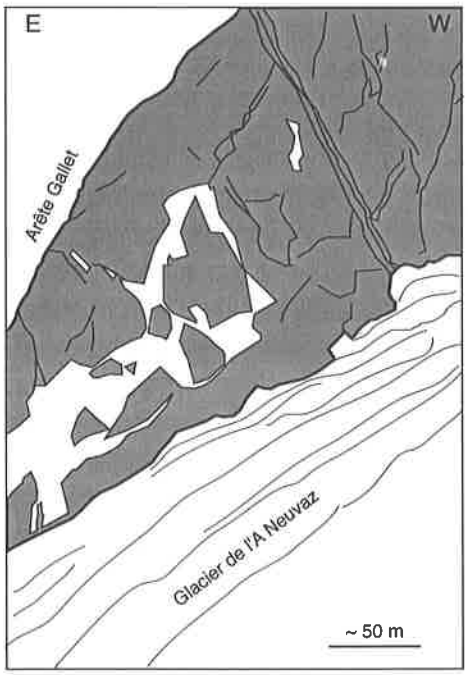

Fig 4.02
Intrusion breccia at the contact of the Mont Blanc granite, drawn after a photograph from Gay (1998). View of the northern slopes of the crest (Arête Gallet) between la Maye and Mt. Dolent from l'A Neuve glacier.
Brèche intrusive au contact du granite du Mont-Blanc, dessiné d'après une photographie de Gay (1998). Vue de la paroi nord de l'Arête Gallet reliant La Maye au Mt. Dolent. (Coord. CH.: 571480/84700).

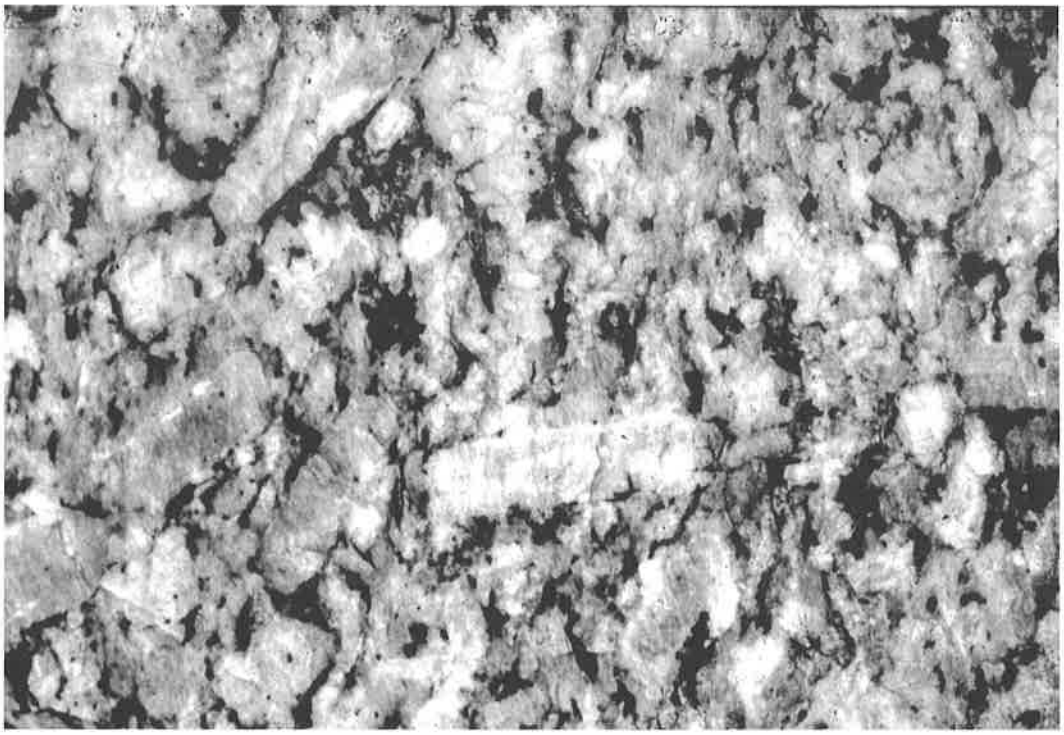

Photo 4.09
Mont Blanc granite, central facies with subvertical Alpine foliation of biotite patches (Coord. CH : 567.675/91.350; 3180m). *Granite du Mont Blanc – faciès central avec foliation alpine subverticale marquée par des agglomérats de biotite. (CoordCH.:567.675/91.350; 3180m).*

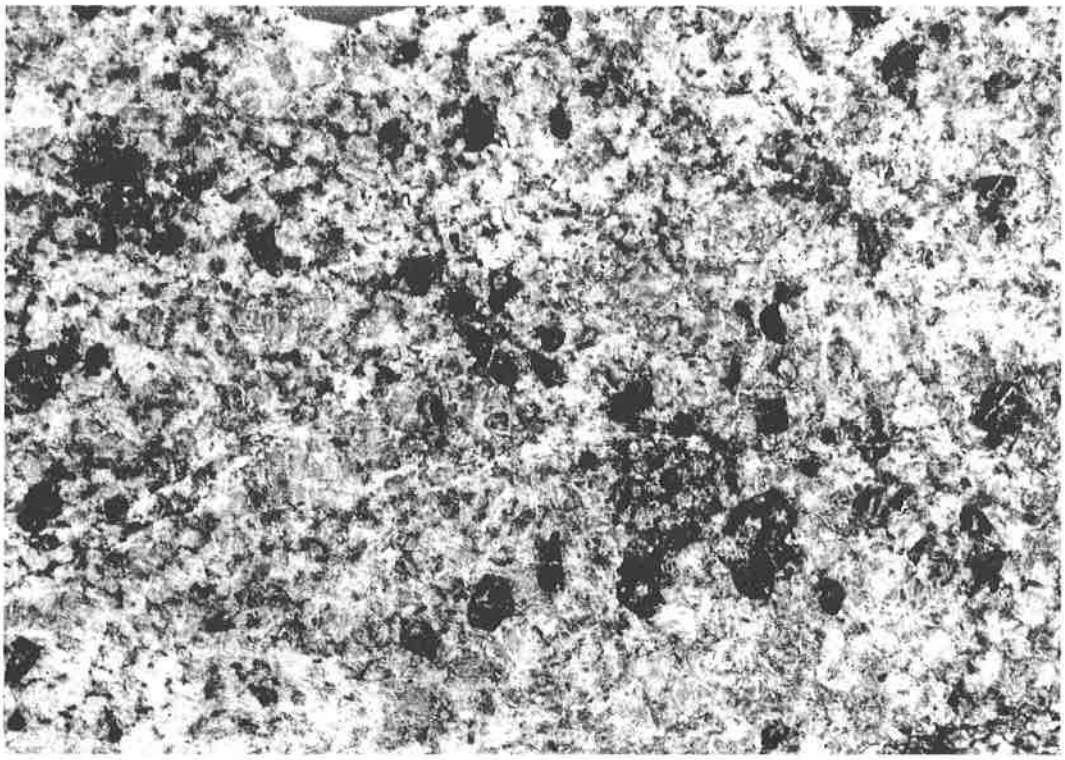

Photo 4.10
Mont Blanc granite, 2nd generation of granitoids with droplets of quartz (dark, size about 4mm). Col des Plines, Trient glacier (Coord. CH: 569.350/93.100; 3270m). *Granite du Mont Blanc, deuxième génération de granite à gouttes de quartz (foncé, taille à peu près 4mm). Col des Plines, Glacier du Trient. (Coord.CH: 569.350/93.100;3270m).*

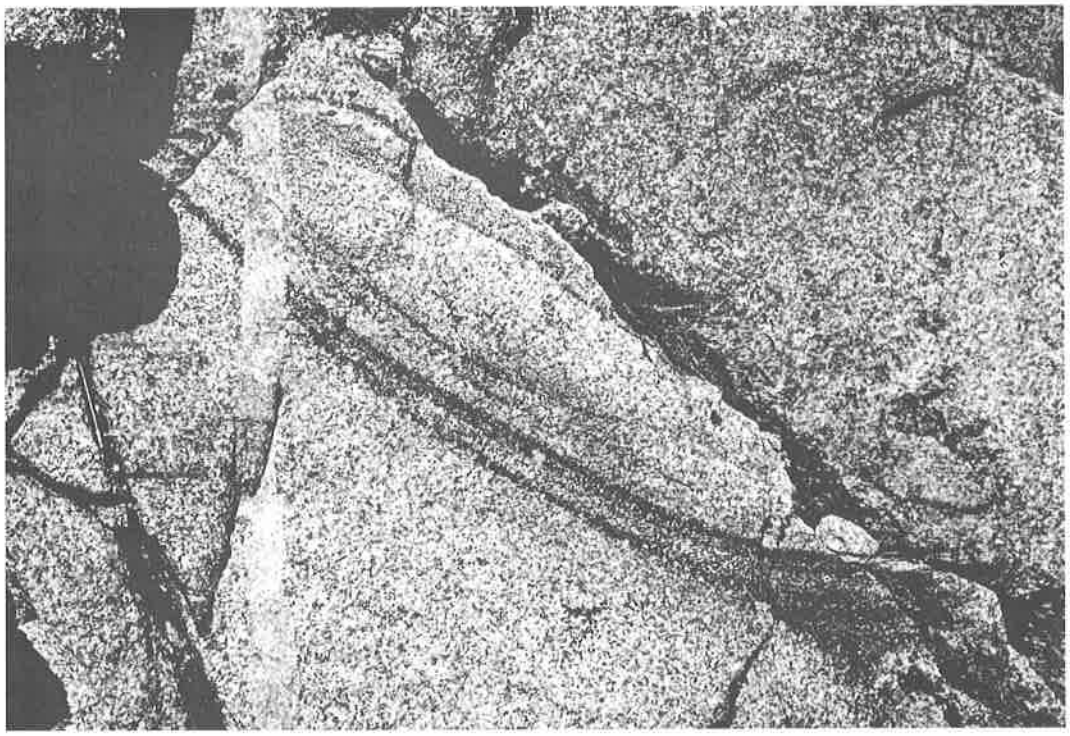

Photo 4.11
Mont-Blanc granite, border facies with biotite containing schlieren of biotite near La Breya. (Coord. CH: 572.935/95.515; 2260m). Width of picture equals 20 cm. *Granite du Mont Blanc – faciès de bordure à schlieren de biotite, voisinage de La Breya (Coord.CH:* 572.935/95.515; 2260m*). Largeur de photo à peu près 20 cm.*

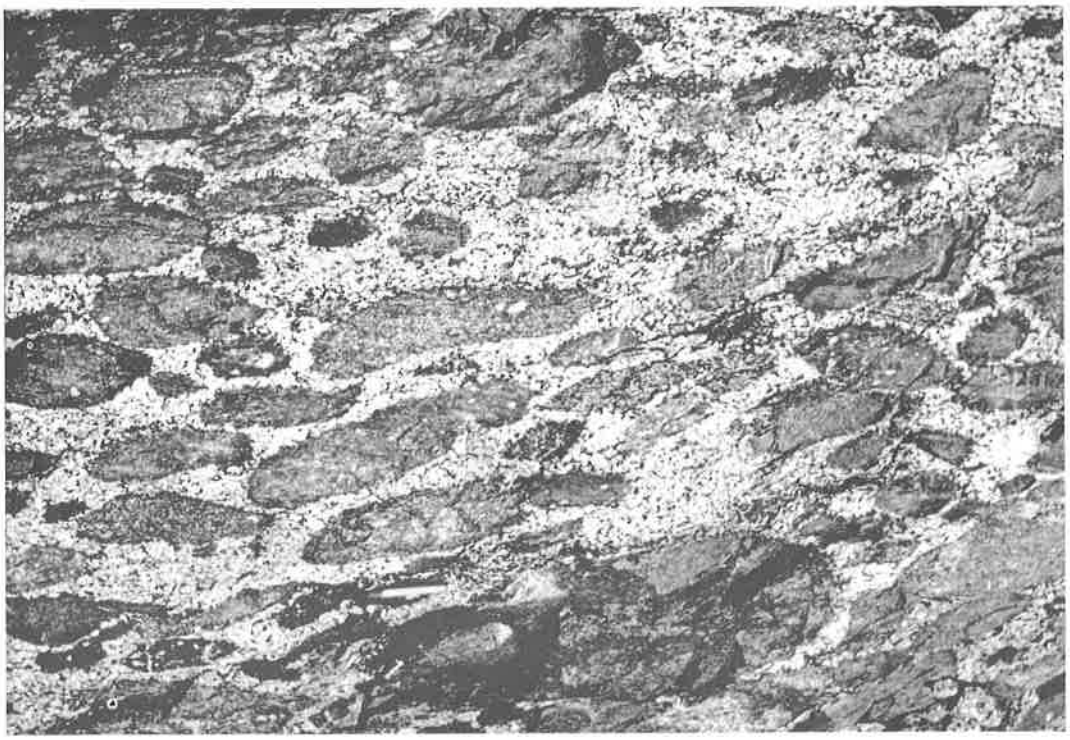

Photo 4.12
Xenoliths (about 10 cm in size) in Mont-Blanc granite at its western contact (boulder at Plan de l'Aiguille, Bosson glacier). *Xénolites (à peu près 10 cm de longueur) dans le Granite du Mont Blanc au contact ouest (grand bloc dans la moraine du Glacier de Bossons, près du Plan de l'Aiguille, Chamonix)*

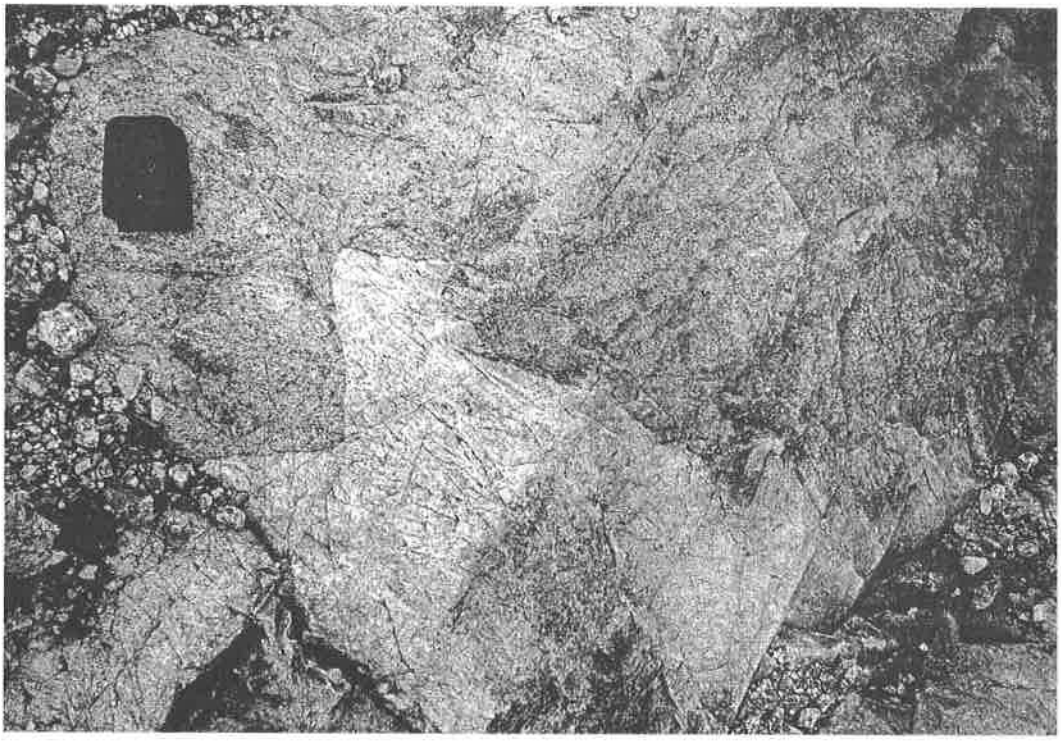

Photo 4.13
Contact between two generations of rhyolites (older leuco-rhyolites) at Reuses de Dolent (see picture 3.4 in Gay 1998; Coord. CH: 571.880/85.390). *Contact fragile entre deux générations de rhyolites, où les leucorhyolites semblent être précoces (voir photo 3.4 dans Gay 1998; Coord. CH: 571.880/85.390).*

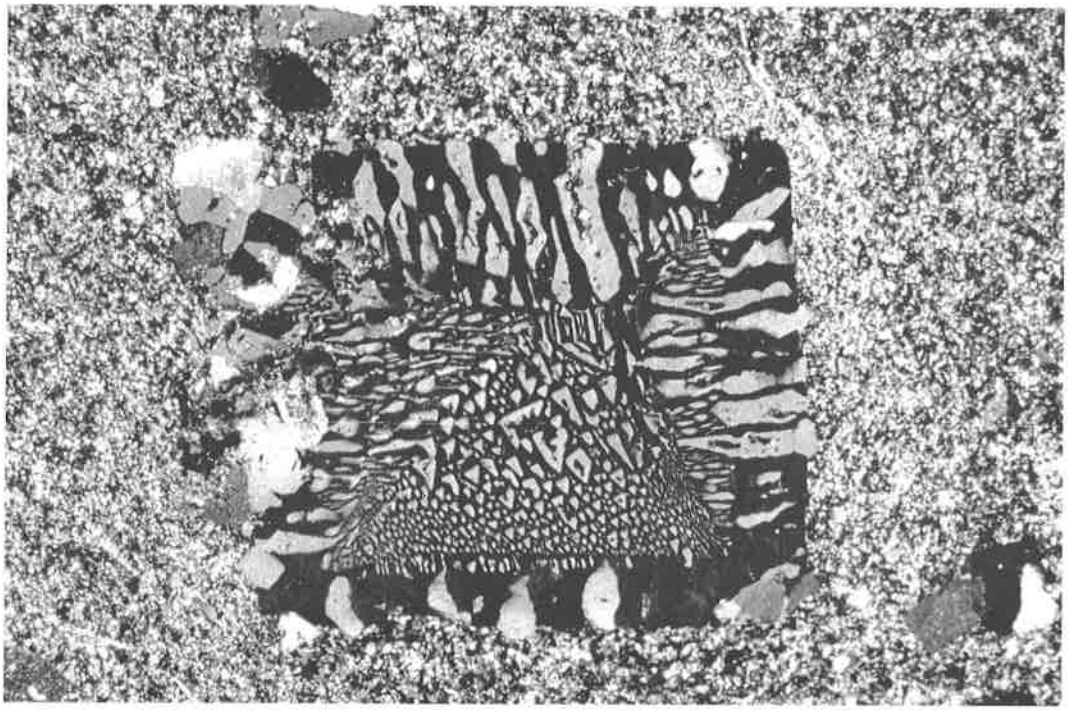

Photo 4.14
Association K-feldpsar/quartz with eutectic texture in a rhyolite (picture from cover; Gay 1998; locality Luys de Dolent, Coord. CH: 571.450/83.998) . *Association quartz/feldspath en structure eutectique dans une rhyolite (Photo de couverture, Gay 1998; localité Luys de Dolent; Coord. CH: 571.450/83.998)*

Rhyolites

The entire southeastern side of the Mont-Blanc granite is juxtaposed, parallel to the Ferret valley, by a long rhyolite complex, already described by Duparc and Pearce (Duparc 1897; Duparc and Pearce 1897), and composed of different generations of rhyolites and leucogranites. Near the type-locality (upper terminal of cable car La Breya, Champex; Coord CH: 574.000/96.675/2190 m), a U/Pb zircon age of 307±3 Ma (Bussy and von Raumer, 1994) has been obtained. In the Dolent area, Gay (1998) distinguished several facies, including microgranites and pre-, syn- and post-plutonic rhyolites (with reference to the Mont Blanc granite). The pre-plutonic dikes (307±3 Ma) are contemporaneous to the major 307 Ma magmatic pulse recorded in the nearby Aiguilles Rouges massif; they appear as leucocratic, microgranular dikes, whereas the second generation appears as darker, biotite-rich rocks, crosscutting the older ones (**Photo 4.13**). The post-plutonic rhyolites might be related to some of the **ash-fall deposits** embedded at different levels in the nearby Salvan-Dorénaz basin, which record a 295 $^{+3}/_{-4}$ Ma old episode of high-explosive volcanism (Capuzzo and Bussy, 2000). Phenocrysts of biotite, plagioclase, K-feldspar, and quartz are observed, K-feldspar and quartz presenting nice examples of eutectic intergrowth (**Photo 4.14**). Alpine deformation is generally low, but replacement of pre-existing minerals is common, like the recrystallisation of brown biotite into green biotite. Neoformation of Alpine stilpnomelane is well observed in such rocks (von Raumer 1968) and, locally, tiny bluish amphiboles can be observed in the fine-grained matrix. Marro (1986) proposed a model of subsurface intrusions accompanied by formation of cauldron-like subsiding structures, and Gay (1998) invoked an evolving magma-chamber through time with intrusion of different types of rhyolites/ microgranites from distinct sources.

IV.2 Zircon typology

Zircon typology of some granites has been published in Bonin et al. (1993), and the corresponding data, as well as more recent ones, are found in Bussy (1990, Mont-Blanc granite), Brändlein (1991, Vallorcine granite), Morard (1998, Montenvers granite), and Bussy et al (2000, Pormenaz monzonite, Montées-Pélissier granite and Fully granodiorite). Morphological features of zircons (Pupin, 1980, 1988) are controlled by the chemical composition of the melt into which they grew, thus allowing the characterizing of different granite types (**Figs. 4.03-4.04**). Among the older granites, large differences appear between the Pormenaz monzonite and the Montées-Pélissier granite, the former corresponding to field 5 (subalkaline FeK granites), whereas the latter plots at the limit between the peraluminous and calc-alkaline granite fields (intrusive monzogranites to granodiorites). The age group of anatectic granites (Vallorcine, Montenvers, microgranular Mont-Blanc granite, Fully granodiorite) occupies uniformly the field of intrusive peraluminous monzogranites and granodiorites, whereas zircon morphology of the Mont-Blanc granites and their enclaves (Bussy 1990) shows an extreme typology with very high A and T indices following the trend typical of alkaline granites. Such differences are the mirror of melting processes of contrasting sources which will be discussed below (IV.4).

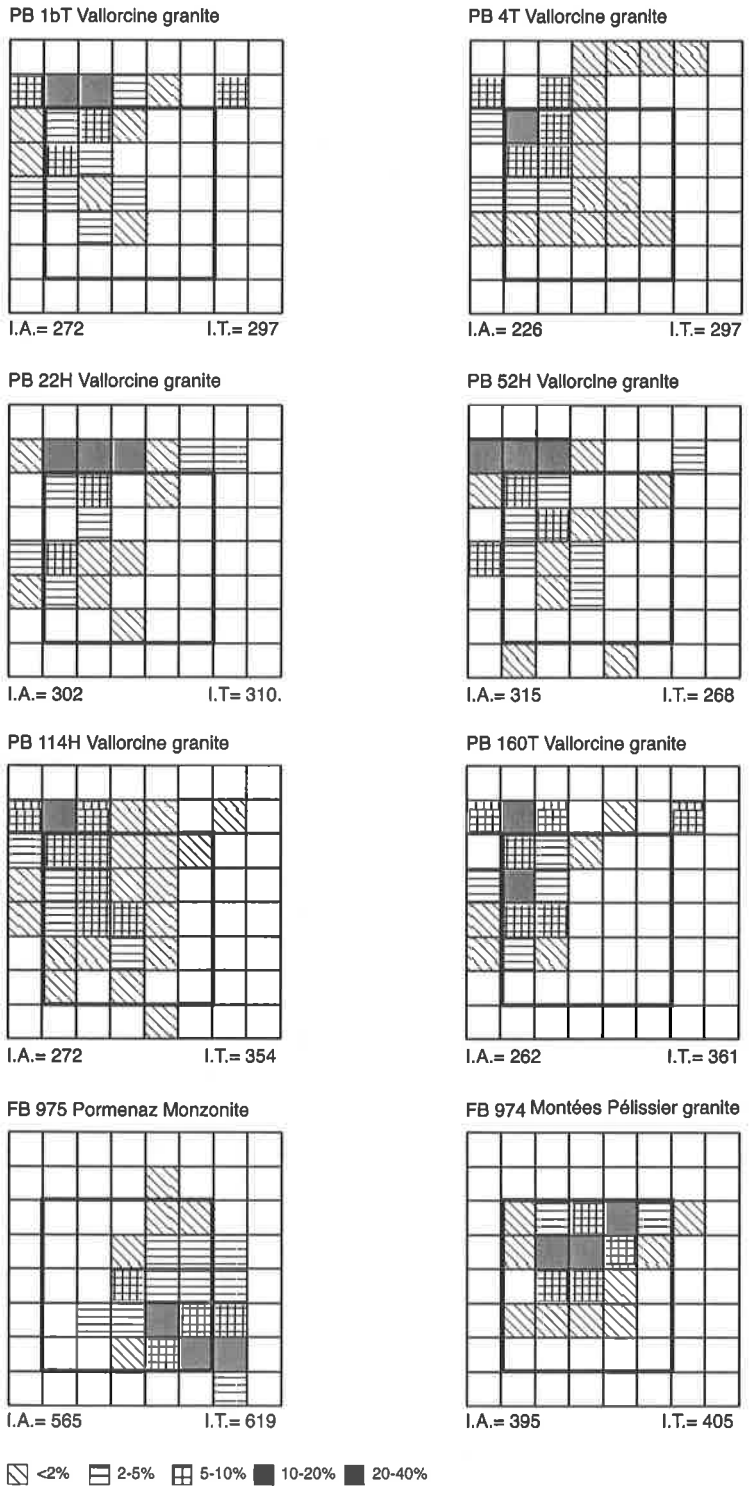

Fig 4.03A
Zircon typology of Carboniferous granitoids after Pupin (1988). Data from Bussy FB (1990); Brändlein PB (1991); Bussy et al. (2000).
Distribution typologique des zircons des granites d'âge carbonifère (d'après Pupin 1988). Données de Bussy FB (1990); Brändlein PB (1991); Bussy et al. (2000).

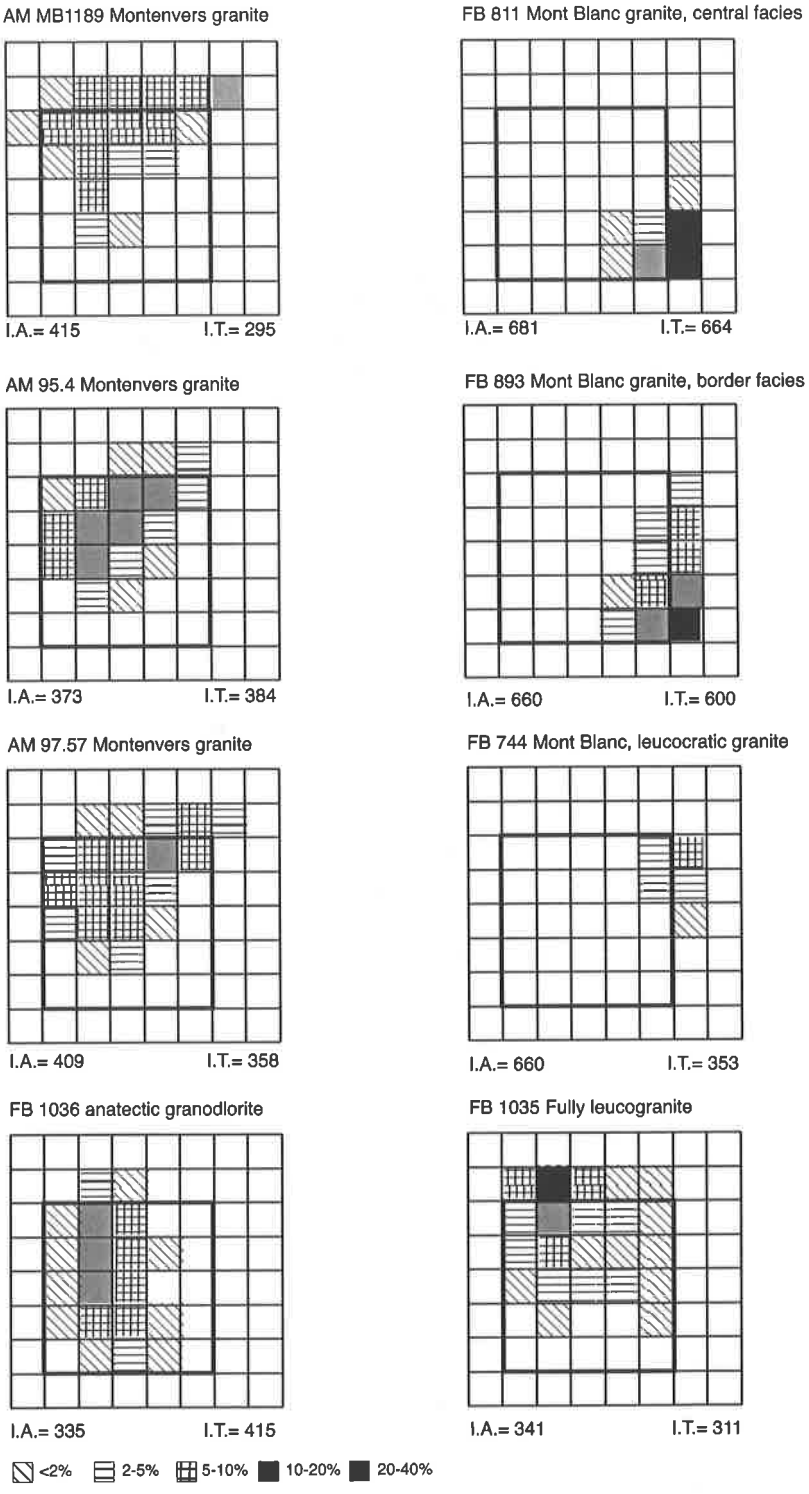

Fig 4.03B
Zircon typology of Carboniferous granitoids after Pupin (1988). Data from Bussy FB (1990); Morard AM (1998); Bussy et al. (2000).
Distribution typologique des zircons des granites d'âge carbonifère (d'après Pupin 1988). Données de Bussy FB (1990); Morard AM (1998); Bussy et al. (2000).

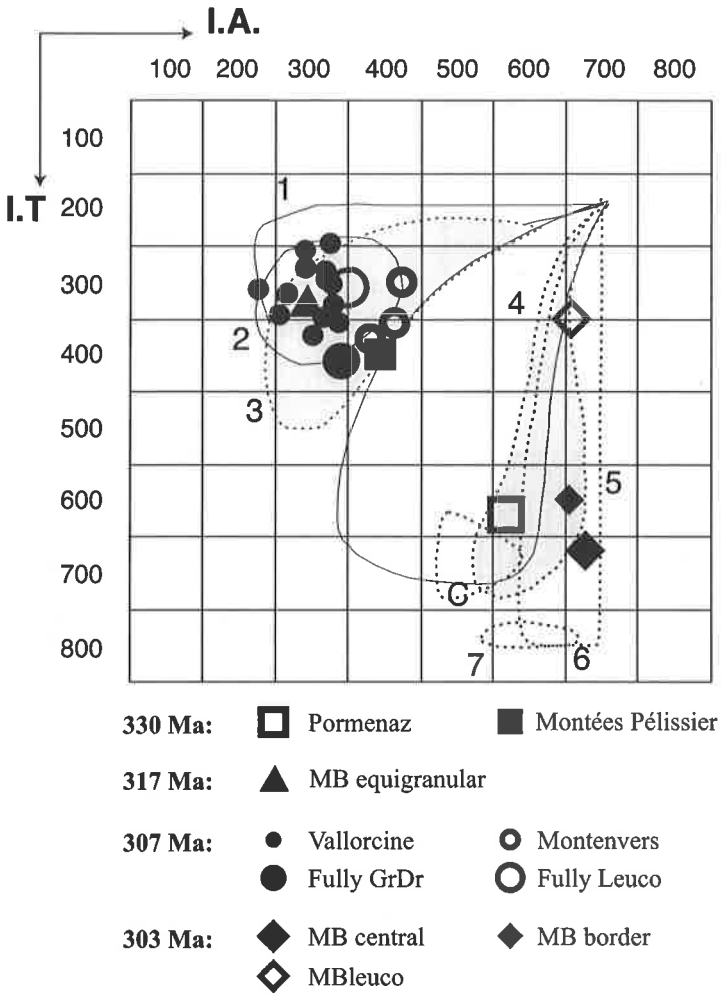

Fig. 4.04
Distribution of zircon populations (mean points) of Variscan granitoïds from the Mont Blanc and Aiguilles Rouges massifs in the classification diagram of Pupin (1988). Data from Fig. 4.03. Significance of the labeled fields: (1) aluminous leucogranites; (2) (Sub)autochtonous monzogranites and granodiorites; (3) intrusive monzogranites and granodiorites; (4) calc-alkaline and K-calc-alkaline series granites; (5) Subalkaline series granites; (6) Alkaline series granites; (7) Oceanic tholeiitic granites (plagiogranites); (C) Continental tholeiitic granites (charnokites).
Distribution des populations de zircons (points moyens) des granites varisques des massifs du Mont Blanc et des Aiguilles Rouges dans le diagramme de classification de Pupin (1988). Données de la figure 4.03. Signification des champs: (1) leucogranites alumineux; (2) monzogranites et granodiorites (sub)autochtones; (3) monzogranites et granodiorites intrusifs alumineux; (4) granites des séries calco-alcalines et calco-alcalines potassiques; (5) granites des séries subalcalines; (6) granites des séries alcalines; (7) granites océaniques tholéiitiques (plagiogranites); (C) granites tholéiitiques continentaux (charnokites).

IV.3 Geochemical characteristics – a summary

The geochemistry of Carboniferous granites has been addressed in many specific studies. The reader is refered to original publications for specific data and details (i.e. Bonin et al., 1993; Bussy et al. 2000; Marro 1986; Schouwey 1988; Bussy 1990; Brändlein 1991, Brändlein et al., 1994; Chiaradia 1993; Dobmeier 1996; Délitroz and Fellay 1997; Gay 1998; Morard 1998) - (Chemical data: **Annex I, Tab VI.12**). Some general chemical features will be reported and discussed below in a number of conventional diagrams. As all these rocks underwent a complex polymetamorphic history, their concentrations in some of the reputedly mobile elements such as Ca, Na, K, Rb, Sr and Ba might have been modified, which would affect their position in some diagrams. For example, some of the samples show dubiously high A/CNK ratios in Fig. 4.8, which might be related to a loss of Ca.

The 330 Ma magmatic association

These rocks present a very wide range of silica contents between 56 and 75 wt% SiO_2 and are relatively high in TiO_2 (**Fig. 4.05**). They plot along a monzonite – monzodiorite - quartz-monzonite - monzogranite trend in the R1-R2 classification (**Fig. 4.07**) and have high MgO/Mg+FeO (>0.5) and K_2O/K_2O+Na_2O (>0.5) ratios (**Fig. 4.10** and **4.11**), like other 330 Ma old monzonitic associations (e.g. French Massif Central (vaugnerites), Belledonne, Vosges, Bohemia (durbachites). They are metaluminous (**Fig. 4.08**) and plot in the Bt+Hbl+Px field of the A-B diagram of Debon and Lefort (1988) (**Fig. 4.06**). The P_2O_5 content of the intermediate facies is strikingly high and corresponds to equilibrium temperatures above 950 to 1000°C according to Harrison and Watson (1984) (**Fig. 4.09**). REE contents are also high (ΣREE=200-400 ppm) and fractionated (La/Lu_N=20), with minor negative Eu anomaly (mean Eu/Eu* = 0.70). Other chemical features include high to very high concentrations in LILE like K, Rb, Ba, Sr, in Mg and transition elements like Cr, Ni and V, and in incompatible elements like LREE, Zr and Th. Conversely, Ca is relatively low in this range of SiO_2 content. The durbachitic enclaves have the same chemical characteristics as the monzonites, reminiscent of lamprophyres. All these features are typical of the so-called magnesio-potassic magmatic association defined Variscides by Rossi and Chevremont (1987) and exemplified by French Variscan associations like the Ballons in the Vosges or the Balagne in Corsica.

The 307 Ma peraluminous magmatic association

The rocks from the Vallorcine and Montenvers intrusions are rather high in silica (65-75 wt% SiO_2) (**Fig. 4.05**) and mostly plot in the monzo- and syenogranite fields of the R1-R2 classification (**Fig. 4.7**). They are peraluminous (**Fig. 4.08**) and plot dominantly in the Ms>Bt field of the A-B diagram of Debon and Lefort (1988) (**Fig. 4.06**). Their P_2O_5 content corresponds to equilibrium temperatures well above 950-1000°C (**Fig. 4.09**), which is certainly too high for this kind of magma and rather denotes low Ca activity, a feature typical of peraluminous melts (Bea et al. 1992). Their mg number is relatively high (40-60) for such evolved compositions (**Fig. 4.11**). Their REE contents are intermediate (ΣREE=100-200 ppm), moderately fractionated (La/Lu_N=5-15), with a marked Eu negative anomaly (Eu/Eu* = 0.37-0.55). These chemical features are typical of cordierite-bearing, peraluminous melts of crustal origin, except may-by for some of their dark microgranular enclaves, which might represent hybrid magmas partly of mantellic origin.

The 300 Ma association

It is essentially represented by the Mont Blanc intrusion and some minor dykes of the Salanfe area. For the Mont Blanc, only compositions of granitic facies are reported, with exclusion of microgranular enclaves and mafic stocks of monzodioritic composition (56 wt% SiO_2, Bussy, 1990). These rocks are highly evolved, generally above 70 wt% SiO_2 (**Fig. 4.05**), metaluminous to slightly peraluminous, definitely peraluminous for the Salanfe dykes (**Fig. 4.8**), and plot in the syenogranite field of the R1-R2 classification diagram (**Fig. 4.07**). Mont-Blanc compositions plot in the Bt±Hbl field of the A-B diagram (**Fig. 4.06**), whereas Salanfe dykes are shifted towards the Ms>Bt field. P_2O_5 concentrations

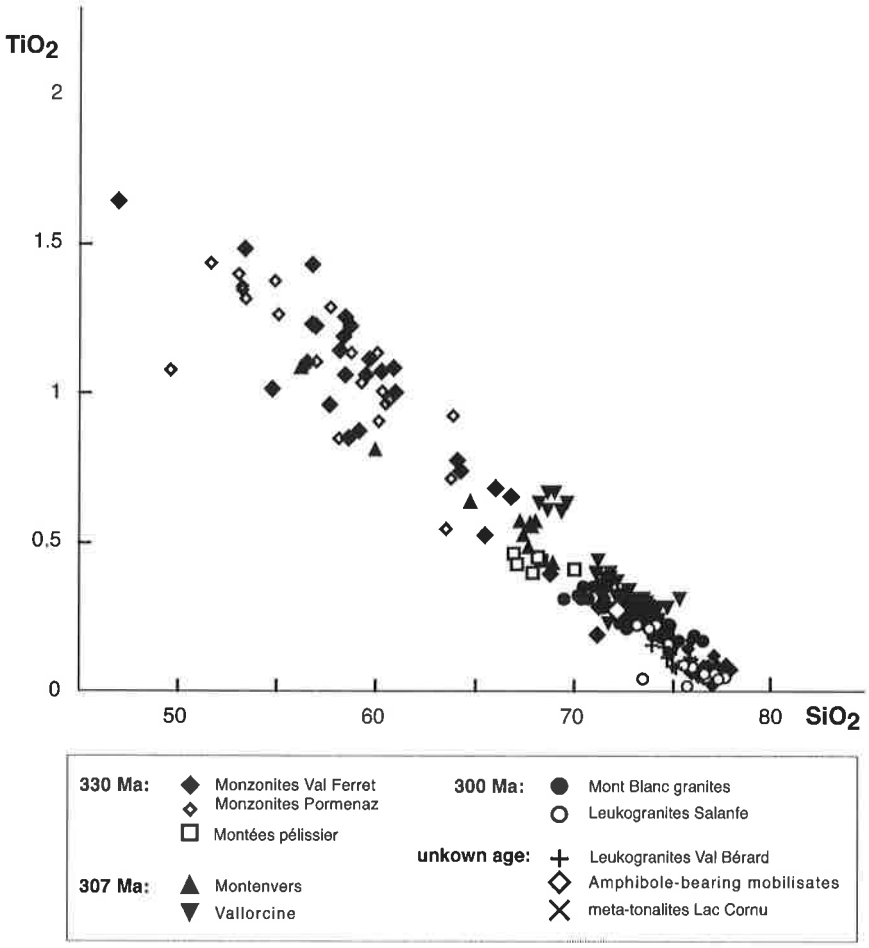

Fig. 4.05
Comparison of chemical composition (TiO_2 – SiO_2) of late Variscan (330-300 Ma) granitoids from the Mont Blanc and Aiguilles Rouges areas (data from Brändlein 1991, Délitroz and Fellay 1997; Dobmeier 1996; Gay 1998; Marro 1986, Morard 1998, Schouwey 1988, Wirsing 1997).
Comparaison du chimisme (TiO_2 - SiO_2) des granitoïdes Varisque (330-300 Ma) du Massif du Mont Blanc et des Aiguilles Rouges (données: Brändlein 1991, Délitroz et Fellay 1997; Dobmeier 1996; Gay 1998; Marro 1986, Morard 1998, Schouwey 1988, Wirsing 1997).

are higher for the more aluminous Salanfe dykes than for the more metaluminous Mont Blanc granites, as expected from the activity of Ca (**Fig. 4.09**). Mg number is especially low for the Mont Blanc granite (**Fig. 4.11**), which is illustrated by iron-rich biotite (Bussy, 1990). Conversely, K is high, as expected from the high K-feldspar content of theses rocks. REE concentrations are intermediate (ΣREE=160-200 ppm), weakly fractionated (La/Lu_N=3-6), with high to very high (leucogranitic facies) Eu negative anomalies (Eu/Eu* = 0.03-0.39). In summary, the chemical characteristics of the Mont Blanc granitic rocks are that of a late orogenic, high-K calc-alkaline to alkali-calcic association, with high Y, Zr contents and Fe/Mg ratios, and a low $^{87}Sr/^{86}Sr$ initial isotopic ratio of 0.705 (Bussy 1990), i.e. a ferro-potassic association as defined by Rossi and Chevremont (1987) with reference to the 300 Ma old Ploumanac'h pink granite in Brittany.

Magmatic rocks of unknown age

Chemical analyses of some magmatic rocks of unknown age and supposedly anatectic origin (leucogranites from Val Bérard, metatonalites and amphibolite-bearing mobilisates from Lac Cornu) have also been reported in some of the reference diagrams for completeness, but will not be commented further on. The Cornu metatonalite often plots away from all other rock analytical points and might not represent a pure melt (e.g. **Figs. 4.08, 4.12**).

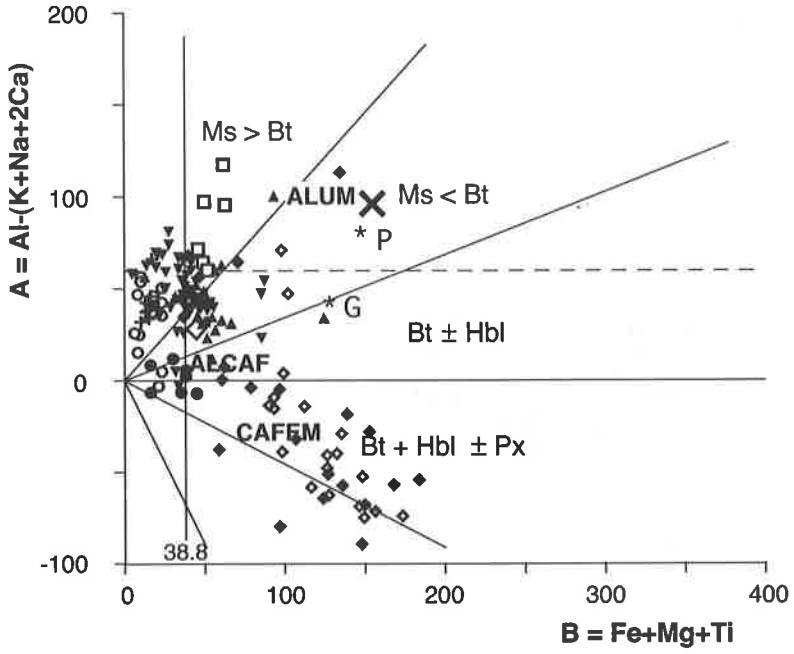

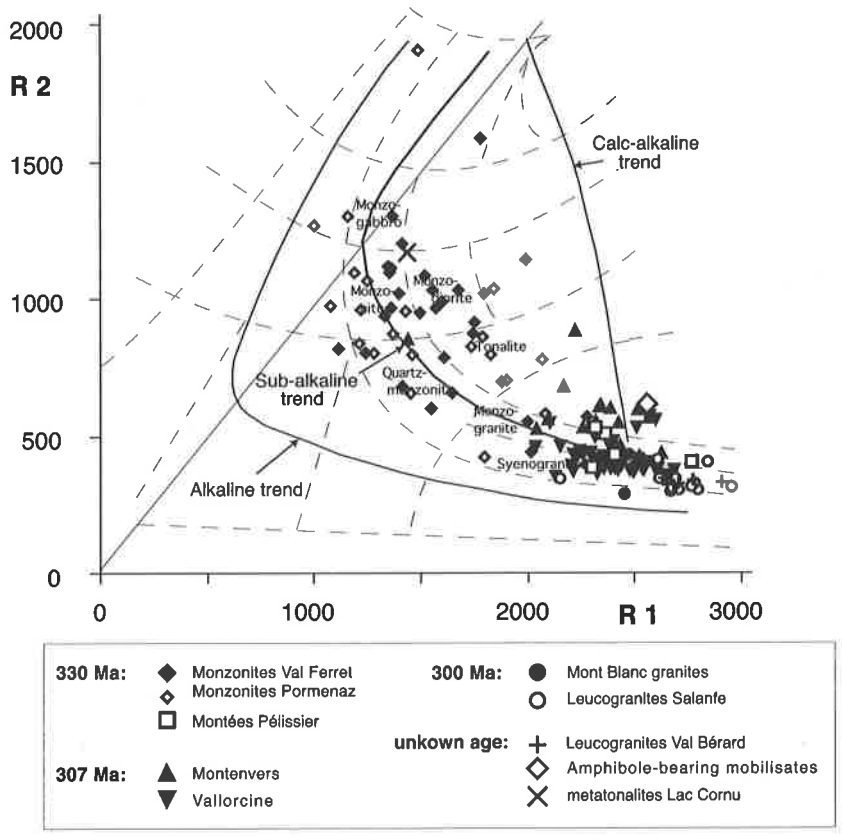

Fig. 4.06
Fields of specific mineral associations in magmatic rocks with discriminants A-B after de Debon & Le Fort (1988). *Diagramme A-B de Debon & Le Fort (1988) et champs de repartition d'associations magmatiques.*

Fig. 4.07
Classification of plutonic rocks after de La Roche et al. (1980). Magmatic trends after Debon et al. (1998); R1 = 4 Si –11 (Na + K) – 2 (Fe + Ti); R2 = Al + 2Mg + 6 Ca. *Diagramme de classification paramétrique des roches plutoniques d'après de La Roche et al. (1980). Tendances d'évolution magmatiques d'après Debon et al. (1998); R1 = 4 Si –11 (Na + K) – 2 (Fe + Ti); R2 = Al + 2Mg + 6 Ca.*

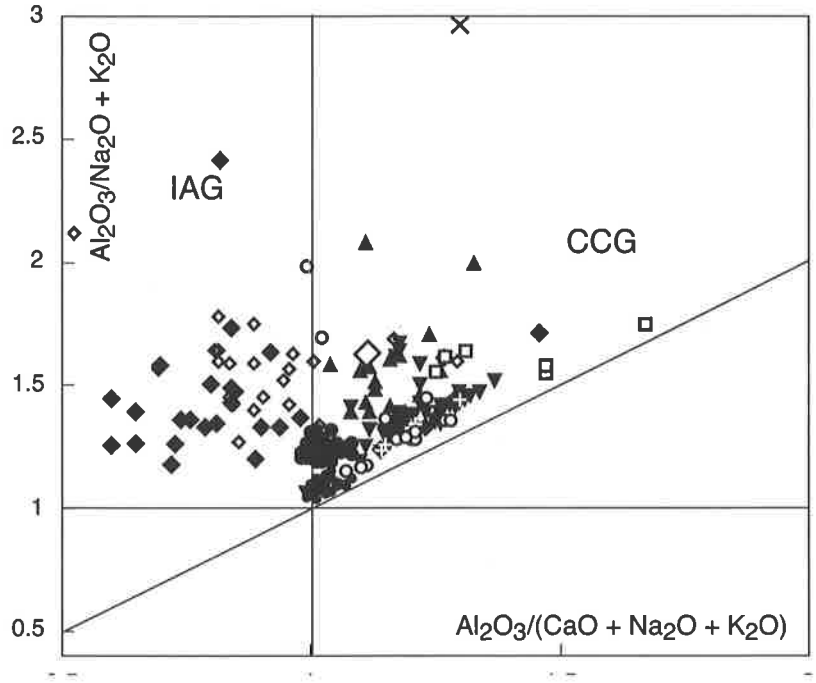

Fig. 4.08
Variscan granites from the Aiguilles Rouges and Mont Blanc massifs in the tectonic discriminant diagram of Maniar and Piccoli (1989). IAG: volcanic arc granites; CCG: continental collision type granites. *Position des granitoïdes varisques des massifs du Mont Blanc et des Aiguilles Rouges dans le diagramme discriminant de Maniar et Piccoli (1989). IAG: granites du type arc volcanique, CCG: granites du type collision continentale.*

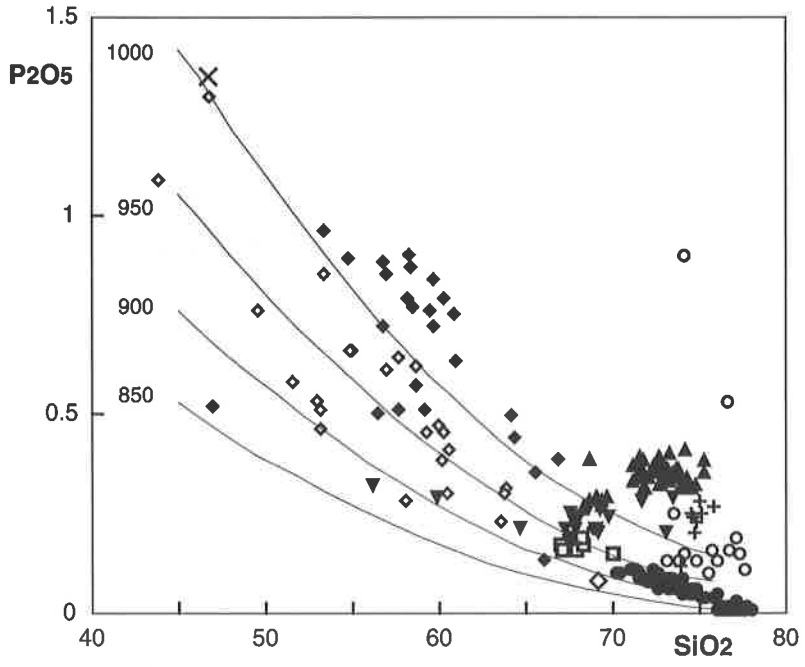

Fig. 4.09
P_2O_5 concentrations in the Variscan granites from the Aiguilles Rouges and Mont Blanc massifs in the diagram of Bea et al. (1992) (see text). Distribution *des concentrations en P_2O_5 des granites varisques des massifs du Mont-Blanc et des Aiguilles Rouges dans le diagram de Bea et al. (1992) (voir texte).*

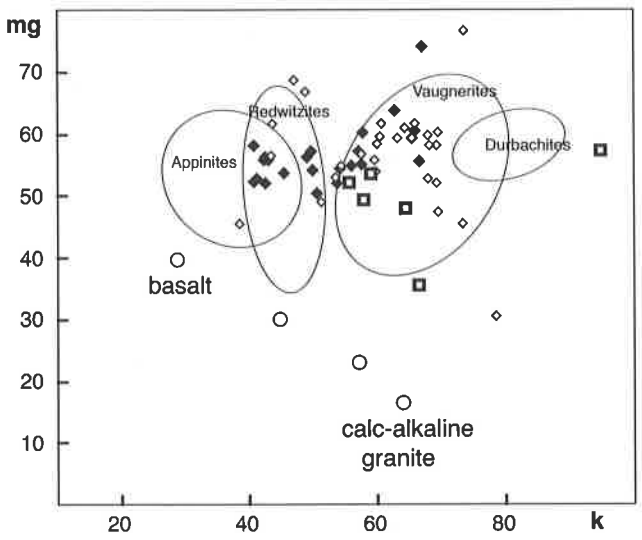

Fig. 4.10
Comparison of chemical composition (values mg = 100*MgO/MgO+FeO; k = 100*K_2O/K_2O + Na_2O) of monzonites/ durbachites from the Val Ferret and Pormenaz areas with comparable rocks from the French Central massif (Sabatier 1991).
*Comparaison de composition chimique (valeurs mg = 100*MgO/ MgO + FeO; k = 100*K_2O/K_2O + Na_2O) de monzonites/durbachites du Val Ferret (massif du Mont Blanc) et de la région de Pormenaz (aiguilles Rouges) avec des roches comparables du Massif central (Sabatier 1991).*

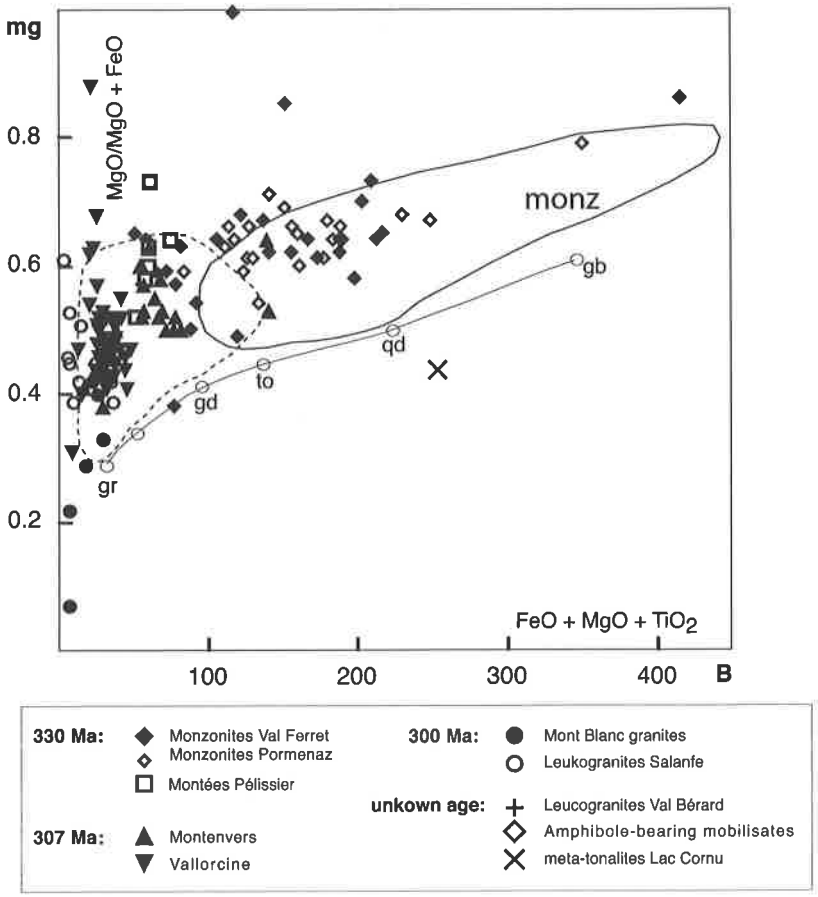

Fig. 4.11
Comparison of chemical composition (values mg = 100*MgO/MgO+FeO; B = FeO + MgO + TiO_2) of monzonites/ durbachites from the Val Ferret and Pormenaz areas with comparable rocks (monz) from the Belledonne massif (Debon et al., 1998).
*Comparaison de composition chimique (valeurs mg = 100*MgO/MgO + FeO; B = FeO + MgO + TiO_2) de monzonites/ durbachites du Val Ferret (massif du Mont Blanc) et de la région de Pormenaz (Aiguilles Rouges) avec des roches comparables (momz) du massif de Belledonne (Debon et al., 1998).*

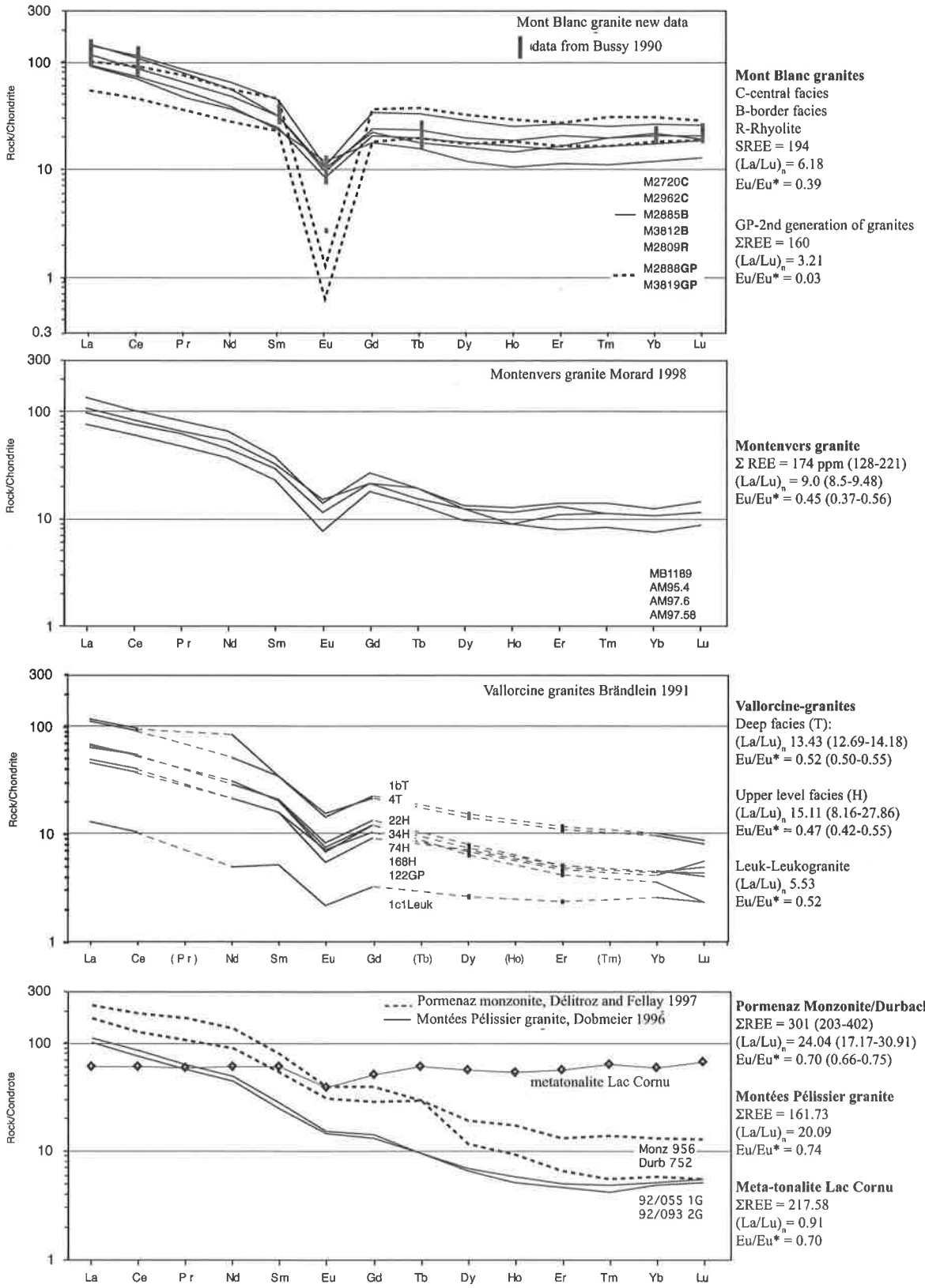

Fig. 4.12

Rare Earth concentration of Late Variscan granites from the Mont-Blanc and Aiguilles-Rouges massifs (chondrite normalized), data from: Bussy 1990, Brändlein 1991, Délitroz and Fellay 1997; Dobmeier 1996; Morard 1998. Mont Blanc granites: new analyses on samples from Marro (M) 1986, and meta-tonalite from Lac Cornu: new data (ICP, CRPG Nancy 1990). (Chemical data: Annex I, Tab.VI.12). *Composition en terres rares (valeurs normalisées aux chondrites) des granites varisques des massifs du Mont Blanc et des Aiguilles Rouges, données: Bussy 1990, Brändlein 1991, Délitroz et Fellay 1997; Dobmeier 1996; Morard 1998. Granites du Mont Blanc: nouvelles analyses sur les échantillons de Marro (M) 1986, métatonalite du Lac Cornu: données nouvelles (ICP, CRPG Nancy 1990). (Données chimiques: Annexe I, Tab. VI.12).*

IV.4 The Carboniferous magmatic evolution

The Carboniferous tectono-magmatic evolution of the Aiguilles Rouges/Mont Blanc area can be synthesized in the following way (Bussy et al. 2000):

(a) Peak T metamorphic conditions are recorded at 327 Ma (peak P is undated, but is probably older) in the Emosson metapelites and isothermal decompression melting at 320 Ma, and pegmatoid veins in eclogites from the Lac Cornu area yielded U/Pb zircon ages of 324 Ma (Bussy, unpublished data). This relatively short time span requires fast uplift rates, accommodated through active tectonic exhumation. According to Thompson and Connolly (1995), decompression melting within the sillimanite-andalusite metamorphic facies cannot occur through simple erosional uplift. Exhumation was thus active already in the Upper Visean, shortly after the transpressive episode recorded by the Montées-Pélissier granite. This is confirmed by $^{39}Ar/^{40}Ar$ cooling ages as old as 331-337 Ma measured on white micas from gneisses adjacent to the Montées-Pélissier granite (Dobmeier 1998). The former nappe stacking which led to the crustal thickening is documented by microstructures (Dobmeier 1996), and is supposed to be of Visean age (Ch. 3.2, von Raumer et al. 2003). In the adjacent Belledonne massif, nappe stacking did not occur before the Visean (Guillot & Ménot 1999) and decompression melting followed quickly during the Westphalian, a timing very similar to that of the Aiguilles Rouges massif.

(b) The 332 Ma Pormenaz monzonite intruded along a high-strain, NNE-SSW trending mylonitic transcurrent fault, which also controlled the position of the adjacent Visean detrital basin. Considering the ultimate mantellic origin of these melts, and their usual syntectonic character in the Variscides, it is inferred that this transcurrent fault zone was one of major crustal- to lithospheric-scale structures, which tapped deep-seated magma chambers or possibly enhanced melting processes, a situation which would allow for rather high temperatures around 900-950°C, as discussed above. The nearby and contemporaneous Montées-Pélissier granite intruded in a similar context. Fluids circulating along the transcurrent fault might have favoured melting of crustal lithologies, triggered by heat transfer from the mantellic magmas (presence of lamprophyric dykes). Von Raumer (1998) suggested a relationship between the Viséan strike-slip evolution and subduction, invoking the model of Chemenda et al (1996), allowing for intrusion of lithospheric melts during slab break-off in a beginning back-arc situation. Considering the most recent plate-tectonic reconstructions for the Lower Carboniferous time span (Stampfli et al., 2002), the formation of the Mg-potassic melts may have been induced, alternatively, by the ongoing subduction of Palaeothetys, or even by subduction of ridge-areas, triggering the intrusion of mantellic melts.

(c) The next recorded event is the simultaneous formation of the Upper Carboniferous detrital basin of Salvan-Dorénaz, starting at 308 Ma (Capuzzo & Bussy 1999), and the 307 Ma magmatic pulse of cordierite-bearing granites. In a Q-Ab-Or diagram, the different types of Vallorcine granite occupy a field stretching from ~5 to 1 Kb eutectic conditions (**Fig. 4.13**; Brändlein, 1991). Considering the shift of eutectic points at reduced water activities to higher values of Q and Or (Ebadi and Johannes, 1991; Holtz et al., 1994), the Vallorcine granitoids are supposed to have been formed under reduced water activities during dehydration melting of granulite type rocks (**Fig. 4.13**; Brändlein, 1991). In comparison, the melts of the contemporaneous Montenvers granite, after their composition Q-Ab-Or, are supposed to have formed at conditions of about 5 Kb/700°C (**Fig. 4.13**; Schouwey 1988). Both granites are supposed to have syntectonically intruded along the border fault of the Carboniferous basin, which is again considered as a major crustal-scale structure. Erosion is very active and thick coarse deposits are accumulating in the basin at least until 295 Ma (Capuzzo & Bussy 1999). This is interpreted as an evidence for continued tectonic exhumation in the latest Carboniferous in an essentially transcurrent to transtensional rather than extensional regime (Capuzzo et al. 2003). In that context, the sedimentary trough could have formed as a kind of pull-apart structure or half-graben in case of oblique sliding (intermediate between normal and transcurrent faulting) along the border

fault. Granodioritic cordierite-bearing melts require temperatures well above 800°C to form (e.g. Patiño-Douce & Harris 1999), and such conditions were not reached through regional metamorphism in the lower-middle crust. Either, the lower crustal magma sources were tapped by the deep transcurrent faults along which progressive restite unmixing (restitic relics of apatite, see above) and crystal fractionation occurred, or additional heat has been supplied by the associated mafic mantellic magmatism.

(d) In the nearby Mont Blanc massif, the larger post-tectonic 303 Ma Mont Blanc acid-basic association intrudes within a pull-apart structure in a continued transcurrent to transtensive regime. Marro (1988) discusses an early stage of liquidus formed at low water activities at considerable depth. After the Q-Ab-Or composition of the second generation leucocratic granites, Marro (1987) deduced cristallisation at pressures about 2 – 0.5 Kb. Following Bussy (1990), the Mont Blanc granite and its enclaves testify for a bimagmatic acid-basic evolution, where the granitic melts formed at depth of a thickened continental crust under granulitic conditions, and the basic melts are supposed to have a mantellic origin. This magmatic evolution in the context of initial Permian rifting occurring in front of the still continuing subduction of Palaeotethys (Stampfli et al., 2002).

The Carboniferous tectono-magmatic evolution outlined above is virtually identical to that observed in the other External Crystalline Massifs and adjacent areas, with minor differences in the timing of events (e.g. Schaltegger 1997; Debon & Lemmet 1999). More generally, it is in good accordance with the overall Carboniferous evolution of the internal Variscides (e.g. Burg et al. 1994; Rey et al. 1997), considered as a period of post-collisional readjustment of a thickened continental crust.

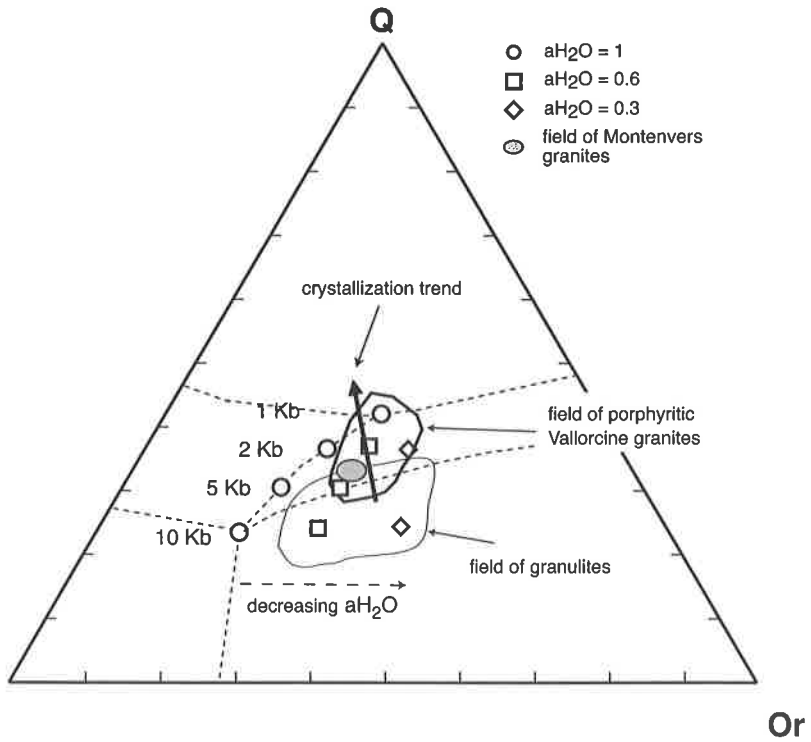

Fig. 4.13
Q-Ab-Or diagram with indication of eutectic compositions of granitic melts at different pressures and water activities (after Johannes and Holtz, 1991; Ebadi and Johannes, 1991; Holtz and Johannes 1994) with interpretation of Vallorcine- and Montenvers granites (Brändlein 1991, Schouwey 1988). Field included by the solid line: chemical variation of Vallorcine-granite (Brändlein 1991) with trend of cristallisation (arrow); Gray elliptic field: composition of Montenvers granites (Schouwey 1988).

Triangle Q-Ab-Or avec indication des compositions eutectiques de granites en fonction de la pression et de l'activité en eau (basé sur Johannes and Holtz, 1991; Ebadi and Johannes, 1991; Holtz et Johannes 1994) et projection des granites de Vallorcine et Montenvers (Brändlein 1991, Schouwey 1988). Champ marqué en gras: variation de compositon chimique des granites de Vallorcine (Brändlein, 1991) avec indication de la tendance de cristallisation (flêche); Ellipse grise:composition des granites de Montenvers (Schouwey, 1988).

Chapter V: Regional Geology – Field Trips

The new geological maps

The Aiguilles Rouges and Mont Blanc massifs offer a variety of rock types to be visited during excursions. For this purpose, in the Aiguilles Rouges massif, visits of the areas around Lac Emosson, Lac Cornu, Lac Salanfe, Val Bérard and the Lac Cornu region are proposed and, in the Mont Blanc massif, the areas around the Argentière glacier (Lognan), the valley of Trient and its glacier, and a walk from La Breya to the alpine huts of Cabane d'Orny and Cabane de Trient may be interesting subjects (see **Fig. 5.01**).

The general geology and petrography is presented in preceding chapters, and the different sketch maps (**Fig. 1.03, 4.01, 5.01**) illustrate the main structural units and the separation of the Mont Blanc and Aiguilles Rouges massifs by a major tectonic line of Alpine age. The latter hosts the Mesozoic sediments of the Chamonix zone, containing the Mesozoic covers of both basement areas (Epard, 2003). Geological details of the basement are given in figures accompanying the different field trips (see **Fig. 5.01**), and in coloured geological maps (Annexes IV-XI) presenting the most recent state of knowledge in geological key areas.

As mentioned already in chapters I and III, the basement areas of both massifs are not only separated by Mesozoic units, but were strongly tectonised before and during the intrusion of Late Variscan granitoids and the formation of syntectonic sedimentary troughs of Late Carboniferous age. Mylonites were already described by Reinhard (1927) from the Miéville region, situated at the southern contact of the Vallorcine granite. In the NW of the Vallorcine granite, Bellière (1958) distinguished two types of rocks, the group of "gneiss du Lac Cornu", metamorphosed rock series of high amphibolite facies grade, and "gneiss de Chésérys", representing a strongly mylonitized zone which may be classified with the older term "blastomylonites", corresponding to a strongly tectonized rock series, where deformation is accompanied by a strong recristallization at amphibolite facies conditions.

The aspect of this mylonite zone, stretching from Miéville in the Rhone valley to the Lac Blanc – Lac de Chésérys area of the Aiguilles Rouges massif, changes considerably when observing the different sections and is characterized by a subvertical north-striking foliation and subhorizontal north-plunging lineations (compare **Figs. 3.11; 3.12**). The evolution from steeply dipping fold-axes to flat-lying sheeth-folds led Joye (1989) to present the model of a major dextral shear-zone. In the west of this large mylonite zone appear normally less deformed rocks like metamorphosed metasdiments, orthogneisses and amphibolites, subject of the proposed field trips (petrography and deformation, see Ch. II, III). The different geological maps published in this volume (annexes IV-XI) represent key areas for specific basement structures, and the corresponding maps (see **Fig.5.01**) will be shortly characterised int he following lines.

The **Emosson region (annexes IV - VI, Figs. 5.02 - 5.05**) is characterised by large-scale folds overprinting an assemblage of former pre-Cambrian to Cambrian metasediments intruded by granitoid orthogneisses of Ordovician age. All rock units reveal a sequence of Variscan folds which may be related to events in the main mylonite zone outcropping in the south of the area (see **Fig. 5.02**).

The **Salanfe area (annex IX, Fig. 5.12)** is situated in the northern prolongation of the Emosson region, and the map gives details of strongly folded Pre-Cambrian to Cambrian metasediments and volcanites intruded by ordovician granitoids. All rock units underwent high-grade metamorphic transformations of Variscan age and, in addition, the former Cambrian carbonate units host gold-bearing scheelite-diopside skarns of Late Carboniferous age.

The **Val Bérard area (annex VII, Fig. 5.07)** again, is characterised by large-scale isoclinal folds in pre-Cambrian to Cambrian metasediments with intruded Ordovician granitoids, and the rock assemblage is surrounded by mylonite zones containing relics of eclogites and/or granulites, and Variscan migmatites and granitoids.

The **Lac Cornu area (annex VIII, Fig. 5.09)**, famous for the historical finding of eclogite, is characterised by a stronly migmatitic assemblage of former metasediments and Ordovician orthogneisses where, parallel to the large-scale synformal structures, large bodies of eclogites and many lumps of granulitic metabasites and ultramafites are observed.

The **Lognan and Trient areas (annexes X, XI, Figs. 5.12, 5.15)**, are situated at the eastern border zone of the Mont Blanc granite. Both are characterised by migmatitic metasediments and orthogneisses (Ordovician granitoids), intersected by Variscan granitoid gneisses (Lognan granite) and limited by the border facies of the Mont Blanc granite. All rocks expose the characteristic features of Alpine metamorphism.

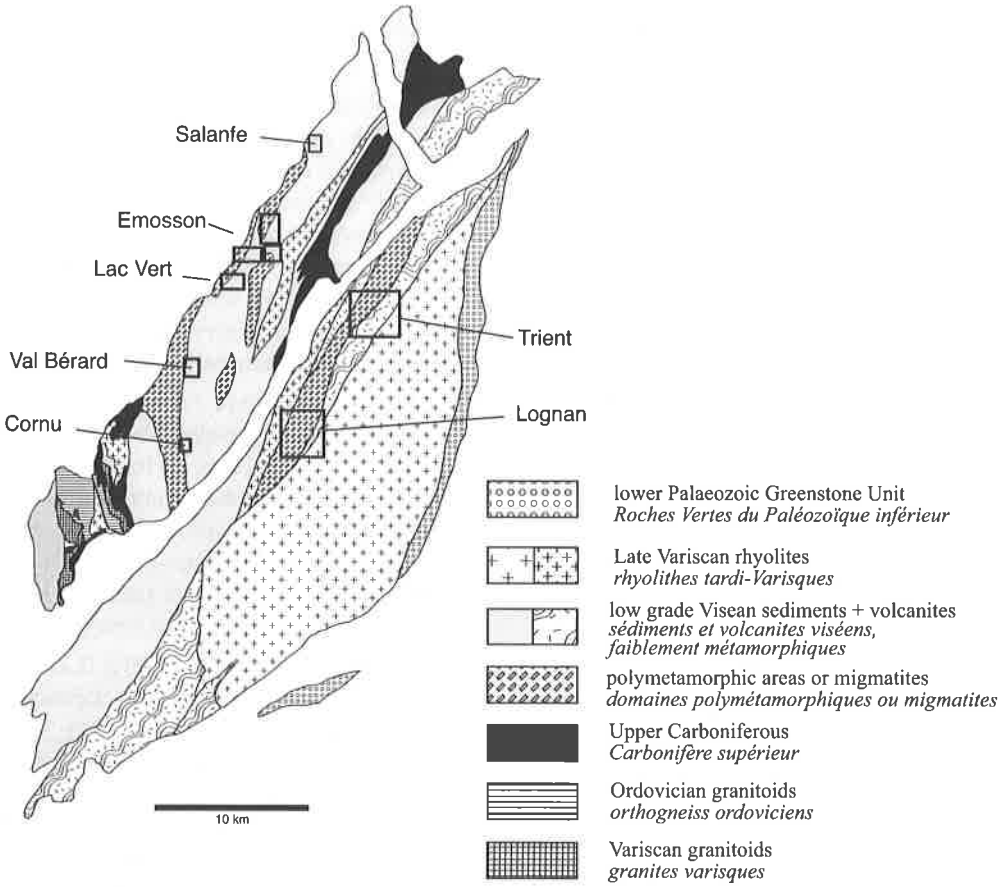

Fig. 5.01

Location of proposed field trip areas and geological maps in the Aiguilles Rouges and Mont Blanc massifs
Loc alisation des excursions et dse cartes géologiques dans les massifs des Aiguilles Rouges et du Mont Blanc.

Emosson field trip (**V.1**): comprising 3 geological maps at the 1: 10 000 scale (annexes IV-VI: Emosson West, Emosson East, Lac Vert) and corresponding field-maps (Figures 5.02, Emosson dam-site; 5.03, Emosson West; Fig. 5.04, Emosson East; Fig. 5.05, Lac Vert) with stop informations.
Emosson: 3 cartes géologiques au 1 : 10 000 (annexes IV-VI: Emosson West, Emosson East, Lac Vert) et figures correspondantes (Fig. 5.02, Emosson barrage; 5.03, Emosson Ouest; Fig. 5.04, Emosson Est; Fig. 5.05, Lac Vert)

Val Bérard field trip (**V.2**): geological map at the 1. 20 000 scale (annex VII); and corresponding field-map Fig. 5.07

Val Bérard: carte géologique au 1: 20 000 (annexe VII) et Fig. 5.07

Lac Cornu field-trip (**V.3**): geological map at the 1 : 10 000 scale (annex VIII) and corresponding field-map Fig. 5.09

Lac Cornu: carte géologique 1 : 10 000 (annexe VIII) et Fig. 5.09

Salanfe field trip (**V.4**): geological map at the 1 : 5 000 scale (annex IX) and corresponding field-map Fig. 5.12;
Salanfe: carte géologique au 1 : 5 000 (annexe IX) et Fig. 5.12.

Lognan (Mont Blanc massif) field-trip (**V.5**): geological map at the 1:20 000 scale (annex XI) and field-map Fig. 5.13

Documentation Lognan (massif du Mont Blanc): carte géologique au1 . 20 000 (annexe XI) et Fig. 5.13

Trient-Petoudes (Mont Blanc massif) field-trip (**V.6**): geological map at the 1: 20 000 scale (annex X) and Fig. 5.15

Trient-Petoudes (massif du Mont Blanc): carte géologique au 1 : 20 000 (annexe X), et Fig. 5.15

V.1. Lac Emosson (Aiguilles Rouges)

Maps: CH: sheet 1324 Barberine (1:25 000); Geological maps 1 : 10 000 East and West Emosson, Lac Vert (Annexes IV, V, VI), Figures 5.02-5.05.

Access: road from Finhaut, parking lot at 1970 m near the dam site (facilities for boarding and lodging). Departure: from the dam site Lac Emosson either towards North along the eastern lake-side to Col de Barberine (**Fig. 5.04**), or across the dam towards West in direction of Vieux Emosson (**Fig. 5.02, 5.03**).

Topic: the polymetamorphic basement of the Aiguilles Rouges massif, its Variscan metamorphism and anatexis, and the Alpine overprint of sedimentary and igneous lithologies.

Outline: The Lake Emosson area is one of the best sites to observe the polymetamorphic basement of the Alpine External Massifs. The oldest lithologies are Late Proterozoic to Early Palaeozoic sediments and volcanites, which were intruded by Ordovician granitoids (orthogneisses), before all rocks underwent Variscan metamorphism. The latter was of high amphibolite facies grade and locally induced partial melting (Genier 2002). Metamorphism was accompanied by long-lasting deformation with superposition of at least three fold generations, the last one being of kilometer scale. The latter is identified by ubiquitous Z-, S- and M-shaped parasitic folds, which allow distinction between adjacent anti- and synforms. A point of discussion remains interpretation of the narrow band of orthogneiss-like rocks, accompanying the main orthogneiss body on the western lake side (**Fig. 5.05, Annex V**). The rocks are strongly sheared, and observation at the western side of the former Barberine dam (june, low water level!) support interpretation as metagreywackes. Consequently, all metasediments of the western Emosson region are comprised in a major synform, which is well visible when regarding the metagreywackes, and this new interpretation is shown in **Fig. 5.05** and in the geological map (Annex IV).

Alpine metamorphism reached low greenschist facies grade. All units are unconformably overlain by sandstones of Triassic age, hosting the famous saurian footprints (Demathieu and Weidmann 1982) in the Vieux Emosson Lake area. The Alpine dome-like structure of the massif is underlined by the position of the Mesozoic sediments, which rest horizontally on top of the basement rocks in the middle of the massif (Aiguille de Belvedere, 2600m; Favre 1867!), whereas they are steeply dipping on both margins of the latter in the Rhone valley (400 m above sea-level).

Alpine metamorphism increases from northwest to southeast throughout the orogen (see Ch. 3.1.1); it is of lowest greenschist facies grade in the Aiguilles-Rouges area (estimated at c. 275°C, on the basis of mineral textures and stability). Most rocks at the dam site show traces of Alpine deformation, where every rock type carries its own characteristics (von Raumer 1974, 1984). Pumpellyite, prehnite and laumontite are found in weakly transformed amphibolites, and stilpnomelane is observed in the matrix of nearly undeformed rhyolites of Late Carboniferous age. Granitoid orthogneisses yield chlorite-albite mineral assemblages when approaching higher levels to the overlying nappes, where small drag-folds also appear. Quartz shows the first stages of undulation and low angle boundary crystallisation (polygonisation). Depending on the lithology, conjugated shear systems with corresponding tension gashes developed at different scales. Orthogneisses developed a general, closely spaced fracture cleavage with tiny chlorite-filled tension gashes, whereas micaschists show two sets of larger shearing planes with growth of fiber quartz crystals parallel to the stretching direction. In the slightly deformed overlying Triassic sandstones, tension gashes are up to 10 cm long. All three types of brittle shear probably represent different answers to the same Alpine deformation in the vicinity of the basal Alpine nappe thrust plane (compare **Fig.3.14**).

Characteristics of outcrops

Stop a, Finhaut (Coord. CH. 565.000/103.860):
On the way to Lac Emosson, road-cut before arriving to the northern entrance of the village of Finhaut (stop **a** in the adjacent figure, in front of the parking facility P before the narrow road bend on the right side).

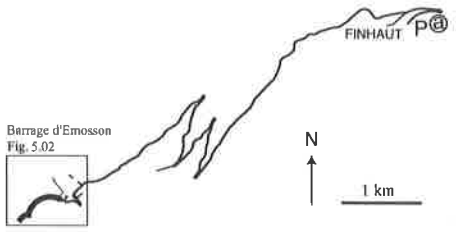

Topic: Mass flow deposits of the Salvan-Dorénaz late Carboniferous sedimentary basin.
In this sedimentary basin, Niklaus and Wetzel (1996) and Capuzzo (2000) distinguished four lithologic units (alluvial fans and braided, anastomosed and meandering river deposits), which record the sedimentary evolution accompanied by a strike-slip tectonic regime. The sedimentary evolution started at the end of the Westphalian (308 ± 3 Ma) with mainly coarse-grained clastics forming an alluvial fan system from the western margin (outcrop area), and the outcrop area represents the corresponding very coarse conglomerates with large boulders of migmatites revealing athe proximal situation at the shoulder of the fan system. The dark couloured fine grained channels underline the quickly changing situation between the deposits in the channel and the very coarse-grained boulder beds.

Stops 1-13, Emosson dam site

Arriving at the dam site, a walk around the lake from east to west, or from the damsite to north, will give the opportunity to recognize the main lithologies of the polymetamorphic basement. The lakeshore is a continuous outcrop, but only a limited number of topics have been selected.

Vallorcine granite

Stop. 1 (Fig. 5.02): The upper facies of the Vallorcine granite is outcropping right after the car park, along the small road to the dam. Compared to the outcrop in the Rhone valley (e.g. Miéville), it is finer-grained with less biotite and almost no enclaves, which is thought to result from an enclave unmixing process during upward motion of the magma. The intrusive contact of the granite with its gneissic host rocks is visible behind the small chapel facing the restaurant (coord. CH 561.310/102.000). It is characterized by a 1 m thick brecciated and silicified band, with fibrous quartz crystallized radially all around the clasts. This spectacular texture has been interpreted as a result of hydraulic brecciation during the shallow level intrusion of a fluid-saturated granitic magma (Genier, 2001).

Mylonite-Zone

Stops 2 and 3 (Fig 5.02): Before arriving to the parking lot, at the entrance of the gallery leading to the eastern side of the lake (stop 2), and at the eastern dam edge (stop 3), a nearly 500 m large mylonite zone separates the Vallorcine granite from the polymetamorphic metasediments located further northwest (see also **Fig. 3.10**). Despite the very strong deformation, former orthogneisses (Ordovician granitoids) and metasediments, like calc-silicate lenses (former calcsilicate marbles) can be recognized. The strike-slip tectonics producing the mylonites probably facilitated intrusion of the Vallorcine granite. The Rb-Sr-thin-slab method of dating (Thöni 1989) produced an age of 300±20 Ma for the general deformation (± 500°C), which corresponds to the age of the Vallorcine granite, 307 Ma, Bussy et al. 2000). Microstructural observations (Joye 1989, **Fig. 3.10**) show that the entire zone is dominated by dextral shearing with formation of a subhorizontal stretching lineation (dip 20° NE) produced through a SSW/NNE tangential compression of pre-existing, more horizontal structures (S_2). Joye (1989) interpreted narrow, very fine-grained, dark veinlets of glassy constitution as probable pseudotachylites.

Retrograded Ordovician orthogneisses

Stop 4 (Fig 5.02): 10m after the western end of the dam, relics of a former Ordovician orthogneiss are visible among the mylonites, the former preserving lens shaped relics of K-feldspar phenocrysts. Some of the dense, light green coloured gneisses show the formation of multiple sets of horizontal kink-bands, corresponding to a horizontal set of slicken sides with a tectonic transport of the hanging parts towards NW. In a lateral view, multiple tiny chlorite-filled tension-gashes correspond to brittle deformation during Alpine NW-directed nappe transport of the hanging parts.

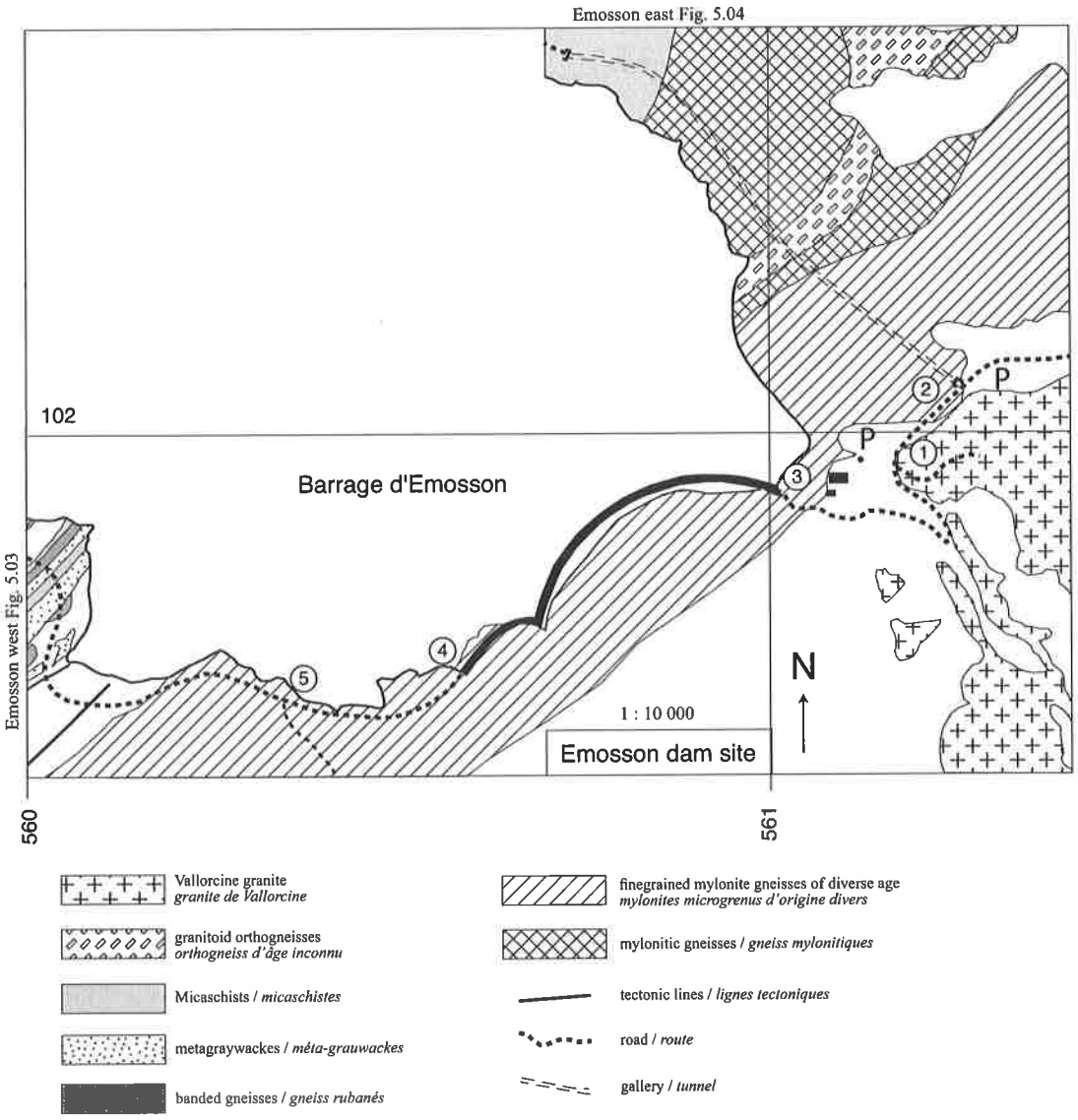

Fig. 5.02
Map of Emosson dam-site with main lithologies and stop numbers. *Lithologies principales observées aux alentours du Barrage d'Emosson avec indication des numéros des arrâts.*

Migmatites

Stop 5 (Fig. 5.02): In the mylonites, partial melting affected former muscovite-bearing (?) metagreywackes, and the orthogneisses. Migmatitic structures are beautifully outcropping along the road west of the dam. Besides local structures due to Alpine metamorphism and deformation, the leucosomes clearly record syn- to post-anatexis dextral shearing. Monazites from one of the thickest leucosome lenses yielded an age of 320 ± 1 Ma (Bussy et al. 2000). The leucosomes mainly consist of K-feldspar (50-60 vol%), quartz (30%) and plagioclase (5-30%) ± muscovite ± biotite (Genier, 2002). These are mostly local melts, which did not substantially migrate. Anatexis is ascribed to the dehydration melting of muscovite during the high-T isothermal decompression of the rocks. Adjacent metapelites host abundant folded quartz veinlets of metamorphic origin, but no leucosomes at all. As pelites melt more readily and at lower temperatures than water unsaturated graywackes, a major tectonic contact is inferred between the migmatitic metagreywackes unit and the non-migmatitic metapelites, for which a lower peak metamorphic temperature is postulated.

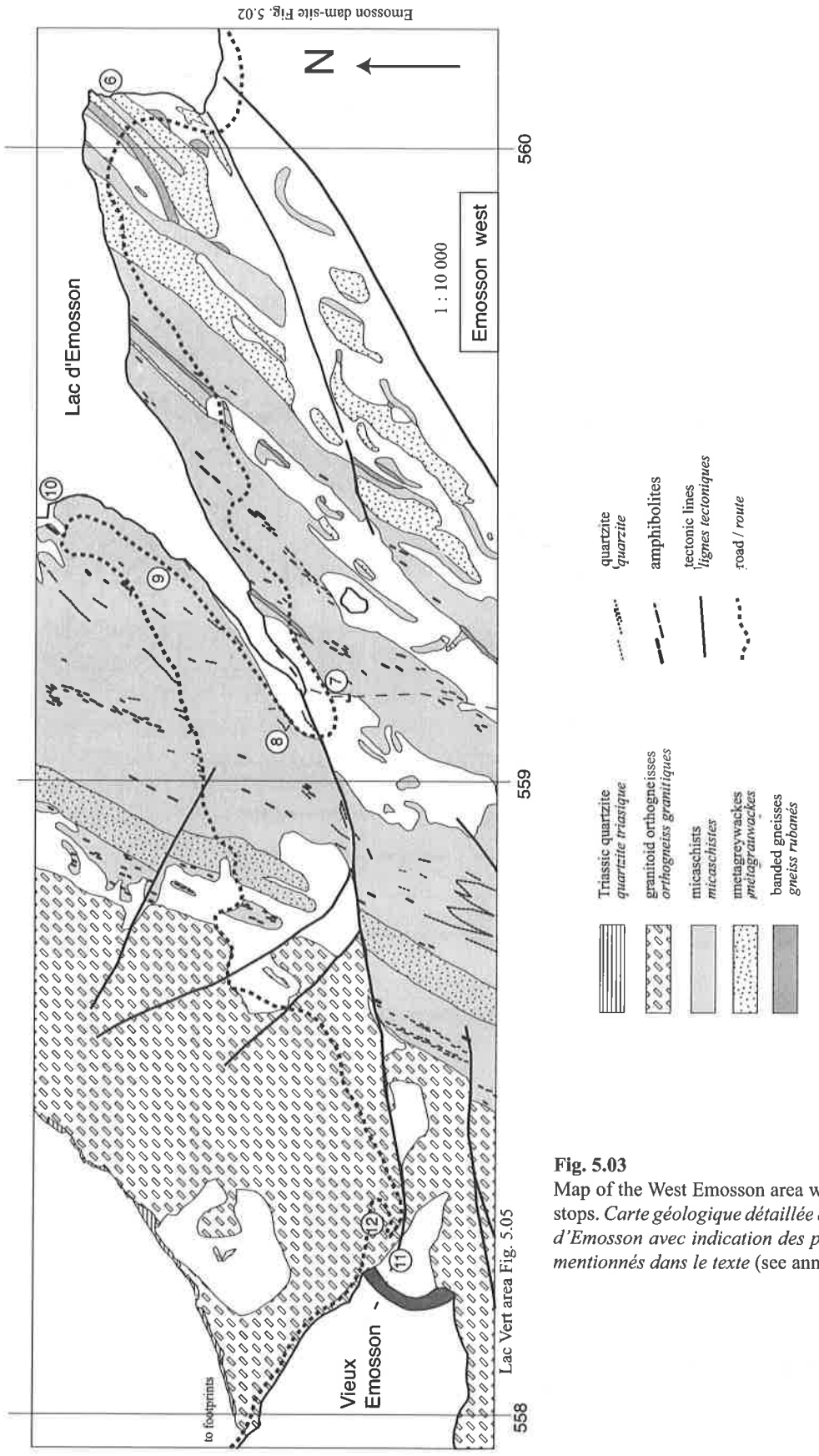

Fig. 5.03
Map of the West Emosson area with numbered field-stops. *Carte géologique détaillée à l'ouest du barrage d'Emosson avec indication des points d'observation mentionnés dans le texte* (see annex V).

Metasedimentary units

Stops 6 – 9 (Fig. 5.03): Complex and superimposed tectonic structures exclude any lithostratigraphic reconstruction in the Aiguilles Rouges massif. Only major sequences or units can be crudely identified at the map scale (see Chapter II, **Fig. 2.19**). They consist of:

(I) a unit of greywackes with metapelitic interlayers;

(II) a mixed unit composed mainly of metapelites with some thin metagreywacke layers, a quartzite horizon, a layer of carbonates (appearing mostly as large boudins), and one or two amphibolite layers (now boudinaged).

(III) a third unit characterized by finely banded metagreywackes and metapelites with a rusty patina.

Many detailed observations are found in von Raumer (1983), von Raumer and Schwander (1985), Schulz & von Raumer (1993), Dupasquier (1996), Schmocker (1996), Fracheboud (1997) and Marquis (1997). A comparison with other European lithostratigraphic sections brings convincing evidence that these lithologies have a Late Proterozoic to Early Palaeozoic age (see general introduction, Ch. I).

Metapelites and metagreywackes record a Barrowian-type of metamorphism with early [biotite-staurolite-kyanite-garnet] assemblages evolving towards [biotite-garnet-sillimanite] parageneses (see Ch. III.2). Joye (1989) locally observed sillimanite and cordierite in strongly sheared rocks among the mylonites. A monazite-in reaction (close to thermal peak?) has been dated at 327 ± 2 Ma (U/Pb on monazite, Bussy et al. 2000). Late stages are quartz segregation lenses with K-feldspar and andalusite. Such a sequence of parageneses does not necessarily represent a continuous PT-path, but could reflect two distinct events, i.e. an early-Variscan high pressure phase and a late-Variscan, more temperature dominated phase. Geochemical data from different localities indicate that metagreywackes carry the fingerprints of an active margin setting (Bhatia 1983), resulting from the erosion of quartzitic lithologies or acidic volcanites (Roser and Korsch 1988). This agrees well with our general interpretation of shelf sediments located at a Gondwana active margin (see Ch. I).

Stop 6 (Fig. 5.03): Metapelites are strongly folded and display either biotite-rich micaschists with some garnet, and /or white patches of plagioclase, elongated parallel to the main foliation plane (**see Photo 3.14**). Nice outcrops are visible, when dam water-level is low.

Stop 7 (Fig. 5.03): Along the road-side, east of the water-channel, erosion uncovered typical F3-folds with steeply dipping fold-axes in metapelitic rocks.

Stop 8 (Fig. 5.03): Metaquartzites form a recognizable white horizon, which can be followed in the field when mapping strongly boudinized pieces preserved in the highly plastic micaschists. They are rather coarse-grained quartzitic sandstones with tiny garnets and a faint layering underlined by biotite.

Stop 9, (Fig. 5.03): Late Variscan tension gash of quartz-andalusite with K-feldspar in metapelitic rocks (**Photo 3.16**). Rather large andalusite crystals are pseudomorphosed by an assemblage of chlorite-white mica (pinite). In the neighborhood, many steeply dipping F3-folds of refolded quartz-veins can be observed in the micaschists.

Metabasites

Metabasites (see Ch. II.2) appear as boudin-shaped amphibolites, mainly concentrated in the micaschist-series, but also as eclogite bodies, as in the Lac Cornu area, situated few kilometers to the southwest. Distribution of amphibolites in km-long strings of boudins point to the former existence of one or two relatively thin layers, best preserved in the fold-hinges. They mainly consist of amphibole – plagioclase ± diopside ± garnet, and pseudomorphs of former zoisite needles (**Photo 2.16**). Von Raumer et al. (1990) distinguished two main groups of amphibolites: plagioclase amphibolites (former spinel-olivine-tholeiites with relatively higher contents in Cr and Ni) and garnet-plagioclase amphibolites (former hypersthene- or quartz-tholeiites with enriched values of V and P), which were considered to represent a magmatic differentiation series. The fine grain size of the amphibolites and high TiO_2 and V-contents (>5% and > 100 ppm, respectively) suggests a volcanic or subvolcanic origin (Pfeifer et al. 1989). The original rocks were interpreted (von Raumer et al. 1990) as transitional MORB volcanites typical for continental rift zones at the onset of ocean floor spreading. Their age could be either Cambrian or Ordovician. Some of the largest amphibolite bodies are accompanied by leucocratic garnet-bearing gneisses, containing

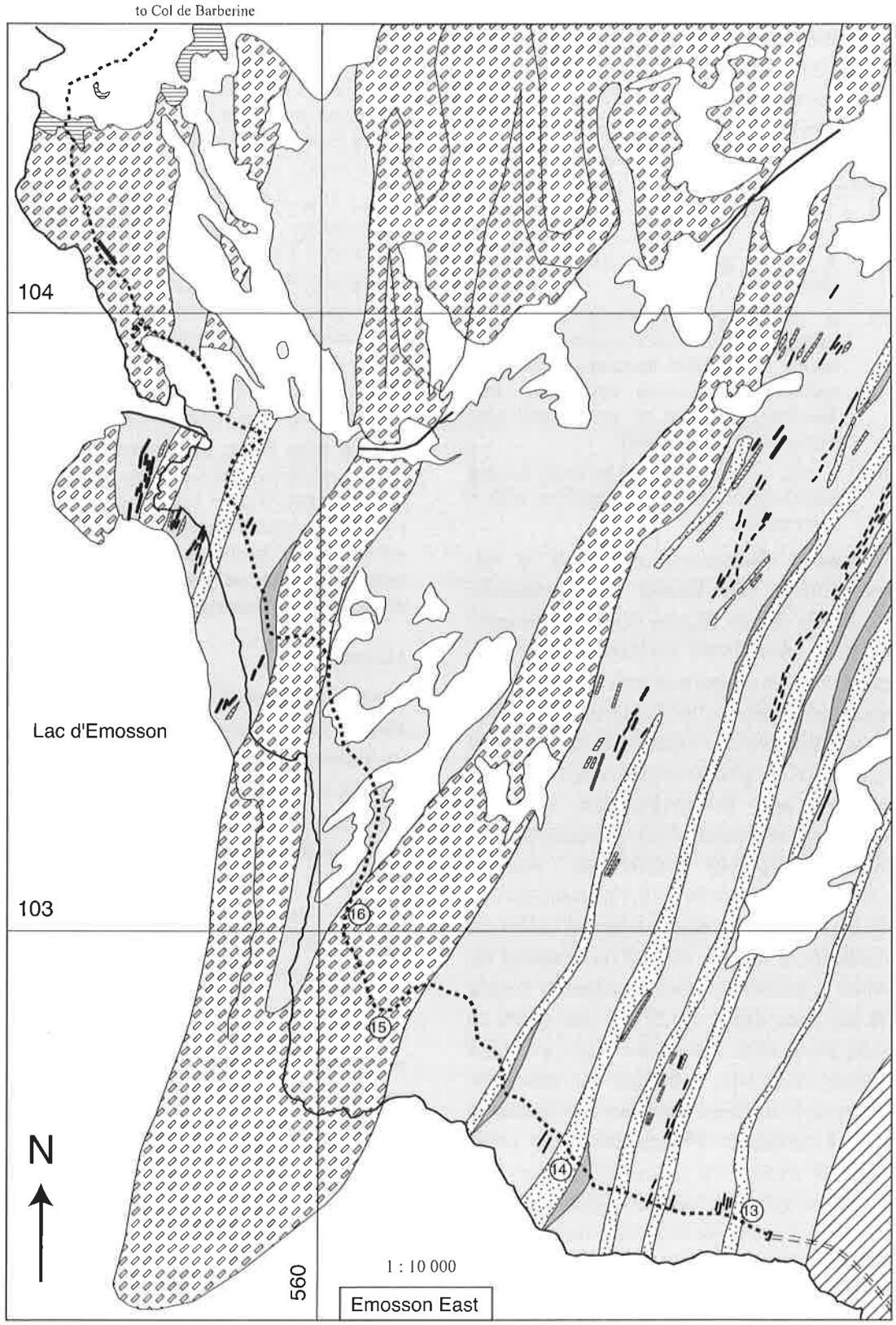

Fig. 5.04
Map of the Eastern Emosson area with numbered field-stops. *Carte géologique détaillée de la côte est du Barrage d'Emosson avec les points d'observation* (Annex IV).

large crystals of staurolite and kyanite, the latter with reaction rims of cordierite and hercynite, interpreted as a HT-decompression reaction (Dupasquier, 1996, Ch. 3.2, **Photo 3.18**). The origin of these leucocratic rocks remains unexplained, but they could result from dehydration melting of amphibolites comparable to those observed in the Lac Cornu area (von Raumer et al. 1996).

Stop 10 (Fig. 5.03): large amphibolite body with plagioclase amphibolites and garnet-amphibolites. Parallel to the foliation planes occur plagioclase-rich mobilisate veins, containing tiny garnets (**Photo 3.17**). The structures are cut by horizontal thrust-planes of Alpine age. At the contact, the amphibolite is transformed into micaschist, and slicken-sides are composed of quartz and chlorite/actinolite.

Orthogneisses

Topic (Fig. 5.03, 5.04): Orthogneisses (see Ch. II.1) occupy large areas in the Emosson region, as large dike-like bodies, which record two phases of folding, as illustrated by the huge, steeply dipping fold structure adjacent to the former Barberine dam site (now flooded by the Emosson lake) (von Raumer 1984). This fold is clearly visible in the landscape (**Photo 2.03**) and helped to understand the complexity of the regional structures during mapping. Both, I-type (hornblende-biotite-bearing granodiorites) and S-type (biotite-bearing porphyritic granites) intrusions were identified (Wirsing, 1997). The Mt. Luisin granodiorite has been dated at 457 ± 2 Ma (U-Pb on zircon, Bussy, unpubl. data), whereas an S-type augengneiss from the nearby Mont Blanc massif intruded at 453 ± 3 Ma (Bussy and von Raumer, 1994). This magmatic event is ascribed to an active margin context, as also documented by the MORB-type mafic rocks of the Lac Cornu area (see general discussion, Ch. III; and von Raumer et al. 2002b). The late Variscan metamorphism is well documented in the orthogneisses, which experienced partial melting. Late Variscan strike-slip deformation is also documented through C-S tectonites.

Stop 11 (Fig. 5.03): The outcrop areas show the typical features of multiple deformation of former Ordovician granitoids. In the Vieux Emosson area, below the dam site, outcrops show the isoclinal folding of these rocks, with intersection of already folded mobilisate veins. Many details about deformation of K-feldspar phenocrysts can be observed.

Stop 12 (Fig. 5.03): Just in the neighbourhood, on the road near the Vieux Emosson dam-site, kink folds of Alpine age (**Photo 2.10**) can be observed, indicating the presence of the Alpine overthrust of the Morcles Nappe units at higher levels.

Additional outcrops

Besides the proposed outcrops, other localities may be of interest, like those at the eastern shore of Lake Emosson (**Annex IV, Fig. 5.04**) or in the Lac Vert area (**Annex VI, Fi.g 5.05**).

Eastern shore of Lake Emosson

Access is easy, as outcrops are located along the road at the eastern shore of Lac Emosson. Crossing the tunnel leading to Barberine, a series of outcrops again show the main lithologies observed on the western side of the lake.

Stop 13 (Fig. 5.04): 50 m after leaving the gallery and crossing a small creek appears a horizon of metagreywackes followed, towards north, by amphibolite-bearing, rusty-weathered micaschists. The latter draw a major subhorizontal fold dipping 37° towards South. The subvertical axial plane is underlined by growth of elongated plagioclase-blasts in the micaschists. The continuation of the cross-section is in micaschists with large plagioclase-blasts.

Stop 14 (Fig. 5.04): Continuing the cross-section in direction NW, after 300 m, again a typical assemblage of rusty weathered banded gneisses is followed by massif metagreywackes and by a large zone of micaschists with large plagioclase-blasts.

Stop 15 (Fig. 5.04): The road cuts a large fold-hinge of orthogneisses with a steeply dipping fold axis. The main structures can be observed best, when water-level is low. Besides this major deformation, many cm-sized chlorite-filled cracks indicate brittle deformation with formation of conjugate sets of slickensides formed during Alpine metamorphic overprint (see **Fig. 3.14**).

Stop 16 (Fig. 5.04): At the northern continuation of the orthogneisses, gneisses change to a more granodioritic composition. Fewer K-feldspar crystals are hosted by a more biotite-rich matrix, which may be either the expression of stronger deformation or a change to more granodioritic composition. Locally, tiny pink-coloured andalusite may be found in these rocks, expression of Late Variscan thermic overprint.

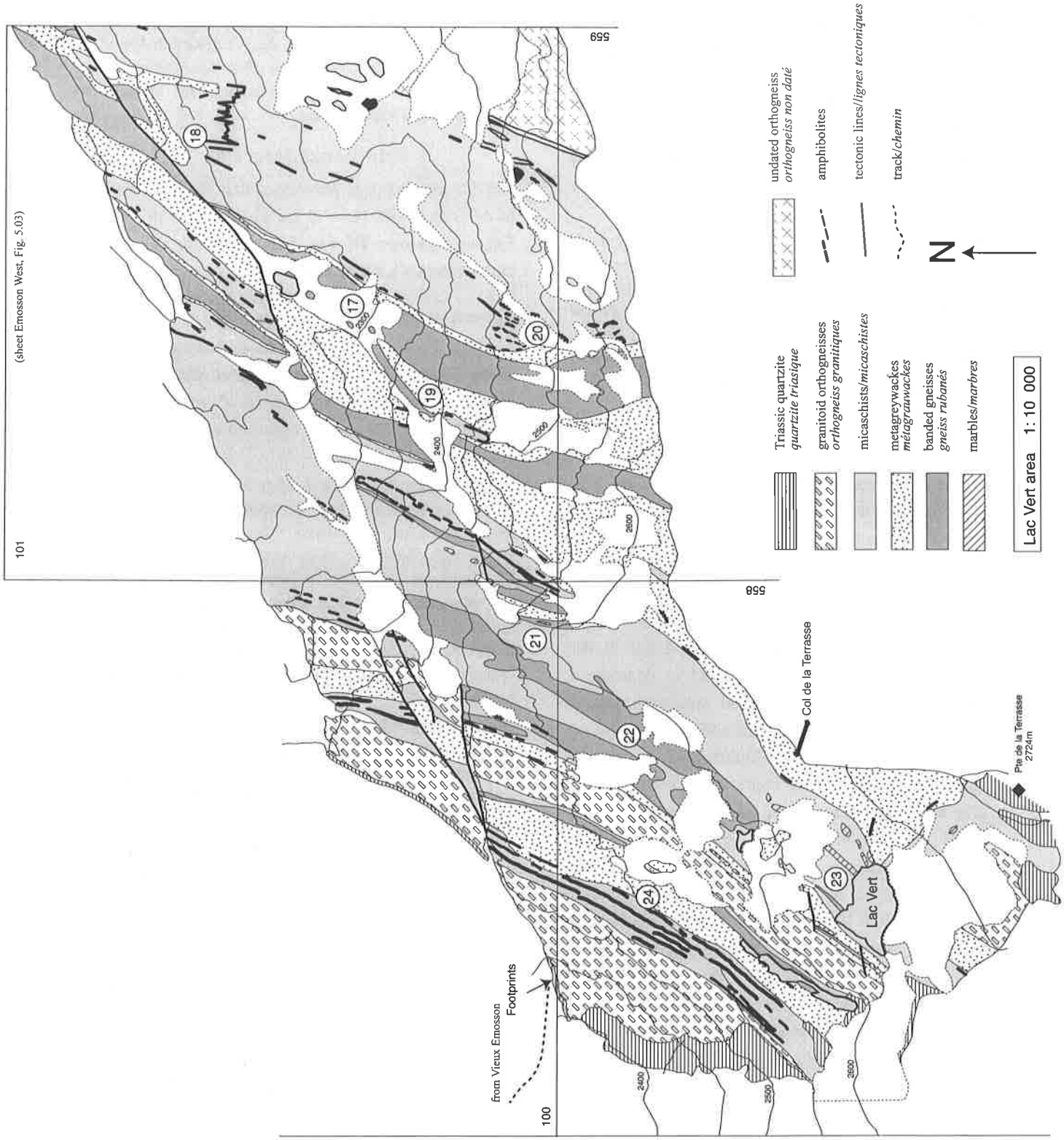

Fig. 5.05
Map of the Lac Vert - Col de la Terrasse area with numbered field-stops. *Carte géologique détaillée des alentours du Lac Vert / Col de la Terrasse avec indication de quelques points d'observation mentionnés dans le texte* (Annex VI).

Lac Vert area

More difficult to attain are the interesting outcrops in the Lac Vert area in the neighbourhood of Col de la Terrasse. They give an insight into the variation of lithologies and their repeated folding, and the many phenomena observed around amphibolite boudins (**Fig. 5.05**).

Stop 17 (Fig. 5.05) (2280m):
Arriving at a small lake, different types of lithologies are exposed in the lake area. Rusty weathering, banded gneisses represent the typical aspect of this type lithology (see Ch. II.4), the adjacent massif gneisses represent the type lithology of the metagreywacke series (see Ch. II.4).

Stop 18 (Fig. 5.05) (2320m):
Following the small valley in NE direction, and after a small climb along a water channel, large-scale folds of amphibolites and their host rocks are exposed. Among the amphibolites, garnet-amphibolites and zoisite-bearing amphibolites (**Photo 2.16**) can be distinguished. Additionally, a leucocratic transition-zone between amphibolites and micaschists is developed, containing plagioclase, biotite, staurolite and kyanite. Host rocks of the amphibolites are micaschists with large patches of plagioclase.

Stop 19 (Fig. 5.05) (2380m):
Returning to the lake and climbing in the metagreywacke unit leads to a large morainic scree, at the level of about 2380 m, the transition from metagreywackes to finely banded turmalinite-bands (**Photo 2.26**) is visible.

Stop 20 (Fig. 5.05) (2380m):
Continuing climbing, at about 2380, m a fold of metagreywackes, micaschists and amphibolites is visible. It is worth to traverse at this level various units of metagreywackes and banded gneisses, and to see the spectacular outcrops of folded amphibolites and micaschists (e.g. **Photo 3.14**).

Stop 21 (Fig. 5.05) (2570m):
Returning to the folded amphibolites and metagreywackes, one might continue climbing to 2400 m to attain a small ridge. Traversing a large zone of micaschists and banded gneisses, a contact-zone between banded gneisses and micaschists is attained. One might find all kinds of interference-patterns of different fold-generations, and spectacular sheath-folds of metagraywackes in micaschists (**Photo 3.25**).

Stop 22 (Fig. 5.05) (2550m):
Continuing in direction of Lac Vert, either following the ridge of the Swiss boundary, or below the ridge, a large area of folded metagreywackes, micaschists and banded gneisses can be observed, as well as some andalusite-bearing tension gashes.

Stop 23 (Fig. 5.05) (2520m):
At Lac Vert, rusty outcrops of marbles, formlarge boudins within micaschists. Marbles are rare, strongly sheared and completely smeared out among the hosting rock series. Larger lenses are locally preserved as banded calcite-diopside rocks. This lens shape is either the result of boudinage during stretching of the hosting micaschists, or might represent former patch-reefs, a well-known lithology in the Cambrian. These calcsilicate lenses are often hosting scheelite, which most probably resulted from metasomatic transfer during late Variscan granite intrusions (Chiaradia 1993).

Stop 24 (Fig. 5.05) (2550m):
A large zone of amphibolite-bearing gneisses is located North of Lac Vert. All phenomena of boudinage and refolding are observed. Again, the amphibolites are surrounded by patchy plagioclase-micaschists.

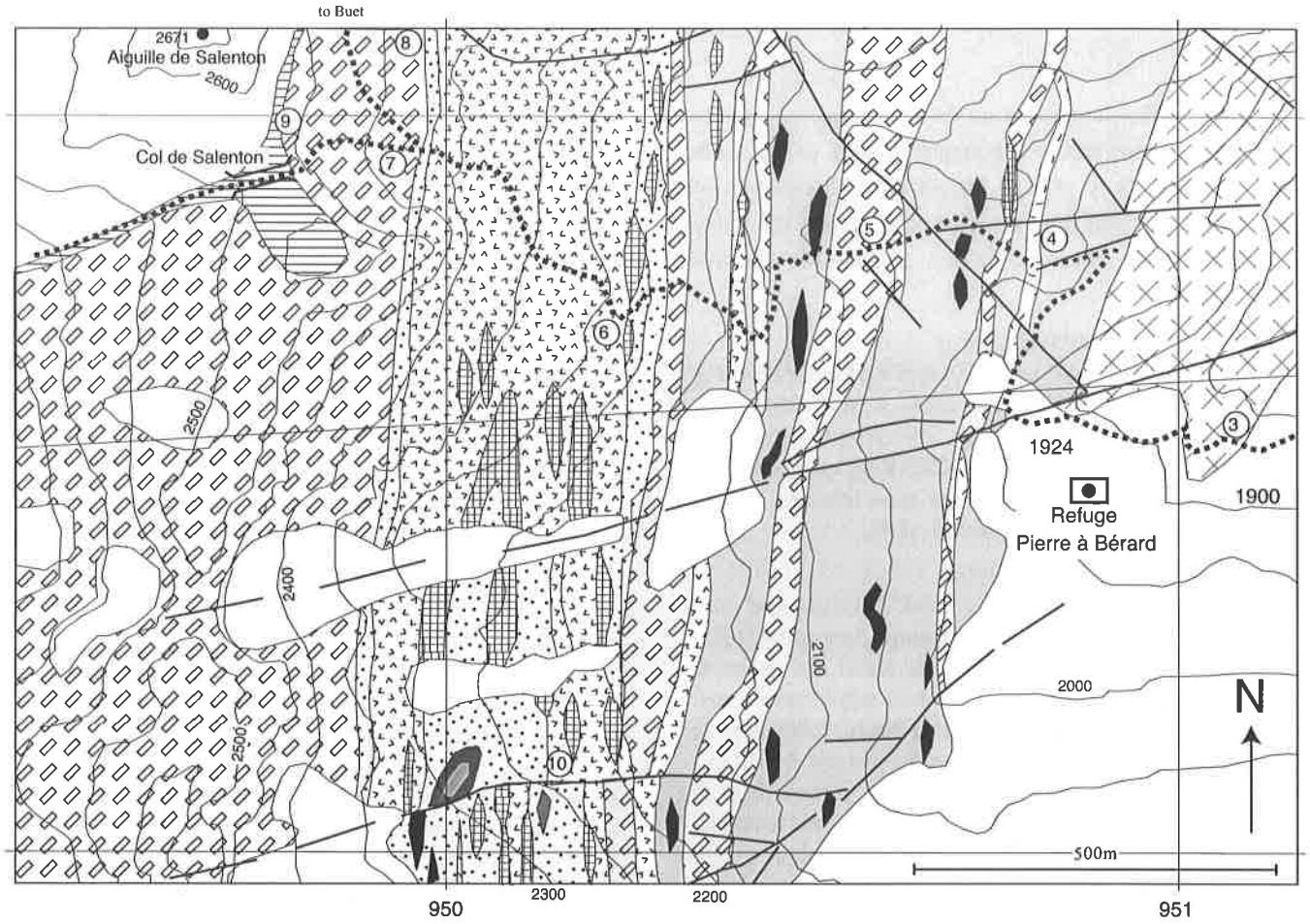

Fig. 5.06
Detail geological map of the northwestern, upper part of Val Bérard between Refuge Pierre à Bérard - Col de Salenton, based on Schulz and von Raumer 1993, Fracheboud 1997, Wirsing 1997 (geological map, annex VII).
Carte géologique de la partie supérieure de Val Bérard entre le refuge Pierre à Bérard et le Col Salenton, basée sur les observations de Schulz et von Raumer 1993, Fracheboud 1997, Wirsing 1997 (carte géologique Annexe VII).

V.2. Val Bérard (Aiguilles Rouges)

Maps: IGN Fr. 1 : 20 000 Chamonix 1-2; IGN Fr. Touristic map 1 : 25 000 Mont-Blanc 1;
CH: 1: 25 000 sheet 1344 Col de Montet; Geological map 1 : 20 000 Tré les Eaux – Val Bérard (Annex VII), Figure 5.06.
References: Bellière 1952; Schulz and von Raumer, 1993; Fracheboud 1997; Wirsing 1997.
Acces: Parking at Gare de Buet (1320m). The visit of this region (Fig. 5.06) needs 1 – 2 hours of walking to reach the Refuge Pierre à Bérard (1924m, lodging and boarding).

Topic: Polymetamorphic basement of the Aiguilles Rouges massif (metasediments, amphibolites, orthogneisses), Late Variscan granitoids and mylonites and the Alpine overprint of sedimentary and igneous lithologies.

Located in the SW prolongation of the Emosson – Lac Vert areas (**Fig. 5.01**), comparable rock units are observed in the Val Bérard area, which is on the way of walking tours to Mt. Buet or across Col de Salenton. Besides the lithologies of the upper Val Bérard (**Fig. 5.06**) mentioned above, a few rocks are visible at the bottom of the valley on the way to the refuge.

Visited outcrops

Stop. 1 (1410m): Down the valley, the first slopes leading to Cascade de Bérard are underlain by the Late Variscan Vallorcine granite (see Ch. IV), and directly after the bridge and the cascade, nice examples of a strongly deformed, coarse K-feldspar augengneiss can be examined (nice boulders in the river). Although undated in the Aiguilles Rouges massif, they undoubtly represent a typical aspect of Ordovician orthogneisses having suffered strong deformation during Late Variscan events.

Stop 2 (Fig. 5.06) (1590m): a huge boulder on the way up, among the trees, consists of granitoid gneisses with a strongly stretched xenolith.
Further up is a complex zone of mylonitic gneisses, well represented in such pebbles (**Photo 5.01**). The latter show various textures such as strongly stretched pencil gneisses, migmatites and granitoids The next outcrops are attained in the neighbourhood of the bridge.

Stop 3 (Fig. 5.06) (1850m): Arriving at the bridge, a great variety of mylonitic gneisses can be observed, where granitoid C-S gneisses (**Photo 5.01**) and migmatised metasediments predominate, representing one aspect of the large mylonite zone mentioned at the beginning of Ch. V.

Stop 4 (Fig. 5.06) (2000m): Around the water gallery, typical examples of the micaschist zone are exposed, being the southwestern continuation of these units in the Emosson – Lac Vert areas. Mostly sheared, they locally contain stretched lenses of plagioclase aggregates. Among the micaschists appear narrow quartz-rich bands, which may represent either mylonitic quartz veins or stretched pieces of former quartzites. Following the old trail towards Col de Salenton, these micaschists are crossed at several places. Locally, boudins of metagraywackes with kyanite or dense garnet-rich gneisses may be found.

Stop 5 (Fig. 5.06) (2050m): In the general structure, the strongly folded micaschists are interesected by coarse biotite-augengneisses, representing the strongly deformed K-feldspar augengneisses (see Ch. II.1), which underwent regional isoclinal folding together with their host-rocks.

Stop 6 (Fig. 5.06) (2270m): After crossing different morainic slopes, a rather narrow band of metasediments delimits an area, exposing rather homogeneous biotite-amphibole gneisses (**Photo 2.11, 2.12**). Biotites, amphiboles and biotite-patches display a strong, subvertical stretching lineation. Relictic lumps of amphibole or pegmatoid patches can be observed. Wirsing (1997, see Ch. II.1) interpreted these rocks as I-type calc-alkaline granodioritic magmatic rocks preceding the K-feldspar-rich augengneisses. The question arises, if these rocks represent Ordovician granodiorites, having received a late Variscan stretching linear, or if only their protoliths represented Ordovician I-type magmatic rocks which, during the late Variscan metamorphic event, underwent anatectic mobilisation and vertical stretching, leading to the present-day equigranular aspect.

Stop 7 (Fig. 5.06) (2300m): Beyond the zone of bi-hbl-gneisses, the main zone of K-feldspar augengneisses is attained, representing granitoid rocks of Ordovician age (see characteristics in Wirsing 1997, Ch. II.1). Their different aspects can be observed on the way up to Col de Salenton, or on the way to Mt. Buet.

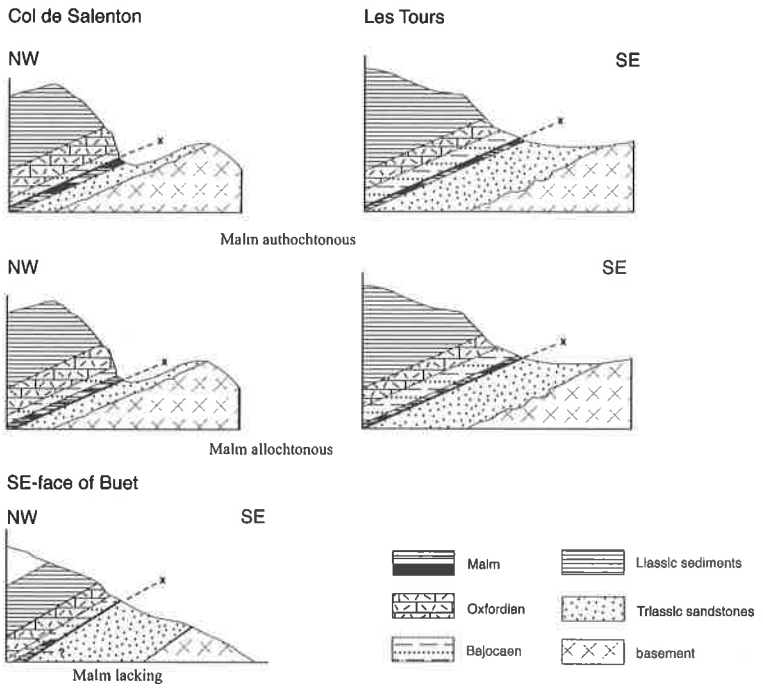

Fig. 5.07
Interpretation of cross-sections in the Mesozoic cover of Val Bérard area (cross-sections at Col Salenton, Les Tours and Buet from Fracheboud (1997). New fossil data (Fracheboud 1997, unpublished) prove the presence of Oxfordian limestones in the cross-section. Consequently, two interpretations can be given for the Malm carbonates, either belonging to the authochtonous cover above the Triassic sandstones, or belonging to the inverse limb of the Morcles Nappe.
Differences d'interprétation des coupes géologiques dans les unités Mésozoïques au Col de Salenton, aux Tours, et au Buet (d'après Fracheboud 1997). L'observation nouvelle de fossiles a permis de dater des calcaires oxfordiens (Fracheboud 1997, non publié). On peut ainsi interprêter les coupes géologiques de deux manières. Ou le Malm (en position normale) fait partie de la couverture autochthone du socle, ou le Malm se trouve en position inverse, sous l'Oxfordien, dans le flanc inverse de la Nappe de Morcles.

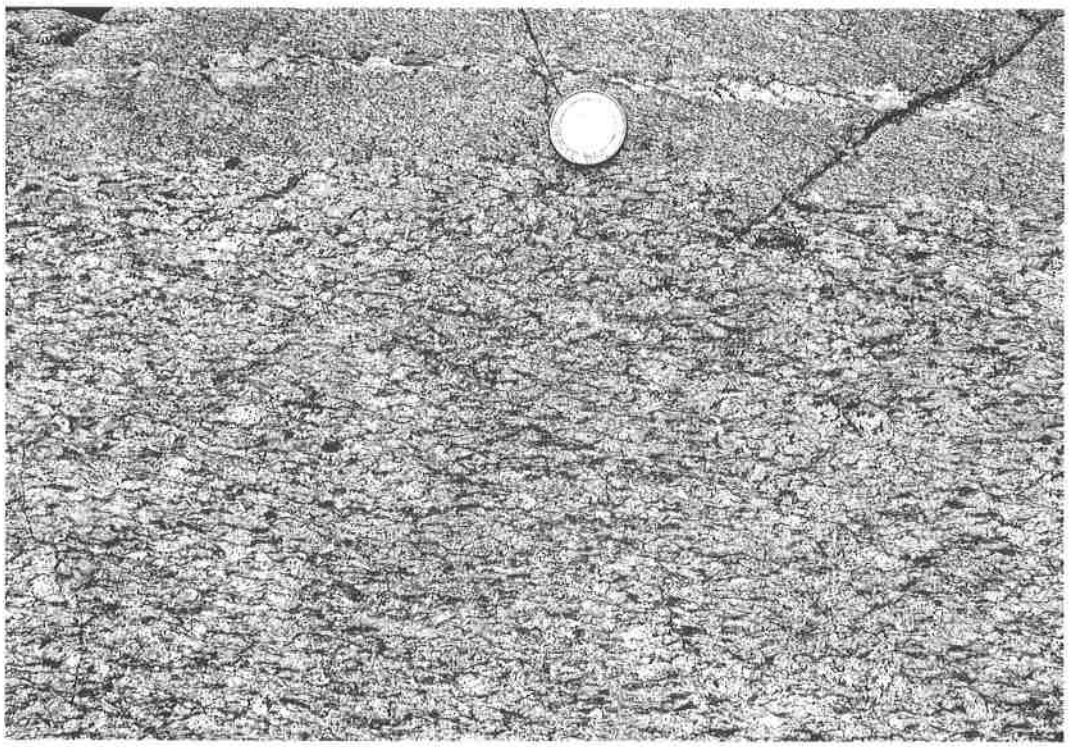

Photo 5.01
Tectonised Late Variscan granitoids (C-S-gneisses). Lower Val Bérard (Coord. FR: 952.280/122.690)
Granite tardi-Varisque déformé (gneiss C-S), Val Bérard inférieur (Coord. FR: 952.280/122.690)

Stop 8 (Fig. 5.06) (2430m):
Below the way in direction of the Mt. Buet, rather large areas of K-feldspat augengneiss are exposed, and leaving the path in southeast direction, their contact with metapelitic sediments, (coarse staur-ky gneisses; see Schulz and von Raumer, 1993) and amphibolite boudins is attained. It is still a question, weather the metasediments have been intruded by the granites, or if they deposited as a former sedimentary cover, before all rocks underwent amphibolite facies late Variscan transformations.

Stop 9 (Fig. 5.06) (2520m):
At Col de Salenton, above the authochtonous Triassic sandstones appear different jurassic carbonates. Calpionellids indicate an upper Jurassic (Malm) age for bluish-gray marbles which were supposed to represent the authochtonous cover. Based on the new findings of *Protoglobigerina* sp. and Radiolarians (Fracheboud 1997, unpublished), the upper sequence of banded marls and carbonates are interpreted to represent the Oxfordian of the invers limb of the Morcles Nappe (see **Fig. 5.07**) and, consequently, the carbonates mentioned before could also belong to the inverse limb of the Morcles Nappe (**Fig. 5.07**).

Additional points of interest

Stop 10 (2280m):
On the way to Col Bérard, a cross-section of about 300 m shows strongly sheared, dense, biotite-garnet-gneisses, which may contain relics of coarse biotite-gneisses, representing probably boudins of former meta-gabbros. A huge lens of eclogite is surrounded by the biotite-garnet gneisses, and farther north, among very coarse biotite schists with locally very large garnets (**Photo 3.11**), a lens of eclogite and serpentinite is outcropping. Such rocks represent the northern-most continuation of eclogites and serpentinites known from the Lac Cornu – Tête de Béchat areas.

Continuing to Col Bérard, a large area of metasedimentary gneisses with amphibolite boudins (**Photo 2.13**) and calc-silicate lenses are crosscut by late Variscan leucogranites, locally with hematite-rich joints.

Stop 11 (not in the map, 2280m):
Away from the path leading to Buet, good climbers may visit the locality of Creux aux Vaches, on the way to Mt. Oreb, where migmatised K-feldspar augengneisses are exposed on the northern river side. On the southern river side, spectecular vertical folds of micaschists and boudinised amphibolites can be observed.

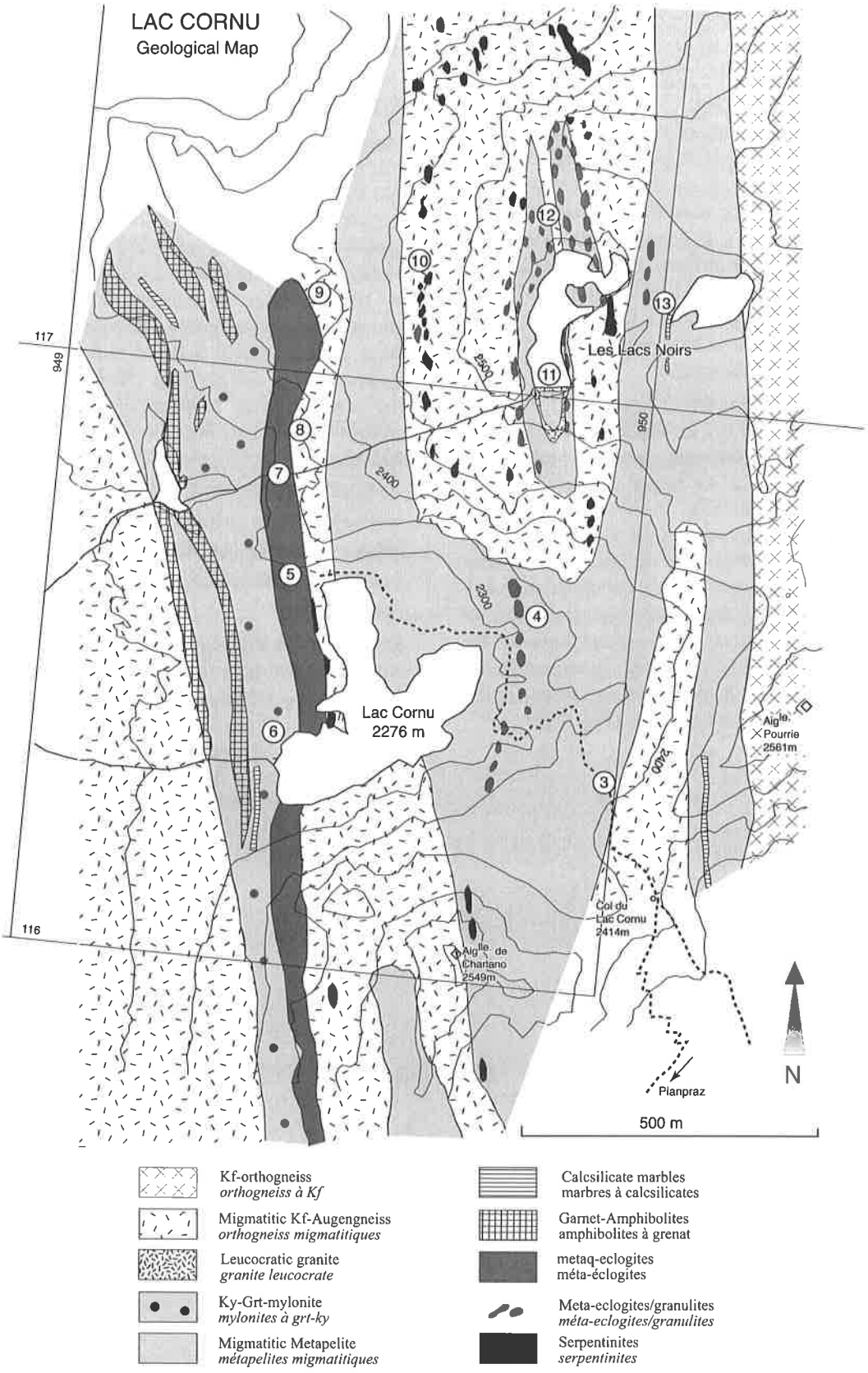

Fig. 5.08
New Geological Map 1 : 10 000 of the Lac Cornu area, with indication of numbered stops (compare with annex VIII). *Nouvelle carte géologique 1 : 10 000 de la region du Lac Cornu, avec les points d'observation (à comparer avec annexe VIII).*

V.3. Lac Cornu (Aiguilles Rouges)

Maps: IGN Fr. 1 : 20 000 Chamonix 1-2; IGN Fr. Touristic map 1 : 25 000 Mont-Blanc 1;
CH: 1: 25 000 sheet 1344 Col de Montet; Geological maps 1 : 10 000 Lac Cornu (Annex VIII), Figure 5.08.

References: Bellière 1952

Access: Cable car Chamonix – Planpraz (2000m); the visit of the Lac Cornu area (Fig. 5.08) needs about 1 – 2 hours of walking from "Altitude 2000" across Col Cornu (2400m).

Topic: Polymetamorphic basement of the Aiguilles Rouges massif (migmatised sediments, amphibolites, orthogneisses), eclogites, ultramafic rocks.

Located in the SW prolongation of the Emosson – Salanfe areas (**Fig. 5.01**), partially comparable rock units are observed in the Lac Cornu area, reminiscent of the micaschist unit with calcsilicate marbles, graphitic layers and boudins of amphibolites, interlayered by K-feldspar augengneisses. In contrast, all units are strongly migmatised. Few outcrops are crossed on the way from the cable-car station to Col Cornu, but many rock types can be observed in the scree.

Visited outcrops

Stop. 1 (2020m) in front of the cable-car station:
white mica-rich gneisses contain some large K-feldspar crystals. These gneisses represent tectonically modified coarse K-feldspar augengneisses, formerly Ordovician granitoids (see Ch. II.1). On the way up to the Restaurant "Altitude 2000" (2060m) and following the bifurcation to Col Cornu, large boulders of migmatised K-feldspar augengneisses can be observed. Granitic mobilisates are visible as microgranular veins and pockets.

Stop 2 (2300m):
After traversing a rather long distance of large slopes, and after crossing a small ridge, on the left side of the path appear massiv migmatic gneisses with a rusty weathering, huge boudin of garnet amphibolite. Following the zig-zag path, Col Cornu (entrance of the Natural Reserve) is attained after 80 m of climbing.

Stop 3 (Fig. 5.08) (2400-2350m):
From the cairn at the entrance of the Natural Reservation onwards, the main rocks represent migmatic gneisses of former sediments, interlayered by zones of migmatised K-feldspar augengneisses. The great variety of these gneisses is well observed when following the path down to the lake. In this area it is difficult to give precise coordinates, but careful observation allows recognition of amphibolite boudins among the migmatites, the latter intersected by leucogranitic veins.

Stop 4 (Fig. 5.08) (2315m):
East of the lake, a small deviation from the main path will lead to rather large boudins of banded meta-eclogites. Among the bands of eclogites of different composition appears a more lens-like microgranular dark eclogite, which may be interpreted as a former basaltic lens among tuff-layers. The rim of the mega-boudin is strongly transformed through migmatisation (see **Photo 3.10**).

Stop 5 (Fig. 5.08):
At the northern end of the lake, a narrow path across a cliff gives insight, from east to west, to a succession of migmatitic metapelites, K-feldpsar augengneisses, the main body of eclogites with different boudins and, at the western contact, homogeneous garnet gneisses. The latter may represent former metagraywackes, but they may also represent a completely recrystallised mylonite zone, forming the western limit of the eclogites.

Stop 6 (Fig. 5.08):
At the western lake shore, near the outlet of the small river, a complete cross-section through the different rock types, the main eclogite body and its host-rocks, can be inspected. In this area of natural reserve, hammering is not allowed. If announcing in advance to the scientific comittee, handspecimens for scientific research may be taken in the large rock-fall at locality (7) 500 m farther to north, at the east of a small lake.

Stop 7 (Fig. 5.08) (2300m):
In the northern prolongation of the eclogite body, to the east of a small lake, a rock-fall in the main eclogite body presents most of the specimens which can be collected in this area.

Stop 8 (Fig. 5.08) (2350m):
In the northern continuation of the eclogite body, at its eastern contact, garnet-bearing granulite-type rocks are at outcrop (**Photo 2.18**), which seem to represent a stage of dehydration melting forming garnet-kyanite-biotite rocks, where kyanite shows reaction rims of spinel and cordierite (see Ch. III.1).

Stop 9 (Fig. 5.08) (2400m):
At the northernmost end of the main eclogite body, the eclogites are surrounded by migmatic rocks, following a steeply dipping syn-form in their main foliation planes. Vein-like garnet-kyanite-biotite granulite-type gneisses are also found. Within the eclogite, red-coloured veins of garnet-quartz can be observed.

Stop 10 (Fig. 5.08) (2470m):
Following the ridge climbing into eastern direction, among metapelitic migmatites appear boudins of ultramafic rocks (see Ch. II.3) from 10 cm to 50m size. The boudins follow the main N-S foliation of the host-migmatites in N-S and are mainly composed of serpentine minerals. Locally appear veins of tremolite, and tension-gashes vertical to the main foliation of the host-rock are filled by talc (**Fig. 2.16**).

Stop 11 (Fig. 5.08) (2480m):
Crossing the ridge in eastern direction (2500m), the western lake of Lac Noirs is attained, which is surrounded by metapelites transformed into migmatites containing many boudins of amphibolite-like granulites. On the northern side of the lake, besides tiny ultramafic lenses, hornblende-bearing anatectic mobilisates (see Ch. IV, **Photo 4.07**) are observed in the migmatites.

Stop 12 (Fig. 5.08) (2480m):
At the southern end of the lake, at the contact with metapelitic rocks, outcrops a white, microgranular, garnet-bearing leucogranitic dike, which hardly shows any alpine deformation. It is probably of Late Variscan age.

Stop 13 (Fig. 5.08) (2538m):
At the eastern lake, different, tectonised gneisses with amphibolite boudins and metapelites are outcropping, and the eastern shore is limited by coarse grained K-feldspar augengneisses. A striking feature at the western shore of the lake are interlayered folded carbonates among the micaschists, which can be followed south among the banded gneisses, and which appear again south of Aiguille Pourrie in the neighbourhood of Col Cornu.

V.4. Lac de Salanfe (Aiguilles Rouges)

Maps: CH: 1: 25 000 sheet 1304 Val d'Illiez; 1324 Barberine; Swiss geological atlas 1 : 25 000, sheet Finhaut; coloured geological map 1 : 5 000 (annex IX); field-map 1 : 10 000: Figure 5.11.

References: Rickenbach and von Kaenel, 1953; Frey and von Raumer 1977; Della Valle et al. 1987; Chiaradia 1993 a,b, 1997.

Acces: Bus Line Martigny - Van d'en Haut; Car: Martigny – Salvan to parking lot Van d'en Haut (1339m). The visit of the Salanfe region needs about 1 hour of walking from the parking to Auberge de Salanfe (1940m, lodging and boarding). To visit the specific region (**Fig. 5.11**), the path towards south across the dam site of Salanfe leads to the former mining site of Salanfe (Mine Robert). After traversing the dam, the path around the lake has to be left after 150 m, to climb the hills in direction South, and at the altitude of 2070m, the easternmost lacet of the former path is attained, which is leading to the mine.

Outline: Located in the NE prolongation of the Emosson area (**Fig. 5.01**), partly comparable rock units are observed in the Salanfe site. The main topic is the former gold-mine located in marbles of the polymetamorphic basement and its skarn-minerals. The polymetamorphic basement is mainly composed by metasediments and Ordovician orthogneisses, transformed during the Late Variscan into migmatites, and intersected by granitoids. The region is known for its gold-mine, and the mining history is described by Rickenbach and von Kaenel (1953). The findings of scheelite by Frey (Frey and von Raumer 1977) drew new interest on this site (Della Valle et al. 1987).

The metasedimentary rocks, probably of Late Precambrian to Early Palaeozoic age, are composed by metagraywackes and metapelites, containing a quartzite-band, dolomitic marbles accompanied by a graphite layer, and a reduced horizon of amphibole-bearing gneisses. They have undergone an amphibolite facies metamorphism, and were overprinted by two coaxial generations of folds ($D_1/F_1/S_1$, $D_2/F_2/S_2$), and a subsequent, non coaxial fold generation (F_3), creating the complex distribution pattern of the metasedimentary lithologies. The metasediments were intruded by granitic and granodioritic magmatic rocks of Ordovician age (see Ch. II.1). The latter are now K-feldspar augengneisses and biotite-gneisses with numerous biotite-rich patches. They underwent two generations of foldings (F_2, F_3), when compared with the metasediments. All these rocks underwent a high-temperature regime of Late Variscan age, leading to anatectis of granitoid gneisses with formation of garnet-bearing leucogranites, accompanied by large-scale transfer of fluids and formation of skarn-minerals in the carbonates of the metasedimentary units. Undeformed, red-coloured Late Variscan rhyolites intersect all structures. Late stage transformations occurred along vertical 120° striking fractures traversing the Triassic sedimentary cover and hosting fluorite-barite mineralisations. The following lines will shortly introduce into the mine site, using the data and interpretation given by Chiaradia (1993).

The ore-site is a scheelite-diopside skarn bound to marble-lenses being in contact with a Late Variscan leucogranite, which resulted from anatectic melting of Ordovician biotite-gneisses. The regional P-T conditions leading to skarn formation and to melting of gneisses were about 700°C / 4Kb (**Fig. 3.05**). The Robert mine is the most important ore-site, where two skarn horizons were distinguished. The main skarn horizon, up to 2 m thick, developed at the contact with the main marble lens (**Fig. 5.09**), and a second, less important skarn horizon formed in marble bands alternating with sedimentary gneisses. Among the newly formed minerals during formation of the skarn, different generations can be distinguished; i.e. the metamorphic minerals, the prograde and the retrograde ore stages (**Fig. 5.10**). The metamorphic stage is characterized by diopside, titanite ± quartz ± plagioclase ± calcite. During the prograde first-stage ore-formation, hedenbergite, a boron-silicate, scheelite I, titanite ± quartz ± plagioclase ± calcite were formed, where scheelite formed in large amount at the skarn/marble limit. The subsequent formation of sulphides started at about 600°C. At about 550°C, Gold I started to precipitate within arsenopyrite in

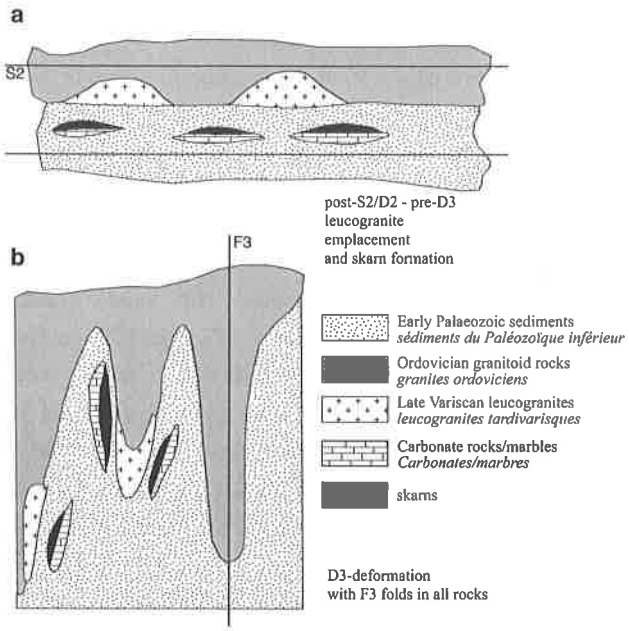

Fig. 5.09
Simplified cross-section of the Salanfe area (from Chiaradia 1993), showing the relationship of deformation 2 and 3 and the skarn formation. **a)** emplacement of the garnet-bearing leucogranite in granitic orthogneisses during a regional thermal static event. Formation of skarns. **b)** Deformation phase F_3, producing the present-day geometry of ore-bodies among the folded metasediments (compare with **Fig. 5.12**).
Coupe horozontale simplifiée de la region de Salanfe (d'après Chiaradia 1993), avec relations d'âge entre déformations 2 et 3 et la formation des skarns. ***a)*** *Emplacement des leucogranites à grenat dans les orthogneiss pendant la phase métamorphique statique à haute température, et formation des skarns.* ***b)*** *Déformation F_3 influençant fortement la distribution actuelle des skarns parmi les roches métamorphisées.*

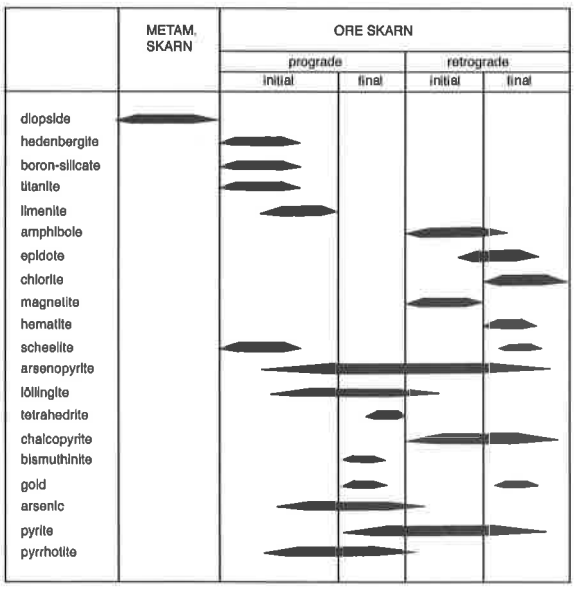

Fig. 5.10
Time-cristallisation table of minerals around the skarn site Mine Robert at Salanfe (from Chiaradia 1993).
Ordre de cristallisation (de Chiaradia 1993) dans les skarns de la Mine Robert à Salanfe.

association with pyrrhotite and bismuthinite, close to the marble. During the final prograde ore-stage, at about 500°C, sulphide-precipitation continued. The precipitated metals are thought to have originated from proto-concentrations in the host sediments or from volcanic horizons, remobilized during the Late Variscan, thus characterising this type of metal concentration as another example of Late Variscan strata-bound W-mineralisation being widespread throughout the European pre-Mesozoic basement areas.

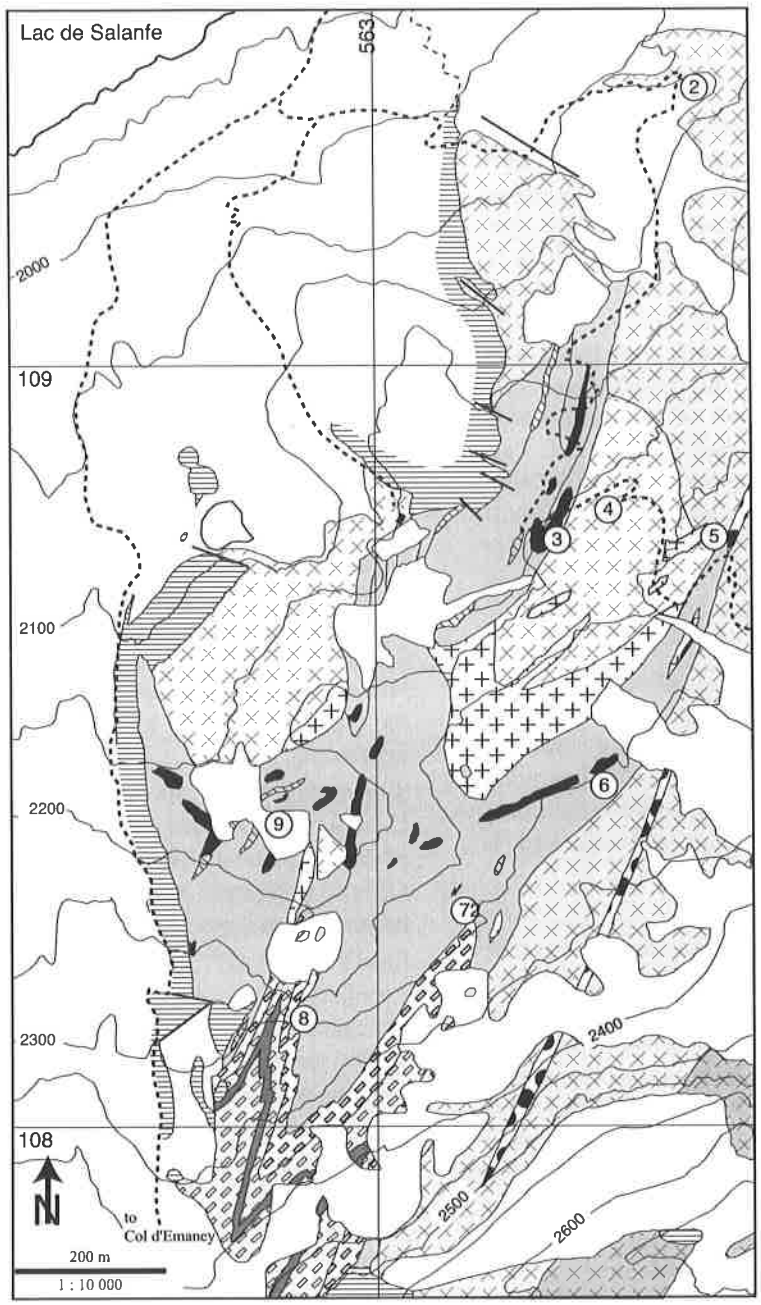

Fig. 5.11
Geological map (1: 10 000) of the Salanfe area (after Chiaradia 1993) with stop numbers stops (compare with annex IX). *Carte géologique de la region de Salanfe (1 : 10 000) avec les numéros des lieux mentionnés (à comparer avec l'annexe IX)..*

Visited outcrops

Stop. 1 (1760m, map **Fig. 5.11**):
Before arriving to the dam site, from the last lacet of the climbing path (1760m) onwards, a series of biotite-rich orthogneisses outcrops along the ice-formed cliffs, part of a former glaciogene channel. These gneisses, containing locally stretched xenoliths, represent the more biotite-rich members of the Ordovician magmatic rocks, as found also in the southern regions of the Salanfe area (see **Fig. 5.11**). Locally, interlayers of migmatites with relics of calcsilicate-lenses may be observed. Two possibilities of interpretation of these migmatites exist, either formed during a late Variscan thermal event, or during an Ordovician thermal event. Near the dam site, at about 1860m, a large, pink-coloured rhyolite-dike crosses the path in NE-SW direction.

Stop 2 (Fig. 5.11) (2100m):
Following the path leading to Mine Robert, on the southern side of the dam, the path crosses a small creek, where Triassic sandstones form the sedimentary cover on the basement rocks. If leaving the path and following across the rocks to the mine, the sedimentary contact can be well observed at different places.

Stop 3 (Fig. 5.11) (2210m):
Mine Robert, the most important mining place in this area. Along the path, different levels of entries into the galleries can be observed, and also surface excavations are visible. Much care has to be taken, when approaching the upper level of the mine, as the entire site is excavated by different galleries, thus leaving huge pits. As the site has been completely exploited, best minerals are only found among the blocks of the tailings.Most of the minerals mentionned in **Fig. 5.10** can be found. A U-V lamp will facilitate the findings of scheelite.

Stop 4 (Fig. 5.11) (2220m):
Continuing the walk on the main path to Goletta pass, the migmatised orthogneiss and, on its southern side (about 2260m), its transformation into garnet-bearing leucogranite can be observed.

Stop 5 (Fig. 5.11) (2270m):
Continuing the walk on the main path to Goletta pass, in the northernmost bend of the path is a small quarry in the pink coloured Late Variscan rhyolite. Completely undeformed, the finegrained matrix of this rock contains tiny stilpnomelane crystals of Alpine age.

Stop 6 (Fig. 5.11) (2300m):
Going 200m back on the main path, and crossing the Combe de Goletta and its small river in SE direction, the micaschist unit with its calcsilicate bands is met again. Crossing a large moraine in SE direction, a NW-SE wall of outcrops shows the sequence from the micaschist unit to biotite-orthogneisses and the intersecting rhyolite.

Stop 7 (Fig. 5.11) (2300m):
Continuing in the same SE direction at the same level of about 2300m, a locality is attained, where isoclinal folds of K-feldspar orthogneisses appear among the migmatitic gneisses.

Stop 8 (Fig. 5.11) (2300m):
Crossing over to the upper part of Comba Rossa, a region of strongly folded augengneisses and banded gneisses are crosscut by leucogranites. In the foldhinges of some of the gneisses, elliptic spots of deformed sillimanite nods can be observed, the long axe of the ellipse being parallel to the axial plane of the fold axes F_3.

Stop 9 (Fig. 5.11) (2160m):
Walking down to the lower part of Comba Rossa, a multitude of small outcrops show small mineralisations and many outcrops of strongly folded calcsilicate-marbles.

V.5 Lognan – Glacier d'Argentière (Mont Blanc massif)

Maps: Topography - IGN Fr 1: 20 000 sheet Chamonix 5-6; IGN Fr 1: 25 000 Tourist map Mont Blanc massif I; Geology – Geological map of the Mont Blanc massif, sheet Argentière 1 : 20 000, Corbin & Oulianoff 1932; coloured geological map 1 : 20 000 (annex XI); field-map 1 : 10 000: Figure 5.12.

References: Corbin & Oulianoff (1932), von Raumer (1971, 1976); Bussy (1990), Morard (1998)

Outline: Taking the cable-car from Argentière to Croix de Lognan (1975m), and following the track to the South leading to the glacier d'Argentière and to the Refuge CAF d'Argentière, a general cross section from N to S is visible, already already described by Corbin and Oulianoff (1932). Three generations of granitoid rocks can be observed from North to South (see map **Fig. 5.12**); the Montenvers granite (Variscan granite), migmatised augengneisses, representing former granitoid rocks of Ordovician age with some relics of strongly deformed metasedimentary units, and the late Variscan Mont Blanc granite. The metamorphic overprint of Alpine age is recognisable in all rock assemblages.

The Montenvers granite, recognised as "granite écrasé" by Corbin & Oulianoff (1932), forms an elongated granite body, and was given its name after its nicest outcrops in the Montenvers region at the foot of the Mer de Glace (von Raumer 1976). It forms an elongated body which can be followed up towards NW in the Trient – area, and was supposed to represent a contemporaneous intrusion to the Vallorcine granite (von Raumer 1976), an assumption confirmed by identical ages (307 Ma, U/Pb zircon; Bussy et al. 2000). Part of the Montenvers granite has been remapped in the Trient – Grands Ottanes area (Nähr 1993), and nice outcrops in the Lognan region were studied more recently (Morard 1998).

The K-feldspar augengneisses have been interpreted as an elongated body of lower Palaeozoic age comparable to the Flüela orthogneisses (Silvretta) or "Ollo de Sapo" orthogneisses from Spain (von Raumer 1971, 1976), intersecting older metasedimentary units. Their U-Pb zircon dating (453±3 Ma, Bussy and von Raumer, 1994) has confirmed the Ordovician age of this rock. Parts of this unit have been remapped by Bauer (1996), Nähr (1996) and Morard (1998), and a summary of petrographic and geochemical observations had been given in Chapter II.1.

The Mont Blanc granite, representing one of the latest and most important Late Variscan granite intrusions in this region, has been subject of specific research (e.g. Bussy 1990), and specific informations are found in Ch. IV.

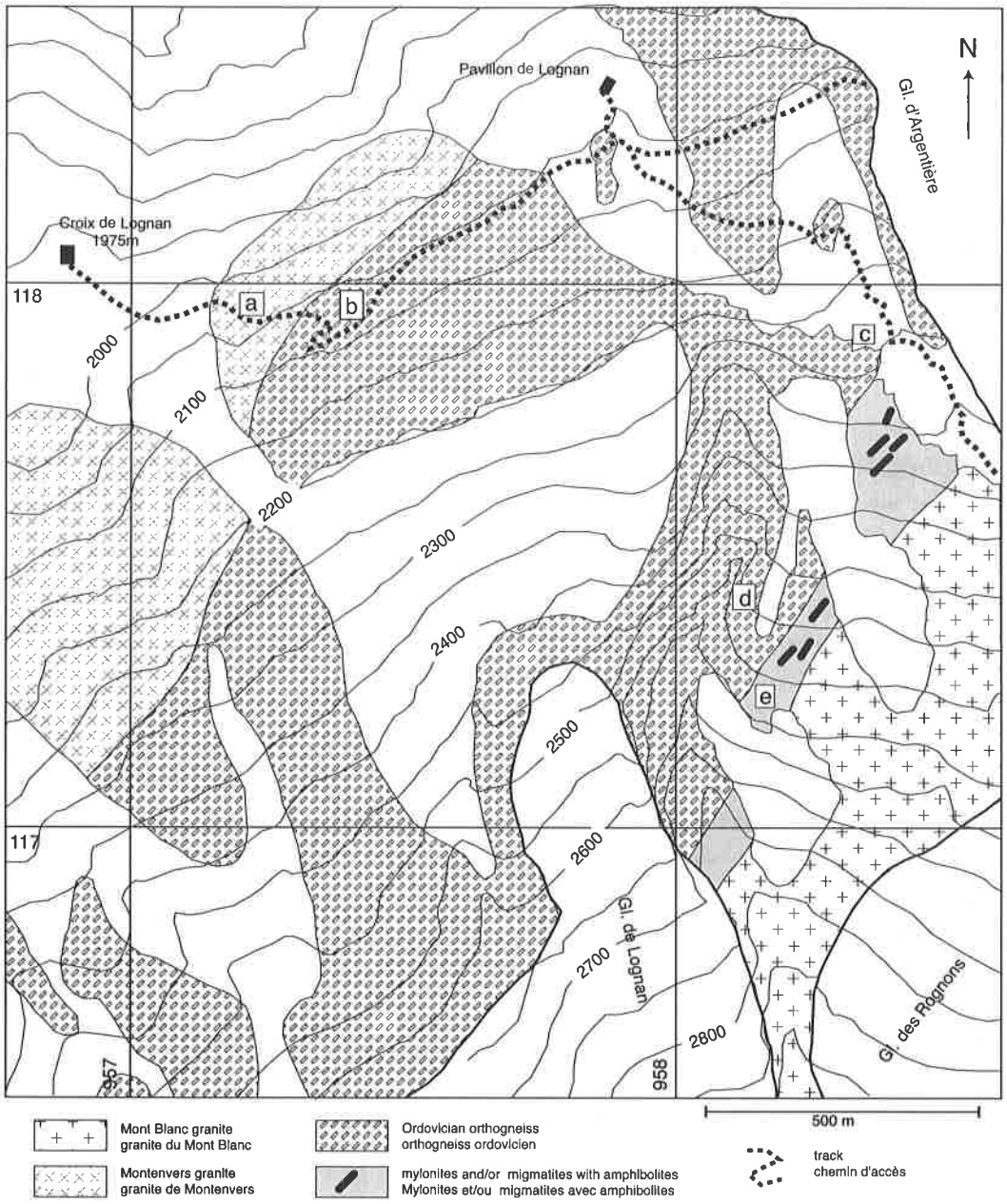

Fig. 5.12
Geological sketch-map of the Lognan region with indication of track or road (dotted line), parallel to the ski-pist, and numbered stops. Swiss topography and coordinates from sheet 1 : 25 000 Col de Balme (annex XI).
Carte géologique des environs de Lognan avec indication du chemin (pointillé) parallèle à la piste de ski, et haltes numérotées. Topographie Suisse et coordonnées de la carte 1: 25 000 feuille Col de Balme (annexe XI)

Stop (a) Montenvers granite:
Ten minutes walk from the Croix de Lognan station leads to the first bend of the road with a first outcrop of typical mylonites (direction 39,85 SE), followed by a rather complete section through the Montenvers granite of Variscan age. The main rock is composed of granitoid gneisses with black coloured, elongated K-feldspar crystals defining a pronounced foliation (43,80 SE). Locally appear strongly elongated enclaves (e.g. **Photo 4.06**), and the main rock is cross-cut by a large number of leucocratic veins, representing former aplitic dikes. All rocks display a strong foliation with a well defined, vertical stretching lineation of Alpine age (**Fig. 5.13**). The cross-section is limited by mylonites, before the former double road-bend is attained (see more details in Ch. IV).

Stop (b) Migmatised orthogneisses:
From the road-bend onwards, rather homogeneous, strongly folded migmatic gneisses are visible in the road cut, which contain irregularly distributed K-feldspar phenocrysts. This rock type can be observed at most of the outcrops, when following the path or the ski track. Two types of structures may be recognised, the steeply dipping fold axes of the migmatites, probably produced during dextral Variscan strike-slip, contemporaneous to the migmatisation of the rocks (see Ch. III, **Fig. 3.09, Fig. 5.13**). Locally, the steeply dipping fold axes are crosscut by horizontal undeformed pegmatoid veinlets, thus prooving the Variscan age of this deformation. A second type of structures, present in all rocks, is a vertical foliation of Alpine age containing a marked vertical stretching lineation (**Fig. 5.13**). Occasionally, thin, orange-coloured garnet-coatings of Alpine age may be observed.

Stop (c) migmatised orthogneiss:
Following the path on the moraine, or following the ski track, at the level of 2240 m, a small cascade on the rock-side is attained. Again, on the ice-polished rock surfaces (locally under water), the migmatised orthogneiss is visible, cross-cut by a regular set of faint fractures, which may contain first anatectic mobilisates (**Photo 2.07**). New veins of mobilisates are visible elsewhere.

Stop (d) migmatised orthogneiss:
The best outcrops of new formed granitic dikes in a ghost-structure of former orthogneisses is attained after climbing offside the track up to 2500 m (**Photo 2.08**), the type locality for dating the migmatisation, as the mobilisates, microgranular granites (Leucogranites of Lognan type), have been dated at 317 ± 2 Ma (U/Pb monazite, Bussy and von Raumer, 1994).

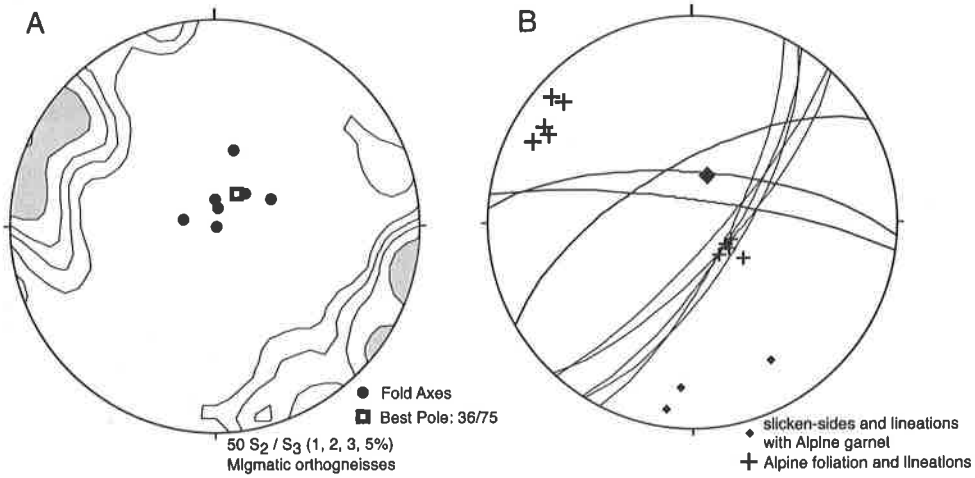

Fig. 5.13
Main structures observed in the Lognan region (see also **Fig. 3.09**). **A**: Late Variscan structures. Statistics of foliation planes in orthogneiss-migmatites (Schmidt net, lower hemisphere) with indication of best pole, coinciding with the distribution of vertical fold axes. **B**: Alpine structures. Foliation planes (poles and great circles) and respective stretching lineations from Montenvers granite, Mont Blanc granite and Ordovician orthogneiss, and garnet-bearing slickensides with lineation from orthogneiss-migmatites.
Structures principales observées dans la region de Lognan (à comparer avec **Fig. 3.09**. ***A**: Structures tardi-varisques. Statistiques des plans de foliation des orthogneiss migmatisés (projection de Schmidt, hémisphère inférieur) avec indication du pôle maximum d'orientation, coïncidant avec la distribution des axes de plis verticaux. **B**: Structures alpines. Plans de foliation (pôles et grands cercles) et linéations correspondantes observées dans le granite de Montenvers, dans le granite du Mont Blanc et dans les orthogneiss ordoviciens. Miroirs de faille à grenat alpins avec linéations dans des orthogneiss migmatisés.*

Stop (e) Mylonite – metasediments
The transition zone to the Mont Blanc granite consists of a complex mylonite zone, hosting strongly deformed migmatic orthogneisses, the contact zone of the Mont Blanc granite, and strongly migmatised metasediments, comparable to the corresponding cross-section in the Trient region further NE.

Among the rusty coloured mylonite-schists appear irregular lumps of amphibolites hosted by migmatites. In the Trient cross section, relics of former calc-silicate rocks are observed, which may be discovered also in the Lognan area.

The chemical composition of one of the amphibolite boudins observed in the Lognan area (Morard 1998) is tholeiitic, chondrite-normalized REE-pattern and multi-element composition pleading for a MORB-type lateral intrusion into a continental back-arc environment.

Stop (f) Mont Blanc granite:
The continuation of the cross-section, either at the level of the glacier, or at 2600 m, leads to the rim of the Mont Blanc granite, a strongly sheared transition zone, where it is difficult to distinguish former migmatites from the granitic border facies. Continuing into the granite body, the increasing size of the K-feldspar phenocrysts is evident. The Alpine foliation is omnipresent, and locally, thin quartz-garnet slicken-sides of Alpine age can be observed. The entire collection of the different aspects of the Mont Blanc granite can be best observed among the boulders in the lateral moraine of the Argentière glacier.

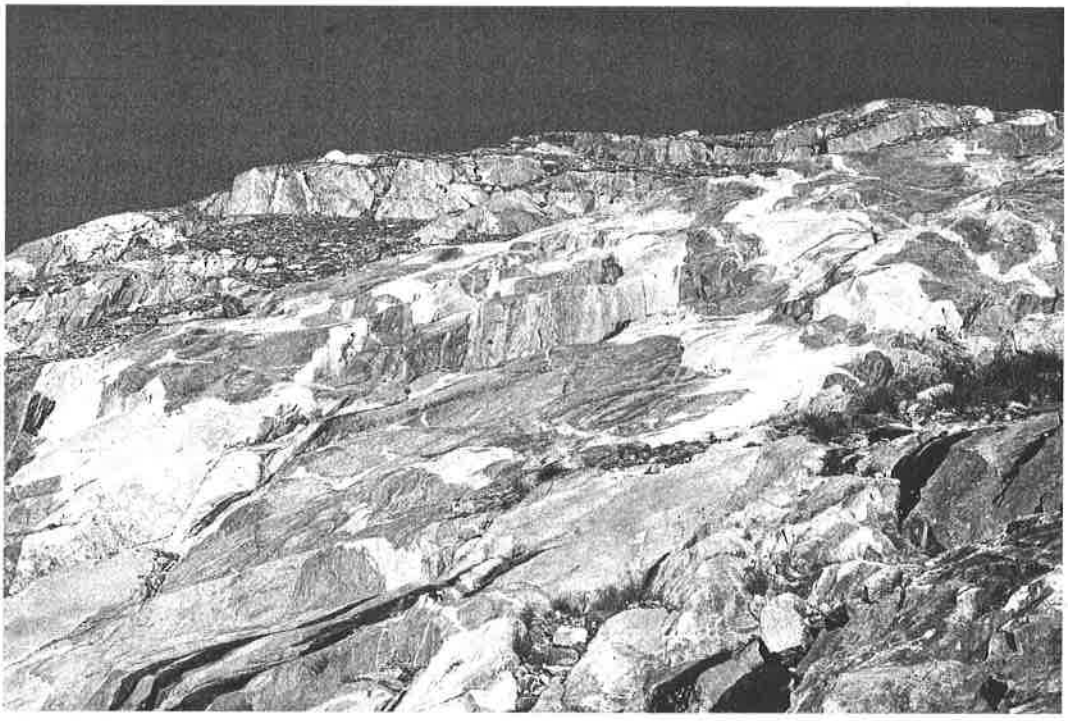

Photo. 5.02
Polymetamorphic basement in the area of Glacier des Petoudes: Sheared migmatites cross-cut by deformed leucogranites. *Socle polymétamorphique dans les environs du Glacier des Petoudes: Migmatites tectonisées avec filons de leucogranites déformés.*

V.6. Trient – Petoudes (Mont Blanc)

Maps: Topography - CH: 1: 25 000 sheets 1324 Barberine; 1325 Sembrancher; 1344 Col de Balme; 1345 Orsières; Swiss geological atlas 1 : 25 000, sheet Finhaut; coloured geological map 1 : 20 000 (annex X); field-map 1 : 10 000: Figure 5.15.

References: Collet et al., 1952; Bauer 1993, Nähr 1993,

Acces: Bus Line Martigny – Col de la Forclaz; Car: Martigny – Col de la Forclaz (1527m; Hotel). The region of Trient – Petoudes is part of the trail around the Mont Blanc massif (section Bovine – Col de la Forclaz – Petoudes – Col de Balme), and its geological features are mainly visible in the ridges of the Trient valley hosting the Glacier de Trient, at present strongly retreated to the level of 2200 m. From Col de la Forclaz, about 1 hour of walking leads to specific outcrops in the neighborhood of the glacier. As torrents are normally very wild and even dangerous, it is difficult to visit outcrops of both sides of the valley during one day.

Outline: The region has become a classical object, as the first section across the northwestern limit of the Mont Blanc massif (Glacier d'Orny – Val de Trient) was already presented by Mrazec (1892), distinguishing the Mont Blanc granite, rimmed at its northwestern limit by its pre-existing basement, containing micaschists and their transformation products ("schistes micacés granulitisés", the present-day migmatites), and the late Variscan granitoids ("granulites"). A section across Col de Balme has been published by Corbin and Oulianoff (1932), and more details are given by Collet et al. (1952), where three sections (4,5,6) illustrate the presence of augengneisses in addition to the gneisses and micaschists of the basement.

Located in the northeastern part of the Mont Blanc massif (**Fig. 5.01**), the northwestern border of the Mont Blanc massif had been subdivided in several longitudinal zones (von Raumer 1976, comprising the metamorphic basement, intersected by the elongated bodies of the K-feldspar augengneiss and the Montenvers granite. The main rocks of the Trient area are comparable to those observed in the Lognan region (see field trip V.5), i. e. a polymetamorphic basement, containing old metasedimentary units and amphibolites, interesected by Ordovician orthogneisses. Most of these rocks were transformed into Late Variscan migmatites and intersected by Late Variscan granitoids (**Photo 5.02**). Additionally, all rocks show a greenschist facies alpine metamorphism with a corresponding foliation plane. All these rocks are illustrated in a NW-SE section, spanning from Col de Balme in SE direction into the Mont Blanc granite (**Fig. 5.14**). Based on unpublished cross-sections (Schouvey, 1988; Nähr 1993), a corresponding cross-section had been mapped in the water-gallery connecting Saleinaz, located in the Mont Blanc granite, and Col de Balme, located in the Mesozoic cover. The opposite cross-section from Col de la Forclaz in southeastern direction to Fenêtre d'Arpette is comparable to that of **Fig. 5.14**, but instead of the Montenvers granite appear strongly deformed gneisses, which may represent relics of the Montenvers granite, but also cordierite-bearing mobilisates, and migmatites of former K-feldspar augengneisses are at outcrop (see Bauer 1993). Small outcrops in front of the Trient glacier (at about 1740m) were visible for the last time in 1974, when they were covered by the advancing ice. They were composed by migmatitic, strongly sheared metasediments, containing stretched lenses of calsilicate marbles, thus representing the northeastern continuation of the corresponding zone at Petoudes du Milieu – Croix de Berons. The very recent retreat of the glacier uncovered a large zone at the level of 1770 – 2150 m (observations september 2003), exposing mainly rocks in continuation from the Pointe des Grands – Croix de Berons areas (**Photo 5.03**).

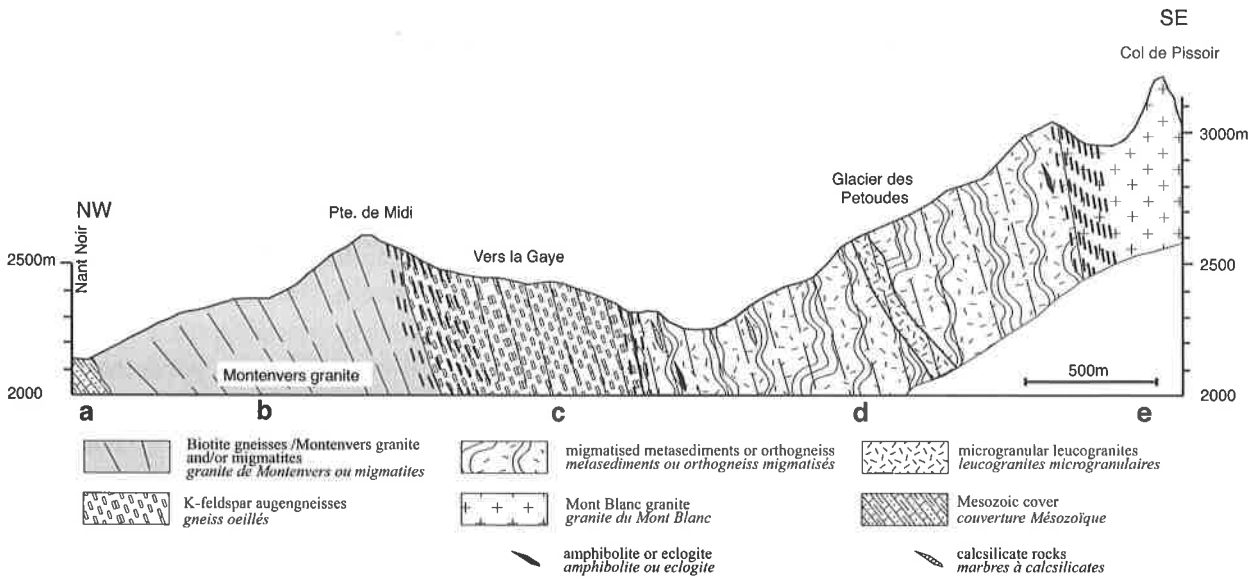

Fig. 5.14
NW-SE section (Col de Balme – Col de Pissoir) through the NW-border of the Mont Blanc massif, containing informations from Schouwey (1988) and Nähr (1993). Main lithologic zones from NW to SE are: a) Mesozoic cover; b) Zone of biotite-gneisses with Alpine foliation, representing the northeastern prolongation of the Montenvers granite; c) K-feldspar augengneisses of Ordovician age; d) zone of migmatites (metasediments and former augengneisses) with leucogranitic dikes (compare **Photo 5.02**); e) Mont Blanc granite, central facies (Ecandies). All units are separated by mylonite zones (dashed zones).
*Section NW-SE (Col de Balme – Col de Pissoir) à travers le bord NO du massif du Mont Blanc, basé sur Schouwey (1988) et Nähr (1993). Les zone lithologiques principales depuis le NO sont: a) couverture mésozoïque; b) gneiss à biotite à schistosité alpine (la continuation NE du granite de Montenvers); c) gneiss oeillés à feldspath potassique d'âge ordovicien; d) zone à migmatites (anciens métasédiments ou orthogneiss) avec des filons leucogranitiques (voir **Photo 5.02**); e) faciès central du granite du Mont Blanc (Ecandies). Les unités sont séparées par des zones à mylonites.*

The **polymetamorphic basement** (**Fig. 5.15**) is represented by mostly migmatic, often strongly tectonised gneisses, either former orthogneisses or former metasediments, containing lens-shaped relics of calcsilicate marbles and irregular lumps or lens-shaped relics of amphibolites and/or eclogites. Such rocks occupy a zone at the northwestern tectonised contact of the Mont Blanc granite, and can be followed up from Alpe Bovine in southwestern direction to Vesevey – Glacier de Trient – Petoudes – Pointe de Berons – Refuge Albert I to the cross-section in the Lognan area (**Fig.5.14**). A second elongated zone of migmatites and tectonized gneisses occupies the most northwestern part of the section, near the contact to the Mesozoic cover (Col de Balme, Forclaz). In this zone, where no relics of metabasic or calsilicate rocks have been observed. Migmatites seem to replace former orthogneisses, and were crosscut by Late Variscan granitoids and pegmatoids of Montenvers resp. Lognan type, when compared to the Lognan cross-section. Both migmatite zones are separated by a large, elongated zone of coarse K-feldspar augengneisses, which can be followed up from the Bovine – Tour Ronde area in southwestern direction to the Lognan area, where they have been dated as Ordovician orthogneisses (Bussy and von Raumer 1994, see Ch. II.1).

Rocks of Late Variscan age are mainly represented, besides the migmatites themselves, by different types of granitoids, corresponding to the intrusions of the Montenvers granite (Col de Balme – Grandes Otanes region), the microgranular leucogranite of Lognan (Petoudes d'en Haut – Pointe de Berons) and in the upper part of the cross-section (**Fig.5.14**) the Mont-Blanc granite (see Ch. IV). Additionally appear coarse-grained pegmatoid veins with large, black coloured K-feldspars (**Photo 5.04**), and crosscutting veins of turmaline.

The proposed stops are introduced after their location at the glacier or at the right or left side of the glacier, as paths leading to those outcrops are distinct. Visitors of the glacier region have to be cautious of rock- or ice-falls.

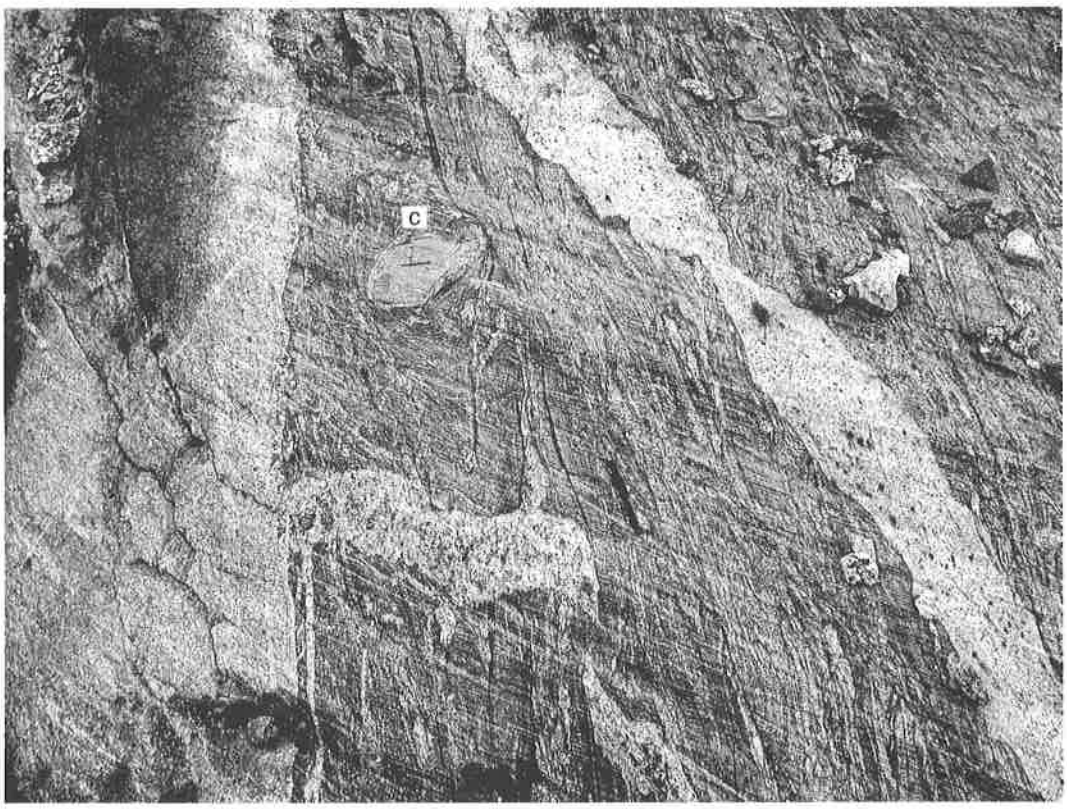

Photo 5.03
Detailed illustration of the polymetamorphic basement at stop 1, pencil as scale, front of Glacier de Trient at 1780 m (Coord. CH: 567.510/96.860). Migmatites with zoned calcsilicate nodule (c), and two generations of granitoid dikes. *Détail du socle polymétamorphique visible au stop 1, crayon comme échelle, front du Glacier de Trient, 1780 m (Coord. CH: 567.510/96.860). Migmatites avec nodule zoné de calcsilicate (c), et deux générations de filons granitiques.*

Stop 1 – Glacier de Trient (1780 m), Polymetamorphic basement (observations september 2003)**:** The retreat of the glacier uncovered a large zone composed of former migmatites (**Photo 5.03**). Relics of calsilicate rocks appear either as long ribbons of large boudins or isolated zonar nodules, and metabasic rocks form irregular lumps. Different generations of granitoids can be observed. Best chances to visit these outcrops exist from september onwards, when snow disappeared, and water of the main torrent is low. In the first outcrops directly in the river at 1780m, the main rocks are dark coloured, microgranular, sheared gneisses, where relics of migmatic structures can be recognised. They had been termed "granulitised micaschists" by Mrazec (1892). They are intersected by already folded leucogranitic dikes, which are either contemporaneous to the Montenvers granite or, more probably, to the microgranular leucogranites as have been dated in the Lognan area (Bussy et al. 2000). Late stage pegmatoid dikes with large black-coloured K-feldspars crosscut the different gneisses (**Photo 5.04**), and latest stages are crosscutting turmalinite veins. All these rocks may be found also among the morainic blocks.

Western side - Petoudes area (Fig. 515)

Stop 2 – Road leading to the water gallery (Coord. CH 565.990/98.460; 1470m), **biotite gneisses, Montenvers granite:** The biotite- K-feldspar gneisses represent a northeastern prolongation of the Montenvers granite. In many outcrops they appear as stretched biotite-rich K-feldspar gneisses (compare with **Photo 4.06**) with a large number of biotite-rich, xenolith-kind patches. In this specific outcrop, they appear as strongly weathering, biotite-rich gneisses, and a normal type of this rock is better preserved in the Grandes Otanes region and on the eastern side of the crest leading to Col de Balme. Dark brown primary biotite is surrounded by small leaves of pale brown Alpine biotite.

Stop 3 – Entrance to the water gallery (Coord. CH 566.570/98.000; 1570m), **K-feldspar augengneisses:** The K-feldspar augengneisses form a heterogeneous assemblage of coarse- and fine-grained gneisses, which in the locality of the gallery appear as foliated augengneisses, where K-feldspar is preserved among the foliation planes.

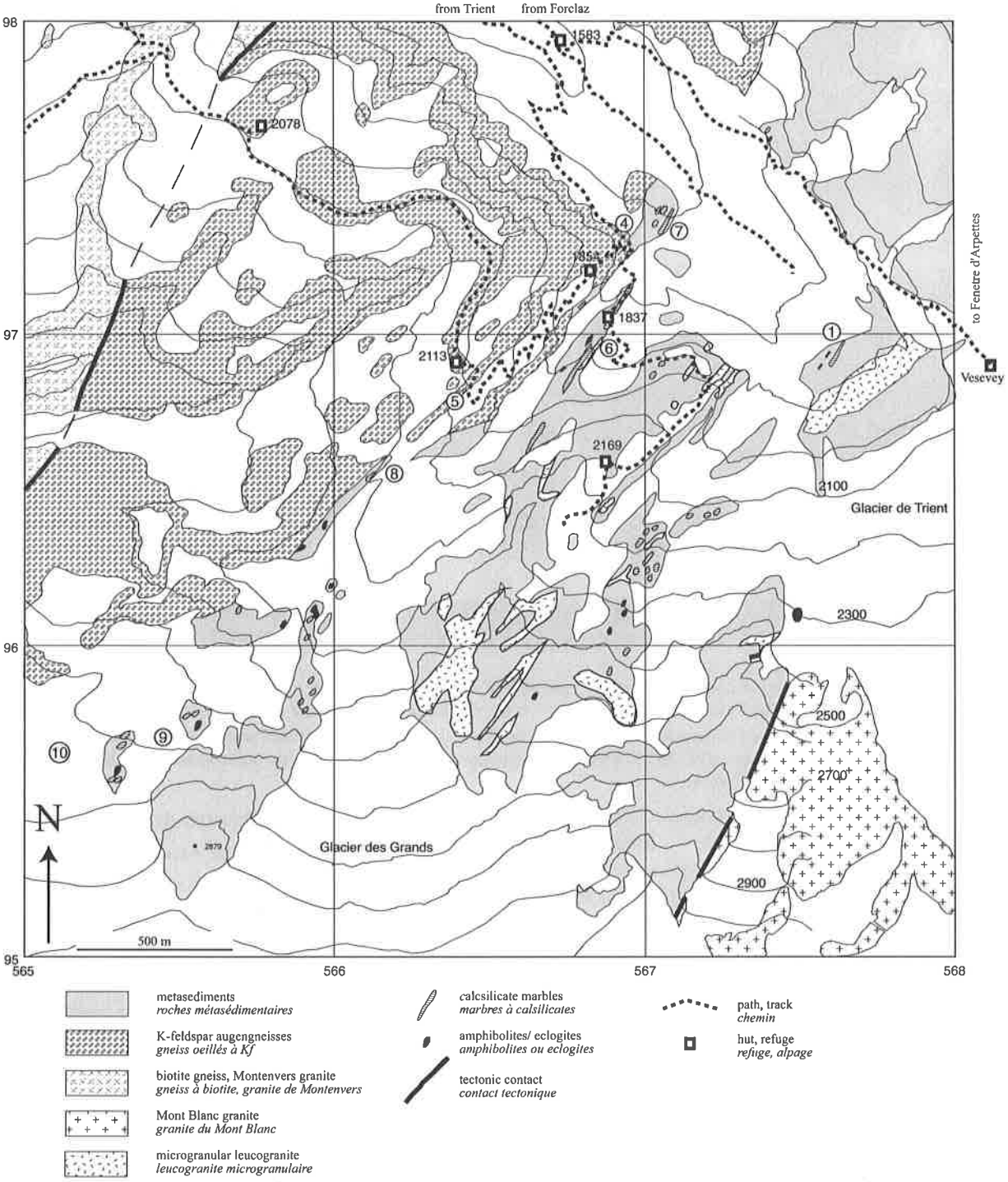

Fig. 5.15
Geological map of the Trient region (Petoudes –Trient area) 1 : 20 000. (Compare annex X).
Carte géologique de la région Trient - Petoudes 1: 20 000 (à comparer avec annexe X).

Stop 4 – Path leading to Petoudes (1730m), **K-feldspar augengneisses:** Typical coarse-grained augengneisses with large K-feldspars are preserved in the massive rocks, which will be the subject of the next outcrop.

Stop 5 – Les Grands - Dessus (2100m), **K-feldspar augengneisses:** Along the stairs across the cliff of the steeply dipping foliation planes of Alpine age, very coarse grained K-feldspars are preserved in the augengneisses. Stretching is considerable, and dark crystals of 10 cm length can be observed, which show white coloured tension gashes filled by albite and quartz (see Ch. II.1, **Photo 2.09**), produced during deformation in the subvertically dipping Alpine stretching lineation. The continuation on the main path leading to Col de Balme exposes outcrops of augengneisses, and from the bifurcation of the path to Trient onwards, the large zone of biotite-gneisses representing the Montenvers granite is traversed.

Stop 6 – Petoudes de Milieu (1837m), **metasediments:** When crossing the main torrent (Jornevette, collecting the water from Pointe des Grands – Pointe de Berons) in southeastern direction, interesting outcrops are visible just above the small hut of Petoudes de Milieu. Strongly sheared metasediments contain elongated lenses of calcsilicate lenses with some scheelite.

Stop 7 – Jornevette river – moraine de Trient (1700), **metasediments and augengneisses:** An interesting group of outcrops can be visited, when leaving the junction of the path leading to Petoudes de Milieu and following the river downward in direction of the junction with the Trient river. The first group of outcrops represents sheared metasediments with different lenses of calcsiliate marbles, cross-cut by a lamprophyric dike. The second group of outcrops, down to the valley in NW direction, shows the tectonised K-feldspar augengneisses.

Western side – Glacier de Berons morainic valley

Stop 8 – moraine de Berons (2300 - 2400m)**:** Continuing, from Les Grands – Dessus in southwestern direction towards Pointe de Berons. Leaving the last outcrops (stretched K-feldspar augengneisses), the small valley "les Chaux" is cut off by the large morainic wall leading to the upper levels of the former Glacier de Berons. At about 2300 m, a torrent from the morainic valley is the place to observe different outcrops on both sides of the morain. At the SE of the moraine (Coord. CH 565.930/96.090; 2270m) outcrop migmatites of former metasediments, containing stretched lenses of calcsilicate lenses and a series of boudinised amphibolites. The outcrops are continuous up to the level of 2400m. On the northwestern side of the moraine, across the torrent mentioned before (2300m), metasedimentary migmatites with relics continue, but at higher levels appear migmatised augengneisses (Coord. CH 565.610/96.020; 2430m; see **Photo 2.05**), thus showing, that all rock units of the basement were transformed by Late Variscan anatexis.

Stop 9 – Moraine in direction Croix de Berons (2500-2600m), **metabasites:** When continuing in direction of the upper Berons morainic valley, two groups of outcrops represent ice-polished rocky buckels, where among dark coloured banded gneisses large boudins of metabasic rocks are preserved. The abundance of garnet and the microscopic structures indicates, that these rocks are meta-eclogites preserved among the migmatites.

Stop 10 – Upper Moraine of Pointe de Berons (2900m), **migmatites:** The upper part of the morain contains many large blocks showing the strong transformation of former K-feldspar augengneisses (**Photo 2.01, 2.02**) into migmatites and microgranular granitoids (see text Ch. II.1). The most advanced transformation stages are leucocratic granular granites (Lognan type) where only black coloured relics of the former K-feldspars have survived. It may be interesting to know, if Ordovician zircons have survived in the phenocrystals.

Eastern side - path to Fenêtre d'Arpette

When walking from Châlet de Glacier in direction to Fenêtre d'Arpette, quality of outcrops is strongly changed by erosion and alteration. Additionally, it is rather difficult to climb all the steep slopes dominating the eastern side of the glacier valley. The entire cross-section is comparable to that presented in **Fig. 5.14** from the Petoudes region. Also on this side, the K-feldspar augengneisses, dominating the Châlet du Glacier (1583m), are in contact with a former metasedimentary series containing many relics of calcsilicates and amphibolites, and are cross-cut by many dikes of leucocratic granitoids. At most outcrops in the area near to the augengneisses, rocks are strongly tectonised. The occurrence of strongly sheared, granulite-like garnet-bearing mylonites of former granitoid dikes (see. **Photo 3.29)** show that the region was transformed by high-temperature mylonites, which are probably related to the intrusion of the Mont Blanc granite. When approaching the contact of the Mont Blanc granite, migmatites are better preserved. Comparable to the Petoudes section, the contact with the Mont Blanc granite is formed by a large mylonite zone, separating migmatic metasediments from the central facies of the Mont Blanc granite.

Near Vesevey (2096m), the large mylonite zone separating migmatites from the Mont Blanc granite is crossed. The limit between both rock types is not evident, and is still covered by the ice sheet. The typical coarse grained granite of the Mont Blanc granite is attained at Fenêtre d'Arpette. The description of a field-trip across the different facies and generations of the Mont Blanc granite are found in Marro (1986) and in the explicative notes to the geological map of Orsières (excursion 1, Burri and Marro, 1993). From Vesevey, a track in southwestern direction is leading to the western foot of the Ecandies, a famous climbing locality in the central facies of the Mont Blanc granite. When in 1965, the climber had still a vertical view from the Ecandies ridge on the ice, at present day, the Col des Ecandies is easily attained across the moraine, as the strong retreat of the ice has unvovered also a great part of the rocks in the upper part of the glacier.

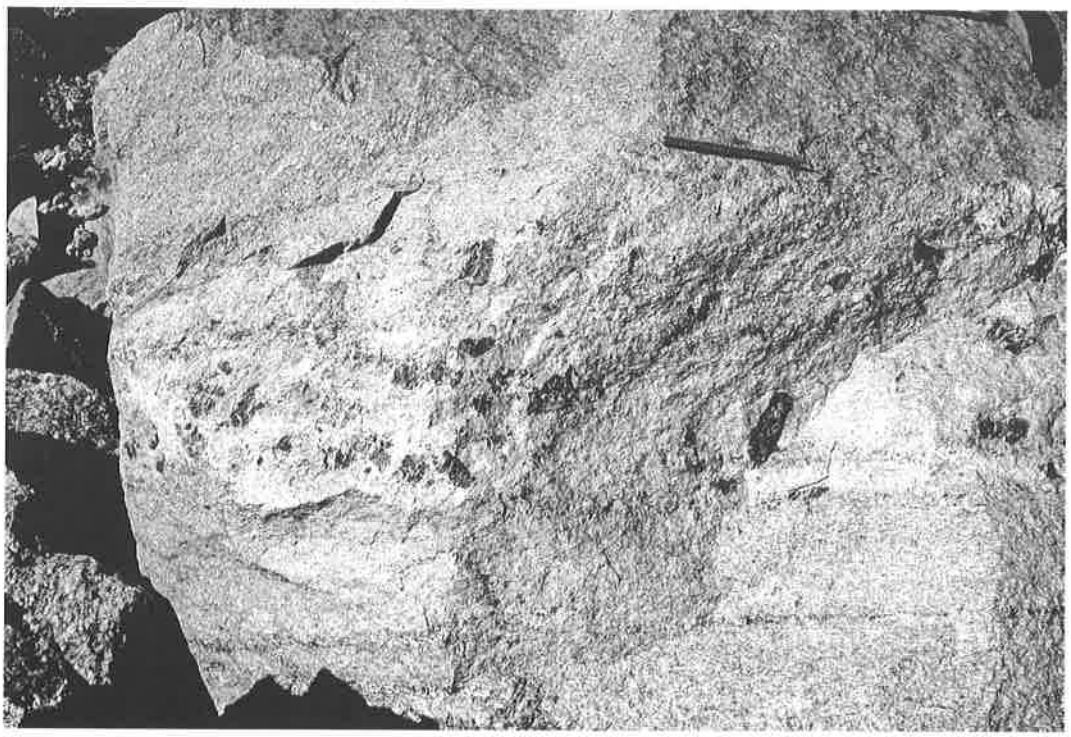

Photo 5.04
Coarse-grained pegmatoid with large black-coloured K-feldspars in leucocratic granite, boulder at foot of Glacier de Trient. *Pegmatoïde grossier avec des grands feldpaths potassiques de couleur noire. Bloc au pied du Glacier du Trient.*

Acknowledgments

This volume is synthesizing 40 years of research of the first author and almost half of that time for the second. It would not have been achieved without the continuous help and encouragement from a large number of institutions and persons, especially to JvR.

More specifically, we would like to sincerely acknowledge the Swiss National Sciences Foundation for many years of financial support, as well as the following institutions for their contribution to the printing costs of this Memoir: Foundation Dr. Joachim de Giacomi (SAS); Fondation B. & S. Tissières, Martigny; Etat du Valais; the Institutes of Geology-Palaeontology and Mineralogy-Geochemistry of the University of Lausanne. We thank the Valais Cadastral Office and the Federal Office for Water and Geology for having supplied us with the topographic basis necessary for the geological mapping. The EDF and Emosson SA companies, as well as the Remontées Téléphériques SA (Argentière) provided us with considerable logistic support. Reception at the huts of the Mountaineering Clubs CAS, CAI et CAF has always been pleasant.

So many years of field work created human contacts, strong ties and invaluable friendship with many inhabitants of these Alpine valleys. JvR is indebted to many of them, who helped and supported him considerably. He is especially grateful to Danièle and Cécile (Refuge Pierre à Bérard), Marc Quebey (Chedde), the Gay-Crosier families (Col de la Forclaz), Mme. Gay-Crosier (Barrage d'Emosson), Madame Cochinal (Argentieres) and Madame Gastaldo (Montroc), Mr. Couvert (Chamonix), Agnès and Patrick Breviglieri (Altitude 2000 and Les Bossons) for their hospitality; to Monsieur l'Abbé Eyheralde, and to Catherine and Jacky Ravanel for their friendly reception in the group of "Réserve Naturelle des Aiguilles Rouges" and at the Châlet du Col de Montets; to Madame Gubler for her special and long-lasting interest in the development of this work.

The authors also benefited from the support of and the discussions with many colleagues and students in Fribourg and Lausanne, especially those who contributed to this memoir via their diploma and/or PhD work, referenced in the text. A special thank is due to H. R. Pfeifer and A. Morard (University of Lausanne) for their active and decisive contribution in this volume, as well as to Jean-Luc Epard for his help and advise in the final steps of the publication process.

Remerciements

Ce volume, qui résume les connaissances acquises durant 40 années de travail géologique sur terrain, n'aurait pas pu être achevé sans l'aide et l'encouragement continu d'une multitude de gens et de nombreuses institutions.

Mes remerciements les plus sincères vont au Fonds National Suisse de la Recherche Scientifique dont l'aide financière substantielle pendant plus de trente ans a considérablement contribué à la progression de la connaissance dans la région concernée. L'impression de ce volume a été facilitée par les contributions financières des institutions suivantes: Fondation Dr. Joachim de Giacomi (ASSN), Fondation B. & S. Tissières (Martigny), Etat du Valais, Instituts de Géologie-Paléontologie et de Minéralogie-Géochimie de l'Université de Lausanne. Le service cadastral de l'Etat du Valais est remercié pour la mise à disposition gratuite des données topographiques pour les cartes géologiques ; l'Office fédéral des eaux et de la géologie (OFEG) a facilité l'accès aux bases topographiques de la Confédération. Un merci sincère pour cette aide considérable. Evidemment, beaucoup d'idées nouvelles ont surgi pendant les discussions avec les étudiants et les collègues. C'est ici une bonne occasion pour remercier les diplômants et doctorants pour les moments de partage durant la recherche et pour leur amitié. Beaucoup de leurs résultats ont été présentés dans ce volume, ils ont donc été cités à de nombreuses occasions.

Pendant les semaines sur terrain, j'ai eu la joie de rencontrer beaucoup d'amis parmi les habitants de la région. C'est grâce à leur soutien moral, leur aide efficace et leur accueil que j'ai pu passer des années extraordinaires dans ces belles régions. Mes remerciements vont aux entreprises électriques EDF et Emosson SA, et aux entreprises mécaniques d'Argentière pour leur aide logistique considérable. L'accueil dans les cabanes et les refuges des Clubs Alpins CAS, CAI et CAF fut toujours agréable. Je remercie tout particulièrement les gardiennes Danièle et Cécile de Pierre-à-Bérard, Marc Quebey (Chedde) pour l'hospitalité dans leur chalet, les familles Gay-Crosier du Col de la Forclaz et Mme. Gay-Crosier au Barrage d'Emosson. Une grande pensée va à Madame Gubler pour son grand intérêt pour l'avancement du travail. Monsieur l'Abbé Eyheralde ainsi que Catherine et Jacky Ravanel sont remerciés pour leur accueil amical dans le groupement de la Réserve Naturelle des Aiguilles-Rouges et au Chalet du Col de Montets. Madame Cochinal (Argentière) et Madame Gastaldo (Montroc) m'ont toujours offert un logement agréable et la famille Couvert (Chamonix), ainsi que Agnès et Patrick Breviglieri (Les Bossons,) ont tout fait pour que je puisse travailler confortablement dans les régions situées au flanc Nord des Aiguilles-Rouges. Un grand merci pour ces moments inoubliables.

Ce volume n'aurait pas vu le jour sans l'aide des collègues de l'institut de Géologie (Université de Fribourg). Les multiples discussions avec les collègues de la Section des Sciences de la Terre (Université de Lausanne) pendant les dernières années et leur encouragement amical ont largement facilité l'achèvement de ce volume. Je remercie H. R. Pfeifer et A. Morard de Lausanne pour leurs contributions à ce volume et Jean-Luc Epard (Lausanne) pour son aide et conseil pendant la phase finale du volume. Bien qu'il ne soit pas d'usage, un chaleureux merci va à François Bussy pour son accompagnement patient et pour ses contributions à ce travail. A toutes et à tous un grand merci!

References

Aeschlimann, H. (1983): Zur Gletschergeschichte des italienischen Mont Blanc Gebietes: Val Veni - Val Ferret - Ruitor. PhD Thesis, Universität Zürich, 105 p

Amberger, G.F. (1960): L'autochthone de la partie nord-ouest du Massiv des Aiguilles Rouges (Haute Savoie et Valais), unpubl. PHD Thesis, Université de Geneve, pp.

Arlt, T. (2004): Strahlen im Mont Blanc-Granit. Schweizer Strahler 2,2004:14-22

Ayrton, S. (1980): La géologie de la zone Martigny-Chamonix (versant suisse) et l'origine de la nappe de Morcles (un exemple de subduction continentale). Eclogae Geologicae Helvetiae, 73: 137-172.

Badoux, H. (1972): Tectonique de la nappe de Morcles entre Rhône et Lizerne. Beiträge zur geologischen Karte der Schweiz Neue Folge, 143: 1-78.

Barbarin, B. (1999): A review of the relationships between granitoid types, their origins and their geodynamic environments. Lithos, 46: 605-626.

Bauer, W. (1993): Petrographie präalpidischer Metamorphite und Geochemie eines Orthogneises im Mont-Blanc-Massiv südlich des Col de la Forclaz (SW Schweiz). Unpubl. Diploma Thesis, Friedrich-Alexander Universität, Erlangen-Nürnberg, 80 pp.

Bayle, L.D. (Editor) (1999): Minéralogie du Massif du Mont-Blanc. Le Règne Mineral, Volume hors série V, 78 pp.

Bea, F., Fershtater, G. and Corretgé, L.G. (1992): The geochemistry of phoshorus in granite rocks and the effect of aluminium. Lithos, 29: 43-56.

Beccaluva, L., Di Girolamo, P., Macciotta, G. and Morra, V. (1983): Magma affinities and fractionation trends in ophiolites. Ofioliti, 8: 307-324.

Bellieni, G., Comin Chiaramonti, P., Marques, L. S., Melli, A. J., Picirillo, P. M., Nardy,A. J. R., Roisenberg, A. (1984): High-and low-TiO2 flood basalts from the Parana plateau (Brazil): petrology and geochemical aspects bearing on their mantle origin. Neues Jahrbuch für Mineralogie Abhandlungen, 150: 273-306.

Bellière, J. (1954): Sur la présence des silicates d'alumine (sillimanite, andalousite, disthène) dans le massif des Aiguilles Rouges (Haute Savoie). Comptes Rendus de l'Académie des Sciences, Partis, 1954: 1395-1397.

Bellière, J. (1958): Contribution à l'étude pétrogénétique des schistes cristallins du massif des Aiguilles Rouges (Haute Savoie). Annales de la Societé Géologique de Belgique, 81: 1-198.

Bellière, J. and Streel, M. (1980): Roches d'âge viséen supérieur dans le massif des Aiguilles Rouges (Haute Savoie). Comptes Rendus Académie des Sciences Paris, 290, D: 1341-1343.

Bermann, R. G. (1988): Internally-consistentthermodynamic data for minerals in the system Na2O-K2O-CaO-MgO-FeO-Fe2O3-Al2O3-SiO2-TiO2-H2O-CO2. Journal of Petrology 29:445-522

Bhatia, M.R. and Crook, K.A. (1986): Trace element characteristics of graywackes and tectonic setting discrimination of sedimentary basins. Contributions of Mineralogy and Petrology, 92: 181-193.

Biino, G. (1994): The pre-Late Ordovician metamorphic evolution of the Gotthard-Tavetsch massifs (Central Alps): from lawsonite to kyanite eclogite to granulite retrogression. Schweizerische Mineralogische und Petrographische Mitteilungen, 74, 87-104.

Bless, R.A. (1984): Beiträge zur spät- und postglacialen Geschichte der Gletscher im nordöstlichen Mont Blanc Gebiet. PhD Thesis, Universität Zürich, 116 pp.

Bonin, B. (coord.), Brändlein P, Bussy F, Desmons J, Eggenberger U, Finger F, Graf K, Marro Ch, Mercolli I, Oberhänsli R, Ploquin A, von Quadt A, von Raumer J, Schaltegger U, Steyrer H P, Visona D, Vivier G (1993): Late Variscan magmatic evolution. In: J. von Raumer and F. Neubauer (Eds.) The Pre-Mesozoic geology in the Alps. Springer, Heidelberg 1993, pp 171-201

Bovay, P. (1988): Pétrographie et géochimie d'une association de roches acides et basiques, Massif cristallin de Fully (Valais). Unpubl. Diploma Thesis, Université de Lausanne, 59 pp.

Brändlein, P. (1991): Petrographische und geochemische Charakteristika des Vallorcine-Granits, Aiguilles-Rouges-Massiv (Westalpen, Schweiz), Unpubl. PHD Thesis, Erlangen, 146 pp.

Brändlein, P., Nollau, G., Sharp, Z. and von Raumer, J. (1994): Petrography and geochemistry of the Vallorcine-Granite (Aiguilles Rouges Massiv, Western Alps). Schweizerische Mineralogische und Petrographische Mitteilungen, 74: 227-243.

Bucher, K. and Frey, M. (1994): Petrogenesis of Metamorphic Rocks. Springer Verlag Berlin Heidelberg, 318 p.

Burg, J.P., van den Driessche, J. and Brun, J. P. (1994): Syn- to post-thickening extension in the Variscan belt of Western Europe. Modes and structural consequences. Géologie de la France, 1994, 3: 33-51.

Bussy, F. (1990): Pétrogenèse des enclaves micro-grenues associées aux granitoïdes calco-alcalins: exemple des massifs varisque du Mont-Blanc (Alpes occidentales) et miocène du Monte Capanne (Ile d'Elbe, Italie). Mémoi-

res de Géologie, Lausanne, 7: 1-309.

Bussy, F., Delitroz, D., Fellay, R. and Hernandez, J. (1998a): The Pormenaz Monzonite (Aiguilles Rouges, Western Alps): an additional evidence for a 330 Ma-old magnesio-potassic magmatic suite in the Variscan. Schweizerische Mineralogische und Petrographische Mitteilungen 78: 193-194

Bussy F, Venturini G, Hunziker J, Martinotti G (1998b): U-Pb ages of magmatic rocks of the western Austroalpine Dent-Blanche-Sesia Unit. Schweizerische Mineralogische und Petrographische Mitteilungen 78: 163-168

Bussy, F., Hernandez, J. and von Raumer, J. (2000): Bimodal magmatism as a consequence of the post-collisional readjustment of the thickened variscan continental lithosphere (Aiguilles Rouges/Mont-Blanc massifs, western Alps). Transactions of the Royal Society of Edinburgh: Earth Sciences, 91,1-2: 221-233.

Bussy, F., Schaltegger, U. and Marro, C. (1989): The age of the Mont-Blanc granite (Western Alps): a heterogeneous isotopic system dated by Rb-Sr whole rock determination on its microgranular enclaves. Schweizerische Mineralogische und Petrographische Mitteilungen, 69: 3-13.

Bussy, F. and von Raumer, J. (1994): U-Pb geochronology of Palaeozoic magmatic events in the Mont-Blanc Crystalline Massif, Western Alps. Schweizerische Mineralogische und Petrographische Mitteilungen, 74: 514-515.

Capuzzo, N. (2000): History of the Late Palaeozoic Salvan-Dorénaz basin revealed from its sedimentary fill. Unpubl. PhD Thesis, Universität Basel, 198 pp.

Capuzzo, N. and Bussy, F. (2001): Syn-sedimentary volcanism in the Late Carboniferous Salvan-Dorénaz basin (Western Alps). Memorie Scienze Naturali Brescia, 25: 203-211.

Capuzzo, N., Handler, R., Neubauer, F. and Wetzel, A. (2003): Post-collisional rapid exhumation and erosion during continental sedimentation: the example of the late Variscan Salvan-Dorénaz basin (Western Alps). International Journal of Earth Sciences, 92: 364-379

Capuzzo, N. and Wetzel, A. (2000): Facies and basin architecture of the Late Carboniferous Salvan-Dorénaz continental basin (Aiguilles-Rouges massif, Western Alps). submitted.

Chemenda, A., Mattauer, M., Bokun, A. N. (1996): Continental subduction and a mechanism for exhumation of high-pressure metamorphic rocks: new modelling and field data from Oman. Earth and Planetary Science Letters 143: 173-182

Chiaradia, M. (1993a): The Scheelite-skarn of Salanfe (Valais, Switzerland), Unpubl. Dr. Thesis, Université de Fribourg, 219 p.

Chiaradia, M. (1993b): The Scheelite-skarn of Salanfe (Valais, Switzerland). Schweizerische Mineralogische und Petrographische Mitteilungen, 73: 41-51.

Chiaradia, M. (1994). "Sedimentary protoconcentrations as a source of tungsten in the W-As-Au skarn of Salanfe (Aiguilles Rouges Massif, Switzerland)." Schweizerische Mineralogische und Petrographische Mitteilungen 74: 329-342.

Chiaradia, M. (1997): Metal source in the W-As-Au skarn of Salanfe (Aiguilles Rouges Massif, Swiss Alps): Attempt of identification using Pb isotopes. In: H. Papunen (Editor), Mineral Deposits: Research and exploration where do they meet? A. A. Balkema, Rotterdam, pp. 621-624.

Collet, L.W. (1924): Description générale du Massif du Mont-Blanc 2: Aperçu sur la géologie du Mont-Blanc et des Aiguilles Rouges. Librairie Fischbacher, Paris, 1-51 pp.

Collet, L.W., Oulianoff, N. and Reinhard, M. (1952): Atlas géologique de la Suisse 1: 25000, Feuille 525 Finhaut, Notice explicative. Kümmerly & Frey S. A., Berne, 52 pp.

Corbin, P. and Oulianoff, N. (1925): Contunité de la tectonique hercynienne dans les massifs du Mont-Blanc et des Aiguilles-Rouges. Bulletin de la Societé géologique de France, (4) 25: 541-553.

Corbin, P. and Oulianoff, N. (1927): Notice explicative. Carte Géologique du Massif du Mont-Blanc. Feuille Servoz-Les Houches, Paris, 26 pp.

Corbin, P. and Oulianoff, N. (1928a): Les roches basiques de la région du Lac Cornu (Aiguilles Rouges) et la question de leur origine. Bulletin de la Societé géologique de France, (4) 28: 43-54.

Corbin, P. and Oulianoff, N. (1928b): Notice explicative. Carte Géologique du Massif du Mont-Blanc. Feuille Chamonix. Imprimerie-Librairie G. Jacquart, Saint-Maur-des-Fosses, 23 pp.

Corbin, P. and Oulianoff, N. (1928c): Notice explicative. Carte Géologique du Massif du Mont-Blanc. Feuille Les Tines. Imprimerie-Librairie G. Jacquart, Saint-Maur-des-Fosses, 23 pp.

Corbin, P. and Oulianoff, N. (1930): Notice explicative. Carte Géologique du Massif du Mont-Blanc. Feuille Vallorcine. Imprimerie-Librairie G. Jacquart, Saint-Maur-des-Fosses, 15 pp.

Corbin, P. and Oulianoff, N. (1931): Notice explicative. Carte Géologique du Massif du Mont-Blanc. Feuille Le Tour. Imprimerie-Librairie G. Jacquart, Saint-Maur-des-Fosses, 16 pp.

Corbin, P. and Oulianoff, N. (1932): Notice explicative. Carte Géologique du Massif du Mont-Blanc. Feuille Argentière. Imprimerie-Librairie G. Jacquart, Saint-Maur-des-Fosses, 16 pp.

Corbin, P. and Oulianoff, N. (1934): Notice explicative. Carte Géologique du Massif du Mont-Blanc. Feuille Mont Dolent. Imprimerie-Librairie G. Jacquart, Saint-Maur-des-Fosses, 16 pp.

Corbin, P. and Oulianoff, N. (1935): Notice explicative. Carte Géologique du Massif du Mont-Blanc. Feuille Talèfre. Imprimerie-Librairie G. Jacquart, Saint-Maur-des-Fosses, 16 pp.

Corbin, P. and Oulianoff, N. (1938): Notice explicative. Carte Géologique du Massif du Mont-Blanc. Feuille Le Tacul - Col du Géant. Imprimerie-Librairie G. Jacquart, Saint-Maur-des-Fosses, 19 pp.

Corbin, P. and Oulianoff, N. (1952): Notice explicative. Carte Géologique du Massif du Mont-Blanc. Feuille Mont Blanc Sommet. Imprimerie-Librairie G. Jacquart, Saint-Maur-des-Fosses, 19 pp.

Corbin, P. and Oulianoff, N. (1956): Notice explicative. Carte Géologique du Massif du Mont-Blanc. Feuille Aiguilles du Midi. Imprimerie-Librairie G. Jacquart, Saint-Maur-des-Fosses, 19 pp.

Corbin, P., Oulianoff, N. and J., B. (1959): Notice explicative. Carte Géologique du Massif du Mont-Blanc. Feuille Miage. Société Française de Stéréophotographie, Paris, 19 pp.

Corbin, P., Oulianoff, N. and J., B. (1969): Notice explicative. Carte Géologique du Massif du Mont-Blanc. Feuille Pormenaz. Société Française de Stéréophotographie, Paris, 19 pp.

Couvert de Crest, R. (1993): Une vallée insolite. Chamonix - Le Mont Blanc - La Savoie. Esope-le Lezard, Chamonix-Le Praz.

Crowley, Q.G., Floyd, P.A., Winchester, J.A., Franke, W. and Holland, J.G. (2000): Early Palaeozoic rift-related magmatism in Variscan Europe: fragmentation of the Armorican Terrane Assemblage. Terra Nova, 12: 171-180.

Dal Piaz, G. V. (1992): Le Alpi dal M Bianco al Lago Maggiore. BE-MA editrice, Padova, 201 pp.

Debon, F. and Le Fort, P. (1988): A cationic classification of common plutonic rocks and their magmatic associations: principles, method, apllications. Bulletin de Minéralogie, 111: 493-510.

Debon, F. and Lemmet, M. (1998): Evolution of Mg/Fe ratios in late Variscan plutonic rocks from the External Crystalline Massifs of the Alps (France, Italy, Switzerland). Journal of Petrology, 40: 1151-1185.

Delamette, M. (1993): Le Pays du Mont-Blanc. Collection Nature, 239 p.

De La Roche, H., Leterrier, J., Grandclaude, P. and Marchal, M. (1980): A classification of volcanic and plutonic rocks using R1 - R2 diagram and major element analyses - its relationship with current nomenclature. Chemical Geology, 29: 183-210.

Délitroz, D. and Fellay, R. (1997): Etude géologique et minéralogique de la région de Pormenaz (Haute Savoie, France). unpubl. Diploma Thesis, Université de Lausanne, 168 pp.

Della Valle, G., Gex, P. and von Raumer, J.F. (1987): Le gîte d'or. d'arsenic et de tungstène de Salanfe. Beiträge zur Geologie der Schweiz, Geotechnische Serie, 72: 118-128.

Demathieu, G. and Weidmann, M. (1982): Les empreintes de pas de reptiles dans le Trias du Vieux Emosson. Eclogae Geoloicae Helvetiae, 75: 721-757.

Dobmeier, C. (1996): Geodynamische Entwicklung des südwestlichen Aiguilles-Rouges-Massivs (Westalpen, Frankreich). Mémoires de Géologie (Lausanne), 29: 1-198.

Dobmeier, C. (1998): Variscan P-T deformation paths from the southwestern Aiguilles Rouges massif (External massif, western Alps) and their implication for its tectonic evolution. Geologische Rundschau, 87: 107-123.

Dobmeier, C., Pfeifer, H.R. and Von Raumer, J.F. (1999): The newly defined „Greenstone Unit" of the Aiguilles-Rouges massif (western Alps); remnant of an early Palaeozoic oceanic island-arc? Schweizerische Mineralogische und Petrographische Mitteilungen, 79: 263-276.

Duparc, L. (1896): Le Mont Blanc au point de vue géologique et pétrographique. Archives des Sciences physiques et naturelles, 4, II: 1-8.

Duparc, L. and Mrazec, L. (1892a): Recherches sur la protogine du Mont-Blanc. Archives des Sciences physiques et naturelles, 3, XXVII: 659-677.

Duparc, L. and Mrazec, L. (1892b): Sur la protogine du Mont-Blanc. Compes Rendus des séances de la Société physique et histoire naturelle Genève (3): 5-7.

Duparc, L. and Mrazec, L. (1893): Roches amphiboliques du Mont-Blanc. Archives des Sciences physiques et naturelles, 3, XXX: 1-22.

Duparc, L. and Mrazec, L. (1894): Le massif de Trient. Archives des Sciences physiques et naturelles, 3, XXXII,9: 1-16.

Duparc, L. and Mrazec, L. (1895): Nouvelles recherches sur le Massif du Mont-Blanc. Archives des Sciences physiques et naturelles, XXXIV: 1-39.

Duparc, L. and Mrazec, L. (1898): Recherches geologiques et petrographiques sur le Massif du Montblanc. Mémoires de la Société de Physique et d'Histoire naturelle XXXIII (1).

Duparc, L. and Pearce, F. (1897): Les porphyres quartzifères du Val Ferret. Archives des Sciences physiques et naturelles, 4, IV: 1-37.

Duparc, L. and Ritter, E. (1894): La nature pétrographique du carbonifère de la zone du Mont-Blanc. Archives des Sciences physiques et naturelles, 3, XXXI: 1-5.

Dupasquier, S. (1996): Géologie et pétrographie de la rive droite du Lac d'Emosson. unpubl. Diploma Thesis, Université de Fribourg, 147 pp.

Ebadi, A. and Johannes, W. (1991): Beginning of melting and composition of first melts in the sytem Qz-Ab-Or-H2O-CO2. Contributions of Mineralogy and Petrolology 106, 286-295

Ehling, B.-C. (1993): Geologie und Geochemie der Scheelitskarnlagerstätte von Delitzsch (NW-Sachsen). Unpubl. PHD Thesis, Bergakademie Freiberg.

Einaudi, M.T., Meinert, L.O. and Newberry, R.J. (1981): Skarn deposits. Economic Geologist, 75th Anniversary Volume: 317-391.

Einfalt, H.C. (1979): Stabilität und Genese von Andalusit in Graniten, unpubl. PHD Thesis Universität Karlsruhe, 140 pp.

Epard, J.-L. (1989): Stratigraphie du Trias et du Lias dauphinois entre Belledonne, Aiguilles-Rouges et Mont-Blanc. Bulletin de la Societé vaudoise des Sciences Naturelles, 79: 301-338.

Epard, J.L. (1990): La nappe de Morcles au sud-ouest du Mont-Blanc. Mémoires de Géologie, 8: 1-152.

Epard, J.L. (2001): The overall tectonic framework of the Externides domain. In: G.M. Stampfli (Editor), Geology of the western Swiss Alps, a guide-book. Mémoires de Géologie (Lausanne), 36: 43-51.

Escher, A., Hunziker, J.C., Masson, H., Sartori, M. and Steck, A. (1997): Geological framework and structural evolution of the western Swiss-latalian Alps. In: O.A. Pfiffner, P. Lehner, P.Z. Heitzmann, S. Müller and A. Steck (Editors), Deep structure of the Swiss Alps – Results from NRP 20. Birkhäuser AG, Basel, pp. 205-222.

Eyheralde, J., Gourreau, J. M., Gubler, Y., Roelly, A., Perret, P., Ravanel, J. (1993): Guide de la Reserve Naturelle des Aiguilles Rouges. Collection Nature, 239 p. pp.

Favre, A. (1867): Recherches geologiques dans les parties de la Savoie, du Piemont et de la Suisse voisins du Mont Blanc. Masson et Fils, Genève.

Fehlmann, H. (1919): Der Schweizerische Bergbau während des Weltkrieges. Kümmerly & Frey, Bern.

Floyd, P.A. & Winchester, J.A. (1975): Magma type and tectonic setting discrimination using immobile elements. Earth and Planetary Science Letters 27: 211-218

Floyd, P.A., Winchester, J., Seston, R., Kryza, R. and Crowley, Q.G. (2000): Review of geochemical variationin Lower Palaeozoic metabasites from the NE Bohemian Massif: intracratonic rifting and plume-ridge interaction. In: W. Franke, R. Altherr, V. Haak, O. Oncken and D. Tanner (Editors), Orogenic processes - quantification and modelling in the Variscan belt of Central Europe. Geological Society of London Special Publications, 179:155-174.

Floyd, P.A., Winchester, J.A. and Park, R.G. (1989): Geochemistry and tectonic setting of Lewisian clastic metasediments from the early Proterozoic Loch Maree Group of Gairloch, NW-Scotland. Precambrian Research, 45: 203-214.

Fodor, R.V. and Vetter, S.K. (1984): Rift-zone magmatism: Petrology of basaltic rocks transitional from CFB to MORB, southeastern Brazil margin. Contributions of Mineralogy and Petrology 88: 307-321

Fracheboud, S. (1997): Géologie et pétrographie du Val Bérard supérieur (Massif des Aiguilles Rouges, France). Unpubl. Diploma Thesis, Université de Fribourg, 136 pp.

Frey, A. (1974): Neue Mineralien aus dem Unterwallis. Schweizer Strahler 3,6,243-248

Frey, A. (1977): Synchisit aus dem Unterwallis. Schweizer Strahler 5, 205-207

Frey, A. (1981): Weiteres Vorkommen seltener Kleinmineralien im Unterwallis. Schweizer Strahler 5,10,434-436.

Frey, A. and von Raumer, J.F. (1977a): Über einen Scheelit-Neufund. Schweizer Strahler, 4-7: 296-298.

Frey, A. and von Raumer, J.F. (1977b): Uranmineralien aus dem Val du Trient. Urner Mineralienfreund, 1977-1: 1-4.

Frey, M., Desmons, J. and Neubauer, F. (Editors) (1999): The new Metamorphic map of the Alps. Schweizerische Mineralogische und Petrographische Mitteilungen, 79/1. Stäubli Verlag AG, Zürich, 230 pp.

Gautron, L. (1999): Les indice minéralogiques du massif du Monr Blanc. Le Regne Minéral 5,59-66

Gay, P. (1998): Pétrographie et géologie de la Combe des Fonds (Val Ferret), Université de Fribourg, Unpubl. Diploma Thesis, Université de Fribourg, 104 pp.

Genier, L. (2001): Etude structurale, pétrographique et géochimique de l'anatexie varisque des gneiss d'Emosson (VS). unpublished Diploma thesis, Université de Lausanne, 120 p.

Genier, L.. (2002): Les Migmatites d'Emosson et leurs encaissants, massif cristallin externe des Aiguilles Rouges (VS), DEA, unpublished, Université de Lausanne 186 p.

Gourlay, P. (1986): La déformation du socle et des couvertures delphino-helétiques dans la region du Mont Blanc (Alpes Occidentales). Bulletin Societé Géologique de France 186: 159-169

Grasmück, K. (1961): Die helvetischen Sedimente am Nordostrand des Mont-Blanc-Massivs. Eclogae Geologicae Helvetiae, 54: 351-450.

Greenwood H. J. (1976): Metamorphism at moderate temperatures and pressures. In: The evolution of the crystalline rocks. D.K. Bailey and R. McDonald (Eds).Academic Press, London

Grubenmann, U. (1892): Über Gesteine des granitischen Kerns im oestlichen Teil des Gotthardmassivs. Mitteilungen der Thurgauischen naturforschenden Gessellschaft 10: 125-144.

Guillemot, J., Guy, M. and Lobjoit, M. (1973): Un système cohérent d'alignements structuraux commun aux Alpes et aux Pyrénées mis en évidence par le satellite ERTS 1. Comptes Rendus Académie des Sciences Paris, 277D: 481-484.

Guillot, S. and Ménot, R.P. (1999): Nappe stacking and first evidence of Late Variscan extension in the Belledonne Massif (External Crystalline Massifs, French Alps). Geodinamica Acta, 12: 97-111.

Harnois, L. (1988): The CIW index: A new chemical index of weathering. Sedimentary Geology, 55: 319-322.

Heim, A. (1919): Geologie der Schweiz. Ed. Tauchnitz, Leipzig.

Holdaway, M. J. (1971): Stability of andalusite and the aluminium silicate phase diagram. Amer. J. Sci., 271, 97-131.

Holtz. F. and Johannes, W. (1994): Maximum and minimum water contents of granitic melts: implications for chemical and physical properties of ascending magmas. Lithos 32: 149-159

Holub, F.V., 1977. Petrology of inclusions as a key to petrogenesis of the durbachitic rocks from Czechoslovakia. Tschermaks Mineralogische und Petrographische Mitteilungen, 24: 133-150.

Huggenberger, P. (1985): Faltenmodelle und Verformungsverteilung in Deckenstrukturen am Beispiel der Morcles Decke, Unpubl. Thesis, ETH Zürich.

Jaquemin, H. & Sider, H. (1989): Aiguilles-Rouges et Mont-Blanc – rencontre au sommet. Les Sciences de la Terre en revue. Cailloux, 8: 1-62.

Johannes, W. and Holtz, F. (1991): Formation and ascent of granitic magmas. Geologische Rundschau 80: 225-231

Jongmans, W.J. (1960): Die Karbonflora der Schweiz. Beiträge zur geologischen Karte der Schweiz Neue Folge, 108: 22-97.

Joukowsky, E. (1902): Sur les eclogites des Aiguilles Rouges. Societe genevoise d'Imprimerie, Geneve, 1-46 pp.

Joye, J.B. (1989): Evolution tectonométamorphique varisque du massif des Aiguilles Rouges, massif cristallin externe alpin, Unpubl. Dr. Thesis, Fribourg, 134 pp..

Jurine (1806): Lettre à Monsieur Gillet-Laumont. Journal des Mines, 19, 113: 367-378.

Kaspar, B. (1997): Geologische und tektonische Aufnahme des oberen Diosaz-Tals, Westalpen, Aiguilles-Rouges-Massiv (Frankreich), Unpubl. Diploma Thesis Univ. Erlangen, 72 pp.

Kerrich, R., Allison, I., Barnett, R.L., Moss, S. and Starkey, J. (1980): Microstrcutural and chemical transformations accompanying deformation of granite in a shear zone at Miéville, Switzerland; with implications for stress corrosion cracking and superplastic flow. Contributions of Mineralogy and Petrology, 73: 221-242.

Krummenacher, D. (1959): Le cristallin de la région de Fully (Valais). Schweizerische Mineralogische und Petrographische Mitteilungen, 39: 151-266.

Laird, J. and Albee, A. L. (1981): Pressure, temperature, and time indicators in mafic schist: their application to reconstructing the polymetamorphic history of Vermont. American Journal of Science 281: 127-175

Laurent, R. (1973a): Metasomatic granitization of ophiolites at the southern tip of the „Aiguilles Rouges" range (Western Alps). Schweizerische Mineralogische und Petrographische Mitteilungen, 53: 33-48.

Laurent, R. (1973b): The origin and kinematic evolution of a metasomatic granite of the Aiguilles Rouges, Western Alps. Special Publications of the Geological Society of South Africa, 3: 499-505.

Laurent, R. and Chessex, R. (1968): Considérations sur le paléozoïque dans les Alpes Occidentales. Eclogae Geologicae Helvetiae, 61: 1-18.

Le Fort, P. (1973): Géologie du Haut-Dauphiné cristallin (Alpes françaises). Sciences de la Terre Mém. 25: 1-373

Liégeois, J.P. and Duchesne, J.C. (1981): The Lac Cornu retrograded eclogites (Aiguilles Rouges Massif, Western Alps, France): evidence of crustal origine and metasomatic alteration. Lithos, 14: 35-48.

Maniar, P.D. and Piccoli, P.M. (1989): Tectonic discrimination of granitoids. Bulletin of the Geological Society of America, 101: 635-643.

Marquis, F.-X. (1997): Géologie et pétrographie du Val de Tré-les-Eaux (Massif des Aiguilles Rouges, France). Unpubl. Diploma Thesis, Université de Fribourg, 110 pp.

Marro, C. (1986): Les Granitoïdes du Mont Blanc en Suisse. Unpubl. Dr. Thesis, Universite de Fribourg, 145 pp.

Marro, C. (1987): Histoire des granitoïdes du Mont Blanc en Suisse. Bulletin de la Société Fribourgeoise de Sciences Naturelles, 76: 73-128.

Marro, C. (1988): Organisation géochimique et intrusion du granite du Mont Blanc et de deux leucogranites. Schweizerische Mineralogische und Petrographische Mitteilungen, 68: 521-529.

Marshall, D., Kirschner, D. and Bussy, F. (1997): A Variscan pressure-temperature-time path for the N-E Mont Blanc massif. Contributions of Mineralogy and Petrology, 126, 416-428.

Meisser, N. (1999) Les gites minéraux du versant suisse du massif du Mont Blanc. Le Règne Minéral 5,29-37

Meyer, J. (1916): Geologisch-petrographische Untersuchungen am Massiv der Aiguilles-Rouges. Eclogae Geologicae Helvetiae, 14: 46-144.

Michel-Lévy, A. (1890): Etudes sur les roches cristallines et eruptives des environs du Mont Blanc. Bulletin de la carte géologique de France 9: 1-54.

Mingram, B. (1996): Geochemische Signaturen der Metasedimente des erzgebirgischen Krustenstapels. Scientific Technical Reports, STR96/04: 1-104.

Mollex, D. (2003): Le magmatisme basique carbonifère dans le massif des Aiguilles Rouges. Unpublished DEA Université de Lausanne, 119 pp

Morard, A. (1998): Pétrographie et cartographie du socle du massif du Mont-Blanc. Dans le secteur de la Montagne de Lognan (Argentière, France). unpubl. Diploma Thesis, Université de Lausanne, 138 pp.

Mrazec, L. (1892): La protogine du Mont-Blanc et les roches eruptives qui l'accompagnent. F. Taponnier, Genève, 1-91 pp.

Mullis, J. (1983): Einschlüsse in Quarzkristallen der Schweizer Alpen und ihre mineralogisch-geologische Bedeutung. Bulletin de la Société Fribourgeoise de Sciences Naturelles, 72: 5-19.

Mullis, J. (1995): Genesis of Alpine fissure minerals. Scientific and Technical Information, XI: 54-64.

Nähr, T. (1993): Kartierung, Petrographie und Geochemie im Altkristallin westlich des Trient-Gletschers (Mont-Blanc Massiv, Westalpen, Schweiz). Unpubl. Diploma Thesis, Friedrich-Alexander Universität, Erlangen-Nürnberg, 104 pp.

Nebbia, G. (1985): Courmayeur Monte Blanco. Guida turistica ed excursionista. Industrie Grafiche Editoriali Musumeci, Quart (Aosta).

Necker, L.A. (1828): Memoire sur la vallée de Valorsine. Mémoires de la Societé de Physique et d' Histoire naturelle Genève IV: 1-37.

Niklaus, P.A. and Wetzel, A. (1996): Faziesanalyse und Ablagerungsmilieu der fluviatilen Sedimentfüllung des Karbontroges von Salvan-Dorénaz. Eclogae Geologicae Helvetiae, 89: 427-437.

Olsen, S.N., Johnson, C.M., Beard, B.L. and Baumgartner, L.. P. (2000): New U-Pb zircon data and constraints on the age and mode of migmatization in the Aar massif, Central Alps. European Journal of Mineralogy, 12: 1245-1260

Oulianoff, N. (1924): La massif de l'Arpille. Matériaux pour la Carte géologique de la Suisse, 54,II: 1-66.

Oulianoff, N. (1946): Infrastructures des Alpes et tremblement de terre du 25 Janvier 1946. Bulletin de la Societé géologique de France, (5) 17: 39-53.

Oulianoff, N. (1953): Superposition successive des chaînes de montagnes. Scientia, 47: 1-5.

Oulianoff, N. (1965): Contribution à l'histoire des massifs du Mont-Blanc et des Aiguilles-Rouges. Bulletin de la Société Vaudoise des Sciences Naturelles, 69(317): 1-11.

Paquette, J.L., Ménot, R.P. and Peucat, J.J. (1989): REE, Sm-Nd and U-Pb zircon study of eclogites from the Alpine External massifs (Western Alps): Evidence for crustal contamination. Earth and Planetary Sciences Letters, 96: 181-198.

Parker, R.L. New edition by Stalder, H. A., De Quervain, F., Niggli, E. and Graeser, S. (1973): Die Mineralfunde der Schweiz. Wepf.& Co., Basel, 433 p.

Patiño-Douce, A.E. and Harris, N. (1998): Experimental constraints on Himalayan anatexis. Journal of Petrology, 39: 689-710.

Pearce, F. (1898): Recherches sur le versant Sud-Est du Massif du Mont-Blanc, PHD Thesis Université de Geneve.

Pearce, J.A. (1980): Geochemical evidence for the genesis and eruptive setting of lavas from Tethyan ophiolites. In: N. Panayiatou (Editor), Proceedings of the international Ophiolite Conference, Nicosia, pp. 261-272.

Pearce, J.A. (1984): A "users guide" to basalt discrimination diagrams, Unpublished manuscript, Milton Keynes, 37.p. pp.

Pearce, J.A. and Cann, J.R. (1973): Tectonic setting of basic volcanic rocks determined using trace element analyses setting of basic volcanic rocks. Earth and Planetary Science Letters, 19: 290-300.

Pearce, J.A., Nigel, B., Harris, W. and Tindle, A.G. (1984): Trace element discrimation diagrams for the tectonic interpretation of granitic rocks. Journal of Petrology, 25: 956-983.

Pearce, J.A. and Norry, M.J. (1979): Petrogenetic implications of Ti, Zr, Y and Nb variations in volcanic rocks. Contribution of Mineralogy and Petrology, 69: 33-47.

Peterson, V.L. and Robinson, P. (1993): Progressive evolution from uplift to orogen-parallel transport in a Late-Acadian, upper amphibolite- to granulite-facies shear zone, South-Central Massachusetts. Tectonics, 12: 550-567.

Pfeifer, H-R. (1990): Major and trace elements discrimination diagrams to determine possible mantle protoliths of orogenic ultramafic rocks. Unpublished manuscript, Centre d'Analyse Minérale, Univ. of Lausanne, 20p

Pfeifer, H.R., Biino, G., Ménot, R.P. and Stille, P. (1993): Ultramafic rocks in the pre-Mesozoic basement of the Central and External Western Alps. In: J. von Raumer and F. Neubauer (Editors), The Pre-Mesozoic geology in the Alps. Springer, Heidelberg, pp. 119-143.

Pfeifer, H.R., Colombi, A. and Ganguin, J. (1989): Zermatt-Saas and Antrona zone: a petrographic and geochemical comparision of polymetamorphic ophiolites of the West-Central Alps. Schweizerische Mineralogische und Petrographische Mitteilungen, 69: 217-236.

Pfeifer, H.R. and von Raumer, J.F. (1996): Lherzolithic and pyroxenitic ultramafics from the Lac Cornu area (Aiguilles Rouges Massif, France). Schweizerische Mineralogisch Petrographische Mitteilungen, 76: 119-120.

Pilloud, C. (1991): Structures de déformation alpine dans le synclinal de permo-carbonifère de Salvan-Dorenaz (massif des Aiguilles Rouges). Mémoires de Géologie (Lausanne) 9: 1-100.

Poty, B. (1969): La croissance des cristaux de quartz dans les filons sur l' exemple du filon de la Gardette et des filons du Massif du Mont-Blanc. Thèse Université de Nancy. Sciences de la Terre, Mémoire 17.

Poty, B. (1999): Roger Fournier (1939-1976) – Cristallier de Chamonix et le renouveau de la recherche des cristaux de Chamonix. Le Règne Minéral, Volume hors série V: 25-28.

Poty, B., Stalder, H.A. and Weisbrod, A.M. (1974): Fluid inclusion studies in quartz from fissures of Western and Central Alps. Schweizerische Mineralogische und Petrographische Mitteilungen, 54: 717-752.

Proyer, A. (2003): Metamorphism of pelites in NKFMASH – a new petrogenetic grid with implications for the preservation of high-pressure mineral assemblages during exhumation. Journal of Metamorphic Geology 21:493-509

Pupin, J.P. (1980): Zircon and granite petrology. Contributions of Mineralogy and Petrology, 73: 207-220.

Pupin, J.P. (1988): Granites as indicators in paleogeodynamics. Rendiconti della Società italiana de Minerlogia e Petrografia 43: 237-262.

Purtscheller, F. (1963): Gefügekundliche Untersuchungen am Granit des Mont-Blanc und an den angrenzenden Gebieten. Sitzungsberichte der Österreichischen Akademie der Wissenschaften Mathematisch-naturwissenschaftliche Klasse, I, 172: 453-522.

Purtscheller, F. (1964): Über gefügekundliche Studien im Mont-Blanc-Gebiet. Schweizerische Mineralogische und Petrographische Mitteilungen, 44: 589-593.

Reinhard, M. and Preiswerk, H. (1927): Über Granitmylonite im Aiguilles-Rouges-Massiv (westl. Wallis). Verhandlungen der Naturforschenden Gesellschaft Basel, 38: 188-200.

Rey, P., Burg, J.P. and Casey, M. (1997): The Scandinavian Caledonides and their relationship to the Variscan belt. In: J.P. Burg and M. Ford (Editors), Orogeny through time, pp. 179-200.

Rickenbach, E. and von Kaenel, F. (1953): Die Arsen-Gold-Lagerstätte von Salanfe (Wallis). Beiträge zur Geologischen Karte der Schweiz, Geotechnische Serie, 31: 1-51.

Ritter, E. (1897): La bordure sud-ouest du Mont-Blanc. Les plis couchés du Mont-Joly et de ses attaches. Bulletin Service Carte géologique France, 60.

Rock, N.M.S. (1991): Lamprophyres. Blackies, Glasgow.

Röllig, G., Kampe, A., Steinbach, V., Ehling, B.-C. and Wasternack, J. (1995): Der Untergrund des Mitteldeutschen Braunkohlereviers. Zeitschrift der Geologischen Wissenschaften, 23: 3-26.

Roser, B.P. and Korsch, R.J. (1988): Provenance signatures of sandstone-mudstone suites using SiO2 contents N, K20/Na2O ratio. Jouranl of Geology, 94: 636-650.

Rossi, Ph and Chevremont, Ph. (1987): Classification des associations magmatiques granitoïdes. Géochronique 21, 14-18

Rutishauser, H. (1973): Die quantitative Erfassung von Migmatiten im Aufschlussbereich (erläutert am Beispiel des Lauterbrunner Kristallins). Schweiz. min. petr. Mitt., 53, 99-124

Sabatier, H. (1991): Special lamprophyre-derivrd mafic enclaves in some Hercynian granites from western and central Europe. In Didier, J. & Barbarin, B. (eds) Enclaves granite petrology. Developments in Petrology 13: 63-81, Elsevier Amsterdam

de Saussure, H.B. (1879): Voyages dans les Alpes, Neuchatel.

Schaltegger, U. (1997): The age of an Upper Carboniferous / Lower Permian sedimentary basin and its hinterland as constrained by U-Pb dating of volcanic and detrital zircons (Northern Switzerland). Schweizerische Mineralogisch Petrographische Mitteilungen, 77: 101-111.

Schardt, H. (1889): Sur l'origine des Prealpes Romandes. Eclogae Geologicae Helvetiae, 4: 129-142.

Schmocker, K. (1996): Géologie et pétrographie de la rive gauche du Lac d'Emosson. Unpubl. Diploma Thesis, Université de Fribourg, 121 pp.

Schouwey, V. (1988): Géologie du Massif de La Croix de Fer entre le Châtelardet et Trient (VS). Unpubl. Diploma Thesis Géologie Univ. de Fribourg, 126 p.

Schulz, B. and von Raumer, J. (1993): Syndeformational uplift of Variscan high-pressure rocks (Col de Bérard, Aiguilles Rouges Massif, Western Alps). Zeitschrift der deutschen geologischen Gesellschaft, 144: 104-120.

Shervais, J.W. (1982): Ti-V plots and the petrogenesis of modern and ophiolitic lavas. Earth and Planetary Science Letters, 59: 101-118.

Spicher, A. (1980): Carte Tectonique de la Suisse au 1 : 500 000. Commission Géologique Suisse.

Stalder, H. A., Wagner, A., Graeser, St. and Stuker, P. (1998): Mineralienlexikon der Schweiz. Wepf. & Co. Basel, 579 p.

Stampfli, G. (1996): The intra-Alpine terrain: a palaeothetyan remnant in the Alpine Variszides. Eclogae Geologicae Helvetiae, 89: 12-42.

Stampfli, G. (Editor) (2001): Geology of the western Swiss Alps, a guide-book. Mémoires de Géologie (Lausanne), 36, 195 pp.

Stampfli, G.M. and Borel, G.D. (2002): A plate tectonic model for the Paleozoic and Mesozoic constrained by dynamic plate boundaries and restored synthetic oceanic isochrons. Earth and Planetary Science Letters, 196: 17-33.

Stampfli, G.M., von Raumer, J. and Borel, G. (2002): The Paleozoic evolution of pre-Variscan terranes: From Gondwana to the Variscan collision:. Geological Society of America Special Paper, 364.

Steck, A. (1966): Petrographische und tektonische Untersuchungen am zentralen Aaregranit und seinen altkristallinenHüllgesteinen im westlichen Aarmassiv im Gebiet Belalp-Grisighorn. Beiträge der geologischen Karte der Schweiz Neue Folge, 130: 1-100.

Steck, A. and Burri, G. (1971): Chemismus und Paragenesen von Granaten aus Granitgneisen der Grünschiefer- und Amphibolitfazies der Zentralalpen. Schweizerische Mineralogische und Petrographische Mitteilungen, 51: 534-539.

Steck, A., Epard, J.L., Escher, A., Gouffon, Y. and Masson, H. (Editors) (2001): Carte tectonique des Alpes de Suisse occidentale. Note explicative, Carte géologique spéciale No. 123. Office fédéral des eaux et de la géologie, Bern.

Steck, A. and Vocat, D. (1973): Zur Mineralogie der Granitmylonite von Miéville, Aiguilles-Rouges-Massiv. Schweizerische Mineralogische und Petrographische Mitteilungen, 54: 474-477.

Sublet, P. (1962): Etude géologique du synclinal Carbonifère de Collonges-Dorénaz (Valais). Eclogae geologicae Helvetiae, 55: 23-76.

Thöni, M. (1989): in Joye, J.B. (1989): Evolution tectonométamorphique varisque du massif des Aiguilles Rouges, massif cristallin externe alpin. Unpubl. Dr. Thesis, Fribourg 1989

Thompson, A. B. (1990): Heat, fluids, and melting in the granulite facies. In: Granulites and crustal evolution (eds. D. Vielzeuf and P. Vidal), Kluver Academic Publishers, 37-57.

Thompson, A. B. and Conolly, J. A. D. (1995): Melting of the continental crust: some thermal and petrological constraints on anatexis in continental collision zones and other tectonic settings. Journal of Geophysical Research 100: 15565-15579

Tièche, J. C. (1969): Les quartzites porphiriques de la bordure Est du Mont Blanc. Unpubl. Diplom Thesis Université de Lausanne, 52 p.

Upton, B.G.J., Emeleus, C.H. and Beckinsale, R.D. (1984): Petrology of the northern east Greenland Tertiary flood basalts: evidence from Hold with Hope and Wollaston Forland. Journal of Petrology, 25: 151-184.

Vernet, J. (1969): Présence d'un synclinal profond de carbonifère dans le massif du Mont Blanc. Comptes Rendus Academie des Sciences, Paris, 268D: 2227-2230.

von Raumer, J.F. (1967): Kristallisation und Gefügebildung im Mont-Blanc-Granit. Schweizerische Mineralogische und Petrographische Mitteilungen, 47: 499-579.

von Raumer, J.F. (1969): Stilpnomelan als alpinmetamorphes Produkt im Mont- Blanc-Granit. Contributions of Mineralogy and Petrology, 21: 257-271.

von Raumer, J.F. (1971): Das Mont-Blanc-Massiv - Altkristallin im Bereich schwacher alpiner Metamorphose. Schweizerische Mineralogische und Petrographische Mitteilungen, 51: 193-225.

Von Raumer, J.F. (1974): Mineralneubildungen im Mont-Blanc-Granit. Schweizer Strahler, 3,7: 303-306.

von Raumer, J.F. (1974): Zur Metamorphose amphibolitischer Gesteine im Altkristallin des Mont-Blanc- und Aiguilles-Rouges-Massivs. Schweizerische Mineralogische und Petrographische Mitteilungen, 54: 471-488.

von Raumer, J.F., 1976. Variszikum in den Zentral- und Westalpen. Nova Acta Leopoldina NF, 45(224): 147-176.

von Raumer, J.F. (1983): Die Metapelite von Emosson (Aiguilles-Rouges-Massiv) als Beispiel spätkaledonisch-frühvariszischer Metamorphose im Altkristallin des helvetischen Bereichs. Schweiz.Min.Petr.Mitt. 63,421-455

von Raumer, J.F. (1984): The external massifs, relics of variscan basement in the Alps. Geologische Rundschau, 73: 1-31.

von Raumer, J.F. (1987): Les massifs du Mont Blanc et des Aiguilles Rouges: témoins de la formation de croûte varisque dans les Alpes Occidentales. Géologie Alpine, 63: 7-24.

von Raumer, J.F. (1998): The Palaeozoic evolution in the Alps - from Gondwana to Pangea. Geologische Rundschau, 87: 407-435.

Von Raumer, J.F. (1999): Les massifs du Mont Blanc et des Aiguilles Rouges – un aperçu géologique. Le Règne Minéral, Vol. hors série V: 13-18.

von Raumer, J.F., Bussy, F. and Sharp, Z.D. (1996): Lac Cornu revisited: the evolution from lower to upper crust (Aiguilles Rouges Massif, Western Alps). Schweizerische Mineralogische und Petrographische Mitteilungen, 76: 120-121.

von Raumer, J.F. and Chiaradia, M. (1992): Bedeutung vor- und frühpaläozoischer Lithologien für Wolfram-Mineralisationen. Zentralblatt für Geologie und Paläontologie I, 1992: 87-91.

von Raumer, J.F. and Neubauer, F. (1993): History of Geological Investigations in the Pre-Triassic Basement of the Alps. In: J.F. von Raumer and F. Neubauer (Editors), The pre-Mesozoic geology in the Alps. Springer, Heidelberg, pp. 55-63.

von Raumer,J.F. & Schwander, H.W. (1985): Garnet evolution in pre-variscan pelitic rocks from the Lake Emosson area, Aiguilles Rouges massif, Western Alps. Journal of Metamorphic Geology 1985:467-479

von Raumer, J.F., Abrecht, J., Bussy, F., Lombardo, B., Ménot, R. P., Schaltegger, U. (1999): The Palaeozoic metamorphic evolution of the Alpine External Massifs. Schweizerische Mineralogische und Petrographische Mitteilungen, 79: 5-22.

von Raumer, J., Dobmeier, C. and Bussy, F. (2002a): Variscan structures in the Aiguilles Rouges - Mont Blanc areas (External Massifs, Alps). Erlanger Geologische Abhandlungen, Sonderband 3: 72-74.

von Raumer, J., Dobmeier, C. and Bussy, F. (2003): Variscan structures in the Aiguilles Rouges – Mont Blanc areas (External Massifs, Alps) Zentralblatt für Geologie und Paläontologie I, 2002,3/4: 237-242

von Raumer, J.F., Galetti, G., Oberhänsli, R. and Pfeifer, H.R. (1990): Amphibolites from Lac d'Emosson/ Aiguilles Rouges (Switrzerland): Tholeiitic basalts at a transition zone between continental and oceanic crust. Schweizerische Mineralogische und Petrographische Mitteilungen, 70: 419-435.

von Raumer, J.F., Stampfli, G.M., Borel, G. and Bussy, F. (2002b): The organization of pre-Variscan basement areas at the north-Gondwanan margin. International Journal of Earth Sciences, 91: 35-52.

von Raumer, J.F., Stampfli, G.M. and Bussy, F. (2003): Gondwana-derived microcontinents - the constituents of the Variscan and Alpine collisional orogens. Tectonophysics, 365: 7-22

Wetter, W. (1987): Gletscherschwankungen im Mont Blanc Gebiet. Gebo Druck AG, Zürich, 267 pp.

Wettlaufer, B. (1(998): Geologie und Petrographie der Montagne de Montjus (Aiguilles-Rouges-Massiv, Westalpen, Frankreich). Unpubl. Diploma Thesis Univ. Erlangen, 103 pp

Wimmenauer, W. (1984): Das prävariskische Kristallin im Schwarzwald. Fortschritte der Mineralogie, 62: 69-86.

Winkler, H. G.F. (1979): Petrogenesis of metamorphic rocks. Springer New York Heidelberg Berlin, 348 p.

Wirsing, A. (1997): Die Orthogneise des oberen Val Bérard (Aiguilles-Rouges-Massiv, Westalpen, Frankreich), Unpubl. Dr.-Thesis, Université de Fribourg, 141 pp.

Wolf, M.R. and Wyllie, P.J. (1994): Dehydration-melting of amphibolite at 10 Kbar: the effects of temperature and time. Contribution of Mineralogy and Petrology, 115: 369-383.

Wyllie, P. J. (1977): Crustal anatexis: an experimental review. Tectonophysics 43:41-71

Zirkel, F. (1863): Mikroskopische Gesteinsstudien. Sitzungs-Berichte der Akademie der Wissenschaften Wien, mathem.-naturw. Kl. 47, 1: 226-270.

Chapter VI

Annexes

ANNEX I : Chemical Data

ANNEXES III-XI: Geological maps: **in pocket**

IV: Eastern side of Lake Emosson 1: 10 000
V: Western side of Lake Emosson 1: 10 000
VI: Lac Vert area (Aiguilles Rouges) 1: 10 000
VII: Val Bérard - Tré les Eaux 1: 25 000
VIII: Lac Cornu area (Aiguilles Rouges) 1: 10 000
IX: Salanfe area (Aiguilles Rouges) 1: 5 000
X: Trient area (Mont Blanc) 1: 25 000
XI: Lognan area (Mont Blanc) 1: 25 000

Tab. VI.1 Chemical data from Early Palaeozoic Granitoids I

Ho-Bi gneisses from Val Bérard

(AW: from Wirsing 1997; 1858-1862: new data)

Major elements (wt %)

	AW1	AW6	AW29	AW55	1858	1859	1860	1861	1862
SiO2	60.85	64.35	64.71	62.34	63.82	62.83	69.47	67	67.26
TiO2	0.65	0.57	0.59	0.64	0.57	0.63	0.37	0.5	0.47
Al2O3	16.17	15.50	15.98	16.23	15.76	16.03	14.52	15.2	15.29
Fe2O3	1.20	1.14	0.91	1.31	0.93	1.13	0.74	0.68	0.57
FeO	4.42	3.55	3.86	4.07	3.93	4.16	2.37	3.22	3.01
MgO	3.39	2.97	2.67	3.38	2.81	3.14	1.8	2.43	2.27
MnO	0.10	0.09	0.10	0.10	0.09	0.1	0.06	0.07	0.07
CaO	4.81	3.57	3.93	4.15	4.47	4.59	1.73	2.95	2.54
K2O	2.54	2.70	2.66	2.48	2.71	2.48	3.45	2.87	3.41
Na2O	2.54	3.14	3.07	3.30	3.04	2.89	3.26	3.43	3.4
P2O5	0.14	0.11	0.12	0.13	0.12	0.14	0.09	0.13	0.11
H2O+	1.98	2.07			1.37	1.59	1.58	1.94	1.59
Loi			1.21	2.00					
CO2	0.95	0.49			0.07	0.22	0.28	0.05	0.08
Total	**99.74**	**100.20**	**99.81**	**100.10**	**99.69**	**99.92**	**99.71**	**100.48**	**100.07**
FeO*t	6.11	5.08	5.20	5.83	5.3	5.75	3.38	4.26	3.92

Trace elements (ppm)

Ba	588	747	675	674	581	625	650	797	793
Be*	1.93	1.35	1.13	1.93					
V	141	112	111	129	111	124	66	98	84
Cr	93	76	53	73	82	91	52	73	68
Ni	20	19	18	19	16	19	13	18	15
Cu	28	8	16	15	9	9	13	14	7
Zn	63	58	67	55	75	79	51	47	42
Ga	16	15	17	16	18	18	14	14	15
Ge	1.39	1.53	1.31	1.28	-	-	-	-	-
As	3.51	1.13	4.21	8.97	-	-	-	-	-
Rb	108	92	97	97	104	90	102	95	106
Sr	229	215	231	295	255	264	175	327	331
Y	24	24	24	27	25	26	22	21	25
Zr	137	140	141	148	137	140	110	141	128
Nb	5	7	7	7	7	6	6	6	6
Mo*	1.47	0.17	1.02	0.51	-	-	-	-	-
Cd*	0.30	0.20	0.41	0.21	-	-	-	-	-
In*	0.04	0.04	0.03	0.05	-	-	-	-	-
Sn*	2.70	3.44	4.74	2.68	-	-	-	-	-
Sb*	1.35	0.47	0.25	0.45	-	-	-	-	-
Cs*	13.50	5.20	7.17	8.91	-	-	-	-	-
Hf*	4.08	4.24	4.54	4.45	-	-	-	-	-
Ta*	1.02	1.06	1.25	1.09	-	-	-	-	-
Pb	1	3	7	1	7	1	14	1	4
Bi*	1.41	0.36	0.12	0.28	-	-	-	-	-

REE-data: Tab VI.7
Sample location: see Annex II

Major elements: XRF data University of Fribourg, Earth Sciences Dept.
Traces: XRF data University of Fribourg, *): ICP-MS, CNRS CRPG Nancy

Tab. VI.2: Chemical data from Early Palaeozoic Granitoids II

K-feldspar augengneisses, Val Bérard: (AW: from Wirsing 1997)
Mt. Luisin Granodiorites: (SD from Chiaradia 1993; 1669 new)

Major elements (wt %)

	AW15	AW37	AW45	AW2	AW33	AW36	1699	SD1	SD2
SiO2	66.49	67.79	67.65	66.92	66.40	67.18	69.58	68.29	64.17
TiO2	0.68	0.59	0.67	0.63	0.73	0.69	0.56	0.83	0.83
Al2O3	15.66	15.71	15.93	15.76	16.26	15.38	14.66	14.78	16.44
Fe2O3	0.88	1.03	0.95	0.80	1.47	1.02	0.5	0.83	1
FeO	3.28	2.64	3.24	3.12	3.05	3.51	3.01	4.09	4.21
MgO	1.54	1.22	1.36	1.34	1.68	1.56	0.07	0.08	0.09
MnO	0.06	0.06	0.06	0.06	0.05	0.06	1.27	2.11	2.27
CaO	1.80	1.39	1.62	1.85	1.37	1.82	1.74	1.01	2.92
K2O	3.95	4.29	4.30	4.05	3.27	3.92	2.61	2.15	3.01
Na2O	3.24	3.08	3.13	3.21	3.29	3.18	4.44	3.2	3.26
P2O5	0.22	0.26	0.27	0.23	0.24	0.23	0.21	0.16	0.23
H2O+	1.63			1.65				2.27	1.37
LOI	1.44	1.21		1.84	1.06	0.76			
CO2	0.29			0.5				0.09	0.04
Total	**99.72**	**99.52**	**100.40**	**100.10**	**99.63**	**99.62**	**99.38**	**99.88**	**99.84**
FeO*t	4.52	3.96	4.55	4.26	4.86	4.92	3.84	5.38	5.68

Trace elements (ppm)

Ba	1117	1224	1179	1155	1083	1101	777	1010	800
Be*	2.93	2.62	2.89	2.93	2.20	2.65	-	-	-
V	66	52	53	61	78	69	48	102	90
Cr	58	29	36	41	44	40	42	64	55
Ni	18	21	21	19	24	27	13	25	24
Cu	16	14	21	14	18	25	3	18	15
Zn	122	64	64	84	70	62	64	170	82
Ga	19	18	20	19	21	19	18	18	18
Ge*	1.36	1.45	1.32	1.49	1.79	1.56	-	-	-
As	2.56	2.73	1.72	1.11	1.00	0.43	-	-	-
Rb	133	136	141	141	98	147	211	116	134
Sr	176	173	180	153	179	172	174	128	239
Y	39	51	47	42	47	45	36	36	36
Zr	213	230	252	228	244	235	187	323	228
Nb	13	16	17	13	16	16	10	17	14
Mo*	0.49	0.46	0.50	0.21	0.51	0.84	-	-	-
Cd*	0.30	0.23	0.15	0.26	0.11	0.14	-	-	-
In*	0.07	0.07	0.07	0.07	0.07	0.06	-	-	-
Sn*	3.26	3.61	3.68	3.85	3.33	3.28	-	-	-
Sb*	0.44	1.46	0.50	0.29	2.18	0.21	-	-	-
Cs*	8.19	10.10	7.93	8.07	4.55	7.22	-	-	-
Hf*	6.25	6.71	7.30	6.93	7.33	6.02	-	-	-
Ta*	1.52	1.66	1.69	1.54	1.68	1.69	-	-	-
Pb*	32	20	17	19	14	9	21	13	1
Bi*	0.14	0.15	0.11	0.18	0.11	0.08	-	-	-
U*	3.90	5.71	4.05	3.73	4.21	4.00	4.6	5.6	3.9
Th*	13	23	19	12	21	17	14.8	213	175

REE-data: Tab VI.7
Sample location: see Annex II

Major elements: XRF data University of Fribourg, Earth Sciences Dept.
Traces: XRF data University of Fribourg, *): ICP-MS, CNRS CRPG Nancy

Tab. VI.3: Chemical data from Early Palaeozoic Granitoids III

K-feldspar augengneisses Lac Emosson: from A. Wirsing (AWAR,1997)

Major elements (wt %)

AWAR	1	2	3	4	5	6	7	8	9	10	11	12
SiO2	69.40	69.16	66.19	67.12	67.44	66.03	67.25	69.12	66.94	64.44	67.96	66.75
TiO2	0.53	0.52	0.75	0.65	0.61	0.70	0.60	0.48	0.69	0.69	0.67	0.67
Al2O3	15.26	15.49	16.14	15.91	15.73	16.06	15.93	15.44	15.29	16.38	15.05	15.72
Fe2O3	0.92	0.82	0.90	0.77	1.20	0.73	1.01	0.74	1.06	1.32	1.14	0.98
FeO	2.57	2.51	3.82	3.24	2.67	3.42	2.68	2.29	3.54	2.96	3.25	3.35
MnO	0.05	0.04	0.07	0.06	0.05	0.06	0.05	0.04	0.07	0.07	0.05	0.06
MgO	1.23	1.15	1.72	1.32	1.36	1.52	1.23	0.94	1.41	1.43	1.62	1.62
CaO	1.12	1.18	1.69	2.04	1.50	1.71	1.93	1.82	1.84	2.28	1.49	1.90
Na2O	3.25	3.41	2.99	3.40	3.17	3.37	3.02	3.20	3.08	2.89	2.96	3.09
K2O	4.38	4.46	4.47	3.88	4.01	4.18	4.15	4.39	4.02	4.55	3.68	3.85
P2O5	0.22	0.22	0.26	0.25	0.24	0.23	0.23	0.24	0.24	0.27	0.24	0.23
H2O+										2.1		
LOI	1.18	1.16	1.18	0.96	1.59	1.55	1.42	1.03	1.41		1.66	1.51
CO2										0.54		
Total	100.12	100.12	100.17	99.60	99.56	99.55	99.50	99.73	99.58	99.91	99.78	99.73
FeO*tot	3.78	3.61	5.14	4.38	4.16	4.53	3.99	3.29	4.99	4.61	4.75	4.71

Trace elements (ppm)

Be									2.18		2.34	3.06
V	43	41	61	54	57	71	51	33	55	63	87	70
Cr	25	18	29	31	38	37	28	28	32	41	51	48
Ni	21	16	21	22	19	20	21	18	20	18	24	23
Cu	10	13	11	15	23	29	23	20	19	33	18	30
Zn	66	64	82	66	58	72	373	57	65	51	64	74
Ga	18	19	19	19	17	18	20	18	20	20	19	19
Ge									1.45		1.42	1.42
As									1.09		1.59	2.51
Rb	157	158	156	136	124	135	135	132	152	180	128	126
Sr	102	102	145	210	155	191	202	169	173	192	141	185
Y	38	37	41	48	44	47	44	43	46	47	38	46
Zr	196	194	242	241	226	243	236	190	229	260	221	234
Nb	16	14	16	15	15	16	14	14	16	15	13	16
Mo									1.13		0.46	1.75
Cd									0.17		0.11	0.23
In									0.08		0.06	0.07
Sn									4.37		3.22	3.61
Sb									0.12		0.21	0.06
Cs									6.32		13.7	5.93
Ba	826	831	11.08	1111	1116	1045	1466	1104	892	1180	1084	1055
Hf									6.88		7.31	7.18
Ta									1.84		1.62	2.14
Pb	17	19	18	14	13	21	89	22	13	10	11	18
Bi									0.13		0.39	0.2
Th	20	20	18	24	21	22	18	20	19	22	16	19
U									4.76		3.62	4.39

REE-data: Tab VI.7
Sample location: see Annex II

Analyses: 1-8, 10: XRF Fribourg University, Earth Sciences Dept.
9,11,12: ICP-MS, CNRS CRPG Nancy

Tab. VI.4: Chemical data from Early Palaeozoic Granitoids IV

K-feldspar augengneisses, Trient (Mont Blanc): (N: Nähr 1996, unpublished)

Major elements (wt %)

	N 186	N 187	N188	N189	N190	N191	N192
SiO2	74.19	74.35	75.63	76.81	74.69	74.92	73.1
TiO2	0.15	0.18	0.2	0.13	0.21	0.21	0.29
Al2O3	14.03	13.57	12.87	12.4	13.32	13.15	13.69
Fe2O3	0.47	0.5	0.55	0.37	0.54	0.49	0.76
FeO	1.06	1.22	1.19	0.97	1.24	1.28	1.53
MnO	0.03	0.03	0.03	0.03	0.03	0.03	0.04
MgO	0.4	0.46	0.49	0.22	0.49	0.48	0.61
CaO	0.48	0.56	0.46	0.46	0.58	0.51	0.94
Na2O	3.55	2.94	2.99	3.28	2.89	2.91	3.13
K2O	5.26	5.01	4.94	4.24	4.64	5.08	4.44
P2O5	0.21	0.22	0.21	0.19	0.22	0.2	0.2
H2O+	0.58	0.84	0.67	0.51	0.77	0.7	0.84
CO2	0.04	0.05	0.04	0.05	0.05	0.05	0.06
Toal	**100.45**	**99.92**	**100.27**	**99.64**	**99.66**	**100.01**	**99.63**
FeTOT	1.65	1.86	1.87	1.44	1.92	1.92	2.46

Trace elements (ppm)

Ba	341	271	292	89	202	299	414
Cr	36	33	43	45	30	43	50
Cu	11	7	8	6	4	6	6
Ga	15	15	14	13	15	15	17
Nb	8	7	7	6	7	8	10
Ni	76	77	115	107	69	125	120
Pb	18	13	13	11	9	11	13
Rb	170	183	175	192	201	205	176
Sr	65	51	53	50	49	55	77
Th	46	30	36	23	29	33	40
V	11	16	11	7	16	20	23
Y	27	22	27	22	30	32	32
Zn	18	27	22	34	42	42	46
Zr	73	79	66	63	85	93	110
U*	3.9	5.2	3	7.9	3.9		
Th*	8.3	13.3	7.6	9.9	9.3		

REE-data: Tab VI.7

Sample location: see Annex II

Analyses: RFX data Fribourg University Earth Science Dept.

* ICP-MS, CNRS CRPG Nancy

Tab. VI.5: Chemical data from Early Palaeozoic Granitoids V

K-feldspar augengneisses, Trient (Mont Blanc): (B: W. Bauer 1996, unpublished)

Major elements (wt %)

	B 293	B 294	B 296	B 297	B 300	B 301	B 302	B 303	B 313	B 313-1
SiO2	70.91	72.29	70.9	72.25	71.65	71.36	71	68	72.55	75.44
TiO2	0.45	0.32	0.41	0.39	0.39	0.36	0.41	0.7	0.2	0.17
AL2O3	14.44	14.39	14.81	14.43	13.87	14.49	14.31	16.23	14.82	12.91
Fe2O3	0.97	0.8	1.07	0.88	0.88	0.96	0.94	0.7	0.48	0.47
FeO	2.43	1.52	1.77	1.83	2.01	1.59	2.05	3.68	1.17	1.18
MnO	0.06	0.03	0.06	0.06	0.06	0.05	0.05	0.07	0.03	0.03
MgO	1.54	0.78	1.13	1.08	0.76	0.71	0.8	2.04	0.48	0.4
CaO	0.3	0.45	0.81	0.67	1.24	1.37	1.43	1.73	0.67	0.41
Na2O	2.41	2.79	3.23	3.84	3.09	3.26	3.1	2.25	3.32	2.77
K2O	3.96	5.21	4.7	3.3	4.38	4.24	4.22	2.53	5.32	4.69
P2O5	0.19	0.2	0.19	0.17	0.25	0.2	0.2	0.26	0.2	0.2
H2O+	1.79	1.17	1.24	1.27	1.01	0.98	1.01	2.19	0.74	0.84
CO2	0.09	0.07	0.04	0.31	0.06	0.06	0.07	0.04	0.04	0.05
Total	**99.54**	**100.03**	**100.35**	**100.48**	**99.66**	**99.63**	**99.59**	**100.4**	**100.01**	**99.56**
FETOT	3.67	2.49	3.03	2.92	3.12	2.73	3.22	4.79	1.78	1.78

Trace elements (ppm)

Ba	717	665	850	610	505	562	667	996	416	129
Cr	65	42	40	36	46	42	62	111	46	37
Cu	9	7	7	9	3	6	10	9	5	5
Ga	16	16	15	15	14	16	17	21	15	16
Nb	10	7	6	9	10	9	10	11	5	10
Ni	85	75	66	59	103	86	150	220	96	91
Pb	4	9	16	11	11	12	10	1	15	8
Rb	170	199	139	133	171	156	149	97	208	209
Sr	76	81	127	105	99	98	108	231	61	30
Th	31	27	28	39	18	23	29	31	32	42
V	71	23	35	32	31	26	31	79	16	11
Y	19	38	31	34	25	20	28	36	34	27
Zn	166	49	60	46	59	51	57	47	39	19
Zr	133	123	129	120	145	121	149	295	74	72
U*	3.4	2.6	3.5	4.5					4.5	
Th*	10.9	12.3	10.7	10.2					13.6	

REE-data: Tab VI.7
Sample location: see Annex II

Analyses: RFX data Fribourg University Earth Sciences Dept.
* ICP-MS, CNRS CRPG Nancy

Tab. VI.6: Chemical data from Early Palaeozoic Granitoids VI

K-feldspar augengneisses, Trient-water gallery (Mont Blanc): (von Raumer, unpublished)

Major elements (wt%)

	MBT70	MBT73	MBT74	MBT75	MBT77	MBT174	MBT175	MB784	MB1184	MB1187
SiO2	73.85	76.1	75.8	77.23	75.49	74.9	75.83	75.82	73.13	73.09
TiO2	0.3	0.17	0.17	0.1	0.17	0.07	0.15	0.2	0.31	0.31
Al2O3	13.8	13.06	12.92	13	13.23	14.29	12.67	13.16	14.26	14.56
Fe2O3	0.64	0.55	0.58	0.5	0.44	0.27	0.5	0.5	0.8	1.04
FeO	1.72	0.94	1.05	0.63	1.14	0.65	0.94	1.36	1.58	1.23
MnO	0.03	0.03	0.04	0.03	0.03	0.03	0.03	0.04	0.04	0.04
MgO	0.68	0.36	0.43	0.13	0.31	0.17	0.26	0.49	0.8	0.72
CaO	0.83	0.48	0.84	0.37	0.49	0.54	0.41	0.43	0.95	0.99
Na2O	3.09	2.78	2.87	3.01	2.82	3.41	2.73	2.92	3.09	2.78
K2O	3.9	4.47	4.12	4.48	4.82	4.8	5.14	5.14	4.84	5.25
P2O5	0.19	0.17	0.19	0.17	0.19	0.12	0.17	0.17	0.21	0.23
H2O+	0.96	0.78	1	0.57	0.78	0.73	0.64	0.78	0.89	0.98
CO2										
Total	**99.99**	**99.89**	**100.01**	**100.22**	**99.91**	**99.98**	**99.47**	**101.01**	**100.82**	**101.22**
FeTOT	2.55	1.59	1.75	1.2	1.71	0.99	1.54	2.01	2.55	2.41

Trace elements (ppm)

Ba	375	169	105	72	99	183	105	-	-	-
Cr	13	8	8	5	8	8	6	-	-	-
Cu	9	12	13	16	10	16	12	-	-	-
Ni	14	9	8	8	9	8	10	-	-	-
Rb	229	231	218	304	283	181	270	-	-	-
Sr	74	62	41	24	28	78	39	-	-	-
Y	42	29	28	18		9		33		42
Zn	71	43	39	56	58	9	22	-	-	-
Zr	120	80	94	61	78	38	77	-	-	-
U*	8	6.5	7.6	14.9		5.2		4.3		7.4
Th*	20.6	9	13	7.7		5.7		10.8		16.6

Sample location: see Annex II
Analyses: RFX data Fribourg University Earth Science Dept.
* ICP-MS, CNRS CRPG Nancy

Tab. VI.7: REE data from Early Palaeozoic Granitoids

Ho-Bi Gneisses Val Bérard (AW: from Wirsing 1997; 1858-1862: new)

	AW1	AW6	AW29	AW55	1858	1859	1860	1861	1862
La	22.60	27.61	29.27	22.53	33.9	32.4	35.1	23.6	24.0
Ce	46.95	54.33	58.71	47.87	57.2	69.7	71.1	47.9	50.9
Pr	5.38	6.24	6.49	5.95	7.1	7.5	7.5	5.6	5.8
Nd	20.58	22.91	25.11	23.12	24.9	28.3	24.8	22.9	21.3
Sm	4.22	4.46	4.98	4.97	4.9	5.7	4.7	4.5	4.8
Eu	1.10	1.07	1.17	1.27	1.36	1.43	1.07	1.32	1.20
Gd	3.52	3.89	4.19	4.11	4.8	5.3	4.2	4.4	4.4
Tb	0.55	0.61	0.62	0.69	0.7	0.8	0.6	0.7	0.7
Dy	3.75	3.85	3.66	4.38	4.4	4.6	4.0	4.1	4.0
Ho	0.85	0.84	0.88	0.92	0.9	0.93	0.81	0.76	0.84
Er	2.08	2.23	2.02	2.39	2.5	2.9	2.5	2.2	2.2
Tm	0.33	0.36	0.33	0.39	0.4	0.4	0.4	0.4	0.4
Yb	2.19	2.36	2.30	2.53	2.7	2.8	2.7	2.4	2.4
Lu	0.36	0.38	0.36	0.41	0.39	0.42	0.44	0.37	0.39

Kf-augengneisses Val Bérard (AW: from Wirsing 1997)

Granodiorites Mt. Luisin (SD: from Chiaradia 1993; 1699: new)

	AW15	AW37	AW45	AW2	AW33	AW36	1699	SD1	SD2
La	46.36	58.57	54.14	50.30	53.13	50.00	36.3	62	52.7
Ce	94.31	109.80	114.40	104.10	103.60	106.10	80.7	121	110
Pr	10.85	14.76	13.62	12.04	12.43	12.78	9	14.2	12.5
Nd	42.45	57.17	51.8	46.45	49.57	49.18	33.3	54.1	47.5
Sm	8.72	12.06	10.9	9.63	10.66	9.98	7.8	10.2	9.5
Eu	1.50	1.76	1.65	1.43	1.80	1.59	1.23	1.81	1.97
Gd	7.34	10.21	9.39	8.10	9.02	8.67	7.5	9.7	9.3
Tb	1.13	1.53	1.43	1.20	1.34	1.28	1.2	1.4	1.3
Dy	7.01	9.12	8.44	7.11	7.70	7.98	7	7.4	7.2
Ho	1.43	1.71	1.67	1.53	1.69	1.53	1.25	1.47	1.46
Er	3.65	4.04	4.12	3.78	3.68	3.60	3.6	4.6	4
Tm	0.48	0.63	0.63	0.53	0.57	0.54	0.5	0.8	0.6
Yb	3.15	3.80	3.78	3.47	3.53	3.38	3.3	5.3	3.8
Lu	0.48	0.60	0.62	0.52	0.54	0.57	0.49	0.79	0.59

Sample location: see Annex II
REE data:ICP-MS, CNRS CRPG Nancy

Tab. VI.7: REE data from Early Palaeozoic Granitoids continuation

Ho-Bi Gneisses Val Bérard (AWAR: from Wirsing 1997)

	Emosson AWAR Wirsing 1997			Trient water gallery Mont Blanc von Raumer, unpublished data						
	9	11	12	MBT70	MBT73	MBT74	MBT75	MBT174	MB784	MB1187
La	45.19	45.33	47.70	31.9	10.8	15.5	5.8	7.2	15	28.1
Ce	96.31	97.16	100.20	67.9	24.4	33.7	13.6	15.6	31.2	63.1
Pr	11.00	11.29	12.05	7.9	2.8	3.9	1.6	1.7	3.7	7.3
Nd	41.6	44.3	45.2	28.9	10	14.7	5.7	6.2	14.9	27.4
Sm	9.04	9.37	9.28	6.6	2.6	3.6	1.6	1.5	3.6	6.5
Eu	1.48	1.40	1.50	0.71	0.29	0.29	0.12	0.32	0.45	0.96
Gd	7.97	7.66	7.91	6.7	3.2	3.6	1.7	1.5	4.1	6.3
Tb	1.22	1.20	1.23	1.2	0.6	0.7	0.4	0.3	0.8	1.2
Dy	7.34	6.77	7.44	7.5	4.5	4.7	2.8	1.6	5.5	7.7
Ho	1.66	1.48	1.60	1.48	0.94	0.97	0.62	0.32	1.12	1.51
Er	4.00	3.50	3.87	4	2.5	2.4	2.2	0.5	3.1	4.4
Tm	0.59	0.56	0.62	0.6	0.5	0.5	0.4	0.2	0.5	0.6
Yb	3.51	3.11	3.78	3.4	3.2	3.4	2.7	1	3.3	4.1
Lu	0.51	0.48	0.56	0.49	0.46	0.45	0.41	0.15	0.46	0.5

	Trient / Mont Blanc; Nähr 1996					Trient/Mont Blanc; Bauer 1996				
	N 186	N 187	N188	N189	N190	B 293	B 294	B 296	B 297	B 313
La	11.6	20	13.3	9.7	19.5	28.1	25.2	27.6	26.7	33.9
Ce	25.3	41.8	29.2	22.2	40.8	57.5	54.2	56.9	53.8	69.4
Pr	2.9	5	3.4	2.7	4.7	6.5	6.3	6.8	6.1	8
Nd	11	18	12.1	9.9	17.4	25.6	23.1	25.4	23.1	29.2
Sm	3	4.3	3.1	2.8	4.1	5.3	5.4	5.4	5.7	6.1
Eu	0.52	0.5	0.44	0.22	0.56	1.25	0.9	1.14	0.9	0.94
Gd	3.6	4.4	3.3	3.3	4.3	5	5.5	5.8	5.3	6
Tb	0.8	0.8	0.7	0.7	0.8	0.8	1	0.9	1.1	1
Dy	6.2	5	4.4	5.2	4.9	4.2	6.4	5.7	5.7	6.3
Ho	1.4	1.02	0.89	1.12	1.07	0.82	1.36	1.17	1.34	1.25
Er	4.4	3	2.8	3.3	3.2	2.2	4.1	3.3	3.5	3.7
Tm	0.6	0.5	0.4	0.6	0.5	0.3	0.6	0.5	0.6	0.6
Yb	4.2	3	2.6	3.7	3	2	3.7	3	3	3.6
Lu	0.6	0.43	0.35	0.51	0.46	0.32	0.52	0.46	0.59	0.51

Sample location: see Annex II
Analyses: ICP-MS, CNRS CRPG Nancy

Tab. VI.8: Chemical data from Ultramafic Rocks

Ultramafic lenses from Lac Emosson and Val Bérard (Aiguilles Rouges)

Major elements (wt%)

	Lac Cornu area (unpunlished data)						Val Bérard area (Fracheboud 1997, unpubl. data)			
	1801[1]	**1725A2**[1]	**1770**[1]	**1758**[1]	**1774**[1]	**1727**[2]	**FS22**[2]	**FS23**[2]	**FS24**[2]	**FS25**[2]
SiO2	36.93	42.19	39.14	38.96	47.84	48.45	39.62	39.86	38.34	38.1
TiO2	0.15	0.07	0.03	0.03	0.46	0.62	0.03	0.03	0.03	0.03
Al2O3	5.15	2.65	2.32	1.73	4.68	7.26	2.2	2.28	2.41	2.24
Fe2O3	5.42	4.06	4.80	5.01	3.39	1.13	6.5	6.53	8.06	7.5
FeO	3.76	3.74	2.48	2.22	5.86	4.60	2.84	3.14	3.33	3.17
MnO	0.13	0.14	0.07	0.04	0.13	0.16	0.09	0.09	0.09	0.09
MgO	29.20	33.28	36.62	39.21	24.58	19.48	36.48	35.98	35.72	36.59
CaO	5.70	2.31	1.11	0.05	6.23	12.33	0.1	0.2	0.04	0.12
Na2O	0.54	0.1	0.00	0.00	0.27	0.71	0.02	0.02	0.03	0.02
K2O	0.08	0.01	0.00	0.00	0.03	0.23	0.01	0.01	0.01	0.01
P2O5	0.01	0	0.00	0.00	0.00	0.03	0.01	0.01	0.01	0.01
Total	**99.06**	**99.93**	**99.74**	**100.27**	**100.16**	**97.59**	**99.3**	**99.31**	**99.36**	**99.52**
$Fe2O3_{tot}$						6.24	9.66	10.02	11.76	11.02
LOI						2.59				
H2O+	7.95	10.1	11.21	12.17	5.08		11.09	10.81	10.93	11.3
H2O-						0.12				
CO2	1.74	0.5	1.33	0.17	1.05					

Trace elements (ppm)

Ba	3	254	3	3	3	39	<1	<1	<1	<1
Cr	2257	3419	2632	2579	3960	3960	4964	4774	5195	4825
Cu	61	<4	4	4	125		51	47	151	154
Ga	6	1	1	1	4					
Nb	5	9	5	5	5		1	1	1	1
Ni	917	1863	1998	2126	882	877	2495	2558	2064	2080
Pb	2	<2	2	2	2		5	3	1	4
Rb	3	3	1	2	2		10	11	12	11
Sr	21	22	15	1	36	96	5	5	4	5
Th	1	<1	1	1	1		<1	<1	<1	<1
V	147	81	61	45	247	288	38	40	38	35
Y	1	<1	1	1	9	22	4	3	4	4
Zn	144	61	29	19	75	45	46	44	61	60
Zr	2	<2	2	2	24	13	3	2	2	2

Sample location: see Annex II

Analyses: 1) RFX data Centre d'Analyses University of Lausanne.
2) RFX data Fribourg University Earth Science Dept

Tab. VI.9: Chemical data from metabasic rocks I

Plagioclase-amphibolites from Lac Emosson (von Raumer et al. 1990)

Major elements (wt%)

	plagioclase-amphibolites (Lac Emosson)						
	1502	**1511**	**1518**	**1526**	**1532**	**1545**	**1547**
SiO2	47.68	47.04	50.72	47.18	45.91	49.70	48.70
TiO2	1.06	0.75	1.39	0.90	0.94	1.13	0.96
Al2O3	16.08	18.23	14.70	15.59	16.20	14.59	15.05
Fe2O3	9.36	8.28	10.71	10.65	11.94	10.84	10.17
MnO	0.18	0.16	0.21	0.21	0.23	0.26	0.20
MgO	8.75	8.23	8.61	9.24	9.76	8.82	9.28
CaO	11.11	10.24	8.72	10.50	10.50	9.49	11.34
Na2O	1.91	2.08	3.11	0.72	1.49	2.29	1.56
K2O	0.48	0.82	0.24	1.21	0.43	0.25	0.44
P2O5	0.14	0.07	0.12	0.08	0.07	0.10	0.09
Total	**99.11**	**99.14**	**99.92**	**99.16**	**99.43**	**99.71**	**99.58**
LOI	2.30	3.18	1.37	2.79	1.88	2.19	1.70
Cr2O3	0.05	0.05	0.02	0.07	0.07	0.03	0.07
NiO	0.02	0.02	0.01	0.02	0.02	0.01	0.01

Trace elements (ppm): LA-ICP-MS (F. Bussy, Lausanne)

Rb	15.84	45.92	5.56	50.50	11.09	5.37	15.71
Sr	333.43	274.45	163.71	322.64	229.24	185.76	171.05
Y	18.50	15.98	29.69	19.45	22.87	30.08	25.95
Zr	72.78	44.44	110.65	50.30	56.80	90.25	66.09
Ba	68.27	320.51	39.51	580.05	147.94	58.49	122.24
Hf	1.54	1.16	2.42	1.15	1.43	2.32	1.46
Ta	0.28	0.29	0.71	0.29	0.32	0.47	0.49
W	96.92	66.20	129.54	85.91	83.10	68.55	98.38
Pb	6.37	12.80	11.37	4.57	1.95	17.49	5.06
Th	0.27	0.12	1.41	0.15	0.25	0.31	0.23
U	0.08	0.06	0.26	0.14	0.11	0.11	0.08

REE (ppm): LA-ICP-MS (F. Bussy, Lausanne)

La	4.21	2.05	8.09	2.28	3.30	3.84	2.91
Ce	10.84	5.45	17.23	5.94	8.43	9.37	7.06
Pr	1.68	0.84	2.34	0.96	1.34	1.55	1.13
Nd	8.63	5.19	11.59	5.03	7.26	9.16	6.13
Sm	2.27	1.93	3.10	1.75	2.96	3.32	2.26
Eu	1.03	0.69	0.86	0.84	1.33	1.08	0.93
Gd	3.28	2.70	4.47	2.56	3.21	3.75	3.04
Tb	0.44	0.35	0.74	0.41	0.54	0.71	0.60
Dy	3.11	2.93	5.32	3.56	3.54	5.15	4.35
Ho	0.80	0.65	1.09	0.64	0.83	1.03	0.96
Er	2.04	1.48	3.10	2.03	2.27	2.83	2.98
Tm	0.25	0.32	0.47	0.26	0.35	0.48	0.35
Yb	1.54	2.23	3.05	1.99	2.18	2.88	3.30
Lu	0.19	0.25	0.42	0.32	0.35	0.52	0.42

Sample location: see Annex II

Tab. VI.9: Chemical data from metabasic rocks II

Garnet-amphibolites from Lac Emosson (von Raumer et al. 1990)

Major elements (wt %): XRF-data; Centre d'analyses, University of Lausanne

	1505	1514	1515	1519	1520	1521	1523
SiO2	49.59	48.97	49.26	49.03	49.60	48.44	50.03
TiO2	1.39	1.41	1.34	1.29	1.33	1.28	1.37
Al2O3	14.59	14.53	15.21	14.95	14.87	16.17	13.97
Fe2O3	11.69	11.50	11.04	11.00	11.10	10.90	11.75
MnO	0.24	0.20	0.19	0.19	0.19	0.20	0.21
MgO	7.95	7.33	7.11	7.33	7.34	7.10	7.82
CaO	9.28	10.38	10.89	11.18	10.62	10.09	10.59
Na2O	1.96	2.87	2.59	2.78	2.35	0.99	1.76
K2O	0.60	0.28	0.15	0.22	0.46	1.59	0.32
P2O5	0.15	0.17	0.16	0.15	0.16	0.17	0.13
Total	**99.05**	**99.18**	**99.32**	**99.23**	**99.26**	**99.13**	**99.00**
LOI	1.61	1.53	1.37	1.11	1.22	2.18	1.01
Cr2O3	0.01	0.01	0.01	0.01	0.01	0.01	0.05
NiO	0.01	0.00	0.01	0.01	0.01	0.01	0.01

Traces (ppm): LA-ICP-MS (F. Bussy, Lausanne)

Rb	27.76	11.76	4.92	9.06	18.18	69.01	10.74
Sr	221.66	258.29	272.08	246.96	246.13	313.75	128.80
Y	24.57	27.31	26.93	25.78	26.74	23.00	32.29
Zr	87.22	96.14	90.49	88.80	95.64	82.94	77.90
Ba	252.47	99.10	50.14	70.07	120.72	734.76	99.38
Hf	2.40	2.19	2.44	2.17	2.53	2.13	1.79
Ta	0.69	0.76	0.79	0.82	0.77	0.67	0.59
W	56.70	127.03	103.52	103.39	105.11	107.10	82.87
Pb	3.75	2.74	3.72	2.99	3.64	3.25	7.91
Th	0.76	0.57	0.59	0.56	0.65	0.52	0.31
U	0.27	0.13	0.15	0.16	0.18	0.18	0.09

REE (ppm): La-ICP-MS (F. Bussy, Lausanne)

La	6.81	7.26	6.91	6.89	7.31	6.88	3.39
Ce	16.63	15.76	15.16	14.22	14.99	14.59	8.95
Pr	2.37	2.23	2.13	2.12	2.25	2.15	1.54
Nd	10.69	12.01	10.98	11.03	11.35	9.78	8.19
Sm	3.10	3.01	3.24	2.92	3.27	4.04	2.53
Eu	1.25	1.31	1.15	1.13	1.01	1.22	1.10
Gd	3.69	4.21	3.99	4.03	4.39	3.42	4.14
Tb	0.53	0.69	0.66	0.63	0.67	0.57	0.72
Dy	4.20	4.54	4.42	4.51	4.87	4.16	5.48
Ho	0.88	1.07	1.04	0.91	1.01	0.92	1.23
Er	2.57	2.79	2.97	2.55	2.69	2.36	3.77
Tm	0.40	0.39	0.48	0.55	0.42	0.34	0.44
Yb	3.13	2.93	2.78	3.15	2.56	2.44	3.69
Lu	0.39	0.43	0.41	0.36	0.45	0.32	0.61

Sample location: see Annex II

Tab. VI.9: Chemical data from metabasic rocks III

contaminated amphibolites from Lac Emosson (von Raumer et al. 1990)
banded eclogites from Lac Cornu

Major elements (wt %): XRF-data; Centre d'analyses, University of Lausanne

	cont amph.			banded eclogites					
	1527	1601	1604	1820	1821	1822	1823	1824	1825
SiO2	51.86	50.00	50.09	46.03	44.54	49.69	50.53	47.71	47.30
TiO2	2.12	2.41	2.77	3.89	5.51	1.47	0.42	3.26	3.28
Al2O3	12.90	13.77	13.17	15.25	14.63	21.97	17.55	16.11	15.52
Fe2O3	14.11	14.29	15.83	15.19	16.42	5.06	6.57	9.13	10.25
MnO	0.20	0.27	0.28	0.28	0.27	0.08	0.12	0.16	0.16
MgO	6.51	5.87	5.74	6.01	5.28	3.62	6.47	7.40	8.37
CaO	6.69	9.54	8.58	8.47	8.95	10.88	12.33	10.53	9.50
Na2O	2.00	0.69	1.46	2.68	2.71	3.42	3.26	2.78	2.82
K2O	0.95	0.66	0.19	0.29	0.40	1.08	0.48	0.48	0.60
P2O5	0.32	0.28	0.30	0.05	0.02	0.02	0.02	0.05	0.06
Total	**99.74**	**99.16**	**99.05**	**99.02**	**99.15**	**99.05**	**99.12**	**99.17**	**99.10**
LOI	2.05	1.34	0.62	0.88	0.43	1.75	1.32	1.51	1.19
Cr2O3	0.02	0.03	0.01	0.01	0.01	0.02	0.04	0.05	0.04
NiO	0.01	0.01	0.01	0.00	0.00	0.00	0.00	0.01	0.01

Traces (ppm): LA-ICP-MS (F. Bussy, Lausanne)

Rb	26.92	32.19	4.38	10.34	15.65	44.75	14.69	17.94	14.90
Sr	114.58	250.61	115.98	242.40	291.38	424.59	311.01	294.12	350.35
Y	93.61	45.49	61.96	13.55	14.04	3.97	8.73	9.33	10.00
Zr	354.89	154.21	211.87	27.67	35.51	6.53	8.52	26.32	35.71
Ba	152.98	257.11	50.24	55.74	44.90	139.08	76.91	79.21	84.33
Hf	9.51	4.31	5.80	1.05	1.15	0.47	0.46	0.91	0.76
Ta	0.89	1.17	1.73	0.66	1.08	0.36	0.33	0.47	0.61
W	78.07	201.19	295.99	157.81	158.47	142.18	125.00	107.75	82.49
Pb	6.18	7.74	16.39	3.18	1.97	1.09	2.75	1.79	9.43
Th	1.79	1.51	2.02	0.06	0.42	0.06	0.06	0.55	0.57
U	0.63	0.35	0.47	0.22	0.60	0.03	0.10	0.20	0.36

REE (ppm): LA-ICP-MS (F. Bussy, Lausanne)

La	12.69	12.26	15.16	1.53	3.44	0.87	1.23	4.21	4.24
Ce	31.87	28.04	29.95	3.39	8.85	1.79	2.63	8.83	8.58
Pr	5.13	4.02	4.78	0.64	1.71	0.22	0.43	1.33	1.23
Nd	27.74	19.17	22.50	4.64	11.68	1.40	2.33	7.50	6.19
Sm	9.25	5.02	7.90	1.53	4.02	0.80	0.87	1.77	1.66
Eu	2.22	1.82	2.10	1.33	2.56	0.82	0.73	0.90	0.79
Gd	12.66	6.69	8.82	2.88	3.92	0.67	1.51	2.31	1.89
Tb	2.20	1.23	1.68	0.34	0.51	0.14	0.29	0.29	0.34
Dy	15.75	8.85	10.66	2.85	2.79	0.76	1.59	1.75	1.74
Ho	3.43	1.56	2.30	0.48	0.53	0.22	0.28	0.30	0.34
Er	10.48	4.72	6.67	1.59	1.34	0.35	0.94	0.97	0.84
Tm	1.58	0.79	0.88	0.24	0.23	0.03	0.18	0.11	0.12
Yb	10.36	4.30	6.63	1.35	1.55	0.34	1.05	0.65	1.19
Lu	1.69	0.77	1.06	0.17	0.15	0.07	0.12	0.18	0.15

Sample location: see Annex II

Tab. VI.9: Chemical data from metabasic rocks IV

eclogitic series from Tête de Béchat

Major elements (wt %): XRF-data; Centre d'analyses, University of Lausanne

	TB1	TB2	TB3	TB4	CV2.1	CV2.2	CV2.4	CV3.1	CV3.2	CV3.3
SiO2	49.12	45.53	48.66	47.95	48.88	49.39	46.44	49.16	47.14	49.65
TiO2	1.17	1.31	1.09	1.83	1.19	0.95	1.71	1.70	2.42	2.03
Al2O3	14.96	15.93	14.70	15.44	15.80	16.96	15.31	13.30	13.41	13.21
Fe2O3	2.04	3.79	2.93	3.76	10.20	6.77	3.51	4.19	3.63	3.12
FeO	8.22	8.33	7.97	9.80	1.09	3.01	9.07	8.62	12.02	10.85
MnO	0.16	0.22	0.19	0.22	0.21	0.19	0.22	0.20	0.26	0.23
MgO	10.06	8.54	8.91	7.66	6.47	6.99	8.08	7.19	7.42	6.75
CaO	7.65	11.70	9.94	8.86	10.37	8.39	8.64	9.68	8.76	10.07
Na2O	2.64	2.48	1.95	2.72	2.89	3.60	2.82	2.50	2.50	2.71
K2O	1.02	0.29	0.44	0.34	0.80	1.31	1.02	0.94	0.27	0.07
P2O5	0.05	0.08	0.07	0.19	0.10	0.05	0.15	0.16	0.23	0.18
Total	**99.97**	**99.98**	**99.83**	**99.76**	**99.51**	**99.82**	**99.81**	**99.96**	**99.83**	**99.87**
H2O+	2.85	1.64	2.95	1.98	1.46	2.18	2.83	2.31	1.76	0.99

Trace elements (ppm): XRF-data; Centre d'analyses, University of Lausanne

Ba	18	23	28	23	64	108	126	123	24	2
Cr	423	468	257	157	481	376	351	258	108	113
Cu	40	8	33	69	24	40	27	15	73	53
Ga	21	20	17	21	18	16	18	20	20	18
Nb	0	0	0	3	0	0	1	3	4	3
Ni	88	147	86	65	118	89	87	63	50	46
Pb	10	11	12	11	15	25	13	13	12	10
Rb	61	19	29	16	33	67	40	43	15	10
Sr	65	139	78	104	197	191	188	115	124	100
Th	12	10	8	10	9	10	10	11	10	9
V	356	364	337	471	294	280	405	429	514	449
Y	32	39	30	41	31	29	35	39	50	43
Zn	106	108	95	138	96	99	118	135	175	122
Zr	46	78	45	81	58	41	74	81	110	96
U	3	3	2	3	3	3	3	4	4	3
Co	70	81	79	80	79	65	63	61	115	98
Ce	11	13	2	20	8	11	17	15	20	18
Nd	8	9	2	11	6	8	10	10	9	9
La	2	9	10	7	2	10	7	3	6	7
S	138	9	181	16	16	9	10	25	181	527
Hf	6	5	6	6	4	5	5	6	6	6
Sc	41	46	44	57	40	37	54	53	63	53
As	4	4	3	0	2	0	0	6	0	0

Sample location: see Annex II

Tab. VI.9: Chemical data from metabasic rocks V

eclogitic series from Tête de Béchat

Major elements (wt %): XRF-data; Centre d'analyses, University of Lausanne

	CP2	CP3	CP4	CP5	CP6	CP7	CP8	CP9	CP11	CP12	CP13	CP14
SiO2	45.19	46.20	43.89	43.82	49.12	48.95	46.12	48.41	56.10	45.54	44.46	49.54
TiO2	1.87	1.50	3.08	2.37	0.91	2.12	2.25	1.05	0.42	2.39	2.05	2.29
Al2O3	15.54	14.59	12.59	12.10	16.29	13.68	13.95	15.42	12.12	13.16	10.64	16.13
Fe2O3	5.28	3.72	4.62	7.10	5.01	4.30	6.05	3.86	1.63	4.66	2.20	2.79
FeO	8.61	9.09	13.99	10.63	4.57	10.24	8.81	6.33	5.80	10.85	9.66	3.49
MnO	0.22	0.22	0.32	0.28	0.17	0.22	0.23	0.20	0.09	0.28	0.18	0.23
MgO	8.42	8.60	7.30	8.43	7.93	6.35	7.69	7.94	10.61	7.34	14.36	2.48
CaO	10.26	9.72	9.44	10.66	7.72	8.75	9.02	11.07	8.02	9.97	10.95	8.77
Na2O	2.21	2.33	2.43	2.23	3.13.	2.34	2.55	2.44	1.44	1.81	1.37	2.27
K2O	1.03	1.40	0.15	0.28	1.91	0.48	0.39	0.87	1.01	0.44	0.59	3.80
P2O5	0.25	0.17	0.26	0.24	0.08	0.21	0.23	0.09	0.20	0.26	0.07	0.25
Total	**99.33**	**100.02**	**100.06**	**99.74**	**99.96**	**99.82**	**99.51**	**99.93**	**99.89**	**100.04**	**99.60**	**99.56**
H2O+	2.43	2.45	1.98	1.59	3.1	2.16	2.21	2.23	2.28	3.32	3.03	7.51

Trace elements (ppm): XRF-data; Centre d'analyses, University of Lausanne

Ba	105	133	0	9	197	39	28	58	151	42	41	94
Cr	245	429	59	162	351	198	221	334	1258	169	363	196
Cu	29	17	67	8	25	20	14	39	4	55	104	82
Ga	20	20	24	25	16	19	21	16	17	21	17	25
Nb	5	2	6	5	0	3	5	0	2	5	6	0
Ni	61	138	64	89	87	63	70	77	103	62	258	31
Pb	15	13	9	12	10	11	10	10	18	12	17	0
Rb	40	52	11	10	89	25	19	45	37	27	15	219
Sr	145	161	72	95	217	72	48	114	89	87	47	135
Th	9	10	11	8	9	10	13	10	16	9	17	11
V	464	364	655	589	293	466	447	296	196	537	522	566
Y	43	37	52	54	30	45	51	28	24	50	35	46
Zn	139	135	186	199	98	130	159	90	133	211	130	3040
Zr	79	74	127	100	52	103	91	51	43	119	49	157
U	3	4	4	4	2	5	5	3	3	5	2	5
Co	69	66	84	90	69	80	86	71	72	86	94	38
Ce	24	23	5	16	15	21	20	3	18	20	39	21
Nd	14	14	2	9	9	11	10	3	10	12	19	13
La	7	7	6	6	6	8	7	9	18	6	21	22
S	149	15	342	22	13	0	78	271	0	478	200	3128
Hf	6	5	6	5	5	6	6	5	9	7	8	2
Sc	60	45	78	72	36	58	65	39	38	61	72	26
As	0	3	0	0	1	0	0	2	15	0	0	3

Sample location: see Annex II

Tab. VI.10: Chemical data from metagraywackes I

Metagraywackes from Lac Emosson
von Raumer, unpublished

Major elements (wt %)

	1661	1663	1666	1674	1675	1676	1679	1681	1684	1688
SiO2	71.55	69.27	66.64	70.76	67.2	68.17	65.05	74.6	70.31	67.47
TiO2	0.86	0.47	0.7	0.69	0.96	0.9	0.86	0.67	0.38	1.02
Al2O3	14.61	15.75	15.57	13.77	14.24	13.91	15.65	11.44	15.6	13.7
Fe2O3	0.44	0.88	0.9	0.94	1.14	1.24	1.88	0.79	0.65	1.49
FeO	1.8	2.08	4.22	3.26	4.08	4.04	4.06	2.65	1.85	4.42
MnO	0.03	0.04	0.08	0.06	0.06	0.06	0.07	0.06	0.03	0.08
MgO	0.67	1.09	2.26	1.82	2.37	2.22	2.54	1.6	0.72	2.16
CaO	1.22	0.92	1.3	1.37	1.9	1.65	1.66	1.09	1.56	2.5
Na2O	3.1	3.11	3.09	3.41	3.42	3.72	3.1	3.29	3.79	3.06
K2O	4.79	3.9	2.15	2.01	1.76	1.4	2.45	1.37	3.67	2.11
P2O5	0.22	0.27	0.18	0.18	0.24	0.22	0.21	0.2	0.24	0.23
Total	**99.69**	**99.43**	**99.54**	**99.47**	**99.24**	**99.23**	**99.14**	**99.21**	**99.73**	**99.05**
FeTOT	2.44	3.2	5.59	4.56	5.67	5.73	6.39	3.73	2.7	6.4
GV	0.91	1.35	2.46	1.51	1.86	1.71	1.11	1.45	0.94	0.81
H2O	0.11	0.16	0.18	0.08	0.13	0.12	0.21	0.13	0.1	0.1

Trace elements (ppm)

Ba	992	1130	471	639	566	563	663	577	981	977
Cr	19	33	81	92	109	96	111	58	14	111
Cu	7	8	32	15	44	7	26	12	5	13
Ga	15	16	16	12	14	15	16	11	16	14
Nb	14	17	15	14	17	16	14	16	15	12
Ni	6	10	36	30	31	34	40	22	8	32
Pb	152	17	3	17	0	0	0	7	29	0
Rb	152	125	99	66	57	45	102	39	105	70
Sr	134	138	167	194	266	574	206	185	192	608
Th	36	41	27	26	23	23	20	35	34	15
V	25	36	123	104	140	149	148	87	29	144
Y	33	51	32	28	32	31	32	25	35	31
Zn	34	43	75	119	68	42	77	51	47	71
Zr	144	203	195	220	249	234	213	248	168	248

Sample location: see Annex II
Analyses: RFX data Earth Sciences Dept., University of Fribourg

Tab. VI.10: Chemical data from metagraywackes II

Metagraywackes from Lac Emosson

von Raumer, Dupasquier (SDU) 1996, and Schmocker (KS) 1996, unpublished

Major elements (wt %)

	1691	1694	1700	1705	1707	1734	SDU 6	KS 134	KS 143	KS 156
SiO2	64.61	74.1	73.25	75.83	65.6	68.32	68.32	65.72	68.85	64.95
TiO2	0.73	0.8	0.78	0.59	0.72	0.81	0.88	0.83	0.77	1.04
Al2O3	16.42	11.57	11.76	11.5	16.5	14.25	15.04	17.47	15.12	16.40
Fe2O3	0.99	0.69	0.73	0.41	0.72	0.8	5.66	6.32	5.48	6.87
FeO	3.52	3.87	4	2.8	3.76	4.45				
MnO	0.06	0.08	0.07	0.06	0.06	0.07	0.09	0.07	0.07	0.08
MgO	1.57	2.05	1.95	1.46	1.52	2.27	2.59	2.73	2.42	2.87
CaO	2.22	1.37	1.69	1.4	1.98	1.66	1.55	0.77	1.41	1.78
Na2O	3.48	2.02	1.99	3.07	2.73	2.98	3.53	2.22	2.81	3.54
K2O	3.62	1.34	2.18	1.4	3.83	1.66	2.13	3.83	2.83	2.28
P2O5	0.27	0.18	0.17	0.17	0.27	0.18	0.25	0.19	0.20	0.25
Total	**99.21**	**99.67**	**99.48**	**99.4**	**99.16**	**99.04**	**100.04**	**100.15**	**99.96**	**100.06**
$Fe2O3_{tot}$	4.9	4.99	5.17	3.52	4.9	5.75	4.03	4.23	3.99	4.95
LOI	1.72	1.62	0.9	0.72	1.48	1.59				
H2O	0.1	0.07	0.06	0.06	0.05	0.13				

Trace elements (ppm)

Ba	1572	462	651	363	1469	451	523	717	847	527
Cr	44	105	84	68	47	107	99	128	102	145
Cu	8	10	12	11	16	12	6	29	25	44
Ga	18	13	12	11	20	16				
Nb	19	12	12	11	14	10	17	14	13	15
Ni	14	36	31	23	17	38	32	38	33	44
Pb	12	16	0	15	24	4	29	24	27	27
Rb	103	50	77	48	122	57	88	147	103	88
Sr	223	148	174	175	190	205	262	157	271	247
Th	34	12	15	12	17	6	14	12	11	8
V	68	117	110	68	67	140	133	140	123	176
Y	45	34	29	25	43	29	34	34	29	37
Zn	71	119	64	44	73	85	79	72	76	101
Zr	272	268	261	209	255	180	284	202	201	244

Sample location: see Annex II

Analyses: RFX data Earth Science Dept, University of Fribourg

Tab. VI.10: Chemical data from metagraywackes III

Metagraywackes from Tré les Eaux (Aiguilles Rouges)
Marquis (FXM)1997, unpublished

Major elements (wt %)

FXM	1	2	3	4	5	6	7	8	9	10	11	12
SiO2	71.88	65.21	72.67	69.76	67.54	67.91	68.98	68.42	71.97	72.71	70.27	71.04
TiO2	0.69	0.83	0.69	0.73	0.75	0.75	0.77	0.81	0.65	0.66	0.64	0.75
Al2O3	13.02	15.72	12.61	13.82	14.85	14.85	13.47	13.65	13.21	12.47	13.98	13.39
Fe2O3	0.5	0.55	0.4	0.52	0.76	0.66	0.76	0.75	0.62	0.45	0.67	0.66
FeO	3.3	4.64	3.37	3.8	4.08	3.91	4.37	4.68	3.29	3.59	3.49	3.47
MnO	0.08	0.11	0.06	0.07	0.05	0.05	0.07	0.08	0.08	0.08	0.08	0.04
MgO	1.83	2.61	1.75	2.07	2.34	2.26	2.5	2.6	1.8	1.84	1.96	1.85
CaO	1.53	1.89	1.41	1.56	0.7	0.6	1.55	1.18	1.25	1.24	1.3	1.19
Na2O	3.11	3.37	3.278	3.26	2.67	3.06	2.73	2.83	3.45	2.95	3.31	3.07
K2O	1.8	2.35	1.79	2.19	2.97	2.82	1.75	2.38	1.88	2.02	1.78	1.75
P2O5	0.2	0.22	0.18	0.19	0.19	0.2	0.18	0.18	0.21	0.18	0.18	0.21
Total	**99.42**	**99.42**	**99.43**	**99.52**	**99.02**	**99.22**	**99.09**	**99.5**	**99.62**	**99.27**	**99.33**	**99.16**
H2O	1.48	1.91	1.23	1.57	2.13	2.15	1.96	1.94	1.22	1.08	1.71	1.75

Trace elements (ppm)

Ba	552	730	489	566	607	643	463	626	375	445	522	520
Cr	83	112	87	96	105	103	129	133	87	79	97	98
Cu	9	12	7	6	20	20	25	43	10	38	5	17
Nb	13	15	13	15	15	15	13	13	13	13	14	15
Ni	26	38	28	33	38	37	36	39	27	28	34	30
Pb	22	25	23	22	17	17	28	26	33	51	22	23
Rb	74	96	72	83	112	102	78	86	74	83	70	67
Sr	272	274	174	180	177	168	247	223	250	210	199	176
Th	12	13	13	13	12	11	14	11	11	11	11	14
V	97	144	94	110	123	118	146	150	100	98	101	97
Y	32	34	31	33	30	30	35	27	33	32	32	37
Zn	67	99	69	90	99	102	119	144	157	309	89	86
Zr	240	237	268	263	217	216	234	242	217	233	211	294

Sample location: see Annex II
Analyses: RFX data Earth Sciences Dept, University of Fribourg

Tab. VI.11: Chemical data from metapelitic rocks I

Micaschists from Lac Emosson (Aiguilles Rouges)

von Raumer, unpublished

Major elements (wt %)

	1040	1082	1124	1126	1303	1326	1328	1331	1334	1339
SiO2	54.13	59.77	38.77	63.47	62.35	45.31	55.58	57.08	64.96	55.02
TiO2	1.10	0.97	1.29	0.88	0.91	1.29	0.95	0.94	0.47	1.02
Al2O3	23.71	17.78	21.82	16.48	17.41	27.22	21.63	21.12	13.66	22.20
Fe2O3	1.23	1.4	6.55	1.37	1.82	1.14	1.14	1.46	2.28	1.14
FeO	5.72	7.39	13.35	6.1	3.96	8.56	6.92	5.97	6.89	7.35
MnO	0.12	0.13	0.33	0.11	0.05	0.09	0.15	0.11	0.07	0.19
MgO	2.44	3.06	6.67	3.47	2.92	2.98	3.24	3	3.56	3.12
CaO	1.79	1.48	1.94	1.24	0.68	0.42	0.51	0.39	1.28	0.52
Na2O	2.58	1.9	0.95	1.31	2.38	1.12	1.38	1.38	0.99	1.4
K2O	3.61	2.81	2.18	2.71	4.29	6.27	4.34	4.23	3.29	3.95
P2O5	0.17	0.12	0.05	0.11	0.23	0.08	0.12	0.12	0.22	0.09
Total	**99.8**	**99.45**	**99.47**	**100.04**	**99.43**	**99.16**	**99.79**	**99.62**	**99.62**	**99.78**
FeTOT	7.59	9.61	3.58	8.16	6.22	10.66	8.83	8.09	9.93	9.3
Loi	3.2	2.65	3.58	2.77	2.43	4.68	3.83	3.82	1.95	3.8
H2O-	0.33	0.26	0.21	0.13	0.38	0.48	0.31	0.24	0.23	0.22
Trace elements (ppm)										
Ba	1671	721	676	769	920	1124	933	834	366	726
Cr	110	115	246	163	110	131	115	107	32	110
Cu	54	215	244	76	25	60	21	40	4	55
Ni	48	42	55	45	16	53	50	50	12	47
Rb	130	105	82	97	183	218	178	173	162	194
Sr	255	103	49	95	132	98	186	122	40	179
Zn	98	99	118	139	79	123	111	100	174	101
Zr	143	223	210	220	190	162	120	135	172	158

Major elements (wt %)

	1340	1348	1350	1351	1352	1353aug	1388B	1388C	1388D	1391aug	1394
SiO2	61.92	57.62	59.73	57.25	51.73	55.69	54.98	54.1	51.73	59.27	48.83
TiO2	1.03	1.13	1	0.99	1.11	1.08	1.53	1.06	1	0.93	3.58
Al2O3	18.87	18.80	20.46	19.35	19.16	20.58	16.64	20.32	23.27	19.47	18.24
Fe2O3	1.08	1.74	0.86	1.69	2.01	1.5	1.48	1.46	1.96	1.31	1.86
FeO	5.05	5.4	5.8	7.17	10.62	7.46	9.66	8.01	6.86	5.73	11.19
MnO	0.11	0.09	0.1	0.13	0.3	0.13	0.16	0.18	0.12	0.11	0.17
MgO	2.54	3.69	2.35	3.29	4.75	3.49	6.6	3.59	3.05	2.55	4.1
CaO	0.59	1.78	0.59	1.44	2.36	0.98	2.1	3.93	4.4	2.68	4.87
Na2O	1.63	4.04	0.8	1.61	1.38	0.94	0.78	2.73	3.23	2.66	2.03
K2O	3.51	3.03	4.23	3.44	2.75	3.95	2.29	1.71	1.78	2.31	1.16
P2O5	0.13	0.25	0.13	0.14	0.17	0.13	0.22	0.11	0.11	0.11	1.06
Total	**99.59**	**100.05**	**99.25**	**99.32**	**98.87**	**99.37**	**100.44**	**99.6**	**100.02**	**99.48**	**99.94**
FeTOT	6.69	7.74	7.31	9.66	13.81	9.79	12.22	10.36	9.58	7.68	14.3
LOI	3.15	2.48	3.21	2.82	2.53	3.46	4.01	2.4	2.51	2.37	2.85
H2O-	0.21	0.38	0.5	0.49	0.36	0.38	0.33	0.34	0.32	0.24	0.12
Trace elements (ppm)											
Ba	685	854	980	943	774	1400	358	330	417	816	218
Cr	92	116	93	128	160	145	71	97	123	110	74
Cu	7	52	97	112	112	121	9	132	139	79	14
Ni	43	53	49	47	44	48	52	48	54	33	65
Rb	176	101	130	124	103	145	146	101	101	111	83
Sr	124	197	68	100	128	75	53	188	223	214	168
Zn	104	175	84	93	95	124	172	112	95	71	165
Zr	227	226	184	190	216	216	99	129	116	178	263

Sample location: see Annex II

Analyses: RFX data Earth Science Dept, University of Fribourg

Tab. VI.11: Chemical data from metapelitic rocks II

Micaschists from Lac Emosson (Aiguilles Rouges)
V: Vallorcine water tunnel Val Bérard-Emosson
von Raumer, unpublished

Major elements (wt %)

	1428	1430	1486	1575	1577	1578	1582	1584	1603	1605
SiO2	63.27	59.38	62.58	55.73	51.3	58.6	58.95	65.05	56.84	57.82
TiO2	0.77	1.0	0.76	0.69	0.93	0.61	1.22	0.76	0.96	0.98
Al2O3	15.05	18.68	17.05	19.14	24.08	16.81	17.83	16.41	23.00	20.01
Fe2O3	1.65	1.2	1.01	1.27	2.06	0.93	1.42	0.98	1.0	1.18
FeO	5.12	6.18	5.98	6.52	7.58	6.46	5.17	4.17	5.19	5.65
MnO	0.2	0.08	0.12	0.15	0.16	0.13	0.12	0.07	0.09	0.14
MgO	3.76	3.3	3.14	5.28	2.53	5.43	3.38	2.56	2.15	2.85
CaO	2.56	0.67	0.64	2.25	2.07	2.59	4.01	1.8	2.39	2.97
Na2O	1.77	0.41	0.95	2.51	2.01	1.95	1.91	2.79	3.44	5.04
K2O	3.88	5.43	4.55	4.09	3.72	3.23	3.37	3.35	2.19	0.82
P2O5	0.14	0.14	0.14	0.13	0.11	0.05	0.27	0.23	0.14	0.16
Total	**99.36**	**99.83**	**99.35**	**99.93**	**99**	**99.03**	**99.34**	**99.99**	**99.4**	**99.36**
FeTOT	7.34	8.07	7.66	8.51	10.48	8.11	7.17	5.62	6.77	7.46
LOI	1.19	3.37	2.44	2.17	2.47	2.25	1.7	1.83	2.02	1.75
H2O-	0.21	0.25	0.17	0.18	0.18	0.11	0.12	0.13	0.16	0.12
Trace elements (ppm)										
Ba	693	752	825	880	1442	605	322	794	780	174
Cr	87	102	117	620	773	671	88	95	141	147
Cu	14	6	25	12	65	5	17	32	45	15
Ni	45	39	49	98	108	113	17	32	39	56
Rb	188	206	188	179	170	129	138	145	124	46
Sr	191	79	148	142	249	144	465	189	504	511
Zn	121	171	92	96	189	115	132	98	65	82
Zr	154	184	122	143	201	123	101	190	142	148

Major elements (wt %)

	V27	V31	V33	V34	V52	V54	V58	V93	V106	V109
SiO2	52.41	50.87	53.64	57.14	53.79	51.31	55.27	55.19	58.7	55.94
TiO2	1.1	1	1.08	0.93	1.31	1.02	0.92	1.09	0.87	0.92
Al2O3	24.05	24.79	24.04	21.42	20.98	25.74	21.85	22.67	22.52	20.82
Fe2O3	0.73	1.47	1	0.15	1.15	1.12	1.11	1.14	1.07	1.08
FeO	9.47	7.29	7.95	7.89	9.49	7.7	6.54	7.41	5.45	6.47
MnO	0.53	0.22	0.52	0.18	0.22	0.43	0.18	0.17	0.08	0.09
MgO	2.66	3.32	2.4	2.54	3.45	2.25	2.86	2.62	1.7	3.56
CaO	0.39	0.33	0.47	0.48	0.5	0.35	2	0.43	0.31	0.93
Na2O	1.12	1.35	1.02	1.48	0.97	0.57	2.4	1.39	0.75	1.55
K2O	3.21	5.1	3.91	3.68	3.63	5.16	3.45	3.7	4.57	4.82
P2O5	0.16	0.06	0.2	0.14	0.05	0.07	0.13	0.14	0.13	0.14
Total	**99.86**	**100.15**	**100.08**	**99.72**	**99.66**	**99.8**	**100.02**	**100.01**	**100.05**	**99.5**
FeTOT	11.25	9.57	9.83	8.92	11.7	9.68	8.38	9.37	7.13	8.27
LOI	4.02	4.35	3.85	3.67	4.12	4.08	3.31	4.04	3.9	3.19
H2O-	0.31	0.4	0.44	0.24	0.22	0.32	0.28	0.33	0.35	0.34
Trace elements (ppm)										
Ba	496	762	546	582	632	950	1269	567	609	1412
Cr	151	145	145	136	179	145	122	145	117	128
Cu	53	136	54	51	45	47	38	11	21	55
Ni	68	46	64	40	67	59	38	42	27	35
Rb	189	294	220	181	207	270	167	210	225	203
Sr	121	116	98	112	75	79	197	138	81	240
Zn	121	156	151	117	159	144	149	117	111	138
Zr	124	141	117	129	207	124	136	163	132	144

Sample locations: see Annex II
Analyses: RFX data Earth Sciences Dept, University of Fribourg

Tab. VI.11: Chemical data from metapelitic rocks III

Micaschists from Lac Emosson (Aiguilles Rouges) (FS: Fracheboud 1997, unpublished)

Major elements (wt %)

	FS1	FS2	FS3	FS4	FS5	FS6	FS7	FS8	FS9
SiO2	54.03	51.15	52.84	65.87	68.73	51.88	54.93	53.05	52.28
TiO2	0.75	0.75	0.8	0.57	0.48	0.76	0.73	0.87	0.86
Al2O3	18.9	21.24	19.75	17.48	16.16	20.66	19.24	22.37	21.96
Fe2O3	1.27	1.66	1.45	0.63	0.64	1.7	1.74	2.39	2.06
FeO	5.91	6.62	6.83	4.64	3.14	6.54	6.7	6.6	7.81
MnO	0.15	0.17	0.16	0.08	0.06	0.14	0.16	0.17	0.2
MgO	4.69	5.16	5.13	1.56	1.55	5.01	4.69	3.34	3.76
CaO	4.77	4.21	4.31	2.59	2.32	4.34	3.69	1.94	2.29
Na2O	2.41	2.43	2.36	2.39	2.37	2.5	2.41	1.47	1.87
K2O	2.9	2.67	2.92	2.2	2.28	3.03	2.66	4.5	4.27
P2O5	0.15	0.17	0.13	0.15	0.18	0.07	0.06	0.09	0.11
Total	**99.86**	**100.24**	**100.27**	**100.02**	**99.64**	**99.86**	**99.75**	**99.74**	**100.41**
FeTOT	7.83	9.02	9.04	5.79	4.13	8.87	9.18	9.73	10.74
H2O	3.28	3.27	2.84	1.34	1.38	2.61	2.01	2.23	2.07
Trace elements (ppm)									
Ba	526	450	527	571	676	615	531	1154	960
Cr	209	248	235	99	64	218	209	251	276
Cu	1	2	1	4	1	1	1	2	2
Ni	46	52	46	25	22	47	45	79	77
Rb	126	135	127	120	120	134	115	205	199
Sr	185	200	186	205	193	203	190	159	156
Zn	116	120	118	40	39	116	95	112	114
Zr	140	150	147	188	168	142	134	156	158

Major elements (wt %)

	FS10	FS11	FS12	FS13	FS14	FS15	FS16	FS17	FS18	FS19
SiO2	65.15	64.88	64.33	64.07	65.83	65.29	54.76	57.39	54.85	50.87
TiO2	0.78	0.79	0.84	0.84	0.81	0.76	0.74	0.73	0.75	1.04
Al2O3	15.87	16.14	15.33	15.07	15.49	15.79	19.85	19.97	20.16	26.54
Fe2O3	1.15	1.07	0.92	0.73	0.86	0.91	1.48	1.21	0.85	1.71
FeO	3.86	3.94	5.16	5.23	4.59	4.54	6.62	6.67	6.89	6.89
MnO	0.06	0.06	0.08	0.09	0.08	0.08	0.11	0.15	0.13	0.16
MgO	2.37	2.38	3.06	3.06	2.43	2.54	4	3.02	4.1	2.07
CaO	1.1	1.6	1.45	1.55	1.02	0.94	2.83	2.15	2.98	2.18
Na2O	3.27	3.28	3.43	3.2	3.12	3.1	3.61	2.98	3.96	2.36
K2O	3.34	3.46	2.36	2.52	2.88	2.87	3.07	3.05	2.92	3.5
P2O5	0.19	0.19	0.22	0.2	0.21	0.2	0.08	0.17	0.09	0.03
Total	**99.64**	**99.71**	**99.95**	**99.68**	**99.7**	**99.74**	**99.74**	**100.07**	**100.2**	**100.1**
FeTOT	5.44	5.45	6.65	6.54	5.96	5.96	8.83	8.62	8.51	9.37
H2O+	2.07	1.91	2.2	2.54	1.87	2.21	1.86	1.84	1.77	1.99
Trace elements (ppm)										
Ba	917	907	556	613	632	679	761	1055	1043	1456
Cr	126	129	137	130	130	120	681	589	686	951
Cu	35	31	40	32	52	34	10	9	32	52
Ni	35	33	43	40	41	44	151	119	117	149
Rb	124	130	102	109	108	105	127	127	111	131
Sr	223	225	191	181	194	186	235	221	229	300
Zn	105	173	83	76	117	131	109	123	108	594
Zr	204	201	202	205	236	198	161	187	164	210

Sample locations: see Annex II
Analyses: RFX data Earth Science Dept, University of Fribourg

Tab. VI.12: Chemical data from Variscan granitoids I

Monzonitic-durbachitic gneisses from the water tunnel Mont Dolent area, SW Mont Blanc massif (von Raumer, unpublished)

Major elements (wt %)

	MBT34	MBT37	MBT44	MBT124	MBT125	MBT134	MBT139	MBT141	MBT148	MBT196	MBT199
SiO2	57.66	56.79	58.35	58.22	58.47	56.54	58.69	61.00	64.17	66.87	65.60
TiO2	0.96	1.43	1.19	1.14	1.06	1.10	0.85	1.00	0.77	0.65	0.52
Al2O3	16.00	15.99	14.95	15.30	14.53	18.21	15.66	14.91	14.93	14.28	15.04
Fe2O3	0.70	1.35	0.61	0.90	0.47	1.21	0.48	0.51	0.93	0.68	0.42
FeO	4.17	4.66	1.72	4.57	1.54	5.56	3.55	3.94	2.59	2.79	1.99
MnO	0.13	0.13	0.10	0.19	0.13	0.16	0.14	0.10	0.09	0.13	0.07
MgO	5.34	4.22	1.37	4.44	1.22	4.30	3.26	3.56	3.06	1.81	1.91
CaO	4.21	2.70	6.72	4.36	7.00	1.02	4.37	2.94	2.35	1.68	2.47
Na2O	3.05	4.13	2.01	2.01	2.26	2.59	2.83	2.50	2.26	3.32	2.61
K2O	4.43	4.83	6.89	6.46	7.27	5.88	6.59	6.55	6.63	5.32	7.57
P2O5	0.51	0.72	0.90	0.79	0.77	0.50	0.57	0.63	0.49	0.38	0.35
Total	**99.60**	**99.54**	**99.98**	**100.15**	**100.27**	**99.63**	**100.18**	**100.15**	**99.82**	**99.82**	**99.69**
FeTOT	5.33	6.52	2.40	5.97	2.18	7.38	4.42	4.88	3.80	3.78	2.63
LOI	2.44	2.59	5.17	1.77	5.55	2.56	3.19	2.51	1.55	1.91	1.14
H2O	0.15	0.33	0.20	0.13	0.16	0.14	0.10	0.15	0.15	0.15	0.12

Trace elements (ppm)

Ba	1949	1143	3154	2457	3057	1727	2596	2612	3861	1625	4146
Cr	202	267	194	153	166	231	124	129	84	71	56
Cu	9	9	36	7	13	6	12	15	11	10	11
Ga	23	24	22	19	18	35	20	17	16	19	16
Nb	7	18	24	23	26	12	22	24	9	15	19
Ni	81	93	22	56	21	93	39	38	31	16	16
Pb	23	3	19	21	17	4	32	26	25	26	39
Rb	259	354	319	343	338	475	332	356	268	320	197
Sr	370	211	393	415	399	118	422	376	367	220	355
Th	17	24	65	73	55	32	74	83	52	63	47
V	109	148	121	114	114	147	93	97	69	54	47
Y	22	38	37	46	35	40	61	48	34	34	46
Zn	151	143	46	184	47	145	112	101	97	90	55
Zr	234	344	500	409	430	290	328	361	310	237	172
U	5	5	21	10	19	4	11	9	9	11	13
Co	40	51	41	44	31	29	37	43	52	52	56
Ce	94	87	123	160	145	117	144	180	151	104	111
Nd	38	39	84	100	101	50	91	104	75	52	75
La	84	44	78	84	93	73	57	68	88	59	48
S	135	15	2920	21	364	67	55	1422	37	973	744
Hf	5	9	21	13	18	7	11	11	12	8	5
Sc	9	16	9	12	8	12	10	11	7	4	7
As	5	5	1	3	3	3	4	3	3	0	3

Analytic data: XRF, Centre d'analyse, University of Lausanne

Tab. VI.12: Chemical data from Variscan granitoids II

Monzonitic-durbachitic gneisses
Val Ferret (Mont Blanc) PG: Gay 1997 unpublished
Pormenaz (Aiguilles Rouges) samples 956, 752: Délitroz and Fellay 1997
Montées Pélissier granite (Aiguilles Rouges) samples 92/055, 92/093: Dobmeier 1996
Tonalitic mobilisate (Lac Cornu, Aiguilles Rouges): 1871: von Raumer unpublished

Major elements (wt %) XRF-data PG: University of Fribourg,
others: Centre d'analyse minérale, University of Lausanne

	PG121	PG450	PG45	PG452	PG453	956	752	92/055 1G	92/093 2G	1871
SiO2	60.92	59.51	59.71	59.74	56.78	60.01	43.87	66.98	69.22	46.68
TiO2	1.08	1.06	0.07	1.11	1.23	1.13	1.10	0.46	0.45	1.79
Al2O3	14.02	14.65	14.30	14.64	14.64	16.19	13.25	15.86	15.41	21.41
Fe2O3	1.12	1.26	1.22	1.17	1.33	1.92	1.85	0.89	1.03	2.43
FeO	4.51	4.01	3.26	2.84	4.85	2.76	5.08	1.56	1.8	9.30
MnO	0.15	0.17	0.17	0.06	0.17	0.06	0.13	0.06	0.04	0.35
MgO	3.88	3.95	3.67	0.95	4.67	2.98	10.62	1.28	1.76	4.10
CaO	3.75	4.00	4.53	4.34	4.66	3.02	10.33	1.48	0.43	5.08
Na2O	2.56	1.85	2.09	1.62	2.08	3.19	1.26	2.51	2.43	2.42
K2O	5.78	6.39	7.30	9.00	6.76	5.73	3.92	5.26	5.3	3.01
P2O5	0.75	0.76	0.72	0.84	0.88	0.47	1.09	0.17	0.19	1.35
Total	**99.34**	**99.39**	**99.52**	**99.69**	**99.32**	**99.15**	**98.73**	**99.28**	**99.05**	**99.99**
FeTOT	6.13	5.72	4.88	4.33	6.72					12.76
LOI	0.82	1.78	1.82	3.36	1.27	1.69	6.23			
H2O+										1.81
H2O-								1.64	1.82	
CO2								1.13	0.17	0.26
Trace elements (ppm)										
Ba	2011	2103	2582	2131	2365	1971	1933	1147	1160	912
Cr	113	122	106	112	161	111	389	121	112	21
Cu						0	0	5.11	4.83	1
Ga						20	9	17	17	37
Nb	20	26	20	30	27	22	7	17.4	14.7	7
Ni	86	85	76	64	92	39	144	96	93	10
Pb	33	32	52	27	37	18	0	33	31.9	1
Rb	255	289	244	433	268	273	275	233	232	141
Sr	428	347	301	354	304	604	429	188	215	200
Th						22	11	39.1	30.8	2.2
V	105	110	94	61	127	109	238	59	55	184
Y	59	55	61	43	56	28	10	12	12	133
Zn	87	110	79	29	114	62	83	32.7	51.9	122
Zr	298	325	190	357	341	349	167	158	154	173
U						9	4	10.8	8.52	2.6
Ce						133	73			
Nd						65	33			
La						72	41			
S						68	52	59	67	
Hf						6	2	5.45	5.06	
REE: ICP-MS, CNRS CRPG Nancy										
La						75	57	33.97	37.84	21.5
Ce						168	113	67.37	74.64	55.5
Pr						23	24.2	7.63	8.45	8.3
Nd						89.1	58.4	29.07	31.81	40.3
Sm						16.4	11.1	5.1	5.78	13.2
Eu						3.07	2.41	1.14	1.2	3.2
Gd						11	8	3.76	4.02	15
Tb						1.5	1	0.48	0.49	3.2
Dy						6.8	4.1	2.3	2.402	20.6
Ho						1.36	0.74	0.402	0.454	4.45
Er						3	1.5	1.063	1.154	13.5
Tm						0.5	0.2	0.151	0.174	2.4
Yb						3	1.3	1.094	1.146	14
Lu						0.45	0.19	0.178	0.19	2.43

Tab. VI.12: Chemical data from Variscan granitoids III

Vallorcine granite - new analyses of samples from Brändlein, 1991, von Raumer unpublished
L: lower facies, H: upper facies; GP: granite-porphyry; leuc: leucocratic granite

Major elements (wt %) XRF-data University of Fribourg,

	1/B L	4 L	22 H	31 H	74 H	168 H	122 GP	1/C/1 leuc
SiO2	68.29	69.39	74.75	74.32	72.97	73.95	74.18	75.77
TiO2	0.63	0.61	0.28	0.28	0.26	0.28	0.14	0.08
Al2O3	15.21	15.22	13.65	13.55	14.29	14.61	14.7	14.49
Fe2O3	3.99	3.92	1.71	1.56	1.45	1.83	1.24	0.36
FeO	2.93	2.61	1.1	1.08	0.86	1.12	0.63	0.41
MnO	0.06	0.05	0.03	0.02	0.05	0.05	0.05	0.02
MgO	1.16	1.28	0.56	0.47	0.47	0.53	0.23	0.15
CaO	1.79	1.28	0.52	0.5	1.58	0.51	0.55	0.54
Na2O	3.35	3.02	3.22	4.51	3.3	3.69	4.33	3.87
K2O	4.87	4.8	4.82	4.97	5.29	4.33	4.42	4.09
P2O5	0.26	0.28	0.32	0.32	0.34	0.31	0.41	0.3
H2O+	0.66	0.96	0.91	1	1.7	1.05	0.95	0.74
H2O-	0.19	0.03	0.02	0.06	0.04	0.1	0.01	0.03
Total	**99.6**	**99.85**	**99.86**	**100.5**	**100**	**100.1**	**100.25**	**100.81**
Fe(tot)	6.92	6.53	2.81	2.64	2.31	2.95	1.87	0.77

Trace elements (ppm) XRF-data University of Fribourg, Earth Sciences Dept.

Nb	14	13	12	15	16	18	23	8
Zr	218	198	113	124	109	100	60	34
Y	25	27	8	15	14	11	7	3
Sr	171	167	83	84	76	60	34	26
Rb	226	229	236	262	293	289	399	225
Th	17	16	17	18	14	11	14	6
Pb	27	28	24	24	25	20	20	16
Ga	22	22	19	19	18	22	24	24
Zn	68	59	36	36	40	33	46	27
Cu	17	11	11	9	9	11	10	11
Ni	50	57	62	43	63	82	35	87
V	47	58	17	16	14	17	7	8
Cr	34	39	31	25	27	35	16	30
Ba	771	662	383	413	376	258	130	91

REE : ICP-MS, CNRS CRPG Nancy

La	38.54	36.95	21.63	22.17	20.74	16.1	15.04	4.29
Ce	83.77	78.93	47.07	45.66	46.46	34.83	32.19	9.11
Nd	53.32	32.35	19.81	19.75	18.4	13.63	13.7	3.16
Sm	7.1	7.08	4.13	4.19	4.32	3.22	3.28	1.06
Eu	1.2	1.11	0.53	0.59	0.64	0.42	0.56	0.17
Gd	5.96	6.24	3.34	3.41	3.68	2.53	2.87	0.9
Dy	4.82	5	2.19	2.56	2.72	2.16	2.32	0.89
Er	2.41	2.54	0.94	1.12	1.16	1.04	1.08	0.53
Yb	2.16	2.27	0.8	0.98	1	1.02	0.93	0.57
Lu	0.28	0.3	0.08	0.17	0.15	0.14	0.19	0.08

Tab. VI.12: Chemical data from Variscan granitoids IV

Montenvers granite (Mont Blanc)

MBT water tunnel and 1189: von Raumer, unpublished data

VS Grandes Otanes: Schouwey 1988, unpublished data

Major elements (wt %)

	MBT166	MBT167	MB T169	MBT170	MB T176	1189
SiO2	67.82	67.89	68.1	64.74	56.21	73.15
TiO2	O.56	0.55	0.57	0.63	1.08	0.28
Al2O3	15.61	16.16	14.94	15.43	20.7	14.54
Fe2O3	0.73	0.86	0.87	0.82	1.14	0.58
FeO	2.54	2.36	2.44	2.66	4.32	1.21
MnO	0.06	0.06	0.06	0.07	0.08	0.05
MgO	1.39	1.33	1.5	1.51	2.68	0.41
CaO	2.06	2.08	1.72	2.8	2.86	1.2
Na2O	2.99	3.06	2.96	3.19	2.53	3.36
K2O	4.46	4.55	4.84	4.18	5.78	4.43
P2O5	0.23	0.21	0.24	O.21	0.32	0.2
Total	**99.59**	**100.26**	**99.78**	**99.57**	**99.76**	**100.15**
FeTOT	3.55	3.48	3.58	3.77	5.94	1.93
H2O+	1.14	1.15	1.54	3.33	2.06	0.74
H2O-	0.11	o.15	0.15	0.13	0.1	0.18
Trace elements (ppm)						
Ba	839	875	929	876	1702	343
Cr	21	27	22	29	53	8
Cu	15	12	11	8	20	11
Ni	15	15	16	16	17	8
Rb	199	193	200	206	217	262
Sr	199	2O9	2O9	205	398	91
Zn	63	65	71	74	80	58
Zr	175	178	188	249	340	126

Major elements (wt %)

	VS2400	VS2410	VS2420	VS2500	VS2530	VS2600	VS2630	VS2640
SiO2	67.65	73.46	69.82	68.7	71.7	69.25	69.19	69.12
TiO2	0.56	0.12	0.45	0.53	0.3	0.45	0.45	0.47
Al2O3	15.36	14.33	14.8	15.4	14.36	15.03	15.03	15.01
Fe2O3	1.51	0.48	1.11	1.5	0.92	1.12	0.94	0.97
FeO	1.88	0.67	1.75	1.86	1.26	1.75	2.12	2.17
MnO	0.06	0.03	0.06	0.06	0.04	0.05	0.06	0.07
MgO	1.44	0.26	1.07	1.29	0.7	1.09	1.3	1.35
CaO	1.3	0.54	1.13	1.81	0.96	1.81	2.16	2.14
Na2O	2.77	3	2.97	2.58	2.96	3.07	3	2.98
K2O	4.88	5.13	4.83	4.47	5.04	4.56	4.27	4.28
P2O5	0.25	0.29	0.24	0.27	0.28	0.26	0.2	0.21
Total								
Fetot	3.6	1.23	3.05	3.57	2.32	3.07	3.3	3.38
Trace elements (ppm)								
Ba	814	296	682	743	434	651	659	659
Cr	30	12	34	36	35	34	43	54
Cu	7	2	8	17	8	7	8	8
Ga	17	16	17	17	17	19	16	15
Nb	15	14	14	16	15	18	15	14
Ni	16	5	13	15	13	15	14	15
Pb	15	20	17	17	22	16	14	15
Rb	224	241	200	199	211	191	171	177
Sr	158	72	135	173	110	164	175	173
Th	21	10	15	10	8	12	7	13
V	60	6	46	55	30	50	48	56
Y	26	15	30	27	23	27	29	29
Zn	63	16	49	59	34	50	50	46
Zr	190	60	153	163	107	152	134	141

Sample location: see Annex II

XRF-data University of Fribourg, Earth Sciences Dept.

Tab. VI.12: Chemical data from Variscan granitoids V

Montenvers granite Lognan area (Mont Blanc)
Morard 1998, unpublished data

Major elements (wt %)

Morard	95.4	97.22	97.6	97.58	96.1
SiO2	68.98	59.92	67.74	67.34	67.53
TiO2	0.43	0.81	0.48	0.57	0.52
Al2O3	14.72	16.18	15.35	15.47	15.47
Fe2O3	1.37	2.61	1.78	2.13	2.07
FeO	1.45	3.35	1.39	1.43	1.59
MnO	0.06	0.09	0.05	0.06	0.06
MgO	1.23	3.33	1.17	1.35	1.17
CaO	1.63	3.68	2.27	1.73	1.51
Na2O	3.62	2.73	3.04	4.2	4.18
K2O	4.31	3.08	4.48	3.59	3.91
P2O5	0.21	0.29	0.19	0.21	0.18
Total	**99.16**	**99.41**	**99.25**	**99.43**	**99.52**
FeTOT					
LOI	1.16	3.33	1.31	1.35	1.33

Trace elements (ppm)

Ba	795	978	917	948	1240
Cr	34	132	35	131	10
Cu	8	19	15	19	43
Ga	19	19	18	20	20
Nb	11	9	10	9	12
Ni	6	21	6	21	2
Pb	26	21	26	21	27
Rb	202	139	173	141	193
Sr	175	329	185	333	199
Th	27	13	27	9	30
V	51	152	57	150	55
Y	25	41	29	41	40
Zn	58	103	58	104	55
Zr	162	121	177	115	262

REE

La	33	-	36.5	46	-
Ce	68	-	74.5	92	-
Pr	8.3	-	8.7	11	-
Nd	29.5	-	35	42	-
Sm	6.2	-	6.8	7.9	-
Eu	0.9	-	1.2	1.1	-
Gd	6.1	-	6	7.5	-
Tb	0.8	-	1	1	-
Dy	4.3	-	4.4	4.7	-
Ho	0.7	-	0.9	1	-
Er	2.5	-	3	3.2	-
Tm	0.4	-	0.4	0.5	-
Yb	2.4	-	2.4	2.8	-
Lu	0.4	-	0.4	0.5	-

Analyses: XRF data: Centre d'analyses, University of Lausanne
REE: neutron activation, XRAL, Ottawa, Canada

Tab. VI.12: Chemical data from Variscan granitoids VI

***Lognan granite (Mont Blanc):** von Raumer, unpublished data
1839 Brévent granite (new rock type): von Raumer, unpublished data
1711 anatectic Ho-granite, Lac Noir (Aiguilles Rouges): von Raumer, unpublished data

Major elements (wt %)

	1118*	1180*	1185*	1186*	1839	1711
SiO2	73.59	73.6	75.22	76.02	72.21	69.17
TiO2	0.33	0.19	0.27	0.15	0.27	0.32
AL2O3	14.16	14.51	13.07	13.27	14.54	15.1
Fe2O3	0.79	0.62	0.81	0.55	0.68	0.54
FeO	1.68	0.97	1.38	1.08	1.42	2.15
MnO	0.04	0.04	0.04	0.07	0.04	0.05
MgO	0.75	0.52	0.63	0.52	0.35	1.35
CaO	0.76	1.55	0.79	0.55	1.6	2.35
Na2O	2.92	4.36	2.91	2.56	3.99	2.66
K2O	4.99	3.26	4.77	5.75	4.71	4.61
P2O5	0.21	0.11	0.19	0.19	0.09	0.08
Total	**101.12**	**100.44**	**100.88**	**101.31**	**100.22**	**99.44**
FeTOT	2.66	1.7	2.34	1.75	2.26	2.93
LOI	0.9	0.71	0.8	0.6		0.87
H2O+					0.26	
H2O-					0.07	0.08

Trace elements (ppm)

Ba	582	536	359	235	461	1643
Cr	18	18	16	13	19	48
Cu	15	17	14	14	7	4
Ga	15	15	18	14	20	15
Nb	8	7	12	6	19	6
Ni	16	15	19	13	7	11
Pb	19	22	16	24	19	11
Rb	182	197	203	207	236	134
Sr	74	81	67	46	102	263
Th	12	12	14	11	17	14
V	21	20	25	8	18	64
Y	38	36	41	32	45	19
Zn	49	46	49	25	35	44
Zr	128	107	123	85	171	104

REE

La	27	21	19.5	13	33
Ce	57	44	42	28.5	68.8
Pr	6.9	5.3	5.1	3.5	7.7
Nd	26.5	20	19	11.5	30
Sm	5.8	5.2	4.7	3.3	6.9
Eu	0.6	0.5	0.4	0.3	0.96
Gd	5.4	5.8	5.1	3.5	7
Tb	1.1	1.1	0.9	0.8	1.3
Dy	6.4	7	5.5	5.2	7.5
Ho	1.4	1.5	1.3	1.2	1.54
Er	4.5	5.2	4.2	3.7	4.3
Tm	0.6	0.8	0.6	0.6	0.7
Yb	4.2	4.7	3.4	3.7	4.4
Lu	0.6	0.6	0.4	0.5	0.7

Analyses: XRF data, University of Fribourg; Earth Sciences Dept.
REE: neutron activation, XRAL, Ottawa, Canada

Tab. VI.12: Chemical data from Variscan granitoids VII

Fully granitoids and gabbros (Mont Blanc)

Mollex 2003, unpublished data

Major elements (wt %)

	DM19	DM1	DM15	DM5	DM8B	DM10	FB987	FB1034
	Granodiorite		Granodiorite		granite	Gabbro	Gabbro	Gabbro
SiO2	65.66	64.90	70.73	49.71	49.62	49.53	52.23	50.14
TiO2	0.91	0.56	0.26	1.28	0.57	1.12	1.01	0.63
Al2O3	16.18	15.76	14.30	15.91	17.52	15.80	18.70	17.46
Fe2O3	4.75	4.57	1.87	9.38	6.26	9.20	7.68	6.74
MnO	0.08	0.07	0.03	0.14	0.14	0.17	0.12	0.13
MgO	2.06	3.10	0.58	9.04	9.02	8.78	6.01	8.31
CaO	3.32	3.22	0.97	7.14	8.61	9.34	6.37	9.75
Na2O	3.30	3.23	3.37	1.01	2.15	2.18	2.88	1.55
K2O	2.48	2.63	5.33	3.26	2.77	1.64	2.40	2.77
P2O5	0.20	0.21	0.26	0.28	0.14	0.22	0.25	0.17
Total	**100.06**	**100.15**	**98.65**	**99.79**	**100.26**	**99.86**	**100.11**	**100.15**
LOI	1.12	1.90	0.95	2.64	3.46	1.88	2.46	2.50

Trace elements (ppm)

V	74	80	15	194	200	227	144	191
Cr	95	74	9	464	197	363	178	183
Ni	6	4	4	116	42	50	11	37
Co	10.26	16.85	2.39	39.68	27.75	34.59	30.21	27.76
Zn	62	65	42	88	69	86	80	65
Cs	7.52	10.60	8.30	10.42	14.82	6.48	11.83	7.63
Rb	104.72	136.05	185.46	144.71	150.29	71.53	91.62	163.47
Ba	404.46	600.84	327.03	381.88	385.40	379.25	687.03	587.36
Th	0.52	11.40	10.95	4.25	2.07	4.21	5.85	2.72
U	1.38	5.18	2.36	1.17	0.55	0.92	1.63	0.61
Nb	14.51	15.27	17.19	15.88	4.05	11.06	8.11	4.13
Ta	1.08	1.64	2.13	0.89	0.25	0.62	0.53	0.24
Pb	15.68	19.41	19.52	3.89	3.34	3.90	11.59	3.93
Sr	272.73	333.54	61.48	257.53	382.44	383.43	532.95	424.24
Zr	152.61	161.85	131.74	121.04	66.69	88.27	134.20	82.97
Hf	3.43	4.34	3.70	3.58	1.73	2.80	3.07	2.00
Y	12.37	30.28	11.97	29.52	17.30	26.08	25.24	16.83

REE

La	6.02	26.61	18.01	19.27	10.54	16.33	19.26	12.10
Ce	12.47	56.51	38.32	47.00	21.62	37.03	39.77	25.85
Pr	1.62	6.89	4.72	6.32	2.78	5.02	4.87	3.29
Nd	6.28	27.14	17.59	26.53	11.76	21.13	20.04	13.92
Sm	1.38	5.79	3.75	5.85	2.71	4.93	4.26	3.19
Eu	0.99	1.03	0.33	1.47	0.89	1.37	1.25	1.06
Gd	1.36	5.65	3.23	5.40	2.99	4.76	4.30	3.22
Tb	0.25	0.86	0.43	0.83	0.47	0.71	0.66	0.49
Dy	1.77	5.02	2.14	4.80	2.81	4.27	4.11	2.96
Ho	0.38	0.97	0.36	0.99	0.61	0.88	0.86	0.60
Er	1.14	2.75	0.92	2.77	1.74	2.50	2.47	1.69
Yb	1.02	2.42	0.80	2.55	1.59	2.21	2.31	1.58
Lu	0.15	0.36	0.12	0.38	0.24	0.35	0.34	0.24

Analyses: Major elemetns XRF data, Centre d'analyses University of Lausanne
Trace elements and REE: LA-ICP-MS data, University of Lausanne

Tab. VI.12: Chemical data from Variscan granitoids VIII

Mont Blanc granite

new analyses on original samples from Marro 1986
von Raumer, unpublished data

Major elements (wt %)

	MGrI 2720	MGrI 2962	MGrIB 2885	MGrIB 3812	MGrII 2888	MGrII 3819	MR 2809
SiO2	70.81	73.2	73.09	74.18	75.35	76.5	73.12
TiO2	0.27	0.2	0.2	0.16	0.04	0.05	0.16
Al2O3	13.41	13.5	12.91	13.69	12.25	12.46	13.51
Fe2O3	2.59	2.09	1.93	1.82	1.18	1.12	2.12
FeO	1.26	0.93	0.83	0.86	0.5	0.38	1.06
MgO	0.35	0.39	0.34	0.2	0.02	0.06	0.39
MnO	0.05	0.04	0.04	0.02	0.02	0.05	0.11
CaO	1.46	1.37	1.41	1.08	0.43	0.48	1.06
K2O	4.94	4.59	4.44	4.8	5.4	4.58	4.85
Na2O	3.5	3.58	3.54	3.57	3.6	3.75	3.66
P2O5	0.17	0.15	0.15	0.14	0.1	0.11	0.15
LOI	0.83	0.66	0.57	0.4	0.27	0.46	0.58
Total	**98.38**	**99.77**	**98.62**	**99.76**	**98.66**	**99.62**	**99.71**

Trace elements (ppm)

Ba	399	462	404	515	23	16	869
Be	5	3.7	4.3	2.5	6	2.4	2.2
Co	72	45	47	51	56	66	45
Cr	5	5	37	6	9	6	36
Cu	15	5	8	5	8	5	9
Ga	12	13	5	12	12	14	8
Nb	19	20	18	17	25	23	11
Ni	5	5	5	5	5	5	5
Rb	304	233	213	217	418	213	142
Sc	7.4	7.3	6	5.5	4.4	3.9	4.09
Sr	92	128	107	79	11	15	174
V	16	16	14	9	5	5	12
Y	50	41	35	35	58	34	20
Zn	45	36	31	36	22	24	82
Zr	194	118	126	147	90	96	113
Th	31.3	29.5	26.6	26.9	48	36.4	18.5
U	11.9	12.1	7.4	9.6	10.3	10.6	8.8

REE

La	48.6	39.8	30.9	49	34.1	18.4	32
Ce	102	76.4	61.3	97.7	81.7	40.9	65.4
Pr	11.4	8.6	6.3	10.5	9.9	4.8	7.2
Nd	41.8	30.7	23.3	36.1	35.6	17.8	24.5
Sm	9.3	6.6	5.1	6.6	9.4	4.7	4.9
Eu	0.85	0.75	0.66	0.81	0.1	0.05	0.95
Gd	9.5	6.7	5.8	6.3	10.2	5.1	5
Tb	1.7	1.2	1	0.9	1.9	1	0.8
Dy	9.9	6.9	6.3	5.7	11.4	6.1	4.2
Ho	1.98	1.47	1.29	1.16	2.29	1.42	0.84
Er	6.1	4.8	3.5	3.8	6.3	3.8	2.6
Tm	0.9	0.7	0.6	0.7	1.1	0.6	0.4
Yb	6	4.9	3.9	4.7	6.9	4.1	2.7
Lu	0.9	0.67	0.65	0.72	1	0.65	0.45

Sample location: see Annex II
Analyses: Major elemetns XRF data, Centre d'analyses University of Lausanne
REE: neutron activation, XRAL, Ottawa, Canada

SAMPLE LOCATION

Coordinates: **CH**: swiss coordinates; **FR**: french coordinates;
MBT: distance in meters from the beginning of the water tunnel (La Fouly, Val Ferret)

Early Palaeozoic granitoids

Ho-Bi-gneiss	Coord.
AW1	FR 950.240/120.670
AW6	FR 949.950/119.450
AW29	FR 950.350/121.070
AW55	FR 950.020/121.830
1858	CH 555.060/097.215
1859	CH 555.110/097.210
1860	CH 555.135/097.190
1861	CH 555.165/097.180
1862	CH 555.200/097.170

KF-gneiss	
AW2	FR 950.270/120.530
AW15	FR 949.820/121.225
AW33	FR 950.480/122.420
AW36	FR 950.670/122.000
AW37	FR 950.000/122.380
AW45	FR 949.350/121.480
AWAR1	CH 560.100/102.890
AWAR2	CH 560.130/102.870

KF-gneiss	Coord.
AWAR3	CH 559.105/102.900
AWAR4	CH 560.075/103.135
AWAR5	CH 559.110/103.530
AWAR6	CH 559.295/102.620
AWAR7	CH 560.650/102.210
AWAR8	CH 559.650/104.050
AWAR9	CH 559.410/103.190
AWAR10	CH 559.450/103.080
AWAR11	CH 558.210/101.440
AWAR12	CH 558.350/101.440
B293	CH 568.970/101.690
B294	CH 568.980/101.675
B296	CH 568.805/101.610
B297	CH 568.805/101.515
B300	CH 568.660/101.490
B301	CH 568.485/101.480
B302	CH 568.670/101.440
B303	CH 568.290/101.515

KF-gneiss	Coord.
B313	CH 566.980/097.940
B313-1	CH 566.300/098.265
N186	CH 568.930/099.740
N187	CH 568.900/099.770
N188	CH 568.735/099.635
N189	CH 568.570/099.675
N190	CH 568.480/099.715
N191	CH 568.330/099.880
N192	CH 568.370/100.150
MBT70	water tunnel 13456m
MBT73	water tunnel 13672m
MBT74	water tunnel 13685m
MBT75	water tunnel 13835m
MBT77	water tunnel 14094m
MBT174	water tunnel 14450m
MBT175	water tunnel 14333m
MB784	CH 566.490/098.040
MB1184	FR 957.720/118.150
MB1187	CH Moraine Petoudes

Amphibolites, Eclogites, Ultramafic rocks

Amph	Coord.
1501	CH 560.750/103.780
1505	CH 560.840/103.840
1511	CH 561.060/103.900
1514	CH 560.790/103.550
1515	CH 560.780/103.540
1518	CH 560.940/103.500
1519	CH 560.800/103.610
1520	CH 560.800/103.610
1521	CH 560.820/103.640
1526	CH 559.880/103.680
1527	CH 559.850/103.840
1532	CH 560.910/104.225
1545	CH 558.440/100.640
1547	CH 558.440/101.070
1601	CH 558.830/100.630
1604	CH 558.830/100.630

Eclogites	Coord.
1820	FR 949 810/116 570
1821	FR 949 810/116 570
1822	FR 949 810/116 570
1824	FR 949 810/116 570
1825	FR 949 810/116 570

Eclogites Béchat	Coord.
TB1	FR 949.212/118.434
TB2	FR 949.220/118.445
TB3	FR 949.175/118.446
TB4	FR 949.123/118.430
CV2.1	FR 949.075/117.120
CV2.2.	FR 949.085/117.117
CV2.4	FR 949.050/117.165
CV3.1	FR 949.356/117.165
CV3.2	FR 949.352/117.152
CV3.3	FR 949.348/117.152
CP2	FR 949.160/118.013
CP3	FR 949.166/118.012
CP4	FR 949.176/118.008
CP5	FR 949.180/118.010
CP6	FR 949.200/118.020
CP7	FR 949.205/118.034
CP8	FR 949.224/118.025
CP9	FR 949.226/118.020
CP11	FR 949.120/118.015
CP12	FR 949.110/118.016
CP13	FR 949.080/118.044
CP14	FR 949.o75/118.045

Ultramafic	Coord.
1725	FR 949 580/117 390
1727	FR 949 580/117 390
1758	FR 949 600/116 870
1770	FR 949 570/117 260
1774	FR 949 530/117 380
1801	FR 949 450/116 460
FS22	FR 950.000/121.120
FS23	FR 950.000/121.120
FS25	FR 950.000/121.120

Variscan granitoids

Durb.-Monz.	Coord.
MBT34	Water Tunnel 937m
MBT37	Water Tunnel 1947m
MBT44	Water Tunnel 1470m
MBT124	Water Tunnel 1490m
MBT125	Water Tunnel 1465m
MBT134	Water Tunnel 2617m
MBT139	Water Tunnel 2860m
MBT141	Water Tunnel 2888m
MBT148	Water Tunnel 3285m
MBT196	Water Tunnel 2498m
MBT199	Water Tunnel 2342m
PG121	CH 571.300/083.925
PG450	CH 571.680/084.810
PG451	CH 571.705/084.670
PG452	CH 571.530/084.700
PG453	CH 571.610/084.720
Lac Cornu	
1871	FR 949.420/117.020
Vallorcine	
1/B L	CH 568.250/110.950
4 H	CH 567.300/109.910

Vallorcine	Coord.
22 H	CH 562.560/102.400
31 H	CH 562.200/102.260
74 H	CH 561.470/102.080
168 H	CH 561.420/100.050
122 GP	CH 564.810/106.700
1/C/1 leuc	CH 568.250/110.950
Montenvers	
MBT166	Water Tunnel 14900m
MBT167	Water Tunnel 14798m
MB T169	Water Tunnel 14753m
MBT170	Water Tunnel 14672m
MB T176	Water Tunnel 15027m
1189	FR 957.080/117.960
VS2400	CH 564.300/096.860
VS2410	CH 564.300/096.850
VS2420	CH 564.310/096.380
VS2500	CH 564.380/096.730
VS2530	CH 564.390/096.710
VS2600	CH 564.500/096.680
VS2630	CH 564.540/096.670
VS2640	CH 564.540/096.640

Montenvers	Coord.
M95.4	CH 561.345/091.870
M97.22	CH 562.140/091.505
M97.6	CH 561.055/089.530
M97.58	CH 561.130/090.000
M96.1	CH 561.875/091.810
Lognan	
1118	FR 957.400/117.920
1180	FR 958.130/117.370
1185	Moraine Petoudes
1186	Moraine Petoudes
Brévent	
1839	FR 948.960/113.680
Lac Noir	
1711	FR 949.890/117.290
Mt Bl granite	
MGrI2720	CH 567.220/094.780
MGrI2962	CH 571.015/094.480
MGrIB2885	CH 570.880/096.630
MGrIB3812	CH 569.475/092.460
MGrII2888	CH 570.880/096.630
MGrII3819	CH 570.420/094.480
MR2809	CH 574.495/102.915

Metasediments

Graywackes	Coord.
1661	CH 561.600/107.010
1663	CH 561.440/105.880
1666	CH 562.560/106.090
1674	CH 557.910/090.790
1675	CH 557.920/090.860
1676	CH 558.180/100.070
1679	CH 557.490/100.045
1681	CH 558.240/100.000
1684	CH 558.020/099.895
1688	CH 557.500/099.940
1691	CH 557.390/099.560

Graywackes	Coord.
1694	CH 562 020/105.280
1700	CH 561.480/105.000
1705	CH 560.110/101.860
1707	CH 950.120/117.250
1734	CH 561.890/104.920
FXM1	FR 125.600/952.175
FXM2	FR 125.600/952.175
FXM3	FR 125.600/952.175
FXM4	FR 125.600/952.175
FXM5	FR 126.000/951.675
FXM6	FR 126.000/951.675

Graywackes	Coord.
FXM7	FR 126.000/951.675
FXM8	FR 125.800/952.200
FXM9	FR 125.800/952.225
FXM10	FR 125.800/952.225
FXM11	FR 125.600/952.350
FXM12	FR 125.600/952.350
KS134	CH 561.475/104.920
KS143	CH 560.750/103.250
KS156	CH 560.725/103.400
SDU6	CH 550.260/101.205

Metapelites	Coord.
1040	CH 560.563/102.549
1082	CH 559.324/101.827
1124	CH 559.295/101.785
1126	CH 559.210/101.770
1303	CH 950.060/117.150
1326	CH 560.614/102.543
1328	CH 560.412/102.586
1331	CH 560.320/102.734
1334	CH 560.075/101.925
1339	CH 560.017/103.408
1340	CH 560.019/103.437
1348	CH 559.849/103.702
1350	CH 559.324/101.827
1351	CH 559.324/101.827
1352	CH 559.324/101.827
1353a	CH 559.867/103.678
1388b	CH 561.090.103.960
1388c	CH 561.090/103.960
1388d	CH 561.090/103.960
1391	CH 561.090/103.960

Metapelites	Coord.
1394	CH 560.380/102.660
1428	CH 563.220/108.790
1430	CH 562.750/108.050
1486	FR 562.875/108.275
1575	FR 950.050/122.200
1577	FR 950.050/122.200
1578	FR 950.050/122.200
1582	FR 953.180/119.390
1584	FR 953.050/119.960
1603	CH 558.790/100.530
1605	CH 558.790/100.530
V27	water tunnel 1000m
V31	water tunnel 600m
V33	water tunnel 394m
V34	water tunnel 432m
V52	water tunnel 1641m
V54	water tunnel 1500m
V58	water tunnel 1220m
V93	water tunnel 987m
V106	water tunnel 2000m

Metapelites	Coord.
V109	water tunnel 2180m
FS1	FR 949.525/120.200
FS2	FR 949.525/120.200
FS3	FR 949.525/120.200
FS4	FR 949.525/120.200
FS5	FR 949.525/120.200
FS6	FR 949.525/120.200
FS7	FR 949.525/120.200
FS8	FR 949.525/120.200
FS9	FR 949.525/120.200
FS10	FR 950.000/120.450
FS11	FR 950.000/120.450
FS12	FR 950.005/120.350
FS13	FR 950.005/120.350
FS14	FR 950.005/120.650
FS15	FR 950.005/120.650
FS16	FR 950.000/122.175
FS17	FR 950.000/122.175
FS18	FR 950.000/122.175
FS19	FR 950.000/122.175

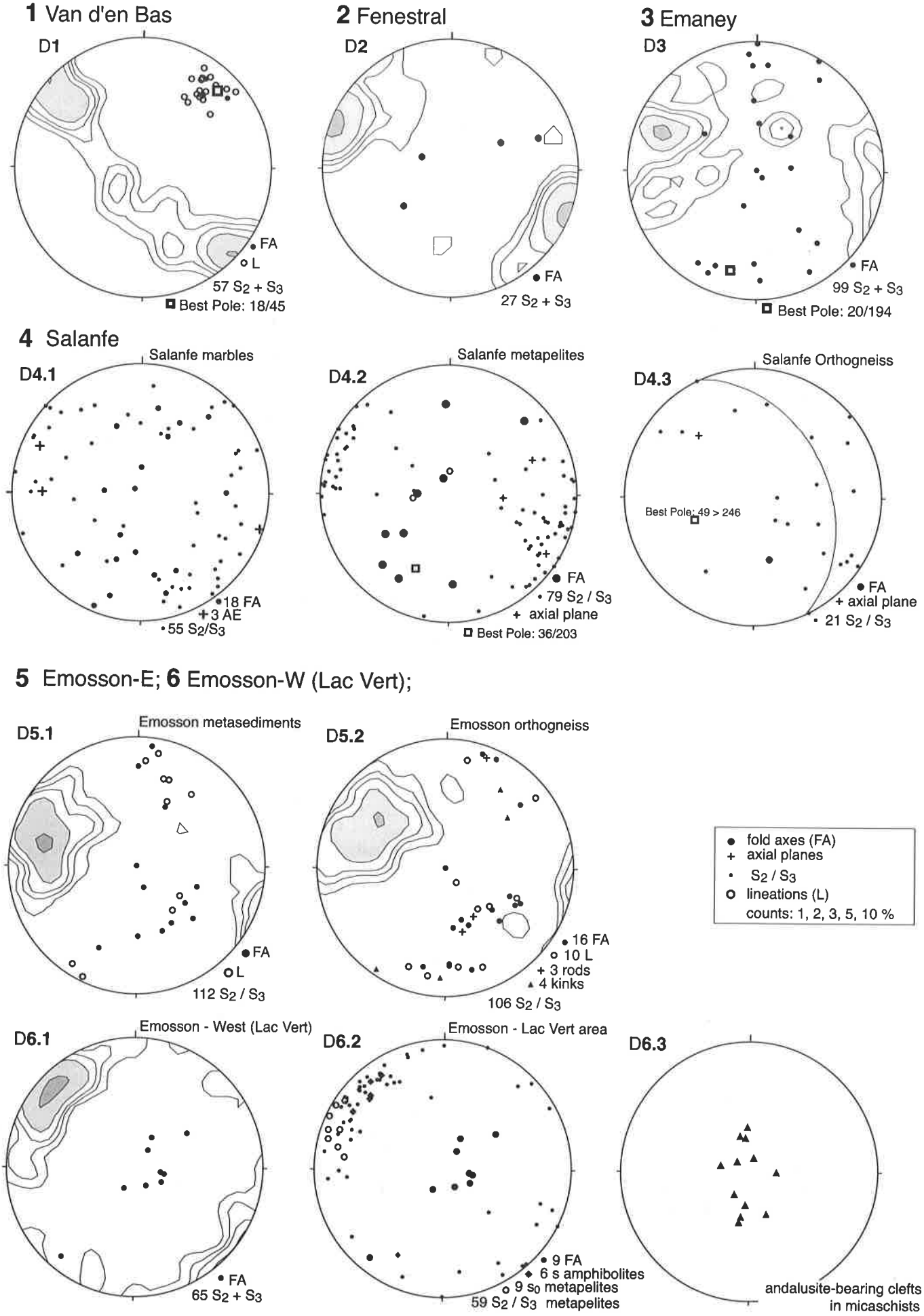
1 Van d'en Bas
D1
FA
L
57 S2 + S3
Best Pole: 18/45
2 Fenestral
D2
FA
27 S2 + S3
3 Emaney
D3
FA
99 S2 + S3
Best Pole: 20/194
4 Salanfe
Salanfe marbles
D4.1
18 FA
3 AE
55 S2/S3
Salanfe metapelites
D4.2
FA
79 S2 / S3
axial plane
Best Pole: 36/203
Salanfe Orthogneiss
D4.3
Best Pole: 49 > 246
FA
axial plane
21 S2 / S3
5 Emosson-E; 6 Emosson-W (Lac Vert);
D5.1
Emosson metasediments
FA
L
112 S2 / S3
D5.2
Emosson orthogneiss
16 FA
10 L
3 rods
4 kinks
106 S2 / S3
fold axes (FA)
axial planes
S2 / S3
lineations (L)
counts: 1, 2, 3, 5, 10 %
D6.1
Emosson - West (Lac Vert)
FA
65 S2 + S3
D6.2
Emosson - Lac Vert area
9 FA
6 s amphibolites
9 s0 metapelites
59 S2 / S3 metapelites
D6.3
andalusite-bearing clefts
in micaschists

7 Tré les Eaux

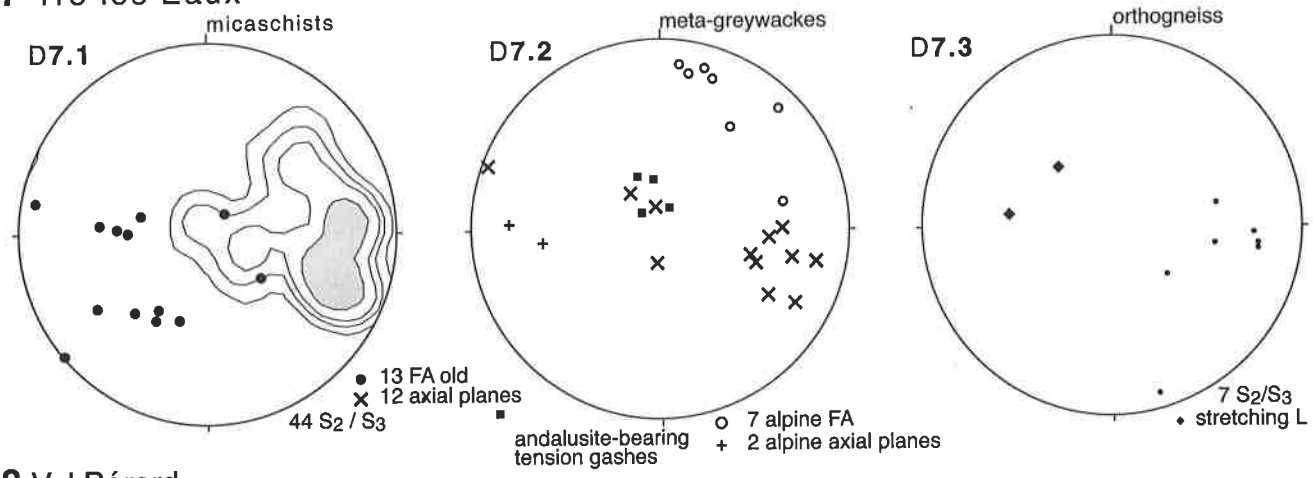

8 Val Bérard

9 Combe de Balme

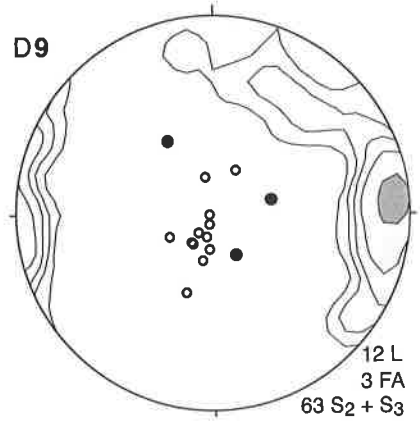

10 Lac Cornu

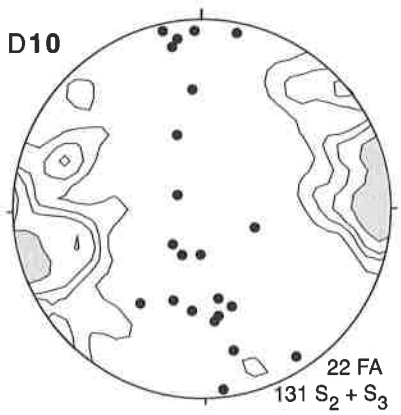

11 Cheserys

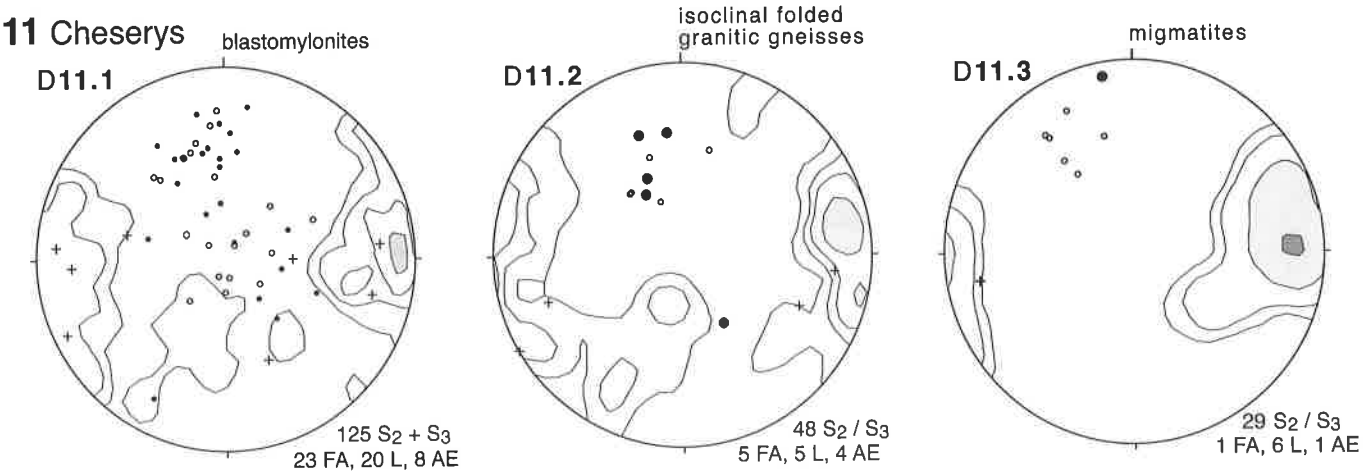

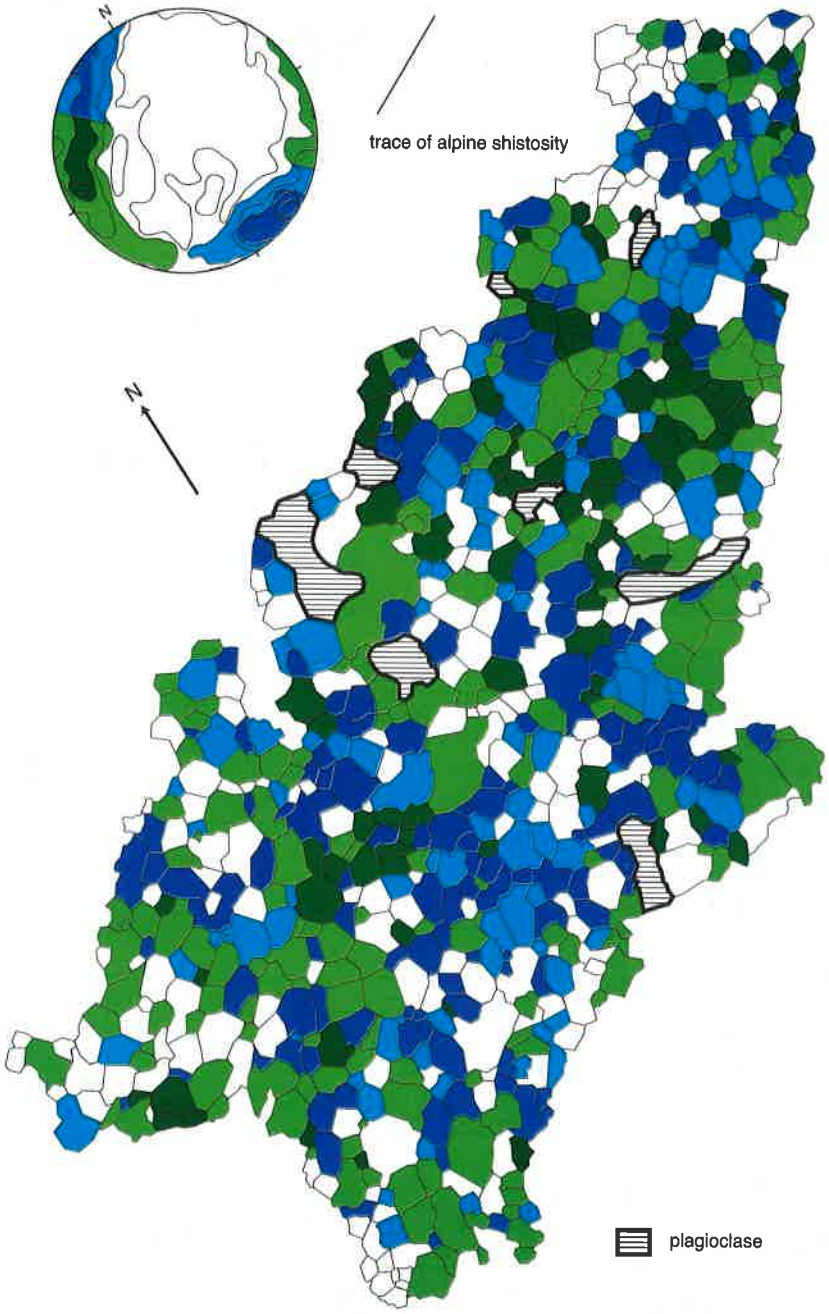

Fig.6.03
Recrystallisation of a former subround granitic quartz grain into a flattened quartz aggregate (length 1 cm) of polygonal quartz grains of Alpine age (see **Photo 3.33**). Statistical distribution analysis of optical c-axes (733 measures on optical universal stage), showing distribution in two main plot maxima (170°, 270°). Colouring: for the 170° maximum: darc green: 3-5% densities, green 1-2% densities; for the 270° maximum: dark blue: maximum 3-5% densities, light blue: 1-2% densities. White: oblique grains. Horizontal pattern: plagioclase.
*Recristallisation d'un ancien grain de quartz granitique arrondi en un aggrégat allongé (1 cm de longueur) de grains polygonaux (**Photo 3.33**). 733 grains de quartz, Analyse statistique d'orientation d'axes optiques c (733 mesures sur platine universelle optique), indiquant une distribution en deux maxima (170°, 270°). Couleurs: Maximum à 170°: Vert foncé - densités de comptage 3-5%, vert clair - densités 1-2% correspondantes. Maximum à 270°: bleu foncé - densités 3-5%, bleu clair - densités 1-2% correspondantes. Blanc: Grains obliques. Hachure horizontale: grains de plagioclase.*

Geological Maps contained in the pocket of this volume:
Cartes géologiques contenues dans la pochette du volume:

Annex III: Geological Map 1: 10 000 Emosson East
Carte géologique 1 : 10 000 Lac Emosson Est

Annex IV: Geological Map 1 : 10 000 Emosson West
Carte géologique 1 : 10 000 Lac Emosson Ouest

Annex V: Geological Map 1 : 10 000 Lac Vert / Vieux Emosson
Carte géologique 1 : 10 000 Lac Vert / Vieux Emosson

Annex VI: Geological Map 1 : 25 000 Val Bérard
Carte géologique 1 : 25 000 Val Bérard

Annex VII: Geological Map 1 : 5 000 Lac Salanfe
Carte géologique 1 : 5 000 Lac Salanfe

Annex VIII: Geological Map 1 : 10 000 Lac Cornu / Aiguilles Rouges massif
Carte géologique 1 : 10 000 Lac Cornu / Aiguilles Rouges massif

Annex IX: Geological Map 1 : 25 000 Lognan / Mont Blanc massif
Carte géologique 1 : 25 000 Lognan / Mont Blanc massif

Annex X: Geological Map 1 : 25 000 Trient / Mont Blanc massif
Carte géologique 1 : 25 000 Trient / Mont Blanc massif

No. 28 HÜRLIMANN A., BESSON-HURLIMANN A and MASSON H. 1995. Stratigraphie et tectonique de la partie orientale de l'écaille de la Gummfluh (Domaine Briançonnais des Préalpes). 132 pp. 62 text-figs., 39 pl.., 6 maps.

No. 29 DOBMEIER C. 1996. Die variskische Entwicklung des südwestlichen Aiguilles Rouges Massives (Westalpen, Frankreich). 191 pp. 70 text-figs., 18 tables., 1 map.

No. 30 BAUD A., POPOVA I., DICKINS J.M., LUCAS S. and ZAKHAROV Y. 1997. Late Paleozoic and early Mesozoic circum-Pacific events : biostratigraphy, tectonic and ore deposits of Primoryie (far East Russia). IGCP Project 272. 202 pp., 71 text-figs., 48 pls.

No. 31 ARMANDO G. 1999. Intracontinental alkaline magmatism : geology, petrography, mineralogy and geochemistry of the Jebel Hayim Massif (Central High Atlas, Morocco). 106 pp. 51 text-figs., 23 tab., 1 map.

No. 32 DEZES P. 1999. Tectonic and metamorphic evolution of the Central Himalayan Domain in Southeast Zanskar (Kashimr, India). 145 pp., 89 text-figs., 1 map.

No. 33 AMODEO F. 1999. Il Triassico terminale- Giurassico del Bacino Lagonegrese. Studi stratigrafici sugli Scisti Silicei della Basilicata (Italia meridionale). 160 pp., 50 text-figs., 10 pl.

No. 34 SAVARY J. and GUEX J. 1999. Discrete biochronological scales and Unitary Associations: Description of the BioGraph computer program. 282 pp. 21 text-figs.

No. 35 GIRARD M. 2001 . Metamorphism and tectonics of the transition between non metamorphic Tethyan Himalaya sediments and the North Himalayan Crystalline Zone (Rupshu area, Ladakh, NW India). 96 pp., 7 pl.

No. 36 STAMPFLI G. M. 2001. Geology of the western Swiss Alps, a guide-book. 195 pp., 67 text-figs., 7 pl.

No. 37 REY D. 2002. Shear2F, un logiciel de modélisation tectonique. 52 pp., 122 text-figs, 1 CD-Rom.

No. 38 TEMGOUA E. 2002. Cuirassement ferrugineux actuel de bas de versant en zone forestière humide du Sud-Cameroun. 134 pp., 83 text-figs., 4 pl.

No. 39 RAKUS M. and GUEX J. 2002. Les ammonites du jurassique inférieur et moyen de la dorsale tunisienne. 217 pp., 109 text-figs., 33 pl.

No. 40 ROBYR M. 2002. Thrusting, extension and doming in the High Himalaya of Lahul-Zanskar area (NW India): structural and pressure-temperature constraints. 127 pp., 62 text-figs., 1 pl.

No. 41 CARRUPT E. 2003. New stratigraphic, geochemical and structural data from the Val Formazza – Binntal area (Central Alps). 116 pp., 46 text-figs., 3 pl.

Annex IV

Mémoires de Géologie (Lausanne) Vol. 42, 2004

Geological Map of the pre-Mesozoic Basement, eastern part of Lac Emosson, Aiguilles Rouges massif

Carte géologique du socle pré-Mésozoique partie Est du Lac Emosson Massif des Aiguilles Rouges

1 : 10 000

Jürgen F. von Raumer, Karin Schmocker

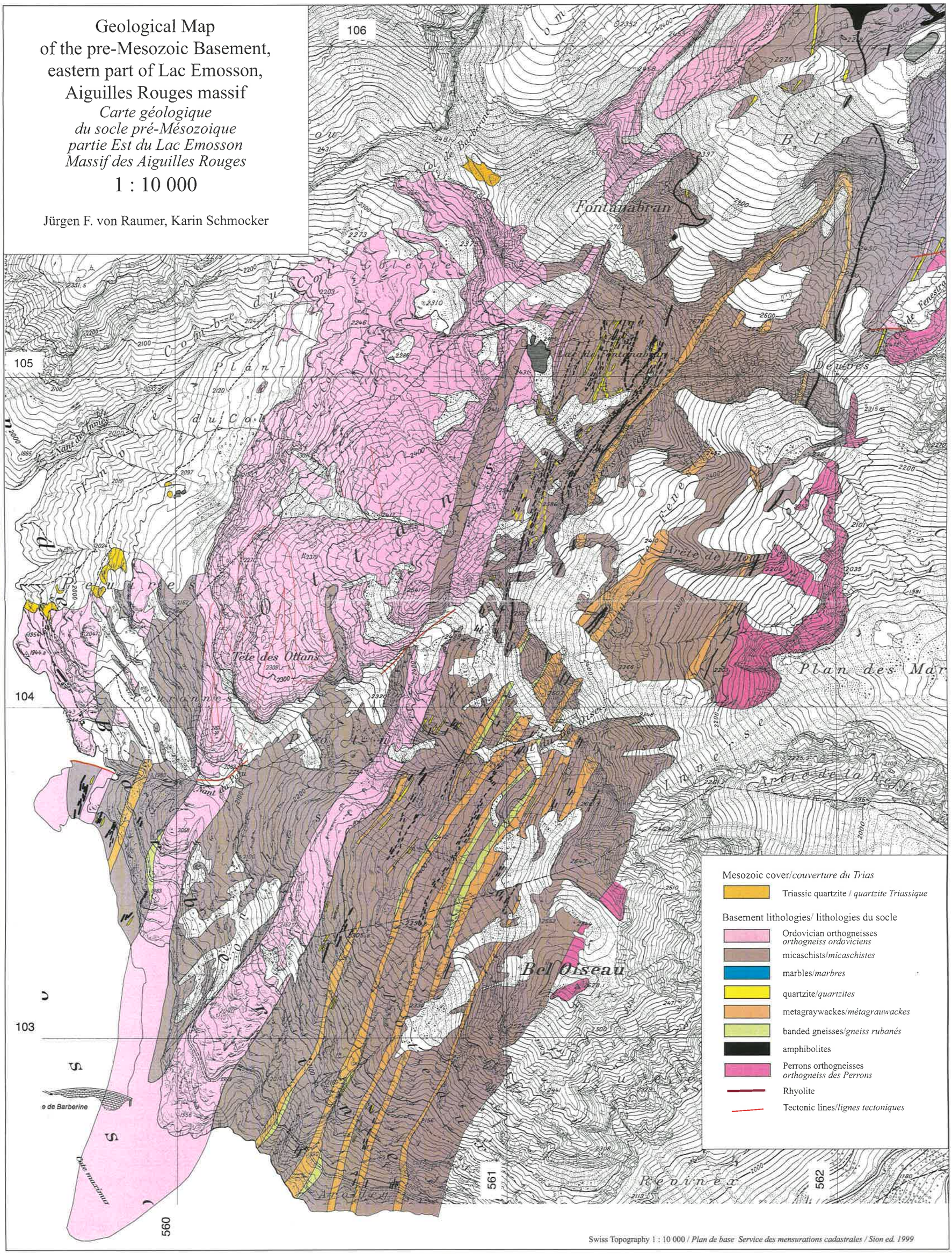

Swiss Topography 1 : 10 000 / *Plan de base Service des mensurations cadastrales / Sion ed. 1999*

Geological Map of the pre-Mesozoic Basement, western part of Lac Emosson, Aiguilles Rouges massif

Carte géologique du socle pré-Mésozoïque partie Ouest du Lac Emosson, Massif des Aiguilles Rouges

1: 10 000

Jürgen F. von Raumer, Stéphane Dupasquier

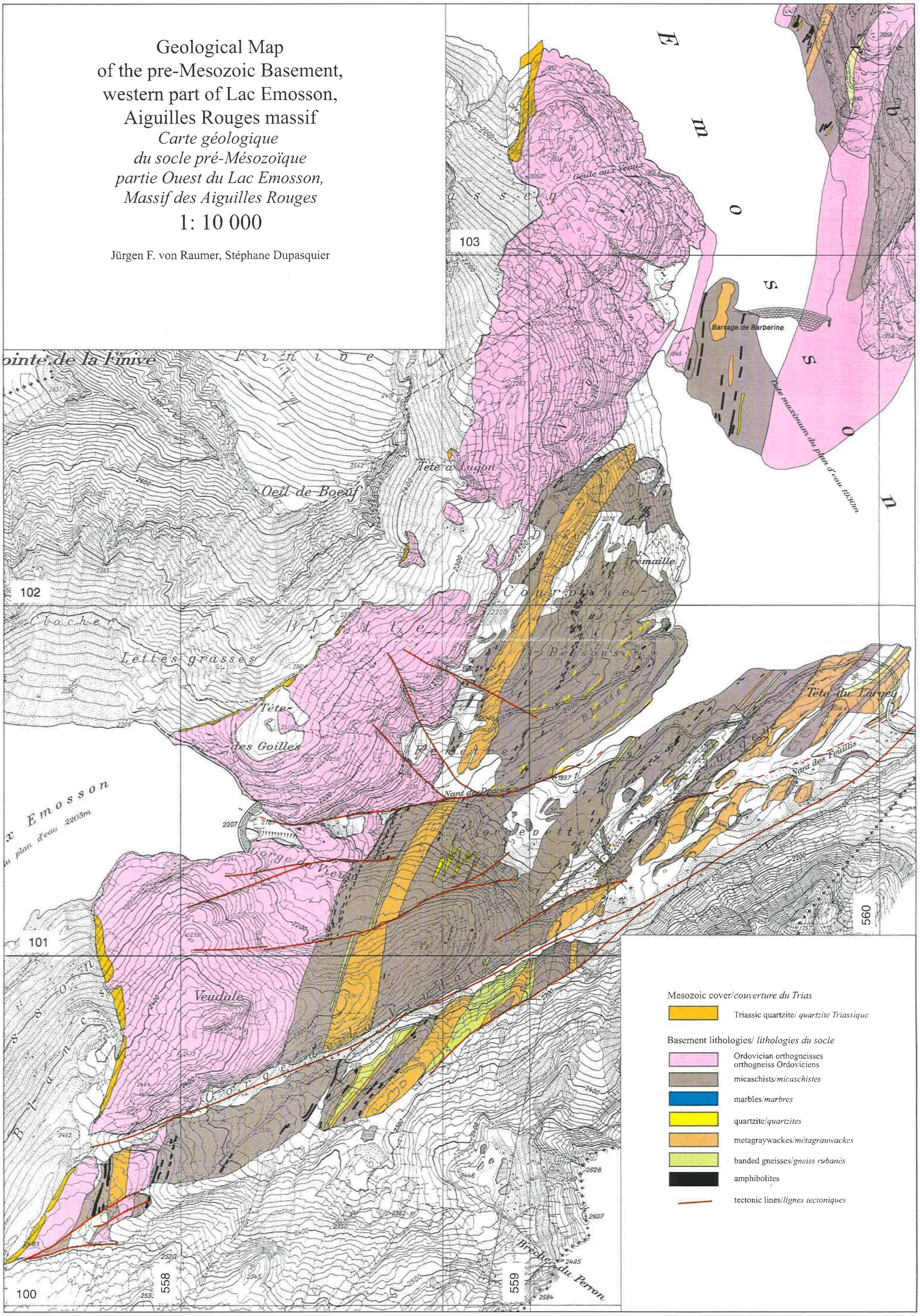

Swiss Topography 1 : 10 000 / *Plan de base Service des mensurations cadastrales / Sion ed. 1999*

Annex VI

Mémoires de Géologie
(Lausanne) Vol. 42, 2004

(sheet Emosson West) - Annex IV

Geological Map
Basement of the Lac Vert area
Aiguilles Rouges massif

Carte géologique du socle
des alentours du Lac Vert
Massif des Aiguilles Rouges

1 : 10 000

J. von Raumer
M. von der Crone, P. Häberle, B. Loup, R. Mayoraz

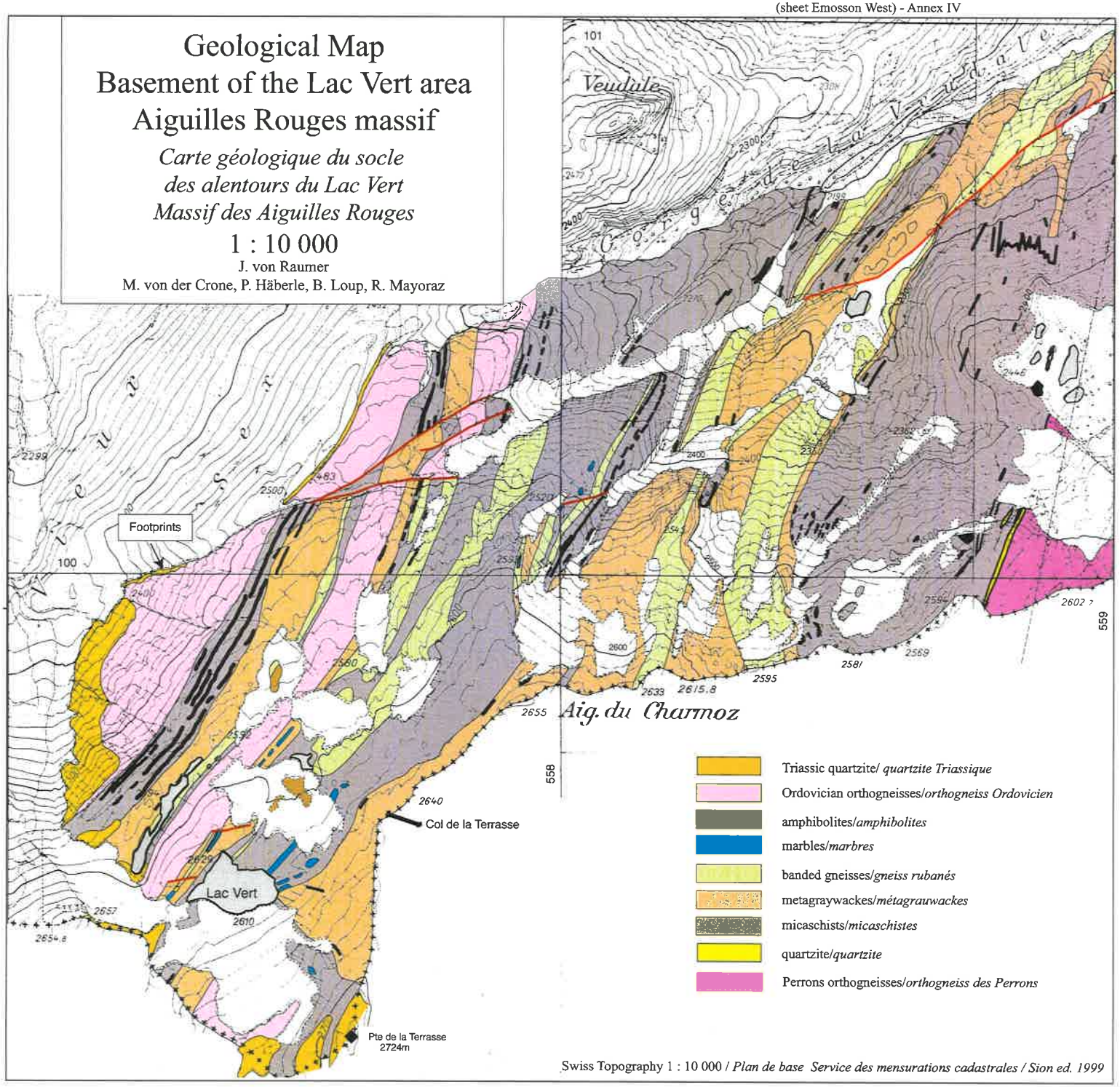

Swiss Topography 1 : 10 000 / *Plan de base Service des mensurations cadastrales / Sion ed. 1999*

Geological map of the pre-Mesozoic basement Val Bérard - Tré les Eaux (Central Aiguilles Rouges)

Carte géologique de Val Bérard - Tré-les-Eaux (Aiguilles Rouges centrales)

1 : 20 000

Jürgen F. von Raumer
Sébastien Fracheboud, Birgit Kaspar, François-Xavier Marquis,
Bernhard Schulz, Bernhard Wettlaufer, Angela Wirsing
with details for Aig. de Belvédère from Corbin & Oulianoff (1928)

Lakes/*Lacs*
Moraines, snow-fields, scree
moraines, nevés, éboulis

undifferentiated Mesozoïc cover
Mésozoïque indifférencié
Triassic autochtonous cover
Trias autochthone

Bi-plg-gneiss
Gneiss à biotite et plagioclase
Micaschist/*micaschiste*
Metagreywacke
méta-grauwacke
Quartzite/*quartzite*
Marble/*marbre*
Amphibolite/*amphibolite*

Ordovician orthogneisses
orthogneiss Ordoviciens
Ho-Bi-gneisses
Gneiss à biotite et hornblende
Garnet-amphibolite and/or eclogite
Amphibolite à grenat ou méta-eclogite
Ultramafic rock/*Ultramafite*
migmatitic gneisses
gneiss migmatiques
leucocratic gneiss/*gneiss clair*
Leucogranite/*granite leucocrate*
mylonitic Variscan orthogneisses
Orthogneiss Varisques mylonitisés

Tectonic line/ *faille*

500m

126
125
124
123
122
121
120

949 950 951 952 953

Topographie IGN 1949
Feuille Chamonix 1-2, 1:20 000

Geological Map of the Lac Cornu area (Aiguilles Rouges massif)

1 : 10 000

Carte Géologique des environs du Lac Cornu (Massif des Aiguilles Rouges)

Jürgen F. von Raumer
Christoph Dobmeier, Philippe Gay

Basement lithologies/ lithologies du socle

- Ordovician orthogneisses *orthogneiss ordoviciens*
- micaschists/*micaschistes*
- banded gneisses/*gneiss rubanés*
- marbles/*marbres*
- grt-gneiss/*gneiss à grenat*
- amphibolites/meta-eclogites/ *amphibolites/méta-eclogites*
- ultramafic rocks/*ultramafites*
- leucogranite/*granite leucocrate*
- leuco-gneiss/*gneiss à muscovite*
- Tectonic lines/*lignes tectoniques*

Base topographique: Feuille Chamonix 5-6 1:20 000, IGN 1949

Annex IX

Mémoires de Géologie (Lausanne) Vol. 42, 2004

Geological Map of the Salanfe area (Aiguilles Rouges massif)

Carte géologique des environs de Salanfe (massif des Aiguilles Rouges)

Massimo Chiaradia and Jürgen F. von Raumer

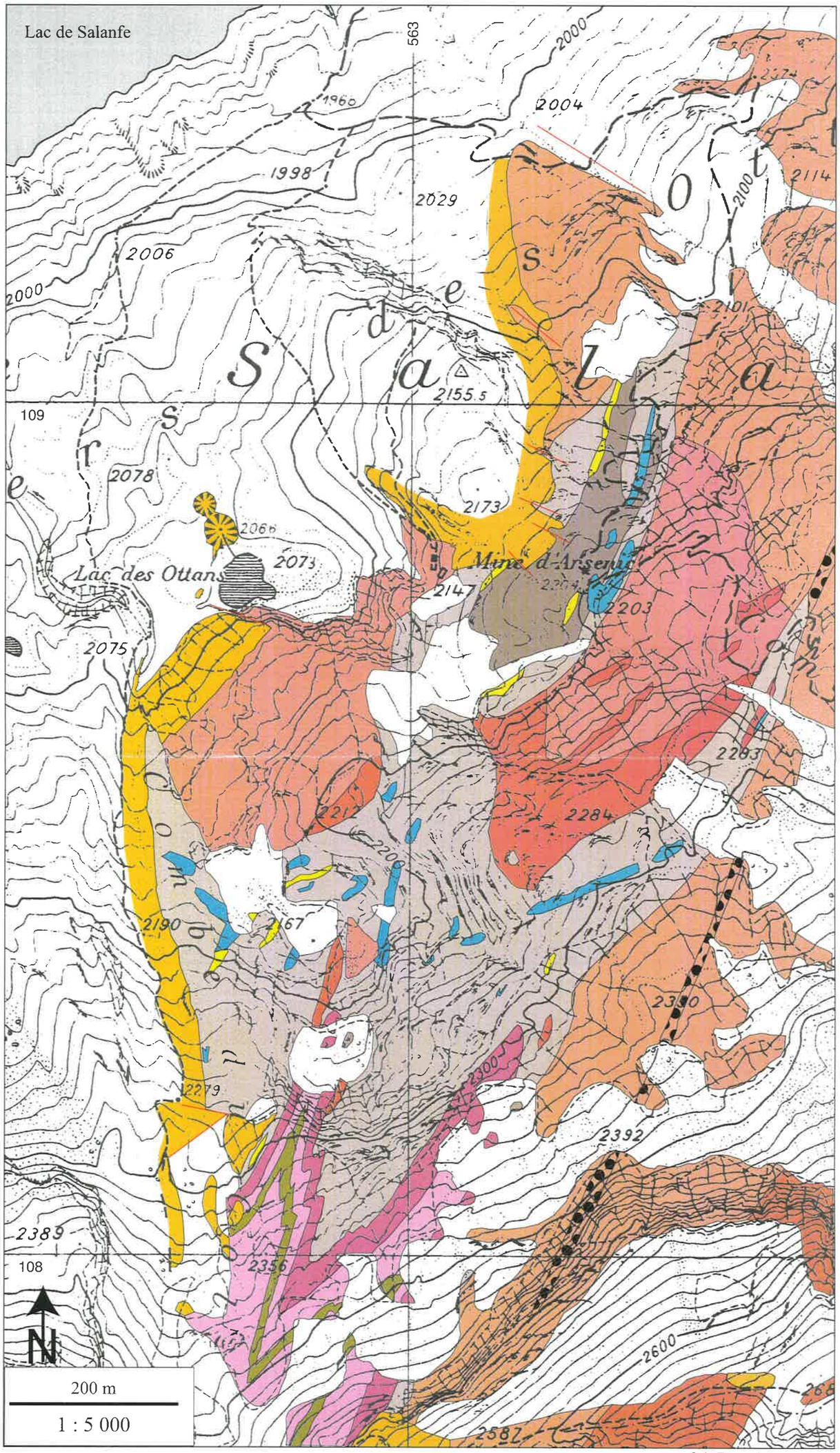

a) paragneiss / *paragneiss*
b) micaschists / *micaschistes*

marble/skarns
marbres/skarns

quartzite/*quartzites*

Triassic cover
couverture triassique

a) Kf-augen-gneiss /*gneiss oeillés*
b) musc-schists/*schistes à muscovite*
c) fine-grained gneiss/*gneiss microgrenus*

a) Bi-orthogneiss/orthogneiss à biotite
b) Bi-orthogneiss with enclaves/*gneiss à enclaves*

a) leucogranite/*leucogranites*
b) diatexite/*diatexites*

rhyolitic dykes
filon rhyolithique

Swiss Topography
Service des mensurations cadastrales / Sion
edition 1999

Annex X

Mémoires de Géologie (Lausanne) Vol. 42, 2004

Geological map of the Trient area pre-Mesozoic basement (Mont Blanc massif)

Carte géologique des alentours du glacier de Trient (Massif du Mont Blanc)

1 : 20 0000

Jürgen F. von Raumer
Wolfgang Bauer, Thomas Nähr

Mesozoic cover/*couverture du Trias*

- Triassic quartzite / *quartzite Triassique*

Basement lithologies/ *lithologies du socle*

- Ordovician orthogneisses *orthogneiss ordoviciens*
- metasediments/*méta-sédiments*
- marbles/*marbres*
- leucogranites/*granites leucocrates*
- Perrons orthogneisses *orthogneiss des Perrons*
- Mont Blanc granite *granite du Mont Blanc*
- Tectonic lines/*lignes tectoniques*

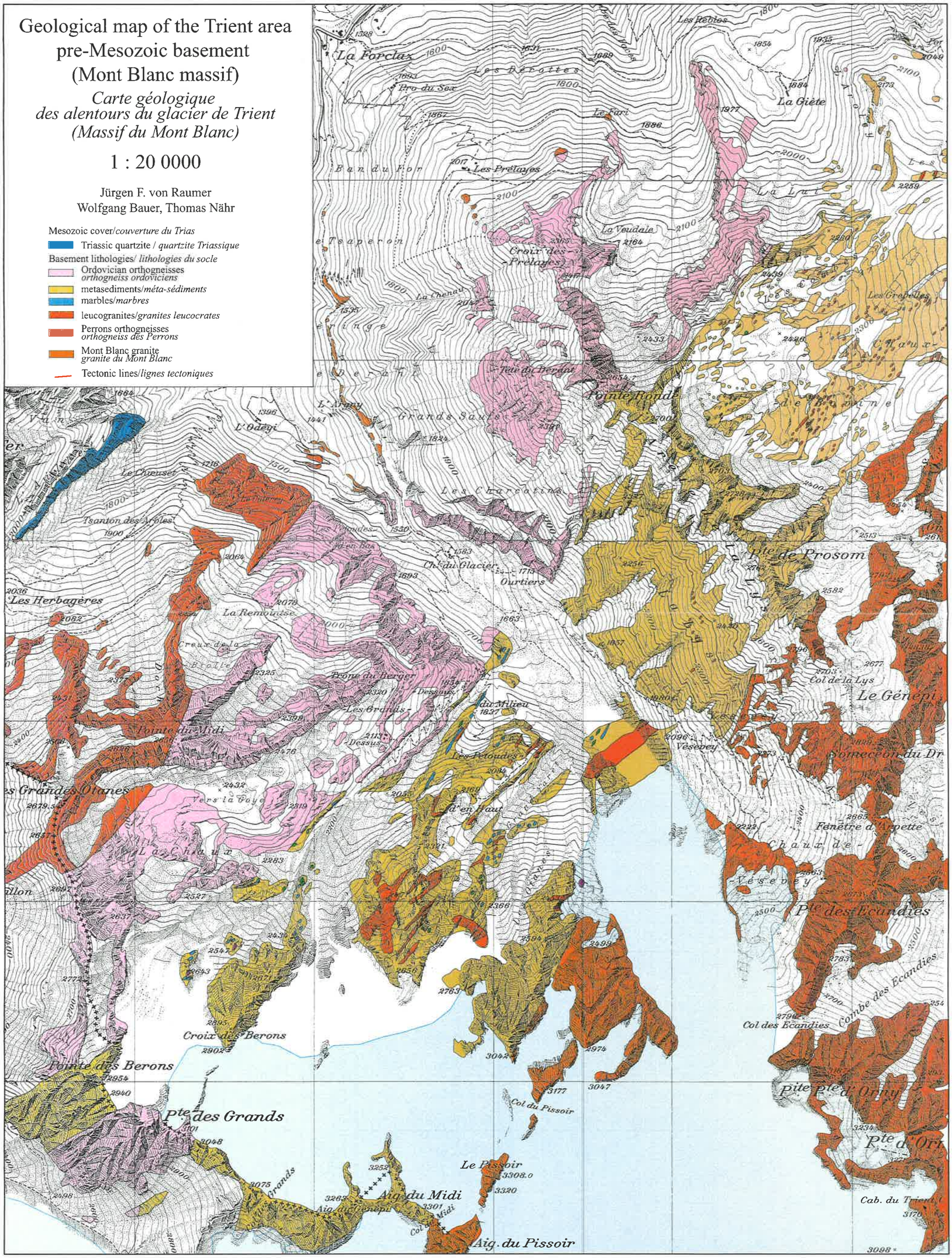

100
99
98
97
96
95

565 566 567 568 569

Annex XI
Mémoires de Géologie (Lausanne) Vol. 42, 2004

Geological map of the Montagne de Lognan area (NW Mont-Blanc massif)

Carte géologique de la Montagne de Lognan (versant NW du massif du Mont-Blanc)

1:20'000

Alain Morard, Jürgen von Raumer & François Bussy

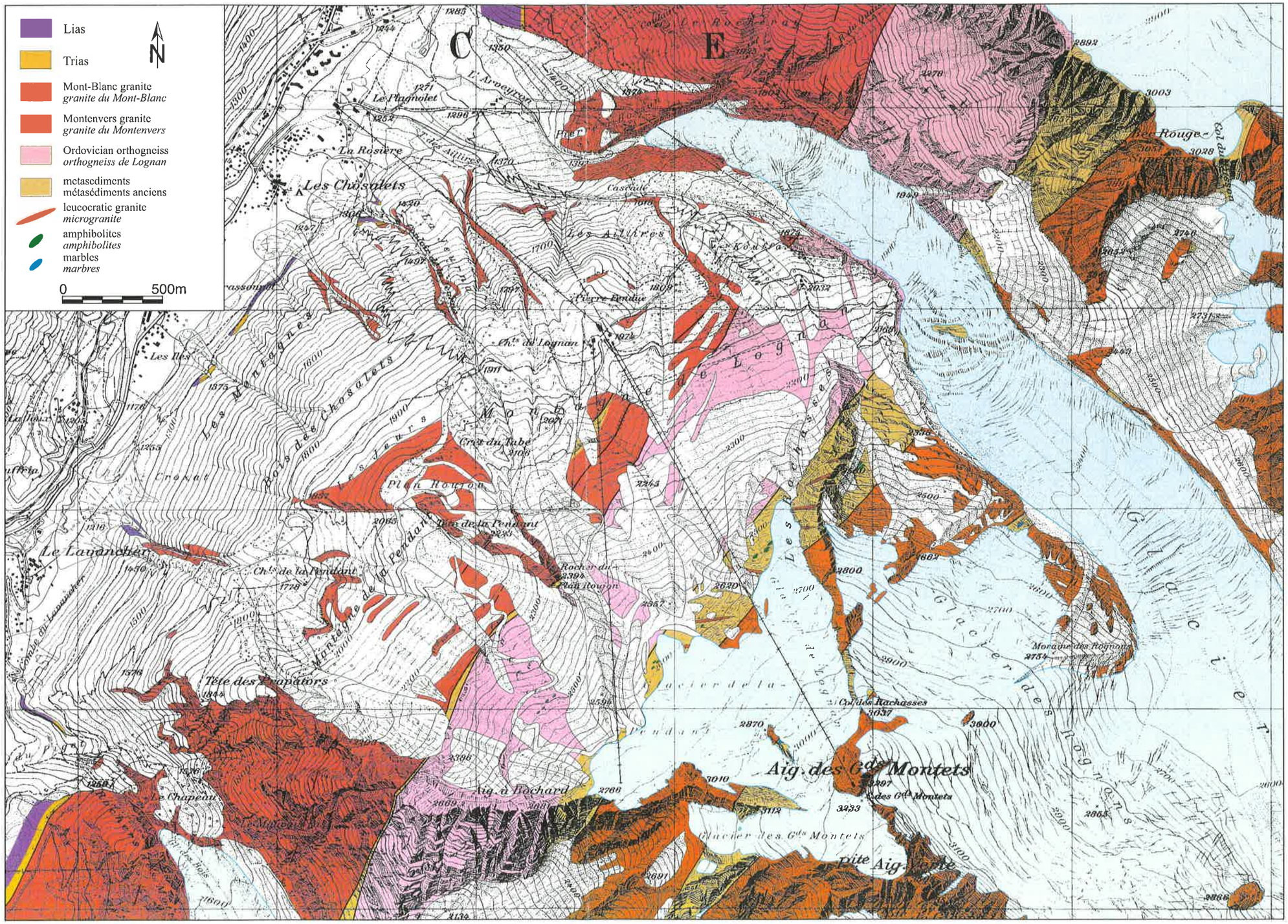

92
91
90
89
88

559 560 561 562 563 564 565

Mémoires de Géologie (Lausanne)

No. 1* BAUD A. 1987. Stratigraphie et sédimentologie des calcaires de Saint-Triphon (Trias, Préalpes, Suisse et France). 202 pp., 53 text-figs., 29 pls.

No. 2 ESCHER A., MASSON H. and STECK A. 1988. Coupes géologiques des Alpes occidentales suisses. 11 pp., 1 text-figs., 1 map.

No. 3* STUTZ E. 1988. Géologie de la chaîne Nyimaling aux confins du Ladakh et du Rupshu (NW-Himalaya, Inde). Evolution paléogéographique et tectonique d'un segment de la marge nord-indienne. 149 pp., 42 text-figs., 11 pls. 1 map.

No. 4 COLOMBI A. 1989. Métamorphisme et géochimie des roches mafiques des Alpes ouest-centrales (géoprofil Viège-Domodossola-Locarno). 216 pp., 147 text-figs., 2 pls.

No. 5 STECK A., EPARD J.-L., ESCHER A., MARCHANT R., MASSON H. and SPRING L. 1989 Coupe tectonique horizontale des Alpes centrales. 8 pp., 1 map.

No. 6 SARTORI M. 1990. L'unité du Barrhorn (Zone pennique, Valais, Suisse). 140 pp., 56 text-figs., 3 pls.

No. 7 BUSSY F. 1990. Pétrogenèse des enclaves microgrenues associées aux granitoïdes calco-alcalins: exemple des massifs varisque du Mont-Blanc (Alpes occidentales) et miocène du Monte Capanne (Ile d'Elbe, Italie). 309 pp., 177 text-figs.

No. 8* EPARD J.-L. 1990. La nappe de Morcles au sud-ouest du Mont-Blanc. 165 pp., 59 text-figs.

No. 9 PILLOUD C. 1991. Structures de déformation alpines dans le synclinal de Permo-Carbonifère de Salvan-Dorénaz (massif des Aiguilles Rouges, Valais). 98 pp., 59 text-figs.

No. 10* BAUD A., THELIN P. and STAMPFLI G. 1991. (Eds.). Paleozoic geodynamic domains and their alpidic evolution in the Tethys. IGCP Project No. 276. Newsletter No. 2. 155 pp.

No. 11 CARTER E.S. 1993 Biochronology and Paleontology of uppermost Triassic (Rhaetian) radiolarians, Queen Charlotte Islands, British Columbia, Canada. 132 pp., 15 text-figs., 21 pls.

No. 12* GOUFFON Y. 1993. Géologie de la "nappe" du Grand St-Bernard entre la Doire Baltée et la frontière suisse (Vallée d'Aoste -Italie). 147 pp., 71 text-figs., 2 pls.

No. 13 HUNZIKER J.C., DESMONS J., and HURFORD AJ. 1992. Thirty-two years of geochronological work in the Central and Western Alps: a review on seven maps. 59 pp., 18 text-figs., 7 maps.

No. 14 SPRING L. 1993. Structures gondwaniennes et himalayennes dans la zone tibétaine du Haut Lahul-Zanskar oriental (Himalaya indien). 148 pp., 66 text-figs, 1 map.

No. 15 MARCHANT R. 1993. The Underground of the Western Alps. 137 pp., 104 text-figs.

No. 16 VANNAY J.-C. 1993. Géologie des chaînes du Haut-Himalaya et du Pir Panjal au Haut-Lahul (NW-Himalaya, Inde). Paléogéographie et tectonique. 148 pp., 44 text-figs., 6 pls.

No. 17* PILLEVUIT A. 1993. Les blocs exotiques du Sultanat d'Oman. Evolution paléogéographique d'une marge passive flexurale. 249 pp., 138 text-figs., 7 pls.

No. 18* GORICAN S. 1994. Jurassic and Cretaceous radiolarian biostratigraphy and sedimentary evolution of the Budva Zone (Dinarides, Montenegro). 120 pp., 20 text-figs., 28 pls.

No. 19 JUD R. 1994. Biochronology and systematics of Early Cretaceous Radiolaria of the Western Tethys. 147 pp., 29 text-figs., 24 pls.

No. 20 DI MARCO G. 1994. Les terrains accrétés du sud du Costa Rica. Evolution tectonostratigraphique de la marge occidentale de la plaque Caraïbe. 166 pp., 89 text-figs., 6 pls.

No. 21* O'DOGHERTY L. 1994. Biochronology and paleontology of Mid-Cretaceous radiolarians from Northern Apennines (Italy) and Betic Cordillera (Spain). 415 pp., 35 text-figs., 73 pls.

No. 22 GUEX J. and BAUD A. (Eds.). 1994. Recent Developments on Triassic Stratigraphy. 184 pp.

No. 23 BAUMGARTNER P.O., O'DOGHERTY L., GORICAN S., URQUHART E., PILLEVUIT A. and DE WEVER P. (Eds.). 1995. Middle Jurassic to Lower Cretaceous Radiolaria of Tethys: Occurrences, Systematics, Biochronolgy. 1162 p.

No. 24 REYMOND B. 1994. Three-dimensional sequence stratigraphy offshore Louisiana, Gulf of Mexico (West Cameron 3D seismic data). 215 pp., 169 text-figs., 49 pls.

No. 25 VENTURINI G. 1995. Geology, Geochronology and Geochemistry of the Inner Central Sezia Zone. (Western Alps - Italy). 183 pp. 57 text-figs, 12 pls.

No. 26 SEPTFONTAINE M., BERGER J.P., GEYER M., HEUMANN C., PERRET-GENTIL G. and SAVARY, J. 1995. Catalogue des types paléontologiques déposés au Musée Cantonal de Géologie, Lausanne. 76 pp.

No. 27 GUEX, J. 1995. Ammonites hettangiennes de la Gabbs Valley Range (Nevada, USA). 130 pp., 22 figs., 32 pl.

*: out of print (continued inside)

Order from **Institut de Géologie et Paléontologie,**
Université de Lausanne. BFSH-2. CH-1015, SWITZERLAND.
http://www-sst.unil.ch/publications/memoires.htm Fax: (41) 21-692.43.05
Bank Transfer: Banque Cantonale Vaudoise 1002 Lausanne
Account Number: **C.323.52.56** Institut de Géologie, rubrique: Mémoires
Price CHF 30 per volume except volume 23 (CHF 100). The price doesn't include postage and handling.
- Please do not send check -